UNIVERSIDAD COMPLUTENSE DE MADRID

FACULTAD DE CIENCIAS QUÍMICAS

Departamento de Bioquímica y Biología Molecular

TESIS DOCTORAL

Análisis molecular del mecanismo de formación de poros por parte de las actinoporinas

Molecular analysis of pore formation mechanism by actinoporins

MEMORIA PARA OPTAR AL GRADO DE DOCTOR

PRESENTADA POR

Sara García Linares

Directores

José G. Gavilanes Franco
Álvaro Martínez del Pozo

Madrid, 2017

Universidad Complutense de Madrid
Facultad de Ciencias Químicas
Departamento de Bioquímica y Biología Molecular I

ANÁLISIS MOLECULAR DEL MECANISMO DE FORMACIÓN DE POROS POR PARTE DE LAS ACTINOPORINAS

MOLECULAR ANALYSIS OF PORE FORMATION MECHANISM BY ACTINOPORINS

TESIS DOCTORAL

Sara García Linares

Directores:
Dr. José G. Gavilanes Franco
Dr. Álvaro Martínez del Pozo

Madrid, 2016

A mis padres.
A Dani.

A mis directores de Tesis, Álvaro y Pepe, por su dedicación (volcándose en todo momento con cada uno de nosotros), por sus acertados consejos y por crear un ambiente de grupo en el que venir al trabajo apetece cada día. Un modelo a seguir como científicos y como personas.

I want to thank Prof. Peter Slotte and his lab (Terhi, Jenny, Thomas, Oskar, Max, Helen, Sazzad) for their warm welcome in their group. It was a great pleasure to visit Turku and work with such a great team.

Queremos agradecer al Dr. Germán Rivas por llamar nuestra atención sobre la existencia de los nanodiscos. Al Dr. Jaime Martín Benito y la Dra. Rocío Arranz, sin cuyo inestimable trabajo no habríamos podido obtener el modelo del poro. A la Dra. Marta Bruix y su laboratorio por años de fructífera colaboración.

A Javier y sus chicos, a Mercedes y a todos los integrantes del Departamento. No se puede desear mejores compañeros de trabajo.

A mis compañeras Sara Abián, Clara, Lucía, Míriam y Laura por todos los buenos momentos dentro y fuera del laboratorio. A mis “pupilos” Espe, Moisés y Juan por las risas en la comida, las búsquedas en la RAE y por su inagotable ayuda haciendo programas, mejorando figuras y buscando dobles espacios.

A Lola, la persona con más talento docente que he conocido y de la cuál sigo aprendiendo. Mis años con ella en el conservatorio han contribuido enormemente a convertirme en la persona que soy hoy en día.

A mi familia. Esa gran tribu que me hace sentir arropada y segura. Y en especial a mis padres. ¿Qué puedo decir? Me lo han dado todo. Han sido un apoyo constante durante toda mi vida. Les debo años de esfuerzo trabajando por mi futuro y toneladas de recuerdos felices.

A Dani, que apareció de sopetón para quedarse. La mejor compañía en los días buenos y mi oasis en el desierto en los que no lo son tanto. Contigo he aprendido a jugar en equipo y quiero seguir haciéndolo durante muchos años.

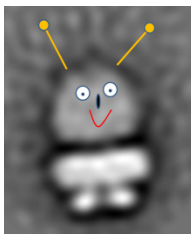

TABLE OF CONTENTS

ABBREVIATIONS

ATR-FTIR	attenuated total reflection-Fourier transform infrared spectra
BA	benzyl alcohol
CD	circular dichroism
CH_2-PSM	PSM analogue with its proximal steric oxygen group replaced by a -CH_2- group
Chol	cholesterol
CPE-Me_2	N-palmitoyl ceramide phosphoethanolamine-N,N-dimethyl
DGR	a mutant version of StnII where Arg141 and Asp143 are substituted by Asp and Arg, respectively
dh-SM	dihydro sphingomyelin
DHPC	dihexanoyl phosphatidylcholine
DOPC	1,2-dioleoyl-*sn*-glycero-3-phosphocholine
DPC	dodecylphosphocholine
DPH	1,6-diphenyl-hexatriene
DPPC	1,2-dipalmitoyl-*sn*-glycero-3-phosphocholine
EAQ	a mutant version of StnII where Arg141, Gly142 and Asp143 are substituted by Glu, Ala and Gln, respectively
EM	electron microscopy
EqtII	equinatoxin II
FraC	fragaceatoxin C
GUV	giant unilamellar vesicles
ITC	isothermal titration calorimetry
LUV	large unilamellar vesicle
MOPS	3-(N-morpholino)propanesulfonic acid
NMR	nuclear magnetic resonance
PC	phosphatidylcholine
PCer	phosphatidyl ceramide
PFT	pore forming toxin
POC	phosphocholine
POPC	1-palmitoyl-2-oleoyl-*sn*-glycero-3-phosphocholine
PSM	palmitoyl sphingomyelin
OSM	oleoyl sphingomyelin
RAD	a mutant version of StnII where Gly142 is substituted by Ala
RHA	relative haemolytic activity
RMB	relative membrane binding
SM	sphingomyelin
SPR	surface plasmon resonance
StnI	sticholysin I

StnII	sticholysin II
T_m	protein denaturation temperature
tPa-SM	*trans*-parinaroyl sphingomyelin
W43F	a mutant version of StnII where Trp43 is substituted by Phe
W43/110F	a mutant version of StnII where Trp43 and Trp110 are substituted by Phe
W43/114F	a mutant version of StnII where Trp43 and Trp114 are substituted by Phe
WquadrupleF	a mutant version of StnII where Trp43, Trp110, Trp114 and Trp115 are substituted by Phe
wt	wild-type
WtripleF	a mutant version of StnII where Trp43, Trp110 and Trp114 are substituted by Phe

RESUMEN / SUMMARY

Introducción

Las actinoporinas constituyen una familia de proteínas tóxicas sintetizadas por anémonas marinas. Son proteínas pequeñas, básicas y normalmente sin cisteínas. Pertenecen al grupo de las toxinas formadoras de poros (PFT en inglés) y su actividad tóxica radica, como su propio nombre indica, en su capacidad para formar poros en las membranas biológicas. Todas las PFT tienen un comportamiento dual según el cual permanecen mayormente en forma monomérica y establemente plegadas en disolución acuosa pero, cuando interaccionan con membranas lipídicas de una composición específica, se integran en la bicapa como estructuras oligoméricas. Las actinoporinas tienen una elevada identidad de secuencia pero muestran grandes diferencias en términos de solubilidad y actividad hemolítica.

Todas las actinoporinas estudiadas hasta ahora se pliegan en forma de sándwich β, compuesto por 10-12 hebras β flanqueadas por dos hélices α. La hélice anfipática en el extremo N-terminal parece ser extremadamente importante para la funcionalidad final del poro, ya que se ha propuesto que se extiende y se inserta en la membrana para formar las paredes del poro. Desde un punto de vista funcional, tres regiones más son importantes en la estructura de las actinoporinas: un sitio de unión a fosfocolina (POC), un racimo de residuos aromáticos y un grupo de aminoácidos básicos. Estas regiones estarían implicadas en el reconocimiento de los lípidos y la unión a la membrana.

Las membranas diana deben contener esfingomielina (SM), pero otras condiciones (como la presencia de esteroles, la coexistencia de fases o dominios, la compactibilidad, la fluidez y la fuerza de la red de puentes de hidrógeno en la interfase) parece que también tienen gran influencia en la formación de los poros.

Existe un consenso general acerca de los pasos que llevan a la formación del poro. Primero, las actinoporinas se unen a la membrana guiadas por la afinidad a alguno de sus componentes, probablemente SM. Esta interacción conllevaría un aumento de la concentración de proteína en la interfase lípido-agua que resultaría en su oligomerización en la superficie de la membrana. Después, la hélice α N-terminal se separaría del sándwich β y se colocaría paralela a la membrana. Al mismo tiempo, tendría lugar la oligomerización. Finalmente, la hélice se insertaría en la membrana. Sin embargo, varios aspectos de este mecanismo, como la estequiometria del poro, el orden de eventos que llevan a la inserción de la hélice o la existencia de un preporo son aún objeto de intenso debate.

Objetivos

Los objetivos de este trabajo son: (i) el estudio de la relevancia de la composición lipídica de la membrana en cada paso del mecanismo de acción de las

actinoporinas; (ii) la producción de actinoporinas naturales y artificiales con el propósito de estudiar sus características estructurales y funcionales y su habilidad para interaccionar con diferentes vesículas lipídicas y/o membranas biológicas; y, finalmente, (iii) el estudio del mecanismo de ensamblaje, estructura y estequiometria de un poro funcional, así como la influencia de la composición de la membrana en su estructura y funcionalidad mediante el uso de diferentes sistemas lipídicos, incluyendo nanodiscos.

Resultados y Discusión

La contribución de los lípidos es relevante en cada paso del mecanismo de acción de las actinoporinas. Como parte del trabajo presentado en esta Tesis, se ha mostrado que el colesterol (Chol) incrementó la cinética de la formación del poro de esticolisina II (StnII), probablemente por el efecto del Chol sobre la orientación y la dinámica de la cabeza de la SM. Por el contrario, la adición de fosfatidil ceramida (PCer) inhibió la unión de StnII a la membrana y por tanto la formación del poro. Se ha interpretado que esto se debe a la interacción de PCer con SM, lo cual lleva a la formación de un dominio altamente ordenado. El Chol es capaz de secuestrar la SM y revertir parcialmente el efecto de la PCer.

Los enlaces de hidrógeno establecidos entre los grupos funcionales 2NH y 3OH de la SM con moléculas de lípidos y/o residuos de las actinoporinas también han demostrado ser importantes para la funcionalidad de las actinoporinas. Los correspondientes análogos metilados fueron incapaces de permitir la unión de StnII a la membrana, como se vio por experimentos de liberación de calceína, ITC y SPR.

Para analizar la influencia de residuos específicos sobre la conformación y actividad de estas proteínas se estudiaron varios mutantes. Los mutantes que afectaban a la región N-terminal han confirmado que dicha región es crucial para la formación del poro pero no parece estar implicada en el reconocimiento de la membrana. Por otro lado, las mutaciones que afectaban a las regiones implicadas en la unión a la membrana, tuvieron un profundo efecto sobre la funcionalidad de las Stn. Como en el caso de la proteína silvestre, el Chol facilitó la interacción con la membrana de la mayoría de los mutantes estudiados, probablemente debido a la modificación de la disponibilidad de las moléculas de SM y la orientación de sus cabezas.

En la secuencia de las actinoporinas hay un motivo conservado Arg-Gly-Asp de unión a integrinas. Sin embargo, en lugar de interaccionar con un receptor de tipo integrina, los resultados han sugerido que este motivo está implicado en el mantenimiento del correcto estado de oligomerización de la proteína. Así, la modificación de la Gly142 por Ala dio lugar a un mutante con la misma capacidad de unión a la membrana que la proteína silvestre pero con una marcada reducción de su actividad hemolítica.

El reemplazo de los residuos de Trp de StnII tuvo un profundo impacto en su capacidad de unión a la membrana pero la formación del poro no se vio tan afectada. Por tanto, se propuso que los residuos de Trp en las actinoporinas juegan un papel importante en el reconocimiento y unión a la membrana pero tienen poca influencia en la difusión y oligomerización necesarias para la formación de un poro funcional.

De todas las actinoporinas conocidas sólo cuatro de ellas han sido caracterizadas con detalle: EqtII, FraC, StnI y StnII. En este trabajo se han comparado las propiedades funcionales y biofísicas de estas proteínas en idénticas condiciones experimentales. Mostraron distintos comportamientos frente a modelos lipídicos simples, lo cual puede deberse a sus distintas especificidades o afinidades de unión a las membranas.

Finalmente, con el objetivo de reconstituir un poro transmembrana funcional de StnII en estado soluble, se han empleado nanodiscos. Los nanodiscos son bicapas lipídicas autoensambladas con la ayuda de una proteína de andamiaje derivada de la apolipoproteína A-1 que han permitido obtener un estructura provisional del poro transmembrana, a 10.0 Å de resolución, reconstruido a partir de imágenes de criomicroscopía electrónica.

Conclusiones

El Chol y la red de puentes de hidrógeno establecida por las moléculas de SM han demostrado ser importantes para la unión de las actinoporinas a la membrana y la formación del poro.

Mutaciones puntuales de residuos localizados en regiones clave de las actinoporinas o que alteren la libertad conformacional y/o la distribución electrostática de regiones bien definidas de la proteína dieron lugar a proteínas que presentaban una disminución en la unión a la membrana y/o formación de poro.

Los nanodiscos han demostrado ser una herramienta muy útil en el estudio de los poros transmembrana de las actinoporinas.

Introduction

Actinoporins constitute a family of toxic proteins synthesized by sea anemones. They are small, basic, and usually cysteinless proteins. They belong to the much larger group of pore forming toxins (PFTs) and their toxic activity relies, as their name suggests, in their capacity to form pores into biological membranes. All PFTs show a very similar dual behaviour by which they remain mostly monomeric and stably folded in aqueous solution but, upon interaction with lipid membranes of specific composition, they become oligomeric integral membrane structures. Actinoporins display high sequence identity but show large functional differences in terms of solubility and haemolytic activity.

All actinoporins studied so far fold as a β-sandwich motif composed of 10-12 β-strands flanked by two α-helices. The amphipathic N-terminal α-helix seems to be extremely important for the final functionality of the pore since it has been proposed to extend and insert into the membrane to form the pore walls. From a functional point of view three more regions appear as very important in actinoporins structure: A phosphocholine (POC) binding site, a cluster of aromatic residues, and an array of basic amino acids, which are involved in lipid recognition and membrane binding.

Target membranes must contain sphingomyelin (SM), but some other conditions, such as the presence of sterols, the coexistence of various phases or domains, compactness, fluidity, and the strength of the interfacial hydrogen bonding network, seem to have a great influence on their membrane pore-forming ability as well.

There is a general consensus in accepting the occurrence of steps in leading to pore-formation. First, actinoporins initially bind to the membrane guided by their affinity to some membrane component, most probably SM. This interaction would result in an increase of protein concentration at the lipid-water interface that would lead to its oligomerization on the membrane surface. Then, the N-terminal α-helix would detach from the β-sandwich, extend, and lie parallel to the membrane. Simultaneously, oligomerization would occur. Finally, the helix would insert into the membrane. However, several aspects of the mechanism, such as the stoichiometry of the pore, the order of events that lead to helix insertion or the existence of a prepore state are still subject of intense debate.

Objectives

The aims of this work were (i) the study of the relevance of lipidic membrane composition in every step of actinoporins' mechanism of action combined with (ii) the production of natural and artificial actinoporins variants with the purpose of studying their structural and functional features and their ability to interact with different lipid

model vesicles and/or biological membranes; and finally, (iii) the elucidation of the assembly mechanism, structure, and stoichiometry of a functional actinoporin pore, and the influence of membrane composition on its structure and functionality by means of the use of different lipidic systems, including nanodiscs platforms.

Results and Discussion

The contribution of lipids is relevant in every step of actinoporins' mechanism of action. As part of the work presented in this Thesis, it has been shown that cholesterol (Chol) increased pore formation kinetics by sticholysin II (StnII), probably because of Chol's effect on SM head group tilt and dynamics. On the contrary, addition of phosphatidyl ceramide (PCer) inhibited StnII binding to the bilayer and consequent pore formation. This was interpreted in terms of PCer interacting with SM, leading to the formation of a highly ordered domain. Consequently, Chol was able to sequester SM and partially reverse the inhibitory effect of PCer.

Hydrogen bonding established between 2NH and 3OH functional groups of SM with lipid molecules and/or actinoporins' residues have been shown also to be important for actinoporins' functionality. The correspondent methylated analogues failed to support stable membrane association of StnII, as it was seen by calcein leakage, ITC and SPR experiments.

In order to analyse the influence of particular residues on the conformation and activity of these proteins many mutant variants were studied. Mutants affecting the amino terminal sequence stretch have confirmed that this region is crucial for pore formation but does not seem to be involved in the arrangements needed for membrane recognition. On the other hand, mutations affecting the regions of the protein involved in membrane recognition and binding had a deep effect on Stn functionality. As with the wild-type protein, Chol significantly favoured interaction with the membrane of most mutants studied, most probably modifying availability of SM molecules and the orientation of their head groups.

Within the sequence of actinoporins there is a conserved integrin-like binding Arg-Gly-Asp motif. However, rather than interacting with an integrin-like receptor, results suggested that this motif is involved in maintaining the correct oligomerization state of the protein. Thus, the modification of Gly142 for Ala yielded a mutant variant with the same membrane binding ability as the wild-type protein but with a markedly reduced haemolysis activity.

Replacing StnII Trp residues had a deep impact on its membrane binding capability but the subsequent step leading to the formation of a functional pore were not so affected. Therefore, it was proposed that Trp residues in actinoporins play a major role in membrane recognition and binding but have only minor influence on the diffusion and oligomerization needed to assemble into a functional pore.

Of all known actinoporins, only four of them have been thoroughly characterized: EqtII, FraC, StnI, and StnII. In this work, functional and biophysical properties of these proteins have been studied in detail under identical experimental conditions. They showed quite different behaviour when studied under simpler lipid model systems, which could be due to their distinct specificities and/or membrane binding affinities.

Finally, with the aim of reconstituting a functional transmembrane pore of StnII in a soluble state, nanodiscs have been employed. They are self-assembled phospholipid bilayers encased within an engineered derivative of apolipoprotein A-1 scaffold protein which have allowed us to obtain a provisional structure of the transmembrane pore, at 10.0 Å resolution, reconstructed from cryo-electron microscopy images.

Conclusions

Chol and hydrogen bonding network established by SM molecules have shown to be important for membrane binding and pore formation by actinoporins.

Single mutations of residues located at crucial regions of actinoporins or altering the strictly required conformational freedom and/or electrostatic distribution of well-defined protein regions yielded proteins with diminished membrane binding and/or pore formation activity.

Nanodiscs have proven to be a very useful tool in the study of the transmembrane pore of actinoporins.

INTRODUCTION

Actinoporins constitute a family of toxic proteins synthesized by sea anemones and most probably stored in their nematocysts *(Basulto et al. 2006)*. They are single polypeptide chains of around 175 amino acids which usually display basic pI and are cysteinless *(Maček 1992, Anderluh et al. 2002, Alegre-Cebollada et al. 2007b)*. They belong to the much larger group of pore forming toxins (PFTs) and their toxic activity relies, as their name suggests, in their capacity to form pores into biological membranes. All PFTs show a very similar dual behaviour by which they remain mostly monomeric and stably folded in aqueous solution but, upon interaction with lipid membranes of specific composition, they become oligomeric integral membrane structures. Thus, this family of proteins represents an optimal system to study the transition from a soluble monomeric folded conformation to an oligomeric transmembrane protein and demonstrates how an identical amino acid sequence can fold into two different structures, showing the environmental influence on the energy landscape of a protein. Pore forming toxins can be classified in α-PFTs or β-PFTs, depending on the structural element that inserts into the membrane *(Parker et al. 2005, Geny et al. 2006, Anderluh et al. 2008, González et al. 2008, Iacovache et al. 2008, Mueller et al. 2009, Law et al. 2010, Mueller et al. 2010)*. Sea anemone actinoporins are α-PFTs because they insert a α-helix stretch. They are believed to participate in functions like predation, defence, and digestion and have been shown to be lethal for small crustaceans, molluscs, and fish *(Basulto et al. 2006)*. They form cation-selective pores with a diameter of 1-2 nm within biological membranes which result in a colloid-osmotic shock that leads to cell death *(Varanda et al. 1980, Maček et al. 1994, Tejuca et al. 1996, De-los-Ríos et al. 1998, Tejuca et al. 2001)*. This is the reason which explains why actinoporins show haemolytic activity when assayed against erythrocytes *(Belmonte et al. 1993, Tejuca et al. 2001)*.

Actinoporins have been so far detected in at least 20 different sea anemone species *(Maček 1992, Alegre-Cebollada et al. 2007b, Bellomio et al. 2009, Monastyrnaya et al. 2010)*, showing their ubiquitous distribution within the Actinaria order. Moreover, they display high sequence identity (between 60% and 80%) (**Fig. 1**) and appear as multigene families *(Anderluh et al. 1999)*, though only a few of the many protein isoforms coded within the same individual are actually produced in detectable amounts *(Turk 1991, Maček 1992, De-los-Ríos et al. 2000, Alegre-Cebollada et al. 2007b, Wang et al. 2008)*. The small number of changes observed can result however in large functional differences in terms of solubility and haemolytic activity *(Alegre-Cebollada et al. 2007b, Wang et al. 2008, Monastyrnaya et al. 2010, Uechi et al. 2010)*, as exemplified by StnI and StnII from *Stichodactyla helianthus*. These two actinoporins are 91% identical but show quite different haemolytic activities. The reason why a single anemone can produce several isoforms of actinoporins in its venom is still not fully understood. One possible explanation would be to expand the range of prey susceptible of being attacked *(Olivera et al. 1990)*. Such a strategy would extend and

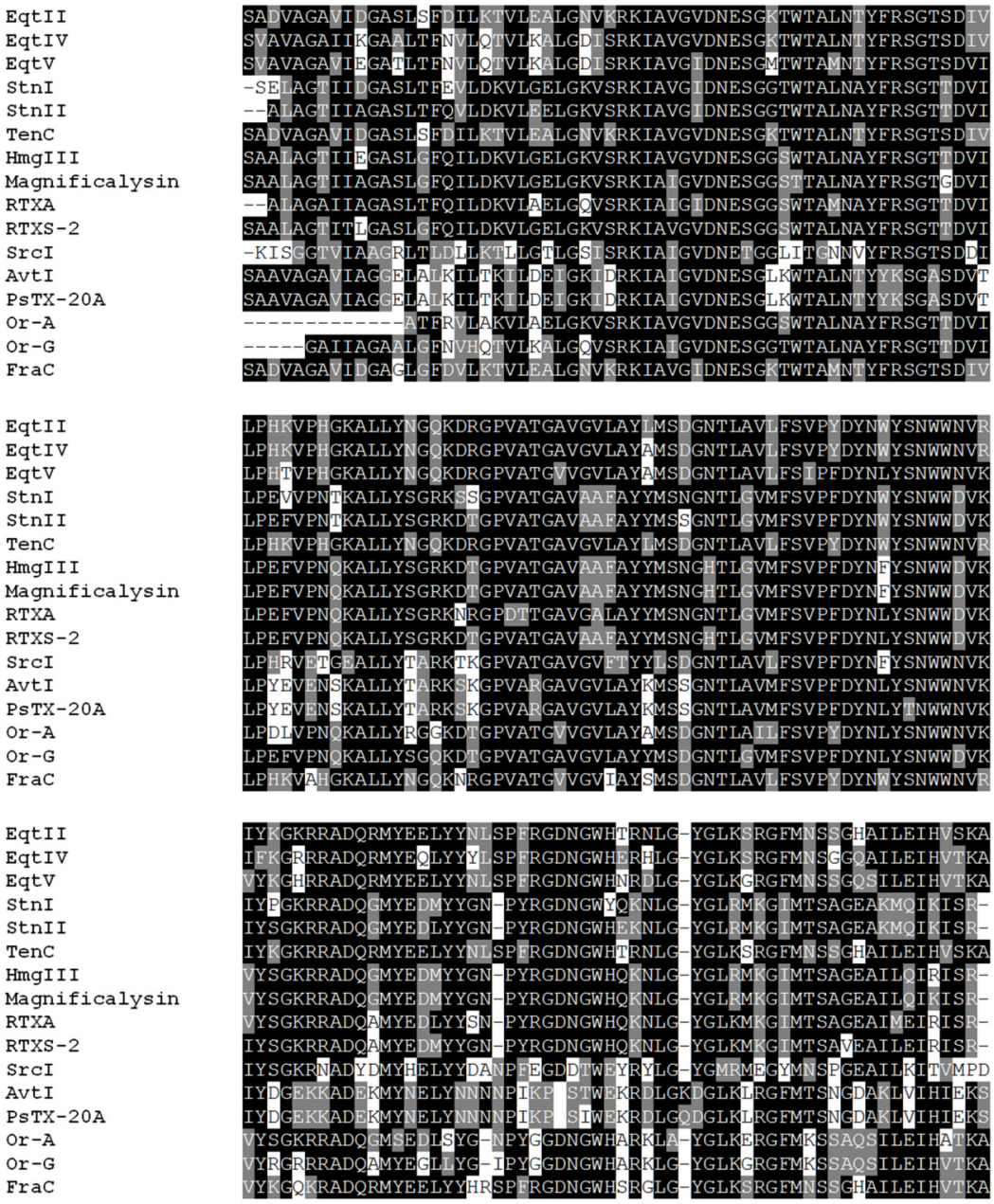

Figure 1. Sequence alignment of all known primary structures from different sea anemone actinoporins.

modulate the range of sea anemones' action. It has even been proposed an analogy with immunoglobulins which suggests that sea anemone tentacles would produce many isoforms of actinoporins because they would represent the embryo of a rudimentary defence system *(Wang et al. 2008)*. It has been recently shown the possibility that these different isoforms show synergistic activity, leading to the production of more efficient and versatile venoms *(Rivera-de-Torre et al. 2016)*. These results not only prove that StnI and StnII potentiate their lytic activity when they act together, but also indicate that they can establish functional heteropores, suggesting that actinoporins have a more complex regulated physiological mode of action than previously believed.

Structure of actinoporins

The water-soluble structures of EqtII *(Athanasiadis et al. 2001, Hinds et al. 2002)*, FraC *(Mechaly et al. 2011, Tanaka et al. 2015)*, StnI *(García-Linares et al. 2013)*, and StnII *(Mancheño et al. 2003)* are known in detail by means of X-ray crystallography and/or NMR determinations. The crystal structure of a FraC octamer, obtained after reconstitution with detergents, has been also reported *(Tanaka et al. 2015)*. All actinoporins studied so far fold as a β-sandwich motif composed of 10-12 β-strands flanked by two α-helices (**Fig. 2**). One of these helices is located near the N-terminal end and is preceded by a short 3_{10} helix *(Athanasiadis et al. 2001, Hong et al. 2002, Mancheño et al. 2003, Norton 2009, Mechaly et al. 2011)*. The first 30 residues (**Fig. 3**) appear to be the longest and only segment of the protein that can adopt alternative conformations without disrupting the fold of the β-sandwich *(Athanasiadis et al. 2001)*. This feature and the amphipathic character of the N-terminal α-helix seem to be extremely important for the final functionality of the pore since it has been proposed to extend and insert into the membrane to form the pore walls *(Malovrh et al. 2003)*. From the functional point of view three more regions appear as very important in actinoporins' structure: A phosphocholine (POC) binding site (**Fig. 4**), a cluster of aromatic residues (**Fig. 5**), and an array of basic amino acids (**Fig. 6**), which are involved in lipid recognition and membrane binding. Determination of the crystal and soluble three-dimensional structures of actinoporins, altogether with different biochemical and biophysical characterization of the natural variants and the high number of mutants of EqtII *(Hong et al. 2002, Kristan et al. 2004, Drechsler et al. 2006, Kristan et al. 2007, Rojko et al. 2013, Wacklin et al. 2016)*, StnI *(García-Linares et al. 2013, Antonini et al. 2014)* and StnII *(Castrillo et al. 2009, Pardo-Cea et al. 2010, García-Linares et al. 2014, García-Linares et al. 2015)*, has led to putative models of their topology and mode of action.

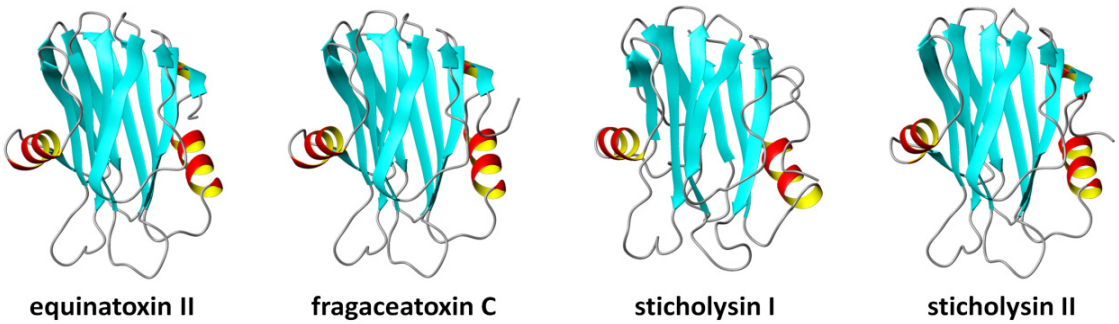

Figure 2. Three-dimensional soluble structure of equinatoxin II (EqtII, PDB 1IAZ), fragaceatoxin C (FraC, PDB 4WDC), sticholysin I (StnI, PDB 2KS4), and sticholysin II (StnII, PDB 1GWY). Diagrams were made using MOLMOL program *(Koradi et al. 1996)*.

As suggested above, the N-terminal end of actinoporins (**Fig. 3**) is essential to exert their pore forming capacity, although it does not seem so implicated in membrane recognition and binding *(Hong et al. 2002, Kristan et al. 2004)*. Depletion of

this region in EqtII or its covalent linking to the β-sandwich by means of an introduced disulfide bond prevented pore formation but did not hinder membrane binding *(Anderluh et al. 1997, Hong et al. 2002, Kristan et al. 2004)*. Even single mutations, like A10P StnII variant, which would prevent the helix extension, can preclude pore formation without affecting membrane attachment *(Alegre-Cebollada et al. 2008, García-Linares et al. 2015)*. Although it is precisely in the first 30 residues where actinoporins show more sequence variability, hydrophobic residues are quite conserved. Thus, the differences are located mainly in the hydrophilic residues, which could result in distinct conductivity across the pore, and therefore, different toxicity of the proteins *(Ros et al. 2015b)*. Peptides mimicking the N-terminal of StnI have been used to study the possible conformation of this region both in water and lipid environment. In both cases the conformation of the first 30 residues corresponded to an α-helix, but the helical content was higher in the lipid environment *(Malovrh et al. 2003)*. On the other hand, the amino-terminal peptides of EqtII and StnII are essentially unstructured and extended in water solution, respectively, but they can also acquire large helical contents in hydrophobic environments *(Casallanovo et al. 2006, Drechsler et al. 2006, Drechsler et al. 2009, Castrillo et al. 2010)*. All the studied peptides seemed to display an environmentally dependent conformational plasticity which may be highly important for exerting their function when included in the complete protein.

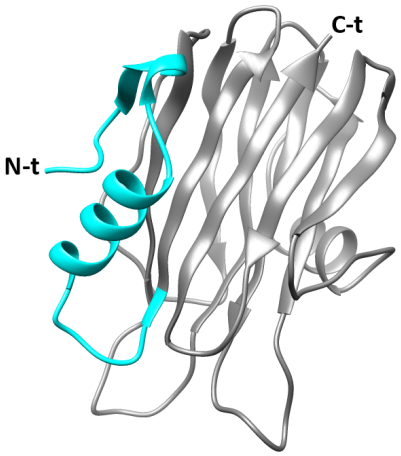

Figure 3. Diagram of StnII three-dimensional structure showing in blue the 30 first amino acids. The image was generated by UCSF Chimera program *(Pettersen et al. 2004)*.

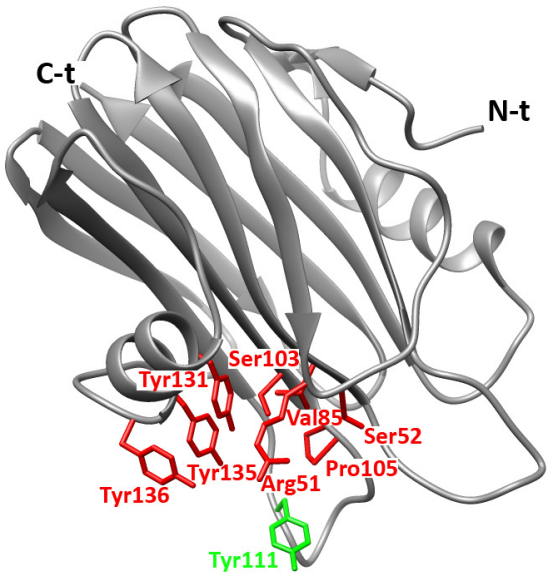

Figure 4. Ribbon representation showing the POC-binding site within the three-dimensional structure of StnII. Tyr111 is labelled in a different colour because its role is particularly discussed. The image was generated by UCSF Chimera program *(Pettersen et al. 2004)*.

Determination of a POC-StnII complex X-ray structure *(Mancheño et al. 2003)* allowed to identify a specific POC binding site composed by both hydrophobic and hydrophilic residues: Arg51, Ser52, Val85, Ser103, Pro105, Tyr111, Tyr131, Tyr135 and Tyr136 in StnII (**Fig. 4**). Some of them are also part of the aromatic cluster. Both overlapping regions seem to

constitute the main recognition and binding sites to the membrane, establishing interactions with the choline moiety and the phosphate group. In particular, Tyr111 is conserved in all the actinoporins known so far and it is located in a very flexible and highly disordered loop. However, in the crystal structure of POC-bound StnII, the aromatic ring of Tyr111 is pointing toward the phosphocholine moiety after a probable conformational change from its exposed free state *(Mancheño et al. 2003)*. Mutation of Tyr111 to Asn resulted in a dramatically decreased haemolytic activity *(Alegre-Cebollada et al. 2004, Alegre-Cebollada et al. 2008, Pardo-Cea et al. 2010, Pardo-Cea et al. 2011)* because this mutant protein is not able to bind to the membrane. The high conformational versatility of this Tyr may indeed facilitate the fast conformational changes needed for the transition from the soluble state to the membrane bound system.

Most of the known actinoporins contain an exposed cluster of aromatic residues: Phe106, Trp110, Tyr111, Trp114, Tyr131, Tyr135, Tyr136 in StnII (**Fig. 5**). Their interaction with the target membrane has been broadly established and mutations affecting this region result in less haemolytic variants with reduced affinity for lipids *(Alegre-Cebollada et al. 2004, Alegre-Cebollada et al. 2008)*. The location of some of these residues is compatible with the surface of the protein that would be in direct contact with the membrane. This observation is in agreement with the fact that aromatic rings have preference for membrane-water interfaces *(De-Planque et al. 1999)*. In this region the key residue for the establishment of the actinoporins-membrane interaction seems to be Trp110 (in close proximity to Tyr111) which penetrates into the hydrophobic core of the membrane. Mutation of the equivalent Trp112 residue in EqtII proved its implication in SM recognition *(Anderluh et al. 2005, Bakrač et al. 2008)*. Consistently, FraC Trp112 appears in the membrane binding region of the octameric crystalline pore structure reported for this protein obtained after reconstitution with detergents and seem to interact directly with lipids. Furthermore, Trp112 would participate in recognizing the lipid located at one of the two high-affinity sites for SM described for FraC oligomers *(Tanaka et al. 2015)*. Finally, the mutant StnI W111C was still able to permeabilize erythrocytes and liposomes, though at a ten-fold higher concentration

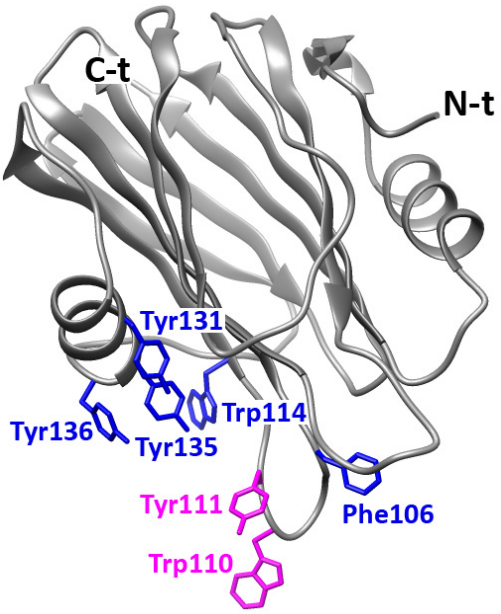

Figure 5. Diagram showing the exposed cluster of aromatic amino acids within the three-dimensional structure of StnII. Trp110 and Tyr111 are labelled in a different colour because their roles are particularly discussed. The image was generated by UCSF Chimera program *(Pettersen et al. 2004)*.

than the wild-type protein due to its lower affinity for the membrane *(Antonini et al. 2014)*. Data suggest that the membrane-recognition key role assigned to the tryptophan residue of the actinoporins represented by StnII Trp110 would be based more on its participation in maintaining a hydrophobic effect that on the establishment of interactions with specific phospholipid chemical groups.

The region rich in basic residues has been proposed to play a role in the initial steps of EqtII membrane recognition via interaction with negatively charged regions of the lipid head groups *(Hinds et al. 2002)*. In StnII this array would be composed of Lys118, Lys123, Arg124, Arg125, Lys149, Arg156, Arg175 (**Fig. 6**). Interestingly, most of the Arg residues in this StnII stretch appear as Lys in EqtII, and vice versa. An additional EqtII Lys residue (Lys123) appears as a Ser in the equivalent StnII position (Ser121). Maybe these small changes are responsible of the apparent different lipid affinities of these two proteins *(De-los-Ríos et al. 2000, Alegre-Cebollada et al. 2007a, Alegre-Cebollada et al. 2008, Bakrač et al. 2008, Bakrač et al. 2010b)*. Although it is not part of this region, Arg29 has revealed itself as very important for StnII structure (**Fig. 6**). It is located at the hinge connecting the N-terminal α-helix to the β-sandwich core and its substitution with Gln provokes long range effects on the interfacial binding site of the protein *(Pardo-Cea et al. 2011)*. The distribution of the electrostatic potential along this surface changes dramatically, with a significant loss of the positive potential. This could affect the efficient targeting of the protein to the membrane and then perturb the specific interactions with the negative phosphate groups of the membrane phospholipids.

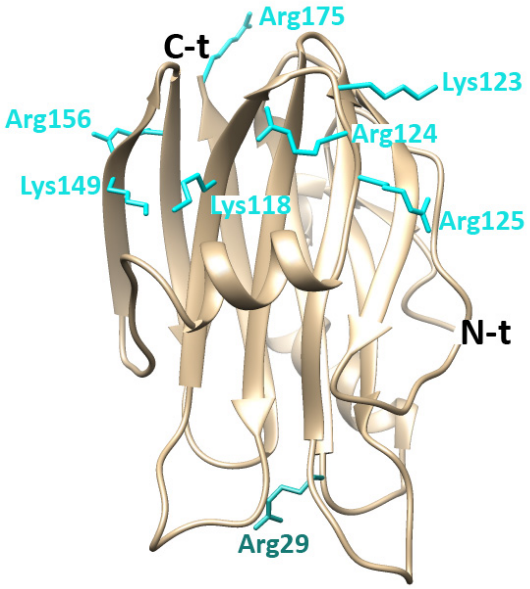

Figure 6. Diagram showing the relative location of the array of basic amino acids (light blue) as well as the side-chain of Arg29 (dark blue) within the three-dimensional structure of StnII. The image was generated by UCSF Chimera program *(Pettersen et al. 2004)*.

Role of lipids in actinoporins' functional activity

There is a great interest in understanding the molecular mechanism of actinoporins' action since they are a very good model for studying different aspects of transmembrane protein structure and function. Binding of water soluble pore forming toxin molecules to the target membrane is usually driven by rather specific interactions between a particular binding site located on the protein and molecules embedded in the membrane moiety *(Rojko et al. 2016)*. In this regard, actinoporins are

not an exception. They are able to form pores within model membranes in the absence of any other protein, showing that they do not need a protein receptor *(Shin et al. 1979, Belmonte et al. 1993, Tejuca et al. 1996, De-los-Ríos et al. 1998)*. Their incorporation into a membrane obviously depends largely on lipid bilayer composition and membrane physicochemical state *(Shin et al. 1979, Belmonte et al. 1993, Tejuca et al. 1996, De-los-Ríos et al. 1998, Valcárcel et al. 2001, Martínez et al. 2007, García-Linares et al. 2016, Palacios-Ortega et al. 2016, Rojko et al. 2016)*. Thus, membranes must contain sphingomyelin (SM) *(Bernheimer et al. 1976, De-los-Ríos et al. 1998, Alegre-Cebollada et al. 2006, Alegre-Cebollada et al. 2008, Bakrač et al. 2008, Maula et al. 2013)*, but some other conditions, such as the presence of sterols, the coexistence of various phases or domains, compactness, fluidity, and the strength of the interfacial hydrogen bonding network, seem to have a great influence on their membrane pore-forming ability as well *(Varanda et al. 1980, De-los-Ríos et al. 1998, Barlič et al. 2004, Martínez et al. 2007, Bakrač et al. 2010a, Pedrera et al. 2014, Alm et al. 2015, Pedrera et al. 2015, García-Linares et al. 2016, Palacios-Ortega et al. 2016)*.

Given the apparent major role of the array of basic amino acids (**Fig. 6**) and the basic pI value of most actinoporins, electrostatic interactions between positively charged residues and negatively charged membranes could be expected, but data suggest that the net charge plays a minor role in actinoporin-membrane interactions *(Hong et al. 2002, Bakrač et al. 2008)*. A close look to EqtII, StnII and the acidic actinoporin from *Sagartia rosea (Jiang et al. 2002)* surface charge distribution reveals that charged residues are not conserved across the protein surface and absent from the region that forms the membrane binding site *(Rojko et al. 2016)*. Instead, it is well accepted that Trp residues play a key role in actinoporins binding to the membranes *(Anderluh et al. 1999, Malovrh et al. 2000, Hong et al. 2002, Malovrh et al. 2003, Alegre-Cebollada et al. 2004, Anderluh et al. 2005, Castrillo et al. 2010)*. Thus, mutating hydrophobic residues Trp112 or Trp116 (EqtII or FraC numbering) lowered binding by more than 90%, implying that protein-membrane interaction is at least partially hydrophobic *(Hong et al. 2002, Alegre-Cebollada et al. 2008, Tanaka et al. 2015)*. ^{19}F labelling of EqtII tryptophans enabled a detailed *in vitro* study of their importance for lipid binding. Accordingly, the most affected ^{19}F resonance in the presence of phospholipid micelles or bicelles was that of Trp112, followed by Trp116 *(Anderluh et al. 2005)*. NMR studies of StnI confirmed that aromatic amino acid residues from the interfacial binding site Trp111, Tyr112, Trp115, Tyr132, Tyr136 and Tyr137 (**Fig. 5**) are inserted into the dodecylphosphocholine (DPC) or dihexanoyl phosphatidylcholine (DHPC) micelles, providing the first contact point with the lipid interface *(Castrillo et al. 2010, López-Castilla et al. 2014)*. It has been recently observed that up to four DHPC molecules can bind to FraC monomer in the crystal structures *(Tanaka et al. 2015)*. Two of these lipid binding sites (L2 and L3 in *Tanaka et al. 2015*) were occupied in independent crystal structures more frequently and could represent the primary sites for protein attachment to lipid membranes. Co-crystallization of StnII with

phosphocholine (POC), which is the essential component of both SM and phosphatidylcholine (PC) head groups (**Fig. 7**), revealed important residues for binding which are also conserved in other actinoporins: Ser52, Val85, Ser103, Pro105, Tyr111, Tyr131, Tyr135 and Tyr136 *(Mancheño et al. 2003)*. Interestingly, POC binds in an orientation that partially overlaps with L2 and L3 binding sites of FraC *(Rojko et al. 2016)*. NMR study of StnI precisely mapped DHPC micelles binding site residues and most of them also overlapped with DHPC and POC binding sites of FraC and StnII, respectively *(Castrillo et al. 2010, López-Castilla et al. 2014)*. Finally, it has been recently published an NMR study that enabled identifying residues involved in binding of EqtII to DPC micelles *(Weber et al. 2015)* and mapping again the interfacial binding site to the same regions of the molecule. Altogether these results allowed identification of the most important residues for lipid recognition, many of them previously identified in mutagenesis studies to be important for actinoporins' permeabilizing activity. Everything suggests then that actinoporins' interfacial binding site allows interaction with several head groups of membrane lipids *(Tanaka et al. 2015)*. The presence of multiple binding sites for SM and PC head group could increase the affinity to lipid membranes during initial membrane interactions *(Rojko et al. 2016)*.

As mentioned above, many factors influence the actinoporins' conformational changes occurring upon the transition from the water media to the inserted state *(Alegre-Cebollada et al. 2008, Ros et al. 2015a)*. Thus, high affinity recognition of SM by the protein seems to be very important for its specific attachment to a particular membrane but the following effects observed probably depend also on the physical properties derived from its particular composition and not only from its SM content. Within this idea, the actinoporins so far studied seem to show different membrane composition preferences, but the specificity of actinoporins for SM has been convincingly demonstrated *(Bakrač et al. 2008)*. For example, incubating sticholysin I with SM prior to erythrocyte addition reduces toxin haemolytic activity *(Valcárcel et al. 2001)*. Identical effect was achieved when SM was removed from erythrocytes by sphingomyelinase *(Bernheimer et al. 1976)*, although recent results seem to indicate that this could be also due to the production of the corresponding ceramides and not

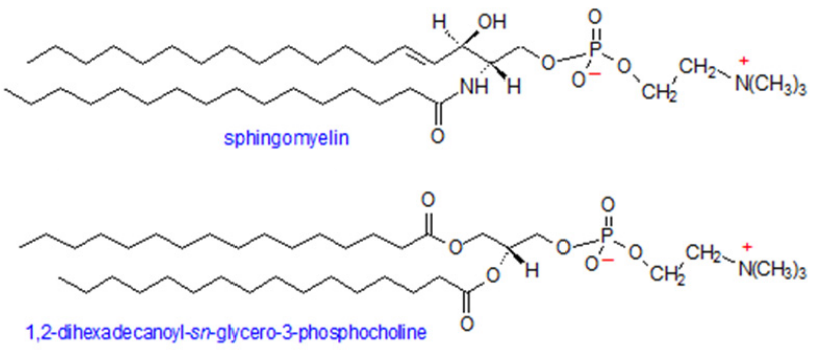

Figure 7. Schematic representation of the molecular structure of SM and DPPC.

only to SM depletion *(Alm et al. 2015)*. This effect was later shown also for EqtII *(Bakrač et al. 2008)*. In a dot-blot binding assay, phosphatidylcholine is not recognized by equinatoxin II, neither is ceramide nor sphingosylphosphorylcholine, so in this case, it has been postulated that SM functions for EqtII as a real membrane receptor but of lipidic nature *(Bakrač et al. 2008)*. Site-directed mutagenesis of EqtII revealed residues Trp112 and Tyr113 to be responsible for specific SM recognition. Interestingly, sea anemones possess within their membranes analogues of SM to which actinoporins do not bind, making them resistant to their own toxins *(Meinardi et al. 1995)*. For example, the haemolytic activity of actinoporin from *Phymactis clematis* was inhibited by SM but not by sphingolipids purified from the same sea anemone. This specific recognition is probably based on the existence of a different phospholipid head group in the SM analogues.

However, it appears that under specific conditions, some actinoporins may show low-affinity interaction with phosphatidylcholines and cause membrane permeabilization in the absence of SM, but only in the presence of phase coexistence, most probably mediated by cholesterol *(De-los-Ríos et al. 1998, Caaveiro et al. 2001, Schön et al. 2008)*. Thus, coexistence of different phases on the membrane seems to be an important factor, if not for attachment, at least for the final formation of the pore *(De-los-Ríos et al. 1998, Menestrina et al. 1999, Alegre-Cebollada et al. 2008)*. For example, studies performed with giant unilamellar vesicles (GUV) have shown that SM strongly enhanced binding of EqtII, but was not sufficient for membrane permeabilization. Pores were formed only when, in addition to the presence of SM, liquid ordered and disordered phases coexisted *(Schön et al. 2008)*. Moreover, there was permeabilization if these GUV were made only of DOPC:DPPC:Chol (1:1:1) mixtures which do not contain SM but do exhibit phase coexistence. Although these experiments were made at far higher concentrations of EqtII compared to the haemolysis assays, the results showed that this actinoporin can also interact with lipid membranes in the absence of SM. In this case, very similar results were obtained for StnII with other membrane systems. According to the results published so far for this particular actinoporin, the presence of SM does not seem to be as crucial as it is for EqtII *(De-los-Ríos et al. 1998, Alegre-Cebollada et al. 2006, Alegre-Cebollada et al. 2007a, Alegre-Cebollada et al. 2008)*.

The presence of microdomains could explain why in Chol-containing bilayer systems actinoporins are much faster in producing calcein leakage. This ability would not necessarily reflect a higher affinity for the membrane but rather an improved easiness to diffuse, oligomerize and penetrate the bilayer, given that membrane binding would not be now the rate-limiting step. Synchrotron radiation CD spectroscopic studies have revealed that the peptide corresponding to residues 1–32 of EqtII adopts very different conformations when examined in water, DPC micelles, or small unilamellar vesicles composed of DOPC or DMPC *(Drechsler et al. 2009)*. These conformations were highly influenced by the presence of SM and Chol, confirming the

importance of the lipid properties arising from the coexistence of liquid ordered and disordered phases and the dual role of SM as a specific attachment and as a promoter of the bilayer organization necessary for membrane lysis *(Drechsler et al. 2009)*. In agreement with all these results, different experiments have shown that StnII is able to promote pore formation in COS-7 cells via its interaction with the domains enriched in SM and Chol known as cellular rafts *(Alegre-Cebollada et al. 2006)*. Cellular membrane is much more complex than binary or ternary model lipid mixtures and liquid ordered/liquid disordered (L_o/L_d) coexistence in model membranes may not be enough to adequately explain lateral heterogeneity in cell membranes.

The role of Chol in actinoporins' function is still controversial. In addition to its presumed favouring pore-formation ability by inducing the existence of lipid-domain boundaries, the latest published results suggest different roles in terms of affecting the physico-chemical state of the membrane. Data and molecular interpretation are compatible with the suggestion that SM-binding toxins (e.g., EqtII) preferentially bind to molecules carrying a phosphocholine head group at the disordered/ordered domain interfaces *(Schön et al. 2008)* since EqtII oligomerization to pores apparently occurs in the liquid disordered phase *(Rojko et al. 2014)*. Furthermore, it has been recently published that StnI binds and permeabilizes with higher efficiency sterol-containing membranes independently of their ability to form domains. The formation of a liquid disordered (L_d) phase has been suggested by these authors out as the most suitable platform for pore formation due to its increased fluidity *(Pedrera et al. 2015)*. It has been also suggested that lipid packing defects arising at the interfaces between coexisting phases may function as preferential binding-sites for the toxin (because SM head group is exposed for easier recognition or because exposing hydrophobic acyl

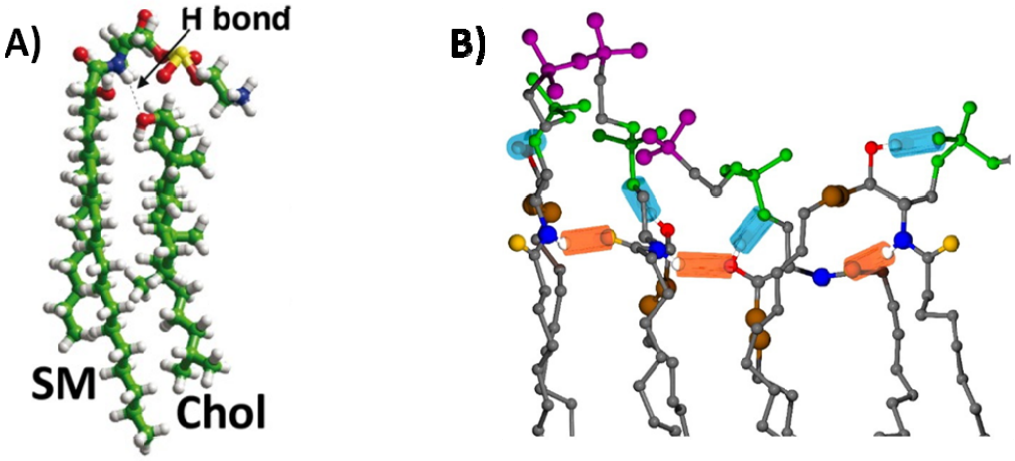

Figure 8. A) SM tilted conformation induced by the hydrogen bond formed between the OH group of Chol and the NH group of the sphingolipids. Atom colors: C (green), H (white), P (yellow), O (red) and N (blue) *(Fantini et al. 2013)*. **B)** Molecular image snapshot of typical intermolecular (orange) and intramolecular (cyan) hydrogen bonding in PSM bilayers. Atom colors: $(CH_3)_3N$ (purple), PO_4 (green), amide N (blue), amide O (orange), hydroxyl O (red), C=C (brown), all other C atoms (gray) *(Venable et al. 2014)*.

chains lowers the energy barrier for helix insertion). Association with these interfaces between domains would function as an efficient concentration strategy confining the toxins to a space where oligomerization and pore formation could take place at very low bulk protein concentrations *(Barlič et al. 2004)*.

Further, Chol appears to affect the SM phosphocholine head group orientation and dynamics (**Fig. 8A**) similarly as shown for glycerophospholipids *(Niemela et al. 2004, Róg et al. 2006, Björkbom et al. 2010)* and may alter the accessibility of phosphocholine group for toxin binding *(Barlič et al. 2004)*. Addition of Chol at about 10 mol% to POPC:PSM vesicles increased pore formation kinetics significantly, while the *trans*-parinaroyl sphingomyelin (tPa-SM) order parameter increased only moderately *(Alm et al. 2015)*. Since the phosphocholine head group is an important recognition site for StnII, it is likely that the Chol's effect on SM head group tilt and dynamics affected StnII binding and/or oligomerization more than Chol's effect on bilayer fluidity. Nevertheless, recent results seem to indicate that some actinoporins' residues can be highly sensitive to the concentration of this lipid within the membrane, such as the conserved Phe16 of FraC, which is critical for pore formation in Chol-rich membranes *(Morante et al. 2015a)*.

Chol is known to affect membrane fluidity via its effects on phospholipid acyl chain order *(Feinstein et al. 1975, Jaikishan et al. 2010)*. In a POPC:PSM (4:1) bilayer model Chol will increase mostly PSM acyl chain order, but will likely also influence POPC acyl chain order to some extent. Given the present state of the actinoporins' membrane-interaction studies, it is very important to remark how Chol will also interfere with SM-SM intra and interlipid hydrogen bonding *(Róg et al. 2006)*, which will likely affect SM properties in the SM rich domains *(Bruzik et al. 1990, Aittoniemi et al. 2006)* as well as the actual lateral packing of the membrane. Phospholipid head group mobility and tilt is indeed known to be different in gel and fluid states *(Cullis et al. 1976)*.

Because SM and PC share phosphocholine head group (**Fig. 7**), other SM regions below phosphocholine head group must be involved in specific interaction with actinoporins *(Bakrač et al. 2008)*. These observations together suggest that both the phosphocholine head group and the hydrogen bonding interfacial groups in SM (the 2NH and the 3OH) (**Fig. 8B**) are important for toxin binding. Using molecular docking of palmitoyl SM (PSM) to a 3D model of StnII, it was suggested that Tyr135 in the POC-binding site stabilized SM binding by interactions with the 2NH and 3OH of PSM, whereas Tyr111 and Tyr136 formed hydrogen bonds to phosphate oxygen, possibly explaining the binding specificity for SM. Methylation of 2NH or 3OH PSM groups or the mutation of any of the mentioned Tyr highly impaired membrane binding and pore formation, according to SPR, ITC and calcein leakage measurements *(Maula et al. 2013, García-Linares et al. 2015)*.

One of the most accepted models for actinoporins' pore formation (see below; **Fig. 9**) involves membrane curving to induce a torus-like channel thanks to the

assistance of PFTs. In this model, the walls of the channel are formed by both polypeptide chains and lipid head groups. To avoid the high energetic cost of exposing their hydrophobic acyl chains to the aqueous environment, lipids bend and form a highly curved non-bilayer structure at the pore edge that connects the two monolayers of the membrane with a continuous surface *(Cosentino et al. 2016)*. If this is correct, minor amounts of lipids favouring non-lamellar organizations should augment the efficiency of pore formation. Accordingly, inclusion of PE in vesicles containing both PC and SM, did not substantially modify the insertion of StnII, but increased the rate of pore formation *(Álvarez et al. 2009)*. Within this same idea, the presence of small quantities of anionic lipids rendered membranes more sensitive to actinoporin-induced permeabilization *(Valcárcel et al. 2001)*. FTIR, ^{31}P NMR, and electron paramagnetic resonance (EPR) experiments have also proven how EqtII induces non-lamellar lipid structures which would be consistent with the formation of a toroidal lipid pore *(Valcárcel et al. 2001, Álvarez et al. 2003, Anderluh et al. 2003, Alegre-Cebollada et al. 2007a)*. In addition, actinoporins are able to induce lipid flip-flop between internal and external leaflets of liposome membranes and to permeabilize liposomes in the presence of phosphatidic acid, a strong inducer of negative membrane curvature *(Valcárcel et al. 2001)*.

It seems clear then that actinoporins' permeabilizing activity depends on membrane lipid composition but ionic concentration and variety of the medium can be also a determinant factor. Results have shown that StnII haemolytic activity is promoted by Ca^{2+} and Mg^{2+} and inhibited by Co^{2+} and Mn^{2+} *(Veitia et al. 1995)*. In particular, some results suggest that StnII pore-forming ability is improved by an increase in intracellular calcium associated to membrane phospholipids translocation elicited by scramblases *(Celedón et al. 2009)*. The oxidative status of the red blood cells, regarding membrane lipid composition, seems to be another feature to take into account when studying actinoporins' effect on cells *(Celedón et al. 2011)*. All these aspects of their function have not been deeply studied yet and deserve future attention and development.

From a very different point of view, it is also remarkable how StnII is about six fold more active than StnI against human red blood cells. Moreover, StnII and EqtII show a very different ability to lyse these cells when tested under the same experimental conditions *(Álvarez et al. 2009)*. Recent studies have shown that the hydrophobicity of the N-terminal 1-30 residues may play a key role in this *(Ros et al. 2015b)*. This region is the most variable sequence in this protein family and data suggest that the higher hydrophobicity of this segment contributes to increase the activity of the protein. This could be due to the N-terminus of StnII being more deeply buried into the hydrophobic core of the bilayer than that of StnI *(Ros et al. 2015b)*. On the other hand, over the other actinoporins studied, StnII seems to show a higher preference for Chol *(De-los-Ríos et al. 1998, Alm et al. 2015, García-Linares et al.*

2015), adding further complexity to the correct understanding of actinoporins' functionality.

Finally, it has been proposed the possibility that other or additional acceptors/receptors for actinoporins are present in cellular membranes besides SM. This proposition is based on the observation that erythrocytes and other mammalian cells were lysed at much lower toxin concentration compared to artificial lipid vesicles containing SM *(Maček 1992, Belmonte et al. 1993)*. It was suggested that an RGD-motif close to the POC binding site could play a role in integrin recognition at the cellular surface *(Monastyrnaya et al. 2010)*. However, some results indicate that the RGD sequence region would be important for maintaining the correct oligomerization state of the protein and the convenient geometric arrangement of the protein monomers in order to form a functional pore *(García-Linares et al. 2014)*. It is a non-reported but well-known fact that actinoporins elute at a delayed position when subjected to size-exclusion chromatography equilibrated in low ionic strength buffer. Much more recently, the ability of FraC to interact weakly with different oligosaccharides has been described (Caaveiro, J. M. M., *personal communication*). Both observations suggest some membrane glycoproteins or glycosphingolipids might play a non-previously foreseen role in the ability of actinoporins to assemble as functional pores on the membrane of their target cells.

Pore formation by actinoporins

Actinoporins must suffer a transformation from a soluble monomeric protein to an oligomeric transmembrane system to form a functional pore *(Parker et al. 2005)*. The mechanism that leads to pore formation is still subject of intense debate. Nevertheless, there is general consensus that independent of the mechanism, in addition to the N-terminal α-helix, the three already mentioned protein regions (**Figs. 4-6**) seem to be especially important from a functional point of view *(García-Ortega et al. 2011)*. The general implication of these clusters in the interaction with membranes has been established through the production of many different mutants with reduced haemolytic activity and diminished affinity for lipids *(Malovrh et al. 2000, Hong et al. 2002, Alegre-Cebollada et al. 2004, Alegre-Cebollada et al. 2007b, Alegre-Cebollada et al. 2008, Pardo-Cea et al. 2010, Pardo-Cea et al. 2011, García-Linares et al. 2013, García-Linares et al. 2015)*. There is however a general consensus in accepting the occurrence of steps in leading to pore-formation, which have been described in high detail before *(Alegre-Cebollada et al. 2007b)* (**Fig. 9**). Thus, it is commonly accepted that actinoporins initially bind to the membrane guided by their affinity to some membrane component, most probably SM or some SM derivative. This interaction would result in an increase of protein concentration at the lipid-water interface that would lead to its oligomerization on the membrane surface. Kinetic measurements using SPR suggest this binding to membranes as a two-step process *(Hong et al. 2002,*

Bakrač et al. 2008). The first one would be driven by the POC-binding site, the aromatic cluster of amino acids, and the array of basic residues. During the second step, the N-terminal α-helix would detach from the β-sandwich, extend, and lie parallel to the membrane. Simultaneously, oligomerization would occur.

A non-active oligomer, often referred as a "prepore" state, would then be formed. The actual existence of this prepore complex is, in fact, one of the most controversial aspects of the mechanism we are describing. Different intermediates and structures which could potentially represent this non-active state have been determined by two-dimensional crystallization on lipid mono-layers and electron and atomic force microscopies, combined with computer assisted docking *(Martín-Benito et al. 2000, Mancheño et al. 2003, Gutiérrez-Aguirre et al. 2004, Mancheño et al. 2006)*. This model shows strong similarities with the prepore structure that precedes pore formation in many β-pore forming toxins (β-PFTs) *(Heuck et al. 2001)* and it has been clearly seen in some α-PFT protein pores such as ClyA *(Mueller et al. 2009)*. Recent studies claim to have identified a prepore species of FraC bound to lipid vesicles by cryo-electron microscopy and atomic force microscopy. In this example of prepore ensemble, the N-terminus would not be inserted in the bilayer but exposed to the aqueous solution *(Morante et al. 2016)*.

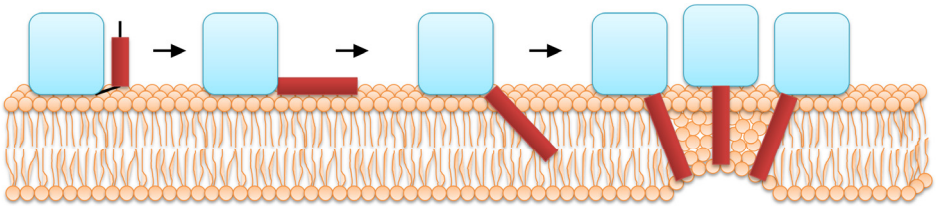

Figure 9. Schematic representation of the pore-forming mechanism of actinoporins. Once the protein is attached to the membrane, the N-terminal α-helix extends and inserts into the bilayer. Finally, oligomerization conduces to a final toroidal pore. The blue shape represents the β-sandwich core. The red dark bars represent the 30 first residues before and after the extension of the α helix.

The order of events leading to the insertion of the N-terminus into the membrane is another of the most controversial steps of the mechanism leading to actinoporins' pore-formation *(Malovrh et al. 2003, Rojko et al. 2013, Tanaka et al. 2015)*. Some results suggest that the insertion of the N-terminal helix in the lipid membrane immediately follows the initial binding of the toxin on the membranes containing SM and imply that the N-terminal region must be inserted into the membrane before the final oligomerization and pore formation occurs. If this were the case, stable prepores would not be needed for actinoporins making a functional pore *(Rojko et al. 2013)*.

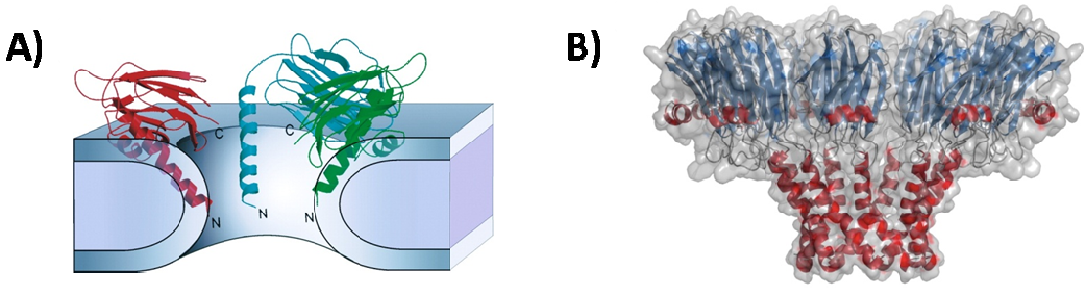

Figure 10. A) Proposed model of the functional tetrameric pore of StnII. Three of the four StnII monomers are shown in different colors. The lipid head group regions are indicated as gray layers. The walls of the pore would be lined by four helices and lipid molecules *(Mancheño et al. 2003)*. **B)** FraC nonameric pore model. The application of 9-fold symmetry to the X-ray crystallographic FraC protomer structure yields a putative model of the functional pore *(Mechaly et al. 2011)*.

Crystallization of StnII on lipid monolayers revealed the presence of stable tetrameric pore-shaped structures where the high resolution water soluble structure could be nicely fitted with only minimal modifications *(Martín-Benito et al. 2000, Mancheño et al. 2003)*. In this tetrameric model, non-interacting helices would be glued together only through the lipids to form the pore walls (**Fig. 10A**). Some years later, results obtained with a crystalline FraC structure in the presence of detergents suggested the existence of a crown-shaped nonamer (**Fig. 10B**) with an external diameter of about 11 nm and an internal diameter of approximately 5.0 nm *(Mechaly et al. 2011)*. In this structure, the detergent molecules appear located at the basal crown rim and the nine N-termini line its inner wall without any need for lipids facing the pore lumen. Most of the residues belonging to the conserved cluster of aromatic amino acids (**Fig. 5**) constitute part of the crown base and their side chains enter into contact with the detergent molecules *(Mechaly et al. 2011)*. The authors of this work state that all these results are compatible with the assumption that this nonameric structure represents a high-resolution model of an actinoporin in its prepore state. However, as it was stated before, the existence of this prepore is still a matter of controversy. In addition to this nonameric FraC assembly, octameric FraC pore-like structures have been also crystallized. Less than two years ago, the crystalline structure of a transmembrane pore exhibiting a unique architecture composed of both protein and lipids was described (**Fig. 11A**) *(Tanaka et al. 2015)*. This pore exhibits lateral fenestrations (**Fig. 11B**) that expose the hydrophobic core of the membrane to the aqueous environment allowing the incorporation of lipids from the target membrane within the structure of the pore, thus providing a membrane-specific trigger for the activation of a haemolytic toxin *(Tanaka et al. 2015)*. The presence of protein-protein interactions in the N-terminal helices, together with the lipids, would help stabilizing the channel needed to make a functional pore *(Tanaka et al. 2015)*. Thus, as it seems obvious from the lines above, and as it is further discussed later, the stoichiometry and final arrangement of the functional pore is still another of the main subjects of scientific debate.

Different biochemical, biophysical and electrophysiological evidences supply support for the different steps of the actinoporins' pore-formation mechanism. For example, EqtII double cysteine mutants, where the N-terminal 1-30 segment was covalently attached to the β-sandwich, exhibited reduced haemolytic activity upon disulfide formation *(Hong et al. 2002)* supporting that N-terminal detachment from the β-sandwich core is a required step. In this same regard, the introduction of Pro residues at StnII position number 10 in order to preclude the needed α-helix extension provided additional evidence *(Alegre-Cebollada et al. 2008)*.

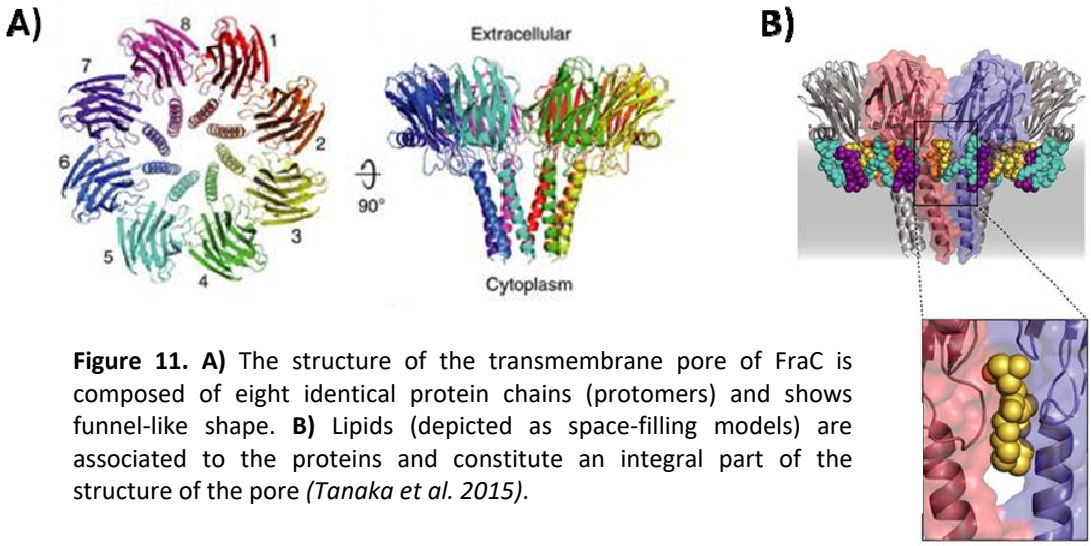

Figure 11. A) The structure of the transmembrane pore of FraC is composed of eight identical protein chains (protomers) and shows funnel-like shape. **B)** Lipids (depicted as space-filling models) are associated to the proteins and constitute an integral part of the structure of the pore *(Tanaka et al. 2015)*.

Mutations of the hydrophobic core resulted in less stable proteins *(Kristan et al. 2004)*, indicating that the β-sandwich does not easily undergo large conformational rearrangements, but it must remain compactly folded for the protein to be fully active. On the basis of the NMR results obtained for StnI in the presence of DPC micelles *(Castrillo et al. 2010)*, during the early steps of the interaction with the lipid bilayer most of the aromatic rings from the cluster (**Fig. 5**) would be in intimate contact with the membrane. The loop comprising Lys27 to Lys31 would be also close to it, and the N-terminal α-helix would remain in its native conformation. Structural and dynamic NMR studies carried out on two disabled variants of the actinoporin sticholysin II, R29Q and Y111N, showed that their lytic activity is not only related to their membrane affinity but also to their long-range interactions along the protein and the overall distribution of the electrostatic potential of the surface facing the membrane (**Fig. 12**). Within this picture, the β-sandwich would be crucial for lipid specificity, membrane targeting, and formation of the final pore structure, because it would constitute the solid scaffold where the distant parts responsible for the different and specific interactions would be positioned precisely to selectively act in the presence of the target *(García-Ortega et al. 2011)*. From this state, membrane permeabilization would be achieved by conformational changes within the toxin, which would expose hydrophobic patches of amino acids required for membrane insertion. One of these conformational changes, most probably the major one, would involve detachment and

extension of the N-terminal α-helix. Finally, the extended N-terminal α-helix would penetrate the membrane to build the pore.

One of the most-accepted models explaining the mechanism of actinoporins' pore formation *(Rojko et al. 2013, Antonini et al. 2014, Baker et al. 2014, Rojko et al. 2014, Subburaj et al. 2015)* assumes a toroidal structure where not only the protein but also the phospholipid head groups would linen the pore walls (**Fig. 9**). This structure would not display a well-defined fixed stoichiometry, but rather heterogeneous *(Antonini et al. 2014, Baker et al. 2014, Rojko et al. 2014, Subburaj et al. 2015)*. EqtII single molecule imaging on living cells showed the existence of a mixture of oligomeric species mostly including monomers, dimers, tetramers and hexamers. Mathematical modelling based on these data supported a model in which toxin clustering proceeded via condensation of EqtII dimer units *(Subburaj et al. 2015)*. The existence of such a toroidal structure has been shown by different means, such as ATR-FTIR of isolated protein-membrane complexes *(Alegre-Cebollada et al. 2007a)* and would explain why these pores are noisy and less stable than those known to be made by β-PFT. On the other hand, the most recent model proposed for pore formation *(Tanaka et al. 2015)*, based on crystal structures of FraC at four different stages of the lytic mechanism, suggests a non-toroidal structure, although the pore would be still composed of both protein and lipids (**Fig. 11**). This model also involves dimerization as an important intermediate step and possibly prepore assembly where α-helices are still attached to the protein core *(Morante et al. 2016)*. In this model it is not clear at which state helices transfer to the bilayer and across the membrane to form a functional pore. Both proposals for pore formation mechanism will probably be subject to experimental validation in the following years, most probably leading to a new scheme reconciling them.

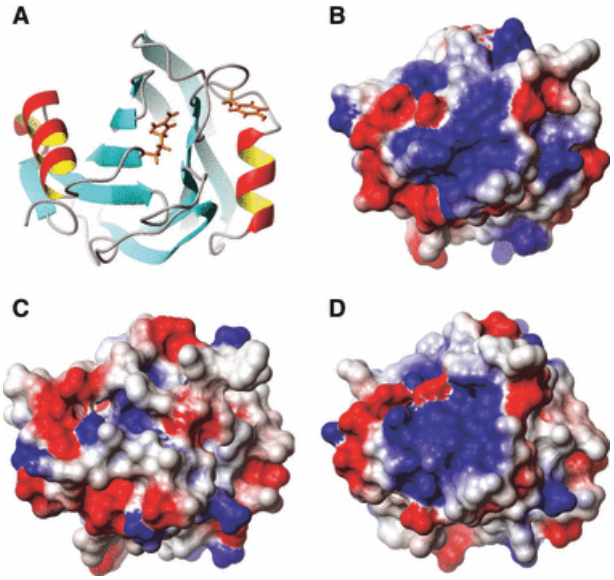

Figure 12. Diagram showing the membrane interaction face of StnII (A) and its electrostatic distribution surface potential for the wild-type protein (B) and the R29Q (C) and Y111N (D) variants. Blue and red correspond to positively and negatively charged areas, respectively. The side chains of R29 and Y111 are shown in (A) *(Pardo-Cea et al. 2011)*.

It is clear that EqtII and StnII form cation selective pores with a hydrodynamic diameter of about 1-2 nm, according to the results of different experiments, including the use of osmotic protectants of different size and conductance measurements in planar bilayers *(Varanda et al. 1980, Belmonte et al. 1993, Maček et al. 1994, Tejuca et al. 1996, De-los-Ríos et al. 1998, Tejuca et al. 2001, Mancheño et al. 2003)*. The helices

from the oligomeric complex are placed approximately perpendicular, with hydrophobic face oriented towards to the outside of the assembly (positively charged residues on the helices interacting with the negative phosphate groups of the membrane lipids) and hydrophilic face towards the pore lumen *(Tanaka et al. 2015)*. Thus, ion selectivity is governed by charged groups facing the conductive channel. Negatively charged residues from the inner part of the helix modulate slight cation selectivity of the pore as revealed by electrophysiological measurements *(Belmonte et al. 1993, Tejuca et al. 1996, Malovrh et al. 2003, Kristan et al. 2007)*. Also, negatively charged lipids enhance cation selectivity, which reinforces the idea that lipid head groups are exposed to the pore lumen *(Anderluh et al. 2003)*. Lipids as pore structural elements could also explain pore instability and broad conductance distribution, a characteristic very different from the stable and well defined barrel-stave pores *(Kristan et al. 2009, Antonini et al. 2014)*. EqtII pores, for example, have a broad conductance distribution *(Kristan et al. 2007)*. However, the size of the pore seems to be independent of protein concentration *(Tejuca et al. 2001)*. Pores seem to have a fixed common predominant structure but may adopt slightly different conformations while keeping constant their size, depending on the protein and the nature of the membrane studied. Variable stoichiometry is a well-known feature among pore forming toxins. There seems to be that EqtII in the membrane exists mostly as monomer, dimer, tetramer and hexamer, but only a small fraction of higher oligomers, like octamer or nonamer, would be present *(Baker et al. 2014, Subburaj et al. 2015)*. FraC octameric structure is probably more stable because protein-protein packing interface in octamer is the most favourable. Kinetic studies of EqtII, StnI and StnII induced pore formation in lipid vesicles suggest predominantly three to four monomers per functional pore *(Belmonte et al. 1993, Tejuca et al. 1996, De-los-Ríos et al. 1998)*. This functional data are in agreement with tetrameric structures observed with electron microscopy of StnII bound to lipid interface *(Mancheño et al. 2003)*. Interestingly, the presence of preassembled StnI dimers, via a disulfide bridge at the N-terminal end, seems to facilitate pore formation *(Valle et al. 2011)*. Data altogether seem to indicate that dimers could be intermediates in the pore formation pathway of actinoporins, as suggested for FraC and EqtII oligomer assembly *(Subburaj et al. 2015, Morante et al. 2015a)*. In summary, all the experiments carried out in model and cellular membranes seem to indicate that only few protein monomers are enough to form a functional pore and that larger oligomers are not the dynamically active predominating form of the protein at the membrane surface *(Tejuca et al. 1996, Rojko et al. 2014)*. The significant differences in actinoporins' N-terminal segments *(Alegre-Cebollada et al. 2007b, Ros et al. 2015b)* could account for differences in activity, size, stability and maybe cation specificity of the resulting pore. Again, much work still needs to be done in order to fully understand the complex mechanism underlying actinoporins' functionality.

OBJECTIVES

(i) Elucidation of the role of the different lipidic membrane components in the actinoporins' mechanism steps leading to pore formation, with special emphasis on the influence of cholesterol and different sphingomyelin analogues and/or other highly related lipids, such as ceramide or dihydro-sphingomyelin.

(ii) Production of natural and artificial actinoporin variants with the purpose of studying their structural and functional features, mapping the key protein regions, and evaluating their ability to interact with lipid model vesicles and/or biological membranes of different composition and physicochemical properties.

(iii) Elucidation of the assembly mechanism, structure, and stoichiometry of a functional actinoporin pore, reconstituted in the absolute absence of detergents, using nanodiscs platforms and cryo-electron microscopy.

RESULTS

SECTION A

A GENERAL VIEW OF ACTINOPORINS

ARTICLE I

The behavior of sea anemone actinoporins at the water-membrane interface

García-Ortega, L., Alegre-Cebollada, J., **García-Linares, S.**, Bruix, M., Martínez-del-Pozo, Á. and Gavilanes, J. G. (2011). *Biochim Biophys Acta* 1808(9): 2275-2288.

Comportamiento de las actinoporinas de anémonas marinas en la interfase agua-membrana

Las actinoporinas constituyen un grupo de toxinas pequeñas y básicas producidas por anémonas marinas. Tienen una alta identidad de secuencia y aparecen como familias multigénicas. Muestran un comportamiento singular en la interfase agua-membrana: en disolución acuosa las actinoporinas permanecen plegadas y estables pero, al interaccionar con bicapas lipídicas, oligomerizan formando estructuras integrales de membrana. Estas membranas deben contener esfingomielina, tener coexistencia de fases o ambas. Las estructuras solubles de las actinoporinas equinatoxina II (EqtII) y esticolisina II (StnII) se conocen con detalle. La estructura cristalina de un nonámero de fragaceatoxina C (FraC) también ha sido determinada. Las tres proteínas se pliegan como un sándwich β flanqueado por dos hélices α, unas de ellas en el extremo N-terminal. Cuatro regiones parecen ser especialmente importantes en la estructura: un racimo de residuos aromáticos, un sitio de unión a fosfocolina, un grupo de aminoácidos básicos y la hélice α N-terminal. La unión de los monómeros solubles a la membrana ocurre a través del racimo de residuos aromáticos, el sitio de unión a fosfocolina y el grupo de aminoácidos básicos. A continuación, la hélice α N-terminal se separa del sándwich β y se extiende paralela sobre la membrana. Simultáneamente tiene lugar la oligomerización de la proteína. Por último, la hélice N-terminal penetra en la membrana para construir un poro toroidal. Este modelo ha sido cuestionado recientemente tras la reconstrucción por microscopía electrónica de FraC unida a vesículas de fosfolípidos. El motivo estructural de las actinoporinas aparece a lo largo de todos los reinos eucariotas en proteínas no relacionadas funcionalmente con ellas. Muchas de estas proteínas no se unen a membranas lipídicas ni inducen lisis celular. Finalmente, existen muchos estudios centrados en el potencial terapéutico de las actinoporinas.

Biochimica et Biophysica Acta 1808 (2011) 2275–2288

Contents lists available at ScienceDirect

Biochimica et Biophysica Acta

journal homepage: www.elsevier.com/locate/bbamem

Review

The behavior of sea anemone actinoporins at the water–membrane interface

Lucía García-Ortega [a], Jorge Alegre-Cebollada [a], Sara García-Linares [a], Marta Bruix [b], Álvaro Martínez-del-Pozo [a,*], José G. Gavilanes [a,*]

[a] Departamento de Bioquímica y Biología Molecular I, Facultad de Ciencias Químicas, Universidad Complutense, 28040 Madrid, Spain
[b] Instituto de Química-Física Rocasolano, CSIC, Serrano 119, 28006 Madrid, Spain

ARTICLE INFO

Article history:
Received 14 March 2011
Received in revised form 10 May 2011
Accepted 11 May 2011
Available online 20 May 2011

Keywords:
Actinoporin
Equinatoxin
Sticholysin
Membrane-pore
Pore-forming-toxin

ABSTRACT

Actinoporins constitute a group of small and basic α-pore forming toxins produced by sea anemones. They display high sequence identity and appear as multigene families. They show a singular behaviour at the water–membrane interface: In aqueous solution, actinoporins remain stably folded but, upon interaction with lipid bilayers, become integral membrane structures. These membranes contain sphingomyelin, display phase coexistence, or both. The water soluble structures of the actinoporins equinatoxin II (EqtII) and sticholysin II (StnII) are known in detail. The crystalline structure of a fragaceatoxin C (FraC) nonamer has been also determined. The three proteins fold as a β-sandwich motif flanked by two α-helices, one of them at the N-terminal end. Four regions seem to be especially important: A cluster of aromatic residues, a phosphocholine binding site, an array of basic amino acids, and the N-terminal α-helix. Initial binding of the soluble monomers to the membrane is accomplished by the cluster of aromatic amino acids, the array of basic residues, and the phosphocholine binding site. Then, the N-terminal α-helix detaches from the β-sandwich, extends, and lies parallel to the membrane. Simultaneously, oligomerization occurs. Finally, the extended N-terminal α-helix penetrates the membrane to build a toroidal pore. This model has been however recently challenged by the cryo-EM reconstruction of FraC bound to phospholipid vesicles. Actinoporins structural fold appears across all eukaryotic kingdoms in other functionally unrelated proteins. Many of these proteins neither bind to lipid membranes nor induce cell lysis. Finally, studies focusing on the therapeutic potential of actinoporins also abound.

Contents

Abbreviations: Avt, actinoporins from *Actineria villosa*; ALP, actinoporin-like protein; ATR, attenuated total reflection; Bc2, actinoporin from *Bunodosoma caissarum*; CD, circular dichroism; Chol, cholesterol; DMPC, dimyristoylphosphatidylcholine; DOPC, dioleylphosphatidylcholine; DPC, dodecylphosphocholine; Drl, ALP from *Danio rerio*; EM, electron microscopy; Ent, actinoporin from *Entacmea quadricolor*; Eqt, equinatoxin; FTIR, Fourier transform infrared spectroscopy, Fra C, actinoporin from *Actinia fragacea*; GUV, giant unilamellar vesicles; ITC, isothermal titration calorimetry; NLP, necrosis and ethylene-inducing peptide 1 (Nep1)-like protein; NMR, nuclear magnetic resonance; PE, phosphatidylethanolamine; PFT, pore forming toxin; PpBP, ALP from *Physcomitrella patens*; Pstx, actinoporins from *Phyllodiscus semoni*; SM, sphingomyelin; SPR, surface plasmon resonance; Stn, sticholysin; TFE, trifluoroethanol.

* Corresponding author.
E-mail addresses: alvaro@bbm1.ucm.es (Á. Martínez-del-Pozo), ppgf@bbm1.ucm.es (J.G. Gavilanes).

0005-2736/$ – see front matter © 2011 Elsevier B.V. All rights reserved.
doi:10.1016/j.bbamem.2011.05.012

"…the native conformation [of a protein] is determined by the totality of interatomic interactions and hence by the amino acid sequence, in a *given environment*"

Christian B. Anfinsen, 1972, Nobel Lecture

Christian B. Anfinsen was well aware of the importance of environment on the acquisition of the final native three-dimensional structure of a polypeptide chain. In fact, the statement shown above summarizes what could be considered as the *dogma of protein folding*. As it is well known, most proteins fold in an aqueous environment and remain soluble in this polar media while functionally active. Another smaller number, though not negligible, have evolved to fold into, or close to, the highly hydrophobic environment of the lipid bilayer. Even the most basic Biochemistry textbooks sustain the clear cut classification that distinguishes between soluble and membrane proteins. Surprisingly, actinoporins, the family of proteins which constitute the subject of this review, escape to this simple classification. They show what can be described as a dual behaviour at the water–membrane interface. In water solution, actinoporins remain mostly monomeric and stably folded but, upon interaction with lipid membranes of specific composition, they become oligomeric integral membrane structures. Thus, this family of proteins represents an optimal system to study the transition from a soluble monomeric folded conformation to an oligomeric transmembrane protein. Indeed, this transition to form a functionally active membrane-bound pore constitutes the core of their biological function. Actinoporins, in short, demonstrate how an identical amino acid sequence can fold into two different structures, showing the environmental influence on the energy landscape of a protein, as essentially stated by Anfinsen more than 35 years ago. They are a natural and beautiful example of protein plasticity.

Sea anemone actinoporins

Actinoporins constitute a widespread family of toxic proteins presumably stored within the nematocysts of sea anemones [1]. Contact with their tentacles triggers injection of these and other toxins into prey, leading to a variety of noxious effects [2]. Actinoporins are produced by different sea anemone species as single polypeptide chains of around 175 amino acids (Fig. 1). They show basic isoelectric point values and are usually cysteinless [3–5].

Actinoporins belong to the much larger group of widely distributed pore forming toxins (PFTs). As it is quite obvious from their denomination, the toxic activity of these proteins relies on the formation of pores within biological membranes [6–13]. All PFTs show this same dual behaviour when encountering a membrane but, in order to study their ability to become integral membrane proteins, actinoporins show precisely the methodological advantage of being small and cysteinless.

The formation of pores by PFTs can be achieved by inserting either α-helices or β-hairpins within the cell membrane [6,9–13]. These structural motifs are employed to classify them into two well-defined groups. Thus, α-PFTs insert α-helices within the membrane, whereas β-PFTs use β-barrels to span it [14]. Actinoporins are α-PFTs since they seem to insert α-helices within the membrane core; a feature that they share with some of the most dangerous toxins known such as diphtheria or anthrax. They show hemolytic activity because they form cation-selective pores with a diameter of 1–2 nm within the membranes of erythrocytes [15–17]. Equinatoxin II (EqtII) from *Actinia equina* and sticholysins I and II (StnI and StnII) from *Stichodactyla helianthus* are the most thoroughly studied actinoporins [5,18].

Biological function

Many carnivorous sea animals possess toxins which function as chemical weapons to paralyze prey such as fish, crabs, worms, or bivalves [2,19,20]. This is particularly important if the considered animal lives a benthic life, spending most of its biological cycle attached to a fixed location. Maybe that is why these animals secrete a wide variety of different toxins including neurotoxins, cytotoxins, cardiotoxins, and hemolysins [2,21–23]. Within this idea, sea anemone actinoporins are believed to participate in functions like predation, defence, and digestion, and have been shown to be lethal to small crustaceans, molluscs, and fish [1], or even parasites such as the unicellular flagellated protozoan *Giardia duodenalis*[24]. The oligomeric cation-selective pores formed by them result in a colloid-osmotic shock that leads to cell death [16,25,26].

So far, actinoporins have been isolated from at least 20 different sea anemone species [3,5,27,28], showing their ubiquitous distribution within the *Actinaria* order. Moreover, they display high sequence identity (between 60% and 80%) (Fig. 1) and appear as multigene families [29], giving rise to many protein isoforms within the same individual [3–5,30–32]. The small number of changes observed, however, result in large functional differences in terms of solubility and hemolytic activity [28,32–34] as exemplified by StnI and StnII. They are 91% identical but show quite different hemolytic activities. The presence of this large number of similar isotoxins in the venom probably helps to broad the range of prey for a given species [35]. Analogous to immunoglobulins, which require a plethora of highly diverse genes to counteract foreign antigens, sea anemone tentacles would produce many actinoporins isoforms. This feature has led some authors to propose that actinoporins could represent the embryo of a rudimentary immune system [32].

Water-soluble three-dimensional structure

The water-soluble structures of EqtII and StnII are known in detail [23,36–38]. The crystal structure of a FraC nonamer, obtained in the presence of detergent, has been also reported [39]. The three proteins fold as a β-sandwich motif composed of 10–12 β-strands flanked by two α-helices which interact with both sides of the β-sandwich (Fig. 2). One of these helices is located near the N-terminal end (Fig. 3) and is preceded by a short 3_{10} helix [23,36–39]. In fact, the first 30 residues appear to be the largest part of the protein that can adopt alternative conformations without disrupting the fold of the β-sandwich [36]. This feature and the amphipathic character of this α-helix seem to be extremely important for the final functionality of the pore since it has been proposed to extend and insert into the membrane to form the pore walls [40]. In addition to the N-terminal α-helix, three more regions of the structure seem to be especially important from a functional point of view: A phosphocholine (POC) binding site, a cluster of aromatic residues, and an array of basic amino acids (Fig. 3). Determination of these crystal and soluble three-dimensional structures of actinoporins, including a StnII–POC complex, altogether with different biochemical and biophysical characterization of a high number of actinoporins mutants and natural variants, has led to putative models of their topology and mode of action.

Fig. 1. Sequence alignment of all known primary structures from different sea anemone actinoporins. Eqt, equinatoxins from *Actinia equina*; Stn, sticholysins from *Stichodactyla helianthus*; Ten, tenebrosins from *Actinia tenebrosa*; Hmg and magnificalysin, magnificalysins from *Heteractis magnifica*; RTX, actinoporins from *Radianthus macrodactylus*; SrcI, acidic cytolysin from *Sagartia rosea*; AvtI, actinoporin from *Actineria villosa*; PSTX-20A, actinoporin from *Phyllodiscus semoni*; Caritoxin, actinoporin from *Actinia cari*; Ent, actinoporin from *Entacmea quadricolor*; SmT, actinoporins from *Stichodactyla mertensii*; Or, actinoporins from *Oulactis orientalis*; FraC, fragaceatoxin C from *Actinia fragacea*. It must be noted that EqtII and TenC have the same sequence. Black, grey, or white boxes indicate the different degree of conservation, in descending order, along all the reported actinoporins sequences.

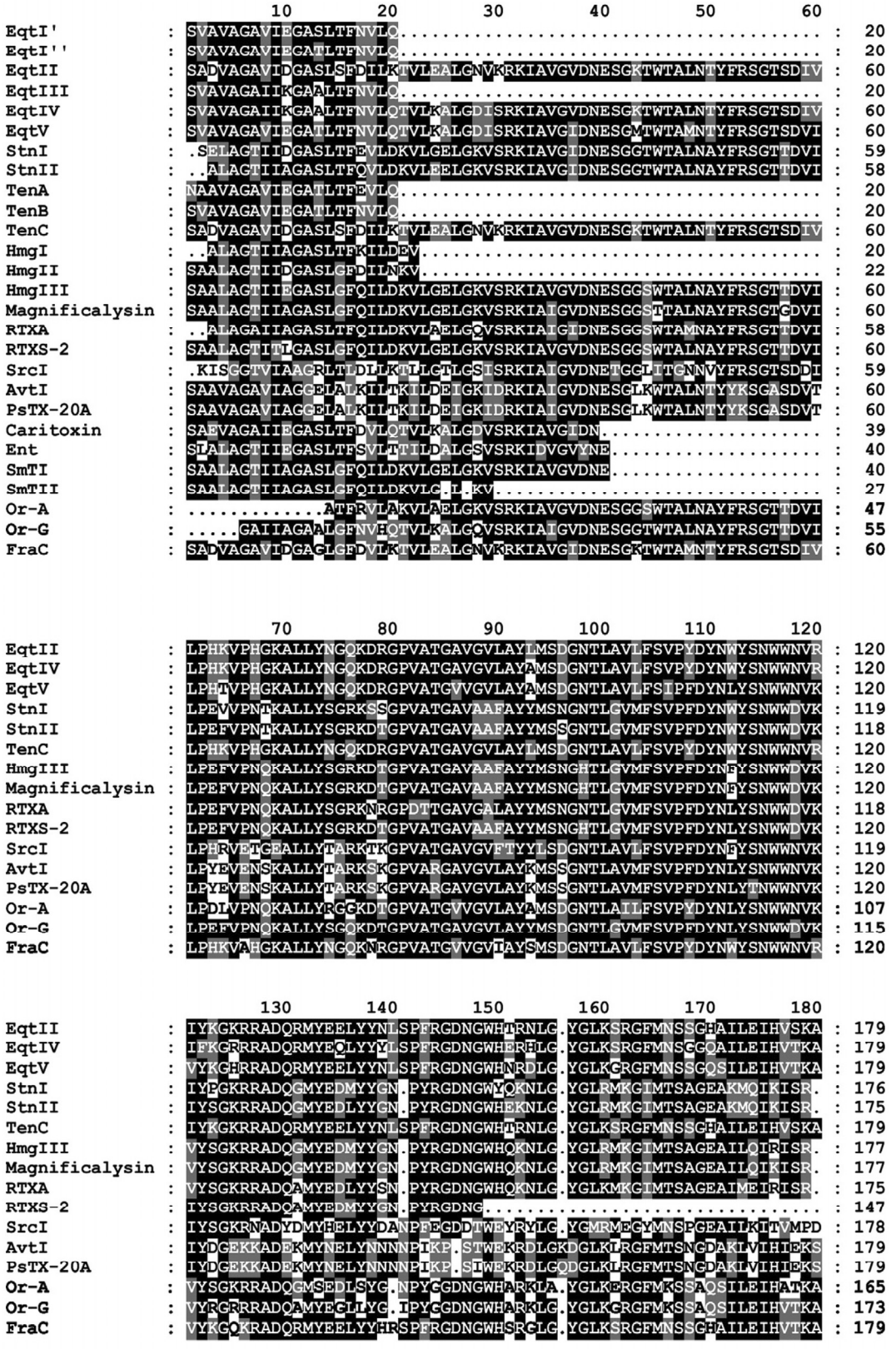
10 20 30 40 50 60
EqtI' : SVAVAGAVIEGASLTFNVLQ : 20
EqtI'' : SVAVAGAVIEGATLTFNVLQ : 20
EqtII : SADVAGAVIDGASLSFDILKTVLEALGNVKRKIAVGVDNESGKTWTALNTYFRSGTSDIV : 60
EqtIII : SVAVAGAIIKGAALTFNVLQ : 20
EqtIV : SVAVAGAIIKGAALTFNVLQTVLKALGDISRKIAVGVDNESGKTWTALNTYFRSGTSDIV : 60
EqtV : SVAVAGAVIEGATLTFNVLQTVLKALGDISRKIAVGIDNESGMTWTAMNTYFRSGTSDVI : 60
StnI : .SELAGTIIDGASLTFEVLDKVLGELGKVSRKIAVGIDNESGGTWTALNAYFRSGTTDVI : 59
StnII : ..ALAGTIIAGASLTFQVLDKVLEELGKVSRKIAVGIDNESGGTWTALNAYFRSGTTDVI : 58
TenA : NAAVAGAVIEGATLTFEVLQ : 20
TenB : SVAVAGAVIEGATLTFNVLQ : 20
TenC : SADVAGAVIDGASLSFDILKTVLEALGNVKRKIAVGVDNESGKTWTALNTYFRSGTSDIV : 60
HmgI : ..ALAGTIIAGASLTFKILDEV : 20
HmgII : SAALAGTIIDGASLGFDIINKV : 22
HmgIII : SAALAGTIIEGASLGFQILDKVLGELGKVSRKIAVGVDNESGGSWTALNAYFRSGTTDVI : 60
Magnificalysin : SAALAGTIIAGASLGFQILDKVLGELGKVSRKIAIGVDNESGGSTTALNAYFRSGTGDVI : 60
RTXA : ..ALAGAIIAGASLTFQILDKVLAELGQVSRKIAIGIDNESGGSWTAMNAYFRSGTTDVI : 58
RTXS-2 : SAALAGTITTGASLGFQILDKVLGELGKVSRKIAVGVDNESGGSWTALNAYFRSGTTDVI : 60
SrcI : .KISGGTVIAAGRLTLDLLKTILGTLGSISRKIAIGVDNETGGLITGNNVYFRSGTSDDI : 59
AvtI : SAAVAGAVIAGGELALKILTKILDEIGKIDRKIAIGVDNESGLKWTALNTYYKSGASDVT : 60
PsTX-20A : SAAVAGAVIAGGELALKILTKILDEIGKIDRKIAIGVDNESGLKWTALNTYYKSGASDVT : 60
Caritoxin : SAEVAGAIIEGASLTFDVLQTVLKALGDVSRKIAVGIDN : 39
Ent : SLALAGTIIEGASLTFSVLTTILDALGSVSRKIDVGVYNE : 40
SmTI : SAALAGTIIAGASLGFQILDKVLGELGKVSRKIAVGVDNE : 40
SmTII : SAALAGTIIAGASLGFQILDKVLG.LLKV : 27
Or-A : .....ATFRVLAKVLAELGKVSRKIAVGVDNESGGSWTALNAYFRSGTTDVI : 47
Or-G : .....GAIIAGAALGFNVLQTVLKALGQVSRKIAIGVDNESGGTWTALNAYFRSGTTDVI : 55
FraC : SADVAGAVIDGAGLGFDVLKTVLEALGNVKRKIAVGIDNESGKTWTAMNTYFRSGTSDIV : 60
70 80 90 100 110 120
EqtII : LPHKVPHGKALLYNGQKDRGPVATGAVGVLAYLMSDGNTLAVLFSVPYDYNWYSNWWNVR : 120
EqtIV : LPHKVPHGKALLYNGQKDRGPVATGAVGVLAYAMSDGNTLAVLFSVPYDYNWYSNWWNVR : 120
EqtV : LPHTVPHGKALLYNGQKDRGPVATGVVGVLAYAMSDGNTLAVLFSIPFDYNLYSNWWNVK : 120
StnI : LPEVVPNTKALLYSGRKSSGPVATGAVAAFAYYMSNGNTLGVMFSVPFDYNWYSNWWDVK : 119
StnII : LPEFVPNTKALLYSGRKDTGPVATGAVAAFAYYMSSGNTLGVMFSVPFDYNWYSNWWDVK : 118
TenC : LPHKVPHGKALLYNGQKDRGPVATGAVGVLAYLMSDGNTLAVLFSVPYDYNWYSNWWNVR : 120
HmgIII : LPEFVPNQKALLYSGRKDTGPVATGAVAAFAYYMSNGHTLGVMFSVPFDYNGYSNWWDVK : 120
Magnificalysin : LPEFVPNQKALLYSGRKDTGPVATGAVAAFAYYMSNGHTLGVMFSVPFDYNGYSNWWDVK : 120
RTXA : LPEFVPNQKALLYSGRKNRGPDTTGAVGALAYYMSNGNTLGVMFSVPFDYNLYSNWWDVK : 118
RTXS-2 : LPEFVPNQKALLYSGRKDTGPVATGAVAAFAYYMSNGHTLGVMFSVPFDYNLYSNWWDVK : 120
SrcI : LPHRVETGEALLYTARKTKGPVATGAVGVFTYYLSDGNTLAVLFSVPFDYNGYSNWWNVK : 119
AvtI : LPYEVENSKALLYTARKSKGPVARGAVGVLAYKMSSGNTLAVMFSVPFDYNLYSNWWNVK : 120
PsTX-20A : LPYEVENSKALLYTARKSKGPVARGAVGVLAYKMSSGNTLAVMFSVPFDYNLYTNWWNVK : 120
Or-A : LPDLVPNQKALLYRGGKDTGPVATGVVGVLAYAMSDGNTLAILFSVPYDYNLYSNWWNVK : 107
Or-G : LPEFVPNQKALLYSGQKDTGPVATGAVGVLAYYMSDGNTLGVMFSVPFDYNLYSNWWDVK : 115
FraC : LPHKVAHGKALLYNGQKNRGPVATGVVGVIAYSMSDGNTLAVLFSVPYDYNWYSNWWNVR : 120
130 140 150 160 170 180
EqtII : IYKGKRRADQRMYEELYYNLSPFRGDNGWHTRNLG.YGLKSRGFMNSSGHAILEIHVSKA : 179
EqtIV : IFKGRRRADQRMYEQLYYYLSPFRGDNGWHERHLG.YGLKSRGFMNSGGQAILEIHVTKA : 179
EqtV : VYKGHRRADQRMYEELYYNLSPFRGDNGWHNRDLG.YGLKGRGFMNSSGQSILEIHVTKA : 179
StnI : IYPGKRRADQGMYEDMYYGN.PYRGDNGWYQKNLG.YGLRMKGIMTSAGEAKMQIKISR. : 176
StnII : IYSGKRRADQGMYEDLYYGN.PYRGDNGWHEKNLG.YGLRMKGIMTSAGEAKMQIKISR. : 175
TenC : IYKGKRRADQRMYEELYYNLSPFRGDNGWHTRNLG.YGLKSRGFMNSSGHAILEIHVSKA : 179
HmgIII : VYSGKRRADQGMYEDMYYGN.PYRGDNGWHQKNLG.YGLRMKGIMTSAGEAILQIRISR. : 177
Magnificalysin : VYSGKRRADQGMYEDMYYGN.PYRGDNGWHQKNLG.YGLRMKGIMTSAGEAILQIKISR. : 177
RTXA : VYSGKRRADQAMYEDLYYSN.PYRGDNGWHQKNLG.YGLKMKGIMTSAGEAIMEIRISR. : 175
RTXS-2 : IYSGKRRADQAMYEDMYYGN.PYRGDNG : 147
SrcI : IYSGKRNADYDMYHELYYDANPFEGDDTWEYRYLG.YGMRMEGYMNSPGEAIIKITVMPD : 178
AvtI : IYDGEKKADEKMYNELYNNNNPIKP.STWEKRDLGKDGLKLRGFMTSNGDAKLVIHIEKS : 179
PsTX-20A : IYDGEKKADEKMYNELYNNNNPIKP.SIWEKRDLGQDGLKLRGFMTSNGDAKLVIHIEKS : 179
Or-A : VYSGKRRADQGMSEDLSYG.NPYGGDNGWHARKLA.YGLKERGFMKSSAQSILEIHATKA : 165
Or-G : VYRGRRRADQAMYEGLLYG.IPYGGDNGWHARKLG.YGLKGRGFMKSSAQSILEIHVTKA : 173
FraC : VYKGQKRADQRMYEELYYHRSPFRGDNGWHSRGLG.YGLKSRGFMNSSGHAILEIHVTKA : 179

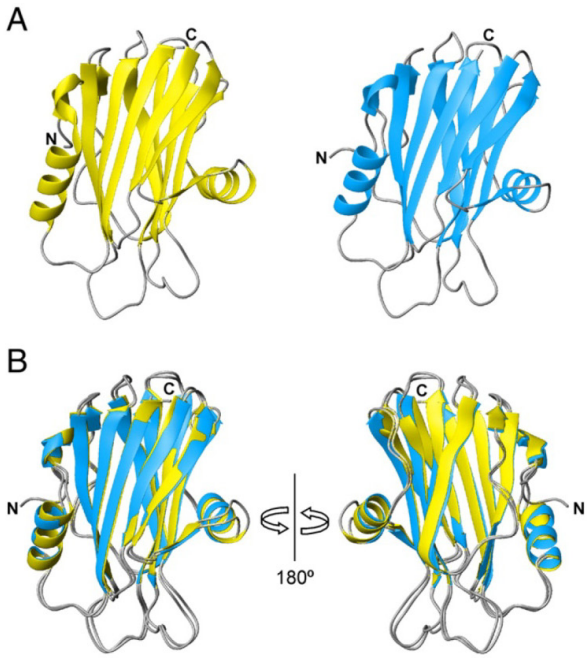

Fig. 2. Ribbon representation of the X-ray structures of EqtII (PDB ID: 1IAZ) and StnII (PDB ID: 1GWY). The N- and C-ends are labelled. A) EqtII is shown in yellow and StnII in blue. B) Two views of the backbone superposition of EqtII and StnII rotated 180º are represented too. Figure prepared with MolMol [150].

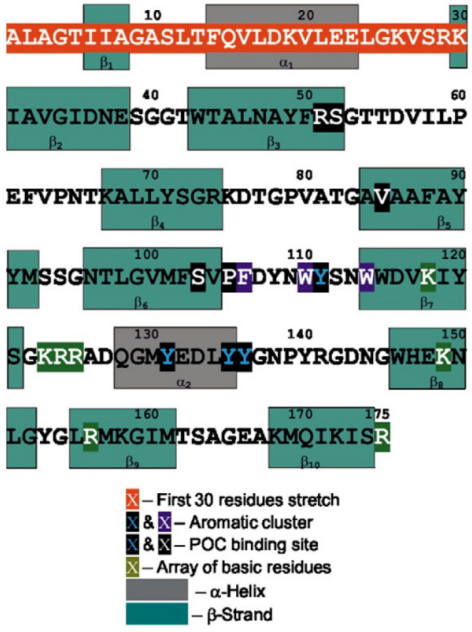

Fig. 3. Diagram showing the distribution of the regular secondary structure elements along the StnII amino acid sequence (grey, α-helix; green, β-strand). The N-terminal 30 first residues are also indicated (red background) as well as those ones conforming the cluster of aromatic amino acids (blue letters with black background and white letters with blue background), the POC-binding site (black background), and the array of basic amino acids (white letters with green background).

The POC binding site

The existence of a specific POC binding site in StnII was determined after solving the X-ray structure of the corresponding complex [38]. This site is partly hydrophobic (side chains of Val-85 and Pro-105, and aromatic rings of Tyr-111 and Tyr-135) and partly hydrophilic (side chains of Ser-52 and Ser-103 and hydroxyl groups of Tyr-131, Tyr-135 and Tyr-136) (Fig. 4). Some of the residues participating in this POC recognition site are also part of the conserved cluster of aromatic residues (Figs. 3 and 5). Altogether, both overlapping regions seem to constitute the main recognition and binding sites to the membrane, as explained below. The positive charge of the choline moiety is stabilized by cation–π interactions with the aromatic rings of Tyr-111 and Tyr-135, whereas the phosphate group interacts with the phenolic hydroxyl groups of again Tyr-111 and Tyr-136, and is probably further stabilized by the cationic side chain of Arg-51 (Fig. 4). Unexpectedly, POC binding does not promote significant conformational changes in StnII apart from minor rearrangements in local side chains and backbone modifications in the β6–β7 loop [38], at least when studied in the absence of lipidic media.

The importance of Tyr-111 is highlighted by the fact that it is 100% conserved among the actinoporins family (Fig. 1). It is located in the very flexible loop linking the β5 and β6 strands (Fig. 5) which appears highly disordered in EqtII [36,37] and StnII [38], both in the free and POC bound forms. However, in the crystal structure of POC-bound Stn II, the aromatic ring of Tyr-111 is pointing toward the phosphocholine moiety after a probable conformational change from its exposed free state [38], a fact that seems confirmed by the behaviour of the corresponding StnI Tyr-112 in the presence of dodecylphosphocholine (DPC) micelles [41]. Also in agreement, mutation of the equivalent Tyr-113 of EqtII diminished specific binding of SM, and prevented insertion of and binding into SM containing lipid monolayers and liposomes [42], suggesting that this residue is strictly required, at least for EqtII SM recognition. Accordingly, mutation of StnII Tyr-111 to Asn (StnII Y111N) resulted in a significantly decreased hemolytic activity and supports the interaction with the positively charged choline [43–46]. Finally, in the recent nonameric FraC structure, detergent molecules cocrystallized in contact with its equivalent Tyr-113 [39]. Surprisingly, StnI Tyr-112 [41,47] is not affected by the micellar environment when studied by NMR in the presence of DPC micelles [41] since it displays identical properties as in the lipid free protein. Thus, either Tyr-112 in StnI does not really interact with the micelle or the mobility of the lipid molecules is larger than in a real membrane, hampering the formation of a pore structure. The higher curvature of the micelle, in comparison to a real membrane, might be another reason to explain the observed absence of effect.

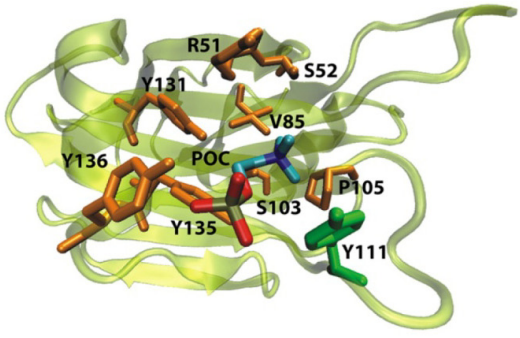

Fig. 4. Ribbon representation showing the POC-binding site within the three-dimensional structure of StnII (PDB ID: 1GWY1O72). This site is composed by the side-chains of residues Arg-51, Ser-52, Val-85, Ser-103, Pro-105, Tyr-111 (shown in green), Tyr-131, Tyr-135, and Tyr-136. A molecule of POC is also shown. Figure produced by VMD [151].

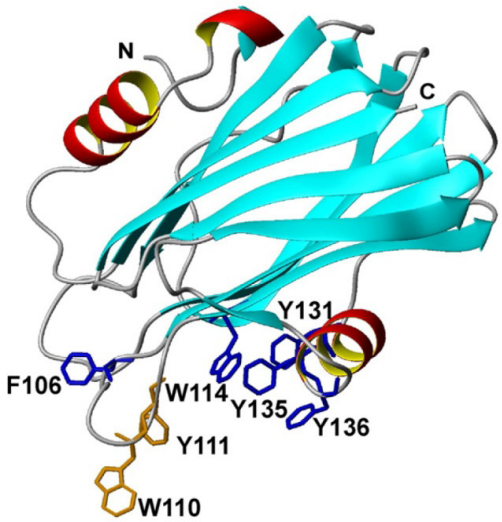

Fig. 5. Diagram showing the exposed cluster of aromatic amino acids within the three-dimensional structure of StnII (PDB ID: 1GWY). This cluster is composed by residues Phe-106, Trp-110, Tyr-111, Trp-114, Tyr-131, Tyr-135, and Tyr-136. The backbone is represented by a ribbon. The side-chains of selected amino acids are shown in blue (Phe-106, Trp-114, Tyr-131, Tyr-135, and Tyr-136) and gold (Trp 110 and Tyr-111). Figure generated by MolMol [150].

Altogether, all these data suggest the existence of a high conformational versatility around this Tyr residue when free in solution or in the presence of lipids. These properties may facilitate the fast conformational arrangements needed upon the environmental change produced when encountering the membrane and could be also responsible, in part, for specific recognition and pore formation.

The exposed cluster of aromatic residues

Most known actinoporins display an exposed and conserved cluster of aromatic amino acids (Figs. 3 and 5), composed mainly of Tyr and Trp residues (Phe-106, Trp-110, Tyr-111, Trp-114, Tyr-131, Tyr-135 and Tyr-136 for StnII). Their implication in the interaction with membranes has been clearly established. In fact, mutations affecting this region result in less hemolytic variants with reduced affinity for lipids [43,44]. More recently, NMR studies of the aromatic resonances of the residues from this cluster, after the interaction of StnI with DPC micelles, have revealed that the motional flexibility of most of them was perturbed when compared with the protein in water [41]. Some of these residues (StnII Tyr-131, 135, and 136, for example) appear along the second α-helix (Fig. 3, α_2 helix). Assuming that the nonameric FraC crystal structure represents a membrane bound state [39], this α_2 helix would lie on the plane of the bilayer providing anchoring sites for attachment and stabilization of the β sandwich [39]. These observations are in good accordance with the very well known fact that aromatic chains preferentially appear at the membrane/water interfaces [48]. Consequently, the cluster seems to play an important role during the first steps of pore formation, most probably during membrane attachment [49,50].

Apart from the already described importance of Tyr-111 (StnII numbering) in POC binding and SM recognition, another important residue for the establishment of the actinoporins-membrane interaction is StnII Trp-110 (Figs. 3 and 5). Its implication in SM recognition has also been proven for the equivalent EqtII Trp-112 [42,51]. However, it can be substituted by any other bulky and hydrophobic amino acid such as Phe or Leu, while still maintaining a wild-type phenotype [42]. Within this same idea, attachment of a short peptide to a Cys residue substituting this Trp in StnI disturbs but does not prevent pore formation [52].

The determination of the soluble three-dimensional structure of a much less hemolytic StnII mutant (R29Q) has also revealed that things are far more complex. This Arg-29 is located at the hinge connecting the N-terminal helix to the β-sandwich core (Fig. 3) and its substitution by Gln has revealed not only a perturbation of this region, but also long range effects affecting most of the residues located in the protein surface that presumably faces the membrane [46]. This perturbation includes the aromatic cluster residues, for example. Indeed, the distribution of the electrostatic potential along this surface changes dramatically, with a significant loss of the positive potential. This could affect the efficient targeting of the protein to the membrane and then perturb the specific interactions with the negative phosphate groups of the membrane phospholipids.

The array of basic amino acids

A region rich in basic residues has been proposed to play a role in the initial steps of EqtII membrane recognition via interaction with negatively charged regions of the lipid head groups [37]. Such a region in StnII would be comprised of Lys-118, Lys-149, Arg-156, and Arg-175, together with the contiguous sequence Lys-123–Arg-124–Arg-125 appearing along the loop linking the strand β7 with the second α-helix (Figs. 3 and 6). Interestingly, most of the Arg in this StnII stretch appear as Lys in EqtII, and vice versa (Lys-118, Lys-149, Arg-156, and Arg-175 in StnII against Arg-120, Arg-152, Lys159, and Lys-178 in EqtII) (Fig. 1). An additional EqtII Lys residue (Lys-123) appears as a Ser in the equivalent StnII position (Ser-121). Maybe these small changes correlate with the apparent different lipid affinities of these two proteins [31,42,44,53,54].

The N-terminal α-helix

Actinoporins N-terminal end, comprising about their first 30 amino acid residues (Fig. 3), is an essential region to achieve the correct formation of the pore and, therefore, to exert their hemolytic activity, although it does not seem to be so important for membrane

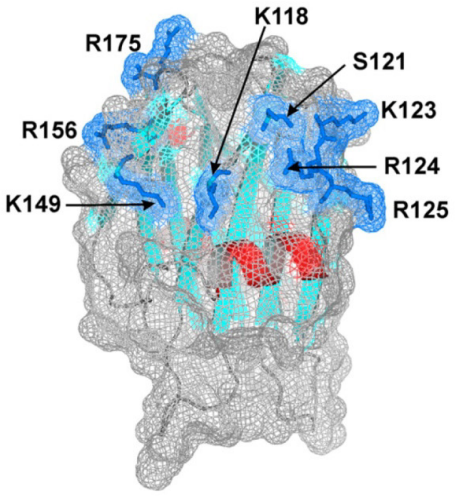

Fig. 6. Diagram showing the protein surface (grey) with the relative location of the array of basic amino acids within the three-dimensional structure of StnII (PDB ID: 1GWY). This array is made of StnII residues Lys-118, Ser-121, Lys-123, Arg-124, Arg-125, Lys-149, Arg-156, and Arg-175. The side-chains corresponding to these residues are shown in blue. The backbone is represented by a ribbon with the α-helices in red and the β-strands in cyan. Figure produced by PyMol (DeLano Scientific LLC).

attachment [49,55]. For example, it is well established how removal of this N-terminus of EqtII precludes pore formation, but does not prevent membrane binding [56]. A more recent characterization of StnII variants where single mutations had been introduced within these first 30 amino acid residues also supported the idea that the N-terminus is not needed for membrane recognition [44]. Furthermore, the use of disulfide mutants that locked the N-terminal helix to the β-sandwich elegantly showed that helix detachment was necessary for pore formation [49,55]. On the other hand, taking into consideration this crucial role of the N-terminal region in the formation of the pore, it is somehow striking that it is precisely the most variable region in the sequence of actinoporins (Fig. 1). However, this variability is located mainly at the hydrophilic residues, whereas a higher degree of conservation is observed for hydrophobic ones, preserving its amphipathic nature. Thus, it seems feasible that distinct actinoporins may form pores with slightly different conductivity properties, resulting in differences in their toxicity. If that is the case, it could help to explain why one specific anemone produces several different isoforms in terms of a strategy of broadening of its venomous condition. In fact, N-terminal sequence differences found between StnI and StnII have been used to explain the observed different hemolytic activity of these two proteins against human erythrocytes [57,58].

The conformation of peptides mimicking the N-terminal of EqtII, StnI, and StnII has been studied in water and in the presence of lipid-like environments such as liposomes, bicelles, micelles, or even trifluoroethanol (TFE) [41,59–62]. All these compounds and materials are generally accepted as a first approximation to mimic the membrane environment of peptides and proteins; and they are thoroughly used with this purpose. Caution must be taken, however, when extrapolating the results obtained to a real membrane bilayer. With this precaution in mind, it still seems clear that this kind of approach has produced a good amount of useful data regarding the conformational possibilities of the N-terminal end of actinoporins. For example, the synthetic peptide corresponding to residues 1–30 of StnI displays a reasonably high tendency to form a helix in water but it is significantly more helical in either TFE or DPC micelles (Fig. 7). In these lipid-mimicking environments it forms a helix–turn–helix motif with the last α-helical segment matching the native N-terminal α-helix (residues 14–24) present in the complete protein, while the first helix (residues 4–9) is less populated and is not present in the water-soluble protein structure [41]. On the other hand, the amino-terminal peptides of EqtII and StnII are essentially unstructured and extended in water solution, respectively, although can also acquire large helical contents in hydrophobic environments like micelles or TFE [59–61]. Simulation of the behaviour in water of a peptide containing the first 32 residues of EqtII [62] revealed the adoption of a flexible loop and turn structures, in contrast to the helical structure seen in DPC micelles [60]. NMR studies confirmed that this peptide in aqueous solution did not adopt an ordered conformation [60] while they showed that it becomes partly helical in the presence of lipids. This helical content is greater when SM is present, in agreement with the increased efficiency of actinoporins in the presence of this lipid [62]. Thus, producing more than one type of protein, such as StnI and StnII, with distinct structural tendencies along an important segment for pore formation, again may endow the anemone with a diverse arsenal suitable for attacking a wider variety of prey, including the possibility of a concerted and more efficient synergic cytotoxic action [41]. Indeed, all the studied peptides seem to display an environmental conformational plasticity which may be highly important for exerting their function when included in the complete protein.

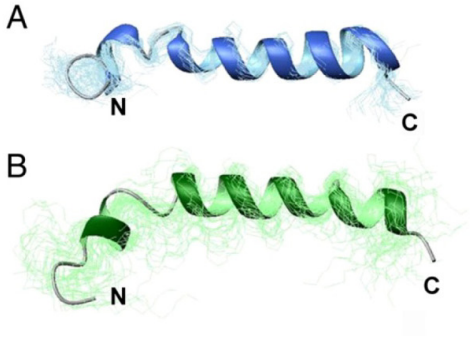

Fig. 7. Representation of the solution structure of a synthetic peptide corresponding to the first 30 amino acids of StnI [40]. Superposition of the backbone atoms of the 25 structures obtained by NMR in 30% TFE (A) or DPC micelles (B). One conformer of each family is represented by a ribbon.

All these NMR studies about the structure of different synthetic peptides and actinoporins in the presence of lipidic environments have rendered clues about their pore-forming mechanism [41,62,63]. For example, NMR analysis of StnI in water and in the presence of membrane-mimicking micelles has shown that the N-terminal α-helix is maintained in its native structure and that this micellar environment does not provoke its detachment from the protein core [41]. This direct observation that the dissociation of the StnI N-terminus does not occur in the presence of micelles [41] is in agreement with previous proposals for the homologous EqtII [51,64] and with the assumption that this region does not participate in the recognition of the membrane [44].

It is suggested that actinoporins do not insert deeply in the membrane except for its N-terminus [49,53]. Within this idea, cysteine-scanning mutagenesis was used to propose that EqtII residues 10–28 are organized as an α-helix in the pore structure [40]. This proposal was later extended to suggest that the adoption of an N-terminal helical conformation would also take place along the first ten amino acids [65]. In fact, addition of an N-terminal 6xHis tag does not preclude pore formation but the channels formed are of lower conductance [65]. Indeed, these tagged proteins show hemolytic activity significantly diminished [33,65,66]. The presence of 3_{10} helices within this protein segment may be indicative of the existence of intermediate structures prone to change their conformation to become elongated α-helices [39]. Such an extended helix would still be amphipathic, forming angle with the membrane normal of about 31° [53]. Accordingly, FTIR [53,67] and CD [68] measurements detected increments in the α-helical content of actinoporins upon lipid binding that were compatible with these observations. Within this same idea, as already mentioned, truncation of the first EqtII residues caused a decrease of its hemolytic activity and pore stability [56,65]. Finally, mutations that confer conformational stiffness, such as the introduction of Pro residues or a disulphide bridge, hamper pore formation most probably by diminishing the propensity to extend and detach the N-terminal helix once the protein is already bound to the membrane [44,49,55]. The already mentioned StnII R29Q mutant shows the existence of an increased dynamic flexibility at the hinge region between the N-terminal α-helix and the protein core [46] which would explain why this impaired variant is however more hemolytic than expected from its membrane binding affinity [46]. On the contrary, the structure of a StnII Y111N mutant [46] suggests not only a rigidification of the POC-binding site but also of the loop comprising residues 25 to 29. This conformational stiffness would hamper detachment of the N-terminal α-helix. Overall there would be a loss of the necessary plasticity to interact with the membrane. Both the local and the long-range effects in this mutant could explain why it is less hemolytic than predicted from its binding affinity [44].

Other protein regions

Regions around the N-terminal and the aromatic and positively charged residues are highly flexible and contribute to membrane

binding as well as undergoing changes in secondary structure during interaction with bilayers [62]. Most actinoporins contain an Arg–Gly–Asp (RGD) motif that might be involved in promoting attachment to integrin receptors on the surface of cells [4,28,69–71], a possibility which does not seem to have been studied yet. The absence of this motif in the sequence of some members of this family, such as Avt-I from *Actineria villosa* or Pstx20 from *Phyllodiscus semoni*[34] (Fig. 1), might be another structural feature to be taken into account when explaining the variety of prey killed by different sea anemones.

Finally, the detailed analysis of the soluble three-dimensional structure of StnII R29Q [46] has revealed the existence of other residues that are affected by conformational exchange processes. These residues are arranged around the β-hairpin composed by residues 145–150 and 156–161. Interestingly, these stretches comprise the RGD motif (StnII Arg-141, Gly-142, and Asp-143) as well as some of the components of the already discussed array of basic amino acids (Fig. 3). It is speculated that these residues could be involved in other type of interactions apart from those directly related to lipid binding and pore formation such as oligomerization, for example. On the basis of the NMR results obtained so far it seems that the atomic determinants for membrane recognition and pore formation by actinoporins rely not only on a structure that provides the correct geometry but also on a finely tuned network arrangement and the adequate dynamic properties of the regions involved [5,46]. These geometric and dynamic arrangements are most probably modified by some of the membrane components when establishing the interactions needed to form the pore. These considerations would help to explain the different nature of the interactions occurring depending on the nature and composition of the bilayer studied.

The nature of the target lipid membrane

Actinoporins seem to be able to form pores within model membranes in the absence of any other protein, showing that they do not need a protein receptor [16,26,72,73]. In fact, the incorporation of the toxin into the bilayer, a crucial step for the final pore formation, depends largely on the composition and physicochemical state of the membrane [73–75]. Both factors influence the actinoporins conformational changes occurring upon the transition from the water media to the inserted state [44,67]. Thus, high affinity recognition of SM by the protein seems to be very important for its specific attachment to a particular membrane but the following effects observed probably depend also on the physical properties derived from its particular composition and not only from its SM content.

The importance of the presence of SM within the membrane has been already highlighted in the previous sections of this review. Many experiments have been performed during the last 15 years to prove the essential role of this lipid in actinoporins function [18,42,51,73–78]. Specific binding of EqtII to SM has been elegantly shown by lipid dot blot assays and surface plasmon resonance (SPR) experiments [41]. This binding is so specific that it has been postulated that SM functions for EqtII as a real membrane receptor but of lipidic nature. The structural basis for this specificity seems to be based on the fact that EqtII could recognize a lipid moiety different from the headgroup, since PC and SM have the same one and POC does not bind with great affinity to actinoporins. A more recent ITC characterization of StnII binding to SM/DOPC/Chol (1:1:1) vesicles has revealed a reversible interaction characterized by a high affinity constant [44], a fact that is contradictory with some previous results [15,76], but compatible with the observation that EqtII can slowly dissociate from DOPC/SM (1:1) membranes [42,49]. Overall, the results so far obtained support the belief that SM is the preferable lipid for EqtII, although permeabilization experiments with other actinoporins may not follow this strict requisite, at least when pore formation is being evaluated [73]. Definitively, this is an aspect that still remains to be completely solved.

Coexistence of different phases on the membrane seems to be another important factor, if not for attachment, at least for the final formation of the pore [44,67,73]. For example, studies performed with giant unilamellar vesicles (GUV) have shown that SM strongly enhanced binding of EqtII, but was not sufficient for membrane permeabilization. Pores were formed only when, in addition to the presence of SM, liquid ordered and disordered phases coexisted [78]. Moreover, there was permeabilization if these GUV were made only of DOPC/DPPC/Chol (1:1:1) mixtures which do not contain SM but do exhibit phase coexistence. Although these experiments were made at far higher concentrations of EqtII compared to the hemolysis assays, the results showed that this actinoporin can also interact with lipid membranes in the absence of SM. In this case, very similar results were obtained for StnII with other membrane systems. According to the results published so far for this particular actinoporin, the presence of SM does not seem to be as crucial as it is for EqtII [44,53,73,79].

Within this same idea, the increased permeabilizing potency of actinoporins observed against PC liposomes in the presence of Chol could be explained by the formation of microdomains, which may alter the accessibility of the phosphorylcholine group for toxin binding [80]. The presence of Chol in membranes exclusively formed by PC leads to pore formation, even under circumstances where little toxin is associated with the lipids [73,81]. Moreover, SM and Chol coexistence in membranes significantly favours binding and permeabilizing activity of StnII. Consequently, solid-state NMR results also indicate that Chol destabilizes the DMPC bilayer in the presence of EqtII but leads to greater disruption when SM is in the bilayer. This supports the proposal that actinoporins are more lytic when both SM and Chol are present as a consequence of the formation of domain boundaries between liquid ordered and disordered phases in lipid bilayers [63,73,75,78]. It seems that lipid packing defects arising at the interfaces between coexisting phases may function as preferential binding-sites for the toxin. Association with these interfaces between domains would function as an efficient concentration strategy confining the toxins to a space where oligomerization and pore formation could take place at very low bulk protein concentrations [80]. If this is correct, minor amounts of lipids favouring non-lamellar organizations should augment the efficiency of pore formation. Accordingly, inclusion of PE in vesicles containing both PC and SM, did not substantially modify the insertion of StnII, but increased the rate of pore formation [81]. Within this same idea, the presence of small quantities of anionic lipids rendered membranes more sensitive to actinoporin-induced permeabilization [74]. FTIR, ^{31}P NMR, and electron paramagnetic resonance (EPR) experiments have also proven how EqtII induces non-lamellar lipid structures which would be consistent with the formation of a toroidal lipid pore [53,74,82,83]. In addition, actinoporins are able to induce lipid flip-flop between internal and external leaflets of liposome membranes and to permeabilize liposomes in the presence of phosphatidic acid, a strong inducer of negative membrane curvature [74]. As mentioned above, synchrotron radiation CD spectroscopic studies have revealed that the peptide corresponding to residues 1–32 of EqtII adopts very different conformations when examined in water, DPC micelles, or small unilamellar vesicles composed of DOPC or DMPC [61]. These conformations were highly influenced by the presence of SM and Chol, confirming the importance of the lipid properties arising from the coexistence of liquid ordered and disordered phases and the dual role of SM as a specific attachment and as a promoter of the bilayer organization necessary for membrane lysis [61]. In agreement with all these results, different experiments have shown that StnII is able to promote pore formation in COS-7 cells via its interaction with the domains enriched in SM and Chol known as cellular rafts [79].

It seems clear then that actinoporins permeabilizing activity depends on membrane lipid composition but ionic concentration and variety of the medium can be also a determinant factor. Results

have shown that StnII hemolytic activity is promoted by Ca^{2+} and Mg^{2+} and inhibited by Co^{2+} and Mn^{2+}[84]. In particular, results recently reported suggest that StnII pore-forming ability is improved by an increase in intracellular calcium associated to membrane phospholipids translocation elicited by scramblases [85]. The oxidative status of the red blood cells, regarding membrane lipid composition, seems to be another feature to take into account when studying actinoporins effect on cells [86]. All these aspects of their function have not been deeply studied yet and deserve future attention and development.

From another point of view, it is also well known how StnII is about six fold more active than StnI against human red blood cells. Moreover, StnII and EqtII show a very different ability to lyse these cells when tested under the same experimental conditions [81]. Therefore, different actinoporins could display distinct lipid requirements to accomplish the formation of the pore, including different efficiencies for SM binding. This is a possibility that still remains as an open question to be answered in the near future.

Finally, sea anemones possess within their membranes analogues of SM to which actinoporins do not bind [87]. This would explain, at least in part, the molecular basis of their self/nonself selectivity. For example, the hemolytic activity of actinoporin from *Phymactis clematis* was inhibited by SM but not by sphingolipids purified from the same sea anemone. This specific recognition is probably based on the existence of a different phospholipid headgroup in the SM analogues.

The current model of pore formation

Actinoporins, as any other PFT, must suffer a transformation from a soluble monomeric protein to an oligomeric transmembrane channel to exert their biological function [6]. The accepted steps of the mechanism of actinoporins pore formation have been described in high detail before [5]. Therefore, only a brief summary of this mechanism (Fig. 8) will be considered in the following lines, with special emphasis on the new results obtained along the last 4 years.

It is generally accepted that these proteins initially bind to the target membrane as monomers guided by their affinity to some membrane component, being SM the preferred candidate. Such an interaction would result in an increase of toxin concentration at the lipid–water interface that would lead to its oligomerization on the membrane surface. Interestingly, the presence of preassembled StnI dimers, via a disulfide bridge at the N-terminal end, seems to facilitate pore formation [88]. Kinetic measurements using SPR suggest this binding to membranes as a two-step process [42,49]. The first one would be driven by the POC-binding site, the aromatic cluster of amino acids, and the array of basic residues. The synergic or cooperative action of these domains seems to be possible, or even probable, but it has not been explicitly measured yet. During the second step, the N-terminal α-helix would detach from the β-sandwich, extend, and lie parallel to the membrane. Simultaneously, oligomerization would occur. A non-active oligomer, often referred as a "prepore" state, would then be formed (represented as T_1 or T_2 in Fig. 8). Different intermediates and structures which could potentially represent this non-active state have been determined by two-dimensional crystallization on lipid mono-layers and electron and atomic force microscopies, combined with computer assisted docking [38,89–91]. Interestingly, in all cases tetrameric ensembles were detected where the high resolution water soluble structure could be nicely fitted with only minimal modifications [38]. However, the recent determination of the FraC crystalline structure has challenged these conclusions. FraC was crystallized in the presence of a detergent [39] resulting in an ensemble consisting of two concentric and identical crown-shaped nonamers. The overall external diameter of each crown was almost double in size that the internal one of approximately 5.2 nm. The detergent molecules appear located at the basal crown rim and the nine N-termini line its inner wall. These N-terminal stretches still retain the conformation of the water soluble structures of actinoporins. Most of the residues belonging to the conserved cluster of aromatic amino acids constitute part of the crown base and their side chains enter into contact with the detergent molecules [39]. The authors of this work state that all these results are compatible with the assumption that this nonameric structure represents a high-resolution model of an actinoporin in its prepore state. Apart from the evident beauty and appeal of this proposal, direct evidence about the existence of this "prepore" as a definite structural intermediate en route to the formation of the pore is still lacking. In contrast, this type of structure seems to have been perfectly identified in some β-PFTs [92].

On the basis of the NMR results obtained for StnI in the presence of DPC micelles [41], during the early steps of the interaction with the lipid bilayer most of the aromatic rings from the cluster would be in intimate contact with the membrane. The loop comprising Lys-27 to Lys-31 would be also close to it, and the N-terminal α-helix would remain in its native conformation. Experiments made with extensive double cysteine scanning mutagenesis [55] confirmed that changes of the β-sandwich structure are not necessary for formation of the pore. Instead, the core of the protein should remain compactly folded in order for the protein to be fully active. The recent determination of the

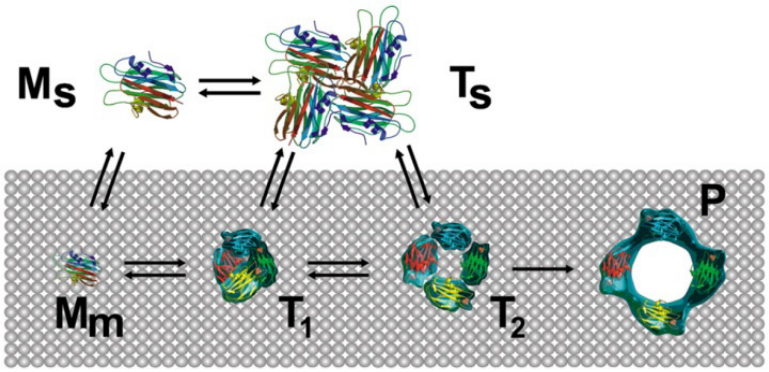

Fig. 8. Scheme showing different steps of the most accepted mechanism of pore formation by actinoporins, exemplified by the proposal that StnII assembles into a tetrameric toroidal pore [5]. M_S: water soluble monomer. T_S: water soluble tetramer. The amount of monomers forming the pore, as well as the particular step where oligomerization occurs, are still matter of study. M_m: monomer bound to the membrane. T_1 and T_2: tetrameric non-conductive lipid-bound forms. P: tetrameric pore. The conformational changes involving detachment and extension of the N-terminal α-helix would take place along the $M_m \leftrightarrow T_1 \leftrightarrow T_2$ transitions.

structures of StnII R29Q and Y111N mutants [46] has revealed, however, the higher complexity of this process, as well as the crucial importance of long-range interactions along the protein and the overall distribution of the electrostatic potential of the surface facing the membrane. Within this picture, the β-sandwich would be crucial for lipid specificity, membrane targeting, and formation of the final pore structure, because it would constitute the solid scaffold where the distant parts responsible for the different and specific interactions would be positioned precisely to selectively act in the presence of the target. From this state, membrane permeabilization would be achieved by conformational changes within the toxin, which would expose hydrophobic patches of amino acids required for membrane insertion. Such lipid–protein interactions may be related to the ability of the protein to adopt a molten-globule state, a conformational intermediate that has been shown to exist for actinoporins under some experimental conditions [37,93–96]. One of these conformational changes would involve the detachment and extension of the N-terminal α-helix. This was shown, for example, by the behaviour of a double cysteine mutant where its N-terminus had been fixed to the protein core by a disulphide bond [49], impairing pore formation. Finally, this extended amino-terminal α-helix would penetrate the membrane to build a toroidal pore [5,97] where not only the protein but also the phospholipid headgroups would linen its walls. The existence of such a structure has been shown by different means, such as ATR-FTIR of isolated protein-membrane complexes [53] and would explain why these pores are noisy and less stable than those known to be made by β-PFT. Usually, pores formed by actinoporins do not seem to require more than 3–4 monomers [16,26,98], while β-PFTs need instead a higher number of units [6] just because the lipid moieties are excluded from the pore lumen. Again, it has to be emphasized how the crystallization of FraC nonameric structure [39] has allowed these authors to build a model, based on cryo-EM results, of the protein bound to phospholipid vesicles, with the nine N-termini assembling as a compact α-helical structure where lipids would not be part of the pore wall. This new model challenges the consensus view in the field of actinoporins, and will probably be subject to experimental validation in the following years.

Furthermore, pore formation by StnII is an enthalpy-driven process [44], which indicates that the strength of interactions between the lipids and the protein is higher than those existing with the solvent [99]. Taking into consideration that ΔS is unfavourable, a higher binding constant is predicted when lowering temperature, which would agree with the higher activity of actinoporins at cooler temperatures [80].

It is clear that EqtII and StnII form cation selective pores with a hydrodynamic diameter of about 1–2 nm, according to the results of different experiments, including the use of osmotic protectants of different size and conductance measurements in planar bilayers [15–17,25,26,38,73]. This size appears to be independent of toxin concentration [17]. Thus, pores seem to have a fixed common predominant structure but may adopt slightly different conformations while keeping constant their size, depending on the protein and the nature of the membrane studied. EqtII pores, for example, have a broad conductance distribution [65]. The positively charged residues on the extended amphipathic N-terminal helices of the oligomer forming the pore would control binding of this protein segment by interacting with the negative phosphate groups of the membrane lipids, while negative charges within the pore lumen would contribute to cation selectivity as well as pore-forming activity [28]. Moreover, negatively charged lipids are able to increase the cationic selectivity of the pore supporting the proposition that lipids are part of the pore lumen [82]. The significant differences in actinoporins N-terminal segments [5,100] (Fig. 1) could account for differences in activity, size, stability and maybe cation specificity of the resulting pore. Much work however still needs to be done in order to fully understand the complex mechanism underlying actinoporins functionality.

Actinoporin-like proteins

Actinoporins constitute a good example of how Nature preserves a common structural fold with different purposes [10]. Until very recently, actinoporins were thought to be restricted to sea anemones, but now actinoporin-like proteins (ALPs) have been identified in other cnidarians and a wide variety of vertebrates, in addition to a small number of plants, mosses, and fungi [101,102]. Surprisingly, many of these proteins, which show high levels of sequence and/or structural similarity with actinoporins, neither bind to lipid membranes nor induce cell lysis.

One of the most remarkable examples of this structural conservation is constituted by a family of fungal lectins, with insecticidal and anti-proliferative properties [103,104], such as XCL from *Xerocomus chrysenteron* or ABL from *Agaricus bisporus*. Although these proteins display less than 15% sequence identity to actinoporins [105,106] they exhibit a protein fold which is almost identical to the three-dimensional structures of EqtII and StnII, except for the absence of the N-terminal α-helix (Fig. 9), in good agreement with their lack of permeabilizing activity. Furthermore, the specific structural features and sequence signatures in this protein family suggest a potential sugar binding site in these lectins, which would be evolutionary related to the actinoporins POC-binding site [105,107].

Very similar structures to actinoporins appear as well in other completely unrelated toxins, such as the necrosis and ethylene-inducing peptide 1 (Nep-1)-like protein (NLP) secreted by the phytopathogenic oomycete *Pythium aphanidermatum*[108]. This toxin belongs to the NLPs superfamily of proteins, produced by various prokaryotic and eukaryotic phytopathogenic microorganisms [109–112]. They trigger leaf necrosis and stimulate immunity associated defences in all dicotyledonous plants tested, but not in monocotyledonous ones [110,111]. Hence, NLPs have been proposed to have dual functions in plant pathogen interactions, acting both as triggers of immune responses and as toxin-like virulence factors [113]. Superimposition of actinoporins and *P. aphanidermatum* NLP three-dimensional structures suggests a significant degree of structural similarity but they are only distantly related proteins [108]. In addition, this ethylene-inducing peptide retains the N-terminal helical segment which in this case seems to be required for inducing necrosis and plant defence activation [114]. This and other membrane permeabilization results suggest that NLPs and actinoporins may share a cytolytic, membrane-disintegrating mode of action [108].

Echotoxins are also actinoporin-related toxins that have been found in the salivary gland of the marine gastropod *Monoplex echo* [115]. They exhibit both hemolytic and mouse-lethal activities that are inhibitable by gangliosides. They share low sequence identity with actinoporins (12–16%), but some of the amino acid residues important for their biological activity are well conserved in both protein families [115]. Therefore, it has been hypothesized that echotoxins may have evolved from actinoporins or, at least, that both toxins originated from a common ancestor.

Bryoporin (PpBP), an ALP produced by the moss *Physcomitrella patens*, must be also mentioned. It shares 50% amino acid identity with EqtII. This protein is upregulated under water stress conditions, and overexpressing PpBP heightens drought resistance in this moss. Therefore, some ALPs might be involved in functions so important to terrestrial plants such as withstanding dehydration [102].

Search in public databases looking for sequences similar to EqtII yielded proteins from three animal and two plant phyla. Sequence conservation located to a region of the β-sandwich involved in membrane binding, suggesting that these homologues should be membrane-binding proteins. Interestingly, most of these sequences were retrieved from fish. One of them, corresponding to DrI, a protein of unknown function from zebra fish (*Danio rerio*), was cloned, isolated, and characterized. Surprisingly, DrI lacked SM specificity, was non-hemolytic and had only weak membrane binding capacity *in vitro*[101]. Clamlysin, another novel SM binding protein, has been purified from the foot muscle of the clam *Corbicula japonica*[116]. This protein shows

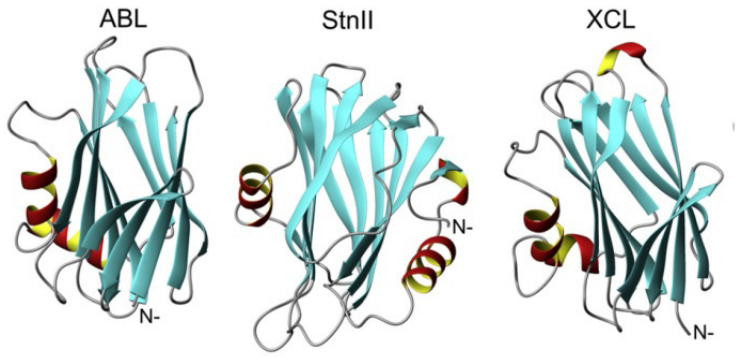

Fig. 9. Diagram showing the three-dimensional structures of XCL (PDB ID: 1XIO), ABL (PDB ID: 1Y2T), and StnII (PDB ID: 1GWY). Images were generated with MolMol [150].

hemolytic activity which can be inhibited by SM, but not other phospholipids or glycosphingolipids. It displays high sequence similarity and a size compatible with actinoporins. However, the reported characterization [116] is still preliminary and much work has to be done yet to include it within the actinoporins family.

Noticeably, actinoporins show weak structural similarity with domain 4 of perfringolysin O (Fig. 10), a Chol-dependent PFT from *Clostridium perfringens*. This domain, which is responsible for the initial membrane recognition and binding of this much larger toxin, lacks the region equivalent to the N-terminal structure of actinoporins, and thus pore-formation requires the intervention of some of its other additional domains [117]. It can be concluded then that the archetypical actinoporin β-sandwich fold is not simply a lipid-recognition motif but it can be also used by other proteins to bind ligands of very different nature and exert a variety of other biological functions apart from pore formation [10].

Eventually some other toxins have been considered ALPs but their classification into this group of proteins is not really established yet. A good example of this situation would be a pore-forming cytolytic protein isolated from the Northern red sea anemone, *Urticina crassicornis*[118]. This cytolysin, named UcI, is able to cause hemolysis as a result of a colloid-osmotic shock caused by the opening of toxin-induced ionic pores. It binds to lipid monolayers and efficiently permeabilizes small lipid vesicles composed of SM and Chol. However, its cytolytic activity is not prevented by preincubation with either any of these two lipids. Sequencing of its N-terminal revealed no sequence similarity with actinoporins but to UpI, another cytolytic protein isolated from a related sea anemone species, *Urticina piscivora*. Both proteins most probably belong to a separate family of sea anemone cytolysins that is pending of being characterized [118]. As a final example, toxins from sea anemones *Gyrostoma helianthus* and *Radianthus koseirensis* have been sometimes classified as actinoporins because they are inhibited by SM [119]. However, this inclusion is rather controversial due to their much smaller size (10 kDa), and should wait for a more detailed inspection of their molecular properties.

In summary, these observations altogether suggest that actinoporins structural motif displays ubiquity and some kind of structural conservation which may be useful to understand protein evolution. Indeed, it seems clear that the archetypal actinoporin fold is widespread and used for specific binding of different proteins to other molecules or surfaces apart from plasmatic membranes.

Therapeutic potential

Finally, similarly to many other toxins, studies focusing on the therapeutic potential of actinoporins abound. These include the

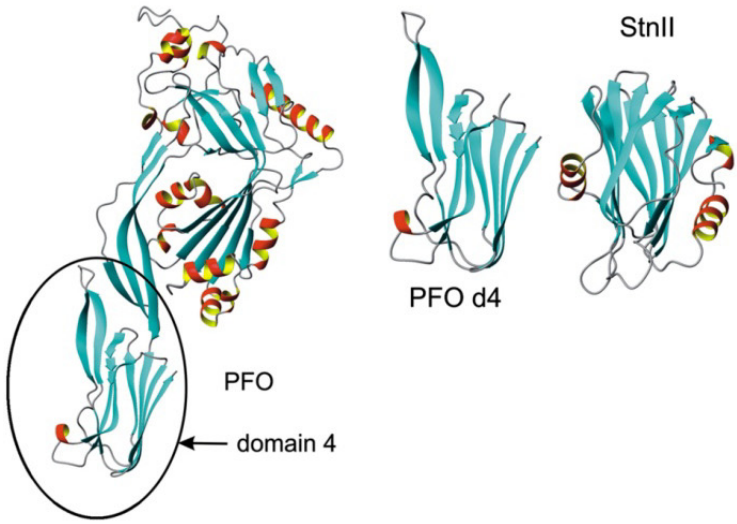

Fig. 10. Diagram showing the three-dimensional structures of Perfringolysin O (PFO; PDB ID: 1M3J) and its domain 4 (PFO d4); and StnII. Images were generated with MolMol [150].

characterization of their different pharmacological effects, their presumable anticancer activities, and their use in the development of highly specific immunotoxins. Cardiostimulatory, anti-tumour, and anti-parasite activity have been reported for some of these toxins from sea anemones [2,24,120–123].

Some actinoporins have been shown to induce concentration dependent inhibition of gamma amino butyric acid and choline uptake into rat brain synaptosomes [124]. Ionotropic, myocardial contractility, hypotension, arrhythmia, and vascular permeability effects have been reported for rats and guinea pigs treated with different doses of actinoporins [125–128], mostly EqtII. Although sometimes transient favourable effects were observed, most of the animals finally died due to a yet unexplained cardio-respiratory arrest [121,127]. StnI and StnII have been shown to display different activities on molluscan nervous system and mammalian cardiac tissues [129]. The effect of the release of different ions such as K^+ or Ca^{2+} due to the administration of actinoporins has been studied without arriving to definitive conclusions about the effect of these toxins on the mammal's cardiovascular system [2,128,130–134].

Cytolysins show anticancer activity but by a mechanism still poorly understood [135–137]. For example, both Bc2, from *Bunodosoma caissarum,* and EqtII decrease U87 glioblastoma cells viability in a concentration dependent manner. Cell death is concomitant with results showing a highly altered membrane permeability leading to cell swelling, activation of different intracellular signalling pathways, and necrosis [136,137]. Actinoporin RTX-A from *Heteractis crispa* has been shown to exhibit cancer preventive and anticancer cytotoxic properties, at low non-cytotoxic concentrations [135], through the induction of p53-independent apoptosis and inhibition of the oncogenic AP-1 and NF-κB nuclear factors activity.

Many viruses, including HIV-1, are suggested to bud from raft-like membrane microdomains [138,139]. Consequently, HIV-1 membrane is highly enriched in Chol, SM, and other raft lipids. Interestingly, treatment of infectious HIV-1 with EqtII showed differential inhibition of infectivity in a SM concentration-dependent manner [140]. However, pores were not being formed into the viral membrane despite complete inactivation of viral infectivity suggesting that inactivation was primarily being caused by the toxin binding to the viral membrane. While pore forming toxins certainly cannot serve in this case as drug candidates, the authors of this work [140] propose testing of other lipophilic compounds which could specifically bind and alter HIV-1 membrane structure.

Actinoporins, or some fragments such as their N-terminal peptide, have also been used in the construction of immunotoxins or tumour protease-activated PFTs, targeted to different cell lines or the parasite *G. duodenalis*[24,141–147]. *Plasmodium falciparum* is another parasite which has been targeted by actinoporins. EqtII has been employed to lyse the limiting membrane of infected and uninfected erythrocytes [148], permeabilizing both cellular populations with similar efficiency but without disrupting the parasitophorus vacuole where the micro-organism resides. This study opened the door to designing new approaches and tools aimed to the analysis of the behaviour of this human pathogen [148].

On a very different register, a GFP-modified version of EqtII has been shown to be an important probe for membrane SM [54] that can be used to monitor the subcellular distribution of this phospholipid. This is a new and important use of actinoporins taking into account that SM is the precursor of many important lipid signalling molecules, such as ceramide and sphingosine or their corresponding phosphorylated versions.

Perspectives

Much work has been done during the last decade in order to explain the behaviour of actinoporins at the water–membrane interface, but many more experiments are still required to fully understand the mechanisms underlying their biological function.

A very important question to be answered is why phase coexistence in the target membrane promotes pore formation and what the precise role of SM in this mechanism is. The use of many more lipid mixtures, containing different amounts of SM and Chol, and their lipid analogues, seems to be a wise line of research to be pursued. In fact, it would be also important to extend many of the experiments made with EqtII and StnII to other actinoporins to confirm the generality of the actual assumptions made about their mechanism. Thermodynamic studies can be of great help in elucidating the influence of temperature. Taking into account that sea anemones live in a rather cool environment, answering this question would be of great importance to understand actinoporins biological function.

Studies targeting the regions of actinoporins whose role has not been assigned yet must be another path to be followed. For example: what are the residues involved in oligomerization? Is there synergy and/or cooperativity among the different regions involved in membrane attachment and oligomerization? Or, what are the determinants of the specific SM recognition? Many more detailed studies regarding the biophysical and structural properties of these proteins are still needed. Characterization of mutants affecting different stages of pore formation will be of the highest interest, as well as, again, the employment of different actinoporins. The wide variety of known proteins from this family, altogether with their high sequence conservation can be considered as a wide natural palette of variants to help in this study of their functionality.

However, the most important and still unanswered question refers to the detailed mechanism of pore formation, as well as the structure of the final functional pore. In this regard, the isolation of a stable pore assembly would be of great help in order to understand the precise role of lipids in the pore, or what is the exact length of the N-terminal helix in the pore. The isolation of water-soluble pore structures seems to be an obliged step in order to solve this problem. Eventually, the discovery of more potential non-conducive "prepore" intermediates would be of great utility to dissect the mechanism of pore formation at the molecular level and establish the final pore structure. Employment of water-soluble lipidic platforms, such as nanodiscs [149], with this purpose seems to be a promising approach. Micelles and bicelles of different nature and composition, although have to be used with caution, represent convenient platforms to mimic the lipidic environment of the final pre and pore structures. Solid-state NMR and cryo-EM stand out as additional useful tools to help unveiling the mechanism of pore formation by actinoporins. Such structural studies may be hindered by the possibility that the pore structure is not a unique entity, as suggested by the broad conductance distribution of actinoporins pores. Again, mutagenesis can be used as a method to "freeze" or isolate some of these intermediate states.

Many more studies must be aimed at searching the distribution of the actinoporins motif within the protein universe and the different roles played in the protein families where it appears. Data mining of genomic and structural data bases must be performed in order to identify the presence of this motif. More experiments should be done in order to clarify if there is a general mechanism, based on protein–lipid interactions, underlying the toxicity of those ALPs with cytotoxic properties. Finally, it must not be forgotten either the potential use of actinoporins, or different modified versions, as diagnostic or therapeutic tools. Their inclusion as part of different immunoconjugates seems to be one of the most promising alternatives in this regard.

Acknowledgments

L.G.-O. is a member of the program Juan de la Cierva from the Spanish Ministerio de Ciencia e Innovación. S.G. L. is recipient of an undergraduate fellowship from the Universidad Complutense.

Dr. Jaime Martín-Benito skilful comments are greatly appreciated. This work was supported by projects CTQ 2008-00080/BQU and BFU2009-10185 from the Spanish Ministerio de Ciencia e Innovación.

References

[1] A. Basulto, V.M. Pérez, Y. Noa, C. Varela, A.J. Otero, M.C. Pico, Immunohistochemical targeting of sea anemone cytolysins on tentacles, mesenteric filaments and isolated nematocysts of *Stichodactyla helianthus*, J. Exp. Zoolog. A Comp. Exp. Biol. 305 (2006) 253–258.

[2] D. Šuput, *In vivo* effects of cnidarian toxins and venoms, Toxicon 54 (2009) 1190–1200.

[3] P. Maček, Polypeptide cytolytic toxins from sea anemones (Actinaria), FEMS Microbiol. Immunol. 5 (1992) 121–129.

[4] G. Anderluh, P. Maček, Cytolytic peptide and protein toxins from sea anemones (Anthozoa: Actinaria), Toxicon 40 (2002) 111–124.

[5] J. Alegre-Cebollada, M. Oñaderra, J.G. Gavilanes, A. Martínez-del-Pozo, Sea anemone actinoporins: the transition from a folded soluble state to a functionally active membrane-bound oligomeric pore, Curr. Protein Pept. Sci. 8 (2007) 558–572.

[6] M.W. Parker, S.C. Feil, Pore-forming protein toxins: from structure to function, Prog. Biophys. Mol. Biol. 88 (2005) 91–142.

[7] B. Geny, M.R. Popoff, Bacterial protein toxins and lipids: pore formation or toxin entry into cells, Biol. Cell. (2006) 667–678.

[8] M.R. González, M. Bischofberger, L. Pernot, F.G. van der Goot, B. Frêche, Bacterial pore-forming toxins: the (w)hole story? Cell. Mol. Life Sci. 65 (2008) 493–507.

[9] I. Iacovache, F.G. van der Goot, L. Pernot, Pore formation: an ancient yet complex form of attack, Biochim. Biophys. Acta 1778 (2008) 1611–1623.

[10] G. Anderluh, J.H. Lakey, Disparate proteins use similar architectures to damage membranes, Trends Biochem. Sci. 33 (2008) 482–490.

[11] M. Mueller, U. Grauschopf, T. Maier, R. Glockshuber, N. Ban, The structure of a cytolytic α-helical toxin pore reveals its assembly mechanism, Nature 459 (2009) 726–730.

[12] M. Mueller, N. Ban, Enhanced SnapShot: pore-forming toxins, Cell 142 (2010) 334.e1.

[13] R.H. Law, N. Lukoyanova, I. Voskoboinik, T.T. Caradoc-Davies, K. Baran, M.A. Dunstone, M.E. D'Angelo, E.V. Orlova, F. Coulibaly, S. Verschoor, K.A. Browne, A. Ciccone, M.J. Kuiper, P.I. Bird, J.A. Trapani, H.R. Saibil, J.C. Whisstock, The structural basis for membrane binding and pore formation by lymphocyte perforin, Nature 468 (2010) 447–451.

[14] E. Gouaux, Channel-forming toxins: tales of transformation, Curr. Opin. Struct. Biol. 7 (1997) 566–573.

[15] W. Varanda, A. Finkelstein, Ion and nonelectrolyte permeability properties of channels formed in planar lipid bilayer membranes by the cytolytic toxin from the sea anemone *Stoichactis helianthus*, J. Membr. Biol. 55 (1980) 203–211.

[16] G. Belmonte, C. Pederzolli, P. Maček, G. Menestrina, Pore formation by the sea anemone cytolysin equinatoxin II in red blood cells and model lipid membranes, J. Membr. Biol. 131 (1993) 11–22.

[17] M. Tejuca, M. Dalla Serra, C. Potrich, C. Álvarez, G. Menestrina, Sizing the radius of the pore formed in erythrocytes and lipid vesicles by the toxin sticholysin I from the sea anemone *Stichodactyla helianthus*, J. Membr. Biol. 183 (2001) 125–135.

[18] B. Bakrač, G. Anderluh, Molecular mechanism of sphingomyelin-specific membrane binding and pore formation by actinoporins, Adv. Exp. Med. Biol. 677 (2010) 106–115.

[19] P. Favreau, R. Stöcklin, Marine snail venoms: use and trends in receptor and channel neuropharmacology, Curr. Opin. Pharmacol. 9 (2009) 594–601.

[20] D. Butzke, A. Luch, High-molecular weight protein toxins of marine invertebrates and their elaborate modes of action, EXS 100 (2010) 213–232.

[21] U. Batista, P. Maček, B. Sedmak, The cytotoxic and cytolytic activity of equinatoxin II from the sea anemone *Actinia equina*, Cell Biol. Int. Rep. 14 (1990) 1013–1024.

[22] R. Zorec, M. Tester, P. Maček, W.T. Mason, Cytotoxicity of equinatoxin II from the sea anemone *Actinia equina* involves ion channel formation and an increase in intracellular calcium activity, J. Membr. Biol. 118 (1990) 243–249.

[23] R.S. Norton, Structures of sea anemone toxins, Toxicon 54 (2009) 1075–1088.

[24] M. Tejuca, G. Anderluh, P. Maček, R. Marcet, D. Torres, J. Sarracent, C. Alvarez, M.E. Lanio, M. Dalla Serra, G. Menestrina, Antiparasite activity of sea-anemone cytolysins on *Giardia duodenalis* and specific targeting with anti-*Giardia* antibodies, Int. J. Parasitol. 29 (1999) 489–498.

[25] P. Maček, G. Belmonte, C. Pederzolli, G. Menestrina, Mechanism of action of equinatoxin II, a cytolysin from the sea anemone *Actinia equina* L. belonging to the family of actinoporins, Toxicology 87 (1994) 205–227.

[26] M. Tejuca, M. Dalla Serra, M. Ferreras, M.E. Lanio, G. Menestrina, Mechanism of membrane permeabilization by Sticholysin I, a cytolysin isolated from the venom of the sea anemone *Stichodactyla helianthus*, Biochemistry 35 (1996) 14947–14957.

[27] A. Bellomio, K. Morante, A. Barlič, I. Gutiérrez-Aguirre, A.R. Viguera, J.M. González-Mañas, Purification, cloning and characterization of fragaceatoxin C, a novel actinoporin from the sea anemone *Actinia fragacea*, Toxicon 54 (2009) 869–880.

[28] M. Monastyrnaya, E. Leychenko, M. Isaeva, G. Likhatskaya, E. Zelepuga, E. Kostina, E. Trifonov, E. Nurminski, E. Kozlovskaya, Actinoporins from the sea anemones, tropical *Radianthus macrodactylus* and northern *Oulactis orientalis*: comparative analysis of structure-function relationships, Toxicon 56 (2010) 1299–1314.

[29] G. Anderluh, I. Križaj, B. Štrukelj, F. Gubenšek, P. Maček, J. Pungerčar, Equinatoxins, pore-forming proteins from the sea anemone *Actinia equina*, belong to a multigene family, Toxicon 37 (1999) 1391–1401.

[30] T. Turk, Cytolytic toxins from sea anemones, J. Toxicol.-Toxin Rev. 10 (1991) 223–262.

[31] V. de los Ríos, M. Oñaderra, A. Martínez-Ruiz, J. Lacadena, J.M. Mancheño, A. Martínez-del-Pozo, J.G. Gavilanes, Overproduction in *Escherichia coli* and purification of the haemolytic protein sticholysin II from the sea anemone *Stichodactyla helianthus*, Protein Expr. Purif. 18 (2000) 71–76.

[32] Y. Wang, L.L. Yap, K.L. Chua, H.E. Khoo, A multigene family of *Heteractis* magnificalysins (HMgs), Toxicon 51 (2008) 1374–1382.

[33] J. Alegre-Cebollada, G. Clementi, M. Cunietti, C. Porres, M. Oñaderra, J.G. Gavilanes, A. Martínez-del-Pozo, Silent mutations at the 5′-end of the cDNA of actinoporins from the sea anemone *Stichodactyla helianthus* allow their heterologous overproduction in *Escherichia coli*, J. Biotechnol. 127 (2007) 211–221.

[34] G. Uechi, H. Toma, T. Arakawa, Y. Sato, Molecular characterization on the genome structure of hemolysin toxin isoforms isolated from sea anemone *Actineria villosa* and *Phyllodiscus semoni*, Toxicon 56 (2010) 1470–1476.

[35] B.M. Olivera, J. Rivier, C. Clark, C.A. Ramilo, G.P. Corpuz, F.C. Abogadie, E.E. Mena, S.R. Woodward, D.R. Hillyard, L.J. Cruz, Diversity of *Conus* neuropeptides, Science 249 (1990) 257–263.

[36] A. Athanasiadis, G. Anderluh, P. Maček, D. Turk, Crystal structure of the soluble form of equinatoxin II, a pore-forming toxin from the sea anemone *Actinia equina*, Structure 9 (2001) 341–346.

[37] M.G. Hinds, W. Zhang, G. Anderluh, P.E. Hansen, R.S. Norton, Solution structure of the eukaryotic pore-forming cytolysin equinatoxin II: implications for pore formation, J. Mol. Biol. 315 (2002) 1219–1229.

[38] J.M. Mancheño, J. Martín-Benito, M. Martínez-Ripoll, J.G. Gavilanes, J.A. Hermoso, Crystal and electron microscopy structures of sticholysin II actinoporin reveal insights into the mechanism of membrane pore formation, Structure 11 (2003) 1319–1328.

[39] A.E. Mechaly, A. Bellomio, D. Gil-Cartón, K. Morante, M. Valle, J.M. González-Mañas, D.M. Guérin, Structural insights into the oligomerization and architecture of eukaryotic membrane pore-forming toxins, Structure 19 (2011) 181–191.

[40] P. Malovrh, G. Viero, M. Della Serra, Z. Podlesek, J.H. Lakey, P. Maček, G. Menestrina, G. Anderluh, A novel mechanism of pore formation: membrane penetration by the N-terminal amphipathic region of equinatoxin, J. Biol. Chem. 278 (2003) 22678–22685.

[41] I. Castrillo, N.A. Araujo, J. Alegre-Cebollada, J.G. Gavilanes, A. Martínez-del-Pozo, M. Bruix, Specific interactions of sticholysin I with model membranes: an NMR study, Proteins 78 (2010) 1959–1970.

[42] B. Bakrač, I. Gutiérrez-Aguirre, Z. Podlesek, A.F. Sonnen, R.J. Gilbert, P. Maček, J.H. Lakey, G. Anderluh, Molecular determinants of sphingomyelin specificity of a eukaryotic pore-forming toxin, J. Biol. Chem. 283 (2008) 18665–18677.

[43] J. Alegre-Cebollada, V. Lacadena, M. Oñaderra, J.M. Mancheño, J.G. Gavilanes, A. Martínez-del-Pozo, Phenotypic selection and characterization of randomly produced non-haemolytic mutants of the toxic sea anemone protein sticholysin II, FEBS Lett. 575 (2004) 14–18.

[44] J. Alegre-Cebollada, M. Cunietti, E. Herrero-Galán, J.G. Gavilanes, A. Martínez-del-Pozo, Calorimetric scrutiny of lipid binding by sticholysin II toxin mutants, J. Mol. Biol. 382 (2008) 920–930.

[45] M.A. Pardo-Cea, J. Alegre-Cebollada, A. Martínez-del-Pozo, J.G. Gavilanes, M. Bruix, ^{1}H, ^{13}C, and ^{15}N NMR assignments of StnII–Y111N, a highly impaired mutant of the sea anemone actinoporin Sticholysin II, Biomol. NMR Assign. 4 (2010) 69–72.

[46] M.A. Pardo-Cea, I. Castrillo, J. Alegre-Cebollada, A. Martínez-del-Pozo, J.G. Gavilanes, M. Bruix, Intrinsic local disorder and a network of charge-charge interactions are key to actinoporin membrane disruption and cytotoxicity, FEBS J. (2011), *in press: doi: 10.1111/j.1742-4658.2011.08123.x.*

[47] I. Castrillo, J. Alegre-Cebollada, A. Martínez-del-Pozo, J.G. Gavilanes, J. Santoro, M. Bruix, ^{1}H, ^{13}C, and ^{15}N NMR assignments of the actinoporin Sticholysin I, Biomol. NMR Assign. 3 (2009) 5–7.

[48] M.R. de Planque, J.A. Kruijtzer, R.M. Liskamp, D. Marsh, D.V. Greathouse, R.E. Koeppe II, B. de Kruijff, J.A. Killian, Different membrane anchoring positions of tryptophan and lysine in synthetic transmembrane α-helical peptides, J. Biol. Chem. 274 (1999) 20839–20846.

[49] Q. Hong, I. Gutiérrez-Aguirre, A. Barlič, P. Malovrh, K. Kristan, Z. Podlesek, P. Maček, D. Turk, J.M. González-Mañas, J.H. Lakey, G. Anderluh, Two-step membrane binding by Equinatoxin II, a pore-forming toxin from the sea anemone, involves an exposed aromatic cluster and a flexible helix, J. Biol. Chem. 277 (2002) 41916–41924.

[50] P. Malovrh, A. Barlič, Z. Podlesek, P. Maček, G. Menestrina, G. Anderluh, Structure–function studies of tryptophan mutants of equinatoxin II, a sea anemone pore-forming protein, Biochem. J. 346 (2000) 223–232.

[51] G. Anderluh, A. Razpotnik, Z. Podlesek, P. Maček, F. Separovic, R.S. Norton, Interaction of the eukaryotic pore-forming cytolysin equinatoxin II with model membranes: ^{19}F NMR studies, J. Mol. Biol. 347 (2005) 27–39.

[52] D. Pentón, V. Pérez-Barzaga, I. Díaz, M.L. Reytor, J. Campos, R. Fando, L. Calvo, E.M. Cilli, V. Morera, L.R. Castellanos-Serra, F. Pazos, M.E. Lanio, C. Alvarez, T. Pons, M. Tejuca, Validation of a mutant of the pore-forming toxin sticholysin-I for the construction of proteinase-activated immunotoxins, Protein Eng. Des. Sel. (2011) *in press.*

[53] J. Alegre-Cebollada, A. Martínez-del-Pozo, J.G. Gavilanes, E. Goormaghtigh, Infrared spectroscopy study on the conformational changes leading to pore formation of the toxin sticholysin II, Biophys. J. 93 (2007) 3191–3201.

[54] B. Bakrač, A. Kladnik, P. Maček, G. McHaffie, A. Werner, J.H. Lakey, G. Anderluh, A toxin-based probe reveals cytoplasmic exposure of Golgi sphingomyelin, J. Biol. Chem. 285 (2010) 22186–22195.

[55] K. Kristan, Z. Podlesek, V. Hojnik, I. Gutiérrez-Aguirre, G. Gunčar, D. Turk, J.M. González-Mañas, J.H. Lakey, P. Maček, G. Anderluh, Pore formation by equinatoxin, a eukaryotic pore-forming toxin, requires a flexible N-terminal region and a stable β-sandwich. J. Biol. Chem. 279 (2004) 46509–46517.

[56] G. Anderluh, J. Pungerčar, I. Križaj, B. Strukelj, F. Gubenšek, P. Maček, N-Terminal truncation mutagenesis of equinatoxin II, a pore-forming protein from the sea anemone *Actinia equina*, Protein Eng. 10 (1997) 751–755.

[57] F. Pazos, A. Valle, D. Martínez, A. Ramírez, L. Calderón, A. Pupo, M. Tejuca, V. Morera, J. Campos, R. Fando, F. Dyszy, S. Schreier, E. Horjales, C. Álvarez, M.E. Lanio, E. Lissi, Structural and functional characterization of a recombinant sticholysin I (rSt I) from the sea anemone *Stichodactyla helianthus*, Toxicon 48 (2006) 1083–1094.

[58] E.M. Cilli, F.T. Pigossi, E. Crusca Jr., U. Ros, D. Martínez, M.E. Lanio, C. Álvarez, S. Schreier, Correlations between differences in amino-terminal sequences and different haemolytic activity of sticholysins, Toxicon 50 (2007) 1201–1204.

[59] F. Casallanovo, F.J. de Oliveira, F.C. de Souza, U. Ros, Y. Martínez, D. Pentón, M. Tejuca, D. Martínez, F. Pazos, T.A. Pertinhez, A. Spisni, E.M. Cilli, M.E. Lanio, C. Alvarez, S. Schreier, Model peptides mimic the structure and function of the N-terminus of the pore-forming toxin sticholysin II, Biopolymers 84 (2006) 169–180.

[60] A. Drechsler, C. Potrich, J.K. Sabo, M. Frisanco, G. Guella, M. Dalla Serra, G. Anderluh, F. Separovic, R.S. Norton, Structure and activity of the N-terminal region of the eukaryotic cytolysin equinatoxin II, Biochemistry 45 (2006) 1818–1828.

[61] A. Drechsler, A.J. Miles, R.S. Norton, B.A. Wallace, F. Separovic, Effect of lipid on the conformation of the N-terminal region of equinatoxin II: a synchrotron radiation circular dichroism spectroscopic study, Eur. Biophys. J. 39 (2009) 121–127.

[62] Y.H. Lam, A. Hung, R.S. Norton, F. Separovic, A. Watts, Solid-state NMR and simulation studies of equinatoxin II N-terminus interaction with lipid bilayers, Proteins 78 (2010) 858–872.

[63] A. Drechsler, G. Anderluh, R.S. Norton, F. Separovic, Solid-state NMR study of membrane interactions of the pore-forming cytolysin, equinatoxin II, Biochim. Biophys. Acta 1798 (2010) 244–251.

[64] A.J. Miles, A. Drechsler, K. Kristan, G. Anderluh, R.S. Norton, B.A. Wallace, F. Separovic, The effects of lipids on the structure of the eukaryotic cytolysin equinatoxin II: a synchrotron radiation circular dichroism spectroscopic study, Biochim. Biophys. Acta 1778 (2008) 2091–2096.

[65] K. Kristan, G. Viero, P. Maček, M. Dalla Serra, G. Anderluh, The equinatoxin N-terminus is transferred across planar lipid membranes and helps to stabilize the transmembrane pore, FEBS J. 274 (2007) 539–550.

[66] I.F. Pazos, D. Martínez, M. Tejuca, A. Valle, A. Martínez-del-Pozo, C. Alvarez, M.E. Lanio, E.A. Lissi, Comparison of pore-forming ability in membranes of a native and a recombinant variant of sticholysin II from *Stichodactyla helianthus*, Toxicon 42 (2003) 571–578.

[67] G. Menestrina, V. Cabiaux, M. Tejuca, Secondary structure of sea anemone cytolysins in soluble and membrane bound form by infrared spectroscopy, Biochem. Biophys. Res. Commun. 254 (1999) 174–180.

[68] N. Poklar, J. Fritz, P. Maček, G. Vesnaver, T.V. Chalikian, Interaction of the pore-forming protein equinatoxin II with model lipid membranes: a calorimetric and spectroscopic study, Biochemistry 38 (1999) 14999 5008.

[69] E. Leininger, M. Roberts, J.G. Kenimer, I.G. Charles, N. Fairweather, P. Novotny, M.J. Brennan, Pertactin, an Arg–Gly–Asp-containing *Bordetella pertussis* surface protein that promotes adherence of mammalian cells, Proc. Natl. Acad. Sci. U.S.A. 88 (1991) 345–349.

[70] E. Ruoslahti, RGD and other recognition sequences for integrins, Annu. Rev. Cell Dev. Biol. 12 (1996) 697–715.

[71] G. Anderluh, P. Maček, Dissecting the actinoporin pore-forming mechanism, Structure 11 (2003) 1312–1313.

[72] M.L. Shin, D.W. Michaels, M.M. Mayer, Membrane damage by a toxin from the sea anemone *Stoichactis helianthus*. II. Effect of membrane lipid composition in a liposome system, Biochim. Biophys. Acta 555 (1979) 79–88.

[73] V. de los Ríos, J.M. Mancheño, M.E. Lanio, M. Oñaderra, J.G. Gavilanes, Mechanism of the leakage induced on lipid model membranes by the haemolytic protein sticholysin II from the sea anemone *Stichodactyla helianthus*, Eur. J. Biochem. 252 (1998) 284–289.

[74] C. Álvarez-Valcarcel, M. Serra, C. Patrich, I. Bernhart, M. Tejuca, D. Martínez, F. Pazos, M.E. Lanio, G. Menestrina, Effects of lipid composition on membrane permeabilization by sticholysin I and II, two cytolysins of the sea anemone *Stichodactyla helianthus*, Biophys. J. 80 (2001) 2761–2774.

[75] D. Martínez, A. Otero, C. Alvarez, F. Pazos, M. Tejuca, M.E. Lanio, I. Gutiérrez-Aguirre, A. Barlič, I. Iloro, J.L. Arrondo, J.M. González-Mañas, E. Lissi, Effect of sphingomyelin and cholesterol on the interaction of St II with lipidic interfaces, Toxicon 49 (2007) 68–81.

[76] J.M. Caaveiro, I. Echabe, I. Gutiérrez-Aguirre, J.L. Nieva, J.L. Arrondo, J.M. González-Mañas, Differential interaction of equinatoxin II with model membranes in response to lipid composition, Biophys. J. 80 (2001) 1343–1353.

[77] B.B. Bonev, Y.H. Lam, G. Anderluh, A. Watts, R.S. Norton, F. Separovic, Effects of the eukaryotic pore-forming cytolysin equinatoxin II on lipid membranes and the role of sphingomyelin, Biophys. J. 84 (2003) 2382–2392.

[78] P. Schön, A.J. García-Sáez, P. Malovrh, K. Bacia, G. Anderluh, P. Schwille, Equinatoxin II permeabilizing activity depends on the presence of sphingomyelin and lipid phase coexistence, Biophys. J. 95 (2008) 691–698.

[79] J. Alegre-Cebollada, I. Rodríguez-Crespo, J.G. Gavilanes, A. Martínez-del-Pozo, Detergent-resistant membranes are platforms for actinoporin pore-forming activity on intact cells, FEBS J. 273 (2006) 863–871.

[80] A. Barlič, I. Gutiérrez-Aguirre, J.M. Caaveiro, A. Cruz, M.B. Ruiz-Argüello, J. Pérez-Gil, J.M. González-Mañas, Lipid phase coexistence favours membrane insertion of equinatoxin-II, a pore-forming toxin from *Actinia equina*, J. Biol. Chem. 279 (2004) 34209–34216.

[81] C. Álvarez, J.M. Mancheño, D. Martínez, M. Tejuca, F. Pazos, M.E. Lanio, Sticholysins, two pore-forming toxins produced by the Caribbean Sea anemone *Stichodactyla helianthus*: their interaction with membranes, Toxicon 54 (2009) 1135–1147.

[82] G. Anderluh, M. Dalla Serra, G. Viero, G. Guella, P. Maček, G. Menestrina, Pore formation by equinatoxin II, a eukaryotic protein toxin, occurs by induction of nonlamellar lipid structures, J. Biol. Chem. 278 (2003) 45216–45223.

[83] C. Álvarez, F. Casallanovo, C.S. Shida, L.V. Nogueira, D. Martínez, M. Tejuca, I.F. Pazos, M.E. Lanio, G. Menestrina, E. Lissi, S. Schreier, Binding of sea anemone pore-forming toxins sticholysins I and II to interfaces—modulation of conformation and activity, and lipid–protein interaction, Chem. Phys. Lipids 122 (2003) 97–105.

[84] R. Veitia, M. Tejuca, C. Alvarez, M.E. Lanio, F. Pazos, Kinetic of a haemolysis induced by a cytolysin from *Stichodactyla helianthus*: effect of temperature and divalent cations, Biologia 9 (2005) 15–22.

[85] G. Celedón, G. González, E. Lissi, T. Cerda, D. Martinez, C. Soto, M. Pupo, F. Pazos, M.E. Lanio, C. Alvarez, Effect of calcium on the haemolytic activity of *Stichodactyla helianthus* toxin sticholysin II on human erythrocytes, Toxicon 54 (2009) 845–850.

[86] G. Celedón, G. González, E. Lissi, T. Cerda, D. Bascuñant, M. Lepeley, F. Pazos, M.E. Lanio, C. Álvarez, Effect of pre-exposure of human erythrocytes to oxidants on the haemolytic activity of Sticholysin II. A comparison between peroxynitrite and hypochlorous acid, Free Radic. Res. 45 (2011) 400–408.

[87] E. Meinardi, M. Florin-Christensen, G. Paratcha, J.M. Azcurra, J. Florin-Christensen, The molecular basis of the self/nonself selectivity of a coelenterate toxin, Biochem. Biophys. Res. Commun. 216 (1995) 348–354.

[88] A. Valle, A. López-Castilla, L. Pedrera, D. Martínez, M. Tejuca, J. Campos, R. Fando, E. Lissi, C. Álvarez, M.E. Lanio, F. Pazos, S. Schreier, Cys mutants in functional regions of Sticholysin I clarify the participation of these residues in pore formation, Toxicon (2011) *in press.*

[89] J. Martín-Benito, F. Gavilanes, V. de Los Ríos, J.M. Mancheño, J.J. Fernández, J.G. Gavilanes, Two-dimensional crystallization on lipid monolayers and three-dimensional structure of sticholysin II, a cytolysin from the sea anemone *Stichodactyla helianthus*, Biophys. J. 78 (2000) 3186–3194.

[90] J.M. Mancheño, J. Martín-Benito, J.G. Gavilanes, L. Vázquez, A complementary microscopy analysis of Sticholysin II crystals on lipid films: atomic force and transmission electron characterizations, Biophys. Chem. 119 (2006) 219–223.

[91] I. Gutiérrez-Aguirre, A. Barli, Z. Podlesek, P. Maček, G. Anderluh, J.M. González-Mañas, Membrane insertion of the N-terminal α-helix of equinatoxin II, a sea anemone cytolytic toxin, Biochem. J. 384 (2004) 421–428.

[92] A.P. Heuck, R.K. Tweten, A.E. Johnson, β-Barrel pore-forming toxins: intriguing dimorphic proteins, Biochemistry 40 (2001) 9065–9073.

[93] V.E. Bychkova, R.H. Pain, O.B. Ptitsyn, The 'molten globule' state is involved in the translocation of proteins across membranes? FEBS Lett. 238 (1988) 231–234.

[94] N. Poklar, F. Lah, M. Salobir, P. Maček, G. Vesnaver, pH and temperature-induced molten globule-like denatured states of equinatoxin II: A study by UV-melting, DSC, far- and near-UV CD spectroscopy, and ANS fluorescence, Biochemistry 36 (1997) 14345–14352.

[95] J.M. Mancheño, V. de los Ríos, A. Martínez-del-Pozo, M.E. Lanio, M. Oñaderra, J.G. Gavilanes, Partially folded states of the cytolytic protein sticholysin II, Biochim. Biophys. Acta 1545 (2001) 122–131.

[96] N.P. Ulrih, G. Anderluh, P. Maček, T.V. Chalikian, Salt-induced oligomerization of partially folded intermediates of equinatoxin II, Biochemistry 43 (2004) 9536–9545.

[97] K.C. Kristan, G. Viero, M. Dalla Serra, P. Maček, G. Anderluh, Molecular mechanism of pore formation by actinoporins, Toxicon 54 (2009) 1125–1134.

[98] V. de los Ríos, J.M. Mancheño, A. Martínez-del-Pozo, C. Alfonso, G. Rivas, M. Oñaderra, J.G. Gavilanes, Sticholysin II, a cytolysin from the sea anemone *Stichodactyla helianthus*, is a monomer-tetramer associating protein, FEBS Lett. 455 (1999) 27–30.

[99] S. Leavitt, E. Freire, Direct measurement of protein binding energetics by isothermal titration calorimetry, Curr. Opin. Struct. Biol. 11 (2001) 560–566.

[100] V. Huerta, V. Morera, Y. Guanche, G. Chinea, L.J. González, L. Betancourt, D. Martínez, C. Álvarez, M.E. Lanio, V. Besada, Primary structure of two cytolysin isoforms from *Stichodactyla helianthus* differing in their haemolytic activity, Toxicon 39 (2001) 1253–1256.

[101] I. Gutiérrez-Aguirre, P. Trontelj, P. Maček, J.H. Lakey, G. Anderluh, Membrane binding of zebrafish actinoporin-like protein: AF domains, a novel superfamily of cell membrane binding domains, Biochem. J. 398 (2006) 381–392.

[102] Q.T. Hoang, S.H. Cho, S.F. McDaniel, S.H. Ok, R.S. Quatrano, J.S. Shin, An actinoporin plays a key role in water stress in the moss *Physcomitrella patens*, New Phytol. 184 (2009) 502–510.

[103] V. Trigueros, A. Lougarre, D. Ali-Ahmed, Y. Rahbe, J. Guillot, L. Chavant, D. Fournier, L. Paquereau, *Xerocomus chrysenteron* lectin: identification of a new pesticidal protein, Biochim. Biophys. Acta 1621 (2003) 292–298.

[104] C. Marty-Detraves, F. Francis, L. Baricault, D. Fournier, L. Paquereau, Inhibitory action of a new lectin from *Xerocomus chrysenteron* on cell-substrate adhesion, Mol. Cell. Biochem. 258 (2004) 49–55.

[105] C. Birck, L. Damian, C. Marty-Detraves, A. Lougarre, C. Schulze-Briese, P. Koehl, D. Fournier, L. Paquereau, J.P. Samama, A new lectin family with structure similarity to actinoporins revealed by the crystal structure of *Xerocomus chrysenteron* lectin XCL, J. Mol. Biol. 344 (2004) 1409–1420.

[106] M.E. Carrizo, S. Capaldi, M. Perduca, F.J. Irazoqui, G.A. Nores, H.L. Monaco, The antineoplastic lectin of the common edible mushroom (*Agaricus bisporus*) has two binding sites, each specific for a different configuration at a single epimeric hydroxyl, J. Biol. Chem. 280 (2005) 10614–10623.

[107] L. Damian, D. Fournier, M. Winterhalter, L. Paquereau, Determination of thermodynamic parameters of *Xerocomus chrysenteron* lectin interactions with N-acetylgalactosamine and Thomsen–Friedenreich antigen by isothermal titration calorimetry, BMC Biochem. 6 (2005) 11.

[108] C. Ottmann, B. Luberacki, I. Küfner, W. Koch, F. Brunner, M. Weyand, L. Mattinen, M. Pirhonen, G. Anderluh, H.U. Seitz, T. Nürnberger, C. Oecking, A common toxin fold mediates microbial attack and plant defence, Proc. Natl. Acad. Sci. U.S.A. 106 (2009) 10359–10364.

[109] C.L. Pemberton, G.P.C. Salmond, The Nep1-like proteins: a growing family of microbial elicitors of plant necrosis, Mol. Plant Pathol. 5 (2004) 353–359.

[110] S. Kamoun, A catalogue of the effector secretome of plant pathogenic oomycetes, Annu. Rev. Phytopathol. 44 (2006) 41–60.

[111] M. Gijzen, T. Nürnberger, Nep1-like proteins from plant pathogens: recruitment and diversification of the NPP1 domain across taxa, Phytochemistry 67 (2006) 1800–1807.

[112] H. Bae, M. Kim, R. Sicher, H.J. Bae, B. Bailey, Necrosis- and ethylene-inducing peptide from *Fusarium oxysporum* induces a complex cascade of transcripts associated with signal transduction and cell death in *Arabidopsis*, Plant Physiol. 141 (2006) 1056–1067.

[113] D. Qutob, B. Kemmerling, F. Brunner, I. Küfner, S. Engelhardt, A.A. Gust, B. Luberacki, H.U. Seitz, D. Stahl, T. Rauhut, E. Glawischnig, G. Schween, B. Lacombe, N. Watanabe, E. Lam, R. Schlichting, D. Scheel, K. Nau, G. Dodt, D. Hubert, M. Gijzen, T. Nürnberger, Phytotoxicity and innate immune responses induced by Nep1-like proteins, Plant Cell 18 (2006) 3721–3744.

[114] G. Fellbrich, A. Romanski, A. Varet, B. Blume, F. Brunner, S. Engelhardt, G. Felix, B. Kemmerling, M. Krzymowska, T. Nürnberger, NPP1, a *Phytophthora*-associated trigger of plant defence in parsley and *Arabidopsis*, Plant J. 32 (2002) 375–390.

[115] K. Gunji, S. Ishizaki, K. Shiomi, Cloning of complementary and genomic DNAs encoding echotoxins, proteinaceous toxins from the salivary gland of marine gastropod *Monoplex echo*, Protein J. 29 (2010) 487–492.

[116] T. Takara, T. Nakagawa, M. Isobe, N. Okino, S. Ichinose, A. Omori, M. Ito, Purification, molecular cloning, and application of a novel sphingomyelin-binding protein (clamlysin) from the brackishwater clam, *Corbicula japonica*, Biochim. Biophys. Acta 1811 (2011) 323–332.

[117] R. Ramachandran, R.K. Tweten, A.E. Johnson, Membrane-dependent conformational changes initiate cholesterol-dependent cytolysin oligomerization and intersubunit β-strand alignment, Nat. Struct. Mol. Biol. 11 (2004) 697–705.

[118] A. Razpotnik, I. Krizaj, W.R. Kem, P. Maček, T. Turk, A new cytolytic protein from the sea anemone *Urticina crassicornis* that binds to cholesterol- and sphingomyelin-rich membranes, Toxicon 53 (2009) 762–769.

[119] D. Mebs, M. Liebrich, A. Reul, Y. Samejima, Hemolysins and proteinase inhibitors from sea anemones of the Gulf of Aqaba, Toxicon 21 (1983) 257–264.

[120] M. Thomson, R.L. Moritz, R.J. Simpson, R.S. Norton, Tenebrosin-A, a new cardiostimulant protein from the Australian sea anemone *Actinia tenebrosa*, Biochem. Int. 15 (1987) 711–718.

[121] R.S. Norton, G. Bobek, J.O. Ivanov, M. Thomson, E. Fiala-Beer, R.L. Moritz, R.J. Simpson, Purification and characterization of proteins with cardiac stimulatory and haemolytic activity from the anemone *Actinia tenebrosa*, Toxicon 28 (1990) 29–41.

[122] R.J. Simpson, G.E. Reid, R.L. Moritz, C. Morton, R.S. Norton, Complete amino acid sequence of tenebrosin-C, a cardiac stimulatory and haemolytic protein from the sea anemone *Actinia tenebrosa*, Eur. J. Biochem. 190 (1990) 319–328.

[123] M.M. Monastyrnaya, T.A. Zykova, O.V. Apalikova, T.V. Shwets, E.P. Kozlovskaya, Biologically active polypeptides from the tropical sea anemone *Radianthus macrodactylus*, Toxicon 40 (2002) 1197–1217.

[124] H.E. Khoo, J.P. Lim, C.H. Tan, Effects of sea anemone (*Heteractis magnifica* and *Actinia equina*) cytolysins on synaptosomal uptake of GABA and choline, Toxicon 33 (1995) 1365–1371.

[125] W.M. Lafranconi, I. Ferlan, F.E. Russell, R.J. Huxtable, The action of equinatoxin, a peptide from the venom of the sea anemone, *Actinia equina*, on the isolated lung, Toxicon 22 (1984) 347–352.

[126] M. Budihna, P. Maček, D. Šuput, Effects of equinatoxin II on the isolated guinea-pig heart, Eur. J. Pharmacol. 5 (1990) 2051–2052.

[127] R.S. Norton, P. Maček, G.E. Reid, R.J. Simpson, Relationship between the cytolysins tenebrosin-C from *Actinia tenebrosa* and equinatoxin II from *Actinia equina*, Toxicon 30 (1992) 13–23.

[128] M. Bunc, G. Drevensek, M. Budihna, D. Šuput, Effects of equinatoxin II from *Actinia equina* (L.) on isolated rat heart: the role of direct cardiotoxic effects in equinatoxin II lethality, Toxicon 37 (1999) 109–123.

[129] T. García, D. Martínez, A. Palmero, C. Soto, M. Tejuca, F. Pazos, R. Menéndez, C. Alvarez, A. Garateix, Pharmacological effects of two cytolysins isolated from the sea anemone *Stichodactyla helianthus*, J. Biosci. 34 (2009) 891–898.

[130] G. Drevensek, M. Bunc, M.V. Budihna, D. Šuput, Lowering of the coronary flow in isolated rat heart by equinatoxin II depends upon extracellular Ca^{2+} concentration, Pflugers Arch. 439 (2000) R150–R151.

[131] G. Drevensek, S. Kirbis, M. Bunc, M. Zitko, M.V. Budihna, D. Šuput, Tezosentan inhibits both equinatoxin II and endotelin-1 induced contractions of isolated porcine coronary artery in a similar way, J. Nat. Toxins 11 (2002) 231–244.

[132] F.A. Meunier, R. Frangez, E. Benoit, G. Ouanounou, B. Rouzaire-Dubois, D. Šuput, J. Molgo, Ca^{2+} and Na^{+} contribute to the swelling of differentiated neuroblastoma cells induced by equinatoxin-II, Toxicon 38 (2000) 1547–1560.

[133] M. Šentjurc, A. Štalc, D. Šuput, Influence of equinatoxin II on coronary smooth muscle membrane fluidity, Pflugers Arch. 431 (1996) R317–318.

[134] D. Šuput, R. Frangez, M. Bunc, Cardiovascular effects of equinatoxin III from the sea anemone *Actinia equina* (L.), Toxicon 39 (2001) 1421–1427.

[135] S. Fedorov, S. Dyshlovoy, M. Monastyrnaya, L. Shubina, E. Leychenko, E. Kozlovskaya, J.O. Jin, J.Y. Kwak, A.M. Bode, Z. Dong, V. Stonik, The anticancer effects of actinoporin RTX-A from the sea anemone *Heteractis crispa* (=*Radianthus macrodactylus*), Toxicon 55 (2010) 811–817.

[136] R.C. Soletti, G.P. de Faria, J. Vernal, H. Terenzi, G. Anderluh, H.L. Borges, V. Moura-Neto, N.H. Gabilan, Potentiation of anticancer-drug cytotoxicity by sea anemone pore-forming proteins in human glioblastoma cells, Anticancer Drugs 19 (2008) 517–525.

[137] R.C. Soletti, T. Alves, J. Vernal, H. Terenzi, G. Anderluh, H.L. Borges, N.H. Gabilan, V. Moura-Neto, Inhibition of MAPK/ERK, PKC and CaMKII signalling blocks cytolysin-induced human glioma cell death, Anticancer Res. 30 (2010) 1209–1215.

[138] D.H. Nguyen, J.E. Hildreth, Evidence for budding of human immunodeficiency virus type 1 selectively from glycolipid-enriched membrane lipid rafts, J. Virol. 74 (2000) 3264–3272.

[139] A. Ono, E.O. Freed, Plasma membrane rafts play a critical role in HIV-1 assembly and release, Proc. Natl. Acad. Sci. U.S.A. 98 (2001) 13925–13930.

[140] M. Lorizate, B. Brügger, H. Akiyama, B. Glass, B. Müller, G. Anderluh, F.T. Wieland, H.G. Kräusslich, Probing HIV-1 membrane liquid order by Laurdan staining reveals producer cell-dependent differences, J. Biol. Chem. 284 (2009) 22238–22247.

[141] A.D. Avila, M.C. de Acosta, A. Lage, A new immunotoxin built by linking a haemolytic toxin to a monoclonal antibody specific for immature T lymphocytes, Int. J. Cancer 42 (1988) 568–571.

[142] A.D. Avila, M.C. de Acosta, A. Lage, A carcinoembryonic antigen directed immunotoxin built by linking a monoclonal antibody to a haemolytic toxin, Int. J. Cancer 43 (1989) 926–929.

[143] C. Pederzolli, G. Belmonte, M. Dalla Serra, P. Maček, G. Menestrina, Biochemical and cytotoxic properties of conjugates of transferrin with equinatoxin II, a cytolysin from a sea anemone, Bioconjug. Chem. 6 (1995) 166–173.

[144] M. Tejuca, I. Díaz, R. Figueredo, L. Roque, F. Pazos, D. Martínez, N. Iznaga-Escobar, R. Pérez, C. Álvarez, M.E. Lanio, Construction of an immunotoxin with the pore forming protein StI and ior C5, a monoclonal antibody against a colon cancer cell line, Int. Immunopharmacol. 6 (2004) 731–744.

[145] M. Tejuca, G. Anderluh, M. Dalla Serra, Sea anemone cytolysins as toxic components of immunotoxins, Toxicon 54 (2009) 1206–1214.

[146] C. Potrich, G. Viero, M. Tejuca, G. Anderluh, P. Maček, G. Menestrina, Construction of new immunotoxins by linking equinatoxin II to monoclonal antibodies via the biotin–avidin interaction. Cytotoxic effects on human tumour cells, Acta Biol. Slov. 43 (2000) 47–51.

[147] C. Potrich, R. Tomazzolli, M. Dalla Serra, G. Anderluh, P. Malovrh, P. Maček, G. Menestrina, M. Tejuca, Cytotoxic activity of a tumor protease-activated pore-forming toxin, Bioconjug. Chem. 2 (2005) 369–376.

[148] K.E. Jackson, T. Spielmann, E. Hanssen, A. Adisa, F. Separovic, M.W. Dixon, K.R. Trenholme, P.L. Hawthorne, D.L. Gardiner, T. Gilberger, L. Tilley, Selective permeabilization of the host cell membrane of *Plasmodium falciparum*-infected red blood cells with streptolysin O and equinatoxin II, Biochem. J. 403 (2007) 167–175.

[149] T.H. Bayburt, S.G. Sligar, Membrane protein assembly into Nanodiscs, FEBS Lett. 3 (2010) 1721–1727.

[150] R. Koradi, M. Billeter, K. Wüthrich, MOLMOL: a program for display and analysis of macromolecular structures, J. Mol. Graph. 14 (1996) 29–32.

[151] W. Humphrey, A. Dalke, K. Schulten, VMD: visual molecular dynamics, J. Mol. Graph. 14 (1996) 33–38, 27–28.

SECTION B

INTERACTION OF ACTINOPORINS WITH LIPID MEMBRANES: THE ROLE OF MEMBRANE COMPOSITION AND BIOPHYSICAL PROPERTIES

ARTICLE II

Cholesterol stimulates and ceramide inhibits sticholysin II-induced pore formation in complex bilayer membranes

Alm, I.*, **García-Linares, S.***, Gavilanes, J. G., Martínez-del-Pozo, Á. and Slotte, J. P. (2015). *Biochim Biophys Acta* 1848(4): 925-931. *equal contribution

El colesterol estimula y la ceramida inhibe la formación de poros inducida por esticolisina II en membranas complejas

Se ha examinado la capacidad de formar poros de esticolisina II (StnII, obtenida de *Stichodactyla helianthus*) en membranas que contienen 1-palmitoil-2-oleoil-*sn*-glicero-3-fosfocolina (POPC), palmitoil esfingomielina (PSM) y colesterol o palmitoil ceramida (PCer). El objetivo del estudio es determinar cómo afecta la presencia de dominios de PSM con diferente grado de orden a la oligomerización y formación de poros por parte de StnII. Se sabe que el colesterol incrementa la formación de poros de StnII y los resultados lo han confirmado y han aportado datos cinéticos del proceso. El efecto del colesterol en la cinética de permeabilización de las bicapas depende de la concentración. En el rango de concentraciones utilizado (2.5-10 nmol en POPC:PSM 80:20), el colesterol también incrementa el orden de los dominios fluidos de PSM y por tanto disminuye la fluidez de la membrana, sugiriendo que la fluidez *per se* no es la responsable del efecto del colesterol. La adición de PCer (2.5-10 nmol) a las bicapas de POPC:PSM (80:20) disminuye la formación de poros por parte de StnII, de nuevo dependiendo de la concentración de PCer utilizada. Esta adición también conduce a la formación de una fase gel enriquecida en PCer. La adición de colesterol a las membranas con PCer puede reducir en parte el efecto inhibidor de la PCer en la formación de poros. Se concluye que el estado físico de la PSM (modificado por colesterol o PCer) afecta a la unión de StnII y a la formación de poros en las condiciones ensayadas.

Biochimica et Biophysica Acta 1848 (2015) 925–931

Contents lists available at ScienceDirect

Biochimica et Biophysica Acta

journal homepage: www.elsevier.com/locate/bbamem

Cholesterol stimulates and ceramide inhibits Sticholysin II-induced pore formation in complex bilayer membranes

Ida Alm [a,1], Sara García-Linares [b,1], José G. Gavilanes [b], Álvaro Martínez-del-Pozo [b], J. Peter Slotte [a,*]

[a] Biochemistry, Department of Biosciences, Åbo Akademi University, Turku, Finland
[b] Departamento de Bioquímica y Biología Molecular I, Universidad Complutense, Madrid, Spain

ARTICLE INFO

Article history:
Received 30 October 2014
Received in revised form 11 December 2014
Accepted 18 December 2014
Available online 27 December 2014

Keywords:
Membrane permeabilization
Surface plasmon resonance
Sphingolipid
Membrane order

ABSTRACT

The pore forming capacity of Sticholysin II (StnII; isolated from *Stichodactyla helianthus*) in bilayer membranes containing 1-palmitoyl-2-oleoyl-sn-glycero-3-phosphocholine (POPC), palmitoylsphingomyelin (PSM) and either cholesterol or palmitoyl ceramide (PCer) has been examined. The aim of the study was to elucidate how the presence of differently ordered PSM domains affected StnII oligomerization and pore formation. Cholesterol is known to enhance pore formation by StnII, and our results confirmed this and provide kinetic information for the process. The effect of cholesterol on bilayer permeabilization kinetics was concentration-dependent. In the concentration regime used (2.5–10 nmol cholesterol in POPC:PSM 80:20 by nmol), cholesterol also increased the acyl chain order in the fluid PSM domain and thus decreased bilayer fluidity, suggesting that fluidity per se was not responsible for cholesterol's effect. Addition of PCer (2.5–10 nmol) to the POPC:PSM (80:20 by nmol) bilayers attenuated StnII-induced pore formation, again in a concentration-dependent fashion. This addition also led to the formation of a PCer-rich gel phase. Addition of cholesterol to PCer-containing membranes could partially reduce the inhibitory effect of PCer on StnII pore formation. We conclude that the physical state of PSM (as influenced by either cholesterol or PCer) affected StnII binding and pore formation under the conditions examined.

1. Introduction

Sticholysin II (StnII) is a member of the actinoporin family of pore forming toxins [1–3]. It is a single polypeptide toxin which in bilayer membranes oligomerizes to a pore structure [4]. StnII pore formation is efficient in sphingomyelin (SM) and cholesterol containing fluid membranes [5,6]. Cholesterol has been shown to enhance pore formation by both StnII and equinatoxin II (EqtII - another member of the actinoporin family of toxins) in a concentration dependent manner [5,7]. In the absence of cholesterol, StnII forms pores only in the presence of hydrogen bonding-competent SM [8]. However, when membranes are rich in cholesterol, pore formation by StnII or EqtII is also possible in bilayers lacking SM [5,9]. It is not fully understood how the bilayer lipid composition or the physical state of the membrane affect pore formation by StnII.

The effects of cholesterol on membrane properties are fairly well known. Cholesterol will abolish the gel phase (decrease acyl chain order or increase fluidity) in simple saturated phospholipid bilayers, but on the other hand it will increase acyl chain order (decrease fluidity) of already disordered phospholipid acyl chains [10,11]. At certain bilayer concentrations, which depend on the co-lipid properties, cholesterol can induce the formation of a liquid-ordered phase together with certain phospholipids [12]. Interestingly, cholesterol has been shown to associate with SM in bilayers [13], and this interaction is in part stabilized by hydrogen-bonding among SMs and between SM and cholesterol [14,15]. It has been speculated that domain formation (ordered cholesterol-enriched domains in an otherwise disordered bilayer) could help StnII or EqtII to form pores, even if the membrane affinity of the toxin is not very high (i.e., in the absence of SM) [5,9].

If membrane SM is partly degraded by a sphingomyelinase enzyme, the resulting ceramide is likely to interact with the remaining SM and form a gel-like ordered domain [16,17]. Cholesterol has been shown to be displaced from such domains [17–19]. It is unclear how StnII activity (i.e., pore formation) is affected in bilayers containing such ceramide-enriched domains. Therefore we have in this study performed detailed

Abbreviations: EqtII, equinatoxin II; LUV, large unilamellar vesicle; POPC, 1-palmitoyl-2-oleoyl-*sn*-glycero-3-phosphocholine; PCer, palmitoyl ceramide; PSM, palmitoyl SM; SM, sphingomyelin; SPR, surface plasmon resonance; StnII, sticholysin II; tPA-SM, *trans* parinaroyl sphingomyelin

* Corresponding author. Tel.: +358 2 215 4689.
E-mail address: jpslotte@abo.fi (J.P. Slotte).

[1] Equal contribution.

http://dx.doi.org/10.1016/j.bbamem.2014.12.017
0005-2736/

studies on the effects of both cholesterol and ceramide, separately and together, on StnII-pore formation in SM containing POPC bilayers. We show that whereas the bilayer presence of cholesterol stimulated StnII pore formation, palmitoylceramide inhibited the process.

2. Materials and methods

2.1. Materials

1-Palmitoyl-2-oleoyl-*sn*-glycero-3-phosphocholine (POPC), palmitoyl ceramide (PCer) and egg SM were obtained from Avanti Polar Lipids (Alabaster, AL, USA). Palmitoyl SM (PSM) was purified from egg SM using preparative HPLC on a reverse phase (C18) column, as described previously [20]. Cholesterol, calcein and Sephacryl S200HR were obtained from Sigma/Aldrich (St. Louis, MO, USA). *trans*-Parinaric acid was synthesized as described in [21]. *trans*-Parinaroyl-SM (tPa-SM) was synthesized from *trans*-parinaric acid and sphingosylphosphorylcholine as described previously [18,22]. StnII was produced in an *E.coli* expression system, and purified, as described previously [23].

2.2. Calcein leakage assay

Calcein-entrapped large unilamellar vesicles (LUVs) were prepared from POPC and PSM (4:1 molar ratio) and contained indicated amounts of cholesterol or PCer. The LUVs were prepared by extrusion through 200 nm filters (Nucleopore, Whatman) at 60 °C. Briefly, the desired lipids were mixed and dried under a stream of nitrogen. The lipids were re-dissolved in chloroform and dried again before removal of any traces of remaining solvent in vacuum for 60 min. Prior to extrusion, the dry lipid films were hydrated for 30 min at 60 °C in Tris buffer (10 mM Tris, 140 mM NaCl, pH 7.4) containing calcein. The calcein concentration was 100 mM, and the total lipid concentration was 1.25 mM. LUVs were separated from non-entrapped calcein by gel filtration on Sephacryl S200HR. The LUVs were used for permeabilization studies within 24 h. The concentration of LUV phospholipids and StnII during calcein leakage experiments were about 70 μM and 80 nM, respectively. Phospholipid concentration was determined from Pi measurement [24] after dilution of vesicles during isolation, and protein concentration was determined from the absorbance at 280 nm (with knowledge of the extinction coefficient of StnII at 280 nm as given in [5]). Emission at 550 nm was followed at 23 °C as a function of time (Excitation at 480 nm). Fluorescence emission was measured with a PTI Quanta-Master spectrofluorimeter (Photon Technology International, Inc. NJ, USA). To ensure that no major spontaneous leakage occurred, the emission was measured for each sample during 5 min before addition of toxin. A steady signal level, indicating intact vesicles, was observed for all samples.

2.3. Surface plasmon resonance spectroscopy

The association of StnII with vesicle-coated gold chips was examined as follows: LUVs were prepared from POPC:PSM (4:1, molar ratio), and the indicated amounts of either cholesterol or PCer, in Tris buffer (10 mM Tris, 140 mM NaCl, pH 7.4) by extrusion through 100 nm polycarbonate filters (Nucleopore, Whatman) at 60 °C. StnII binding to the vesicles was studied at 23 °C with a BioNavis SPR Navi 200 instrument (BioNavis Ltd, Tampere, Finland). The sensor gold chip was coated with a carboxymethylated dextran layer which was treated with N-hydroxysuccinimide and N-ethyl-N′(dimethylaminopropyl) carbodiimide to activate the surface for capturing phospholipid membranes. All solutions used for SPR were filtered through 0.2 μm membrane filters and degassed by bath sonication before use. The running buffer was 10 mM Tris, 140 mM NaCl, pH 7.4 and the flow rate was 10 μl/min. First, the chip surface was cleaned (or regenerated after being coated with lipid) with two injections of 50 mM regeneration solution (NaOH:isopropanol, 2:3 by vol). Then extruded LUVs (0.5 mM lipid concentration) were applied on the surface (10 min injection) and unbound vesicles were removed by one (2 min) injection of 50 mM NaOH. Bovine serum albumin (0.1 mg/ml, 5 min injection) was used to verify that the chip did not have uncovered areas. The very limited binding of albumin to uncoated parts of the chips (data not shown) did not vary with liposome type, suggesting that coverage was similar within experimental error for all liposome types used in this study. Finally StnII (4 μM) was applied for 10 min. The chip was regenerated between different vesicle compositions with 50 mM regeneration solution (NaOH:isopropanol, 2:3 by vol).

2.4. Steady-state anisotropy measurements

Multilamellar vesicles were prepared by bath sonication, as described previously [25]. The final lipid concentration was 50 μM and tPa-SM was included at 1 mol%. The steady-state anisotropy measurements were performed with a T-format Quanta-Master spectrofluorimeter (Photon Technology International, Birmingham, NJ, USA) between 10 and 57 °C. The probe was excited at 305 nm and emission was detected at 410 nm. Steady state anisotropy values were calculated according to Lakowicz [26].

2.5. Binding of StnII to bilayer membranes measured with isothermal titration calorimetry

The interaction between StnII and LUVs prepared from POPC and SM (4:1 molar ratio, 100 nm diameter) with cholesterol or PCer was measured using a VP-ITC (MicroCal, Northampton, MA, USA), as described previously [27]. Briefly, protein solutions at 10 μM were titrated by injection of 20 μL aliquots of lipid suspensions (phospholipid concentration: 5 mM). Two separate injections for each compositon was performed. Binding isotherms were adjusted to a model were the protein binds the membrane involving n lipid molecules. ΔG and ΔS were calculated from the following relationship:

$$\Delta G = -RT\ln(K/0.8n) \text{ and } \Delta G = \Delta H - T\Delta S$$

([27]).

3. Results

3.1. Cholesterol enhances StnII pore formation kinetics

The pore-forming capability of actinoporins is often detected from their membrane permeabilization capacity [28]. Using POPC and PSM as the main bilayer components, at a 4:1 molar ratio, we measured how addition of cholesterol to the unilamellar bilayers affected the kinetics of StnII-induced calcein release from the vesicle-entrapped aqueous compartment. The ratio of vesicles to StnII was adjusted so that the POPC:PSM (80:20 nmol) system gave "intermediate" kinetics for calcein release (Fig. 1A). Addition of cholesterol to the bilayers (up to 10 nmol) increased the kinetics of calcein release in a concentration-dependent manner (Fig. 1B shows the concentration-dependence at time 200 s after StnII addition from several experiments). Triton X-100 addition to the LUVs at the end of the experiment (at time ~1300 sec) resulted in signals equivalent to the normalized value of 1 (one Triton X-100 addition is shown for curve 1). This suggest that the LUVs were not completely unilamellar. Since we did not measure calcein release to the end-point, and because of some apparent multilamellarity, comparison of the maximal extent of calcein-release as a function of cholesterol was not made. It is also evident from Fig. 1A that the calcein signal (after the plateau was reached) decreased slightly, most probably due to light-induced quenching.

Measuring StnII binding to bilayers on a solid support (using surface plasmon resonance), we observed that addition of increasing amounts of cholesterol to the POPC:PSM (80:20 nmol) bilayer led to increased

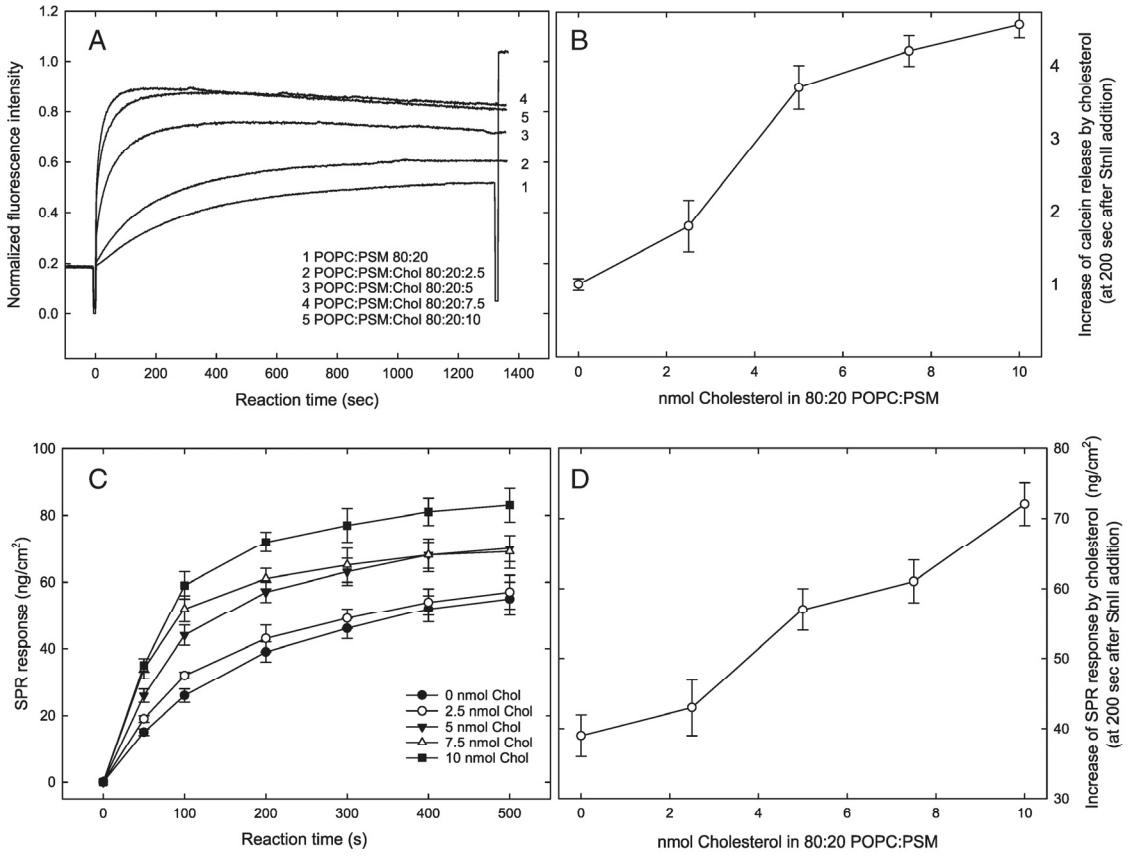

Fig. 1. Effect of cholesterol on StnII interaction with bilayer membranes. Calcein-entrapped vesicles were prepared with extrusion, and contained POPC and PSM (80:20 nmol) and increasing amounts of cholesterol (0 to 10 nmol). Calcein release was measured at 23 °C (panel A). All intensities were normalized. Towards the end of the measurement, Triton X-100 was added to dissolve the LUVs and release all calcein. In panel B, the cholesterol-induced calcein increase (fold increase relative to 0 cholesterol) is shown for the situation 200 s after StnII addition (average ± SEM). Panel C gives the SPR sensogram showing the binding of StnII to immobilized vesicles of different lipid composition. The vesicles consisted of POPC and PSM (80:20 nmol) and the indicated amounts of cholesterol (0 to 10 nmol). Each value is the average ± SEM (n = 3) from measurements at 23 °C. Panel D shows the cholesterol concentration dependence of StnII binding at 200 s after StnII addition.

SPR response (Fig. 1C). The concentration dependence of the SPR signal at 200 s is also shown (Fig. 1D). Taken together, both calcein release kinetics and the SPR response suggest that cholesterol addition to the POPC:PSM (80:20 nmol) system facilitated the StnII/bilayer interaction and the subsequent formation of StnII pores.

ITC analysis of StnII binding to POPC:PSM (80:20 by mol) bilayers is shown in Fig. 2 and Table 1. The binding constant of StnII for POPC:PSM bilayers was $2.1 \pm 0.3 \times 10^{-6}$ M^{-1}, whereas inclusion of cholesterol (POPC:PSM:Chol 80:20:10 by mol) increased the K to $6.1 \pm 0.1 \times 10^{-6}$ M^{-1}. The binding of StnII to cholesterol-containing bilayers was thermodynamically slightly more favorable (ΔG -6.8 ± 0.2 kcal/mol) compared to the cholesterol-free bilayers (ΔG -6.4 ± 0.8 kcal/mol).

3.2. Palmitoylceramide attenuates the formation of StnII pores in POPC:PSM 4:1 bilayers

To measure the effects of PCer on StnII pore formation kinetics, we measured both calcein release-kinetics and SPR response as a function of added PCer to POPC:PSM LUVs. As shown in Fig. 3, addition of up to 10 nmol PCer to POPC:PSM (80:20 nmol) bilayers led to decreased calcein release (Fig. 3A), again in a concentration-dependent manner (Fig. 3B, shows concentration-dependence at 200 s after addition of StnII from several experiments). The SPR response was similarly attenuated when the bilayers contained increasing amounts of PCer (Fig. 3C). In Fig. 3D, the concentration-dependence of the SPR signal to PCer addition is shown at time 200 s post StnII addition.

Binding of StnII to POPC:PSM bilayers containing PCer (POPC:PSM: PCer 80:20:10 by mol) was reduced, as determined by ITC analysis (Fig. 2). The K-value was 0.4 ± 0.1 x10^{-6} M^{-1}, down from the control value of $2.1 \pm 0.3 \times 10^{-1}$ M^{-1} (Table 1). Binding of StnII to PCer-containing membranes was again accompanied by a slightly less favorable free energy (ΔG 5.2 ± 0.2 kcal/mol), when compared to control bilayers (ΔG -6.4 ± 0.8 kcal/mol; Table 1).

3.3. How does cholesterol or PCer addition to POPC:PSM bilayers affect bilayer properties?

Both cholesterol and PCer are able to interact with PSM in the bilayers. With cholesterol, PSM becomes more liquid-ordered [20], and with PCer a gel phase is likely to arise [18,29]. To test for these possibilities, the steady-state anisotropy of tPa-SM was measured. This SM probe partitions into the PSM-rich domains [18], since it can hydrogen-bond to PSM as well as native SM, and since the *all trans* parinaroyl chain is extended and also prefers ordered domains [30,31]. As shown in Fig. 4, the POPC:PSM 80:20 (nmol) bilayers did not show domain

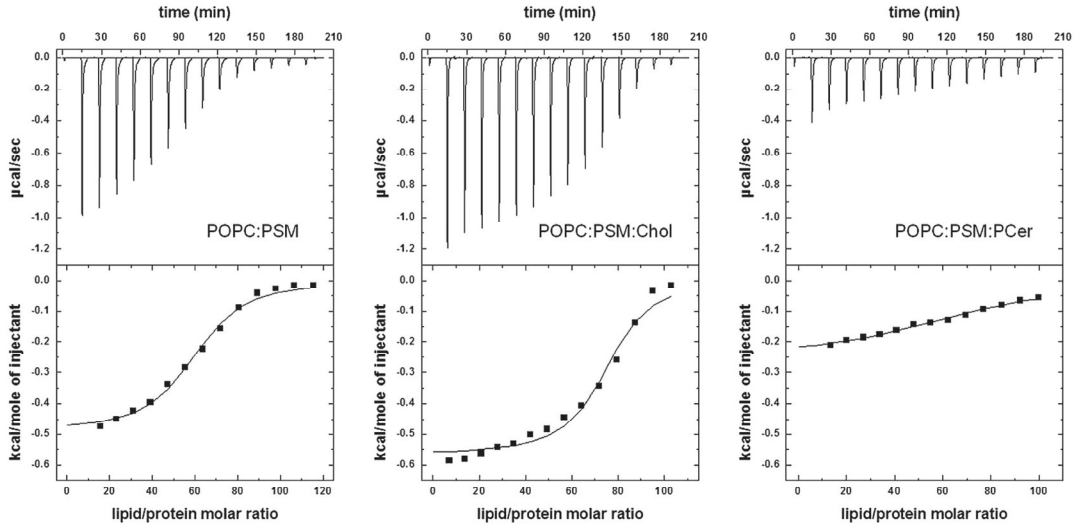

Fig. 2. Interaction of StnII with lipid vesicles as determined with isothermal titration calorimetry. To a StnII solution at 10 μM was added a 20 μL aliquot of vesicles of indicated composition (by molar ratio: 80:20 POPC:PSM or 80:20:10 POPC:PSM:cholesterol or PCer, or PSM alone) about every 15 min, until binding enthalpy approached zero (for a total of 14 injections). Binding isotherms were adjusted to a model were the protein binds the membrane involving *n* lipid molecules.

melting at temperatures above 20 °C, suggesting that PSM in the POPC matrix was disordered by the POPC and was not present as a gel phase. This interpretation is fully consistent with phase diagrams of POPC and PSM at ambient temperature [32]. Addition of cholesterol to the POPC:PSM bilayer (POPC:PSM:Chol 80:20:10 nmol) increased the tPa-SM anisotropy value slightly, suggesting an ordering effect of cholesterol on the acyl chains of PSM (and tPa-SM; Fig. 4). However, when PCer was added to the POPC:PSM fluid bilayer (POPC:PSM:PCer 80:20:10 nmol), a highly ordered (gel) phase was clearly seen at temperatures below 35 °C (Fig. 4). At temperatures above this, the apparent gel phase melted (complete melting around 42–43 °C), but even in the melted state the acyl chains of PSM and tPa-SM were more ordered by the presence of PCer.

3.4. Can cholesterol overcome the inhibition caused by PCer?

To test the pore-forming properties of StnII in POPC:PSM (80:20 nmol) bilayers which simultaneously contain both PCer and cholesterol, we measured calcein-release kinetics from different bilayer systems (Fig. 5). Addition of 20 nmol PCer to POPC:PSM (80:20 nmol) bilayers decreased the calcein release signal by about 90% (Fig. 5). Addition of 2.5 nmol cholesterol to this bilayer increased StnII-induced calcein release slightly, and at 5 nmol cholesterol (in POPC:PSM:PCer 80:20:20 nmol) increased calcein-release significantly despite the presence of PCer (Fig. 5). This increase was not due to surface dilution of PCer (bars 3 vs 2), but to the presence of cholesterol. However, PCer still inhibited calcein release by StnII, since the addition of 5 nmol cholesterol to POPC:PSM (without PCer) enhanced calcein release significantly (Fig. 1A and Fig. 5). These results show that cholesterol and PCer modulate the StnII pore formation process, and that they appear to compete with each other reversibly.

4. Discussion

Although SM is not obligate for StnII pore formation in bilayers [5], it greatly facilitates bilayer binding of StnII and pore formation [27]. It is likely that the hydrogen-bonding groups of SM (2-NH and 3-OH) stabilize the interaction between the SM head group and the POC binding site of StnII [8] and EqtII [7]. If this interaction is crucial also for pore formation, alterations of the SM head group orientation or dynamics may have consequences for StnII pore formation.

Cholesterol is known to affect membrane fluidity via its effects on phospholipid acyl chain order [20]. With our bilayer model (POPC:PSM 4:1) cholesterol will increase mostly PSM acyl chain order (Fig. 4), but will likely also influence POPC acyl chain order to some extent. Cholesterol will also interfere with SM-SM interlipid hydrogen bonding [33], which is likely to slightly affect SM properties in the SM-rich domains [34,35]. Phospholipid head group mobility and tilt is known to be different in gel and fluid states [36]. Further, cholesterol appears to affect the SM phosphocholine head group orientation and dynamics similarly as seen with glycerophospholipids [33,37,38]. In this study, cholesterol at about 10 mol% increased pore formation kinetics significantly (Fig. 1), while the tPa-SM order parameter increased only moderately (Fig. 4). Since the phosphocholine head group is an important recognition site for StnII, we find it likely that that cholesterol's effect on SM head group tilt and dynamics affected StnII binding and/or oligomerization more than cholesterol's effect on bilayer fluidity. In the POPC:PSM:Chol 80:20:10 (by mol) system, a gel phase-restricted mobility of SM is not a likely explanation of cholesterol's effect on

Table 1
Interaction of StnII with LUVs prepared to the indicated compositions. To a buffer solution containing 10 μM of StnII, 20 μl injections of a 5 mM solution of LUVs were performed (see Fig. 2). Values are average ± deviation from two separate measurements.

Vesicles	n	$K \times 10^{-6}$ (M^{-1})	ΔG (kcal mol^{-1})	ΔH (kcal mol^{-1})	ΔS (cal mol^{-1} K^{-1})
POPC:PSM	54 ± 5	2.1 ± 0.3	−6.4 ± 0.8	−29.0 ± 0.2	−76 ± 1
POPC:PSM:Chol	75 ± 2	6.1 ± 0.1	−6.8 ± 0.2	−40.5 ± 0.8	−113 ± 3
POPC:PSM:PCer	66 ± 8	0.4 ± 0.1	−5.2 ± 0.2	−16.2 ± 2.6	−36 ± 8

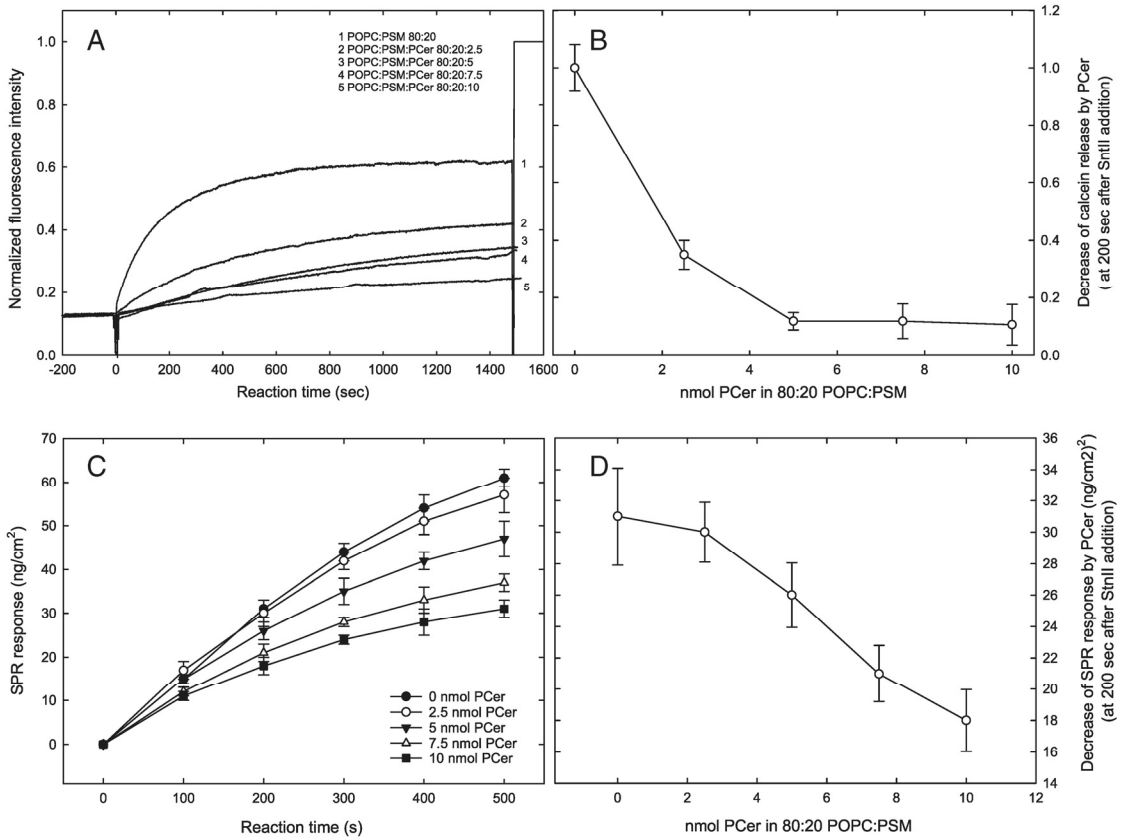

Fig. 3. Effect of PCer on StnII interaction with bilayer membranes. Calcein-entrapped vesicles were prepared with extrusion, and contained POPC and PSM (80:20 nmol) and increasing amounts of PCer (0 to 10 nmol). Calcein release was measured at 23 °C (panel A). All intensities were normalized. Towards the end of the measurement, Triton X-100 was added to dissolve the LUVs and release all calcein. In panel B, the effect of PCer addition on calcein release is given, relative to the PCer-free system, for the situation 200 s after StnII addition. Panel C gives the SPR sensogram showing the binding of StnII to immobilized vesicles of different lipid composition. The vesicles consisted of POPC and PSM (80:20 nmol) and the indicated amounts of PCer (0 to 10 nmol). Each value is the average + SEM (n = 3) from measurements at 23 °C. Panel D shows the PCer concentration dependence of StnII binding at 200 s after StnII addition.

StnII pore formation (Fig. 4). ITC data further suggest that StnII binding and pore formation led to an ordering effect in the bilayer (large negative ΔS, Table 1), possibly reflecting in part ordering of the SM head group by StnII binding. Our data and molecular interpretation is compatible with the suggestion that SM-binding toxins (e.g., EqtII) preferentially bind to molecules, carrying a phosphocholine head group, at

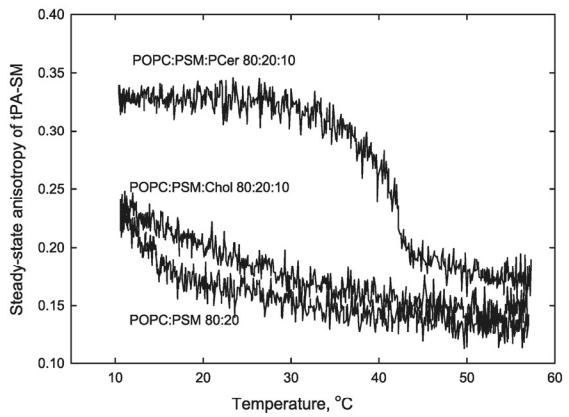

Fig. 4. Determination of steady-state anisotropy of tPa-SM in multilamellar vesicles. Vesicles were prepared to contain POPC and PSM (80 and 20 nmol) and either 10 nmol of cholesterol or PCer. The temperature gradient was 5 °C/min, and each curve is representative of at least three separate measurements.

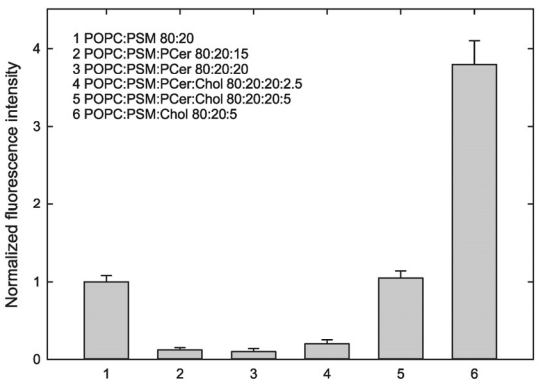

Fig. 5. Effect of the simultaneous presence of cholesterol and PCer (at different ratios) on StnII pore formation in POPC:PSM bilayers. Calcein release was determined from LUVs containing POPC:PSM at 80 and 20 nmol, to which indicated amounts of cholesterol and/or PCer were added. Calcein release at 200 s after StnII addition is shown, normalized to the POPC:PSM system. Values are averages ± SEM for two or three separate experiments for each composition.

the disordered/ordered domain interfaces [39]. Toxin (EqtII) oligomerization to pores apparently occurs in the liquid disordered phase [40].

Addition of PCer to SM-containing bilayers is known to lead to the formation of SM and PCer-rich domains [29,41], mainly because of their mutual affinity for each other and because of entropically favored mixing. In this study, PCer addition to POPC:PSM bilayers markedly inhibited StnII bilayer binding (Fig. 2) and pore formation (Fig. 3). PCer prefers to interact with PSM over POPC [42–44], and the resulting interaction leads to the formation of a highly ordered PCer- and PSM-rich domain [45,46], as also demonstrated by the high tPA-SM anisotropy at ambient temperature (Fig. 4). The shift of PSM from a fluid to a gel-like state (by PCer) will affect SM phosphocholine head group orientation and dynamics [47], in addition to increasing acyl chain order and lateral packing. The gel-phase formation most likely also sequesters SM (together with PCer [29]) and in that way may affect SM availability to StnII for binding. Our results do not allow us to distinguish the mechanism for how PCer addition to SM-domains hinder StnII-pore formation so markedly.

Both cholesterol and ceramide compete for interacting with PSM under certain conditions [18,19]. Usually cholesterol gets displaced from PSM domains by PCer, probably because PCer has higher affinity for PSM compared to cholesterol [18], but the ratios of cholesterol to ceramide, or cholesterol/ceramide to PSM also affect the final outcome of interaction [48]. In our present study, cholesterol was able to (partially) reverse the inhibitory effect of PCer on StnII pore formation, as determined from calcein release kinetics (Fig. 5). While cholesterol at the concentration used (about 4 mol%) was not likely to affect the over-all gel nature of the PSM/PCer domains (16 mol% each), it is possible that cholesterol affected properties of PSM in the POPC-rich phase, or of PSM at the gel phase boundary in a way that facilitated StnII/SM interaction and pore formation.

Considering the biological implications of our results, we may first speculate that since StnII is most likely targeted to SM-rich membranes, the protein was apparently evolutionarily optimized to function best in cholesterol-containing membranes, since cholesterol and SM coexist in membranes [49,50]. If that is the case, is it not surprising that pore formation is attenuated in SM-containing membranes in the absence of cholesterol. Secondly, we may conclude that the inhibitory effects of SM degradation (by sphingomyelinase) on red blood cell hemolysis by StnII [6] is probably not caused by SM depletion from membranes per se, but rather from ceramide generation. We conclude that StnII/membrane interaction, leading to pore formation, may critically respond to changes in PSM head group properties, which can be efficiently modulated by cholesterol or ceramide.

Acknowledgments

The work was funded by generous grants from the Sigrid Juselius Foundation (JPS), the Åbo Akademi Foundation (JPS), and BFU2012-32404 from the Spanish Ministerio de Ciencia e Innovación (JGG and AMP) and one FPU fellowship granted to S.G.-L.

References

[1] V. De Los Rios, J.M. Mancheno, P.A. Martinez de, C. Alfonso, G. Rivas, M. Onaderra, J.G. Gavilanes, Sticholysin II, a cytolysin from the sea anemone Stichodactyla helianthus, is a monomer-tetramer associating protein, FEBS Lett. 455 (1999) 27–30.
[2] C. Alvarez, J.M. Mancheno, D. Martinez, M. Tejuca, F. Pazos, M.E. Lanio, Sticholysins, two pore-forming toxins produced by the Caribbean Sea anemone Stichodactyla helianthus: their interaction with membranes, Toxicon 54 (2009) 1135–1147.
[3] L. García-Ortega, J. Alegre-Cebollada, S. García-Linares, M. Bruix, A. Martínez-Del-Pozo, J.G. Gavilanes, The behavior of sea anemone actinoporins at the water-membrane interface, Biochim. Biophys. Acta 1808 (2011) 2275–2288.
[4] J. Alegre-Cebollada, M. Onaderra, J.G. Gavilanes, A.M. del Pozo, Sea anemone actinoporins: the transition from a folded soluble state to a functionally active membrane-bound oligomeric pore, Curr. Protein Pept. Sci. 8 (2007) 558–572.
[5] V. De Los Rios, J.M. Mancheno, M.E. Lanio, M. Onaderra, J.G. Gavilanes, Mechanism of the leakage induced on lipid model membranes by the hemolytic protein sticholysin II from the sea anemone Stichodactyla helianthus, Eur. J. Biochem. 252 (1998) 284–289.
[6] A.W. Bernheimer, L.S. Avigad, Properties of a toxin from the sea anemone Stoichacis helianthus, including specific binding to sphingomyelin, Proc. Natl. Acad. Sci. U. S. A. 73 (1976) 467–471.
[7] B. Bakrac, I. Gutierrez-Aguirre, Z. Podlesek, A.F. Sonnen, R.J. Gilbert, P. Macek, J.H. Lakey, G. Anderluh, Molecular determinants of sphingomyelin specificity of a eukaryotic pore-forming toxin, J. Biol. Chem. 283 (2008) 18665–18677.
[8] T. Maula, Y.J.E. Isaksson, S. Garcia-Linares, S. Niinivehmas, O.T. Pentikainen, V. Kurze, S. Yamaguchi, T. Yamamoto, S. Katsumura, J.G. Gavilanes, A. Martinez-Del-Pozo, J.P. Slotte, 2NH and 3OH are crucial strctural requirements in sphingomyelin for sticholysin II binding and pore formation in bilayer membranes, Biochim. Biophys. Acta 1828 (2013) 1390–1395.
[9] A. Barlic, I. Gutierrez-Aguirre, J.M. Caaveiro, A. Cruz, M.B. Ruiz-Arguello, J. Perez-Gil, J.M. Gonzalez-Manas, Lipid phase coexistence favors membrane insertion of equinatoxin-II, a pore-forming toxin from Actinia equina, J. Biol. Chem. 279 (2004) 34209–34216.
[10] P.L. Yeagle, Modulation of Membrane Function by Cholesterol, Biochimie 73 (1991) 1303–1310.
[11] T.P. McMullen, R.N. Lewis, R.N. McElhaney, Differential scanning calorimetric study of the effect of cholesterol on the thermotropic phase behavior of a homologous series of linear saturated phosphatidylcholines, Biochemistry 32 (1993) 516–522.
[12] J.H. Ipsen, G. Karlstrom, O.G. Mouritsen, H. Wennerstrom, M.J. Zuckermann, Phase equilibria in the phosphatidylcholine-cholesterol system, Biochim. Biophys. Acta 905 (1987) 162–172.
[13] J.P. Slotte, Sphingomyelin-cholesterol interactions in biological and model membranes, Chem. Phys. Lipids 102 (1999) 13–27.
[14] A. Bjorkbom, T. Rog, P. Kankaanpaa, D. Lindroos, K. Kaszuba, M. Kurita, S. Yamaguchi, T. Yamamoto, S. Jaikishan, L. Paavolainen, J. Paivarinne, T.K. Nyholm, S. Katsumura, I. Vattulainen, J.P. Slotte, N- and O-methylation of sphingomyelin markedly affects its membrane properties and interactions with cholesterol, Biochim. Biophys. Acta 1808 (2011) 1179–1186.
[15] M. Lonnfors, J.P. Doux, J.A. Killian, T.K. Nyholm, J.P. Slotte, Sterols Have Higher Affinity for Sphingomyelin than for Phosphatidylcholine Bilayers even at Equal Acyl-Chain Order, Biophys. J. 100 (2011) 2633–2641.
[16] F.M. Goni, A. Alonso, Biophysics of sphingolipids I. Membrane properties of sphingosine, ceramides and other simple sphingolipids, Biochim. Biophys. Acta 1758 (2006) 1902–1921.
[17] J. Sot, M. Ibarguren, J.V. Busto, L.R. Montes, F.M. Goni, A. Alonso, Cholesterol displacement by ceramide in sphingomyelin-containing liquid-ordered domains, and generation of gel regions in giant lipidic vesicles, FEBS Lett. 582 (2008) 3230–3236.
[18] S.M. Alanko, K.K. Halling, S. Maunula, J.P. Slotte, B. Ramstedt, Displacement of sterols from sterol/sphingomyelin domains in fluid bilayer membranes by competing molecules, Biochim. Biophys. Acta 1715 (2005) 111–121.
[19] Megha, E. London, Ceramide selectively displaces cholesterol from ordered lipid domains (rafts): implications for lipid raft structure and function, J. Biol. Chem. 279 (2004) 9997–10004.
[20] S. Jaikishan, A. Bjorkbom, J.P. Slotte, Sphingomyelin analogs with branched N-acyl chains: The position of branching dramatically affects acyl chain order and sterol interactions in bilayer membranes, Biochim. Biophys. Acta 1798 (2010) 1987–1994.
[21] D.V. Kuklev, W.L. Smith, Synthesis of four isomers of parinaric acid, Chem. Phys. Lipids 131 (2004) 215–222.
[22] R. Cohen, Y. Barenholz, S. Gatt, A. Dagan, Preparation and characterization of well defined D-*erythro* sphingomyelins, Chem. Phys. Lipids 35 (1984) 371–384.
[23] J. Alegre-Cebollada, G. Clementi, M. Cunietti, C. Porres, M. Onaderra, J.G. Gavilanes, A.M. Pozo, Silent mutations at the 5'-end of the cDNA of actinoporins from the sea anemone Stichodactyla helianthus allow their heterologous overproduction in Escherichia coli, J. Biotechnol. 127 (2007) 211–221.
[24] G. Rouser, S. Fleischer, A. Yamamoto, Two dimensional thin layer chromatographic separation of polar lipids and determination of phospholipids by phosphorus analysis of spots, Lipids 5 (1970) 494–496.
[25] S. Jaikishan, J.P. Slotte, Stabilization of sphingomyelin interactions by interfacial hydroxyls - A study of phytosphingomyelin properties, Biochim. Biophys. Acta 1828 (2013) 391–397.
[26] J.R. Lakowicz, Principles of Fluorescence Spectroscopy, Kluwer Academic/Plenum Publishers, New York, 1999.
[27] J. Alegre-Cebollada, M. Cunietti, E. Herrero-Galan, J.G. Gavilanes, A. Martinez-Del-Pozo, Calorimetric scrutiny of lipid binding by sticholysin II toxin mutants, J. Mol. Biol. 382 (2008) 920–930.
[28] G. Anderluh, P. Macek, Dissecting the actinoporin pore-forming mechanism, Structure 11 (2003) 1312–1313.
[29] L.C. Silva, R.F. de Almeida, B.M. Castro, A. Fedorov, M.J. Prieto, Ceramide-domain formation and collapse in lipid rafts: membrane reorganization by an apoptotic lipid, Biophys. J. 92 (2006) 502–516.
[30] L.A. Sklar, B.S. Hudson, R.D. Simoni, Conjugated polyene fatty acids as fluorescent probes: synthetic phospholipid membrane studies, Biochemistry 16 (1977) 819–828.
[31] L.A. Sklar, G.P. Miljanich, E.A. Dratz, Phospholipid lateral phase separation and the partition of cis-parinaric acid and trans-parinaric acid among aqueous, solid lipid, and fluid lipid phases, Biochemistry 18 (1979) 1707–1716.
[32] R.F. de Almeida, A. Fedorov, M. Prieto, Sphingomyelin/phosphatidylcholine/cholesterol phase diagram: boundaries and composition of lipid rafts, Biophys. J. 85 (2003) 2406–2416.
[33] T. Rog, M. Pasenkiewicz-Gierula, Cholesterol-sphingomyelin interactions: a molecular dynamics simulation study, Biophys. J. 91 (2006) 3756–3767.

[34] J. Aittoniemi, P. Niemela, M.T. Hyvonen, M. Karttunen, I. Vattulainen, Insight into the Putative Specific Interactions Between Cholesterol, Sphingomyelin and Palmitoyl-Oleoyl Phosphatidylcholine, Biophys. J. 92 (2006) 1125–1137.
[35] K.S. Bruzik, B. Sobon, G.M. Salamonczyk, Nuclear magnetic resonance study of sphingomyelin bilayers, Biochemistry 29 (1990) 4017–4021.
[36] P.R. Cullis, K.B. De, R.E. Richards, Factors affecting the motion of the polar headgroup in phospholipid bilayers. A 31P NMR study of unsonicated phosphatidylcholine liposomes, Biochim. Biophys. Acta 426 (1976) 433–446.
[37] A. Bjorkbom, T. Rog, K. Kaszuba, M. Kurita, S. Yamaguchi, M. Lonnfors, T.K. Nyholm, I. Vattulainen, S. Katsumura, J.P. Slotte, Effect of sphingomyelin headgroup size on molecular properties and interactions with cholesterol, Biophys. J. 99 (2010) 3300–3308.
[38] P. Niemela, M.T. Hyvonen, I. Vattulainen, Structure and Dynamics of Sphingomyelin Bilayer: Insight Gained Through Systematic Comparison to Phosphatidylcholine, Biophys. J. 87 (2004) 2976–2989.
[39] P. Schon, A.J. Garcia-Saez, P. Malovrh, K. Bacia, G. Anderluh, P. Schwille, Equinatoxin II permeabilizing activity depends on the presence of sphingomyelin and lipid phase coexistence, Biophys. J. 95 (2008) 691–698.
[40] N. Rojko, B. Cronin, J.S. Danial, M.A. Baker, G. Anderluh, M.I. Wallace, Imaging the lipid-phase-dependent pore formation of equinatoxin II in droplet interface bilayers, Biophys. J. 106 (2014) 1630–1637.
[41] B.M. Castro, R.F. de Almeida, L.C. Silva, A. Fedorov, M. Prieto, Formation of ceramide/sphingomyelin gel domains in the presence of an unsaturated phospholipid. A quantitative multiprobe approach, Biophys. J. 93 (2007) 1639–1650.
[42] T. Maula, M. Kurita, S. Yamaguchi, T. Yamamoto, S. Katsumura, J.P. Slotte, Effects of sphingosine 2 N- and 3O-methylation on palmitoyl ceramide properties in bilayer membranes, Biophys. J. 101 (2011) 2948–2956.
[43] S. Nybond, Y.J. Bjorkqvist, B. Ramstedt, J.P. Slotte, Acyl chain length affects ceramide action on sterol/sphingomyelin-rich domains, Biochim. Biophys. Acta 1718 (2005) 61–66.
[44] T.K. Nyholm, P.M. Grandell, B. Westerlund, J.P. Slotte, Sterol affinity for bilayer membranes is affected by their ceramide content and the ceramide chain length, Biochim. Biophys. Acta 1798 (2010) 1008–1013.
[45] I. Artetxe, C. Sergelius, M. Kurita, S. Yamaguchi, S. Katsumura, J.P. Slotte, T. Maula, Effects of sphingomyelin headgroup size on interactions with ceramide, Biophys. J. 104 (2013) 604–612.
[46] T. Maula, I. Artetxe, P.M. Grandell, J.P. Slotte, Importance of the sphingoid base length for the membrane properties of ceramides, Biophys. J. 103 (2012) 1870–1879.
[47] R. Metcalf, S.A. Pandit, Mixing properties of sphingomyelin ceramide bilayers: a simulation study, J. Phys. Chem. B 116 (2012) 4500–4509.
[48] B.M. Castro, L.C. Silva, A. Fedorov, R.F. de Almeida, M. Prieto, Cholesterol-rich fluid membranes solubilize ceramide domains: implications for the structure and dynamics of mammalian intracellular and plasma membranes, J. Biol. Chem. 284 (2009) 22978–22987.
[49] H. Ohvo-Rekila, B. Ramstedt, P. Leppimaki, J.P. Slotte, Cholesterol interactions with phospholipids in membranes, Prog. Lipid Res. 41 (2002) 66–97.
[50] S. Patton, Correlative relationship of cholesterol and sphingomyelin in cell membranes, J. Theor. Biol. 29 (1970) 489–491.

ARTICLE III

2NH and 3OH are crucial structural requirements in sphingomyelin for sticholysin II binding and pore formation in bilayer membranes

Maula, T., Isaksson, Y. J., **García-Linares, S.**, Niinivehmas, S., Pentikainen, O. T., Kurita, M., Yamaguchi, S., Yamamoto, T., Katsumura, S., Gavilanes, J. G., Martínez-del-Pozo, Á. and Slotte, J. P. (2013). *Biochim Biophys Acta* 1828(5): 1390-1395.

Los grupos 2NH y 3OH son elementos cruciales en la estructura de la esfingomielina para la unión de la esticolisina II a la membrana y la formación del poro

Esticolisina II (StnII) es una toxina formadora de poros de la anémona marina *Stichodactyla helianthus* que pertenece a la familia de las actinoporinas. La proteína se une a membranas que contengan esfingomielina (SM) y muestra una alta especificidad de unión por este lípido. En este trabajo se ha examinado el papel de los grupos formadores de enlaces de hidrógeno 2NH y 3OH de la esfingomielina en el reconocimiento por parte de la StnII. Para ello se han preparado dos derivados de la esfingomielina en los que se han metilado los grupos 2NH y 3OH, de manera que su capacidad para formar enlaces de hidrógeno está reducida. Tanto las medidas por resonancia de plasmones superficiales como de calorimetría de titulación isotérmica indican que la StnII no se une a las membranas que contienen los derivados metilados, mientras que sí lo hace a las membranas con SM. La StnII tampoco induce liberación de calceína (es decir, formación de poros) de las vesículas con los derivados metilados, pero sí de las que contienen SM. El modelado molecular de la SM unida al sitio de unión a fosfocolina de la StnII indica que los grupos 2NH y 3OH probablemente formen enlaces de hidrógeno con la Tyr135. Además, parece que las Tyr111 y Tyr136 podrían formar enlaces de hidrógeno con el grupo fosfato de la esfingomielina, estabilizando su unión a la proteína. Se concluye que las propiedades de la esfingomielina para formar enlaces de hidrógeno en la interfase proteína-membrana, junto con el grupo fosfocolina, son cruciales para la interacción de alta afinidad entre la esfingomielina y la StnII.

Biochimica et Biophysica Acta 1828 (2013) 1390–1395

Contents lists available at SciVerse ScienceDirect

Biochimica et Biophysica Acta

journal homepage: www.elsevier.com/locate/bbamem

2NH and 3OH are crucial structural requirements in sphingomyelin for sticholysin II binding and pore formation in bilayer membranes

Terhi Maula [a], Y. Jenny E. Isaksson [a], Sara García-Linares [b], Sanna Niinivehmas [c], Olli T. Pentikäinen [c], Mayuko Kurita [d], Shou Yamaguchi [d], Tetsuya Yamamoto [d], Shigeo Katsumura [d], José G. Gavilanes [b], Álvaro Martínez-del-Pozo [b], J. Peter Slotte [a,*]

[a] Biochemistry, Department of Biosciences, Åbo Akademi University, Turku, Finland
[b] Departamento de Bioquímica y Biología Molecular I, Universidad Complutense, Madrid, Spain
[c] Department of Biological and Environmental Science, University of Jyväskylä, Jyväskylä, Finland
[d] School of Science & Technology, Kwansei Gakuin University, 2-1 Gakuen, Sanda City, Hyogo 669-1337, Japan

ARTICLE INFO

Article history:
Received 27 November 2012
Received in revised form 9 January 2013
Accepted 22 January 2013
Available online 30 January 2013

Keywords:
Molecular docking
Membrane permeabilization
Isothermal titration calorimetry
Surface plasmon resonance

ABSTRACT

Sticholysin II (StnII) is a pore-forming toxin from the sea anemone *Stichodactyla heliantus* which belongs to the large actinoporin family. The toxin binds to sphingomyelin (SM) containing membranes, and shows high binding specificity for this lipid. In this study, we have examined the role of the hydrogen bonding groups of the SM long-chain base (i.e., the 2NH and the 3OH) for StnII recognition. We prepared methylated SM-analogs which had reduced hydrogen bonding capability from 2NH and 3OH. Both surface plasmon resonance experiments, and isothermal titration calorimetry measurements indicated that StnII failed to bind to bilayers containing methylated SM-analogs, whereas clear binding was seen to SM-containing bilayers. StnII also failed to induce calcein release (i.e., pore formation) from vesicles made to contain methylated SM-analogs, but readily induced calcein release from SM-containing vesicles. Molecular modeling of SM docked to the phosphocholine binding site of StnII indicated that the 2NH and 3OH groups were likely to form a hydrogen bond with Tyr135. In addition, it appeared that Tyr111 and Tyr136 could donate hydrogen bonds to phosphate oxygen, thus stabilizing SM binding to the toxin. We conclude that the interfacial hydrogen bonding properties of SM, in addition to the phosphocholine head group, are crucial for high-affinity SM/StnII-interaction.

1. Introduction

Sticholysin II (StnII) is a pore-forming single-peptide toxin isolated from the sea anemone *Stichodactyla heliantus* [1]. Structurally, it is highly related to other single peptide toxins in the actinoporin family, including equinatoxin II (EqtII) [1,2]. The StnII structure is based on a β-sandwich fold composed of 10 β-strands, with two α-helices interacting with both sides of the β-sandwich [3]. The N-terminal helix is amphiphilic and has been proposed to extend and be inserted into the bilayer, to form the pore walls [4,5]. Incorporation of the toxin into the bilayer depends largely on the composition and physicochemical state of the membrane [6–8]. A common and functionally important feature of actinoporins is their high specificity for sphingomyelin (SM) [9,10], but actinoporin/membrane association is also influenced by the physical properties of the bilayer membranes [7,11–13].

StnII binds to SM-containing phospholipid-membranes with high affinity ($K = 1.7 \times 10^8\ M^{-1}$) [11]. Mutation of a tyrosine residue (Y111N) in the phosphocholine (POC) binding site on StnII was shown by isothermal titration calorimetry (ITC) to reduce the bilayer binding constant of StnII by two orders of magnitude [11]. Since this residue was located in the POC-binding site, the results suggested that binding to SM was crucial for the high membrane affinity of StnII. However, the exact nature of SM/StnII interaction is not known, since no 3D structure of StnII is available with bound SM.

The specificity of actinoporins for SM has been convincingly demonstrated [10]. However, it appears that under specific conditions, some actinoporins may show low-affinity interaction with phosphatidylcholines and cause membrane permeabilization, but only in the presence of phase coexistence, most probably mediated by cholesterol [7,13,14]. In a dot-blot binding assay, phosphatidylcholine is not recognized by equinatoxin II, neither is ceramide nor sphingosylphosphorylcholine [10]. These observations together suggest that both the phosphocholine head group and the hydrogen bonding interfacial groups in SM (the 2NH and the 3OH) are important for toxin binding. Sphingomyelinase, which is specific for SM and does not degrade phosphatidylcholine,

Abbreviations: EqtII, equinatoxin II; ITC, isothermal titration calorimetry; LUV, large unilamellar vesicle; pbSM, procine brain sphingomyelin; POC, phosphocholine (binding site); POPC, 1-palmitoyl-2-oleoyl-*sn*-glycero-3-phosphocholine; PSM, palmitoyl SM; SM, sphingomyelin; pbSM, porcine brain SM; sSM, truncated SM analog used for docking optimization; SPR, surface plasmon resonance; StnII, sticholysin II

* Corresponding author. Tel.: +358 22154689.
E-mail address: jpslotte@abo.fi (J.P. Slotte).

0005-2736/$ – see front matter © 2013 Elsevier B.V. All rights reserved.
http://dx.doi.org/10.1016/j.bbamem.2013.01.018

also uses the interfacial hydrogen bond donating functional groups (in addition to the phosphocholine head group) of SM to stabilize binding to the active site [15,16].

In this study, we examine the importance of the 2NH and 3OH in SM for pore formation by StnII. By chemical synthesis, we have prepared SM analogs in which either the 2NH or the 3OH is methylated [17], to yield 2NMeSM and 3OMeSM, respectively. We have prepared 1-palmitoyl-2-oleoyl-*sn*-glycero-3-phosphocholine (POPC) bilayers containing either palmitoyl SM (PSM), or one of the methylated PSM analogs (POPC:SM molar ratio 4:1). With such bilayers, we found that StnII caused extensive calcein leakage only in PSM-containing bilayers. With surface plasmon resonance (SPR) analysis, only PSM containing vesicles caused StnII binding. Very similar results were shown using isothermal titration calorimetry (ITC) to study toxin binding to bilayer membranes. StnII was found to interact only with PSM-containing vesicles. Finally, using molecular docking of PSM to a 3D model of StnII, we suggest that Y135 in the POC-binding site stabilized SM binding by interactions with the 2NH and 3OH of PSM, whereas Y111 and Y136 formed hydrogen bonds to phosphate oxygen, possibly explaining the binding specificity for SM.

2. Materials and methods

2.1. Material

POPC, porcine brain SM (pbSM), and egg SM were obtained from Avanti Polar Lipids (Alabaster, AL, USA). PSM was purified from egg SM using preparative HPLC on a reverse phase (C18) column, as described previously [18]. The acyl chains of pbSM are mostly saturated (50% 18:0 and19% other saturated) while 24:1 is present at 21% (Avanti Polar Lipids). Methylated analogs of PSM (i.e., 2NMeSM and 3OMeSM) were prepared by chemical synthesis, as described previously [17]. Calcein and Sephacryl S200HR were obtained from Sigma/Aldrich (St. Louis, MO, USA). StnII was produced in an *E.coli* expression system, and purified, as described previously [19].

2.2. Calcein leakage assay

Calcein-entrapped large unilamellar vesicles (LUVs) were prepared from POPC and a SM-analog (4:1 molar ratio), by extrusion through 200 nm filters at 60 °C [20]. Briefly, the desired lipids were mixed and dried under a stream of nitrogen. The lipids were redissolved in chloroform and dried again before removal of any traces of remaining solvent in vacuum for 60 min. Prior to extrusion, the dry lipid films were hydrated for 30 min at 60 °C in Tris buffer containing calcein. The calcein concentration was 100 mM (10 mM Tris, 140 mM NaCl, pH 7.4), and the total lipid concentration was 1.25 mM. LUVs were separated from non-entrapped calcein by gel filtration on Sephacryl S200HR. The LUVs were used for permeabilization studies within 24 h. The concentration of LUV and StnII during calcein leakage experiments was 2.5 μM and 20 nM, respectively. Emission at 550 nm was followed at 23 °C as a function of time (Ex 480 nm). Fluorescence emission was measured on a PTI Quanta-Master spectrofluorimeter (Photon Technology International, Inc. NJ, USA). The released fraction of calcein was determined based on the maximum calcein release which was induced by Triton X-100 induced LUV disintegration. To ensure that no spontaneous leakage occurred, the emission was measured for each sample for 5 min before addition of toxin. A steady signal level, indicating intact vesicles, was observed for all samples.

2.3. Surface plasmon resonance spectroscopy

The association of StnII with vesicle-coated gold chips were performed as follows: LUVs were prepared from POPC or POPC/SM analog (4:1, molar ratio) in Tris buffer (10 mM Tris, 140 mM NaCl, pH 7.4) by extrusion through 100 nm polycarbonate filters at 60 °C. StnII binding to the vesicles was studied at 23 °C with a BioNavis SPR Navi 200 instrument (BioNavis Ltd, Tampere, Finland). The sensor gold chip was coated with a carboxymethylated dextran layer which was treated with N-hydroxysuccinimide and N-ethyl-N′ (dimethylaminopropyl) carbodiimide to activate the surface for capturing phospholipid membranes [21]. All solutions used for SPR were filtered through 0.2 μm membrane filters and degassed by bath sonication before use. The running buffer was 10 mM Tris, 140 mM NaCl, pH 7.4 and the flow rate was 5 μl/min. First, the chip surface was cleaned with two injections of 10 mM CHAPS. Then extruded LUVs (0.5 mM lipid concentration) were applied on the surface (12 min injection) and unbound vesicles were removed by one (3 min) injection of 50 mM NaOH. Bovine serum albumin (0.1 mg/ml, 3 min injection) was used to verify that the chip did not have uncovered areas. Finally StnII (1.0 μM) was applied for 22–24 min after which buffer alone was injected for 10 min to study toxin dissociation. The chip was regenerated with CHAPS as in the beginning of the experiment.

2.4. Isothermal titration calorimetry

The interaction between StnII and LUVs prepared from POPC and SM analogs (4:1 molar ratio, 100 nm diameter) was measured using a VP-ITC (MicroCal, Northampton, MA, USA), as described previously [11].

2.5. Computational studies

The structure of SM was sketched and energy minimized in SYBYL-X2.0 (Tripos, St. Louis, MO, USA) using the conjugate gradient method with MMFF94s charges [22] and a dielectric constant of 10. The termination gradient was set to 0.05 kcal/mol, and calculations were iterated until convergence was reached. PSM was drawn with two different configurations: PSM and a shortened version composed of the phosphocholine part, the long-chain base until C5, and the *N*-linked acyl chain until the Cα (sSM).

The 3D structure of StnII (PDB: 1O72 [3]) was acquired from the Protein Data Bank [23]. Hydrogen atoms were added into the StnII structure using TLEAP in ANTECHAMBER 1.27 [24]. The docking of PSM to the phosphocholine binding site of StnII was performed flexibly with GOLD 5.0 [25] using ChemScore scoring function, diverse solutions option, and the most accurate (slow) docking. Docking atom selection was not restricted entirely to the solvent-accessible surface. Both PSM and the sSM were used in docking experiments. However, due to the conformational space that the docking should cover for PSM, and since the main focus was on the exploring of the interfacial portion of the SM, the docking of sSM was studied more thoroughly. In addition, the stability of the ligand-protein complex was studied with molecular dynamics (MD) simulations. MD simulations were done as described previously [16]. Multiple starting conformations of PSM (obtained via molecular docking) were used in the MD.

3. Results

3.1. StnII pore formation and membrane binding

The importance of specific functional groups in SM structure for StnII binding to bilayers, and for subsequent pore formation, was examined using chemically synthesized SM analogs in which either the 2NH or the 3OH was methylated (see Scheme 1 for molecular structures). The methylated SM analogs have markedly reduced capability to form hydrogen bonds compared to unmodified SM [17].

StnII binding to SM-rich bilayers is known to lead to pore formation, and to membrane permeabilization for small solutes. We measured calcein leakage from LUVs which were prepared to contain POPC and one of the SM analogs (4:1 molar ratio; Fig. 1). While PSM-containing membranes were permeabilized efficiently by StnII, both

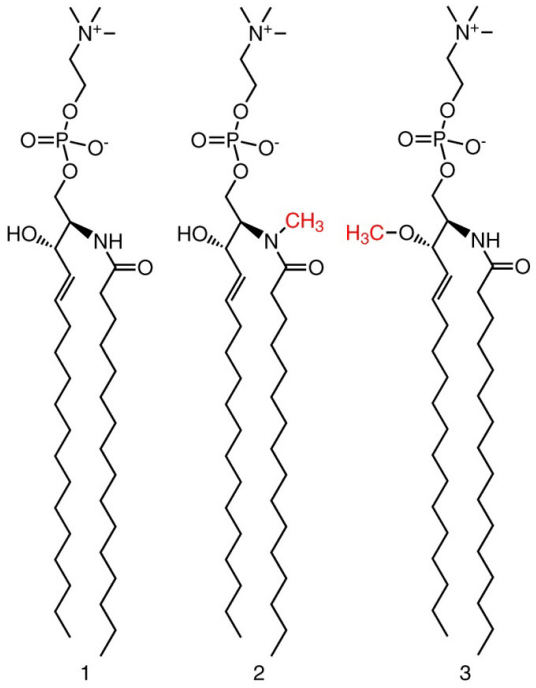

Scheme 1. Molecular structures of the three SM analogs used in the study: (1) palmitoyl SM, (2) 2NMe palmitoyl SM, and (3) 3OMe palmitoyl SM.

of the methylated PSM analogs failed to support StnII pore formation. The leakage from POPC LUVs was also very slow under the conditions used (Fig. 1).

Since calcein leakage only indicates pore formation, but gives no information about StnII binding to vesicles *per se*, we next used SPR to examine StnII binding to gold chips coated with different vesicles containing POPC and PSM or one of the methylated PSM analogs (Fig. 2). The SPR sensogram showed efficient binding of StnII to bilayers containing PSM, but not to bilayers containing methylated PSM, or POPC alone. The off-rate of StnII from PSM-containing bilayers was also negligible, indicating high affinity binding. The small initial deviations in the SPR response after injection of StnII could relate to mismatch in solvents (vesicle loading solvent versus StnII-containing solvent).

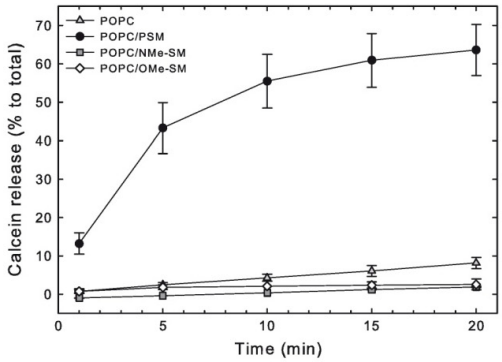

Fig. 1. The StnII-induced release of calcein from LUVs containing POPC and SM analogs was examined at 23 °C. The LUVs contained POPC and SM in a 4:1 molar ratio. StnII was added to the sample cell at time zero, and the RF (%) was calculated at time points indicated. Each value is the average from 3 to 5 separate experiments ± SD.

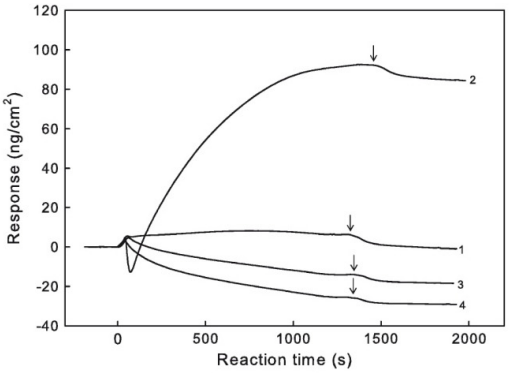

Fig. 2. SPR sensogram showing the binding of StnII to immobilized vesicles of different lipid composition. The vesicles consisted of 1: POPC, 2: POPC/PSM (4:1), 3: POPC/NMe-SM (4:1) or 4: POPC/OMe-SM (4:1). Vesicles (0.5 mM total lipid) were first immobilized on the chip surface for 12 min. Then StnII (1.0 μM) was allowed to bind for 22–24 min (starting at 0 s). The arrows indicate the injection of buffer (10 mM Tris, 140 mM NaCl, pH 7.4) to study toxin dissociation. The flow rate was 5 μl/min and the temperature was 23 °C. The figure shows representatives of at least 3 independent experiments.

In order to study direct toxin/bilayer binding with another method, we measured StnII/vesicle interaction by using ITC, which in addition also gives thermodynamic data for the binding process. The heat released after injection of POPC bilayers to StnII was close to zero (Fig. 3), indicating no substantial binding of StnII to POPC. Inclusion of PSM in the POPC bilayers resulted in clear exothermic signals when StnII was added. The calculated K for StnII binding to POPC/PSM (4:1 molar ratio) was $1.80 \times 10^6\ M^{-1}$ (Table 1). A very similar result ($K = 1.44 \times 10^6\ M^{-1}$, Table 1) was obtained when using pbSM containing vesicles. pbSM has a very different composition from PSM in terms of fatty acids composition (see Section 2). With methylated PSM analogs in the POPC vesicles, StnII failed to interact with the bilayers, since the interaction energy was close to zero (Fig. 3).

3.2. Computational studies of sphingomyelin binding to sticholysin II

To deduce the structural details that are important for SM recognition by StnII, and to outline the binding interactions of SM with StnII, SM was docked to the POC binding site of StnII. Overall, the docking pose of the phosphocholine moiety of SM is relatively similar to the pose appeared in the StnII crystal structure complexed with phosphocholine (PDB:1O72 [3]). sSM was used in the initial docking experiments, because interactions of the toxin with the phosphocholine moiety and with both 2NH and 3OH are likely to be important for SM recognition. Additionally, there are no clear grooves on the surface of the toxin for the hydrocarbon chains, and thus, the chains are not supposed to interact with the binding site of StnII, as suggested before [10].

The ligand binding cavity of StnII contains a cluster of aromatic amino acids, and is partly hydrophobic and partly hydrophilic. For example side chains of Val85, Pro105, and Trp114, and aromatic rings of several tyrosine residues (Tyr111, Tyr131, Tyr135, and Tyr136) are hydrophobic, whereas side chains of Ser52, and Ser103, and phenolic hydroxyl groups of the above-mentioned tyrosine residues add hydrophilic properties to the binding site [3]. Docking results suggested that the 2NH and 3OH groups of SM donate a hydrogen bond to the phenolic hydroxyl group of Tyr135 (Fig. 4). Furthermore, Tyr111 and Tyr136 could form hydrogen bonds to the oxygen atoms of the phosphate moiety through the phenolic hydroxyl groups (Fig. 4). Additionally, the phosphate moiety could be further stabilized by the cationic side chain of Arg51. Throughout the MD simulation, the phosphocholine moiety of PSM remains similarly bound into the ligand binding site. However, the long hydrocarbon chains do not find stable conformation but remain flexible as there are no grooves on the surface of the protein

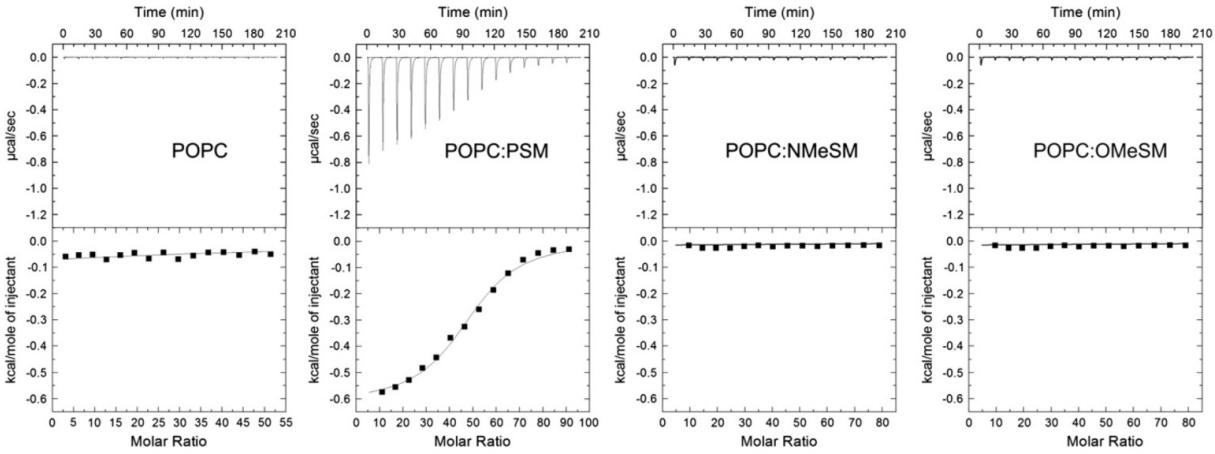

Fig. 3. Binding of StnII to POPC/SM analog vesicles at 25 °C. Protein solutions at 10 µM were titrated by injection of 20 µL aliquots of lipid suspensions (5 mM). Binding isotherms were adjusted to a model were the protein binds the membrane involving *n* lipid molecules [11].

for the hydrocarbon chains. This observation is also in good agreement with the pbSM ITC results which indicate that the fatty acid chain length is not important for binding (Table 1).

4. Discussion

Sphingomyelins are important phospholipids in animal cell membranes [26]. They often have saturated or monounsaturated acyl chains, and are thus ordered lipids [26,27]. Their ordered nature, and their extensive hydrogen bonding properties help to form SM-rich ordered domains in cell membranes [28]. Cholesterol associates with SM-rich domains and helps to keep them in a liquid ordered state [29]. In addition to maintaining membrane structure, and serving as precursors for many bioactive sphingolipids [30], SMs are also used by extracellular proteins as "receptors" to which they may bind [31]. This is also evidenced by the toxins from the actinoporin family, which are known to lyse membranes which contain SM [1,2,8,32,33].

The lipid specificity of equinatoxin II (EqtII) binding has been shown to be very high, since only SM is recognized by the toxin, from a range of other sphingolipids or glycerophospholipids [10]. However, EqtII is known to penetrate into monolayers from both SM and phosphatidylcholine, if the initial surface pressure is below 25–26 mN/m [14]. The toxin was also shown to cause bilayer permeabilization in vesicles made from cholesterol and phosphatidylcholine [7,14]. It appears that while binding of SM to StnII is of high affinity, phosphatidylcholine can bind to StnII but with much less affinity, and somehow cholesterol appears to facilitate this at least in *in vitro* studies.

All the results in this study clearly show that StnII failed to interact with or cause pore formation with bilayers which contained SM analogs in which the 2NH and 3OH functional properties were compromised. It therefore appears that these two functional groups are important for giving specificity and high affinity for StnII/membrane interaction and for pore formation. Methylation of the 2NH of SM was recently shown to reduce its gel-phase stability [17], suggesting that hydrogen-bonding involving the 2NH are important for SM–SM interlipid interactions. The 3OMe analog also showed slightly decreased gel-phase stability, but much less than for 2NMe. Sterol affinity for bilayers containing the methylated SM analogs was markedly lowered compared to PSM.

The 2NH and 3OH in SM have in many studies been shown to be of critical importance for the biophysical membrane properties of SM [17,34], and for the specificity of sphingomyelinase for SM [15,16]. The amino acid residues in the phospholipid binding site of StnII (or EqtII), which are most likely to give specificity for SM, are Tyr 111 (Tyr 113 in EqtII) and Trp 110 (Trp 112 in EqtII). Replacing Trp112 in EqtII with more polar residues led to loss of pore formation in DOPC:SM bilayers (as deduced from membrane permeabilization) [10,35]. Conversion of Tyr113 in EqtII to Ala113 also led to loss of pore formation in DOPC:SM bilayers, but Tyr113 could be converted

Table 1
Isothermal titration calorimetric analysis of the binding of StnII to POPC:PSM or POPC:pbSM (4:1) vesicles at 25 °C.

Vesicles	*n*	$K\times10^{-6}$ (M^{-1})	ΔG (kcal/mol)	ΔH (kcal/mol)	ΔS (cal mol^{-1} K^{-1})
POPC:PSM	48±1	1.80±0.32	−6.4±0.8	−29.3±1.5	−77±7
POPC:SM	45±1	1.44±0.22	−6.3±0.5	−25.4±1.1	−64±6

Values are the mean of at least two independent determinations (±SEM). Binding isotherms were adjusted to a model were the protein binds the membrane involving *n* lipid molecules [11].

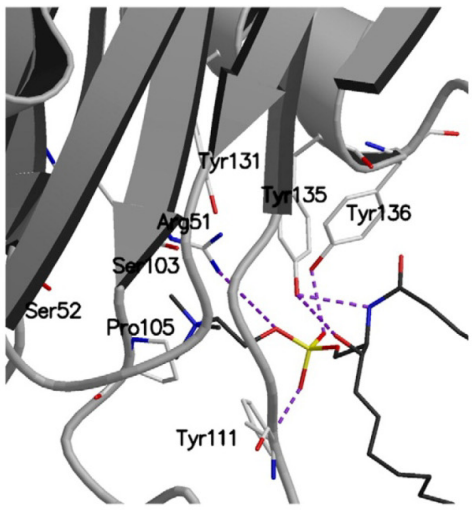

Fig. 4. Molecular docking of SM to the POC binding site of StnII. The protein structure (PDB: 1O72 [3]) is shown with secondary structure in gray whereas SM and key amino acids are shown in stick models. Hydrogen bonds are indicated with purple dashed lines. The 2NH and 3OH groups form a hydrogen bond with Tyr135. Additionally, Tyr111 and Tyr136 donate hydrogen bonds to the phosphate group. The figure was prepared using BODIL [36], MOLSCRIPT v 2.1.2 [37], and the RASTER3D package [38].

to Phe113 without significant loss of membrane association or pore formation [10]. In StnII, mutation of Tyr111 to Asn111 significantly reduced hemolytic activity of the toxin. This mutation also led to a 2 orders of magnitude less membrane affinity, compared to the wild type StnII [11].

Our SM docking model suggests that the phosphate oxygens interact with Tyr111 and Tyr136, while the 2NH and 3OH engage in electrostatic interactions with Tyr135. Additionally, the phosphate moiety could be further stabilized by the cationic side chain of Arg51. Methylation of 2NH and 3OH would prevent such interactions. Also MD simulations support the stable positioning of the phosphocholine head group of the SM into the ligand binding site.

It remains unclear what contribution, if any, the steric size (and hydrophobicity) of the methyl group would impose on SM/POC binding site interactions. However, in the case where these methylated SM analogs were allowed to interact with the binding site of sphingomyelinase, it was reasoned that attenuated hydrogen bonding was a more important factor than the steric size of the methyl, to eliminate their substrate capability [15,16]. This model does not contradict results from mutation studies involving Tyr111 (or Trp112 and Tyr113 in EqtII). It suggests, however, that mutation studies in which Tyr135 and Tyr136 would be changed, would be worthwhile to undertake, in order to better clarify the role of these residues for stabilizing SM/toxin interaction in the POC site.

The results of this study do not directly address questions related to the role of 2NH or 3OH in the SM structure for (i) membrane binding of StnII, and (ii) for the subsequent oligomerization and pore formation. However, the lack of apparent membrane binding of the methylated SM analogs (SPR and ITC data, Figs. 2 and 3), and the failure to cause significant membrane permeabilization (Fig. 1), suggest that the methylated SM analogs failed to support stable membrane association of StnII. This would confirm that high affinity interaction between StnII and SM is required for stable membrane association of StnII. The slow kinetics (relatively speaking) of both membrane permeabilization (calcein leakage) and membrane association (SPR sensogram) suggest that pore formation (i.e., oligomerization) is rate limiting relative to membrane association.

This study is the first to have used SM analogs with compromised hydrogen bonding properties, in the characterization of SM/StnII interaction. With the help of mutational studies with actinoporin toxins, the amino acid residues important for SM recognition have been identified. Our results with the methylated SM analogs complement the current understanding of SM/toxin interaction, and provide further evidence for the mechanisms involved in the high affinity binding of StnII to SMs.

Acknowledgments

The Turku group thanks Sofie Kvarnström and Josefin Halin for their help with some of the experiments. The work was funded by generous grants from the Sigrid Juselius Foundation (JPS), the Åbo Akademi Foundation (JPS), National Doctoral Programme in Nanoscience (SN), Grant-in-Aid for Science Research on Priority Areas 16073222 from the Ministry of Education, Culture, Sports, Science and Technology (SK) and also the Matching Fund Subsidy for a Private University, Japan (SK), and BFU2009-10185 from the Spanish Ministerio de Ciencia e Innovación (JGG and AMP).

References

[1] L. García-Ortega, J. Alegre-Cebollada, S. García-Linares, M. Bruix, A. Martínez-Del-Pozo, J.G. Gavilanes, The behavior of sea anemone actinoporins at the water-membrane interface, Biochim. Biophys. Acta 1808 (2011) 2275–2288.
[2] G. Anderluh, P. Macek, Dissecting the actinoporin pore-forming mechanism, Structure 11 (2003) 1312–1313.
[3] J.M. Mancheno, J. Martin-Benito, M. Martinez-Ripoll, J.G. Gavilanes, J.A. Hermoso, Crystal and electron microscopy structures of sticholysin II actinoporin reveal insights into the mechanism of membrane pore formation, Structure 11 (2003) 1319–1328.
[4] A. Athanasiadis, G. Anderluh, P. Macek, D. Turk, Crystal structure of the soluble form of equinatoxin II, a pore-forming toxin from the sea anemone *Actinia equina*, Structure 9 (2001) 341–346.
[5] K. Kristan, Z. Podlesek, V. Hojnik, I. Gutierrez-Aguirre, G. Guncar, D. Turk, J.M. Gonzalez-Manas, J.H. Lakey, P. Macek, G. Anderluh, Pore formation by equinatoxin, a eukaryotic pore-forming toxin, requires a flexible N-terminal region and a stable beta-sandwich, J. Biol. Chem. 279 (2004) 46509–46517.
[6] C.A. Valcarcel, S.M. Dalla, C. Potrich, I. Bernhart, M. Tejuca, D. Martinez, F. Pazos, M.E. Lanio, G. Menestrina, Effects of lipid composition on membrane permeabilization by sticholysin I and II, two cytolysins of the sea anemone *Stichodactyla helianthus*, Biophys. J. 80 (2001) 2761–2774.
[7] V. de los Rios, J.M. Mancheno, M.E. Lanio, M. Onaderra, J.G. Gavilanes, Mechanism of the leakage induced on lipid model membranes by the hemolytic protein sticholysin II from the sea anemone *Stichodactyla helianthus*, Eur. J. Biochem. 252 (1998) 284–289.
[8] D. Martinez, A. Otero, C. Alvarez, F. Pazos, M. Tejuca, M.E. Lanio, I. Gutierrez-Aguirre, A. Barlic, I. Iloro, J.L. Arrondo, J.M. Gonzalez-Manas, E. Lissi, Effect of sphingomyelin and cholesterol on the interaction of St II with lipidic interfaces, Toxicon 49 (2007) 68–81.
[9] M. Tejuca, M.D. Serra, M. Ferreras, M.E. Lanio, G. Menestrina, Mechanism of membrane permeabilization by sticholysin I, a cytolysin isolated from the venom of the sea anemone *Stichodactyla helianthus*, Biochemistry 35 (1996) 14947–14957.
[10] B. Bakrac, I. Gutierrez-Aguirre, Z. Podlesek, A.F. Sonnen, R.J. Gilbert, P. Macek, J.H. Lakey, G. Anderluh, Molecular determinants of sphingomyelin specificity of a eukaryotic pore-forming toxin, J. Biol. Chem. 283 (2008) 18665–18677.
[11] J. Alegre-Cebollada, M. Cunietti, E. Herrero-Galan, J.G. Gavilanes, A. Martinez-Del-Pozo, Calorimetric scrutiny of lipid binding by sticholysin II toxin mutants, J. Mol. Biol. 382 (2008) 920–930.
[12] B. Bakrac, G. Anderluh, Molecular mechanism of sphingomyelin-specific membrane binding and pore formation by actinoporins, Adv. Exp. Med. Biol. 677 (2010) 106–115.
[13] P. Schon, A.J. Garcia-Saez, P. Malovrh, K. Bacia, G. Anderluh, P. Schwille, Equinatoxin II permeabilizing activity depends on the presence of sphingomyelin and lipid phase coexistence, Biophys. J. 95 (2008) 691–698.
[14] J.M. Caaveiro, I. Echabe, I. Gutierrez-Aguirre, J.L. Nieva, J.L. Arrondo, J.M. Gonzalez-Manas, Differential interaction of equinatoxin II with model membranes in response to lipid composition, Biophys. J. 80 (2001) 1343–1353.
[15] M.D. Lister, Z.S. Ruan, R. Bittman, Interaction of sphingomyelinase with sphingomyelin analogs modified at the C-1 and C-3 positions of the sphingosine backbone, Biochim. Biophys. Acta 1256 (1995) 25–30.
[16] C. Sergelius, S. Niinivehmas, T. Maula, M. Kurita, S. Yamaguchi, T. Yamamoto, S. Katsumura, O.T. Pentikainen, J.P. Slotte, Structure-activity relationship of sphingomyelin analogs with sphingomyelinase from *Bacillus cereus*, Biochim. Biophys. Acta 1818 (2012) 474–480.
[17] A. Bjorkbom, T. Rog, P. Kankaanpaa, D. Lindroos, K. Kaszuba, M. Kurita, S. Yamaguchi, T. Yamamoto, S. Jaikishan, L. Paavolainen, J. Paivarinne, T.K. Nyholm, S. Katsumura, I. Vattulainen, J.P. Slotte, N- and O-methylation of sphingomyelin markedly affects its membrane properties and interactions with cholesterol, Biochim. Biophys. Acta 1808 (2011) 1179–1186.
[18] S. Jaikishan, A. Bjorkbom, J.P. Slotte, Sphingomyelin analogs with branched N-acyl chains: the position of branching dramatically affects acyl chain order and sterol interactions in bilayer membranes, Biochim. Biophys. Acta 1798 (2010) 1987–1994.
[19] J. Alegre-Cebollada, G. Clementi, M. Cunietti, C. Porres, M. Onaderra, J.G. Gavilanes, A.M. Pozo. Silent mutations at the 5′-end of the cDNA of actinoporins from the sea anemone *Stichodactyla helianthus* allow their heterologous overproduction in *Escherichia coli*, J. Biotechnol. 127 (2007) 211–221.
[20] T.K. Nyholm, P.M. Grandell, B. Westerlund, J.P. Slotte, Sterol affinity for bilayer membranes is affected by their ceramide content and the ceramide chain length, Biochim. Biophys. Acta 1798 (2010) 1008–1013.
[21] S. Löfås, B. Johnsson, A novel hydrogel matrix on gold surfaces in surface plasmon resonance sensors for fast and efficient covalent immobilization of ligands, J. Chem. Soc., Chem. Commun. (1990) 1524–1526.
[22] T. Halgren, Merck molecular force field. I. Basis, form, scope, parameterization, and performance of MMFF94, J. Comput. Chem. 17 (1996) 490–519.
[23] H.M. Berman, J. Westbrook, Z. Feng, G. Gilliland, T.N. Bhat, H. Weissig, I.N. Shindyalov, P.E. Bourne, The Protein Data Bank, Nucleic Acids Res. 28 (2000) 235–242.
[24] J. Wang, W. Wang, P.A. Kollman, D.A. Case, Automatic atom type and bond type perception in molecular mechanical calculations, J. Mol. Graph. Model. 25 (2006) 247–260.
[25] G. Jones, P. Willett, R.C. Glen, Molecular recognition of receptor sites using a genetic algorithm with a description of desolvation, J. Mol. Biol. 245 (1995) 43–53.
[26] Y. Barenholz. Sphingomyelin–lecithin balance in membranes: composition, structure, and function relationships, in: M. Shinitzky (Ed.), Physiology of Membrane Fluidity, vol. 1, CRC Press, Boca Raton, 1984, pp. 131–174.
[27] Y. Barenholz, T.E. Thompson, Sphingomyelins in bilayers and biological membranes, Biochim. Biophys. Acta 604 (1980) 129–158.
[28] K. Simons, W.L. Vaz, Model systems, lipid rafts, and cell membranes, Annu. Rev. Biophys. Biomol. Struct. 33 (2004) 269–295.
[29] J.P. Slotte, Sphingomyelin–cholesterol interactions in biological and model membranes, Chem. Phys. Lipids 102 (1999) 13–27.
[30] Y.A. Hannun, The sphingomyelin cycle and the second messenger function of ceramide, J. Biol. Chem. 269 (1994) 3125–3128.
[31] V.R. Gupta, H.K. Patel, S.S. Kostolansky, R.A. Ballivian, J. Eichberg, S.R. Blanke, Sphingomyelin functions as a novel receptor for *Helicobacter pylori* VacA, PLoS Pathog. 4 (2008) e1000073.

[32] V. de los Rios, J.M. Mancheno, P.A. Martinez del, C. Alfonso, G. Rivas, M. Onaderra, J.G. Gavilanes, Sticholysin II, a cytolysin from the sea anemone *Stichodactyla helianthus*, is a monomer–tetramer associating protein, FEBS Lett. 455 (1999) 27–30.
[33] P.S. Garcia, G. Chieppa, A. Desideri, S. Cannata, E. Romano, P. Luly, S. Rufini, Sticholysin II: a pore-forming toxin as a probe to recognize sphingomyelin in artificial and cellular membranes, Toxicon 60 (2012) 724–733.
[34] R. Bittman, C.R. Kasireddy, P. Mattjus, J.P. Slotte, Interaction of cholesterol with sphingomyelin in monolayers and vesicles, Biochemistry 33 (1994) 11776–11781.
[35] Q. Hong, I. Gutierrez-Aguirre, A. Barlic, P. Malovrh, K. Kristan, Z. Podlesek, P. Macek, D. Turk, J.M. Gonzalez-Manas, J.H. Lakey, G. Anderluh, Two-step membrane binding by Equinatoxin II, a pore-forming toxin from the sea anemone, involves an exposed aromatic cluster and a flexible helix, J. Biol. Chem. 277 (2002) 41916–41924.
[36] J.V. Lehtonen, D.J. Still, V.V. Rantanen, J. Ekholm, D. Bjorklund, Z. Iftikhar, M. Huhtala, S. Repo, A. Jussila, J. Jaakkola, O. Pentikainen, T. Nyronen, T. Salminen, M. Gyllenberg, M.S. Johnson, BODIL: a molecular modeling environment for structure-function analysis and drug design, J. Comput. Aided Mol. Des. 18 (2004) 401–419.
[37] P. Kraulis, MOLSCRIPT: a program to produce both detailed and schematic plots of protein structures, J. Appl. Crystallogr. 24 (1991) 946–950.
[38] E.A. Merritt, D.J. Bacon, Raster3D: photorealistic molecular graphics, Methods Enzymol. 277 (1997) 505–524.

ARTICLE IV

Toxin-induced pore formation is hindered by intermolecular hydrogen bonding in sphingomyelin bilayers

García-Linares, S., Palacios-Ortega, J., Yasuda, T., Åstrand, M., Gavilanes, J. G., Martínez-del-Pozo, Á. and Slotte, J. P. (2016). *Biochim Biophys Acta* 1858(6): 1189-1195.

Los enlaces de hidrógeno intermoleculares entre las esfingomielinas de las membranas impiden la formación de poros inducida por toxinas

Esticolisinas I y II (StnI y StnII) son toxinas formadoras de poros que utilizan esfingomielina (SM) para unirse a las membranas. Se ha examinado cómo los enlaces de hidrógeno entre las moléculas de esfingomielina de la membrana afectan al proceso de formación de poros inducido por las esticolisinas, que lleva a la permeabilización de la bicapa. Se ha comparado la permeabilización inducida por toxinas en membranas que contienen esfingomielina o dihidro-esfingomielina (que carece del doble enlace trans Δ^4 en la cadena larga), ya que se sabe que su red de enlaces de hidrógeno es muy distinta. Se ha observado que tanto StnI como StnII son capaces de formar poros en vesículas unilamelares que contienen palmitoil-SM (PSM) u oleoil-SM (OSM), pero esto no ocurre si las vesículas se preparan con dihidro-PSM o dihidro-OSM. En bicapas que contienen OSM, la StnII es capaz de unirse a la membrana, como se ha podido determinar por resonancia de plasmones superficiales. Sin embargo, la unión de StnII a bicapas con dihidro-OSM es muy baja en condiciones experimentales similares. La asociación de StnII cargada positivamente (a pH 7) con vesículas unilamelares de OSM da lugar a un aumento de la carga de las vesículas dependiente de la concentración de proteína, según las medidas de potencial ζ. Con vesículas de dihidro-OSM no se observa esta respuesta. El alcohol bencílico, un pequeño compuesto capaz de formar enlaces de hidrógeno con afinidad por la superficie de bicapas lipídicas, facilita enormemente la formación de poros por parte de StnII en vesículas de dihidro-OSM, sugiriendo que los enlaces de hidrógeno en la interfase de la membrana son la causa de que en un principio la StnII no pueda unirse a la membrana ni formar poros. Se concluye que los enlaces de hidrógeno en la interfase son capaces de afectar a la asociación entre StnI y StnII con la membrana y, por tanto, a su capacidad para formar poros. Los resultados sugieren que otros tipos de interacciones entre proteínas y bicapas se pueden ver afectadas por los enlaces de hidrógeno intermoleculares originados por las esfingomielinas.

Biochimica et Biophysica Acta 1858 (2016) 1189–1195

Contents lists available at ScienceDirect

Biochimica et Biophysica Acta

journal homepage: www.elsevier.com/locate/bbamem

Toxin-induced pore formation is hindered by intermolecular hydrogen bonding in sphingomyelin bilayers

Sara García-Linares [a,b], Juan Palacios-Ortega [a,b], Tomokazu Yasuda [b,c], Mia Åstrand [b], José G. Gavilanes [a], Álvaro Martínez-del-Pozo [a], J. Peter Slotte [b,*]

[a] Departamento de Bioquímica y Biología Molecular I, Universidad Complutense, Madrid, Spain
[b] Biochemistry, Faculty of Science and Engineering, Åbo Akademi University, Turku, Finland
[c] Department of Chemistry, Graduate School of Science, Osaka University, Osaka, Japan

ARTICLE INFO

Article history:
Received 11 January 2016
Received in revised form 23 February 2016
Accepted 10 March 2016
Available online 11 March 2016

Keywords:
Permeabilization
Surface plasmon resonance
Sphingomyelinase
Sticholysin

ABSTRACT

Sticholysin I and II (StnI and StnII) are pore-forming toxins that use sphingomyelin (SM) for membrane binding. We examined how hydrogen bonding among membrane SMs affected the StnI- and StnII-induced pore formation process, resulting in bilayer permeabilization. We compared toxin-induced permeabilization in bilayers containing either SM or dihydro-SM (lacking the *trans* Δ^4 double bond of the long-chain base), since their hydrogen-bonding properties are known to differ greatly. We observed that whereas both StnI and StnII formed pores in unilamellar vesicles containing palmitoyl-SM or oleoyl-SM, the toxins failed to similarly form pores in vesicles prepared from dihydro-PSM or dihydro-OSM. In supported bilayers containing OSM, StnII bound efficiently, as determined by surface plasmon resonance. However, StnII binding to supported bilayers prepared from dihydro-OSM was very low under similar experimental conditions. The association of the positively charged StnII (at pH 7.0) with unilamellar vesicles prepared from OSM led to a concentration-dependent increase in vesicle charge, as determined from zeta-potential measurements. With dihydro-OSM vesicles, a similar response was not observed. Benzyl alcohol, which is a small hydrogen-bonding compound with affinity to lipid bilayer interfaces, strongly facilitated StnII-induced pore formation in dihydro-OSM bilayers, suggesting that hydrogen bonding in the interfacial region originally prevented StnII from membrane binding and pore formation. We conclude that interfacial hydrogen bonding was able to affect the membrane association of StnI- and StnII, and hence their pore forming capacity. Our results suggest that other types of protein interactions in bilayers may also be affected by hydrogen-bonding origination from SMs.

1. Introduction

Actinoporins are a group of soluble monomeric peptide toxins that have evolved to use sphingomyelin (SM) as their membrane recognition target [1–7]. These actinoporins include toxins such as sticholysin I and II (StnI and StnII, from *Stichodactyla helianthus* [8–10]), equinatoxin II (EqtII, from *Actina equina* [11]), and fragaceatoxin C (FraC, from *Actina fragacea* [12]). The water-soluble structure of the toxins is known in detail [13–16]. They have a β-sandwich motif consisting of 10 β-strands flanked by two α-helices, which interact with both sides of the β-sandwich. For the actinoporins, it is generally believed that monomeric peptides bind to the membrane interface (aided by SM) before oligomerization takes place, and a functional pore is finally formed [6,7].

The effects of membrane properties on toxin binding and pore formation by actinoporins have received a lot of attention over the years (for recent reviews, see [6,7,17]). Quite a lot is known about how membrane and SM properties affect pore formation by different actinoporins. In the absence of cholesterol, pore formation by StnII requires the hydrogen-bonding competent SM [18]. Indeed, all examined actinoporins appear to require the presence of SM in their target membranes [8,18–20]. However, under some conditions, both EqtII and StnII have been shown to increase bilayer permeability in the absence of SM [8,20]. Cholesterol has been shown to affect the pore-formation kinetics and efficiency of actinoporins [21,22]. The actual mechanism by which cholesterol affects rates and efficiency of pore formation is not fully understood, but cholesterol is known to abolish a gel phase in which SM could form in a unsaturated phospholipid bilayer (in the absence of cholesterol). In so doing, cholesterol increases diffusion in the SM-rich domain, but decreases diffusion in the unsaturated phospholipid domain [23,24]. Cholesterol may also affect hydrogen bonding in the membrane

Abbreviations: BA, benzyl alcohol; DPH, diphenyl hexatriene; EqtII, equinatoxin II; LUV, large unilamellar vesicle; FraC, fragaceatoxin C; OSM, *N*-oleoyl-D-*erythro*-sphingomyelin; POPC, 1-palmitoyl-2-oleoyl-*sn*-glycero-3-phosphocholine; PSM, *N*-palmitoyl-D-*erythro*-sphingomyelin; SM, sphingomyelin; StnI, sticholysin I; StnII, sticholysin II.

* Corresponding author.
E-mail address: jpslotte@abo.fi (J.P. Slotte).

http://dx.doi.org/10.1016/j.bbamem.2016.03.013
0005-2736/

interface, since its polar hydroxyl can act as both hydrogen bond donor and acceptor. Palmitoyl ceramide, which interacts strongly with SM and induces gel phase formation [25,26], is known to abolish StnII-induced pore formation [21].

SM is a hydrogen-bonding molecule, and many of its bilayer properties (e.g., interaction with other co-lipids) are affected by hydrogen bonding [27,28]. Intermolecular hydrogen-bonding origination from the 2NH function of the sphingoid base is thought to result in SM clustering in the bilayer phase [29]. Intramolecular hydrogen bonding involving the 3OH of the sphingoid base and phosphate oxygens of the phosphocholine headgroup is very prevalent and is likely to regulate head group dynamics and orientation in SM [30,31]. The formation of StnII-pores was abolished when hydrogen bonding from both 2NH and 3OH was prevented by methylation [18]. This result was interpreted to be a consequence of decreased binding of toxin to methylated SM analogs. However, it is possible that intermolecular hydrogen bonding among SMs also affects the way in which pores are formed.

Most SM species have a *trans* Δ^4 double bond in their long-chain base. However, dihydro-SM, which lacks the unsaturation in the long-chain base, is a fairly common SM present in most cells [32,33]. Dihydro-SM is the predominant SM present in the eye-lens membrane [34]. SM and dihydro-SM are known to display very different intra- and intermolecular hydrogen-bonding properties [30,31,35]. Hydrogen bonding among dihydro-SM molecules was recently shown to contribute to the lateral segregation and stabilization of a fluid dihydro-SM domain in disordered PC bilayers at high temperature [36]. A similar segregation of a fluid SM domain was not observed. The much stronger hydrogen bonding in dihydro-SM bilayers, as compared to acyl-chain matched SM bilayers, was also shown to have a fairly large effect on cholesterol and ceramide interactions with SMs [37].

Now, we have examined how pore formation by two different toxins, with highly similar structures but quite different hemolytic activities [19,38], is affected by the differing hydrogen-bonding properties of SM and dihydro-SM bilayers. We used *N*-palmitoyl-SM (PSM) or dihydro-PSM in mixed bilayers with 1-palmitoyl-2-oleoyl-*sn*-glycero-3-phosphocholine (POPC) (1:4 molar ratio) and *N*-oleoyl-SM (OSM) or dihydro-OSM in pure SM bilayers (the latter was possible because of the low gel–liquid crystalline-phase transition temperature of OSM/dihydro-OSM [39]). Our results show that StnII binding to bilayers and the subsequent pore formation were dramatically attenuated in bilayers containing dihydro-SM bilayers as compared to SM-containing bilayers. The addition of benzyl alcohol rescued the pore formation process in dihydro-SM bilayers, possibly by rearranging interfacial hydrogen bonding in a way that favored pore formation also in dihydro-OSM bilayers. We speculate that also other protein-driven processes in membranes may be affected by strong interfacial hydrogen bonding among dihydro-SM molecules.

2. Materials and methods

2.1. Materials

POPC, egg SM, sphingosyl-phosphorylcholine (lyso SM), sphinganin-phosphorylcholine (lyso dihydro-SM), and OSM were obtained from Avanti Polar Lipids (Alabaster, AL, USA). PSM was purified from egg SM as described previously [40]. Dihydro-PSM was prepared from PSM by hydrogenation using H_2-gas and palladium (10%) on charcoal (Sigma-Aldrich, St. Louis, MO, USA) as a catalyst, as described previously [39]. Dihydro-OSM was prepared from oleic acid anhydride (Sigma-Aldrich) and sphinganin–phosphorylcholine, as described previously [41]. Benzyl alcohol and calcein were obtained from Sigma-Aldrich. DPH was obtained from Molecular Probes (Eugene OR, USA). StnI and StnII were produced in an *Escherichia coli* expression system and purified, again, as previously [38].

2.2. Calcein release from LUVs

Calcein-entrapped large unilamellar vesicles (LUVs) were prepared from POPC/PSM and POPC/dihydro-PSM (4:1 molar ratio) and from pure OSM and dihydro-OSM by extrusion through 200-nm filters at 60 °C [18]. Briefly, the desired lipids were mixed and dried under a stream of nitrogen. Prior to extrusion, the dry lipid films were hydrated for 30 min at 60 °C in Tris buffer (10 mM Tris, 140 mM NaCl, pH 7.4) containing calcein. The calcein concentration was 100 mM, and the final lipid concentration was 1.25 mM. LUVs were separated from non-entrapped calcein by gel filtration on Sephacryl S200HR. The LUVs were used for permeabilization studies within 12 h. The concentrations of LUV and StnII during calcein leakage experiments were 2.5 μM and 20 nM, respectively. Emission at 550 nm was followed at 23 °C as a function of time (Ex 480 nm). Fluorescence emission was measured in a PTI Quanta-Master spectrofluorimeter (Photon Technology International, Inc. NJ, USA). The released fraction of calcein was determined based on the maximum calcein release induced by Triton X-100. To ensure that no spontaneous leakage occurred, the emission was measured for each sample for 5 min before addition of toxin. A steady signal level, indicating intact vesicles, was observed for all samples. When benzoyl alcohol was used, it was added to preformed LUVs 30 min prior to initiation of experiments.

2.3. Surface plasmon resonance measurements

The association of StnII with lipid bilayers on coated gold chips was performed as follows. LUVs were prepared from OSM and dihydro-OSM in Tris buffer by extrusion through 100 nm polycarbonate filters at 60 °C. StnII binding to the coated bilayers was studied at 23 °C with a BioNavis SPR Navi 200 instrument (BioNavis Ltd., Tampere, Finland). The sensor gold chip was coated with a carboxymethylated dextran layer treated with N-hydroxysuccinimide and N-ethyl-N′(dimethylaminopropyl) carbodiimide to activate the surface for capture of phospholipid membranes [18]. All solutions used for SPR were filtered through 0.2 μm membrane filters and degassed by bath sonication before use. The running buffer was 10 mM Tris, 140 mM NaCl, pH 7.4, and the flow rate was 5 μl/min.

First, the chip surface was cleaned with two injections of 10 mM CHAPS. Then, extruded LUVs (0.5 mM lipid concentration) were applied on the surface (10 min injection) and unbound vesicles were removed by one (2 min) injection of 50 mM NaOH. Bovine serum albumin (0.1 mg/ml, 2 min injection) was used to verify that the chip did not have uncovered areas. Finally StnII (1.0 μM) was applied for 10 min, after which buffer alone was injected for 2 min to study toxin dissociation. The chip was regenerated with CHAPS, as in the beginning of the experiment.

2.4. ζ-Potential measurements

To measure toxin/LUV bilayer interactions, vesicles were prepared from OSM and dihydro-OSM in Tris buffer (pH 7.4, 140 mM NaCl). They were exposed to increasing concentrations of StnII for 20 min prior to measuring the ζ-potential of the aggregates. A Malvern Zetasizer ZS (Worcestershire, UK) was used for the measurements. Values given are averages ± SD of $n = 3$.

2.5. Interaction of StnII with OSM or dihydro-OSM monolayers

To measure the penetration of StnII into OSM and dihydro-OSM monolayers, these were spread to an initial surface pressure of 9 mN/m. Following injection of StnII into the buffer subphase of the monolayers (0.8 μM final concentration), which were kept at constant surface area, the penetration of toxin into the monolayer led to a time-dependent increase in lateral surface pressure [42]. The experiments were repeated three times, and a set of representative penetration curves are shown.

2.6. Effects of benzyl alcohol on bilayer fluidity

To determine the bilayer acyl chain order in the presence of increasing amounts of benzyl alcohol (BA), steady state fluorescence anisotropy of DPH was measured on a PTI QuantaMaster spectrofluorimeter operating in the T-format, essentially following the procedure described in [43]. Briefly, OSM and dihydro-OSM LUVs were prepared and exposed to increasing amounts of BA for 30 min. After this period, DPH anisotropy was measured at the indicated temperature as a function of BA concentration. DPH was used at 1 mol% of the total lipid. The wave lengths of excitation and emission of DPH were 360 nm and 430 nm, respectively. The steady state anisotropy was calculated as described previously [44].

3. Results

3.1. Bilayer permeabilization by sticholysins

We have examined pore formation by StnI and StnII in bilayers containing SM and dihydro-SM. It has previously been shown that interfacial hydrogen bonding is very different in SM and dihydro-SM containing bilayers [30,31,35,36]. This difference results mainly from the increased flexibility of the 3OH in the long-chain base of dihydro-SM [37,45]. Our main aim was to study how such strong intermolecular hydrogen bonding (in dihydro-SM) may affect sticholysin-induced pore formation and membrane permeabilization. Pore formation was assessed by measuring calcein release from large unilamellar vesicles (200 nm diameter). The binding of both StnI and StnII to bilayers is mediated by SM, which acts as a recognition target for the pore-forming toxins. After monomer binding to the bilayer, an oligomerization process takes place in the membrane, followed eventually by the formation of a pore that allows calcein to be released from the entrapped volume within the LUVs. Pore formation by sticholysins is concentration-dependent. We used a concentration of 20 nM, which corresponds to a lipid:StnII (or StnI) ratio of about 125:1. As shown in Fig. 1A, the addition of StnI or StnII to LUVs prepared from POPC and PSM (4:1 molar ratio) led to a time-dependent release of calcein from the vesicles. The rate and extent of pore formation was more efficient with StnI than with StnII. However, when the LUVs contained dihydro-PSM instead of PSM, the pore formation by both StnI and StnII was very low and hardly above background leakage (Fig. 1A) under the conditions used. The temperature for the experiment shown in Fig. 1A was 23 °C. At this temperature the SM is more ordered than the POPC, but a gel phase is not present [46]. When LUVs were made of pure OSM or pure dihydro-OSM (Fig. 1B), a similar calcein release pattern, induced by StnII, was observed as for the saturated SMs. StnII efficiently formed pores in OSM bilayers, which led to calcein release, but the pore formation and subsequent calcein release was much less efficient in dihydro-OSM bilayers, under the conditions used. The calcein release from OSM and dihydro-OSM LUVs was performed at 24 °C and 28 °C, respectively. At these temperatures, the bilayers are fluid and the acyl chain order in the two populations of LUVs is the same ([37]); see also Fig. 6).

3.2. Analysis of bilayer association of StnII, using SPR, ζ-potential measurements, or a competition assay

To further assess StnII binding to and pore formation in bilayers formed from OSM and dihydro-OSM, we next performed surface plasmon resonance measurements. As shown in Fig. 2, the SPR sensogram indicated efficient binding of StnII to and accumulation in bilayers formed from OSM. However, StnII binding to bilayers made from dihydro-OSM was markedly attenuated (Fig. 2). The SPR data are consistent with the very low rate of calcein-release from dihydro-OSM vesicles after exposure to StnII.

Since StnII is a positively charged toxin at pH 7 (the isoelectric point of StnII is above 9.5 [19]), we measured StnII/LUV interaction based on

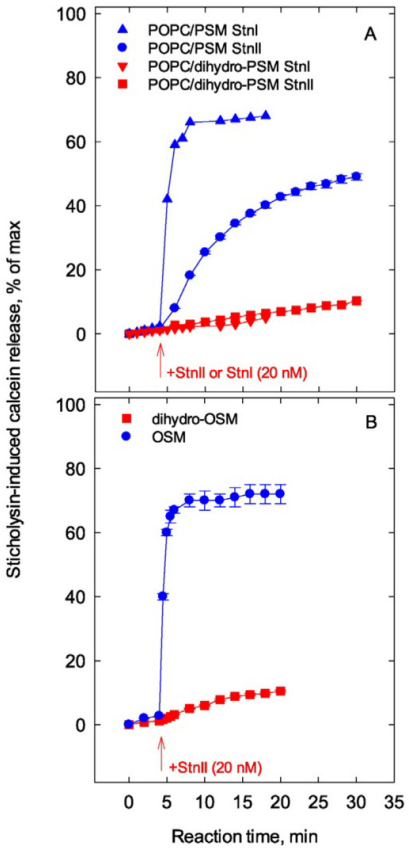

Fig. 1. Calcein release by StnI or StnII from SM or dihydro-SM LUVs. 200 nm LUVs were prepared either from POPC/PSM or POPC/dihydro-PSM (4:1 molar ratio; panel A, 37 °C), or pure OSM (24 °C) or dihydro-OSM (28 °C) (panel B). At the indicated time (red arrow 1n figure), StnI (Panel A) or StnII was added to give final concentration of 20 nM. The total lipid:StnII molar ratio was about 125:1. Each value is the average ± SEM from n = 2.

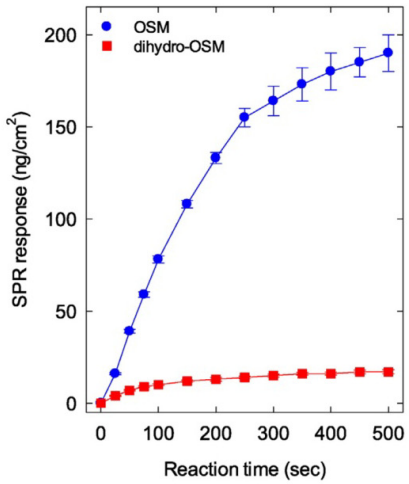

Fig. 2. Interaction of StnII with supported bilayers of OSM or dihydro-OSM as analyzed by SPR. For SPR measurements, StnII was added at time 0, and the bilayer association of StnII was determined as a function of time. The chip temperature was maintained at 23 °C. Each value is average ± SEM from n = 2.

ζ-potential measurements. SM is a zwitter-ionic phospholipid, and LUVs prepared from SM should have a net charge at pH 7, which is close to zero. In fact, the LUVs had a small negative overall charge (−1.4 mV and −2.1 mV for OSM and dihydro-OSM LUVs at pH 7, respectively Fig. 3). The addition of StnII to LUVs prepared from OSM led to a concentration-dependent increase in the net charge (positive). However, with LUVs containing dihydro-OSM, StnII addition did not result in the accumulation of the positively charged StnII in the LUVs. Instead a small decrease in the overall dihydro-OSM LUV charge was observed (Fig. 3).

Finally, we measured calcein-release from OSM vesicles (with constant ratio of calcein vesicles and StnII), in the presence of increasing amounts of unlabeled LUVs prepared from either OSM or dihydro-OSM. Since StnII also should bind to unlabeled OSM LUVs, the effective ratio of calcein-entrapped LUVs and StnII should decrease with increasing presence of un-labeled OSM vesicles, and the amount of calcein-release should decrease. The same should happen in the presence of dihydro-OSM LUVs if StnII bound to these bilayers. The results in Fig. 4 show a concentration-dependent reduction in maximum calcein release when OSM vesicles were added. However, StnII failed to bind similarly to dihydro-OSM vesicles, and hence the effect of unlabeled dihydro-OSM vesicles on calcein release from OSM LUVs was small. Clearly, the binding of StnII to LUVs was very different according to whether they were prepared from OSM or dihydro-OSM. Altogether, the results obtained with StnII (Figs. 1–4) suggest that binding to dihydro-SM, and/or oligomerization to functional pores is substantially compromised when compared to binding and pore-formation in SM-containing bilayers.

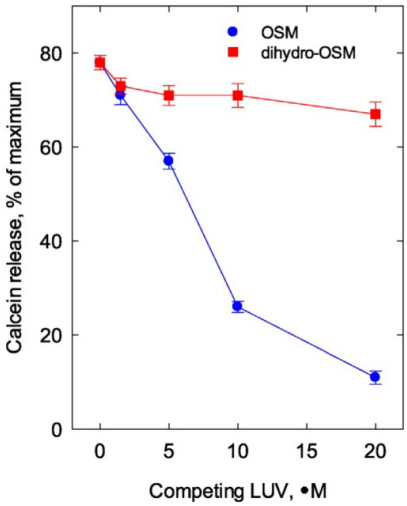

Fig. 4. Competition assay for StnII-induced calcein release from OSM LUVs. Calcein-entrapped OSM LUVs (200 nm diameter) were exposed to increasing concentrations of unlabeled OSM or dihydro-OSM LUVs (200 nm diameter) for a few minutes before StnII was added (20 nM final concentration). The maximum release of calcein after 5 min was determined. Maximum release was achieved before 5 min in each sample. The concentration of calcein-entrapped OSM vesicles was 3 μM. Each value is average ± SEM from n = 2. The experimental temperature was 23 °C.

3.3. Monolayer penetration of StnII

Sticholysin is known to bind to monolayers containing SM [42], and if the monolayer is kept at constant area, its lateral surface pressure will increase as more toxin accumulates in the monolayer. We examined StnII interaction with OSM and dihydro-OSM monolayers at the air/buffer interface. The monolayers were spread to a lateral surface pressure of 9 mN/m, and after 5 min equilibration time, StnII (final subphase concentration 0.8 μM) was injected into the stirred subphase. The initial kinetics of toxin penetration into both OSM and dihydro-OSM bilayers were similar (Fig. 5). However, after reaching a surface pressure of about 28 mN/m, the toxin penetration into the dihydro-OSM monolayer ceased and the monolayer surface pressure stabilized at 30 mN/m after 10 min of toxin exposure. With OSM monolayers, toxin penetration continued to higher surface pressures when compared to dihydro-OSM monolayers, and after 10 min a surface pressure of about 34 mN/m was reached. These results suggest that as packing became tighter (at increased surface pressure), intermolecular hydrogen bonding among

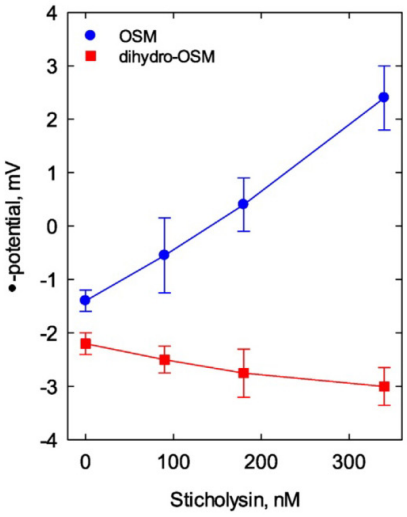

Fig. 3. Interaction of StnII with LUVs prepared from OSM and dihydro-OSM, as analyzed ζ-potential. For ζ-potential, 200 nm LUVs were exposed to indicated amounts of StnII for 20 min prior to measurement of ζ-potential (total lipid:StnII molar ratio 30:1 to 10:1). OSM vesicles were measured at 24 °C and dihydro-OSM vesicles at 28 °C. Each value is average ± SEM from n = 2. The diameter of the LUVs was 200 ± 20 nm before and after addition of StnII.

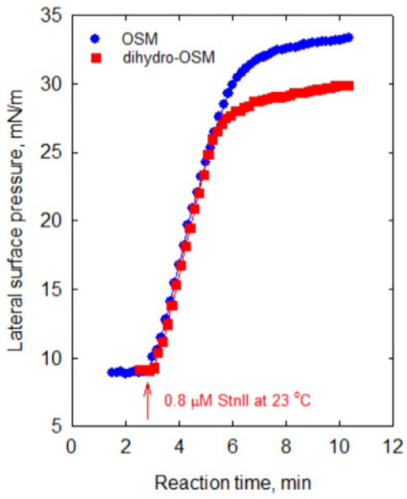

Fig. 5. Penetration of StnII into OSM or dihydro-OSM monolayers. The monolayer was spread to an initial surface pressure of about 9 mN/m, and after 5 min equilibration time, StnII was injected into the stirred buffer subphase to a final concentration of 0.8 μM. The increase in surface pressure, following toxin penetration into the monolayer, was followed as a time function at 23 °C. The curves shown are representative of three identical experiments performed with OSM or dihydro-OSM monolayers.

dihydro-OSM molecules became stronger (compared to the situation in OSM monolayers) and toxin penetration ceased at a lower effective surface pressure.

3.4. Does interference with interfacial hydrogen bonding affect membrane association and pore formation by StnII?

Finally, to further examine how hydrogen bonding in the SM domains affected StnII membrane binding and subsequent pore formation, we used increasing concentrations of BA to interfere with interfacial hydrogen bonding in OSM and dihydro-OSM LUV bilayers. We observed that whereas BA enhanced StnII-induced pore formation in dihydro-OSM bilayers (Fig. 6), it did not show a similar stimulatory effect on StnII-induced pore formation in OSM LUV bilayers, under the conditions used (suggesting that pore formation with OSM at the toxin concentration used was not hydrogen-bonding limited). In addition to affecting hydrogen bonding at the bilayer interface, BA also affected acyl chain order, as determined from DPH anisotropy measurements (Fig. 7). However, the concentration-dependent effect of BA on acyl chain order was equal in both (OSM and dihydro-OSM) bilayers.

4. Discussion

In this study we present evidence that sticholysin interaction with SM membranes is very different from sticholysin interaction with dihydro-SM membranes. The differences were clearly revealed using different experimental approaches: (i) we observed much slower sticholysin-induced calcein release from dihydro-SM bilayers than from SM bilayers (Fig. 1); (ii) we measured much less total binding of StnII to supported bilayers (SPR, Fig. 2) and LUVs (ζ-potential, Fig. 3) prepared from dihydro-OSM as compared to OSM bilayers; (iii) dihydro-OSM vesicles failed to efficiently compete with OSM vesicles for StnII binding, as determined from a competition assay (Fig. 4); (iv) StnII penetration into dihydro-OSM monolayers was less efficient at higher surface pressures as compared to OSM monolayers (Fig. 5). Our working hypothesis is that the differing intermolecular hydrogen bonding properties of SM and dihydro-SM may explain all our results.

Let us first review the literature evidence that hydrogen bonding among dihydro-SMs is stronger than (or at least different from) that between SMs. The first studies on the properties of SM and dihydro-

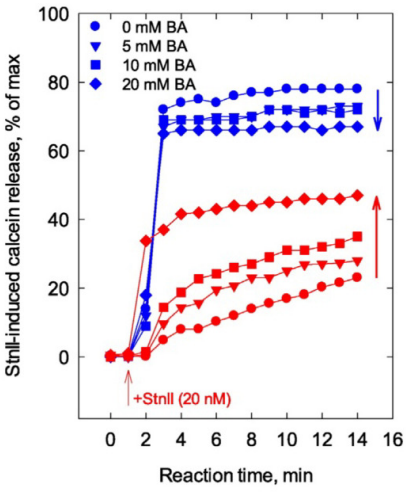

Fig. 6. Effects of benzyl alcohol on StnII-induced calcein release in LUVs prepared from OSM (blue symbols, top four lines) or dihydro-OSM (red symbols, bottom four lines). Calcein-entrapped LUVs were exposed to indicated concentrations of BA (for 30 min), and then StnII was added (red arrow). Each value is average ± SEM from n = 2. Identical red and blue symbols have indicated BA concentrations.

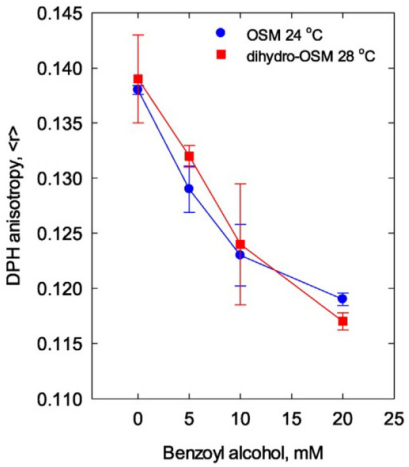

Fig. 7. Effects of benzyl alcohol on acyl chain order in LUVs prepared from OSM or dihydro-OSM. The effect of BA on acyl chain order was measured from the steady-state anisotropy of DPH in OSM and dihydro-OSM LUVs. Each value is the average ± SEM from n = 3.

SM by FTIR and NMR suggested that both intra- and intermolecular hydrogen bonding was different in bilayers prepared from saturated SM and from dihydro-SM [30,31]. Further, although PSM and dihydro-PSM occupy the same mean molecular area in monolayer membranes, their gel–liquid crystalline-phase transition temperature is different by about 6.5 °C (higher for dihydro-PSM [47]), suggesting a hydrogen-bonding stabilization of the gel phase of dihydro-SM. It was also noted that the rotational correlation time of *N*-DPH-SM was different for PSM and dihydro-PSM bilayers in their fluid phase, and that Prodan partitioning into dihydro-PSM bilayers, as compared to PSM bilayers, was much reduced [47]. Such observations are most likely explained by differing hydrogen-bonding properties of SM and dihydro-SM bilayers.

Furthermore, Kinoshita and coworkers have recently demonstrated that dihydro-18:0-SM shows liquid/liquid phase immiscibility in di-oleoyl-PC bilayers above 60 °C, which was not seen in 18:0-SM/di-oleoyl-PC bilayers [36]. Again, stronger hydrogen bonding in dihydro-SM bilayers was cited as the most likely reason for such a thermostable liquid phase. Finally, we showed that the lateral segregation of dipalmitoyl glycerol is much more enhanced in dihydro-OSM bilayers than in OSM bilayers at equal acyl chain order [37]. It appeared that strong intermolecular hydrogen bonding among dihydro-OSM bilayers caused the segregation of dipalmitoyl glycerol into its own phase, whereas the monomer solubility of dipalmitoyl glycerol in OSM bilayers was much less affected (at comparable bilayer compositions and temperature). All these previous observations are compatible with the present findings, that pore formation by StnI and StnII was markedly different in SM and dihydro-SM bilayers.

Sticholysin-induced calcein release was markedly attenuated in dihydro-SM containing bilayers. This finding could result from weaker sticholysin monomer binding to bilayers, or from hindered lateral diffusion, oligomerization, and pore formation in dihydro-SM containing bilayers. Both processes are likely to be affected by strong intermolecular hydrogen bonding among dihydro-SM molecules. However, we cannot exclude the possibility that the 3OH in SM would be closer to the interface, as compared to the 3OH in dihydro-SM, since the *trans* double bond has a partly polar nature when compared to a single C–C bond. A deeper localization of the 3OH in dihydro-SM could possibly hinder sticholysin association with the bilayer interface in a way observed here.

Our SPR and ζ-potential measurements suggest that total StnII binding to bilayers was reduced in dihydro-SM bilayers. It is therefore possible that strong intermolecular hydrogen bonding between dihydro-SM

molecules can increase the energy barrier for toxin penetration into the interfacial region of the bilayer. Support for this interpretation was given by our monolayer experiments, which showed that StnII penetration into dihydro-OSM monolayers was less efficient at high lateral surface pressures, when compared to OSM monolayers.

Additional support for the involvement of intermolecular hydrogen bonding in regulating membrane association of StnII is given by our BA data. The hydroxyl group of BA allows it to participate in hydrogen bonding similarly as cholesterol. Cholesterol is known to facilitate pore formation by different actinoporins [8,21,48,49]. BA showed a strong activation of StnII-dependent calcein release from dihydro-OSM bilayers. This effect was not dependent on altered packing properties in the bilayer, as evidenced by the similar effects of BA on acyl chain order in both OSM and dihydro-OSM bilayers. OSM bilayers were not affected by BA under the conditions used, probably because pore formation was already maximal and could not further be enhanced. We have observed that BA is capable of enhancing StnII-induced calcein release in any SM-containing bilayer, provided that sub-saturation levels of toxins are used (data not shown). It has previously been shown that EqtII-induced calcein release from LUVs is facilitated by different alkanols [50]. It is likely that the effect of alkanols, BA, and cholesterol on pore formation by actinoporins could be due to effects of the compounds on interfacial hydrogen bonding in SM-containing bilayers. However, we cannot rule out that the free hydroxyl on these compounds could interact with sticholysin and somehow stabilize the membrane association of the toxin.

To conclude, we have shown that pore formation by sticholysins is markedly restricted in bilayers containing dihydro-SM when compared to acyl-chain-matched normal SM. We have preliminary evidence that similar restrictions apply to EqtII-induced pore formation in dihydro-SM-containing bilayers (data not shown). We would not be surprised if other diffusion related or bilayer penetration processes by other proteins are similarly affected by strong intermolecular hydrogen bonding in dihydro-SM-containing bilayers. In fact, it has been observed that enrichment of dihydro SM in cells reduced infectivity of the HIV-1 virus, a process which likely was sensitive to interactions among the dihydro-SMs [51].

Author contributions

All authors contributed in the execution and completion of the study and in the writing of the manuscript. All authors have seen and accepted the final submitted version of the manuscript.

Acknowledgments

The work was funded by generous grants: BFU2012 32404 from the Spanish Ministerio de Ciencia e Innovación (JGG and AMP), a FPU fellowship grant (S.G.-L); the Academy of Finland, the Sigrid Juselius Foundation, and the Åbo Akademi Foundation (JPS). TY was supported in part by the International Collaboration Promotion Program from Osaka University.

References

[1] J. Alegre-Cebollada, M. Oñaderra, J.G. Gavilanes, A. Martínez-del-Pozo, Sea anemone actinoporins: the transition from a folded soluble state to a functionally active membrane-bound oligomeric pore, Curr. Protein Pept. Sci. 8 (2007) 558–572.
[2] G. Anderluh, P. Maček, Cytolytic peptide and protein toxins from sea anemones (*Anthozoa*: *Actiniaria*), Toxicon 40 (2002) 111–124.
[3] B. Bakrač, G. Anderluh, Molecular mechanism of sphingomyelin-specific membrane binding and pore formation by actinoporins, Adv. Exp. Med. Biol. 677 (2010) 106–115.
[4] P. Maček, Polypeptide cytolytic toxins from sea anemones (Actiniaria), FEMS Microbiol. Immunol. 5 (1992) 121–129.
[5] N. Rojko, S.M. Dalla, P. Maček, G. Anderluh, Pore formation by actinoporins, cytolysins from sea anemones, Biochim. Biophys. Acta (2015), http://dx.doi.org/10.1016/j.bbamem.2015.09.007.
[6] G. Anderluh, P. Maček, Dissecting the actinoporin pore-forming mechanism, Structure 11 (2003) 1312–1313.
[7] L. Garcia-Ortega, J. Alegre-Cebollada, S. García-Linares, M. Bruix, A. Martínez-del-Pozo, J.G. Gavilanes, The behavior of sea anemone actinoporins at the water–membrane interface, Biochim. Biophys. Acta 1808 (2011) 2275–2288.
[8] V. De Los Ríos, J.M. Mancheño, M.E. Lanio, M. Oñaderra, J.G. Gavilanes, Mechanism of the leakage induced on lipid model membranes by the hemolytic protein sticholysin II from the sea anemone *Stichodactyla helianthus*, Eur. J. Biochem. 252 (1998) 284–289.
[9] M. Tejuca, M.D. Serra, M. Ferreras, M.E. Lanio, G. Menestrina, Mechanism of membrane permeabilization by sticholysin I, a cytolysin isolated from the venom of the sea anemone *Stichodactyla helianthus*, Biochemistry 35 (1996) 14947–14957.
[10] W.R. Kem, B.M. Dunn, Separation and characterization of four different amino acid sequence variants of a sea anemone (*Stichodactyla helianthus*) protein cytolysin, Toxicon 26 (1988) 997–1008.
[11] I. Ferlan, D. Lebez, Equinatoxin, a lethan protein from *Actinia equina* — purification and characterization, Toxicon 12 (1974) 57–61.
[12] A.E. Mechaly, A. Bellomio, K. Morante, J.M. González-Mañas, D.M. Guérin, Crystallization and preliminary crystallographic analysis of fragaceatoxin C, a pore-forming toxin from sea anemone *Actinia fragacea*, Acta Crystallogr. F 65 (2009) 357–360.
[13] A. Athanasiadis, G. Anderluh, P. Maček, D. Turk, Crystal structure of the soluble form of equinatoxin II, a pore-forming toxin from the sea anemone *Actinia equina*, Structure 9 (2001) 341–346.
[14] S. García-Linares, I. Castrillo, M. Bruix, M. Menendez, J. Alegre-Cebollada, A. Martínez-del-Pozo, J.G. Gavilanes, Three-dimensional structure of the actinoporin sticholysin I. Influence of long-distance effects on protein function, Arch. Biochem. Biophys. 532 (2013) 39–45.
[15] J.M. Mancheño, J. Martin-Benito, M. Martinez-Ripoll, J.G. Gavilanes, J.A. Hermoso, Crystal and electron microscopy structures of sticholysin II actinoporin reveal insights into the mechanism of membrane pore formation, Structure 11 (2003) 1319–1328.
[16] K. Tanaka, J.M. Caaveiro, K. Morante, J.M. Gonzalez-Manas, K. Tsumoto, Structural basis for self-assembly of a cytolytic pore lined by protein and lipid, Nat. Commun. 6 (2015) 6337.
[17] U. Ros, A.J. Garcia-Saez, More than a pore: the interplay of pore-forming proteins and lipid membranes, J. Membr. Biol. 248 (2015) 545–561.
[18] T. Maula, Y.J.E. Isaksson, S. Garcia-Linares, S. Niinivehmas, O.T. Pentikainen, V. Kurze, S. Yamaguchi, T. Yamamoto, S. Katsumura, J.G. Gavilanes, A. Martínez-del-Pozo, J.P. Slotte, 2NH and 3OH are crucial strctural requirements in sphingomyelin for sticholysin II binding and pore formation in bilayer membranes, Biochim. Biophys. Acta 1828 (2013) 1390–1395.
[19] C. Alvarez, J.M. Mancheno, D. Martinez, M. Tejuca, F. Pazos, M.E. Lanio, Sticholysins, two pore-forming toxins produced by the Caribbean Sea anemone *Stichodactyla helianthus*: their interaction with membranes, Toxicon 54 (2009) 1135–1147.
[20] B. Bakrač, I. Gutierrez-Aguirre, Z. Podlesek, A.F. Sonnen, R.J. Gilbert, P. Maček, J.H. Lakey, G. Anderluh, Molecular determinants of sphingomyelin specificity of a eukaryotic pore-forming toxin, J. Biol. Chem. 283 (2008) 18665–18677.
[21] I. Alm, S. García-Linares, J.G. Gavilanes, A. Martínez-del-Pozo, J.P. Slotte, Cholesterol stimulates and ceramide inhibits sticholysin II-induced pore formation in complex bilayer membranes, Biochim. Biophys. Acta 1848 (2015) 925–931.
[22] M.Z. Islam, J.M. Alam, Y. Tamba, M.A. Karal, M. Yamazaki, The single GUV method for revealing the function of antimicrobial, pore-forming toxin, and cell-penetrating peptides or proteins, Phys. Chem. Chem. Phys. 14 (2014) 15752–15767.
[23] A. Filippov, G. Oradd, G. Lindblom, Lipid lateral diffusion in ordered and disordered phases in raft mixtures, Biophys. J. 86 (2004) 891–896.
[24] A. Filippov, G. Oradd, G. Lindblom, Sphingomyelin structure influences the lateral diffusion and raft formation in lipid bilayers, Biophys. J. 90 (2005) 2086–2092.
[25] L. Silva, R.F. de Almeida, A. Fedorov, A.P. Matos, M. Prieto, Ceramide-platform formation and -induced biophysical changes in a fluid phospholipid membrane, Mol. Membr. Biol. 23 (2006) 137–148.
[26] I. Artetxe, C. Sergelius, M. Kurita, S. Yamaguchi, S. Katsumura, J.P. Slotte, T. Maula, Effects of sphingomyelin headgroup size on interactions with ceramide, Biophys. J. 104 (2013) 604–612.
[27] Y. Barenholz, T.E. Thompson, Sphingomyelins in bilayers and biological membranes, Biochim. Biophys. Acta 604 (1980) 129–158.
[28] M. Lonnfors, J.P. Doux, J.A. Killian, T.K. Nyholm, J.P. Slotte, Sterols have higher affinity for sphingomyelin than for phosphatidylcholine bilayers even at equal acyl-chain order, Biophys. J. 100 (2011) 2633–2641.
[29] E. Mombelli, R. Morris, W. Taylor, F. Fraternali, Hydrogen-bonding propensities of sphingomyelin in solution and in a bilayer assembly: a molecular dynamics study, Biophys. J. 84 (2003) 1507–1517.
[30] S.R. Ferguson-Yankey, D. Borchman, K.G. Taylor, D.B. DuPre, M.C. Yappert, Conformational studies of sphingolipids by NMR spectroscopy. I. Dihydrosphingomyelin, Biochim. Biophys. Acta 1467 (2000) 307–325.
[31] C.M. Talbott, I. Vorobyov, D. Borchman, K.G. Taylor, D.B. DuPre, M.C. Yappert, Conformational studies of sphingolipids by NMR spectroscopy. II. Sphingomyelin, Biochim. Biophys. Acta 1467 (2000) 326–337.
[32] J.W. Kok, M. Nikolova-Karakashian, K. Klappe, C. Alexander, A.H. Merrill Jr., Dihydroceramide biology. Structure-specific metabolism and intracellular localization, J. Biol. Chem. 272 (1997) 21128–21136.
[33] P.B. Schneider, E.P. Kennedy, Metabolism of labeled dihydrosphingomyelin in vivo, J. Lipid Res. 9 (1968) 58–64.
[34] D. Borchman, M.C. Yappert, Lipids and the ocular lens, J. Lipid Res. 51 (2010) 2473–2488.
[35] R.M. Epand, Cholesterol in bilayers of sphingomyelin or dihydrosphingomyelin at concentrations found in ocular lens membranes, Biophys. J. 84 (2003) 3102–3110.

[36] M. Kinoshita, N. Matsumori, M. Murata, Coexistence of two liquid crystalline phases in dihydrosphingomyelin and dioleoylphosphatidylcholine binary mixtures, Biochim. Biophys. Acta 1838 (2014) 1372–1381.
[37] T. Yasuda, Md.A. Al Sazzad, N.Z. Jäntti, O.T. Pentikäinen, J.P. Slotte, The influence of hydrogen bonding on sphingomyelin/colipid interactions in bilayer membranes, Biophys. J. (2016) (in press).
[38] J. Alegre-Cebollada, G. Clementi, M. Cunietti, C. Porres, M. Oñaderra, J.G. Gavilanes, A.M. Pozo, Silent mutations at the 5′-end of the cDNA of actinoporins from the sea anemone *Stichodactyla helianthus* allow their heterologous overproduction in *Escherichia coli*, J. Biotechnol. 127 (2007) 211–221.
[39] M. Kuikka, B. Ramstedt, H. Ohvo-Rekilä, J. Tuuf, J.P. Slotte, Membrane properties of D-erythro-N-acyl sphingomyelins and their corresponding dihydro species, Biophys. J. 80 (2001) 2327–2337.
[40] B. Terova, J.P. Slotte, T.K. Nyholm, Miscibility of acyl-chain defined phosphatidylcholines with N-palmitoyl sphingomyelin in bilayer membranes, Biochim. Biophys. Acta 1667 (2004) 182–189.
[41] R. Cohen, Y. Barenholz, S. Gatt, A. Dagan, Preparation and characterization of well defined D-*erythro* sphingomyelins, Chem. Phys. Lipids 35 (1984) 371–384.
[42] L. Pedrera, M.L. Fanani, U. Ros, M.E. Lanio, B. Maggio, C. Alvarez, Sticholysin I-membrane interaction: an interplay between the presence of sphingomyelin and membrane fluidity, Biochim. Biophys. Acta 1838 (2014) 1752–1759.
[43] S. Jaikishan, A. Bjorkbom, J.P. Slotte, Sphingomyelin analogs with branched N-acyl chains: the position of branching dramatically affects acyl chain order and sterol interactions in bilayer membranes, Biochim. Biophys. Acta 1798 (2010) 1987–1994.
[44] J.R. Lakowicz, Principles of Fluorescence Spectroscopy, Kluwer Academic/Plenum Publishers, New York, 1999.
[45] J.P. Slotte, The importance of hydrogen bonding in sphingomyelin's membrane interactions with co-lipids, Biochim. Biophys. Acta 1858 (2015) 304–310.
[46] V. Lukacova, M. Peng, R. Tandlich, A. Hinderliter, S. Balaz, Partitioning of organic compounds in phases imitating the headgroup and core regions of phospholipid bilayers, Langmuir 22 (2006) 1869–1874.
[47] T. Nyholm, M. Nylund, A. Soderholm, J.P. Slotte, Properties of palmitoyl phosphatidylcholine, sphingomyelin, and dihydrosphingomyelin bilayer membranes as reported by different fluorescent reporter molecules, Biophys. J. 84 (2003) 987–997.
[48] J. Alegre-Cebollada, A. Martínez-del-Pozo, J.G. Gavilanes, E. Goormaghtigh, Infrared spectroscopy study on the conformational changes leading to pore formation of the toxin sticholysin II, Biophys. J. 93 (2007) 3191–3201.
[49] D. Martinez, A. Otero, C. Alvarez, F. Pazos, M. Tejuca, L.M. Eliana, I. Gutierrez-Aguirre, A. Barlic, I. Iloro, A.J. Luis, J.M. Gonzalez-Manas, E. Lissi, Effect of sphingomyelin and cholesterol on the interaction of St II with lipidic interfaces, Toxicon 49 (2007) 68–81.
[50] P. Maček, M. Zecchini, K. Stanek, G. Menestrina, Effect of membrane-partitioned n-alcohols and fatty acids on pore-forming activity of a sea anemone toxin, Eur. Biophys. J. 25 (1997) 155–162.
[51] C.R. Vieira, J.M. Munoz-Olaya, J. Sot, S. Jimenez-Baranda, N. Izquierdo-Useros, J.L. Abad, B. Apellaniz, R. Delgado, J. Martinez-Picardo, A. Alonso, J. Casas, J.L. Nieva, G. Fabrias, S. Manes, F.M. Goni, Dihydrosphingomyelin impairs HIV-1 infection by rigidifying liquid-ordered membrane domains, Chem. Biol. 17 (2010) 766–775.

SECTION C

THE ROLE OF PARTICULAR RESIDUES
OF ACTINOPORINS

ARTICLE V

Three-dimensional structure of the actinoporin sticholysin I. Influence of long-distance effects on protein function

García-Linares, S., Castrillo, I., Bruix, M., Menéndez, M., Alegre-Cebollada, J., Martínez-del-Pozo, Á. and Gavilanes, J. G. (2013). *Arch Biochem Biophys* 532(1): 39-45.

Estructura tridimensional de la actinoporina esticolisina I. Influencia de efectos a larga distancia en la función de la proteína

Las actinoporinas son proteínas solubles en agua con la habilidad de formar poros mediante su inserción en membranas biológicas. Constituyen una familia de proteínas con un alto grado de identidad de secuencia pero distintas actividades hemolíticas, lo que sugiere que mínimos cambios conformacionales se traducen en diferencias funcionales importantes. Un buen ejemplo de esta situación es el caso de la anémona *Stichodactyla helianthus*, que produce dos actinoporinas muy similares, esticolisina I (StnI) y II (StnII), cuya eficiencia hemolítica es muy diferente. Con esta idea, dado que ya se conoce la estructura tridimensional de StnII en alta resolución, se ha resuelto la correspondiente a StnI, de manera que podamos analizar la influencia de residuos específicos en la conformación y actividad de estas proteínas. Además, se han obtenido cinco mutantes de StnI menos hemolíticos por mutagénesis al azar. Todas estas mutaciones se encuentran en regiones relevantes para la proteína porque posiblemente están involucradas en cambios conformacionales asociados a la formación del poro, que ocurre después de la unión de la proteína a la membrana y suponen reordenamientos a larga distancia de la cadena polipeptídica de las actinoporinas.

Archives of Biochemistry and Biophysics 532 (2013) 39–45

Contents lists available at SciVerse ScienceDirect

Archives of Biochemistry and Biophysics

journal homepage: www.elsevier.com/locate/yabbi

Three-dimensional structure of the actinoporin sticholysin I. Influence of long-distance effects on protein function

Sara García-Linares [a], Inés Castrillo [b], Marta Bruix [b], Margarita Menéndez [c], Jorge Alegre-Cebollada [a,1], Álvaro Martínez-del-Pozo [a,*], José G. Gavilanes [a,*]

[a] Departamento de Bioquímica y Biología Molecular I, Facultad de Ciencias Químicas, Universidad Complutense, 28040 Madrid, Spain
[b] Departamento de Química Física Biológica, Instituto de Química Física "Rocasolano", CSIC, Serrano 119, 28006 Madrid, Spain
[c] Instituto de Química-Física "Rocasolano", C.S.I.C., and Centro de Investigación Biomédica en Red de Enfermedades Respiratorias (CIBERES), Madrid, Spain

ARTICLE INFO

Article history:
Received 10 October 2012
and in revised form 18 January 2013
Available online 29 January 2013

Keywords:
Actinoporin
Sticholysin
NMR structure
Dynamics
Equinatoxin

ABSTRACT

Actinoporins are water-soluble proteins with the ability to form pores upon insertion into biological membranes. They constitute a family of proteins with high degree of sequence identities but different hemolytic activities, suggesting that minor conformational arrangements result in major functional changes. A good example of this situation is the sea anemone *Stichodactyla helianthus* which produces two very similar actinoporins, sticholysins I (StnI) and II (StnII), but of very different hemolytic efficiency. Within this idea, given that the high resolution three-dimensional structure of StnII is already known, we have now solved that one corresponding to StnI in order to analyze the influence of particular residues on the conformation and activity of these proteins. In addition, random mutagenesis has been also used to produce five less hemolytic variants of StnI. All these mutations map to functionally relevant regions because they are probably involved in conformational changes associated with pore formation, which take place after membrane binding, and involve long-distance rearrangements of the polypeptide chain of actinoporins.

Introduction

Actinoporins are an intriguing family of unique proteins produced by different sea anemone species from the *Actinaria* order [1–7]. They are highly basic, made of a single polypeptide chain of around 175 amino acid residues and remain stable as monomeric water-soluble proteins, yet they can oligomerize and integrate into lipid membranes [1–7]. Actinoporins are members of the larger family of pore-forming toxins [2](PFTs) [8] and are classified as α-PFTs because their mechanism of pore formation involves the insertion of an α-helix within the cell membrane [8–12]. These pore-forming properties explain their fast and efficient hemolytic activity [12–15].

Actinoporins from each anemone species appear as multigene families displaying high sequence similarity (between 60% and 80% of identity) [1–3,7,16–19]. Unexpectedly, a small number of sequence changes results in large differences in terms of aqueous solubility and hemolytic activity [7,19–21]. This observation has been functionally explained assuming that the presence of a large number of similar isotoxins in a single venomous secretion probably increases the prey range for a particular species [22]. A good representative example of this situation can be found in the tentacles of the sea anemone *Stichodactyla helianthus* which produce sticholysins I (StnI) and II (StnII), two actinoporins displaying 91.0% sequence identity but showing quite different hemolytic activities [4,20].

The three-dimensional monomeric structure of several actinoporins is already known [23–27], including that one corresponding to StnII [25]. All of them display a common fold characterized by a β-sandwich of 10–12 β-strands flanked by two α-helices which interact with both sides of the β-sandwich. This can be seen in Fig. 1, where the new structure reported now (StnI, in red) is compared with those ones of StnII (Fig. 1B, StnII blue) and EqtII (Fig. 1C, EqtII blue), which were already known [23–27]. One of the helices is always located near the N-terminal end. This N-terminal portion, about 30 residues long, can adopt alternative conformations without disrupting the β-sandwich motif [23], and has been proposed to form the pore walls [27–30]. Three additional regions have been also shown to participate in membrane recognition: an exposed cluster of

* Corresponding authors. Fax: +34 91 394 4159.
E-mail addresses: alvaro@bbm1.ucm.es (Á. Martínez-del-Pozo), ppgf@bbm1.ucm.es (J.G. Gavilanes).
[1] Present address: Dept. of Biological Sciences, Columbia University, 808 Northwest Corner Bldg., 550 W. 120th St., New York, NY 10027, USA.
[2] *Abbreviations used:* Chol, Cholesterol; CD, circular dichroism; DOPC, dioleylphosphatidylcholine; Fra, fragaceatoxins produced by *Actinia fragacea*; Eqt, equinatoxins produced by *Actinia equina*; MOPS, 3-(N-morpholino)propanesulfonic acid; PFT, pore-forming toxin; POC, phosphocholine; SM, sphingomyelin; Stn, sticholysins produced by *Stichodactyla helianthus*; wt, wild-type.

0003-9861/$ - see front matter © 2013 Elsevier Inc. All rights reserved.
http://dx.doi.org/10.1016/j.abb.2013.01.005

aromatic residues, an array of basic amino acids, and a phosphocholine (POC) binding site [24,25,27,30–32]. Thus, the conservation of amino acid sequences is not only reflected but rather supported by the high degree of conformational identity. From this point of view, the observations made allow drawing two main conclusions. First, the general overall fold of actinoporins is absolutely required for their unique function and, therefore, it has been conserved along evolution [31]. Second, minor changes produce subtle conformational modifications with deep impact on the function of these proteins. However, very little is known regarding these conformational transitions and the residues that participate in the intramolecular communication between the membrane-binding regions and the N-terminal α-helix that irreversibly inserts into the membrane.

Within this idea, we have solved the monomeric three-dimensional structure of StnI in aqueous solution by NMR and studied its dynamical properties. Random mutagenesis has been used to select five StnI mutants that display decreased hemolytic activity. Altogether, the results obtained are discussed in terms of the involvement of particular actinoporins regions in the changes that occur after membrane binding.

Experimental procedures

Proteins production and purification

The cDNA coding for StnI mutants G26D, V28E, S53T, D57A, and E62G were obtained by random mutagenesis as described elsewhere [32] and selected after screening for a less hemolytic phenotype using blood-agar plates [32]. The unlabeled versions of the wild-type and the different mutants of StnI, as well as the double uniformly labeled $^{13}C/^{15}N$ wild-type StnI samples, were produced using an *Escherichia coli* expression system following a protocol previously described [20]. For the labeled form, cells were grown in a M9 minimal medium with $^{15}NH_4Cl$ (1 g/l) and $^{13}C_6$-glucose (4 g/l) as the sole nitrogen and carbon sources. Protein purification was achieved by ion exchange chromatography on CM52 cellulose equilibrated in 50 mM Tris–HCl at different pH values, depending on the estimated pI value of the protein purified (pH 6.0 for V28E and G26D; pH 6.8 for S53T; pH 7.8 for D57A and E62G). The homogeneity of all protein samples used was analyzed by SDS–PAGE and amino acid analysis after acid hydrolysis of the proteins (5.7 M HCl, 24 h, 110 °C). These amino acid analyses were

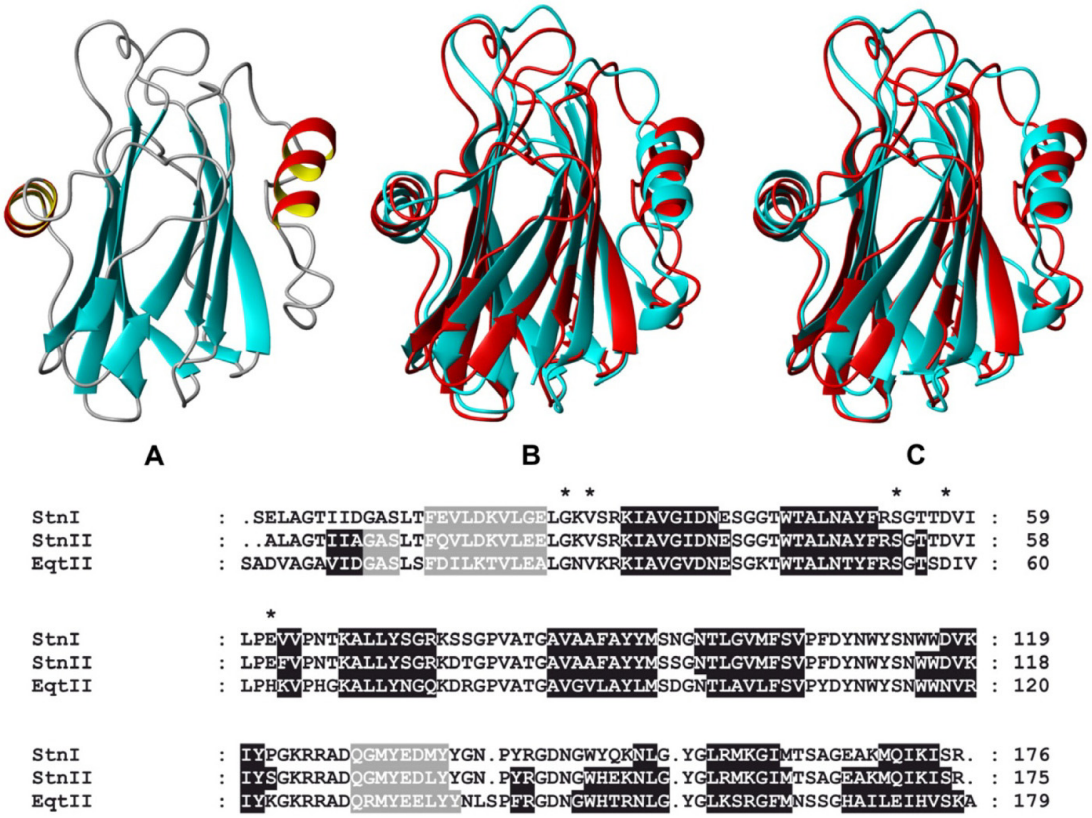

Fig. 1. *Upper panel*: Diagrams corresponding to the 3D structure of StnI (A) as well as its comparison (StnI in red) with those ones of StnII (B, StnII blue) [25] and EqtII (C, EqtII blue) [23]. Diagrams were constructed from the atomic coordinates deposited in PDB (Protein Data Bank, references 2KS4 for StnI, 1GWY for StnII, 1IAZ for EqtII). Structures were fitted by considering the atoms of the peptide bonds of residues 15–24, 68–75, 85–93, 97–105 and 129–136 (StnI), 14–23, 67–74, 84–92, 96–104 and 128–135 (StnII), and 16–25, 69–76, 86–94, 99–106 and 130–137 (EqtII). These peptide segments correspond to the two helical segments of the three proteins as well as three of their longer β strands. The resulting RMSD values were 1.355 Å for the pair StnI/StnII and 1.194 Å for StnI/EqtII. Images and fittings were generated by the MOLMOL program [41]. *Lower panel*: Sequence alignment of the three considered actinoporins, indicating the stretches corresponding to their different elements of ordered secondary structure (helical segments in grey, and β strands in black). The residues mutated in the StnI variants studied appear labeled with an asterisk. (For interpretation of the references to color in this figure legend, the reader is referred to the web version of this article.)

Table 1
Amino acid changes in StnI correspond to the mutations detected in the plasmids isolated from the less-hemolytic colonies of transformed *E. coli* RB791 cells that still produced significant amounts of the protein. This table summarizes some of the features of the purified proteins.

StnI variants[a]	Purification yield (mg/L)	$E_{(0.1\%,\ 280\ nm,\ 1\ cm)}$	Q^b	$HC_{50}{}^c$ (nM)	Relative HC_{50} value[d]	T_m (°C)[e]
G26D	15	2.8	1.06	49.8	11.3	58
V28E	27	2.7	1.05	101.6	23.1	59
S53T	18	2.7	1.12	25.2	5.7	62
D57A	14	2.7	0.99	69.1	15.7	59
E62G	7	2.6	1.00	94.1	21.4	64
Wild-type	13[f]	2.6	1.00	4.4	1.0	65

[a] Amino acid numeration is given according to the sequence of the wild-type protein produced by the anemone *S. helianthus*.
[b] Relative fluorescence quantum yield for excitation at 275 nm to that of wild-type StnI considered as 1.00.
[c] Concentration (nM) of actinoporin required for 50% hemolysis. The corresponding value for StnII is 1.4 nM [32].
[d] Relative HC_{50} value is defined as mutant HC_{50}/wild-type HC_{50}. This value increases as the hemolytic activity is reduced.
[e] Mid point temperature of the thermal denaturation transition.
[f] Taken from Alegre-Cebollada et al., 2007 [20].

performed on a Biochrom 20 automatic analyzer (Pharmacia, Uppsala, Sweden). The results were in agreement with those expected and were used to estimate extinction coefficients (Table 1) and protein concentrations for each mutant.

Spectroscopic characterization

Absorbance measurements were carried out on an Uvikon 930 spectrophotometer (Kontron Instruments, Milan, Italy). CD spectra were obtained on a Jasco 715 spectropolarimeter (Easton, MD) at 50 nm/min scanning speed. Optical path cells (0.1 cm) were employed in the far-UV region, whereas 1-cm optical path cells were used in the 250–350 nm range. Proteins were dissolved in 15 mM MOPS buffer, pH 7.5, containing 0.1 M NaCl (0.2–1 mg/mL protein concentration). At least four spectra were averaged to obtain the final spectrum. CD measurements were also employed to study the thermal stability of the mutants, as described before [33,34]. At neutral pH, thermal denaturation of StnI occurs simultaneously with a fast aggregation, which can be monitored as optical path clarification (aggregates settling) by CD measurements at 218 nm. Temperature scans were carried out at a rate of 0.5 °C/min. Results are expressed as percentages of the total CD variation versus temperature. T_m values correspond to the temperature at the midpoint of the monophasic thermal transition.

NMR samples and assignment

Typically, samples contained up to 0.5 mM of protein and were prepared in both 90% H_2O/10% D_2O and D_2O at pH 4.0 (uncorrected for deuterium isotope effects). Sodium-4,4-dimethyl-4-silapentane-1-sulfonate (DSS) was used as internal ^1H chemical shift reference. Protein NMR assignment was previously described [35] and the ^1H, ^{13}C and ^{15}N chemical shifts are deposited in the BioMagResBank (http://www.bmrb.wisc.edu/) under accession number 15927.

NMR structure calculation

The NMR spectra used to obtain the protein structure were recorded in a Bruker AV-800 instrument equipped with cryoprobe and field gradients. All data were acquired and processed with TOPSPIN (version 1.3) (Bruker, Germany) at 25 °C. NOE assignments were obtained from 3D ^{15}N-NOESY-HSQC, ^{13}C-NOESY-HSQC spectra with 50 ms mixing times and 2D ^1H-^1H NOESY spectra with 80 ms mixing time in 90% H_2O/10% D_2O and D_2O solutions. The spectral analysis was performed with the program Sparky (version 3.1) [36] on the bases of the published assignments [35]. The structure calculation was performed with CYANA [37] using the automatic NOE assignment facility combined with lists of manually assigned NOEs. NOE intensities were calibrated with CYANA and used as upper distance limit constraints in the calculations. Moreover, backbone dihedral angle constraints were determined from chemical shift values using TALOS [38] and incorporated into the structure calculation protocol. Initially, 100 conformers were generated that were forced to satisfy the experimental data during a standard automatic CYANA protocol based on simulated annealing using torsion angle dynamics. The 20 conformers with the lowest final CYANA target function values were selected and subjected to 2000 steps of energy minimization, in the presence of the NMR restraints, using the generalized Born continuum solvation model implemented in AMBER9 [39] with a non-bonded cutoff of 10 Å. The final structure quality was checked with PROCHECK-NMR [40]. The coordinates have been deposited in the PDB under the accession number 2KS4. Statistics of the calculation are summarized in Table 2. The program MOLMOL [41] was used for molecular display and structure analysis.

NMR dynamics

All NMR relaxation experiments were carried out at the same conditions described above. Conventional ^{15}N heteronuclear relaxation rates R_1, R_2 and NOE data were determined. To this end, a series of 2D heteronuclear correlated spectra using sensitivity enhanced gradient pulse scheme [42] were recorded. The relaxation delay times were set as follows for R_1: 5, 50, 150, 300, 600, 800, 1000 and 1200 ms; and for R_2: 15.6, 31.3, 46.8, 62.5, 78.2, 93, 109.4 and 125 ms. The relaxation rate constants R_1 and R_2 were obtained from the exponential fits of the measured crosspeak intensities. The uncertainty was taken as the error in the fit of the decay function. For the NOE measurement, the experiments with and without proton saturation were acquired simultaneously in an interleaved manner with a recycling delay of 5 s, and were splitted during processing into separate spectra for analysis. The values for the heteronuclear NOEs were obtained from the ratio intensities of the resonances according to: I_{sat}/I_{ref}. Here, the uncertainty was estimated to be about 5%.

Analytical ultracentrifugation

Ultracentrifugation was performed on a Beckman-Coulter OPTIMA XL-1 analytical ultracentrifuge at 20 °C. The sample solution contained StnI in water at pH 4.0. Both equilibrium sedimentation (final velocity 25,000 rpm and 500 μM protein concentration) and sedimentation velocity (final velocity 45,000 rpm and 5.0 μM StnI) experiments were conducted. Differential sedimentation coefficients, c(s), were calculated by least squares boundary modeling of sedimentation velocity data using the program SEDFIT [43]. The SEDNTERP program [44] was used to calculate protein specific

Table 2
Structural statistics of the 20 best NMR structures of sticholysin I.

NOE distances and diedral constraints	*Number*
No. of short-range distances ($\|i-j\| \leqslant 1$)	1282
No. of medium-range distances ($1 < \|i-j\| < 5$)	303
No. of long-range distances ($\|i-j\| \geqslant 5$)	1116
No. of angular restraints (ϕ, ψ)	182
No. of total restraints	2883
Structure calculation (20 structures)	*Mean, (max to min)*
CYANA target function value	0.70±0.22 (0.22 to 1.09)
Total AMBER energy (kcal/mol)	−5895.6 (-5761.3 to −5983.7)
van der Waals energy (kcal/mol)	−1245.5 (−1213.3 to −1284.7)
Electrostatic energy (kcal/mol)	−10668.3 (−9989.6 to −11358.7)
RMSD (Å)	*Backbone, heavy atoms*
All residues	1.21 ± 0.23, 1.87 ± 0.23
Secondary structure	0.59 ± 0.12, 1.26 ± 0.16
Well defined regions: 1–24,31–75,85–105,117–162,170–176	0.78 ± 0.14, 1.36 ± 0.14
Ramachandran plot analysis (%)	
Most favored	74.7
Allowed	24.9
Add. allowed	0.4
Disallowed	0.0

volumes from the amino acid sequences, and the buffer viscosity and density. The HeteroAnalysis program [45] was used to analyze the equilibrium results.

Hemolysis assay

Hemolysis assays were performed in 96-multiwell plates as previously described [20,32,33]. Briefly, erythrocytes from heparinized sheep blood were washed in 10 mM Tris–HCl buffer, pH 7.4, containing 0.145 M NaCl, and diluted with the same buffer to a final OD_{655} of 0.5. The hemolysis was followed as a decrease in OD_{655} after addition of the erythrocyte suspension to twofold serial dilutions of the proteins. An Expert 96 microplate reader (Asys Hitech, GmbH, Eugendorf, Austria) was employed to measure OD_{655}. The value obtained with 0.1% (w/v) Na_2CO_3 was considered as 100% hemolysis. HC_{50} (Table 1) is the protein concentration required to produce 50% hemolysis.

Assay of phospholipid vesicle binding

SM/DOPC/Chol (1:1:1) phospholipid vesicles were prepared as previously described [46]. A phospholipid (1–5 mg) solution in 2:1 (v/v) chloroform/methanol was dried under a flow of nitrogen, and the dry film obtained was used to prepare a lipid dispersion by adding 1–5 mL Tris/NaCl (10 mM Tris–HCl, pH 7.4, 145 mM NaCl), briefly vortex-mixing, and incubating for 1 h at 37 °C. This suspension of multilamellar vesicles was further subjected to five cycles of extrusion through polycarbonate filters (100-nm pore size) to obtain a homogeneous population of unilamellar vesicles. Binding assays were performed by ultracentrifugation essentially as previously described [46,47]. Several protein/vesicle samples were prepared at different lipid to protein molar ratios. The samples were incubated at 37 °C for 1 h and then centrifuged at 164,000 g for 1 h 45 min at 4 °C in a 42.2 Ti rotor, using Beckman cellulose propionate tubes (7 × 20 mm). When centrifuged under these conditions, lipid vesicles sediment, as checked by using both traces of radioactive phospholipids and light dispersion measurements. There was no significant protein adsorption to the centrifuge tubes. The amount of StnI that did not co-sediment with the vesicles was determined from the absorbance spectra of the supernatant, and the concentration of protein bound to the liposomes was then calculated taking into account the initial concentration of protein (10 μM in all cases) and the absorption coefficient of the protein (Table 1) [20].

Results

Global fold of actinoporin StnI

Figs. 1 and 2, and Supplementary 1 show the three-dimensional structure of StnI in solution determined on the basis of the NMR restraints summarized in Table 2. The resulting structure is well defined and satisfies the experimental constraints with small deviations from the idealized covalent geometry. The global fold is very similar to that one shown by the other actinoporins whose monomeric water-soluble structure has been previously solved: wild-type StnII [25] (Fig. 1B), its R29Q and Y111N variants [48,49], FraC [27], and EqtII [23,24] (Fig. 1C).

Structure and dynamic properties of StnI

The secondary structure of StnI is composed of two α-helices (residues 15–24 and 129–136) and ten β strands (31–38, 44–51, 63–64, 68–75, 85–93, 97–105, 117–121, 151–152, 156–161 and 170–174) arranged according to the classical β-sheet actinoporin structural motif (Figs. 1 and 2 and S1). Structural variability was only observed in segments corresponding to the loops connecting these regular secondary elements. This is especially evident for loops 76–84 and 106–116 (Fig. S1) which have RMSD values above the mean. These loops are topologically located in the same region of the protein which also would correspond to the membrane interaction face, based on the studies performed for this and other actinoporins [50].

^{15}N NMR relaxation was used to characterize the dynamic properties of StnI in solution. Relaxation data were obtained for 147 of the 176 residues present in StnI (Fig. 2). Good correlations could be established between structure and experimental relaxation data. Thus, most residues appearing along the regular secondary structure elements exhibited heteronuclear NOE values close to the theoretical maximum as an indication of high rigidity existing in those regions. In contrast, N- and C-terminal residues, and some loop regions, showed decreased longitudinal relaxation rates (R_1), variable transversal relaxation rates (R_2) and low NOE values suggesting a much higher mobility on the ps-time scale.

Differences in R_1 values were not significant along the sequence (mean values 0.9 s^{-1}). More variability was certainly observed in the NOE and R_2 data, with mean values of 0.8 and 21.9 s^{-1}, respectively. Low R_2 values correlate with a decrease in the NOE ratio in the N-terminus, residues 27 and 28, and residues in the segment 78–86, showing that these regions are the most flexible ones of the protein structure. As observed in R29Q and Y111N StnII variants [51], other regions of StnI with low or average NOE values present higher R_2 values with respect to the mean. These correspond to the C-terminal part of the protein sequence (residues 106–176), with the highest values in the stretch 108–114 in the membrane interaction face. This suggests that these regions are affected by conformational exchange processes in the μs-ms time scale.

Characterization of purified StnI mutant variants

Using a PCR-based random mutagenesis approach, five different StnI mutant variants showing a less hemolytic phenotype, were selected and purified to homogeneity with yields ranging from 7 to 25 mg/L of culture medium (Table 1). The location of the mutations found is shown in Figs. 1 and 2.

As expected, taking into account that no aromatic residues were changed, the measured $E_{(0.1\%,\ 280\ nm,\ 1\ cm)}$ values were within the 5%

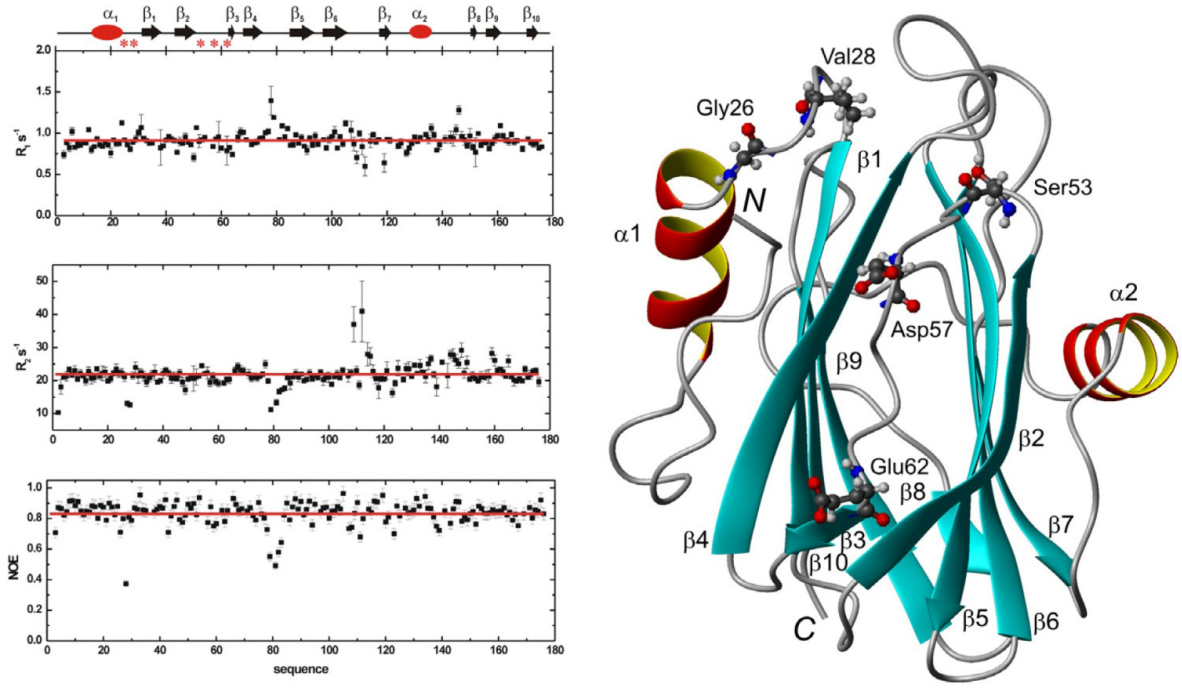

Fig. 2. *Left panel.* Distribution of the relaxation parameters R_1, R_2 and heteronuclear NOE of StnI as a function of the protein sequence. Red horizontal lines represent the mean values. The different secondary structural elements are represented at the top part of the figure. Ellipses for α-helices and arrows for β-strand regions. The residues mutated in the StnI variants studied appear labeled with an asterisk. *Right panel.* Diagram of the three-dimensional structure of StnI indicating the location of the five mutated positions Gly26, Val28, Ser53, Asp57 and Glu62. The different elements of ordered secondary structure, as well as the N- and C-terminal ends, are also labeled. Diagram was constructed from the atomic coordinates deposited in PDB (Protein Data Bank, reference 2KS4 for StnI). Image was generated by the MOLMOL program [41]. (For interpretation of the references to colour in this figure legend, the reader is referred to the web version of this article.)

range of the corresponding value of wild-type StnI (Table 1). Far-UV circular dichroism spectra of these protein variants revealed a similar secondary structure compared to that of wild-type StnI (Fig. S2A). No more than 10% variation in secondary structure content was compatible with the obtained spectra. The fluorescence emission spectra of the mutant forms were also very similar to that of the wild-type protein (Fig. S2B). Finally, the thermal denaturation profiles (Fig. S2C) showed that all the mutant variants exhibited only slightly lower T_m values (Table 1), indicating that the stability of the mutants was not greatly altered by the mutations.

In perfect agreement with the procedure followed to select them, all the purified mutant variants exhibited a decreased hemolytic activity (Fig. 3), confirming the original phenotype. This diminished activity was reflected in higher HC_{50} values ranging from 4.4 nM for the wild-type protein to 101.6 nM for the V28E variant (Table 1).

Binding to SM:DOPC:Chol lipid vesicles

Binding of the isolated StnI mutant variants to lipid vesicles was studied by ultracentrifugation. The results obtained are shown in Fig. 4. Saturation of the protein binding to the vesicles was observed at about 150–200 lipid to protein molar ratio, irrespective of the mutant variant considered. The StnI S53T mutant was the only one showing a significantly different binding behavior.

Diffusion properties of StnI studied by analytical ultracentrifugation

At the NMR concentration (0.50 mM) of StnI (MW 19410 Da), the data obtained from equilibrium sedimentation are best fitted by monomer ↔ dimer equilibrium. The apparent molecular weight was 27800 Da indicating that under conditions used for the NMR relaxation and structural studies StnI showed tendency to associate. A very similar situation has been also demonstrated before for the wild-type StnII [52] and the two StnII mutants with decreased lytic activity mentioned above [48,49,51]. Sedimentation velocity experiments performed at 5 μM protein concentration revealed that StnI behaves as a monomeric species in diluted solution (Fig. S3), as well as the mutants studied (data not shown).

Discussion

The reported three-dimensional structure of StnI corroborates the extremely high similarity characterizing actinoporins (Fig. 1), confirming that the fold of actinoporins is an optimized structure for full performance of these proteins, thus limiting three-dimensional structure variability along the evolution [31].

Most of the mutated positions selected in this study are conserved within the amino acid sequences of actinoporins. Thus, residues at positions 26, 53 and 57 are maintained for all the actinoporins known. In some instances Val28 appears as Ile, but it is still maintained for most of them too. The residue at position 62 is the most variable one among those five mutated. Nevertheless, among the 27 actinoporin sequences known so far it is still Glu in all them except for seven proteins where it appears substituted by His or Tyr. All the five mutated residues correspond to positions where no regular secondary structure is observed for StnI (Figs. 1 and 2). Thus, Gly26 and Val28 are part of the loop connecting the N-terminal α-helix (α1 helix; residues 15–24) and the β1-strand (residues 31–38). Ser53 flanks the C-terminal end of the β2-strand (residues 44–51). Altogether with Asp57 and Glu62, the three of

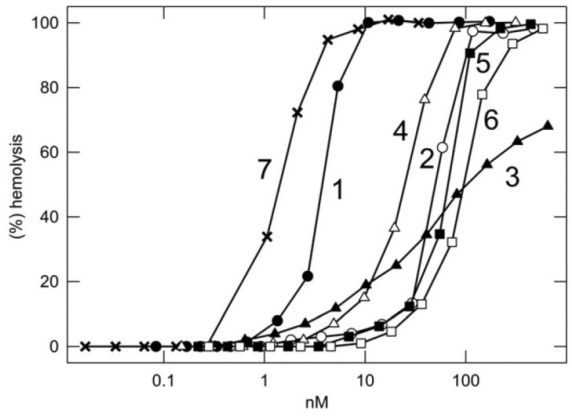

Fig. 3. Hemolytic activity (% hemolysis) of sticholysin variants: (1, solid circles) StnI; (2, empty circles) G26D; (3, solid triangles) V28E; (4, empty triangles) S53T; (5, solid squares) D57A; (6, empty squares) E62G; (7, crosses) Stn II. Results are expressed as percentages of the hemolysis produced by 0.1% (w/v) Na_2CO_3.

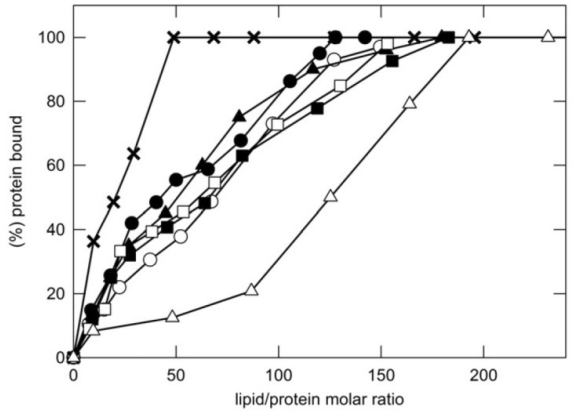

Fig. 4. Binding of sticholysin variants to SM:DOPC:Chol (1:1:1) vesicles. Protein bound (expressed as percentage) was calculated as the difference of total protein *minus* protein remaining in the supernatant after co-sedimentation of the protein-lipid vesicles complexes by ultracentrifugation (100% being the total protein amount present in the assay): (solid circles) StnI; (empty circles) G26D; (solid triangles) V28E; (empty triangles) S53T; (solid squares) D57A; (empty squares) E62G; (crosses) StnII.

them belong to the loop linking β2 and β3 strands (β3-strand; residues 63–64). However, only the relaxation data corresponding to position 28 suggest the presence of high flexibility as they are characterized by low NOE and relaxation rates values (Fig. 2). The other four residues at positions 26, 53, 57 and 62 of StnI show relaxation parameters in the mean R_1, R_2 and NOE values, indicating that they behave as part of the rigid protein core, with no important dynamics in the time scales explored by NMR.

Colony screening involved a heating step at 53 °C which precludes the selection of protein variants denaturing below that temperature value. This methodological approach may explain why mutants located at regions showing regular secondary structure were not detected. Most probably, mutations within the β-barrel or the helices would involve a high level of structure destabilization making these protein species unable to survive the mentioned thermal treatment. Interestingly, none of the mutations appeared at the loops 76–84 and 106–116, characterized by RMSDs values above the mean and also showing the highest variability of R_2 values. Taking into account that theses loops are located at the membrane interaction face, this observation can be also used to explain the minimal changes found in the membrane binding behavior of most of the mutants studied (Fig. 4). On the other hand, these two loops are also the sequence stretches showing the highest structural variability when compared to StnII (Fig. 1B) what could help to explain the different hemolytic properties of both proteins.

Interestingly, four of the mutations found (G26D, V28E, D57A, and E62G) showed reduced hemolytic activity but intact ability to bind to model lipid vesicles (Fig. 4). Consequently, they must be defective in some of the steps following membrane binding. It is generally accepted that the N-terminal α-helix detachment is a crucial step for pore formation [28–30,33,51]. Therefore, mutations affecting this step should yield less hemolytic proteins. This could be the case in at least two of the mutations selected along the present study. Thus, the reduced hemolytic activity of StnII G26D (relative HC_{50} value of 11.3; Table 1) might be explained by the potential establishment of a new electrostatic interaction between the introduced Asp residue and Arg75 and/or Lys76 side-chains (the α-carbons of positions 26 and 75/76 are located at only around 10 Å of distance). An identical explanation can be given for V28E (relative HC_{50} value of 23.1; Table 1) located only two residues away. In this case, the presence of Glu side-chain could also result in an electrostatic interaction with the same positive charges at positions 75 and 76 (in this case, the distance between α-carbons is even shorter, around 7 Å). Then, in both cases (G26D and V28E) these new interactions could hinder the detachment of the N-terminal helix required for pore formation.

Within the same idea, in the wild-type protein Asp57 is electrostatically interacting with Lys 27, but it is also near to Glu2 and Glu62 (the distance among α-carbons is around 8 Å), creating a repulsion effect in an area that should be important for the conformational change involving helix detachment for pore formation. In the D57A mutant, substitution of Asp by Ala in position 57 would in this case eliminate negative charge, favoring the interactions of the helix with the hinge loop (for example between Glu2 and Lys27) or/and with the β-sandwich residues (between Glu2 and Lys75), impairing helix detachment and thus decreasing the hemolytic activity of this mutant (relative HC_{50} value of 15.7; Table 1). If such were the case, it seems clear that identical arguments can be used for the decreased activity of StnI E62G (relative HC_{50} value of 21.4; Table 1), since it also involves loss of negative charge. Additionally, substitution of Glu by Gly might reinforce the close interaction existing between Lys68 and Asp9, and also interfere with helix detachment.

In summary, the lower hemolytic effect of four of the five mutations selected, altogether with their strategic situation in the vicinity of the N-terminal α-helix, could be interpreted as the result of impediments for its detachment while leaving membrane binding unaffected. Overall, these results add up to a plethora of previous observations obtained with two other actinoporins, EqtII and StnII, reinforcing the role of this conformational change for pore formation. This observation is not trivial given that this protein stretch is the segment showing the highest sequence variability among all actinoporins known.

The StnI mutant S53T seems to be the only one behaving significantly different, among the five selected during this study, given its location and membrane binding behavior. Its relative HC_{50} value is 5.7 (Table 1). Therefore, it is the variant which shows the highest hemolytic activity. On the other hand, it is the only one whose binding behavior to lipid vesicles is altered (Fig. 4). Maybe this effect is enough to explain its diminished hemolytic potency. In fact, cysteine-scanning mutagenesis had been used before to identify the equivalent residue in EqtII (Ser54) as a crucial amino acid for correct pore formation [29,30]. Substitution of this Ser54 by a

Cys residue yielded a less active mutant (relative HC_{50} value of 20) [29]. This mutant was even less hemolytic if the thiol group was chemically modified to add positive or negative charge [53]. Considering that the equivalent Ser52 in StnII (Fig. 1B) belongs to the phosphocholine (POC)-binding site, it is safe to assume that Ser53 is also one of the residues conforming this site in StnI. Within this idea, it is also highly probable that mutations at this position, even if they involve such an small change as introducing a Thr, can imply enough distortion within the POC-binding site to explain the deficient binding to DOPC:SM:Chol vesicles (Fig. 4). It is not easy to understand why this marked decrease in binding is not directly related to a much lower hemolytic activity. However, we interpret these apparently contradictory results as StnI S53T being less effective in membrane binding but at the same time, once bound to the membrane, more efficient in the pore forming process. Long-range effects can have deep impact in actinoporins behavior. Buried Ser53 is indeed in close contact with residues in the segment 75–86, located on the membrane interaction face of the protein and one of the stretches showing the highest conformational flexibility. Therefore, this segment has to be also capable of accommodating structural rearrangements. In fact, it has been proven before for a StnII mutant [51] that the structure and dynamic properties of this region highly depend on the long-range contacts of residues placed around the hinge region. Conversely, changes in the structure of region 75–86 due to the Ser to Thr substitution at position 53 could change interactions within the hinge loop facilitating N-terminal α-helix detachment, thus compensating its altered membrane binding behavior. Furthermore, as discussed above, this segment might be involved in the different hemolytic activities observed for StnI and StnII.

In summary, the obtained results agree with the accepted notion that the N-terminal region of actinoporins, the helical portion related to pore formation, is not directly involved in membrane recognition. In addition, they provide additional evidence that single modifications of actinoporins residues located at positions not taking part in the interactions needed for membrane binding or insertion may largely affect the proper functionality of these proteins by just altering the strictly required conformational freedom and/or electrostatic distribution of well-defined protein regions.

Acknowledgments

This work was supported by the Spanish *Ministerio de Ciencia e Innovación* through projects CTQ2008-00080/BQU, CTQ2011-22514, and BFU2009-10185, and one FPU fellowship granted to S.G.-L.

Appendix A. Supplementary data

Supplementary data associated with this article can be found, in the online version, at http://dx.doi.org/10.1016/j.abb.2013.01.005.

References

[1] P. Maček, FEMS Microbiol. Immunol. 5 (1992) 121–129.
[2] G. Anderluh, P. Maček, Toxicon 40 (2002) 111–124.
[3] J. Alegre-Cebollada, M. Oñaderra, J.G. Gavilanes, A. Martínez-del-Pozo, Curr. Protein Pept. Sci. 8 (2007) 558–572.
[4] C. Álvarez, J.M. Mancheño, D. Martínez, M. Tejuca, F. Pazos, M.E. Lanio, Toxicon 54 (2009) 1135–1147.
[5] L. García-Ortega, J. Alegre-Cebollada, S. García-Linares, M. Bruix, A. Martínez-del-Pozo, Biochim. Biophys. Acta 1808 (2011) 2275–2288.
[6] A. Bellomio, K. Morante, A. Barlič, I. Gutiérrez-Aguirre, A.R. Viguera, J.M. González-Mañas, Toxicon 54 (2009) 869–880.
[7] M. Monastyrnaya, E. Leychenko, M. Isaeva, G. Likhatskaya, E. Zelepuga, E. Kostina, E. Trifonov, E. Nurminski, E. Kozlovskaya, Toxicon 56 (2010) 1299–1314.
[8] M.W. Parker, S.C. Feil, Prog. Biophys. Mol. Biol. 88 (2005) 91–142.
[9] I. Iacovache, F.G. van der Goot, L. Pernot, Biochim. Biophys. Acta 1778 (2008) 1611–1623.
[10] M. Mueller, U. Grauschopf, T. Maier, R. Glockshuber, N. Ban, Nature 459 (2009) 726–730.
[11] N. Mueller, N. Ban, Cell 142 (2010) 334 e1.
[12] R.H. Law, N. Lukoyanova, I. Voskoboinik, T.T. Caradoc-Davies, K. Baran, M.A. Dunstone, M.E. D'Angelo, E.V. Orlova, F. Coulibaly, S. Verschoor, K.A. Browne, A. Ciccone, M.J. Kuiper, P.I. Bird, J.A. Trapani, H.R. Saibil, J.C. Whisstock, Nature 468 (2010) 447–451.
[13] W. Varanda, A. Finkelstein, J. Membr. Biol. 55 (1980) 203–211.
[14] G. Belmonte, C. Pederzolli, P. Maček, G. Menestrina, J. Membr. Biol. 131 (1993) 11–22.
[15] M. Tejuca, M. Dalla Serra, C. Potrich, C. Álvarez, G. Menestrina, J. Membr. Biol. 183 (2001) 125–135.
[16] T. Turk, J. Toxicol. Toxin Rev. 10 (1991) 223–262.
[17] G. Anderluh, I. Križaj, B. Štrukelj, F. Gubenšek, P. Maček, J. Pungerčar, Toxicon 37 (1999) 1391–1401.
[18] V. De los Ríos, M. Oñaderra, A. Martínez-Ruiz, J. Lacadena, J.M. Mancheño, A. Martínez-del-Pozo, J.G. Gavilanes, Protein Expr. Purif. 18 (2000) 71–76.
[19] Y. Wang, L.L. Yap, K.L. Chua, H.E. Khoo, Toxicon 51 (2008) 1374–1382.
[20] J. Alegre-Cebollada, G. Clementi, M. Cunietti, C. Porres, M. Oñaderra, J.G. Gavilanes, A. Martínez-del-Pozo, J. Biotechnol. 127 (2007) 211–221.
[21] G. Uechi, H. Toma, T. Arakawa, Y. Sato, Toxicon 56 (2010) 1470–1476.
[22] B.M. Olivera, J. Rivier, C. Clark, C.A. Ramilo, G.P. Corpuz, F.C. Abogadie, E.E. Mena, S.R. Woodward, D.R. Hillyard, L.J. Cruz, Science 249 (1990) 257–263.
[23] A. Athanasiadis, G. Anderluh, P. Maček, D. Turk, Structure 9 (2001) 341–346.
[24] M.G. Hinds, W. Zhang, G. Anderluh, P.E. Hansen, R.S. Norton, J. Mol. Biol. 315 (2002) 1219–1229.
[25] J.M. Mancheño, J. Martín-Benito, M. Martínez-Ripoll, J.G. Gavilanes, J.A. Hermoso, Structure 11 (2003) 1319–1328.
[26] R.S. Norton, Toxicon 54 (2009) 1075–1088.
[27] A.E. Mechaly, A. Bellomio, D. Gil-Cartón, K. Morante, M. Valle, J.M. González-Mañas, D.M. Guérin, Structure 19 (2011) 181–191.
[28] P. Malovrh, G. Viero, M. Della Serra, Z. Podlesek, J.H. Lakey, P. Maček, G. Menestrina, G. Anderluh, J. Biol. Chem. 278 (2003) 22678–22685.
[29] G. Anderluh, A. Barlic, Z. Podlesek, P. Maček, J. Pungerčar, F. Gubensek, M.L. Zecchini, M.D. Serra, G. Menestrina, Eur. J. Biochem. 263 (1999) 128–136.
[30] K. Kristan, Z. Podlesek, V. Hojnik, I. Gutiérrez-Aguirre, G. Guncar, D. Turk, J.M. González-Mañas, J.H. Lakey, P. Maček, G. Anderluh, J. Biol. Chem. 279 (2004) 46509–46517.
[31] G. Anderluh, J.H. Lakey, Trends Biochem. Sci. 33 (2008) 482–490.
[32] J. Alegre-Cebollada, V. Lacadena, M. Oñaderra, J.M. Mancheño, J.G. Gavilanes, A. Martínez-del-Pozo, FEBS Lett. 575 (2004) 14–18.
[33] J. Alegre-Cebollada, M. Cunietti, E. Herrero-Galán, J.G. Gavilanes, A. Martínez-del-Pozo, J. Mol. Biol. 382 (2008) 920–930.
[34] J.M. Mancheño, V. De los Ríos, A. Martínez-del-Pozo, M.E. Lanio, M. Oñaderra, J.G. Gavilanes, Biochim. Biophys. Acta 1545 (2001) 122–131.
[35] I. Castrillo, J. Alegre-Cebollada, A. Martínez-del-Pozo, J.G. Gavilanes, J. Santoro, M. Bruix, Biomol. NMR Assign. 3 (2009) 5–7.
[36] T.D. Goddard, D.G. Kneller, SPARKY 3, University of California, San Francisco, 2005.
[37] P. Güntert, Methods Mol. Biol. 278 (2004) 353–378.
[38] G. Cornilescu, F. Delaglio, A. Bax, J. Biomol. NMR 13 (1999) 289–302.
[39] D.A. Case, T.E. Cheatham 3rd, T. Darden, H. Gohlke, R. Luo, K.M. Merz Jr., A. Onufriev, C. Simmerling, B. Wang, R.J. Woods, J. Comput. Chem. 26 (2005) 1668–1688.
[40] R.A. Laskowski, J.A. Rullmannn, M.W. MacArthur, R. Kaptein, J.M. Thornton, J. Biomol. NMR 8 (1996) 477–486.
[41] R. Koradi, M. Billeter, K. Wüthrich, J. Mol. Graph. 14 (51–55) (1996) 29–32.
[42] N.A. Farrow, R. Muhandiram, A.U. Singer, S.M. Pascal, C.M. Kay, G. Gish, S.E. Shoelson, T. Pawson, J.D. Forman-Kay, L.E. Kay, Biochemistry 33 (1994) 5984–6003.
[43] P. Schuck, Biophys. J. 78 (2000) 1606–1619.
[44] T.M. Laue, B.D. Shah, T.M. Ridgeway, S.L. Pelletier, in: S.E. Harding, A.J. Rowe, J.C. Horton (Eds.), Analytical Ultracentrifugation in Biochemistry and Polymer Science, Royal Soc. Chem., Cambridge, UK, 1992, pp. 90–125.
[45] J.L. Cole, J.W. Lary, HeteroAnalysis, Bioservices Center, University of Connecticut, Storrs, CT, Analytical Ultracentrifugation Facility, 2009.
[46] A. Martínez-Ruiz, L. García-Ortega, R. Kao, J. Lacadena, M. Oñaderra, J.M. Mancheño, J. Davies, A. Martínez-del-Pozo, J.G. Gavilanes, Methods Enzymol. 341 (2001) 335–351.
[47] J. Alegre-Cebollada, I. Rodríguez-Crespo, J.G. Gavilanes, A. Martínez-del-Pozo, FEBS J. 273 (2006) 863–871.
[48] I. Castrillo, J. Alegre-Cebollada, A. Martínez-del-Pozo, J.G. Gavilanes, M. Bruix, Biomol. NMR Assign. 3 (2009) 239–241.
[49] M.A. Pardo-Cea, J. Alegre-Cebollada, A. Martínez-del-Pozo, J.G. Gavilanes, M. Bruix, Biomol. NMR Assign. 4 (2010) 69–72.
[50] I. Castrillo, N.A. Araujo, J. Alegre-Cebollada, J.G. Gavilanes, A. Martínez-del-Pozo, M. Bruix, Proteins 78 (2010) 1959–1970.
[51] M.A. Pardo-Cea, I. Castrillo, J. Alegre-Cebollada, A. Martínez-del-Pozo, J.G. Gavilanes, M. Bruix, FEBS J. 278 (2011) 2080–2089.
[52] V. De los Ríos, J.M. Mancheño, A. Martínez-del-Pozo, C. Alfonso, G. Rivas, M. Oñaderra, J.G. Gavilanes, FEBS Lett. 455 (1999) 27–30.
[53] G. Anderluh, A. Barlic, C. Potrich, P. Maček, G. Menestrina, J. Membr. Biol. 173 (2000) 47–55.

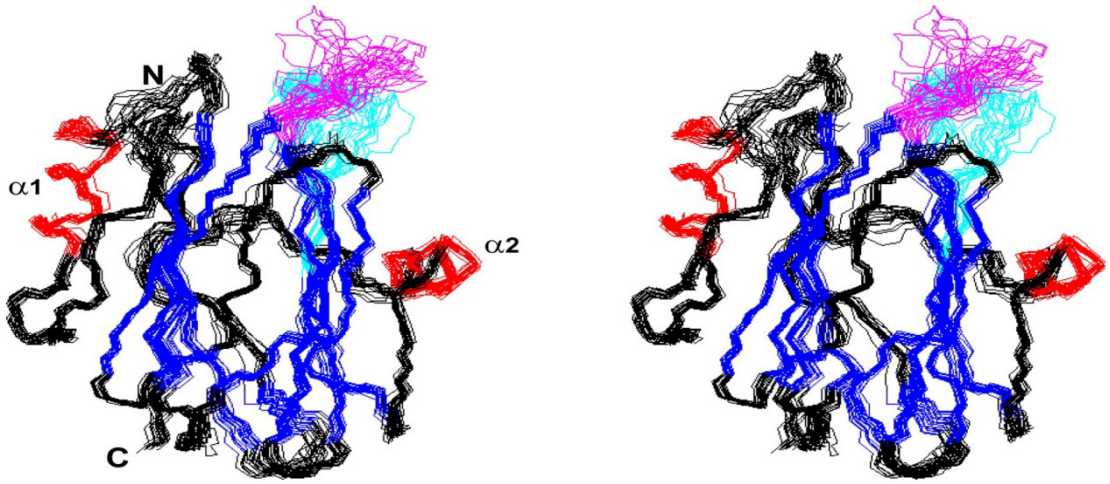

Supplementary Fig. 1 Stereo representation of the family of 20 lowest-energy NMR structures documented in <ce:cross-ref refid="t0010"> Table 2</ce:cross-ref> . The orientation of the structure corresponds to the one shown in <ce:cross-ref refid="...

Sara Garc?a-Linares , In?s Castrillo , Marta Bruix , Margarita Men?ndez , Jorge Alegre-Cebollada , ?lvaro Mart?nez...

Three-dimensional structure of the actinoporin sticholysin I. Influence of long-distance effects on protein function

Archives of Biochemistry and Biophysics Volume 532, Issue 1 2013 39 - 45

http://dx.doi.org/10.1016/j.abb.2013.01.005

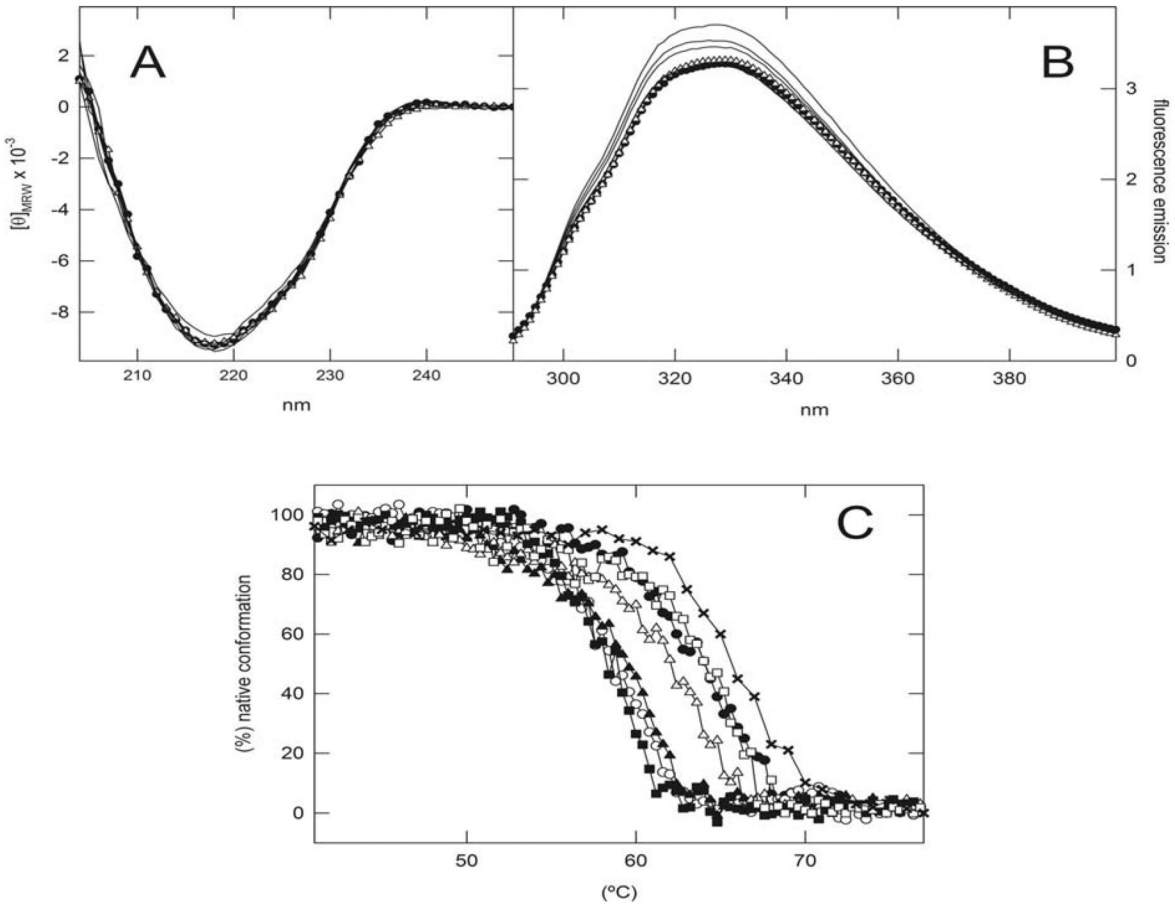

Supplementary Fig. 2 Spectroscopic characterization of sticholysin variants. (A) Far-UV circular dichroism spectra. Results are expressed in [?]MRW, mean residue weight ellipticity, in units of degree<ce:hsp sp="0.25"/> ?<ce:hsp sp="0.25"/> cm 2 ...

Sara Garc?a-Linares , In?s Castrillo , Marta Bruix , Margarita Men?ndez , Jorge Alegre-Cebollada , ?lvaro Mart?nez...

Three-dimensional structure of the actinoporin sticholysin I. Influence of long-distance effects on protein function

Archives of Biochemistry and Biophysics Volume 532, Issue 1 2013 39 - 45

http://dx.doi.org/10.1016/j.abb.2013.01.005

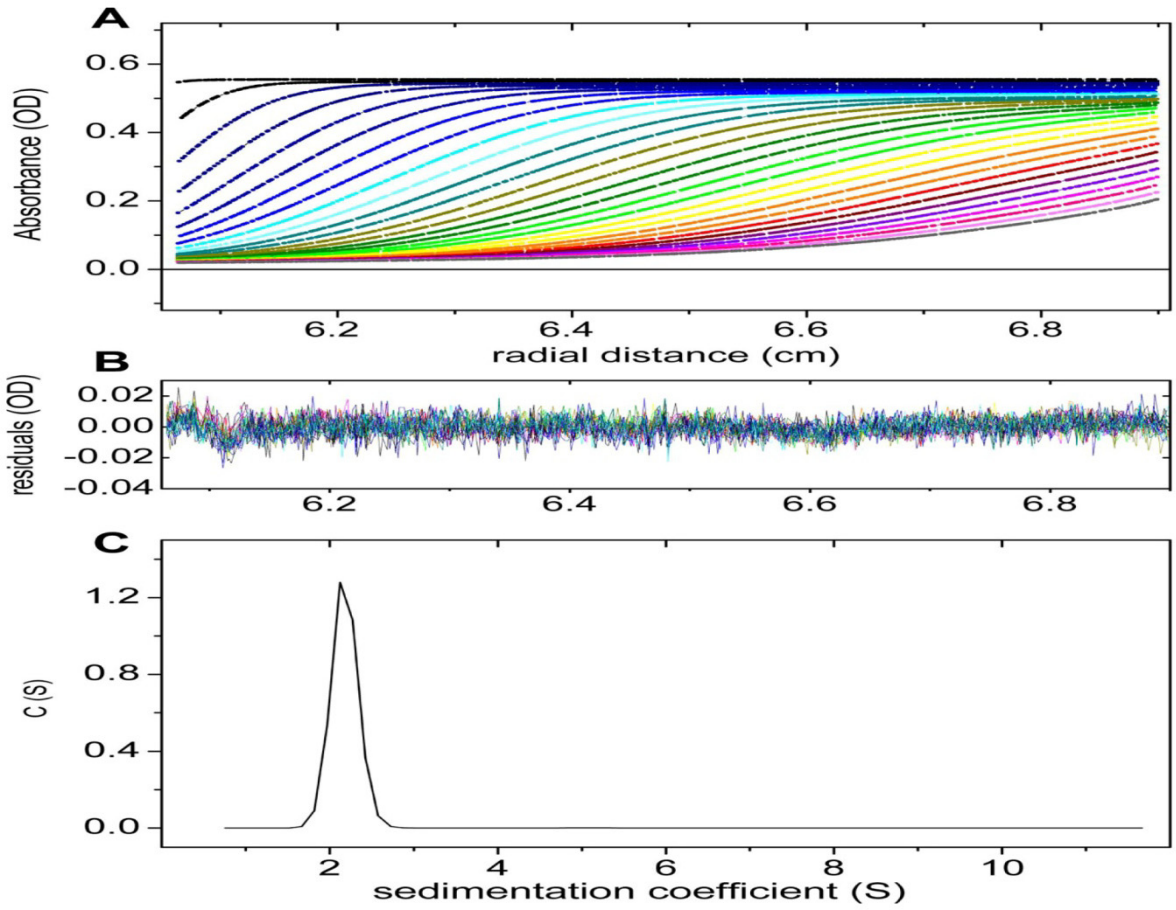

Supplementary Fig. 3 Sedimentation velocity behavior of wild-type StnI at 5<ce:hsp sp="0.25"/> ?M concentration. (A) Absorbance as a function of radial position and (B) residuals are shown for sedimentation at 45,000<ce:hsp sp="0.25"/> rpm. (C) F...

Sara Garc?a-Linares , In?s Castrillo , Marta Bruix , Margarita Men?ndez , Jorge Alegre-Cebollada , ?lvaro Mart?nez...

Three-dimensional structure of the actinoporin sticholysin I. Influence of long-distance effects on protein function

Archives of Biochemistry and Biophysics Volume 532, Issue 1 2013 39 - 45

http://dx.doi.org/10.1016/j.abb.2013.01.005

ARTICLE VI

The effect of cholesterol on the long-range network of interactions established among sea anemone sticholysin II residues at the water-membrane interface

García-Linares, S., Alm, I., Maula, T., Gavilanes, J. G., Slotte, J. P. and Martínez-del-Pozo, Á. (2015). *Mar Drugs* 13(4): 1647-1665.

Efecto del colesterol en las interacciones establecidas a larga distancia entre los residuos de la interfase proteína-membrana de la actinoporina de anémona marina StnII

Las actinoporinas son proteínas formadoras de poros de tipo α con potencial terapéutico, producidas por anémonas marinas. La StnII de *Stichodactyla helianthus* es uno de los miembros mejor caracterizados. Estas proteínas permanecen solubles y plegadas en medios acuosos, pero al interaccionar con membranas lipídicas oligomerizan y forman un poro. Esto ocurre gracias a la presencia de SM en la membrana, pero el Chol también facilita la formación del poro. La unión a la membrana y la formación del poro requieren que se produzcan reordenamientos a larga distancia de los residuos localizados en la interfase proteína-membrana. La influencia del Chol en el reconocimiento de la membrana, la oligomerización de la proteína y la formación del poro se han estudiado utilizando una batería de mutantes de StnII, caracterizados en función de su habilidad para interaccionar con membranas modelo en presencia o ausencia de colesterol. Los resultados obtenidos muestran que el Chol no sólo colabora con la SM en el reconocimiento de la membrana, si no que reduce significativamente los requerimientos estructurales para que los reordenamientos mencionados anteriormente tengan lugar. Sin embargo, dado que las vesículas de DOPC:SM:Chol empleadas tienen coexistencia de fases y dominios diferenciados, los efectos observados podrían deberse también a la presencia de dichas fases en la membrana.

Mar. Drugs **2015**, *13*, 1647-1665; doi:10.3390/md13041647

OPEN ACCESS

marine drugs

ISSN 1660-3397

www.mdpi.com/journal/marinedrugs

Article

The Effect of Cholesterol on the Long-Range Network of Interactions Established among Sea Anemone Sticholysin II Residues at the Water-Membrane Interface

Sara García-Linares [1], Ida Alm [2], Terhi Maula [2], José G. Gavilanes [1,*], Johan Peter Slotte [2] and Álvaro Martínez-del-Pozo [1,*]

[1] Department of Biochemistry and Molecular Biology I, Complutense University, 28040 Madrid, Spain; E-Mail: saraglinares@gmail.com

[2] Biochemistry, Department of Biosciences, Åbo Akademi University, 20520 Turku, Finland; E-Mails: iasalm@tutu.fi (I.A.); terhi.kuru@abo.fi (T.M.); jpslotte@abo.fi (J.P.S.)

* Authors to whom correspondence should be addressed; E-Mails: ppgf@bbm1.ucm.es (J.G.G.); alvaromp@quim.ucm.es (Á.M.-P.); Tel.: +34-91-394-4158; Fax: +34-91-394-4159.

Academic Editor: Keith Glaser

Received: 23 January 2015 / Accepted: 16 March 2015 / Published: 25 March 2015

Abstract: Actinoporins are α-pore forming proteins with therapeutic potential, produced by sea anemones. Sticholysin II (StnII) from *Stichodactyla helianthus* is one of its most extensively characterized members. These proteins remain stably folded in water, but upon interaction with lipid bilayers, they oligomerize to form a pore. This event is triggered by the presence of sphingomyelin (SM), but cholesterol (Chol) facilitates pore formation. Membrane attachment and pore formation require changes involving long-distance rearrangements of residues located at the protein-membrane interface. The influence of Chol on membrane recognition, oligomerization, and/or pore formation is now studied using StnII variants, which are characterized in terms of their ability to interact with model membranes in the presence or absence of Chol. The results obtained frame Chol not only as an important partner for SM for functional membrane recognition but also as a molecule which significantly reduces the structural requirements for the mentioned conformational rearrangements to occur. However, given that the DOPC:SM:Chol vesicles employed display phase coexistence and have domain boundaries, the observed effects could be also due to the presence of these different phases on the membrane. In addition, it is also shown that the Arg51 guanidinium group is strictly required for membrane recognition, independently of the presence of Chol.

Keywords: actinoporin; equinatoxin; sphingomyelin; pore-forming toxin; sphingomyelin

1. Introduction

Sea anemones are a group of benthic marine animals which secrete various toxins [1] including a group of small and basic α-pore forming proteins known as actinoporins [2]. These actinoporins form cation-selective pores on the cell membranes, causing colloid-osmotic shock that leads to cells death [3–5]. They are believed to participate in anemone functions such as predation, defense, and digestion, and have been shown to be lethal to small crustaceans, mollusks, fish [6], and parasites [7]. All known actinoporins display high sequence identity and appear as multigene families [8,9]. However, only four of them have been characterized in deep detail: Equinatoxin II (EqtII) from *Actinia equina* [8], Sticholysins I and II (StnI and StnII) from *Stichodactyla helianthus* [10,11], and Fragaceatoxin C (Fra C) from *Actinia fragacea* [12]. Like many other marine toxins, actinoporins show some therapeutic potential, including different pharmacological effects, presumable anticancer activities, and use in the construction of specific immunotoxins [1,7,13–18].

In addition to their potential as therapeutic drugs, actinoporins have gained remarkable attention because they show a singular behavior at the water–lipid membrane interface. In aqueous solution they remain stably folded, but they become integral membrane structures upon interaction with lipid bilayers, oligomerizing to form pores [10,11,19]. It is widely accepted that the bilayers targeted must contain sphingomyelin (SM) and/or display phase coexistence [20–25]. In fact, the effect of not only SM but also Chol on the membrane pore-forming ability of StnII has been thoroughly studied [21,22,25–29]. According to those results, it is now quite clear that the presence of Chol eases the formation of pores by StnII, a conclusion which is in agreement with the coexistence of Chol and SM in biological membranes [27,30–33]. However, what still remains poorly studied is the nature of the protein determinants which explain this effect. To answer this question, we have studied a battery of different StnII mutants affecting different protein regions presumably involved in pore formation.

The water-soluble structure of StnII is known in detail [34]. It folds as a β-sandwich motif composed of 10 β-strands flanked by two α-helices which interact with both sides of the β-sandwich (Figure 1). One of these helices (α1) is located near the *N*-terminal end. In fact, the first 30 residues appear to be able to adopt alternative conformations without disrupting the fold of the β-sandwich [35]. This feature, altogether with the amphipathic character of this stretch, seems to be extremely important for the final functionality of the pore, since the α1 helix has been proposed to extend and further insert into the membrane to form the pore walls [17,36,37]. The most recent model explaining the mechanism of actinoporins' pore formation [17,37–39] assumes a toroidal protein-lipid structure without a well-defined fixed stoichiometry [17,38–40], although an alternative model has been proposed for Fra C [41]. Nevertheless, it is reasonably well-proven that insertion of the *N*-terminus into the membrane takes place in anon-coordinate way, shortly after the binding of the toxin and before their oligomerization into the final pore [37]. In addition to this *N*-terminal α-helix, three more regions of the structure seem to be especially important from a functional point of view: a phosphocholine (POC) binding site, a cluster of aromatic residues, and an array of basic amino acids [11].

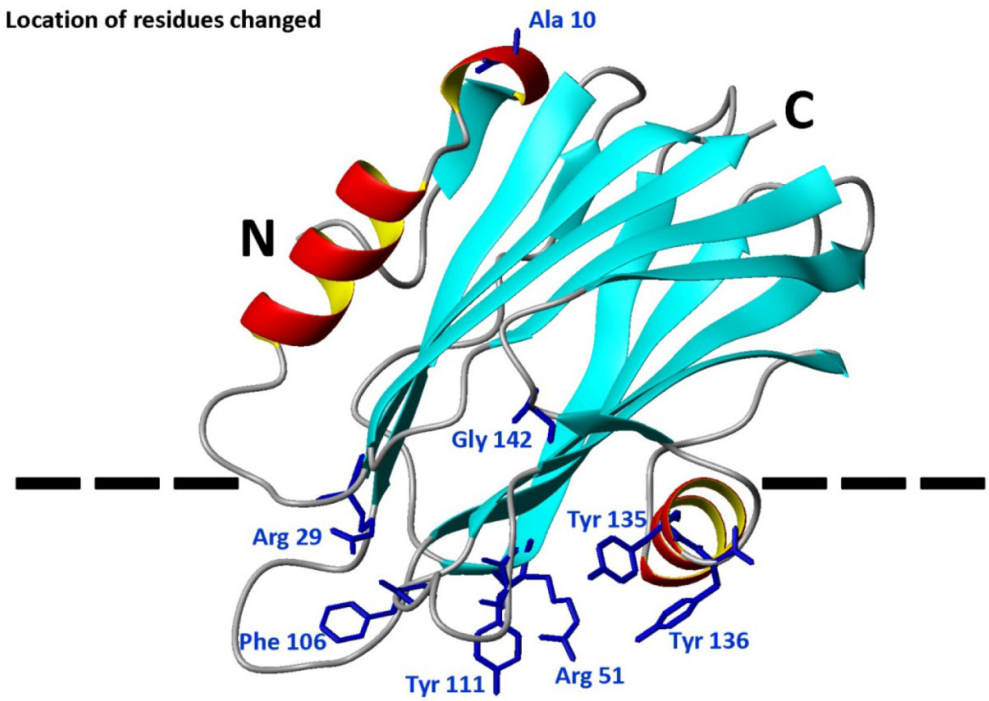

Figure 1. Diagram of the three-dimensional structure of StnII indicating the location of the eight mutated positions: Ala10, Arg29, Arg51, Phe106, Tyr111, Tyr135, Tyr136, and Gly142. The different elements of ordered secondary structure, as well as the *N*- and *C*-terminal ends, are also indicated. The dotted line is a representation of the membrane surface. The diagram was constructed from the atomic coordinates deposited to the PDB (Protein Data Bank, reference 1GWY for StnII). The image was generated by the MolMol Program [42].

The work presented here studies the effect of Chol on the membrane-interacting behavior of eight different StnII mutants affecting the stretch of the 30 first residues (A10P and R29Q), the aromatic cluster (F106L, Y111N, Y135F, and Y136F), the POC binding site (R51Q, Y111N, Y135F, and Y136F), and a residue involved in maintaining the pore-competent state of protein oligomerization (G142A).

2. Results

2.1. Protein Purification and Characterization

All proteins used in the study were purified to homogeneity according to their behavior in SDS-PAGE. Their amino acid compositions were consistent with the introduced mutations. The calculated $E^{0.1\%}$ (280 nm, 1 cm) values were also in good agreement with the amino acid changes made (Table 1). All far-UV CD spectra of the individual mutants were indistinguishable from that corresponding to the wild-type StnII (data not shown). In summary, all eight mutants retained the overall native water-soluble conformation.

The hemolytic activity was diminished in all the mutants studied (Table 1). This may not be a surprise, given that all the residues changed are presumably involved in essential steps for the formation of the final functional pore [10,11,37]. This effect was especially evident for mutants R29Q, Y111N, and G142A (Table 1) [29,43,44].

Stability analyses also revealed the importance of some of these residues (Arg29 and Gly142) in maintaining the protein conformation as deduced from the large decrease of the T_m values for R29Q and G142A mutant variants (Table 1). It is also remarkable that substitution of Tyr111 by Asn and Tyr136 by Phe produced mutant proteins with higher T_m values (Table 1). All mutants studied showed values high above the temperatures used along the study and, therefore, the results described below should not be attributed to thermal denaturing effects.

Table 1. Structural and functional parameters of the proteins used in the study.

StnII Variant	$E^{0.1\%}$ (280 nm, 1 cm)	T_m (°C)	Relative Hemolytic Activity [c]
Wild-type	2.54 [a]	67 [a]	1.00
A10P	2.69 [a]	66 [a]	0.26 [a]
R29Q	2.54 [a]	60 [a]	<0.10 [a]
R51Q	2.38	67	0.30
F106L	2.62 [a]	66 [a]	0.39 [a]
Y111N	2.58 [a]	70 [a]	<0.10 [a]
Y135F	2.47	66	0.26
Y136F	2.66	69	0.26
G142A	2.30 [b]	61 [b]	0.13 [b]

[a] [29]; [b] [44]; [c] Relative hemolytic activity calculated as HC_{50}(WT)/HC_{50}(mut).

2.2. Protein Binding to the Two Different Lipid Model Vesicles Employed

ITC was used to measure the interaction of the StnII mutants with DOPC:SM:Chol (1:1:1) or POPC:PSM (4:1) vesicles (Figures 2 and 3). The interaction of wild-type StnII with POPC:PSM (4:1) vesicles in the presence of low amounts of Chol has been recently described [27]. In the present work DOPC:SM:Chol (1:1:1) vesicles were chosen because they are considered a model of coexistence between liquid-disordered and liquid-ordered phases [31,45–47]. All mutants studied were observed to bind to the DOPC:SM:Chol (1:1:1) vesicles (Figure 2) although with evident differences in terms of relative membrane binding affinity values (Table 2). Thus, while A10P still bound with almost identical affinity to the wild-type StnII, and F106L showed only a reduction of about 2.5-fold (Table 2), all the other mutants displayed values about one to two orders of magnitude smaller. The most dramatic differences in affinity were observed for the R29Q, R51Q, Y111N, and Y135F mutants (Table 2). Binding to the POPC:PSM (4:1) vesicles was about 100-fold lower than to the Chol-containing ones for wild-type StnII (Table 2) and most of the mutants did not produce a detectable signal in these experiments (Figure 3). Only binding of the A10P protein variant was measurable, showing again a very similar relative binding affinity to the wild-type protein (Table 2).

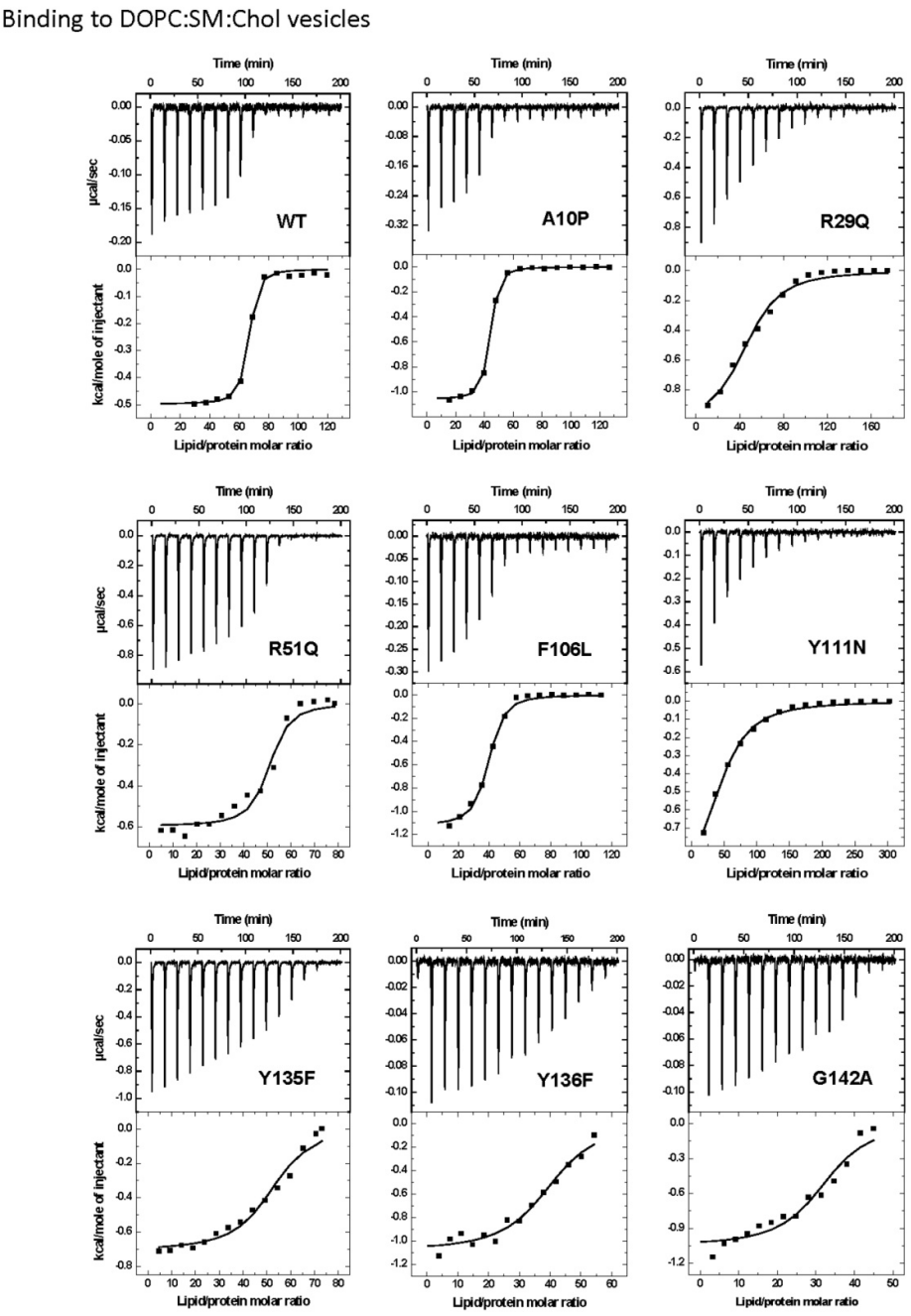

Figure 2. Binding of StnII and its mutants to DOPC:SM:Chol (1:1:1) 100-nm-diameter vesicles studied by ITC. Reactant concentrations were as follows: WT (P_0 = 1.2 µM, L_0 = 0.56 mM), A10P (P_0 = 1.1 µM, L_0 = 0.55 mM), R29Q (P_0 = 2.3 µM, L_0 = 1.8 mM), R51Q (P_0 = 10.4 µM, L_0 = 3.6 mM), F106L (P_0 = 1.1 µM, L_0 = 0.53 mM), Y111N (P_0 = 1.2 µM, L_0 = 1.6 mM), Y135F (P_0 = 10.4 µM, L_0 = 3.4 mM), Y136F (P_0 = 1.0 µM, L_0 = 0.25 mM), and G142A (P_0 = 1.2 µM, L_0 = 0.25 mM). Binding isotherms were adjusted to a model in which protein membrane binding involves the participation of "*n*" lipid molecules. The c values ($c = K \times P_0$) for all the graphs are in the range 1–1000.

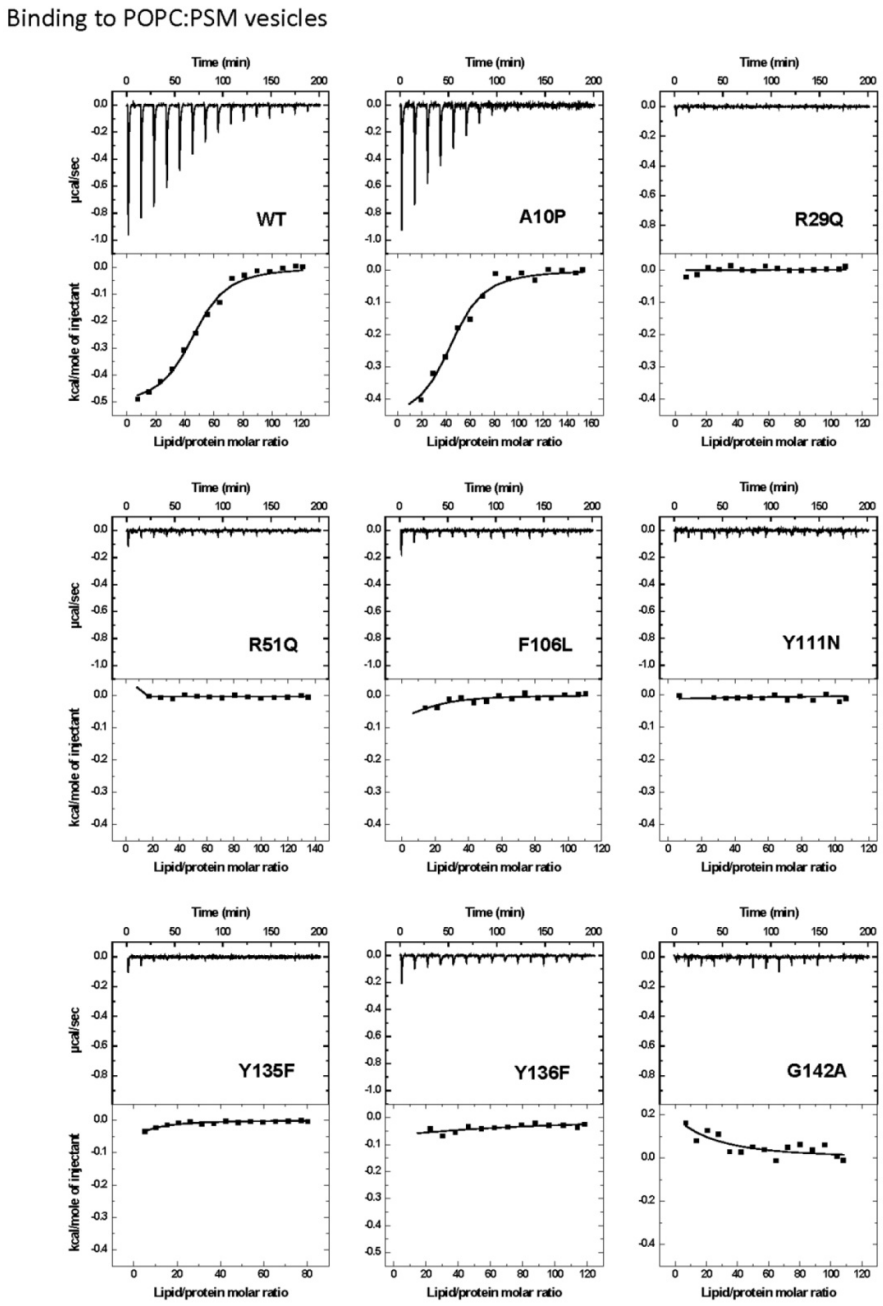

Figure 3. Binding of StnII and its mutants to POPC:PSM (4:1) 100-nm-diameter vesicles studied by ITC. Reactant concentrations were as follows: WT (P_0 = 10.0 µM, L_0 =5.4 mM), A10P (P_0 = 8.0 µM, L_0 = 5.4 mM), R29Q (P_0 = 9.9 µM, L_0 = 4.8 mM), R51Q (P_0 = 10.5 µM, L_0 = 6.3 mM), F106L (P_0 = 9.1 µM, L_0 = 4.9 mM), Y111N (P_0 = 10.1 µM, L_0 = 5.1 mM), Y135F (P_0 = 10.3 µM, L_0 = 3.7 mM), Y136F (P_0 = 9.6 µM, L_0 = 5.1 mM), and G142A (P_0 = 9.4 µM, L_0 = 5.0 mM). Binding isotherms were adjusted to a model in which protein membrane binding involves the participation of "*n*" lipid molecules. Given the low affinity of most of the mutants for the vesicles assayed, in this case only the c values ($c = K \times P_0$) for WT and A10P are in the range 1–1000.

Table 2. Binding of StnII protein variants to DOPC:SM:Chol (1:1:1) and POPC:PSM (4:1) vesicles studied by ITC. The interaction of some mutants with POPC:PSM (4:1) vesicles was too weak to be detected by ITC in the conditions used for these experiments (see Figure 3) (data not shown in the Table).

StnII Variant	*n*	K × 10^{-8} (M^{-1})	ΔG (kcal/mol)	ΔH (kcal/mol)	ΔS (cal·mol^{-1}·K^{-1})	Relative Membranebinding [a]
DOPC:SM:Chol (1:1:1)						
WT	39 ± 4 [b]	1.700 ± 0.900 [b]	−9.1 ± 0.5 [b]	−44.0 ± 3.0 [b]	−115.0 ± 9.0 [b]	1.000 [b]
A10P	37 ± 4 [b]	1.900 ± 0.900 [b]	−9.3 ± 0.4 [b]	−39.0 ± 6.0 [b]	−99.0 ± 20.0 [b]	1.180 [b]
R29Q	51 ± 8 [b]	0.031 ± 0.002 [b]	−6.7 ± 0.2 [b]	−45.0 ± 3.0 [b]	−129.0 ± 8.0 [b]	0.014 [b]
R51Q	49 ± 2	0.140 ± 0.070	−7.6 ± 0.2	−29.0 ± 1.0	−72.0 ± 4.0	0.082
F106L	36 ± 3 [b]	0.600 ± 0.100 [b]	−8.6 ± 0.1 [b]	−37.0 ± 7.0 [b]	−94.0 ± 24.0 [b]	0.380 [b]
Y111N	46 ± 7 [b]	0.025 ± 0.004 [b]	−6.6 ± 0.1 [b]	−47.0 ± 2.0 [b]	−134.0 ± 4.0 [b]	0.012 [b]
Y135F	51 ± 2	0.039 ± 0.013	−6.8 ± 0.2	−36.0 ± 2.0	−99.0 ± 6.0	0.023
Y136F	40 ± 1	0.270 ± 0.080	−8.1 ± 0.1	−43.0 ± 1.0	−117.0 ± 4.0	0.160
G142A	32 ± 1	0.250 ± 0.100	−8.2 ± 0.1	−33.0 ± 1.0	−83.0 ± 4.0	0.150
POPC:PSM (4:1)						
WT	45 ± 2	1.5 ± 0.3	−6.3 ± 0.1	−23.0 ± 1.0	−57.0 ± 3.0	1.000
A10P	44 ± 3	1.2 ± 0.4	−6.2 ± 0.2	−20.0 ± 2.0	−48.0 ± 6.0	0.800

[a] [n(WT) × K(mut)]/[n(mut) × K(WT)] as explained in [29]; [b] [29].

2.3. Pore Formation

Pore formation was monitored by recording the fluorescence emission of calcein released from lipid model vesicles. These vesicles are only a simplified version of a real membrane. This would explain why, in general, actinoporins seem to be more effective against erythrocytes. However, this approach is extremely useful because it allows the determination of different biophysical parameters and, most of all, the dissection of the individual roles of different types of lipid molecules, as is the case in this work. Within this idea, wild-type StnII and the A10P, F106L, Y136F, and G142A variants displayed an indistinguishable kinetic of calcein release from DOPC:SM:Chol (1:1:1) vesicles (Figure 4A). The R29Q and Y135F mutants were able to induce calcein leakage but exhibited a largely decreased velocity constant. The R51Q and Y111N mutants, on the other hand, were unable to release the entrapped fluorophore (Figure 4).

For POPC:PSM (4:1) vesicles, only the A10P mutant variant was able to induce calcein release, although to a lower extent than the wild-type protein (Figure 4B). This would be explained by the conformational stiffness introduced in this StnII mutant by the substitution of an Ala residue by Pro that would hamper pore formation without loss of binding affinity [29].

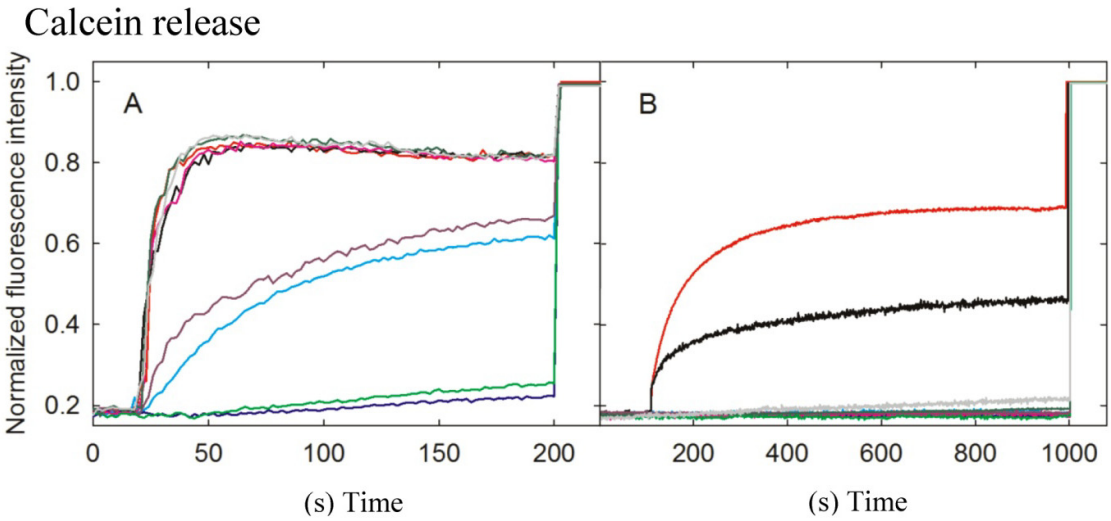

Figure 4. Release of calcein entrapped in DOPC:SM:Chol (1:1:1) (**A**) or POPC:PSM (4:1) (**B**) vesicles by wild-type StnII (red) or its A10P (black), R29Q (light blue), R51Q (dark blue), F106L (magenta), Y111N (light green), Y135F (purple), Y136F (dark green), and G142A (gray) mutants. Calcein-entrapped vesicles were prepared with extrusion and release was measured at 23 °C. All intensities were normalized. Towards the end of the measurement (at 200 s in A and 800 s in B), Triton X-100 was added to dissolve the LUVs and release all calcein. The results shown are representative of two different independent experiments.

3. Discussion

Pore formation by actinoporins is the result of a series of well coordinated events. The recently refined model of this mechanism [37,39,40] predicts that, after an extremely fast toxin binding to the membrane, major conformational changes occur, resulting in the simultaneous presence of several distinct membrane-bound protein forms (Figure 5). These conformational changes involve long-distance rearrangements [48,49] which complicate the interpretation of the effects produced by individual mutations, especially if these changes affect the protein face involved in recognizing the membrane. According to the mentioned mechanism, one of the first distinct conformational species to appear would be represented by a molecule in which an extended *N*-terminal α1 helix would lie more or less parallel to the membrane surface [50]. Then, this elongated α1 helix would be inserted into the membrane, a step which would be faster than the oligomerization step [37]. Finally, functional pore formation would take place as the result of a mechanism which begins with the formation of dimers and ends in a toroidal protein-lipid structure (Figure 5) lacking a well-defined fixed stoichiometry [17,38–40]. A stable prepore structure is not required according to this model, in clear contrast to β-pore forming toxin behavior [51,52]. However, an alternative non-toroidal nonameric pore based on a detergent-containing crystalline structure, has been also proposed for the actinoporin Fra C [41]. Independently of the pore formation mechanism, it is well-established that Chol enhances pore formation by actinoporins not only because induces the formation of raft-like domains but also because, even at low concentrations, it still affects the physical state of SM [21,22,26–29]. The results

presented here reveal the influence of this lipid on the essential long-distance rearrangements required for pore-formation, since the StnII variants that were studied harbor mutations that affect residues in protein regions with assigned key roles in pore formation (Figures 1 and 5).

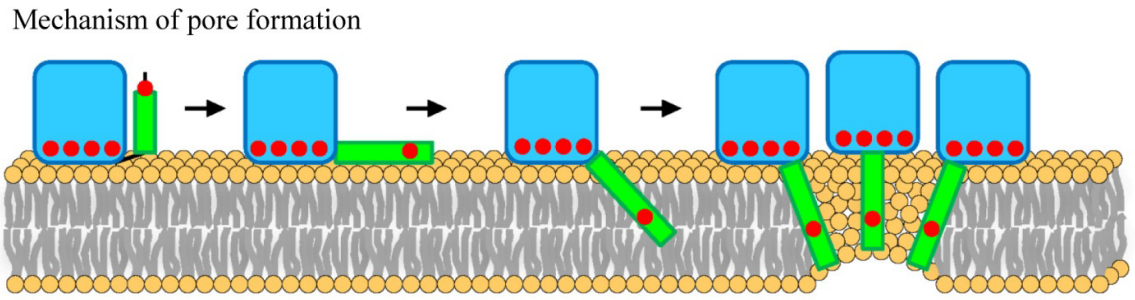

Figure 5. Illustration representing the pore-forming mechanism of actinoporins. Once the protein is attached to the membrane, the *N*-terminal α1 helix extends and inserts into the bilayer. Finally, oligomerization conduces to a final toroidal pore. The blue shape represents the β-sandwich core. The green dots represent the 30 first residues before and after the extension of the α1 helix extension. Red dots represent the approximate location of the residues mutated in the work presented here. This figure has been adapted from [37].

3.1. StnII Mutants Affecting the 30 First Residues Sequence Stretch

StnII Ala10 is located at the edge of the region thought to become α-helical to form the pore [50]. Thus, StnII A10P contains a mutation which is located far away from the membrane binding surface (Figures 1 and 5) and therefore does not participate directly in the long-distance rearrangements needed for membrane recognition. This mutation has been shown to provide enough conformational stiffness so as to hamper the required α1 helix extension [29,43,53] (Figure 5). This is in good agreement with the behavior of a double cysteine mutant of EqtII, which was also designed to increase the stiffness of this protein region [54]. It was then proposed that neither the presence of the *N*-terminal stretch region nor the conformational changes occurring along this sequence after membrane binding would provide higher affinity of StnII for the bilayer. Binding of A10P was not substantially affected by the presence or absence of Chol. However, hemolysis and calcein leakage activity in the absence of Chol were clearly diminished (Tables 1 and 2; Figure 4B), thus suggesting that pore formation, but not membrane recognition, is impaired in this mutant. On the other hand, like the wild-type protein, A10P was observed to bind with greater affinity to Chol-containing lipid vesicles (Tables 1 and 2), which explains the differences observed between both types of vesicles in terms of calcein leakage. Thus, A10P could be considered a reference for efficient protein binding without pore formation. The presence of Chol (Figure 4A) allows leakage of water soluble solutes even in the absence of a completely extended *N*-terminal α-helix, a result that would reinforce the hypothesis in favor of the toroidal nature of the pore [17,38,39].

The other residue mutated along this polypeptide region, Arg29, is a conserved amino acid [11] located at the *C*-terminal end of this 30 residues long protein stretch (Figure 1). This residue has been shown to be crucial because of its involvement in membrane recognition and also in sustaining the

necessary conformational changes leading to pore formation [29]. A rotation between StnII Ser28 and Arg29 might occur after membrane binding [34], inducing these conformational changes. In addition, Arg29 and Phe106 establish a cation-π interaction, which is needed to provide the protein with the right conformational flexibility [43]. This interaction is not possible in the R29Q mutant, which results in an increased conformational freedom of this region that, in turn, greatly distorts the distribution of the electrostatic potential along the surface of the protein face involved in recognizing the membrane [48]. Relative membrane binding affinity for the DOPC:SM:Chol (1:1:1) was greatly diminished (Table 2; Figure 2), in agreement with less hemolytic (Table 1) and calcein release activities, (Figure 4). In the absence of Chol, binding and calcein leakage were not detectable (Figures 3 and 4B). Altogether, these results reveal a key role for Chol in the correct binding and positioning of the region around StnII Arg29 on the membrane in order to produce a functional pore.

3.2. StnII Mutants Affecting the Aromatic Cluster

The mutations affecting the aromatic cluster of StnII were F106L, Y111N, Y135F, and Y136F. NMR analysis of the aromatic resonances of the equivalent StnI groups in the presence of dodecylphosphocholine micelles revealed a high motional flexibility of StnI Tyr-136 and Tyr-137 (Tyr 135 and 136 in StnII) [55]. From this point of view, given that the hydrophobicity of the side chain of these two residues is maintained in the mutants, it can be explained why they still interact fairly well with the Chol containing vesicles (Figures 2 and 4A) while they are completely unable to maintain the specific contacts in the absence of Chol (Figures 3 and 4B; see also below). Interestingly, StnITyr-112 (Tyr111 in StnII) was not affected by the micellar media [55]. Detailed inspection of the water soluble forms of EqtII and StnII reveals that the loop containing this residue (segment spanning StnII Tyr108 to Tyr111) is completely disordered and displays high conformational flexibility [34,35,56]. In the crystal structure of the StnII:POC complex [34], the aromatic ring of Tyr111 is pointing towards the POC moiety after a probable conformational change from its exposed POC-free state [55]. Indeed, it has also been proposed that Tyr111 would induce a necessary disorder in exposed hydrophobic chains to promote their interaction with the membrane [48]. Finally, as stated above, Phe106 and Arg29 establish an interaction which may function like a switch to turn on the conformational changes needed for protein binding to the membrane [43,48].

Taking all this into account, the results presented here agree with the existence of the aforementioned network of long-range interactions, given that any of the single mutations studied rendered protein variants completely unable to interact with the POPC:PSM (4:1) vesicles (Figures 3 and 4). This situation changed significantly in the presence of Chol (Figures 2 and 4) since some of the residues involved are also part of the POC-binding site, as explained below.

3.3. StnII Mutants Affecting the POC-Binding Site

The StnII mutants affecting the POC-binding site studied herein were R51Q, Y111N, Y135F, and Y136F. Three of these mutated amino acids are involved in the aromatic cluster, and all four participate in specific interactions with the POC moiety and/or the 2NH and 3OH groups of SM [24,29,34,41,43,48,55,57]. Therefore, these four mutants displayed diminished hemolytic activities (Table 1) and lacked the ability to interact with PSM containing vesicles in the absence of Chol

(Table 2; Figures 3 and 4). However, they behave differently when studied against DOPC:SM:Chol (1:1:1) vesicles (Table 2; Figures 3 and 4) and could be ascribed to three different behavior patterns.

First, in the presence of Chol, Y136F was quite similar to the wild-type StnII in terms of membrane affinity (Figure 2) and calcein release activity (Figure 4A) but was not able to interact with the POPC:PSM (4:1) vesicles (Figure 3). These results agree with the role assigned to Tyr136 in interacting specifically with the phosphate oxygens of the POC moiety [24], contributing to its stabilization within the POC-binding pocket. In the absence of Chol, this interaction would then be essential for maintaining the SM molecule at the right position, and therefore this mutant failed in binding efficiently enough to the vesicles.

The second pattern would correspond to the Y135F mutant. Tyr135 is a residue which has been related to interactions with the SM 2NH and 3OH groups through the phenolic hydroxyl group [24]. Both interactions would be absent in the mutant assayed. This would explain the obtained results in terms of lower hemolytic activity (Table 1) and much lower relative membrane binding affinity (Table 2) as well as the dampened calcein release properties (Figure 4A) against DOPC:SM:Chol (1:1:1) vesicles. However, this mutant was completely unable to bind to the POPC:PSM (4:1) vesicles, and therefore it can be inferred that the interactions with the SM molecule involving Tyr135 are enhanced in the presence of Chol.

Regarding the third pattern, the last two mutants studied, R51Q and Y111N, displayed quite low hemolytic activity (especially Y111N) and a rather low affinity for both types of vesicles studied (Table 2).They were also completely inactive in the calcein release experiments (Figure 4). It has been proposed that the POC phosphate moiety could be further stabilized by the cationic side chain of Arg51 [24]. Thus, these results would also support the abovementioned role of Tyr111 in the observed conformational change from its exposed free state to the POC-bound complex [34]. The Y111N mutant would not be able to provide the required interactions and therefore would fail to produce a functional pore even in the presence of Chol (Figure 4A). Finally, according to the present results, it can also be stated that the interaction provided by the side chain of StnII Arg51 is strictly required for membrane recognition independently of Chol.

3.4. StnII Mutant Affecting the Pore-Competent State of Protein Oligomerization

StnII Gly142 belongs to a conserved RGD motif which has been related to maintaining the protein in the correct aggregation competent state, not only in its water-soluble state, but also in its membrane bound configuration [44]. Therefore, it would not be a residue directly involved in membrane recognition, nor in pore formation (Figure 1). In good agreement with this hypothesis, in the presence of Chol, both the G142A mutant and the wild-type protein showed similar behaviors in terms of membrane binding (Table 2; Figure 2) and calcein release activity (Figure 4A). However, this mutant failed to bind to the POPC:PSM (4:1) vesicles (Figure 3). Inspection of the relative orientation of Gly142 within the StnII three-dimensional structure (Figures 1 and 6) suggests how this residue could also be involved in the required long-distance rearrangements [48,49] for its correct attachment to the membrane. The presence of an additional obstructing methyl group in the G142A mutant would distort not only a well-established ionic interaction between Arg141 and Asp143, but also the stabilization of Gly142 by the hydroxyl group of Ser163 (Figure 6). Mutation to Ala would then interfere with these

rearrangements, leading to a more aggregation-prone protein that is nonetheless unable to bind to the membrane in a pore-competent state. This effect would be especially evident in the absence of Chol.

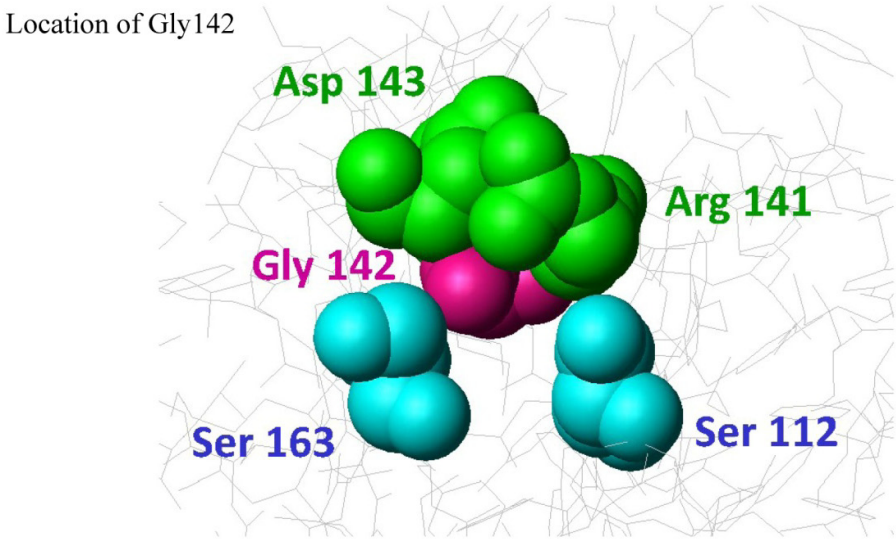

Figure 6. Close-up diagram representation of the residues presumably affected by substitution of StnII Gly142 (red) by an Ala residue: Ser112 (blue), Arg141 (green), Asp143 (green), and Ser163 (blue). Image was generated by the MolMol Program [42].

4. Experimental Section

4.1. Materials

1-Palmitoyl-2-oleoyl-*sn*-glycero-3-phosphocholine (POPC), 1,2-dioleoyl-sn-glycero-3-phosphocholine (DOPC), cholesterol (Chol), and porcine brain sphingomyelin (SM) were obtained from Avanti Polar Lipids. Palmitoyl-SM (PSM) was purified from egg SM using preparative HPLC on a reverse phase (C18) column, as described previously [58,59]. Calcein was from Fluka/Sigma-Aldrich (St. Louis, MO 63103, USA). Sephacryl S200HR was obtained from GE Healthcare. The cDNA coding for the StnII mutants were obtained by the overlap extension mutagenesis method [60], also as described [61]. Wild-type StnII and all the mutants used in this study were produced in an *E. coli* expression system, and purified as described previously [29,43,61].The homogeneity of all protein samples used was analyzed by SDS/PAGE and amino acid analysis after acid hydrolysis of the proteins (5.7 M HCl, 24 h, 110 °C). These amino acid analyses were performed on a Biochrom 20 automatic analyzer (Pharmacia, Cambridge, UK).

4.2. Spectroscopic Characterization

Spectroscopic characterization was essentially performed as previously described [29,44,49,62–64]. Absorbance measurements were carried out on a Uvikon 930 spectrophotometer (Kontron Instruments, Madrid, Spain). The individual $E^{0.1\%}$ (280 nm, 1 cm) coefficients were calculated for every single protein species as described [21,29,44], using their amino acid compositions and specific

UV-absorption spectra [9,21,65]. Far-UV circular dichroism (CD) spectra were obtained on a Jasco 715 spectropolarimeter at50 nm/min scanning speed. Optical path cells of 0.1 cm were employed. Proteins were dissolved in 15 mM MOPS buffer, pH 7.5, containing 100 mM NaCl (0.2 mg/mL protein concentration). At least four spectra were averaged to obtain the final spectrum. CD measurements were also employed to study the thermal stability of the mutants, as described before [29,49,62]. T_m values correspond to the temperature at the midpoint of the monophasic thermal denaturation transition.

4.3. Hemolysis Assay

Hemolysis assays were performed in 96-multiwell plates as previously described [29,61]. Briefly, erythrocytes from heparinized sheep blood were washed in 10 mM Tris buffer, pH 7.4, containing 0.145 M NaCl, to a final OD_{655} of 0.5 when mixing equal volumes of the cell suspension and buffer. The hemolysis was followed as a decrease in OD_{655} after addition of the erythrocyte suspension to twofold serial dilutions of the proteins. An Expert 96 microplate reader (AsysHitech, GmbH, Eugendorf, Austria) was employed to measure OD_{655}. The value obtained with 0.1% (w/v) Na_2CO_3 was considered 100% hemolysis. HC_{50} is the protein concentration required to produce 50% hemolysis.

4.4. Binding of StnII to Bilayer Membranes

Binding was measured using isothermal titration calorimetry (ITC) as described before [24,29,44], using a VP-ITC calorimeter (MicroCal). Briefly, protein solutions at 10 μM were titrated by injection of 20 μL aliquots of lipid suspensions (phospholipid concentration: 5 mM). Binding isotherms were adjusted to a model were the protein binds the membrane involving “n” lipid molecules [29].

4.5. Calcein Leakage Assay

Calcein-entrapped POPC:PSM (4:1) or DOPC:SM:Chol (1:1:1) large unilamellar vesicles (LUVs) were prepared as described [27] by extrusion through 200 nm filters (Nucleopore, Whatman) at 37 °C, or 60 °C if Chol was not present. Briefly, the desired lipids were mixed and dried under a stream of nitrogen. The lipids were re-dissolved in chloroform and dried again before removal of any traces of remaining solvent in vacuum for 60 min. Prior to extrusion, the dry lipid films were hydrated for 30 min at 60 °C (or 37 °C if Chol was present) in Tris buffer (10 mM Tris, 140 mM NaCl, pH 7.4) containing calcein at a concentration of 100 mM. The total lipid concentration was 1.25 mM. LUVs were separated from non-entrapped calcein by gel filtration on Sephacryl S200HR. These LUVs were used for permeabilization studies within 24 h. Phospholipid concentration was determined from P_i measurement [66] after elution of vesicles during isolation. The concentration of LUV phospholipids and StnII during calcein leakage experiments were about 7.5 μM and 20 nM, respectively. Emission at 550 nm was followed at 23 °C as a function of time (excitation at 480 nm). Fluorescence emission was measured with a PTI Quanta-Master spectrofluorimeter (Photon Technology International, Inc., Edison, NJ, USA). To ensure that no major spontaneous leakage occurred, the emission was measured for each sample during 5 min before addition of toxin. A steady signal level, indicating intact vesicles, was observed for all samples.

5. Conclusions

One major conclusion of the results presented here is that Chol is a key molecule in the correct and efficient interaction of StnII with its target membranes in order to produce a functional pore. It is now proven that this lipid molecule is even able to circumvent the impairment produced by the substitution of residues specifically involved in SM recognition and/or membrane surface attachment. Thus, although SM would definitively be the crucial molecule for specific membrane recognition, Chol would also act as a highly important partner in this interaction. At the temperatures employed in these experiments, POPC:SM (4:1) bilayers exist in a liquid disordered phase. However, the DOPC:SM:Chol vesicles employed display liquid disordered-liquid ordered phase coexistence and have domain boundaries. Therefore, the observed effects of Chol could be due not only to the reported specific influence on the SM physical state [27] but also to coexistence of different phases on the membrane. Similar effects have been reported already, if not for attachment, at least for the final formation of the pore [21,25,29,67].

It has been previously acknowledged that a series of conformational changes involving long-distance rearrangements of the residues on the protein side facing the membrane must occur for the correct attachment of StnII to the membrane surface. Substitution of individual residues involved in these rearrangements has a dramatic impact on the interaction of StnII with PSM containing vesicles in the absence of Chol, but the impact of these mutations is nearly negligible if Chol is present. Therefore, it can also be concluded that the presence of Chol would ease the requirements needed for these conformational rearrangements to occur.

Acknowledgments

The work was funded by generous grants from the Sigrid Juselius Foundation (JPS), the Åbo Akademi Foundation (JPS), and BFU2012-32404 from the Spanish Ministerio de Ciencia e Innovación (JGG and AMP) and a FPU fellowship granted to S.G.-L.

Author Contributions

Conceived and designed the experiments: JGF, JPS, AMP. Performed the experiments: SGL, IA, TM. Analyzed and discussed the data: SGL, TM, JGF, JPS, AMP. Wrote the paper: JGF, JPS, AMP.

Conflicts of Interest

The authors declare no conflict of interest.

References

1. Suput, D. *In vivo* effects of cnidarian toxins and venoms. *Toxicon* **2009**, *54*, 1190–1200.
2. Anderluh, G.; Macek, P. Cytolytic peptide and protein toxins from sea anemones (Anthozoa: Actiniaria). *Toxicon* **2002**, *40*, 111–124.

3. Belmonte, G.; Pederzolli, C.; Macek, P.; Menestrina, G. Pore formation by the sea anemone cytolysin equinatoxin-II in red blood cells and model lipid membranes. *J. Membr. Biol.* **1993**, *131*, 11–22.
4. Macek, P.; Belmonte, G.; Pederzolli, C.; Menestrina, G. Mechanism of action of equinatoxin II, a cytolysin from the sea anemone *Actinia equina* l. Belonging to the family of actinoporins. *Toxicology* **1994**, *87*, 205–227.
5. Tejuca, M.; Serra, M.D.; Ferreras, M.; Lanio, M.E.; Menestrina, G. Mechanism of membrane permeabilization by sticholysin I, a cytolysin isolated from the venom of the sea anemone *Stichodactyla helianthus*. *Biochemistry* **1996**, *35*, 14947–14957.
6. Basulto, A.; Pérez, V.M.; Noa, Y.; Varela, C.; Otero, A.J.; Pico, M.C. Immunohistochemical targeting of sea anemone cytolysins on tentacles, mesenteric filaments and isolated nematocysts of *Stichodactyla helianthus*. *J. Exp. Zoolog. A Comp. Exp. Biol.* **2006**, *305*, 253–258.
7. Tejuca, M.; Anderluh, G.; Macek, P.; Marcet, R.; Torres, D.; Sarracent, J.; Alvarez, C.; Lanio, M.E.; Dalla Serra, M.; Menestrina, G. Antiparasite activity of sea-anemone cytolysins on *Giardia duodenalis* and specific targeting with anti-*Giardia* antibodies. *Int. J. Parasitol.* **1999**, *29*, 489–498.
8. Anderluh, G.; Krizaj, I.; Strukelj, B.; Gubensek, F.; Macek, P.; Pungercar, J. Equinatoxins, pore-forming proteins from the sea anemone *Actinia equina*, belong to a multigene family. *Toxicon* **1999**, *37*, 1391–1401.
9. De los Ríos, V.; Oñaderra, M.; Martínez-Ruiz, A.; Lacadena, J.; Mancheño, J.M.; Martínez-del-Pozo, A.; Gavilanes, J.G. Overproduction in *Escherichia coli* and purification of the hemolytic protein sticholysin II from the sea anemone *Stichodactyla helianthus*. *Protein Expr. Purif.* **2000**, *18*, 71–76.
10. Alegre-Cebollada, J.; Oñaderra, M.; Gavilanes, J.G.; Martínez-del-Pozo, A. Sea anemone actinoporins: The transition from a folded soluble state to a functionally active membrane-bound oligomeric pore. *Curr. Protein Pept. Sci.* **2007**, *8*, 558–572.
11. García-Ortega, L.; Alegre-Cebollada, J.; García-Linares, S.; Bruix, M.; Martínez-del-Pozo, A.; Gavilanes, J.G. The behavior of sea anemone actinoporins at the water-membrane interface. *Biochim. Biophys. Acta* **2011**, *1808*, 2275–2288.
12. Bellomio, A.; Morante, K.; Barlic, A.; Gutiérrez-Aguirre, I.; Viguera, A.R.; Gonzalez-Mañas, J.M. Purification, cloning and characterization of fragaceatoxin c, a novel actinoporin from the sea anemone *Actinia fragacea*. *Toxicon* **2009**, *54*, 869–880.
13. Thomson, M.; Moritz, R.L.; Simpson, R.J.; Norton, R.S. Tenebrosin-A, a new cardiostimulant protein from the australian sea anemone *Actinia tenebrosa*. *Biochem. Int.* **1987**, *15*, 711–718.
14. Norton, R.S.; Bobek, G.; Ivanov, J.O.; Thomson, M.; Fiala-Beer, E.; Moritz, R.L.; Simpson, R.J. Purification and characterisation of proteins with cardiac stimulatory and haemolytic activity from the anemone *Actinia tenebrosa*. *Toxicon* **1990**, *28*, 29–41.
15. Simpson, R.J.; Reid, G.E.; Moritz, R.L.; Morton, C.; Norton, R.S. Complete amino acid sequence of tenebrosin-C, a cardiac stimulatory and haemolytic protein from the sea anemone *Actinia tenebrosa*. *Eur. J. Biochem.* **1990**, *190*, 319–328.
16. Monastyrnaya, M.M.; Zykova, T.A.; Apalikova, O.V.; Shwets, T.V.; Kozlovskaya, E.P. Biologically active polypeptides from the tropical sea anemone *Radianthus macrodactylus*. *Toxicon* **2002**, *40*, 1197–1217.

17. Antonini, V.; Perez-Barzaga, V.; Bampi, S.; Penton, D.; Martinez, D.; Dalla Serra, M.; Tejuca, M. Functional characterization of sticholysin I and W111C mutant reveals the sequence of the actinoporin's pore assembly. *PLoS ONE* **2014**, *9*, e110824.
18. Penton, D.; Perez-Barzaga, V.; Diaz, I.; Reytor, M.L.; Campos, J.; Fando, R.; Calvo, L.; Cilli, E.M.; Morera, V.; Castellanos-Serra, L.R.; *et al*. Validation of a mutant of the pore-forming toxin sticholysin-I for the construction of proteinase-activated immunotoxins. *Protein Eng. Des. Sel.* **2011**, *24*, 485–493.
19. Bakrac, B.; Anderluh, G. Molecular mechanism of sphingomyelin-specific membrane binding and pore formation by actinoporins. *Adv. Exp. Med. Biol.* **2009**, *677*, 106–115.
20. Bernheimer, A.W.; Avigad, L.S. Properties of a toxin from the sea anemone *Stoichactis helianthus*, including specific binding to sphingomyelin. *Proc. Natl. Acad. Sci. USA* **1976**, *73*, 467–471.
21. De los Ríos, V.; Mancheño, J.M.; Lanio, M.E.; Oñaderra, M.; Gavilanes, J.G. Mechanism of the leakage induced on lipid model membranes by the hemolytic protein sticholysin II from the sea anemone *Stichodactyla helianthus*. *Eur. J. Biochem.* **1998**, *252*, 284–289.
22. Barlic, A.; Gutiérrez-Aguirre, I.; Caaveiro, J.M.; Cruz, A.; Ruiz-Argüello, M.B.; Pérez-Gil, J.; González-Mañas, J.M. Lipid phase coexistence favors membrane insertion of equinatoxin-II, a pore-forming toxin from *Actinia equina*. *J. Biol. Chem.* **2004**, *279*, 34209–34216.
23. Bakrac, B.; Gutierrez-Aguirre, I.; Podlesek, Z.; Sonnen, A.F.; Gilbert, R.J.; Macek, P.; Lakey, J.H.; Anderluh, G. Molecular determinants of sphingomyelin specificity of a eukaryotic pore-forming toxin. *J. Biol. Chem.* **2008**, *283*, 18665–18677.
24. Maula, T.; Isaksson, Y.J.; García-Linares, S.; Niinivehmas, S.; Pentikainen, O.T.; Kurita, M.; Yamaguchi, S.; Yamamoto, T.; Katsumura, S.; Gavilanes, J.G.; *et al.* 2NH and 3OH are crucial structural requirements in sphingomyelin for sticholysin II binding and pore formation in bilayer membranes. *Biochim. Biophys. Acta* **2013**, *1828*, 1390–1395.
25. Schön, P.; Garcia-Saez, A.J.; Malovrh, P.; Bacia, K.; Anderluh, G.; Schwille, P. Equinatoxin II permeabilizing activity depends on the presence of sphingomyelin and lipid phase coexistence. *Biophys. J.* **2008**, *95*, 691–698.
26. Varanda, W.; Finkelstein, A. Ion and nonelectrolyte permeability properties of channels formed in planar lipid bilayer membranes by the cytolytic toxin from the sea anemone, *Stoichactis helianthus*. *J. Membr. Biol.* **1980**, *55*, 203–211.
27. Alm, I.; García-Linares, S.; Gavilanes, J.G.; Martínez-del-Pozo, A.; Slotte, J.P. Cholesterol stimulate and ceramide inhibit sticholysin II-induced pore formation in complex bilayer membranes. *Biochim. Biophys. Acta Biomembr.* **2014**, *1848*, 925–931.
28. Martínez, D.; Otero, A.; Alvarez, C.; Pazos, F.; Tejuca, M.; Lanio, M.E.; Gutierrez-Aguirre, I.; Barlic, A.; Iloro, I.; Arrondo, J.L.; *et al.* Effect of sphingomyelin and cholesterol on the interaction of St II with lipidic interfaces. *Toxicon* **2007**, *49*, 68–81.
29. Alegre-Cebollada, J.; Cunietti, M.; Herrero-Galán, E.; Gavilanes, J.G.; Martínez-del-Pozo, A. Calorimetric scrutiny of lipid binding by sticholysin II toxin mutants. *J. Mol. Biol.* **2008**, *382*, 920–930.
30. Barenholz, Y.; Thompson, T.E. Sphingomyelins in bilayers and biological membranes. *Biochim. Biophys. Acta* **1980**, *604*, 129–158.

31. Alegre-Cebollada, J.; Rodríguez-Crespo, I.; Gavilanes, J.G.; Martínez-del-Pozo, A. Detergent-resistant membranes are platforms for actinoporin pore-forming activity on intact cells. *FEBS J.* **2006**, *273*, 863–871.
32. Patton, S. Correlative relationship of cholesterol and sphingomyelin in cell membranes. *J. Theor. Biol.* **1970**, *29*, 489–491.
33. Ohvo-Rekilä, H.; Ramstedt, B.; Leppimaki, P.; Slotte, J.P. Cholesterol interactions with phospholipids in membranes. *Prog. Lipid Res.* **2002**, *41*, 66–97.
34. Mancheño, J.M.; Martín-Benito, J.; Martínez-Ripoll, M.; Gavilanes, J.G.; Hermoso, J.A. Crystal and electron microscopy structures of sticholysin II actinoporin reveal insights into the mechanism of membrane pore formation. *Structure* **2003**, *11*, 1319–1328.
35. Athanasiadis, A.; Anderluh, G.; Macek, P.; Turk, D. Crystal structure of the soluble form of equinatoxin II, a pore-forming toxin from the sea anemone *Actinia equina*. *Structure* **2001**, *9*, 341–346.
36. Malovrh, P.; Viero, G.; Serra, M.D.; Podlesek, Z.; Lakey, J.H.; Macek, P.; Menestrina, G.; Anderluh, G. A novel mechanism of pore formation: Membrane penetration by the *N*-terminal amphipathic region of equinatoxin. *J. Biol. Chem.* **2003**, *278*, 22678–22685.
37. Rojko, N.; Kristan, K.C.; Viero, G.; Zerovnik, E.; Macek, P.; Dalla Serra, M.; Anderluh, G. Membrane damage by an alpha-helical pore-forming protein, equinatoxin II, proceeds through a succession of ordered steps. *J. Biol. Chem.* **2013**, *288*, 23704–23715.
38. Rojko, N.; Cronin, B.; Danial, J.S.; Baker, M.A.; Anderluh, G.; Wallace, M.I. Imaging the lipid-phase-dependent pore formation of equinatoxin II in droplet interface bilayers. *Biophys. J.* **2014**, *106*, 1630–1637.
39. Baker, M.A.; Rojko, N.; Cronin, B.; Anderluh, G.; Wallace, M.I. Photobleaching reveals heterogeneous stoichiometry for equinatoxin II oligomers. *Chembiochem* **2014**, *15*, 2139–2145.
40. Subburaj, Y.; Ros, U.; Hermann, E.; Tong, R.; García-Sáez, A.J. Toxicity of an α-pore-forming toxin depends on the assembly mechanism on the target membrane as revealed by single-molecule imaging. *J. Biol. Chem.* **2015**, *290*, 4856–4865.
41. Mechaly, A.E.; Bellomio, A.; Gil-Carton, D.; Morante, K.; Valle, M.; Gonzalez-Mañas, J.M.; Guerin, D.M. Structural insights into the oligomerization and architecture of eukaryotic membrane pore-forming toxins. *Structure* **2011**, *19*, 181–191.
42. Koradi, R.; Billeter, M.; Wüthrich, K. MolMol: A program for display and analysis of macromolecular structures. *J. Mol. Graph.* **1996**, *14*, 29–32, 51–55.
43. Alegre-Cebollada, J.; Lacadena, V.; Oñaderra, M.; Mancheño, J.M.; Gavilanes, J.G.; Martínez-del-Pozo, A. Phenotypic selection and characterization of randomly produced non-haemolytic mutants of the toxic sea anemone protein sticholysin II. *FEBS Lett.* **2004**, *575*, 14–18.
44. García-Linares, S.; Richmond, R.; García-Mayoral, M.F.; Bustamante, N.; Bruix, M.; Gavilanes, J.G.; Martínez-del-Pozo, A. The sea anemone actinoporin (Arg-Gly-Asp) conserved motif is involved in maintaining the competent oligomerization state of these pore-forming toxins. *FEBS J.* **2014**, *281*, 1465–1478.

45. Nyholm, T.K.; Lindroos, D.; Westerlund, B.; Slotte, J.P. Construction of a dopc/psm/cholesterol phase diagram based on the fluorescence properties of trans-parinaric acid. *Langmuir* **2011**, *27*, 8339–8350.
46. De Almeida, R.F.; Fedorov, A.; Prieto, M. Sphingomyelin/phosphatidylcholine/cholesterol phase diagram: Boundaries and composition of lipid rafts. *Biophys. J.* **2003**, *85*, 2406–2416.
47. Veatch, S.L.; Keller, S.L. Miscibility phase diagrams of giant vesicles containing sphingomyelin. *Phys. Rev. Lett.* **2005**, *94*, 148101.
48. Pardo-Cea, M.A.; Castrillo, I.; Alegre-Cebollada, J.; Martínez-del-Pozo, A.; Gavilanes, J.G.; Bruix, M. Intrinsic local disorder and a network of charge-charge interactions are key to actinoporin membrane disruption and cytotoxicity. *FEBS J.* **2011**, *278*, 2080–2089.
49. García-Linares, S.; Castrillo, I.; Bruix, M.; Menéndez, M.; Alegre-Cebollada, J.; Martínez-del-Pozo, A.; Gavilanes, J.G. Three-dimensional structure of the actinoporin sticholysin I. Influence of long-distance effects on protein function. *Arch. Biochem. Biophys.* **2013**, *532*, 39–45.
50. Alegre-Cebollada, J.; Martínez-del-Pozo, A.; Gavilanes, J.G.; Goormaghtigh, E. Infrared spectroscopy study on the conformational changes leading to pore formation of the toxin sticholysin II. *Biophys. J.* **2007**, *93*, 3191–3201.
51. Miller, C.J.; Elliott, J.L.; Collier, R.J. Anthrax protective antigen: Prepore-to-pore conversion. *Biochemistry* **1999**, *38*, 10432–10441.
52. Heuck, A.P.; Tweten, R.K.; Johnson, A.E. Assembly and topography of the prepore complex in cholesterol-dependent cytolysins. *J. Biol. Chem.* **2003**, *278*, 31218–31225.
53. Kristan, K.; Podlesek, Z.; Hojnik, V.; Gutiérrez-Aguirre, I.; Guncar, G.; Turk, D.; González-Mañas, J.M.; Lakey, J.H.; Macek, P.; Anderluh, G. Pore formation by equinatoxin, a eukaryotic pore-forming toxin, requires a flexible *N*-terminal region and a stable β-sandwich. *J. Biol. Chem.* **2004**, *279*, 46509–46517.
54. Hong, Q.; Gutiérrez-Aguirre, I.; Barlic, A.; Malovrh, P.; Kristan, K.; Podlesek, Z.; Macek, P.; Turk, D.; Gonzalez-Mañas, J.M.; Lakey, J.H.; *et al.* Two-step membrane binding by equinatoxin II, a pore-forming toxin from the sea anemone, involves an exposed aromatic cluster and a flexible helix. *J. Biol. Chem.* **2002**, *277*, 41916–41924.
55. Castrillo, I.; Araujo, N.A.; Alegre-Cebollada, J.; Gavilanes, J.G.; Martínez-del-Pozo, A.; Bruix, M. Specific interactions of sticholysin I with model membranes: An nmr study. *Proteins* **2010**, *78*, 1959–1970.
56. Hinds, M.G.; Zhang, W.; Anderluh, G.; Hansen, P.E.; Norton, R.S. Solution structure of the eukaryotic pore-forming cytolysin equinatoxin II: Implications for pore formation. *J. Mol. Biol.* **2002**, *315*, 1219–1229.
57. Pardo-Cea, M.A.; Alegre-Cebollada, J.; Martínez-del-Pozo, A.; Gavilanes, J.G.; Bruix, M. ^{1}h, ^{13}C, and ^{15}NNMR assignments of stnII-Y111N, a highly impaired mutant of the sea anemone actinoporin sticholysin ii. *Biomol. NMR Assign.* **2010**, *4*, 69–72.
58. Jaikishan, S.; Björkbom, A.; Slotte, J.P. Sphingomyelin analogs with branched n-acyl chains: The position of branching dramatically affects acyl chain order and sterol interactions in bilayer membranes. *Biochim. Biophys. Acta* **2010**, *1798*, 1987–1994.

59. Terová, B.; Heczko, R.; Slotte, J.P. On the importance of the phosphocholine methyl groups for sphingomyelin/cholesterol interactions in membranes: A study with ceramide phosphoethanolamine. *Biophys. J.* **2005**, *88*, 2661–2669.
60. Sambrook, J.; Fritsch, E.F.; Maniatis, T. *Molecular Cloning: A Laboratory Manual*, 2nd ed.; Cold Spring Harbor Laboratory: Cold Spring Harbor, NY, USA, 1989.
61. Alegre-Cebollada, J.; Clementi, G.; Cunietti, M.; Porres, C.; Oñaderra, M.; Gavilanes, J.G.; Martínez-del-Pozo, A. Silent mutations at the 5'-end of the cDNA of actinoporins from the sea anemone *Stichodactyla helianthus* allow their heterologous overproduction in *Escherichia coli*. *J. Biotechnol.* **2007**, *127*, 211–221.
62. Mancheño, J.M.; de los Ríos, V.; Martínez-del-Pozo, A.; Lanio, M.E.; Oñaderra, M.; Gavilanes, J.G. Partially folded states of the cytolytic protein sticholysin II. *Biochim. Biophys. Acta* **2001**, *1545*, 122–131.
63. Álvarez-García, E.; Martínez-del-Pozo, A.; Gavilanes, J.G. Role of the basic character of α-sarcin's NH_2-terminal β-hairpin in ribosome recognition and phospholipid interaction. *Arch. Biochem. Biophys.* **2009**, *481*, 37–44.
64. De Antonio, C.; Martínez-del-Pozo, A.; Mancheño, J.M.; Oñaderra, M.; Lacadena, J.; Martínez-Ruiz, A.; Pérez-Cañadillas, J.M.; Bruix, M.; Gavilanes, J.G. Assignment of the contribution of the tryptophan residues to the spectroscopic and functional properties of the ribotoxin α-sarcin. *Proteins* **2000**, *41*, 350–361.
65. De los Ríos, V.; Mancheño, J.M.; Martínez-del-Pozo, A.; Alfonso, C.; Rivas, G.; Oñaderra, M.; Gavilanes, J.G. Sticholysin II, a cytolysin from the sea anemone *Stichodactyla helianthus*, is a monomer-tetramer associating protein. *FEBS Lett.* **1999**, *455*, 27–30.
66. Rouser, G.; Fkeischer, S.; Yamamoto, A. Two dimensional thin layer chromatographic separation of polar lipids and determination of phospholipids by phosphorus analysis of spots. *Lipids* **1970**, *5*, 494–496.
67. Menestrina, G.; Cabiaux, V.; Tejuca, M. Secondary structure of sea anemone cytolysins in soluble and membrane bound form by infrared spectroscopy. *Biochem. Biophys. Res. Commun.* **1999**, *254*, 174–180.

ARTICLE VII

The sea anemone actinoporin (Arg-Gly-Asp) conserved motif is involved in maintaining the competent oligomerization state of these pore-forming toxins

García-Linares, S., Richmond, R., García-Mayoral, M. F., Bustamante, N., Bruix, M., Gavilanes, J. G. and Martínez-del-Pozo, Á. (2014). *FEBS J* 281(5): 1465-1478.

El dominio conservado (Arg-Gly-Asp) de las actinoporinas de anémonas marinas está implicado en el mantenimiento del estado competente de oligomerización de estas toxinas formadoras de poros

Las actinoporinas de anémonas marinas constituyen un modelo ideal para investigar mecanismos de formación de poros de membrana. Todas las actinoporinas conocidas tienen la misma estructura general compuesta por un sándwich β flanqueado por dos hélices α. El componente crucial para la formación del poro parece ser la hélice localizada en el extremo N-terminal. El papel de otras regiones de la proteína en la unión a la membrana también está ampliamente establecido. Sin embargo, no se sabe mucho sobre los residuos implicados en la oligomerización necesaria para la formación del poro. El análisis detallado de las estructuras tridimensionales de las formas solubles de las actinoporinas producidas por *Stichodactyla helianthus*, sugiere qué residuos pueden estar implicados en dicha oligomerización. Una de estas regiones contiene una secuencia conservada compatible con un motivo RGD de unión a integrinas. Los resultados que se presentan en este trabajo corresponden a mutantes que afectan a este motivo en una de las actinoporinas más estudiadas, StnII. Pequeñas modificaciones en esta secuencia de tres residuos tienen efectos cruciales en la solubilidad de la proteína. Un único grupo metilo (RAD) produce un mutante con una actividad hemolítica altamente disminuida y un patrón de oligomerización alterado. Los resultados obtenidos se han discutido en términos de un papel clave del motivo RGD en el mantenimiento de un estado de oligomerización competente para que las actinoporinas puedan formar el poro.

the FEBS Journal

The sea anemone actinoporin (Arg-Gly-Asp) conserved motif is involved in maintaining the competent oligomerization state of these pore-forming toxins

Sara García-Linares[1], Ryan Richmond[1], María F. García-Mayoral[2], Noemí Bustamante[2], Marta Bruix[2], José G. Gavilanes[1] and Álvaro Martínez-del-Pozo[1]

1 Departamento de Bioquímica y Biología Molecular I, Facultad de Ciencias Químicas, Universidad Complutense, Madrid, Spain
2 Instituto de Química-Física Rocasolano, Madrid, Spain

Keywords
actinoporin; equinatoxin; haemolysis; integrin; pore formation; sticholysin

Correspondence
J. G. Gavilanes, Departamento de Bioquímica y Biología Molecular I, Facultad de Ciencias Químicas, Universidad Complutense, 28040 Madrid, Spain
Fax: +34 91 934 4159
Tel: +34 91 394 4158
E-mail: ppgf@bbm1.ucm.es
A. Martínez-del-Pozo, Departamento de Bioquímica y Biología Molecular I, Facultad de Ciencias Químicas, Universidad Complutense, 28040 Madrid, Spain
Fax: +34 91 934 4159
Tel: +34 91 394 4158
E-mail: alvaromp@quim.ucm.es

(Received 30 October 2013, revised 12 December 2013, accepted 31 December 2013)

doi:10.1111/febs.12717

Sea anemone actinoporins constitute an optimum model to investigate mechanisms of membrane pore formation. All actinoporins of known structure show a general fold of a β-sandwich motif flanked by two α-helices. The crucial structure for pore formation seems to be the helix located at the N-terminal end. The role of several other protein regions in membrane attachment is also well established. However, not much is known about the protein residues involved in the oligomerization required for pore formation. Previous detailed analysis of the soluble three-dimensional structures of different wild-type and mutant actinoporins from *Stychodactyla helianthus* suggested residues which could be involved in this oligomerization. One of these stretches contains a conserved sequence compatible with an integrin-binding RGD motif. The results presented now deal with mutants affecting this motif in the well-characterized actinoporin sticholysin II. Small modifications along this three-residue sequence had profound effects on its solubility. Just a single methyl group yielded an RAD mutant version with a highly diminished haemolytic activity and altered oligomerization behaviour. The results obtained are discussed in terms of a key role for the RGD motif in maintaining the actinoporins' pore-competent state of protein oligomerization.

Structured digital abstract
- StnII and StnII bind by molecular sieving (1, 2)

Introduction

Sea anemone actinoporins constitute an interesting group of small and basic α-pore-forming toxic proteins [1–4]. They not only represent an ideal system to study water-soluble to integral membrane protein transitions but are also optimal to investigate the mechanisms of membrane pore formation. Studies using synthetic liposomes, or different mammalian erythrocytes, have shown how the oligomeric cation selective pores formed by actinoporins result in colloid-osmotic shocks that lead to cell death [5–7]. It has also been demonstrated that the lipidic composition is a key factor for actinoporin membrane integration and pore formation. Thus, their target membranes must contain sphingomyelin (SM), display phase coexistence, or both [3,8–17]. In fact, binding of these proteins to SM is so specific that it has even been postulated that this

Abbreviations
Chol, cholesterol; DGR, a mutant version of StnII where Arg141 and Asp143 are substituted by Asp and Arg, respectively; DOPC, 1,2-dioleoyl-*sn*-glycero-3-phosphocholine; EAQ, a mutant version of StnII where Arg141, Gly142 and Asp143 are substituted by Glu, Ala and Gln, respectively; POC, phosphocholine; RAD, a mutant version of StnII where Gly142 is substituted by Ala; SM, sphingomyelin; Stn, sticholysin.

lipid might behave as a real membrane receptor [10,15,17]. However, although it is quite obvious that their natural function must be related to defence and/or predation, and although they have been shown to be lethal to some small crustaceans, molluscs and fish [18,19], their natural specific targets are not really known yet at the molecular level.

The structures of several actinoporins are known [20–24], including the crystal structure of a nonamer obtained in the presence of detergent [25]. They all show a general fold of a β-sandwich motif composed of 10–12 β-strands flanked by two α-helices (α1 and α2) which interact with both sides of the β-sandwich (Fig. 1). One of these helices (α1) is located near the N-terminal end and appears to be crucial for the final functionality of the pore since it has been proposed to detach from the β-sandwich and then extend and insert into the membrane to form the pore wall [26–33]. However, short peptides containing the sequence corresponding to this N-terminus show poor haemolytic activity [34]. This observation has been interpreted as the bulk of the protein being essential for efficient pore formation. In fact, at least three more regions of the structure seem to be especially important from a functional point of view: a phosphocholine (POC) binding site [14,16,22,33,35–37], a cluster of aromatic residues [16,27,33,35,38] and an array of basic amino acids [21].

The sea anemone *Stychodactyla helianthus* produces two very similar actinoporins named sticholysins I and II (StnI and StnII, respectively). Detailed analysis of the soluble 3D structures of wild-type StnI [24] and an StnII R29Q mutant [36] revealed the existence of residues affected by conformational exchange processes which were not among those just mentioned above. Hence, it was speculated that these residues could be involved in other types of interaction apart from those directly related to lipid binding and pore formation, such as oligomerization for example. Three of them comprise a stretch that contains a sequence compatible with an integrin-binding RGD motif (Arg141, Gly142 and Asp143 for StnII). In fact, most actinoporins contain this three amino acid long sequence, which might then play an important role by directing protein attachment to integrin-like receptors on the cell surface [1,39,40], a possibility that has not yet been studied.

Given this premise, the work presented here describes the production of three different mutants affecting this RGD motif which was changed to RAD, DGR and EAQ. Only the first of these three protein variants was soluble enough to be purified in the amount required for an exhaustive characterization, suggesting a key role for the RGD motif in protein oligomerization. The results obtained with this StnII G142A mutant (RAD variant) show the crucial role of the RGD motif in maintaining the pore-competent state of protein oligomerization.

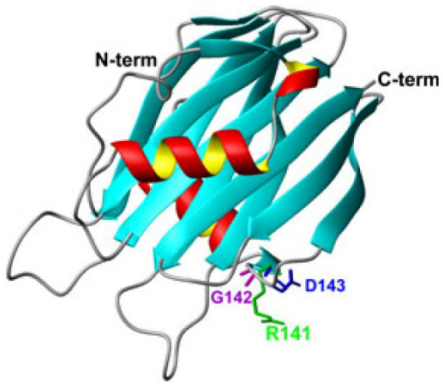

Fig. 1. Ribbon diagram showing the 3D structure of StnII. The location of the RGD motif is indicated showing the side chains of the three different amino acids involved: Arg141 (green), Gly142 (magenta) and Asp143 (blue). The N- and C-terminal ends are also labelled. The helix appearing at the foreground of the diagram corresponds to the N-terminal α1-helix. The image was constructed from the atomic coordinates deposited in the PDB (reference 1GWY) and was generated with the MOLMOL program [73].

Results

Protein production and structural characterization

Wild-type StnII and the corresponding RAD mutant (G142A) were purified to SDS/PAGE homogeneity with yields comparable to those described before for other mutants (Table 1) [41] (Fig. S1). Production of the other two mutants, EAQ and DGR, gave insoluble precipitates which were useless for purification (Fig.

Table 1. Features summary of the purified proteins. *Q* is the relative fluorescence quantum yield for excitation at 275 nm to that of wild-type StnII considered as 1.00. HC_{50} is the concentration (nM) of actinoporin required for 50% haemolysis under the assay conditions. The relative HC_{50} value is defined as mutant HC_{50}/wild-type HC_{50}. This value increases as the haemolytic activity is reduced. T_m is the mid-point temperature of the thermal denaturation transition.

StnII	Purification yield ($mg \cdot L^{-1}$)	$E^{0.1\%}$ (280 nm, 1 cm)	*Q*	HC_{50}	Relative HC_{50} value	T_m (°C)
RAD	7.5	2.30	1.04	10.6	7.6	61
Wild-type	5.2	2.54	1.00	1.4	1.0	67

S1). Therefore, the work was finally conducted on the RAD variant only.

As expected, taking into account that no aromatic residues were changed, the measured $E^{0.1\%}$ (280 nm, 1 cm) value was 2.30, still within the 10% range of the corresponding value of wild-type StnII (Table 1). Far and near-UV CD spectra of the RAD protein variant revealed also very similar secondary and tertiary structures compared with the wild-type protein (Fig. S2A, B). Only very small variations were observed in terms of the fluorescence emission (Fig. S2C,D) and near-UV CD spectra (Fig. S2B). Finally, the thermal denaturation profile showed a significantly lower T_m value (Table 1), but still quite high above the temperatures used in all the experiments described below.

NMR characterization

NMR signal assignment revealed the absence of major conformational changes within the RAD mutant compared with the wild-type protein, in good agreement with the CD and fluorescence emission characterization. Only minor modifications were observed in the vicinity of the mutated region. Wild-type StnII 3D conformation has only been determined by X-ray diffraction of its crystalline structure [22]. However, two different mutants (R29Q and Y111N) have been characterized in deep detail using multidimensional NMR spectroscopy [36,42,43]. Consequently, to estimate the chemical shift changes (Δδ Cα) of the RAD mutant with respect to the wild-type protein (Fig. 2A), we used previous data corresponding to the R29Q mutant (BMRB deposition number 16362) except for the stretch 27–31, which contains the residue mutated and was instead taken from the Y111N mutant (BMRB deposition number 16630). Apart from Gly142, major changes were only observed for regions spatially close to the position changed such as those around Asn113 and Thr162. In fact, close inspection of the wild-type StnII structure revealed the existence of a hydrogen bond between both of these residues while simultaneously Asn113 is also hydrogen bonded to Gly142. Therefore, it seems that only this network of interactions was observably disrupted by the introduced mutation.

Interestingly, although studied in identical conditions (around 0.5 mM protein concentration), the NMR signals of the RAD mutant were much broader than those of other previously characterized StnII mutants [36,42,43], suggesting the contribution of higher-order aggregation processes (see below). Mean relaxation rates reported for the R29Q and Y111N mutants were R_1 0.9 and 1.0 s^{-1}, R_2 21 and 18 s^{-1}, respectively. In contrast, ^{15}N heteronuclear relaxation data of the RAD mutant (Fig. 2B–D) revealed a smaller R_1 value (0.8 s^{-1}) and a much higher R_2 value

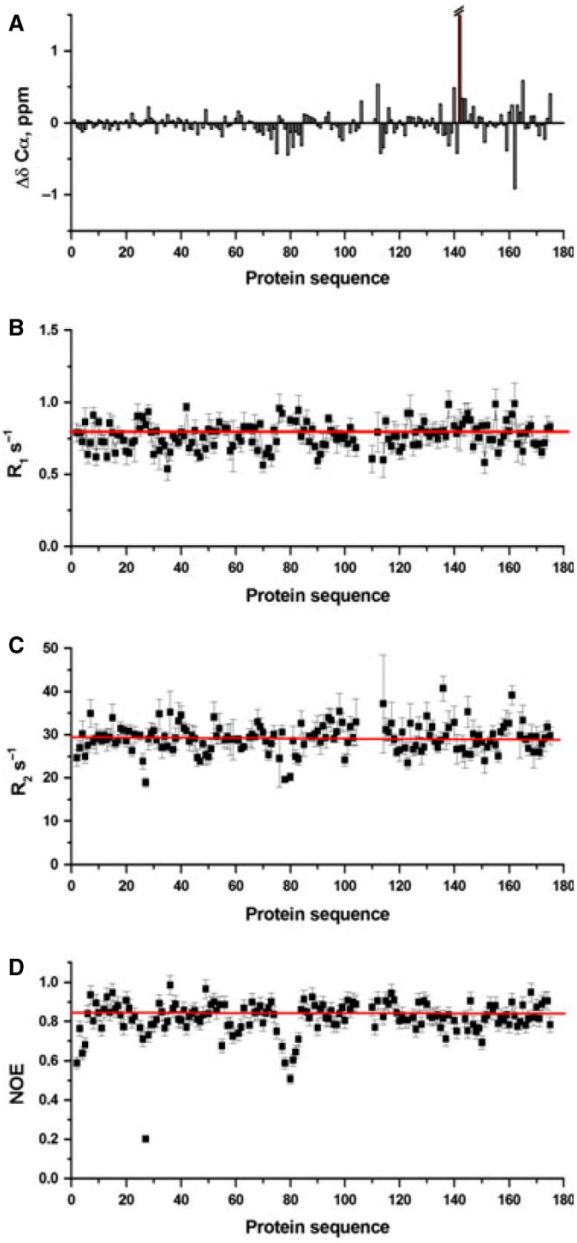

Fig. 2. NMR characterization of the StnII G142A mutant. (A) Comparison of the Δδ Cα chemical shifts of the RAD mutant and the R29Q and Y111N stretches corresponding to the wild-type sequences. (B) R_1 heteronuclear relaxation rates as a function of the protein sequence. (C) R_2 heteronuclear relaxation rates as a function of the protein sequence. (D) NOE heteronuclear relaxation values as a function of the protein sequence. Red lines indicate the mean value. Experimental conditions: 800 MHz, 0.5 mM, pH 4.0 and 25 °C.

(29.2 s^{-1}), which gave an R_2/R_1 ratio compatible with a molecular entity of much higher correlation time [44] and suggested the existence of protein aggregation [45].

Analytical ultracentrifugation analysis

In the light of the results reported above, ultracentrifugation studies were performed for the RAD mutant protein solution used in the NMR characterization. Sedimentation velocity (560 μM protein concentration in water) experiments were conducted (Fig. 3). The sedimentation coefficients obtained for the StnII RAD mutant in these conditions indicated the presence of different species in the sample – monomer ($s_{20,w}$ = 2.2 S, 56%), dimer ($s_{20,w}$ = 3.1 S, 42%) and tetramer ($s_{20,w}$ = 5.25 S, 2%) – suggesting an aggregation-prone behaviour of this mutant in solution. Not surprisingly, equilibrium sedimentation analysis of this sample after an almost 40-fold dilution (15 μM protein concentration) yielded results compatible with only a single monomer species (Fig. 3) with an average molecular mass (MW_{app}) of 20.7 ± 0.7 kDa (average of all velocities assayed).

Functional characterization

The RAD mutant functionality was assayed by measuring its haemolytic activity against sheep erythrocytes. As can be observed in Fig. 4, this mutant showed an HC_{50} value of 10.6 nM, significantly higher than that of wild-type StnII (1.4 nM) under identical conditions (Table 1). This decreased haemolytic activity could be due to a diminished ability to form the final pore or to a reduction of its binding affinity, or both. To distinguish between these possibilities, binding experiments were done. Unfortunately, direct binding to erythrocytes cannot be accurately quantitated given that the proteins studied produce haemolysis. Thus, a standard ultracentrifugation binding assay was performed. This assay is based on the employment of SM : DOPC : Chol (1 : 1 : 1) lipid vesicles which are routinely used as a lipid-only system to study the interaction with sticholysins [24,33,46]. The results obtained, shown in Fig. 5, revealed an indistinguishable behaviour compared with the wild-type protein and suggested that the region mutated was not involved in lipid recognition.

Altogether, these results seemed to suggest the presence of an integrin-like receptor in the erythrocytes used. However, such a receptor does not seem to be present in the red blood cells' membrane [47]. Taking into account that RGD-mediated interactions can be inhibited by short peptides encompassing the RGD sequence [48,49], haemolysis assays were also performed with the wild-type StnII in the presence of increasing concentrations of a GRGDTP hexapeptide [49]. However, changes in the haemolytic behaviour

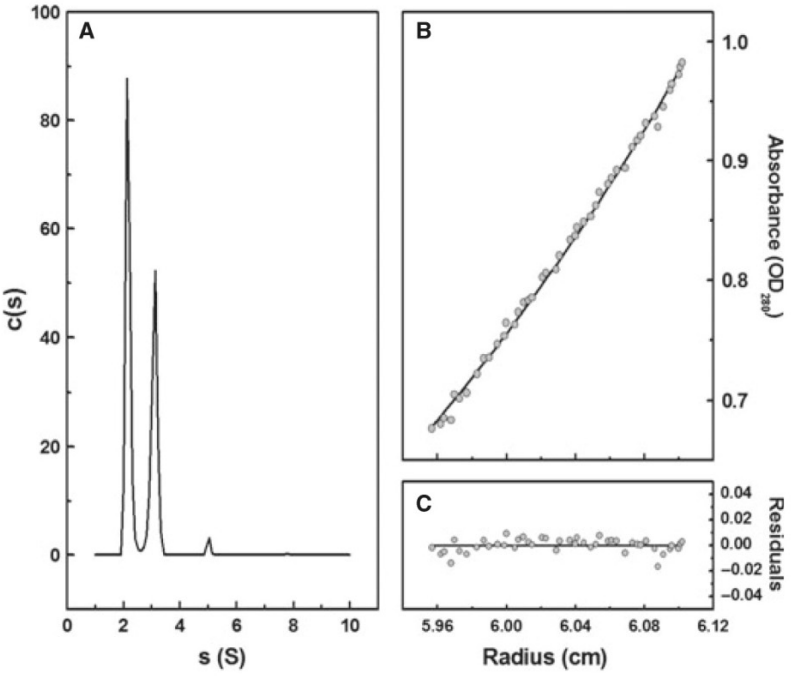

Fig. 3. Characterization of the StnII G142A mutant by analytical ultracentrifugation. (A) Distribution of sedimentation coefficients measured at 182 900 ***g*** and 560 μM. (B) Sedimentation equilibrium profile of the experimental data (grey circles) at 14 500 ***g*** with an average mass of 20.5 ± 0.2 kDa. The continuous line shows the best fit of the experimental data to a single species. The concentration of the sample was 15 μM. (C) Residual distribution of experimental data. Both equilibrium and velocity sedimentation measurements were performed in water at 20 °C.

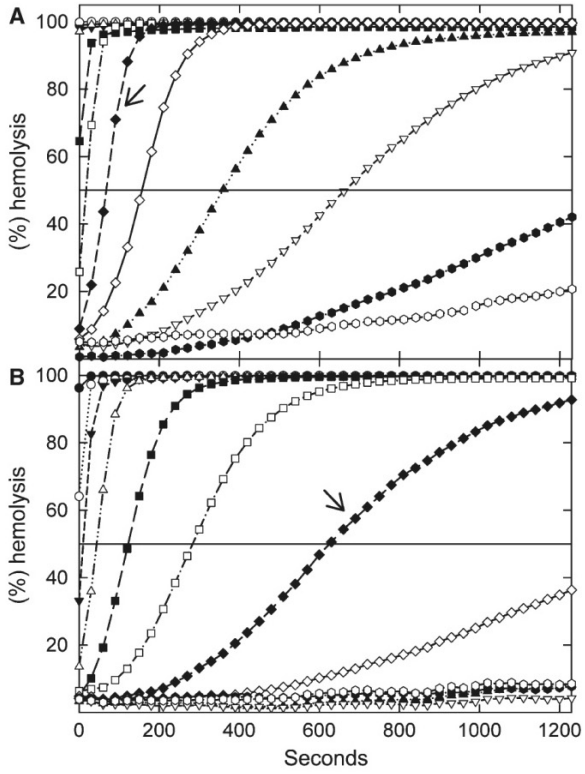

Fig. 4. Haemolytic activity (% haemolysis) of wild-type StnII (A) and its RAD mutant (B). Results are expressed as percentages of the haemolysis produced by 0.1% (w/v) Na_2CO_3 as a function of time. The protein concentrations shown are 640.0 (black dots), 320.0 (white dots), 160.0 (black down triangles), 80.0 (white up triangles), 40.0 (black squares), 20.0 (white squares), 10.0 (black diamonds), 5.0 (white diamonds), 2.5 (black up triangles), 1.25 (white down triangles); 0.63 (black hexagons) and 0.31 nM (white hexagons). The arrows indicate the traces corresponding to the 10 nM concentration of protein in both graphs.

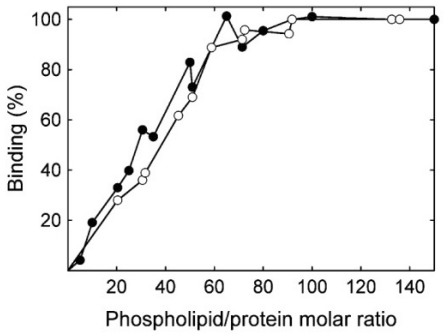

Fig. 5. Binding of wild-type StnII and its RAD mutant to SM : DOPC : Chol (1 : 1 : 1) vesicles. The protein bound to the vesicles (expressed as a percentage) was calculated by subtracting the amount of protein remaining in the supernatant after co-sedimentation of the protein–lipid vesicle complexes by ultracentrifugation to the total amount of protein (100% being the total protein amount present in the assay). WT, solid circles; RAD, empty circles.

were not observed within the 20 nM to 175 μM peptide concentration range assayed, a range quite far above the expected values for showing specific integrin-binding inhibition [49]. This lack of inhibition would also be in agreement with the mentioned absence of integrin-like receptors on the erythrocyte membrane.

Haemolysis experiments were also carried out using combined amounts of wild-type and RAD StnII proteins. These experiments, shown in Fig. 6, were made maintaining a final actinoporin concentration value of 8.0 nM but changing the molar ratio of both species as [wt]/([wt] + [RAD]), where [wt] and [RAD] are the protein molar concentrations of the wild-type and RAD mutant proteins, respectively. The result revealed a behaviour which did not differ from that expected if both protein species behaved independently (see Fig. 6B). Thus, as the RAD mutant proportion increased, the percentage of haemolysis did not change significantly in comparison with the expected values for the wild-type protein behaviour. Accordingly, the mutant would retain the ability to bind to a membrane (Fig. 5) but would not be able to interact with the wild-type protein, at least in terms of competing with the association of wild-type protein monomers required to form a productive pore.

Effect of dilution on the NMR spectra

In view of the above results, NMR characterization of the StnII RAD mutant was attempted then at the low concentration value (15 μM) where only the monomer species had been observed in ultracentrifugation studies (Fig. 3). The NMR assignment was done as for the concentrated solutions. In these conditions, some signals were found to change their position in the spectra after dilution (Fig. 7). Interestingly, R_1 values also increased significantly (mean value 1.0 s^{-1}), suggesting a marked decrease in the amount of aggregates present in the molecular equilibrium, in good agreement with the ultracentrifugation results (Fig. 3). R_2 was not measurable at these low concentration conditions. Thus, taking into account the specific residues that changed their chemical shifts after dilution, it was possible to construct a surface map revealing the regions presumably involved in the aggregation process (Fig. 7).

According to these results, residues 28, 51, 82–84, 119, 128, 131, 134, 135 and 137 (Fig. 7) and the

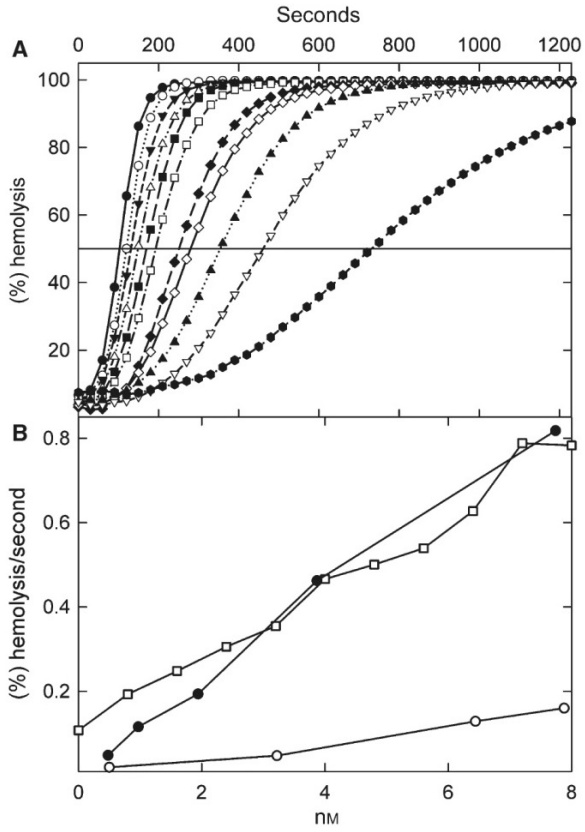

Fig. 6. Haemolytic activity of different mixtures of wild-type StnII and its RAD mutant. The total actinoporin concentration was always 8.0 nM. (A) The percentage of haemolysis is represented for the different wild-type StnII molar fractions ([wild-type]/([wild-type] + [RAD]) used: 1.0 (black dots), 0.9 (white dots), 0.8 (black down triangles), 0.7 (white up triangles), 0.6 (black squares), 0.5 (white squares), 0.4 (black diamonds), 0.3 (white diamonds), 0.2 (black up triangles), 0.1 (white down triangles) and 0.0 (black hexagons). (B) Different haemolytic rates, calculated from the graphs in Fig. 4 as the slope of the linear segment of the kinetic traces and expressed as haemolysis (%)/second, were plotted as a function of the different protein concentrations of wild-type (black dots) and RAD mutant (white dots) employed. The result of plotting the rates calculated from the mixtures shown in (A) as a function of only the wild-type StnII concentration in each of these mixtures (white squares) is also shown.

regions nearby are the most affected by protein concentration and would therefore play a major role in these protein–protein interactions. Most of the changes observed were concentrated in the loop and flexible regions, but some residues in β-strands (β_6 111–120, β_7 148–151) and the helix α2 (128–137) were also affected. Interestingly, if we consider the structure of this protein as a β-sandwich flanked by two α-helices which interact with both of its sides, the surface most affected by the aggregation observed at high concentration would be located opposite to the side containing the N-terminal α-helix, which was not found to be perturbed (Fig. 7).

Model construction

Taking into account this surface map, and the ultracentrifugation results that suggested that a tetramer could be present in the NMR studied concentrated samples, models compatible with the NMR dilution data were built to describe possible assemblies of the StnII RAD variant. Different solutions were obtained with HADDOCK [50], all of them with spatial arrangements where the helix α1, apparently not involved in the aggregation process described now, appeared exposed on the oligomeric protein surface while the helix α2 remained buried. As an example of this situation, two representative models are shown in Fig. 8. Interestingly, most of the residue side chains involved in binding to the membrane (the POC binding site, the cluster of aromatic residues and the array of basic amino acids) [4] remained freely available to interact with the phospholipid vesicles within the reconstructions made. Among them, only Arg51 and Val85, presumably belonging to the POC binding site, and the basic C-terminal Arg175 residue seemed affected by the oligomerization observed in solution after NMR characterization at high protein concentration (Fig. 7A). On the other hand, the location of the α1-helices would not be compatible with the association assembly needed to constitute the pore [51].

Overall, these models could explain why the mutant protein behaves indistinguishably from the wild-type StnII upon binding to the vesicle model membranes but at the same time shows a highly diminished haemolytic activity. Within this idea, the RAD mutant would tend to oligomerize giving rise to non-productive tetramers which would compete with the right competent oligomerization state. This competition would result in significantly lower haemolysis efficiency (Fig. 4).

Discussion

Much work has been done in order to elucidate the mechanism of pore formation by actinoporins. Accordingly, it is fairly well accepted that the N-terminal α1-helix plays a key role in making a conductive pore. Even considering the actual controversy regarding the stoichiometry and/or toroidal nature of this pore [3,4,25,51,52], there is general agreement accepting that helix detachment and elongation are essential

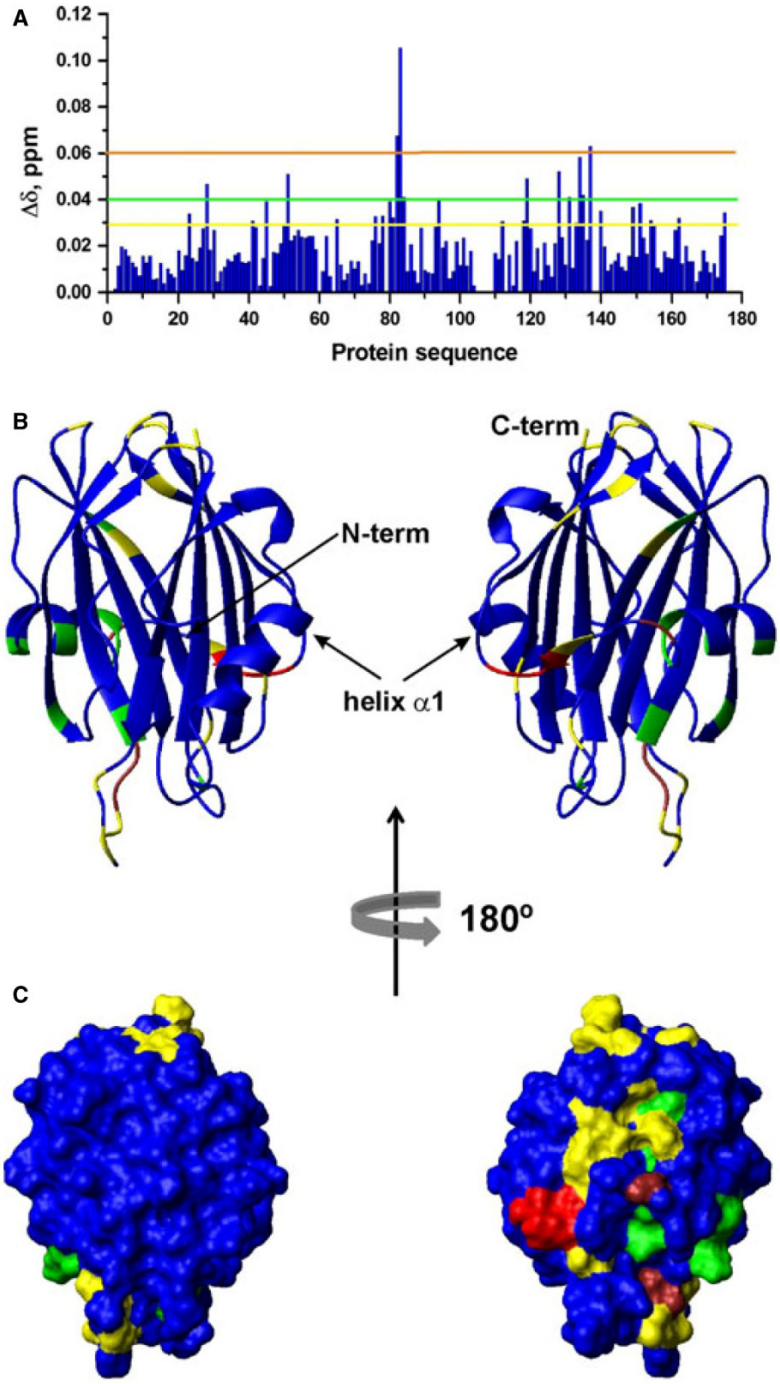

Fig. 7. Effect of dilution on the NMR parameters of StnII G142A. (A) Changes in the chemical shifts of the amide $^{1}H-^{15}N$ correlations measured at 560 μM and 15 μM as a function of the protein sequence. Δδ values were calculated using the formula $\{\Delta\delta(^{1}H)^2 + [\Delta\delta(^{15}N)/5]^2\}^{1/2}$, where $\Delta\delta(^{1}H)$ and $\Delta\delta(^{15}N)$ are the differences between the chemical shifts in the concentrated and dilute conditions. Horizontal lines represent Δδ variations in three ranges: brown $\Delta\delta > 0.06$ ppm, green $0.04 < \Delta\delta < 0.06$, and yellow $0.03 < \Delta\delta < 0.04$. This colour code is maintained in (B) and (C). (B) Ribbon representation of the X-ray structure of StnII (PDB 1GWY) coloured with the Δδ perturbation values. (C) Interacting surface of StnII G142A self-association mapped according to the NMR data. Right and left views are rotated 180º. Residues R141, G142 and D143 are represented in red. The N-term, C-term and helix α1 are labelled.

events for its correct establishment [26–30,32,52,53]. There is also consensus about the fact that the β-sandwich would constitute a membrane recognition motif behaving quite independently from the actual formation of the pore. This concept is supported not only by many experiments carried out with different actinoporin mutants but also by the fact that many other proteins use it as an archetypal fold for specific binding to other molecules or surfaces apart from plasmatic membranes [54–58]. In particular, three protein regions have been shown to participate in membrane recognition: an exposed cluster of aromatic residues,

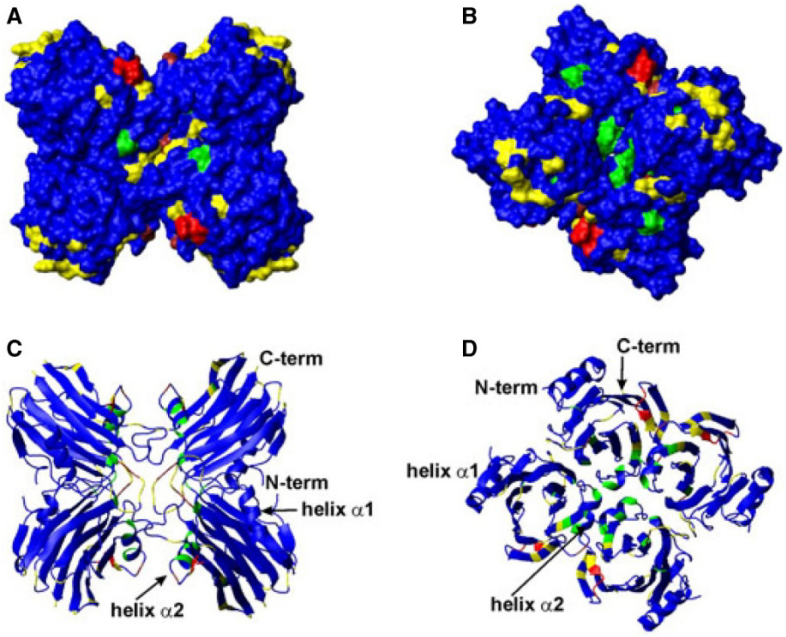

Fig. 8. Unproductive aggregation model. Two StnII tetramer docked structures (A–C; B–D) obtained with HADDOCK in surface (A and B) and ribbon representation (C and D). The colour code is the same as in Fig. 7. N-term, C-term, α1- and α2-helices are labelled in one monomer of each tetramer.

an array of basic amino acids, and a POC binding site [24,28,35,37,56,59]. All these regions seem to be located on the protein surface facing the phospholipid membrane and consequently play important roles in membrane recognition and attachment. However, a large part of the protein still remains unexplored, with no known function yet assigned in the protein–protein interactions involving the oligomerization needed for pore formation.

With this in mind, previous analysis revealed the existence of residues that could be involved in interactions leading to protein oligomerization [24,36]. Inspection of these sequences revealed that they contained the conserved potential integrin-binding RGD motif (Arg141, Gly142 and Asp143 for StnII), suggesting that it might participate in promoting attachment to integrin-like receptors on the surface of cells [1,39,40]. The results shown here support a different hypothesis. The RGD sequence region would be important for maintaining the correct oligomerization state of the protein and the convenient geometric arrangement of the protein monomers in order to form a functional pore.

First, as stated above, even minimal modifications of this sequence (RGD changed to DGR or EAQ) led to protein precipitation, making insoluble aggregates and showing its importance in maintaining the solubility of the monomeric species and therefore monomer–monomer interactions. Only a very minor change was allowed, the introduction of just a single methyl group, which yielded a soluble mutant (StnII RAD). It thus seems clear that this three amino acid long sequence plays a crucial role in maintaining the water-soluble state. This hypothesis was corroborated by the ultracentrifugation analysis which showed how after the NMR analysis at high concentration the RAD mutant displayed a significant proportion of a tetrameric species which disappeared upon dilution (Fig. 3).

On the other hand, binding of this StnII RAD mutant to phospholipid model vesicles was indistinguishable from wild-type StnII (Fig. 5), confirming the apparent lack of direct involvement of the RGD motif in bilayer attachment and/or recognition, in accordance with the many different studies carried out before with proteins belonging to the actinoporin family [2–4,60]. However, the RAD mutant also showed a highly diminished haemolytic activity (Fig. 4 and Table 1). This functional impairment could not be attributed to misrecognition of integrin-like receptors on the erythrocyte membrane because of their absence in such membranes, suggesting that a different mechanism should be found to explain these results.

The NMR characterization of the RAD mutant at two very different concentrations allowed the construction of a map revealing the residues and surfaces involved in the interactions conducing to the dimer and tetramer species observed at 0.5 mM protein concentration (Fig. 7). This map was used to dock the monomers *in silico* into tetramers, obtaining a collection of different structures which shared the common feature of displaying the N-terminal α1-helix in an

exposed position but unable to participate in pore formation (Fig. 8). A careful inspection of the geometry of the tetramers not only revealed that the elongation of this α-helix towards the membrane recognition face in one monomer was sterically blocked by the adjacent molecule but also suggested that these helices were too far apart to associate into a functional pore (Fig. 8). This could explain the impaired ability of the StnII RAD mutant to form native pores resulting in its low haemolytic activity.

In summary, the long known actinoporins' RGD motif seems to contribute to maintaining the proteins in the correct competent state of aggregation, not only in their water-soluble state but also in their membrane-bound configuration. Otherwise, given that binding appears unaffected, differences in haemolytic activity would have been negligible. However, since the natural targets of these proteins do not seem to be mammalian erythrocytes, but instead some small fishes or crustaceans [18,19], the possibility for the RGD sequence motif being also involved in binding to some integrin-like receptor when encountering the right prey cannot be discarded by the results presented now.

Experimental procedures

Protein production and purification

Wild-type StnII and its mutants were produced in an *Escherichia coli* expression system that has been described before [24,33,41]. The cDNAs coding for the three StnII mutants RAD, DGR and EAQ were obtained by the overlap extension mutagenesis method [61], also as described elsewhere [41]. Inserts from the final expression plasmids were sequenced to assure that no mutations other than the expected were present. DNA manipulations were performed according to standard procedures [61].

The unlabelled versions of the wild-type and the different mutants of StnII, as well as the double uniformly labelled $^{13}C/^{15}N$ StnII RAD variant, were produced by following a protocol previously described [41]. For the labelled form, cells were grown in an M9 minimal medium with $^{15}NH_4Cl$ (1 g·L^{-1}) and $^{13}C_6$-glucose (4 g·L^{-1}) as the sole nitrogen and carbon sources. Wild-type and RAD StnII purification was achieved by ion exchange chromatography on CM52 cellulose equilibrated in 50 mM Tris/HCl at pH 7.8. The homogeneity of all protein samples used was analysed by SDS/PAGE and amino acid analysis after acid hydrolysis of the proteins (5.7 M HCl, 24 h, 110 °C). These amino acid analyses were performed on a Biochrom 20 automatic analyser (Pharmacia, Uppsala, Sweden).The results were in agreement with those expected and were used to estimate extinction coefficients and protein concentrations.

Spectroscopic characterization

Spectroscopic characterization was essentially as previously described [24,33,62,63]. Absorbance measurements were carried out on an Uvikon 930 spectrophotometer (Kontron Instruments, Milan, Italy). CD spectra were obtained on a Jasco 715 spectropolarimeter (Easton, MD, USA) at 50 nm·min^{-1} scanning speed. Optical path cells of 0.1 cm were employed in the far-UV region, whereas optical path cells of 1.0 cm were used in the 250–350 nm range. Proteins were dissolved in 15 mM MOPS buffer, pH 7.5, containing 100 mM NaCl (0.2–1.0 mg·mL^{-1} protein concentration). At least four spectra were averaged to obtain the final spectrum. CD measurements were also employed to study the thermal stability of the mutants, as described before [24,33,62]. Fluorescence emission spectra were recorded on an SLM Aminco 8000 spectrofluorimeter at 25 °C using a slit width of 4 nm for both excitation and emission beams. The spectra were recorded for excitation at 275 and 295 nm and both were normalized by considering that Tyr emission above 380 nm is negligible. The Tyr contribution was calculated as the difference between the two normalized spectra. Thermostatted cells with a path length of 0.4 and 1.0 cm for the excitation and emission beams, respectively, were used. The temperature was controlled using a circulating water bath.

NMR samples, assignment and dynamics

Typically, samples contained up to 0.5 mM protein and were prepared in both 90% H_2O/10% D_2O and D_2O at pH 4.0 (uncorrected for deuterium isotope effects). Sodium-4,4-dimethyl-4-silapentane-1-sulfonate was used as internal ^1H chemical shift reference, and both ^{13}C and ^{15}N chemical shifts were calibrated through indirect referencing [64]. The NMR spectra were recorded in a Bruker AV-800 instrument equipped with cryoprobe and field gradients. All data were acquired and processed with TOPSPIN (version 2.1) (Bruker, Germany) at 25 °C. The acquisition data matrix was zero-filled to double the number of original points in all dimensions and shifted squared sine-bell apodization functions were applied in all dimensions prior to Fourier transformation. Baseline correction was applied in all dimensions. NMR assignments were performed following the heteronuclear strategy by using a standard suite of heteronuclear 2D and triple resonance 3D spectra, ^1H-^{15}N-HSQC, ^1H-^{13}C-HSQC, HN(CO)CA, HNCA, CBCA(CO)NH, CBCANH, HNCO, HC(C)H-TOCSY (12 ms) and (H)CCH-TOCSY (12 ms), as previously described [65]. The spectral analysis was performed with the program SPARKY (version 3.1) [66]. Conventional ^{15}N heteronuclear relaxation rates R_1, R_2 and NOE data were determined. To this end, series of 2D heteronuclear correlated spectra using a sensitivity enhanced gradient pulse scheme [67] were recorded. The relaxation delay times were set as follows: for R_1, 5, 50, 150, 300, 600, 800, 1000 and 1200 ms; and

for R_2, 15.6, 31.3, 46.8, 62.5, 78.2, 93, 109.4 and 125 ms. The relaxation rate constants R_1 and R_2 were obtained from the exponential fits of the measured cross-peak intensities. The uncertainty was taken as the error in the fit of the decay function. For the heteronuclear NOE measurement, the experiments with and without proton saturation were acquired simultaneously in an interleaved manner with a recycling delay of 7 s and were split during processing into separate spectra for analysis. The values for the heteronuclear NOEs were obtained from the intensity ratio of the resonances according to I_{sat}/I_{ref}. Here, the uncertainty was estimated to be about 5%.

Analytical ultracentrifugation

Sedimentation velocity experiments with the RAD StnII mutant were carried out in a Beckman-Coulter Optima XL-I (interference optics) analytical ultracentrifuge at 20 °C. Measurements were performed in water at pH 4.0 using a protein concentration of 560 μM and a velocity of 182 900 ***g***. Differential sedimentation coefficients $c(s)$ were calculated by least squares boundary modelling of sedimentation velocity profiles using the program SEDFIT [68]. Equilibrium measurements (15 μM RAD StnII, in water at pH 4.0) were performed at 7 950, 14 500, 24 000 and 47 650 ***g*** in an Optima XL-A (absorption optics) at 20 °C. Conservation of mass was checked for all velocities used, and the equilibrium profiles were analysed using a single species sedimentation model as previously described [69]. The SEDNTERP program was used to calculate the protein specific volume from the amino acid sequences and the buffer viscosity and density [70].

Haemolysis assays

Haemolysis assays were performed in 96-multiwell plates as previously described [24,35,41,62]. Briefly, erythrocytes from heparinized sheep blood were washed in 10 mM Tris/HCl buffer, pH 7.4, containing 145 mM NaCl, and diluted with the same buffer to a final A_{655} value of 0.5 (1 cm optical path). The haemolysis was followed as a decrease in this A_{655} after addition of the erythrocyte suspension to two-fold serial dilutions of the proteins. An Expert 96 microplate reader (AsysHitech GmbH, Eugendorf, Austria) was employed to do the measurements. The value obtained with 0.1% (w/v) Na_2CO_3 was considered as 100% haemolysis. The HC_{50} value is the protein concentration required to produce 50% haemolysis. These assays were also made in the presence of different concentrations of a GRGDTP hexapeptide which was obtained from Sigma (St. Louis, MO, USA).

Phospholipid vesicle binding assay

All lipids were obtained from Avanti Polar Lipids Inc. (Alabaster, AL, USA). Phospholipid vesicles made of brain SM, 1,2-dioleoyl-*sn*-glycero-3-phosphocholine (DOPC) and cholesterol (Chol) (SM : DOPC : Chol, 1 : 1 : 1) were prepared as previously described [24,46] in 10 mM Tris/HCl, pH 7.4, 145 mM NaCl. Binding assays were performed by ultracentrifugation also as reported before [24,46,71]. The amount of protein that did not co-sediment with the vesicles was determined from the absorbance spectra of the supernatants, and the concentration of protein bound to the liposomes was then calculated taking into account the initial concentration of protein (10 μM in all cases) and the absorption coefficient [41].

HADDOCK docking

Models of tetramer associations of StnII were built using the HADDOCK webserver with the multi-body interface [50] (http://haddock.chem.uu.nl/services/HADDOCK). The X-ray structure of StnII [22] (PDB reference 1GWY) and the NMR-monitored chemical shift perturbation data of the RAD mutant together with the residue accessible surface area were used to define the sets of active and passive residues for the four protein monomers. Monomers N- and C-termini were conveniently charged with the PYMOL program [72]. Active residues (solvent-accessible residues identified to be involved in the interaction) were 28, 50–52, 55–58, 62, 81–83, 112, 128, 131, 135, 137, 140. Passive residues (solvent-accessible residue neighbours of active residues) were 41, 42, 49, 53, 54, 65, 76–78, 80, 93, 94, 118, 133, 149, 154, 162, 175. The classification was made on the basis of the magnitude of chemical shift perturbations and the CPORT interface predictor. Calculations were run imposing C2 symmetry restraints in the HADDOCK protocol. Final structures were analysed and two docked complexes shown to fulfil the imposed restraints were selected as representative models.

Acknowledgements

This work was supported by the Spanish Ministerio de Economía y Competitividad through projects CTQ2011-22514, BFU2012-32404 and BFU2009-10185, and one FPU fellowship granted to S.G.-L.

References

1 Anderluh G & Maček P (2002) Cytolytic peptide and protein toxins from sea anemones (Anthozoa: Actinaria). *Toxicon* **40**, 111–124.
2 Alegre-Cebollada J, Oñaderra M, Gavilanes JG & Martínez-del-Pozo A (2007) Sea anemone actinoporins: the transition from a folded soluble state to a functionally active membrane-bound oligomeric pore. *Curr Protein Pept Sci* **8**, 558–572.
3 Bakrač B & Anderluh G (2010) Molecular mechanism of sphingomyelin-specific membrane binding and pore

formation by actinoporins. *Adv Exp Med Biol* **677**, 106–115.

4 García-Ortega L, Alegre-Cebollada J, García-Linares S, Bruix M, Martínez-del-Pozo A & Gavilanes JG (2011) The behaviour of sea anemone actinoporins at the water–membrane interface. *Biochim Biophys Acta* **1808**, 2275–2288.

5 Belmonte G, Pederzolli C, Maček P & Menestrina G (1993) Pore formation by the sea anemone cytolysin equinatoxin II in red blood cells and model lipid membranes. *J Membr Biol* **131**, 11–22.

6 Maček P, Belmonte G, Pederzolli C & Menestrina G (1994) Mechanism of action of equinatoxin II, a cytolysin from the sea anemone *Actinia equina L.* belonging to the family of actinoporins. *Toxicology* **87**, 205–227.

7 Tejuca M, Dalla Serra M, Ferreras M, Lanio ME & Menestrina G (1996) Mechanism of membrane permeabilization by Sticholysin I, a cytolysin isolated from the venom of the sea anemone *Stichodactyla helianthus*. *Biochemistry* **35**, 14947–14957.

8 De los Ríos V, Mancheño JM, Lanio ME, Oñaderra M & Gavilanes JG (1998) Mechanism of the leakage induced on lipid model membranes by the haemolytic protein sticholysin II from the sea anemone *Stichodactyla helianthus*. *Eur J Biochem* **252**, 284–289.

9 Álvarez-Valcarcel C, Serra M, Patrich C, Bernhart I, Tejuca M, Martínez D, Pazos F, Lanio ME & Menestrina G (2001) Effects of lipid composition on membrane permeabilization by sticholysin I and II, two cytolysins of the sea anemone *Stichodactyla helianthus*. *Biophys J* **80**, 2761–2774.

10 Caaveiro JM, Echabe I, Gutiérrez-Aguirre I, Nieva JL, Arrondo JL & González-Mañas JM (2001) Differential interaction of equinatoxin II with model membranes in response to lipid composition. *Biophys J* **80**, 1343–1353.

11 Bonev BB, Lam YH, Anderluh G, Watts A, Norton RS & Separovic F (2003) Effects of the eukaryotic pore-forming cytolysin equinatoxin II on lipid membranes and the role of sphingomyelin. *Biophys J* **84**, 2382–2392.

12 Anderluh G, Razpotnik A, Podlesek Z, Maček P, Separovic F & Norton RS (2005) Interaction of the eukaryotic pore-forming cytolysin equinatoxin II with model membranes: ^{19}F NMR studies. *J Mol Biol* **347**, 27–39.

13 Martínez D, Otero A, Alvarez C, Pazos F, Tejuca M, Lanio ME, Gutiérrez-Aguirre I, Barlič A, Iloro I, Arrondo JL *et al.* (2007) Effect of sphingomyelin and cholesterol on the interaction of St II with lipidic interfaces. *Toxicon* **49**, 68–81.

14 Bakrač B, Gutiérrez-Aguirre I, Podlesek Z, Sonnen AF, Gilbert RJ, Maček P, Lakey JH & Anderluh G (2008) Molecular determinants of sphingomyelin specificity of a eukaryotic pore-forming toxin. *J Biol Chem* **283**, 18665–18677.

15 Schön P, García-Sáez AJ, Malovrh P, Bacia K, Anderluh G & Schwille P (2008) Equinatoxin II permeabilizing activity depends on the presence of sphingomyelin and lipid phase coexistence. *Biophys J* **95**, 691–698.

16 Castrillo I, Araujo NA, Alegre-Cebollada J, Gavilanes JG, Martínez-del-Pozo A & Bruix M (2010) Specific interactions of sticholysin I with model membranes: an NMR study. *Proteins* **78**, 1959–1970.

17 Barlič A, Gutiérrez-Aguirre I, Caaveiro JM, Cruz A, Ruiz-Arguello MB, Pérez-Gil J & González-Mañas JM (2004) Lipid phase coexistence favors membrane insertion of Equinatoxin-II, a pore forming toxin from *Actinia equina*. *J Biol Chem* **279**, 34209–34216.

18 Basulto A, Pérez VM, Noa Y, Varela C, Otero AJ & Pico MC (2006) Immunohistochemical targeting of sea anemone cytolysins on tentacles, mesenteric filaments and isolated nematocysts of *Stichodactyla helianthus*. *J Exp Zoolog A Comp Exp Biol* **305**, 253–258.

19 Šuput D (2009) *In vivo* effects of cnidarian toxins and venoms. *Toxicon* **54**, 1190–1200.

20 Athanasiadis A, Anderluh G, Maček P & Turk D (2001) Crystal structure of the soluble form of equinatoxin II, a pore-forming toxin from the sea anemone *Actinia equina*. *Structure* **9**, 341–346.

21 Hinds MG, Zhang W, Anderluh G, Hansen PE & Norton RS (2002) Solution structure of the eukaryotic pore-forming cytolysin equinatoxin II: implications for pore formation. *J Mol Biol* **315**, 1219–1229.

22 Mancheño JM, Martín-Benito J, Martínez-Ripoll M, Gavilanes JG & Hermoso JA (2003) Crystal and electron microscopy structures of sticholysin II actinoporin reveal insights into the mechanism of membrane pore formation. *Structure* **11**, 1319–1328.

23 Norton RS (2009) Structures of sea anemone toxins. *Toxicon* **54**, 1075–1088.

24 García-Linares S, Castrillo I, Bruix M, Menéndez M, Alegre-Cebollada J, Martínez-del-Pozo A & Gavilanes JG (2013) Three-dimensional structure of the actinoporin sticholysin I. Influence of long-distance effects on protein function. *Archiv Biophys Biochem* **532**, 39–45.

25 Mechaly AE, Bellomio A, Gil-Cartón D, Morante K, Valle M, González-Mañas JM & Guérin DM (2011) Structural insights into the oligomerization and architecture of eukaryotic membrane pore-forming toxins. *Structure* **19**, 181–191.

26 Anderluh G, Pungerčar J, Križaj I, Strukelj B, Gubenšek F & Maček P (1997) N-terminal truncation mutagenesis of equinatoxin II, a pore-forming protein from the sea anemone *Actinia equina*. *Protein Eng* **10**, 751–755.

27 Hong Q, Gutiérrez-Aguirre I, Barlič A, Malovrh P, Kristan K, Podlesek Z, Maček P, Turk D, González-Mañas JM, Lakey JH *et al.* (2002) Two-step membrane binding by Equinatoxin II, a pore-forming toxin from the sea anemone, involves an exposed aromatic cluster and a flexible helix. *J Biol Chem* **277**, 41916–41924.
28 Malovrh P, Viero G, Dalla Serra M, Podlesek Z, Lakey JH, Maček P, Menestrina G & Anderluh G (2003) A novel mechanism of pore formation: membrane penetration by the N-terminal amphipathic region of equinatoxin. *J Biol Chem* **278**, 22678–22685.
29 Gutiérrez-Aguirre I, Barli A, Podlesek Z, Maček P, Anderluh G & González-Mañas JM (2004) Membrane insertion of the N-terminal α-helix of equinatoxin II, a sea anemone cytolytic toxin. *Biochem J* **384**, 421–428.
30 Kristan K, Podlesek Z, Hojnik V, Gutiérrez-Aguirre I, Gunčar G, Turk D, González-Mañas JM, Lakey JH, Maček P & Anderluh G (2004) Pore formation by equinatoxin, a eukaryotic pore-forming toxin, requires a flexible N-terminal region and a stable β-sandwich. *J Biol Chem* **279**, 46509–46517.
31 Pazos F, Valle A, Martínez D, Ramírez A, Calderón L, Pupo A, Tejuca M, Morera V, Campos J, Fando R *et al.* (2006) Structural and functional characterization of a recombinant sticholysin I (rSt I) from the sea anemone *Stichodactyla helianthus*. *Toxicon* **48**, 1083–1094.
32 Cilli EM, Pigossi FT, Crusca E Jr, Ros U, Martínez D, Lanio ME, Álvarez C & Schreier S (2007) Correlations between differences in amino-terminal sequences and different haemolytic activity of sticholysins. *Toxicon* **50**, 1201–1204.
33 Alegre-Cebollada J, Cunietti M, Herrero-Galán E, Gavilanes JG & Martínez-del-Pozo A (2008) Calorimetric scrutiny of lipid binding by sticholysin II toxin mutants. *J Mol Biol* **382**, 920–930.
34 Drechsler A, Potrich C, Sabo JK, Frisanco M, Guella G, Dalla Serra M, Anderluh G, Separovic F & Norton RS (2006) Structure and activity of the N-terminal region of the eukaryotic cytolysin equinatoxin II. *Biochemistry* **45**, 1818–1828.
35 Alegre-Cebollada J, Lacadena V, Oñaderra M, Mancheño JM, Gavilanes JG & Martínez-del-Pozo A (2004) Phenotypic selection and characterization of randomly produced non-haemolytic mutants of the toxic sea anemone protein sticholysin II. *FEBS Lett* **575**, 14–18.
36 Pardo-Cea MA, Castrillo I, Alegre-Cebollada J, Martínez-del-Pozo A, Gavilanes JG & Bruix M (2011) Intrinsic local disorder and a network of charge–charge interactions are key to actinoporin membrane disruption and cytotoxicity. *FEBS J* **278**, 2080–2089.
37 Maula T, Isaksson J, García-Linares S, Niinivehmas S, Pentikäinen OT, Kurita M, Yamaguchi S, Yamamoto T, Katsumura S, Gavilanes JG *et al.* (2013) 2NH and 3OH are crucial structural requirements in sphingomyelin for sticholysin II binding and pore formation in bilayer membranes. *Biochim Biophys Acta* **1828**, 1390–1395.
38 Malovrh P, Barlič A, Podlesek Z, Maček P, Menestrina G & Anderluh G (2000) Structure–function studies of tryptophan mutants of equinatoxin II, a sea anemone pore-forming protein. *Biochem J* **346**, 223–232.
39 Anderluh G & Maček P (2003) Dissecting the actinoporin pore-forming mechanism. *Structure* **11**, 1312–1313.
40 Monastyrnaya M, Leychenko E, Isaeva M, Likhatskaya G, Zelepuga E, Kostina E, Trifonov E, Nurminski E & Kozlovskaya E (2010) Actinoporins from the sea anemones, tropical *Radianthus macrodactylus* and northern *Oulactisorientalis*: comparative analysis of structure–function relationships. *Toxicon* **56**, 1299–1314.
41 Alegre-Cebollada J, Clementi G, Cunietti M, Porres C, Oñaderra M, Gavilanes JG & Martínez-del-Pozo A (2007) Silent mutations at the 5′-end of the cDNA of actinoporins from the sea anemone *Stichodactyla helianthus* allow their heterologous overproduction in *Escherichia coli*. *J Biotechnol* **127**, 211–221.
42 Castrillo I, Alegre-Cebollada J, Martínez-del-Pozo A, Gavilanes JG & Bruix M (2009) ^{1}H, ^{13}C, and ^{15}N NMR assignments of StnII-R29Q, a defective lipid binding mutant of the sea anemone actinoporin Sticholysin II. *Biomol NMR Assign* **3**, 239–241.
43 Pardo-Cea MA, Alegre-Cebollada J, Martínez-del-Pozo A, Gavilanes JG & Bruix M (2010) ^{1}H, ^{13}C, and ^{15}N NMR assignments of StnII-Y111N, a highly impaired mutant of the sea anemone actinoporin Sticholysin II. *Biomol NMR Assign* **4**, 69–72.
44 Kay LE, Torchia DA & Bax A (1989) Backbone dynamics of proteins as studied by ^{15}N inverse detected heteronuclear NMR spectroscopy: application to staphylococcal nuclease. *Biochemistry* **28**, 8972–8979.
45 Clubb RT, Omichinski JG, Sakaguchi K, Appella E, Gronenborn AM & Clore GM (1995) Backbone dynamics of the oligomerization domain of p53 determined from ^{15}N NMR relaxation measurements. *Protein Sci* **4**, 855–862.
46 Alegre-Cebollada J, Rodríguez-Crespo I, Gavilanes JG & Martínez-del-Pozo A (2006) Detergent-resistant membranes are platforms for actinoporin pore-forming activity on intact cells. *FEBS J* **273**, 863–871.
47 De Oliveira S & Saldanha C (2010) An overview about erythrocyte membrane. *Clin Hemorheol Microcirc* **44**, 63–74.
48 Hostetter MK (2000) RGD-mediated adhesion in fungal pathogens of humans, plants and insects. *Curr Opin Microbiol* **3**, 344–348.
49 Tanabe N, Wheal BD, Kwon J, Chen HH, Shugg RP, Sims SM, Goldberg HA & Dixon SJ (2011) Osteopontin signals through calcium and nuclear factor

of activated T cells (NFAT) in osteoclasts: a novel RGD-dependent pathway promoting cell survival. *J Biol Chem* **286**, 39871–39881.
50 De Vries SJ, Van Dijk M & Bonvin AM (2010) The HADDOCK web server for data-driven biomolecular docking. *Nat Protoc* **5**, 883–897. (http://haddock.chem.uu.nl/services/HADDOCK)
51 Rojko N, Kristan KČ, Viero G, Žerovnik E, Maček P, Dalla Serra M & Anderluh G (2013) Membrane damage by an α-helical pore-forming protein, Equinatoxin II, proceeds through a succession of ordered steps. *J Biol Chem* **288**, 23704–23715.
52 Kristan K, Viero G, Maček P, Dalla Serra M & Anderluh G (2007) The equinatoxin N-terminus is transferred across planar lipid membranes and helps to stabilize the transmembrane pore. *FEBS J* **274**, 539–550.
53 Alegre-Cebollada J, Martínez-del-Pozo A, Gavilanes JG & Goormaghtigh E (2007) Infrared spectroscopy study on the conformational changes leading to pore formation of the toxin sticholysin II. *Biophys J* **93**, 3191–3201.
54 Birck C, Damian L, Marty-Detraves C, Lougarre A, Schulze-Briese C, Koehl P, Fournier D, Paquereau L & Samama JP (2004) A new lectin family with structure similarity to actinoporins revealed by the crystal structure of *Xerocomus chrysenteron* lectin XCL. *J Mol Biol* **344**, 1409–1420.
55 Gutiérrez-Aguirre I, Trontelj P, Maček P, Lakey JH & Anderluh G (2006) Membrane binding of zebra fish actinoporin-like protein: AF domains, a novel superfamily of cell membrane binding domains. *Biochem J* **398**, 381–392.
56 Anderluh G & Lakey JH (2008) Disparate proteins use similar architectures to damage membranes. *Trends Biochem Sci* **33**, 482–490.
57 Hoang QT, Cho SH, McDaniel SF, Ok SH, Quatrano RS & Shin JS (2009) Actinoporin plays a key role in water stress in the moss *Physcomitrella patens*. *New Phytol* **184**, 502–510.
58 Ottmann C, Luberacki B, Küfner I, Koch W, Brunner F, Weyand M, Mattinen L, Pirhonen M, Anderluh G, Seitz HU *et al.* (2009) A common toxin fold mediates microbial attack and plant defence. *Proc Natl Acad Sci USA* **106**, 10359–10364.
59 Anderluh G, Barlic A, Podlesek Z, Maček P, Pungerčar J, Gubenšek F, Zecchini ML, Dalla Serra M & Menestrina G (1999) Cysteine-scanning mutagenesis of an eukaryotic pore-forming toxin from sea anemone: topology in lipid membranes. *Eur J Biochem* **263**, 128–136.
60 Kristan KC, Viero G, Dalla Serra M, Maček P & Anderluh G (2009) Molecular mechanism of pore formation by actinoporins. *Toxicon* **54**, 1125–1134.
61 Sambrook J & Russell DW (2001) Molecular Cloning: A Laboratory Manual. Cold Spring Harbor Laboratory Press, Cold Spring Harbor, NY.
62 Mancheño JM, De los Ríos V, Martínez-del-Pozo A, Lanio ME, Oñaderra M & Gavilanes JG (2001) Partially folded states of the cytolytic protein sticholysin II. *Biochim Biophys Acta* **1545**, 122–131.
63 Álvarez-García E, Martínez-del-Pozo A & Gavilanes JG (2009) Role of the basic character of α-sarcin's NH_2-terminal β-hairpin in ribosome recognition and phospholipid interaction. *Arch Biochem Biophys* **481**, 37–44.
64 Wishart DS, Bigam CG, Yao J, Abildgaard F, Dyson HJ, Oldfield E, Markley JL & Sykes BD (1995) ^{1}H, ^{13}C and ^{15}N chemical shift referencing in biomolecules. *J Biomol NMR* **6**, 135–149.
65 Castrillo I, Alegre-Cebollada J, Martínez-del-Pozo A, Gavilanes JG, Santoro J & Bruix M (2009) ^{1}H, ^{13}C, and ^{15}N NMR assignments of the actinoporin Sticholysin I. *Biomol NMR Assign* **3**, 5–7.
66 Goddard TD & Kneller DG (2005) SPARKY 3. University of California, San Francisco, CA.
67 Farrow NA, Muhandiram R, Singer AU, Pascal SM, Kay CM, Gish G, Shoelson SE, Pawson T, Forman-Kay JD & Kay LE (1994) Backbone dynamics of a free and phosphopeptide-complexed Src homology 2 domain studied by ^{15}N NMR relaxation. *Biochemistry* **33**, 5984–6003.
68 Schuck P (2000) Size-distribution analysis of macromolecules by sedimentation velocity ultracentrifugation and lamm equation modeling. *Biophys J* **78**, 1606–1619.
69 Varea J, Sáiz JL, López-Zumel C, Monterroso B, Medranos FJ, Arrondo JL, Lloro I, Laynez J & García LG (2000) Do sequence repeats play an equivalent role in the choline-binding module of pneumococcal LytA amidase? *J Biol Chem* **275**, 26842–26855.
70 Laue TM, Shah BD, Ridgeway TM & Pelletier SL (1992) Analytical ultracentrifugation. In Biochemistry and Polymer Science (Harding SE, Rowe AJ & Horton JC, eds), pp. 90–125. Royal Society of Chemistry, Cambridge, UK.
71 Martínez-Ruiz A, García-Ortega L, Kao R, Lacadena J, Oñaderra M, Mancheño JM, Davies J, Martínez-del-Pozo A & Gavilanes JG (2001) RNase U2 and α-sarcin: a study of relationships. *Methods Enzymol* **341**, 335–351.
72 DeLano WL (2008) The PyMOL Molecular Graphics System. DeLano, Schrödinger, LLC, San Francisco, CA.
73 Koradi R, Billeter M & Wüthrich K (1996) MOLMOL: a program for display and analysis of macromolecular structures. *J Mol Graph* **14**, 51–55, 29–32.

Supporting information

Additional supporting information may be found in the online version of this article at the publisher's web site:

Fig. S1. (A) SDS/PAGE analysis of the different fractions obtained during the purification of the RAD mutant: Molecular mass markers (Bio-Rad) (lane 1), *E. coli* RB791 cells culture harboring the plasmid, just before and after 4 h of induction by 1 mM IPTG, respectively (lanes 2 and 3), cell lysate (lane 4), the soluble protein fraction loaded onto the CM52 cellulose column (lane 5), the corresponding non retained proteins (lane 6), proteins eluted with the wash (lane 7), and purified StnII G142A mutant (RAD) eluted from the CM52 cellulose column (lane 8).

Fig. S2. (A) Far-UV and (B) near-UV circular dichroism spectra of RAD (continuous lines) and wild-type StnII (dashed lines).

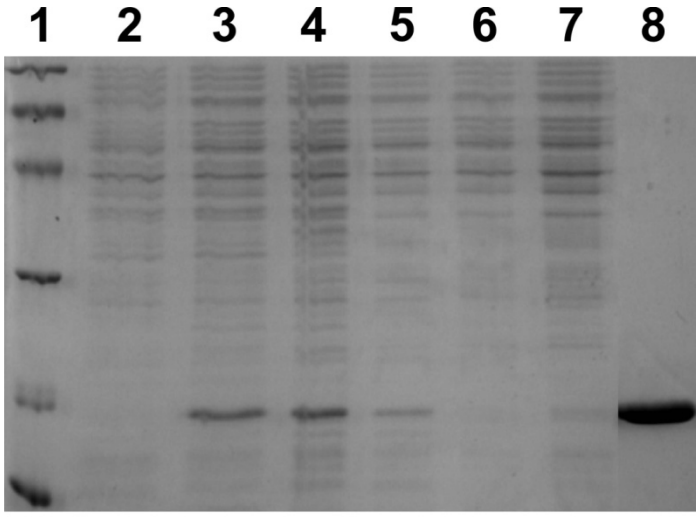

(A)

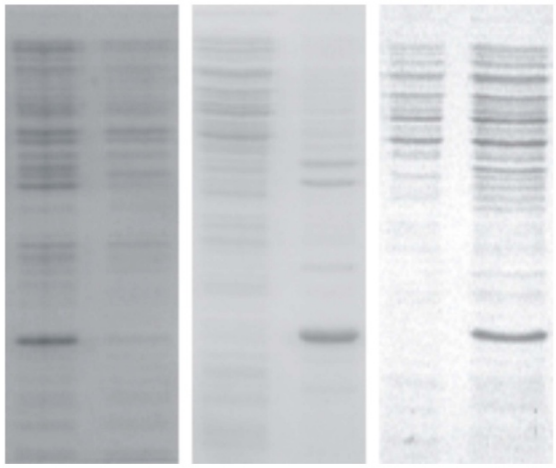

(B)

Figure S1

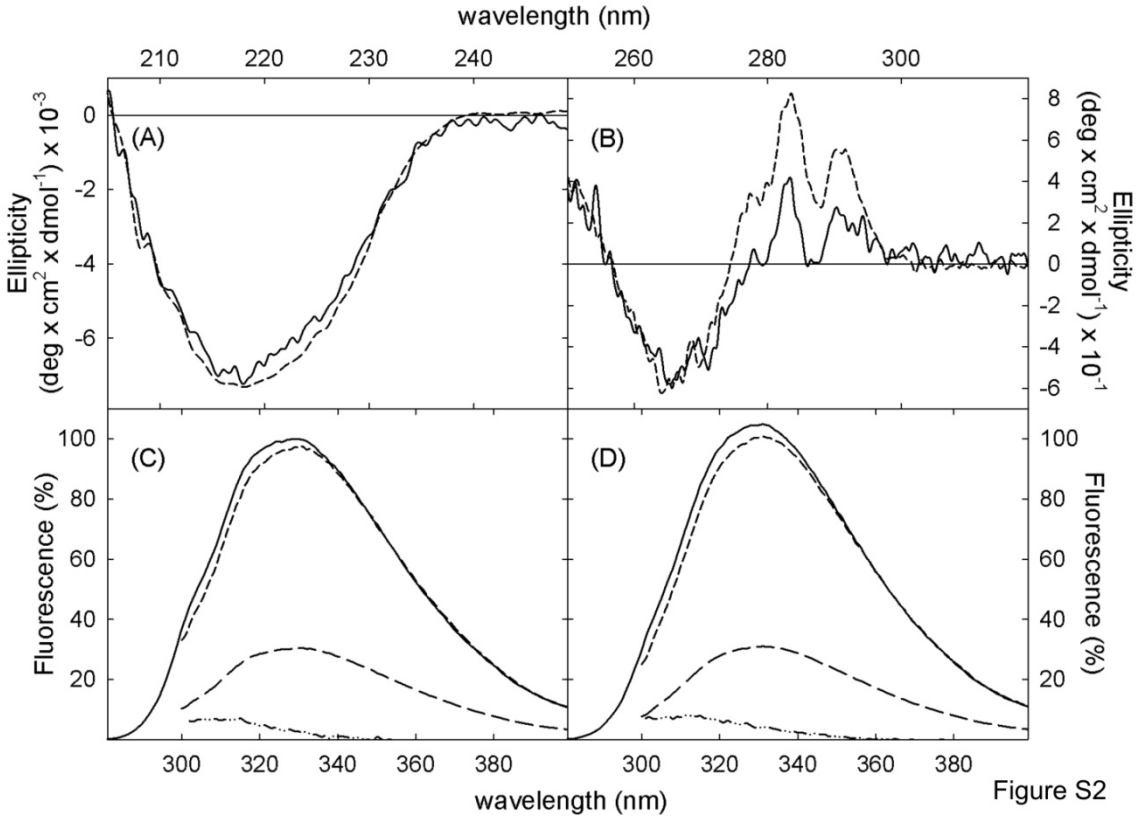
wavelength (nm)
210
220
230
240
260
280
300
(A)
(B)
(C)
(D)
Ellipticity (deg x cm^2 x dmol^{-1}) x 10^{-3}
Ellipticity (deg x cm^2 x dmol^{-1}) x 10^{-1}
Fluorescence (%)
Fluorescence (%)
300
320
340
360
380
wavelength (nm)

Figure S2

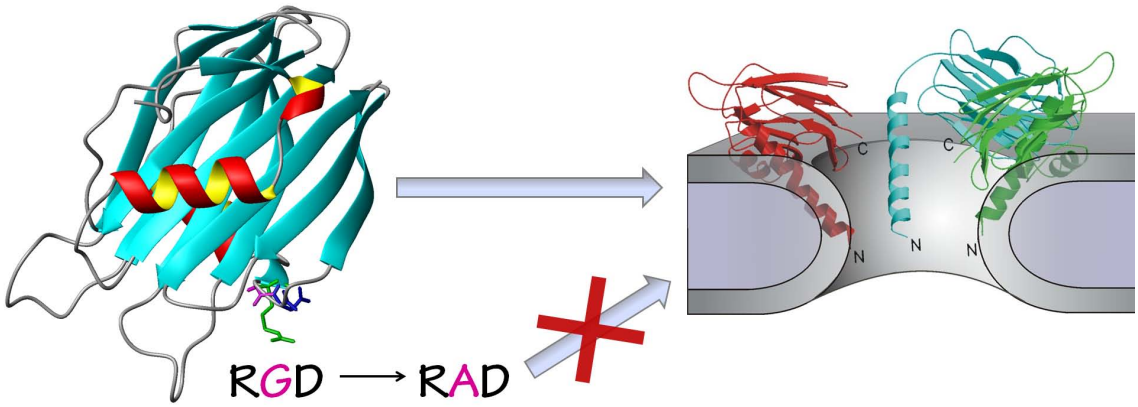
RGD → RAD
C
C
N
N
N

ARTICLE VIII

Role of the tryptophan residues in the specific interaction of the sea anemone *Stichodactyla helianthus*'s actinoporin sticholysin II with biological membranes

García-Linares, S., Maula, T., Rivera-de-Torre, E., Gavilanes, J. G., Slotte, J. P., Martínez-del-Pozo, Á. (2016). In press in *Biochemistry* (DOI: 10.1021/acs.biochem.6b00935).

Papel de los residuos de triptófano en la interacción específica de la actinoporina StnII de la anémona marina *Stichodactyla helianthus* con membranas biológicas

Las actinoporinas son un grupo de toxinas formadoras de poros secretadas por anémonas marinas que, ante la interacción con una bicapa lipídica que contenga esfingomielina, se convierten en proteínas integrales de membrana que oligomerizan y forman un poro. En su estructura hay un conjunto de aminoácidos aromáticos conservados que están involucrados en dicha interacción. StnII de *Stichodactyla helianthus*, una de las actinoporinas mejor caracterizadas, contiene cinco triptófanos conservados localizados en posiciones estratégicas, incluido el mencionado conjunto de aminoácidos aromáticos. Este trabajo se centra en el estudio sistemático de varios mutantes de StnII en los que se han sustituido los residuos de triptófano por fenilalaninas y en su potencial intervención en la unión a la membrana y la formación del poro. Los resultados muestran que Trp43 y Trp115 juegan un papel importante en el mantenimiento de la alta termoestabilidad de la proteína. También confirman que Trp146 participa en interacciones específicas que favorecen la interacción entre protómeros. En relación a su comportamiento frente a membranas que contienen esfingomielina, en presencia de colesterol, el efecto hidrofóbico que aportan Trp110 y Trp114 es una de las principales fuerzas que dirigen la unión a la membrana. Sin embargo, en ausencia de colesterol, la unión y la formación del poro requieren una participación adicional de estos residuos, que deben interaccionar específicamente con la esfingomielina. Estas conclusiones fueron confirmadas utilizando dos análogos de esfingomielina, uno de los cuales tiene una capacidad muy limitada para formar enlaces de hidrógeno. En conjunto, los resultados obtenidos son compatibles con la idea de que los residuos de triptófano de las actinoporinas juegan un papel importante en el reconocimiento y unión a la membrana, pero tienen poca influencia en los procesos de difusión y oligomerización necesarios para ensamblar un poro funcional.

BIOCHEMISTRY
including biophysical chemistry & molecular biology

Article

pubs.acs.org/biochemistry

Role of the Tryptophan Residues in the Specific Interaction of the Sea Anemone *Stichodactyla helianthus*'s Actinoporin Sticholysin II with Biological Membranes

Sara García-Linares,[†,‡] Terhi Maula,[‡] Esperanza Rivera-de-Torre,[†] José G. Gavilanes,[†] J. Peter Slotte,[‡] and Álvaro Martínez-del-Pozo*[,†]

[†]Departamento de Bioquímica y Biología Molecular I, Universidad Complutense, Madrid, Spain
[‡]Biochemistry, Faculty of Science and Engineering, Åbo Akademi University, Turku, Finland

Supporting Information

ABSTRACT: Actinoporins are pore-forming toxins from sea anemones. Upon interaction with sphingomyelin-containing bilayers, they become integral oligomeric membrane structures that form a pore. Sticholysin II from *Stichodactyla helianthus* contains five tryptophans located at strategic positions; its role has now been studied using different mutants. Results show that W43 and W115 play a determinant role in maintaining the high thermostability of the protein, while W146 provides specific interactions for protomer−protomer assembly. W110 and W114 sustain the hydrophobic effect, which is one of the major driving forces for membrane binding in the presence of Chol. However, in its absence, additional interactions with sphingomyelin are required. These conclusions were confirmed with two sphingomyelin analogues, one of which had impaired hydrogen bonding properties. The results obtained support actinoporins' Trp residues playing a major role in membrane recognition and binding, but their residues have an only minor influence on the diffusion and oligomerization steps needed to assemble a functional pore.

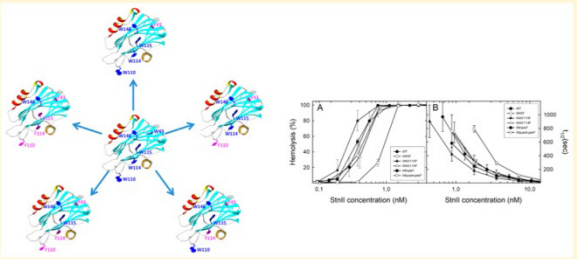

Actinoporins make up a group of small, basic α-pore-forming toxins secreted by sea anemones.[1] They are believed to participate in functions such as predation, defense, and digestion and have been shown to be lethal to small crustaceans, mollusks, fish, and protozoans.[2,3] Cell death takes place after a colloid-osmotic shock induced by cation-selective pores formed on cell membranes.[4−6] All proteins of this family show a high degree of sequence identity and appear as multigene families.[7−9] Four of them have been characterized in great detail: sticholysins I and II (StnI and StnII, respectively) from *Stichodactyla helianthus*,[10,11] equinatoxin II (EqtII) from *Actinia equina*,[7,12] and fragaceatoxin C (FraC) from *Actinia fragacea*.[13]

Actinoporins are globular proteins that remain stably folded in aqueous solution, but upon interaction with lipid bilayers, they become integral membrane structures that oligomerize to form a pore.[10−12,14] Their incorporation into a membrane depends largely on lipid bilayer composition and membrane physicochemical state.[4,6,12,14−20] Thus, membranes must contain sphingomyelin (SM),[16,21−23] but some other conditions, such as the presence of sterols, the coexistence of various phases or domains, compactness, fluidity, and the strength of the interfacial hydrogen bonding network, seem to have a strong influence on their membrane pore-forming ability, as well.[14,16,18−20,24−30]

Monomeric and water-soluble actinoporins appear as a β-sandwich motif composed of 10−12 β-strands flanked by two α-helices that interact with both sides of the β-sandwich (Figure 1A).[31−36] One of these helices (α1) is located near the N-terminal end (Figure 1A) and has been shown to be extremely important for the final function of the pore. This helix seems to extend to the first 30 residues of the protein and become inserted into the membrane to form its walls.[20,31,37−39] This feature, together with the amphipathic character of this stretch, seems to be extremely important for the final functionality of the pore.[37−39]

The formation of a functional pore is, however, still the subject of intense debate. One of the most accepted models explaining the mechanism of actinoporins' pore formation[20,38−42] assumes a toroidal protein−lipid structure without a well-defined fixed stoichiometry.[39−42] Alternative models for FraC have been also proposed on the basis of octameric or nonameric nontoroidal crystalline structures.[34,36] Within this context, the order of events leading to the insertion of the N-terminus into the membrane is also controversial.[36,38,43] Nevertheless, there is general consensus that independent of the mechanism, in addition to the N-terminal α-helix, three

Received: September 12, 2016
Revised: November 2, 2016
Published: November 2, 2016

DOI: 10.1021/acs.biochem.6b00935
Biochemistry XXXX, XXX, XXX−XXX

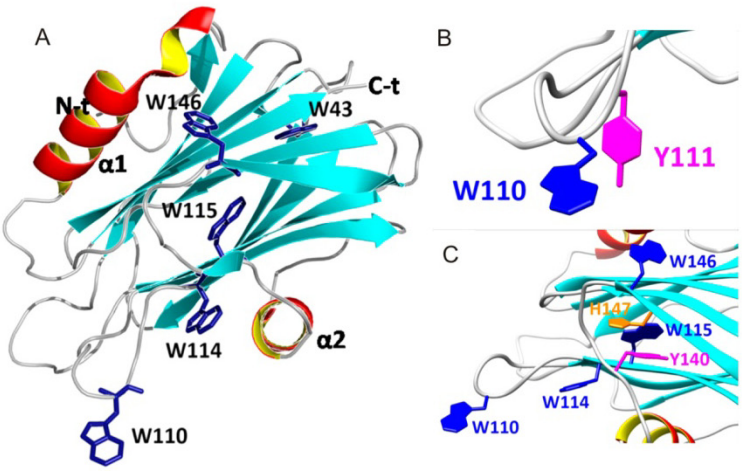

Figure 1. (A) Diagram representing the three-dimensional, water-soluble backbone structure of StnII oriented with its membrane-facing side down. The locations and side chains of all its W residues are also colored blue. The N- and C-terminal ends are indicated as well as both α-helix stretches (α1 and α2). The diagram was constructed from the atomic coordinates deposited in the Protein Data Bank (entry 1GWY for StnII). The image was generated with PyMOL.[70] (B) Diagram showing the relative positions of StnII, W110, and Y111 at the POC binding site. (C) Diagram showing the relative locations among StnII residues W115, Y140, and H147. Side chains of W110, W114, and W146 are also shown.[71]

additional regions of the structure seem to be especially important from a functional point of view: a phosphocholine (POC) binding site, an array of basic amino acids, and a W- and Y-containing cluster of aromatic residues.[11,20,22] The general implication of this cluster in the interaction with membranes has been established through the production of mutants, which results in a reduced level of hemolytic character and a reduced affinity for lipids.[10,27,44−48] However, a detailed study of this region has not yet been performed.

StnII contains five tryptophans, which are conserved in most other known actinoporins and located at strategic positions (Figure 1), including the mentioned cluster of aromatic amino acids (Figure 2).[11] Therefore, this work is focused on the detailed study of the spectroscopic features of various mutants affecting these StnII W residues and the determination of their potential role in membrane binding and pore formation.

■ MATERIALS AND METHODS

Materials. 1-Palmitoyl-2-oleoyl-*sn*-glycero-3-phosphocholine (POPC), 1,2-dioleoyl-*sn*-glycero-3-phosphocholine (DOPC), cholesterol (Chol), and egg sphingomyelin (SM) were obtained from Avanti Polar Lipids. Palmitoyl-SM (PSM) was purified from egg SM using preparative high-performance liquid chromatography on a reverse-phase (C18) column, as described previously.[49] *N*-Palmitoyl ceramide phosphoethanolamine-*N*,*N*-dimethyl (CPE-Me_2) and a PSM analogue with its proximal esteric oxygen group replaced by a -CH_2- group (CH_2-PSM) were obtained as described previously.[50] Calcein and Sephacryl S200HR were obtained from GE Healthcare. The cDNA encoding the StnII mutants was obtained via the overlap extension mutagenesis method,[51] also as described previously.[52] Wild-type StnII and all the mutants used in this study were produced in an *Escherichia coli* expression system and purified as described previously.[27,46,52] The homogeneity of all protein samples used was analyzed via sodium dodecyl sulfate−polyacrylamide gel electrophoresis (SDS−PAGE) and amino acid analysis after the acid hydrolysis of the proteins (5.7 M HCl, 24 h, 110 °C). These amino acid analyses were performed on a Biochrom 20 automatic analyzer (Pharmacia).

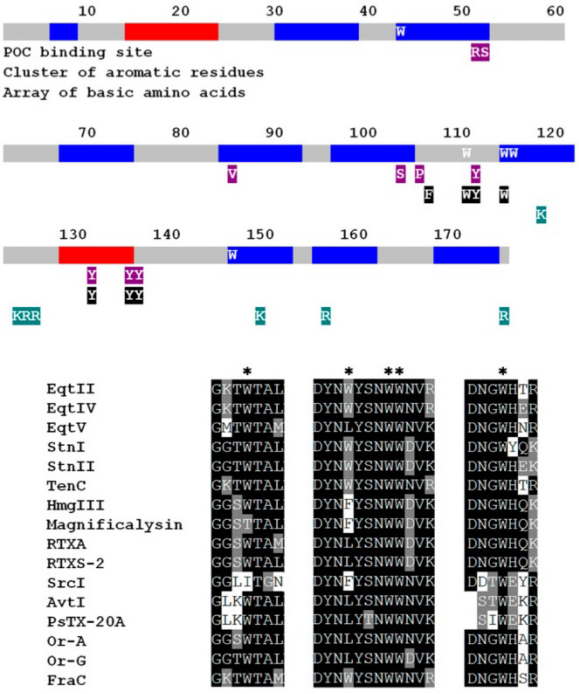

Figure 2. Schematic representation (top) of the actinoporins' secondary structure arrangement: α-helices (red), β-strands (blue), and disordered connecting loops (gray). The W residues and the amino acids constituting the POC binding site (purple), the cluster of aromatic residues (black), and the array of basic amino acids (green) are also indicated. Sequence alignment (bottom) of the stretches containing the amino acids flanking the W residues for all 16 actinoporins whose primary structure is completely known.[11] Asterisks indicate the W residues.

Spectroscopic Characterization. Spectroscopic characterization was essentially performed as previously described.[27,35,53−56] Absorbance measurements were taken on a

DOI: 10.1021/acs.biochem.6b00935
Biochemistry XXXX, XXX, XXX−XXX

Uvikon 930 spectrophotometer (Kontron Instruments). The individual $E^{0.1\%}$ (280 nm, 1 cm) coefficients were calculated for every single protein species as described previously,[16,27,56] using the amino acid analysis results and their specific UV absorption spectra.[8,15,56] Far-UV circular dichroism (CD) spectra were recorded on a Jasco 715 spectropolarimeter at a scanning speed of 50 nm/min. Optical path cells of 0.1 cm were employed. The proteins were dissolved in 15 mM MOPS buffer (pH 7.5) containing 100 mM NaCl (protein concentration of 0.2 mg/mL). At least six spectra were averaged to obtain the final spectrum. CD measurements were also employed to study the thermal stability of the mutants, as described above.[27,35,54] The T_m values correspond to the temperatures at the midpoint of the monophasic thermal transition.

Fluorescence emission spectra were recorded on an SLM Aminco 8000 spectrofluorimeter, using 4 nm slits for both excitation and emission beams as described previously.[53] The spectra were recorded for excitation at 275 and 295 nm. These two spectra were normalized by considering that the tyrosine contribution above 380 nm is negligible. The Tyr contribution was calculated as the difference between the two mentioned normalized spectra. Thermostated cells with 0.2 and 1.0 cm optical paths for the excitation and emission beams, respectively, were used. The temperature was controlled with a circulating water bath (Huber Polystat).

Hemolysis Assay. Hemolysis assays were performed in 96-multiwell plates as previously described.[27,35,52,56] Briefly, erythrocytes from heparinized sheep blood were washed in 10 mM Tris buffer (pH 7.4) containing 0.145 M NaCl, to a final OD_{655} of 0.5. Hemolysis was followed by a decrease in OD_{655} after the addition of the erythrocyte suspension to 2-fold serial dilutions of the proteins. An Expert 96 microplate reader (Asys Hitech, GmbH, Eugendorf, Austria) was used to measure OD_{655}. The value obtained with 0.1% (w/v) Na_2CO_3 was considered to represent 100% hemolysis. HC_{50} is the protein concentration required to produce 50% hemolysis.

Binding of StnII to Bilayer Membranes. This binding was assessed via isothermal titration calorimetry (ITC), as described previously,[23,27,56,58] using a VP-ITC instrument (MicroCal). Briefly, 10 μM protein solutions were titrated via the injection of 20 μL aliquots of lipid suspensions (phospholipid concentration of 5 mM). Binding isotherms were adjusted to a model, described previously,[27] in which the protein binds the membrane, involving "n" lipid molecules.

Surface Plasmon Resonance. The association of StnII and the W mutants studied by surface plasmon resonance (SPR) with vesicle-coated gold chips was performed as follows. LUVs were prepared from POPC/PSM (4:1) or DOPC/SM/Chol (1:1:1) large unilamellar vesicles (LUVs)[28] in Tris buffer [10 mM Tris and 140 mM NaCl (pH 7.4)] via extrusion through 100 nm polycarbonate filters at 60 °C. Binding of protein to the vesicles was studied at 23 °C with a BioNavis SPR Navi 200 instrument (BioNavis Ltd., Tampere, Finland). The gold sensor chip was coated with a carboxymethylated dextran layer, which was treated with *N*-hydroxysuccinimide and *N*-ethyl-*N*′-(dimethylaminopropyl) carbodiimide to activate the surface for capturing phospholipid membranes. All solutions used for SPR were filtered through 0.2 μm membrane filters and degassed via bath sonication before use. The running buffer consisted of 10 mM Tris and 140 mM NaCl (pH 7.4), and the flow rate was 10 μL/min. First, the chip surface was cleaned with two injections of 50 mM regeneration solution [2:3 (v/v) NaOH/isopropanol]. Then, the extruded LUVs (0.5 mM lipid) were applied to the surface (10 min injection), and the unbound vesicles were removed by one (2 min) injection of 50 mM NaOH. Bovine serum albumin (0.1 mg/mL, 5 min injection) was used to verify that the chip did not have uncovered areas. Finally, StnII (4 μM) was applied for 10 min. The chip was regenerated between the various vesicle compositions by first applying two injections of 10 mM CHAPS and then injecting the aforementioned regeneration solution for an additional 3 min.

Calcein Leakage Assay. Calcein entrapped in POPC/PSM (4:1) or DOPC/SM/Chol (1:1:1) LUVs was prepared as described previously[28] via extrusion through 200 nm filters (Nucleopore, Whatman) at 60 °C. Briefly, the desired lipids were mixed and dried under a stream of nitrogen. The lipids were redissolved in chloroform and dried again before the removal of any traces of the remaining solvent in a vacuum for 60 min. Prior to extrusion, the dry lipid films were hydrated for 30 min at 60 °C in Tris buffer [10 mM Tris and 140 mM NaCl (pH 7.4)] containing calcein at a concentration of 100 mM. The total lipid concentration was 1.25 mM. The LUVs were separated from nonentrapped calcein via gel filtration on a Sephacryl S200HR instrument. These LUVs were used for permeabilization studies within 24 h. The phospholipid concentration was determined via P_i measurement[59] after the dilution of the vesicles during isolation. The concentrations of LUV phospholipids and StnII during calcein leakage experiments were approximately 7.5 μM and 1−200 nM, respectively. Emission at 550 nm was followed as a function of time (excitation at 480 nm) at 23 °C. Fluorescence emission was measured with a PTI Quanta-Master spectrofluorimeter (Photon Technology International, Inc.). To ensure that no major spontaneous leakage occurred, the emission was measured for each sample during the 5 min before the addition of the toxin. A steady signal level, indicating intact vesicles, was observed for all samples. The released fraction of calcein was determined on the basis of the maximal calcein release, which was induced by Triton X-100-induced LUV disintegration.

RESULTS

Protein Production and Purification. The cDNAs for 15 StnII W to F mutants were constructed and employed to produce them in *E. coli* using the standard conditions routinely employed for the wild-type protein.[52] Unfortunately, most proteins harboring mutations affecting W146 showed such a dramatic reduction in solubility (Figure S1) that their purification was rendered impractical at the amounts needed to perform the planned experiments (Table 1). Therefore, ultimately, only five of the most soluble variants were selected for purification and characterization (Table 1). This selection was made considering not only the solubility criteria but also the maintenance of minimal coherence in the structural and functional relationships. Thus, the proteins purified were wild-type (WT) StnII, single mutant W43F, two double mutants (W43/110F and W43/114F), one triple mutant (W43/110/114F or WtripleF), and one quadruple variant (W43/110/114/115F or WquadrupleF) (Table 1). This quadruple mutant contained only a single W, specifically W146.

Wild-type StnII and the five mutant proteins were purified to homogeneity on the basis of their SDS−PAGE behavior (Figure 3) and in terms of milligram amounts (Table 2). Their amino acid compositions were consistent with the introduced mutations, and the calculated $E^{0.1\%}$ (280 nm, 1 cm) values were

DOI: 10.1021/acs.biochem.6b00935
Biochemistry XXXX, XXX, XXX−XXX

Table 1. Solubilities of the Various W Mutants Produced in *E. coli*[a]

StnII variant	solubility	abbreviation used in this article
wild-type	++++	WT
W43F	++++	W43F
W43F/W110F	++++	W43/110F
W43F/W114F	++++	W43/114F
W43F/W110F/W114F	++++	WtripleF
W43F/W110F/W114F/W115F	+++	WquadrupleF
W110F	++++	
W110F/W146F	++++	
W43F/W110F/W146F	++	
W110F/W114F/W146F	++	
W114F/W146F	++	
W43F/W114F/W146F	++	
W43F/W110F/W114F/W146F	+	
W110F/W114F/W115F/W146F	+	
W43F/W110F/W115F/W146F	–	
W43F/W114F/W115F/W146F	–	

[a]The proteins that were finally purified and characterized were those indicated in the third column. Solubility is indicated by plus or minus symbols, where four pluses indicate that the solubility was estimated to be equal to or larger than that of wild-type StnII.

Table 2. Structural and Functional Parameters of the Proteins Used in This Study

StnII variant	purification yield (mg/L of the original culture)	$E^{0.1\%}$ (280 nm, 1 cm)	T_m (°C)[a]	relative hemolytic activity[b]
WT	5.2	2.54	67	1.00 ± 0.05
W43F	2.4	2.45	53	0.93 ± 0.09
W43/110F	5.3	2.26	57	1.33 ± 0.10
W43/114F	8.1	2.24	57	0.89 ± 0.06
WtripleF	3.4	2.20	59	1.08 ± 0.06
WquadrupleF	1.4	1.60	53	0.65 ± 0.03

[a]T_m values are in the range of ±0.5 °C. [b]$HC_{50}(WT)/HC_{50}(mut)$.[27]

also in good agreement with the amino acid changes made (Table 2).[60]

Spectroscopic Characterization. All far-UV CD spectra of the individual mutants were very similar to that corresponding to wild-type StnII (Figure 3). The small changes observed can be easily explained by taking into account the potential contributions of the side chains of the W residues in this wavelength region. In fact, it is well-established that these contributions are especially significant in proteins with high β-sheet structure content,[53,61] as in this case. In summary, it is safe to conclude that all five mutants retained the overall native water-soluble conformation.

On the other hand, the CD spectra in the near-UV wavelength range (Figure S2) showed major changes that could be attributed to the sequential replacement of the W residues with F. In agreement with this observation, the fluorescence emission characterization also revealed very important differences (Figure 4 and Table 3). First, the W emission yield decreased as the number of residues substituted with F increased, given the extremely low quantum yield of the benzyl side chain of this aromatic amino acid. Nevertheless, except for the WquadrupleF mutant, the emission per W residue remained fairly constant for all the other proteins studied (Table 3), suggesting that only small conformational changes took place in the mutations created. On the other hand, the emission of Y increased concomitantly, indicating the existence of nonradiative energy transfer phenomena from Y to W residues in the wild-type protein (Table 3). This effect was

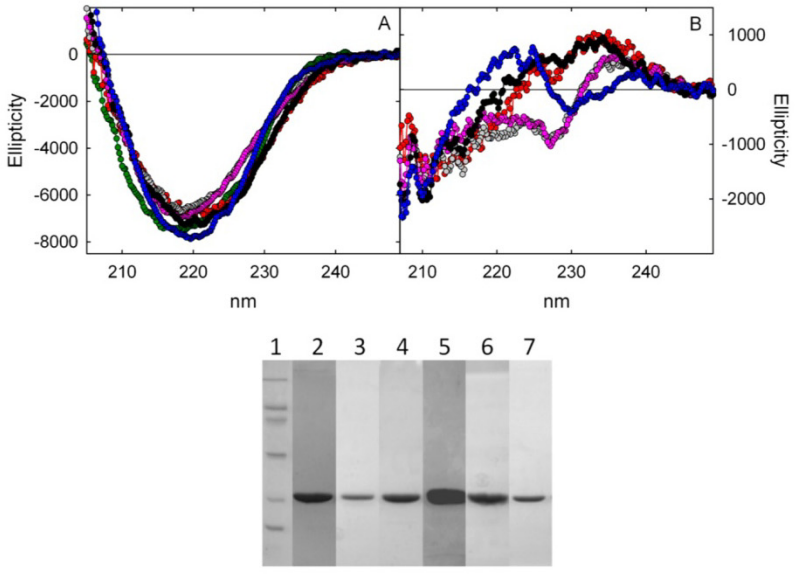

Figure 3. (A) Far-UV circular dichroism spectra of wild-type StnII (green dots) and the W mutants studied: W43F (red), W43/110F (gray), W43/114F (pink), WtripleF (black), and WquadrupleF (blue). (B) Calculated difference spectra for the wild-type protein minus the corresponding mutant. The mean residue weight ellipticity is expressed in units of degrees square centimeter per decimole. The bottom panel shows a 0.1% SDS–15% PAGE analysis of purified wild-type StnII (lane 2) and the five W mutants studied: W43F (lane 3), W43/110F (lane 4), W43/114F (lane 5), WtripleF (lane 6), and WquadrupleF (lane 7). Lane 1 corresponds to the BioRad low-range molecular weight marker (14.4, 21.5, 31.0, 45.0, 66.2, and 97.4 kDa).

DOI: 10.1021/acs.biochem.6b00935
Biochemistry XXXX, XXX, XXX–XXX

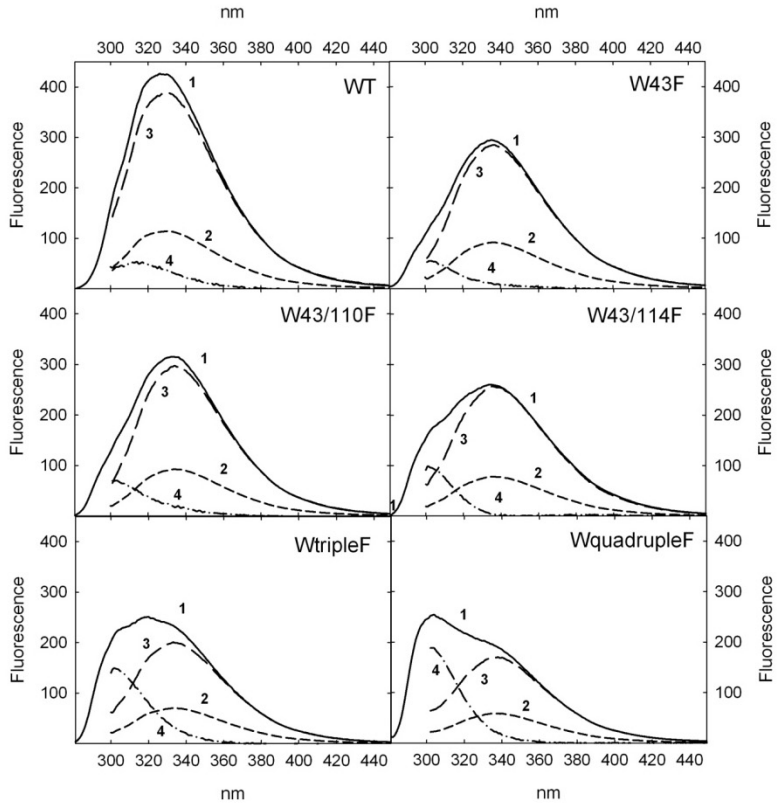

Figure 4. Fluorescence emission spectra of wild-type StnII and the various W mutants studied. All spectra were recorded at identical protein concentrations. Spectra labeled 1 resulted from excitation at 275 nm, and spectra labeled 2 resulted from excitation at 295 nm. These spectra were normalized at wavelengths above 380 nm to produce spectra 3 (tryptophan contribution). Spectra 4 (tyrosine contribution) were calculated by subtracting spectra 3 from spectra 1. The fluorescence emission is proportional in all cases but expressed in arbitrary units.

Table 3. W and Y Fluorescence Emission Yield Values (Q_W and Q_Y) of the Proteins Used in This Study[a]

StnII variant	Q_W	Q_Y	Q_W/number of W
WT	1.00	1.00	1.00
W43F	0.74	0.86	0.95
W43/110F	0.76	1.20	1.25
W43/114F	0.67	1.22	1.10
WtripleF	0.52	2.21	1.30
WquadrupleF	0.46	2.70	2.30

[a]The spectra recorded for excitation at 275 and 295 nm were normalized by considering that the Y contribution above 380 nm is negligible. The Y contribution was calculated as the difference between the two mentioned normalized spectra. The area under these normalized Y and W emission spectra was used to calculate the emission yield obtained for W or Y in the proteins studied. The number shown is referred to the value obtained for each of the two types of amino acids in wild-type StnII. Because the number of W residues differs among the mutants studied, a third column with the relative W emission yield divided by the number of W residues present is also shown, taking 1.00 as the reference value obtained for wild-type StnII.

especially evident after the removal of W110 and W115, as can be seen in the corresponding spectra of the WtripleF and WquadrupleF mutants (Figure 4 and Table 3). Finally, as mentioned above, the removal of W115 yielded a WquadrupleF mutant with only one remaining W (W146), which showed a >2-fold increase in its tryptophan fluorescence emission (Figure 4 and Table 3).

Hemolytic Activity. Quite surprisingly, hemolysis was barely affected in all of the mutants studied (Figure 5 and Table 2). Most observed differences were roughly within the error limits of the experiment (Figure 5). Only the WquadrupleF mutant showed significantly different behavior, which resulted in slightly diminished hemolytic activity, at least in terms of its relative hemolytic activity (RHA) value [an ~35% reduction (Table 2)].

Interaction of Protein with Various Lipid Model Vesicles. Erythrocytes are complex systems that do not easily allow researchers to draw conclusions about the nature of the lipid molecules involved in membrane binding and pore formation. Therefore, functional comparison was continued using LUVs made of two different but well-controlled lipidic compositions: POPC/PSM (4:1) and DOPC/SM/Chol (1:1:1). Both types of vesicles can be considered standard systems for actinoporins because they have been widely employed with the aim of studying actinoporins' functional properties.[19,23,26−28,56,62]

ITC experiments revealed that in the Chol-containing vesicles, all studied proteins showed the characteristic high-affinity and enthalpy-driven binding process of wild-type StnII[27] (Figure 6), though not all showed identical relative membrane binding [RMB (see Table 4 for a definition of this concept)] affinities (Table 4). Thus, whereas the membrane

DOI: 10.1021/acs.biochem.6b00935
Biochemistry XXXX, XXX, XXX−XXX

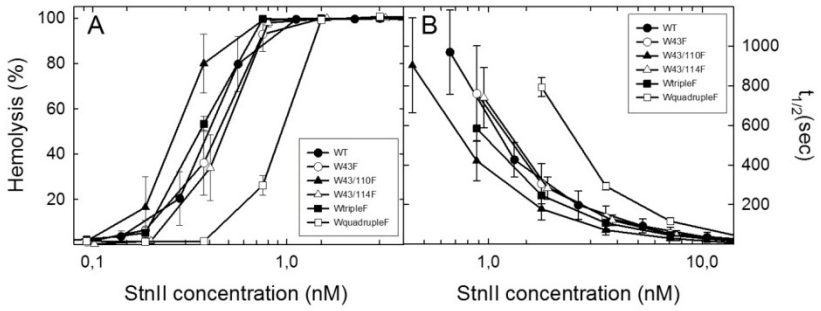

Figure 5. Hemolytic activity of wild-type StnII (●) and W43F (○), W43/110F (▲), W43/114F (△), WtripleF (■), and WquadrupleF (□) mutants. Results are expressed as percentages of hemolysis produced after protein addition for 10 min (A) or as the time needed ($t_{1/2}$, in seconds) to reach 50% complete hemolysis (B). Both terms operate as a function of protein concentration. The maximal hemolysis value considered (100.0%) was that produced by 0.1% (w/v) Na_2CO_3.

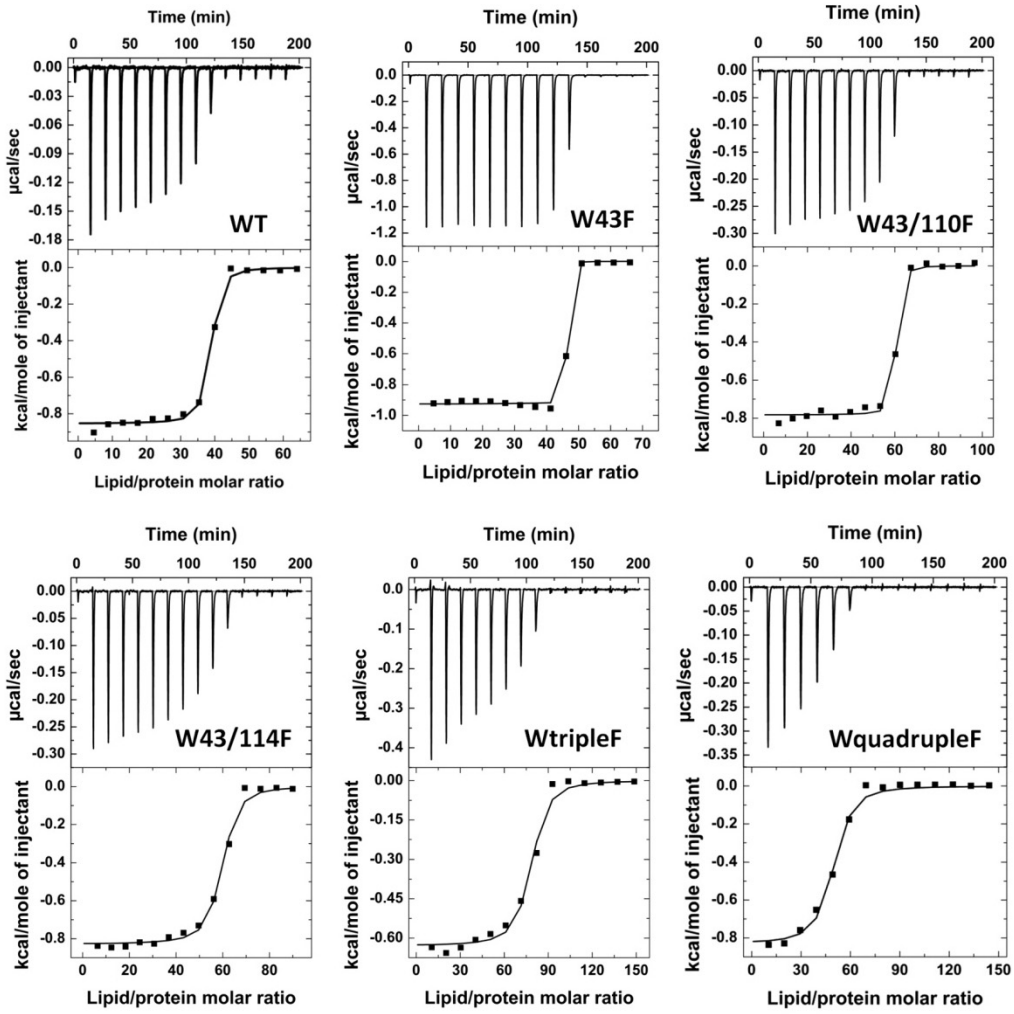

Figure 6. Interaction of StnII and its W mutants with DOPC/SM/Chol (1:1:1) 100 nm diameter LUVs, studied via ITC. Isotherms were adjusted to a model in which the protein binds the membrane involving *n* lipid molecules.[27,58] The *c* values ($c = KP_0$, where P_0 is the protein concentration assayed) for all the graphs are in the range of 1−1000.

binding ability was improved in both W43F and W43/110F mutants, it was impaired in all the other mutants studied. In the absence of Chol, however, the affinity values of all mutants were strongly reduced (Figure 7), as has been described previously for the wild-type protein,[28,62] which showed an RMB value at least 125-fold lower (Table 4). Nevertheless, in relative

DOI: 10.1021/acs.biochem.6b00935
Biochemistry XXXX, XXX, XXX−XXX

Table 4. Binding to DOPC/SM/Chol (1:1:1) or POPC/PSM (4:1) Vesicles by StnII and Its Mutants, Studied via ITC

DOPC/SM/Chol (1:1:1)						
StnII variant	n	K ($\times 10^{-8}$ M^{-1})	ΔG (kcal/mol)	ΔH (kcal/mol)	ΔS (cal mol^{-1} K^{-1})	RMB[a]
WT	39 ± 4	1.70 ± 0.90	−9.1 ± 0.5	−44.0 ± 3.0	−115.0 ± 9.0	1.00
W43F	51 ± 6	4.64 ± 0.36	−9.6 ± 0.1	−39.2 ± 1.0	−99.4 ± 3.5	2.09
W43/110F	55 ± 2	12.45 ± 0.38	−10.1 ± 0.1	−41.8 ± 2.5	−106.1 ± 8.0	5.19
W43/114F	65 ± 8	1.59 ± 0.11	−8.9 ± 0.2	−46.8 ± 0.3	−127.4 ± 0.6	0.56
WtripleF	72 ± 2	0.86 ± 0.10	−8.4 ± 0.1	−48.2 ± 1.6	−133.3 ± 5.3	0.27
WquadrupleF	47 ± 1	0.38 ± 0.08	−8.2 ± 0.2	−36.9 ± 1.2	−96.3 ± 3.7	0.19
POPC/PSM (4:1)						
StnII variant	n	K ($\times 10^{-6}$ M^{-1})	ΔG (kcal/mol)	ΔH (kcal/mol)	ΔS (cal mol^{-1} K^{-1})	RMB[a]
WT	45 ± 2	1.50 ± 0.30	−6.3 ± 0.1	−23.0 ± 1.0	−57.0 ± 3.0	1.00[b]
W43F	47 ± 11	1.20 ± 0.11	−6.2 ± 0.2	−22.4 ± 3.5	−54.5 ± 12.5	0.77
W43/110F	53 ± 9	1.03 ± 0.45	−5.9 ± 0.4	−24.3 ± 2.6	−61.6 ± 10.0	0.58
W43/114F	39 ± 2	0.21 ± 0.02	−5.2 ± 0.1	−1.6 ± 0.4	12.0 ± 1.9	0.16
WtripleF	54 ± 2	0.01 ± 0.01	−4.5 ± 1.2	−1.8 ± 0.2	9.0 ± 4.8	–
WquadrupleF	nd[c]	nd[c]	nd[c]	nd[c]	nd[c]	–

[a]RMB is the relative membrane binding, which equals $[n(\mathrm{WT}) \times K(\mathrm{mut})]/[n(\mathrm{mut}) \times K(\mathrm{WT})]$ (this approximation is valid if L_T is in excess with respect to P_T and $L_T \ll n/K$).[27,57] [b]This RMB value refers to the result obtained for the WT protein in the absence of Chol, but it is at least 125-fold lower than the value calculated for the same protein when it is assayed against the DOPC/SM/Chol (1:1:1) vesicles. [c]Not detectable.

terms, the binding pattern was roughly maintained, with the W43/114F, WtripleF, and WquadrupleF mutants showing the lowest RMB values (Table 4). These ITC results were indeed in good agreement with the SPR measurements (Figure 8). In this case, the presence of Chol minimized binding kinetic differences, while its absence deeply affected the same mutant proteins when their behavior was compared with the wild-type behavior (Table 5). As also revealed by the ITC experiments, in the absence of the sterol component, W43/114F, WtripleF, and WquadrupleF did not even yield an observable SPR signal (Figure 8).

Pore Formation. Actinoporins' pore formation is usually studied following the leakage of calcein encapsulated in different model lipid vesicles, such as the ones used in this study: POPC/PSM (4:1) and DOPC/SM/Chol (1:1:1) (Figures 9 and 10). These types of experiments reveal information about two aspects of the mechanism behind making a functional pore. First, the kinetics of the process can shed light on the ability of the protein monomers involved to bind to and diffuse along the membrane to oligomerize into the required final structure (Figure 9). Second, once equilibrium is reached, the percentage of leakage can reveal the extent of pore formation on the studied membrane (Figure 10).

Considering this idea, all six proteins studied, wild-type StnII included, showed very low calcein release rates when assayed against POPC/PSM (4:1) LUVs, as can be observed in Figure 9. However, the wild-type protein and the W43F and W43/110F mutants were still able to produce the maximal degree of leakage observed after incubation for 10 min (Figure 10). Under identical conditions, the other mutant proteins assayed did not produce observable leakage, even at the highest protein concentrations employed (Figure 10).

As observed previously,[28,62] the presence of Chol dramatically increased the rate of pore formation of all proteins studied to promote pore formation (Figure 9). Indeed, when assayed against DOPC/SM/Chol (1:1:1) vesicles, the wild-type protein and three of the mutants (W43F, W43/110F, and W43/114F) were practically indistinguishable in kinetic terms, while the WtripleF and WquadrupleF proteins, although still much less effective, showed a significant kinetic improvement in terms of the maximal pore formation rate values (Figure 9). On the other hand, all proteins studied were indistinguishable when the final extent of leakage was the parameter measured, showing saturation at much lower concentrations than in the absence of Chol (Figure 10), even though the final extent of calcein release was smaller in the presence of the sterol than in its absence.

SM Analogues. The employment of methylated SM analogues with reduced hydrogen bonding capability from 2NH and 3OH has previously been used to show that StnII failed to bind to lipid bilayers containing these analogues.[23] As mentioned above, some of the W residues mutated in this work have been shown to play crucial roles in SM recognition.[22,45] Therefore, the membrane binding and pore forming abilities of the wild-type protein and the W mutants studied were also assayed against model vesicles containing two new PSM analogues: CPE-Me_2 and CH_2-PSM (Figure 8).

In the absence of Chol, neither the W mutants studied nor the wild-type protein showed any detectable SPR signal against vesicles containing either of the two analogues (Figure 8). This impairment of the establishment of protein−lipid interactions was practically overcome when the same StnII variants were assayed against DOPC/CPE-Me_2/Chol (1:1:1) vesicles (Figure 8). Only the WquadrupleF mutant still showed very low rates of binding to the vesicles, though even in this particular mutant, a detectable signal was also observed. This set of results was consistent with the results of the calcein release experiments, in which leakage was undetectable for all the protein variants and concentrations used in the absence of Chol but became apparent when this lipid was present (Figure 10). Again, the WtripleF and WquadrupleF mutants showed the least ability to induce calcein release in these CPE-Me_2-containing vesicles (Figure 10). These results suggest that even a minor modification at the phospholipid head choline moiety can have strong consequences regarding the behavior of actinoporins at the water−membrane interface, specifically an impairment that can be largely reversed by the mere presence of Chol within the membrane involved in the interaction.

A very similar set of results was obtained with the vesicles containing the CH_2-PSM analogue. In the absence of Chol, all proteins studied, the wild type included, failed to produce a detectable SPR signal, suggesting that binding was strongly impaired. In this particular case, Chol rescued only the SPR

DOI: 10.1021/acs.biochem.6b00935
Biochemistry XXXX, XXX, XXX−XXX

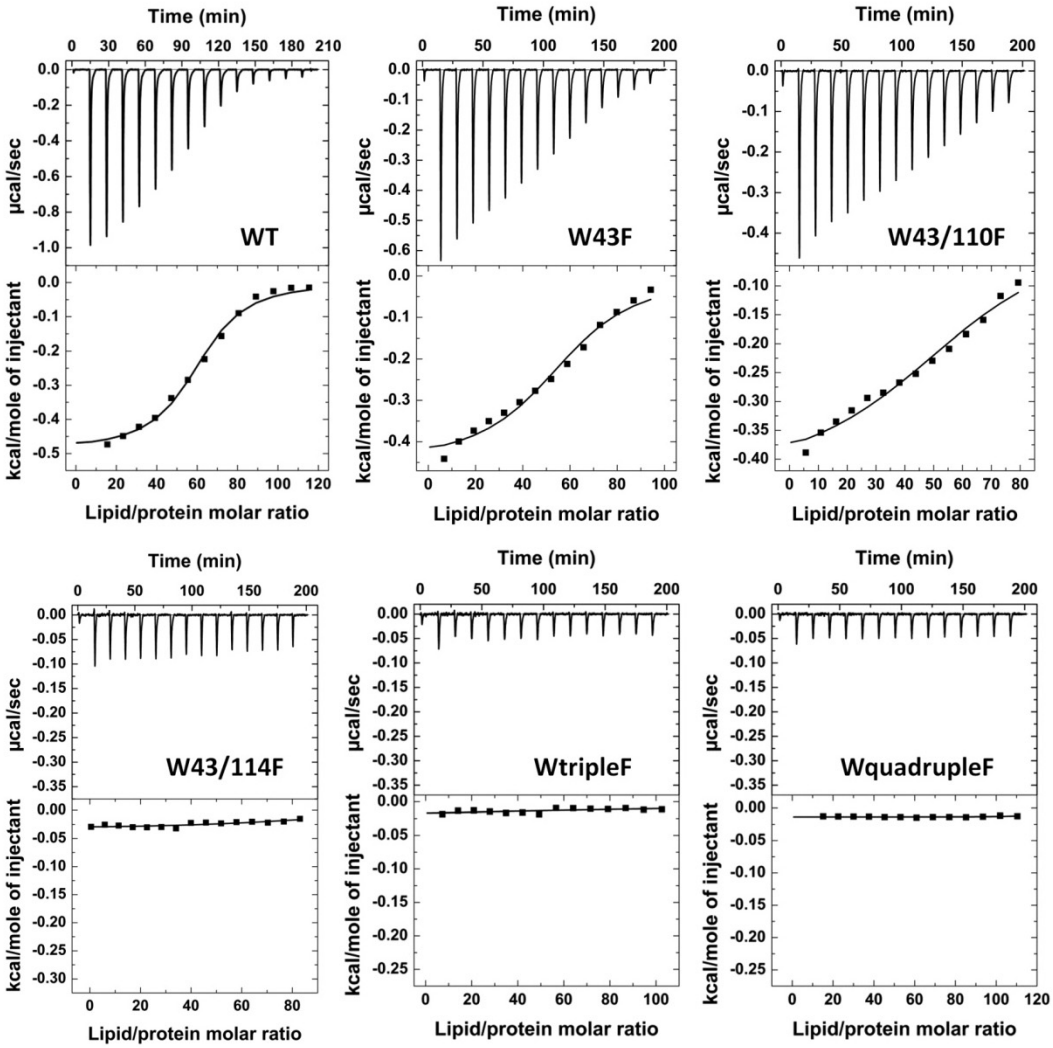

Figure 7. Interaction of StnII and its W mutants with POPC/PSM (4:1) 100 nm diameter LUVs, studied via ITC. Isotherms were adjusted to a model in which the protein binds the membrane involving n lipid molecules.[27,58] The c values ($c = KP_0$, where P_0 is the protein concentration assayed) for all the graphs are in the range of 1−1000, except for the experiment shown for WquadrupleF, because its binding affinity is so low as to preclude working within this range.

signal of wild-type StnII and its W43F and W43/110F mutants (Figure 8). Both set of results were in perfect agreement with those obtained when calcein release was analyzed (Figure 10). In this case, the SM modification resides just at the other end of the SM phosphocholine head because one of the phosphate oxygen atoms has been substituted with a -CH_2- group, which obviously displays a very different geometry and electronic configuration and, most importantly, lacks hydrogen bonding ability.

■ DISCUSSION

It is generally accepted that actinoporins' W residues play a pivotal role in membrane binding and recognition. This hypothesis has been specifically proven for some of these tryptophans,[10,27,44−48] but a study as systematic as this one has not been performed previously. The inspection of the three-dimensional water-soluble structure of StnII suggests that the cluster of amino acids, which seems to be critical to interaction with membranes, is comprised of F106, W110, Y111, W114, Y131, Y135, and Y136[33] (Figure 2). On the other hand, W43 and W115 seem to be located at positions that play major roles in stabilizing the β-sandwich (Figure 1). Finally, in the three-dimensional structures of the two oligomeric complexes formed by FraC, the interface between adjacent subunits exhibits high shape complementarity, in which a valine residue from one promoter protrudes into a cavity within the opposing promoter lined by aromatic residues, namely the tryptophan equivalent to StnII W146,[36,63] which has been assigned as a key residue for the stabilization of the oligomers needed to produce a functional pore. In light of these initial observations, a rather conservative approach was taken when performing this work, which explains why all mutants made were on the basis of the replacement of W with F residues. Both types of amino acids have been shown to be quite hydrophobic residues according to several experimental scales,[64] and though there seems to be a consensus that W side chains show exceptionally strong

DOI: 10.1021/acs.biochem.6b00935
Biochemistry XXXX, XXX, XXX−XXX

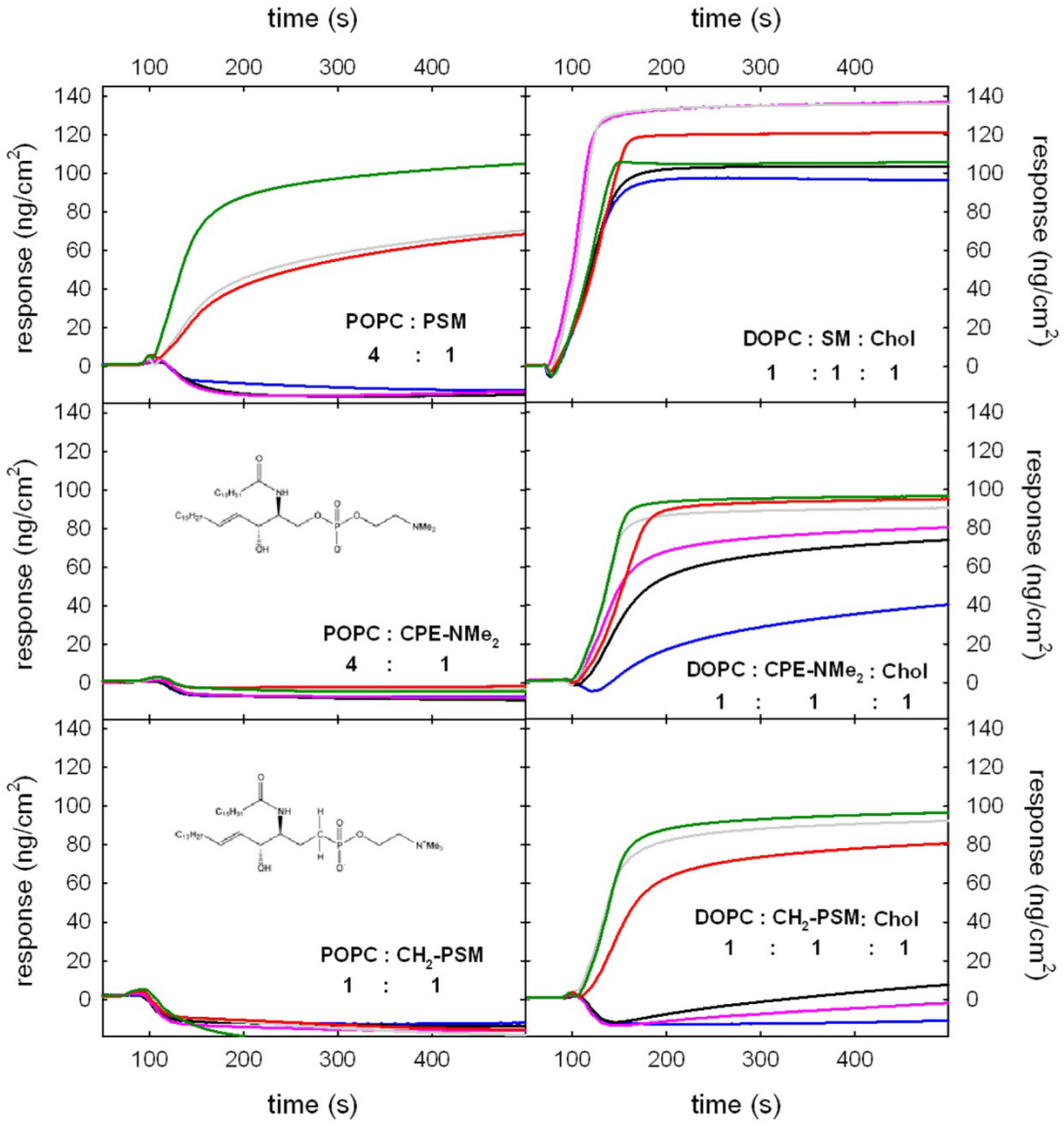

Figure 8. SPR sensorgrams showing the binding of wild-type StnII and the studied W mutants to immobilized vesicles of various lipidic compositions, as indicated in each panel. The traces shown correspond to the wild type (green), W43F (red), W43/110F (gray), W43/114F (pink), WtripleF (black), and WquadrupleF (blue). Chemical formulas of the SM analogues CPE-Me_2 and CH_2-PSM are inserted in panels C and E, respectively.

Table 5. Normalized Increase in SPR Response (nanograms per square centimeter) 200 s after Protein Addition[28,a]

protein	POPC/PSM (4:1)	POPC/CPE-Me_2 (4:1)	POPC/CH_2-PSM (4:1)	DOPC/SM/Chol (1:1:1)	DOPC/CPE-Me_2/Chol (1:1:1)	DOPC/CH_2-PSM/Chol (1:1:1)
WT	1.0	0.0	0.0	1.0	0.9	0.8
W43F	0.5	0.0	0.0	1.1	0.8	0.6
W43/110F	0.5	0.0	0.0	1.3	0.8	0.8
W43/114F	0.0	0.0	0.0	1.3	0.6	0.0
WtripleF	0.0	0.0	0.0	1.0	0.5	0.0
WquadrupleF	0.0	0.0	0.0	0.9	0.2	0.0

[a]The values corresponding to wild-type StnII against either POPC/PSM (4:1) or DOPC/SM/Chol (1:1:1) vesicles were taken as the reference for normalization.

partitioning into the membrane interface, it is generally accepted that this is mainly due to the hydrophobic effect. Therefore, the effects observed and discussed below should not be systematically attributed to changes in the hydrophobicity of

DOI: 10.1021/acs.biochem.6b00935
Biochemistry XXXX, XXX, XXX−XXX

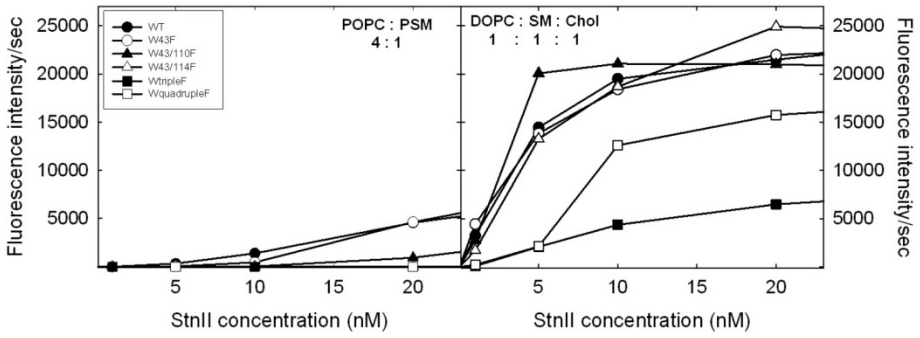

Figure 9. Maximal rates of calcein release (expressed as normalized fluorescence intensity increment per second) vs the total protein concentration added to POPC/PSM (4:1) or DOPC/SM/Chol (1:1:1) (as indicated) calcein-containing LUVs. The following proteins were assayed: wild-type StnII (●), W43F (○), W43/110F (▲), W43/114F (△), WtripleF (■), and WquadrupleF (□). Each plot was constructed from duplicate measurements with a maximum ± SEM value of 3800 in units of fluorescence intensity per second.

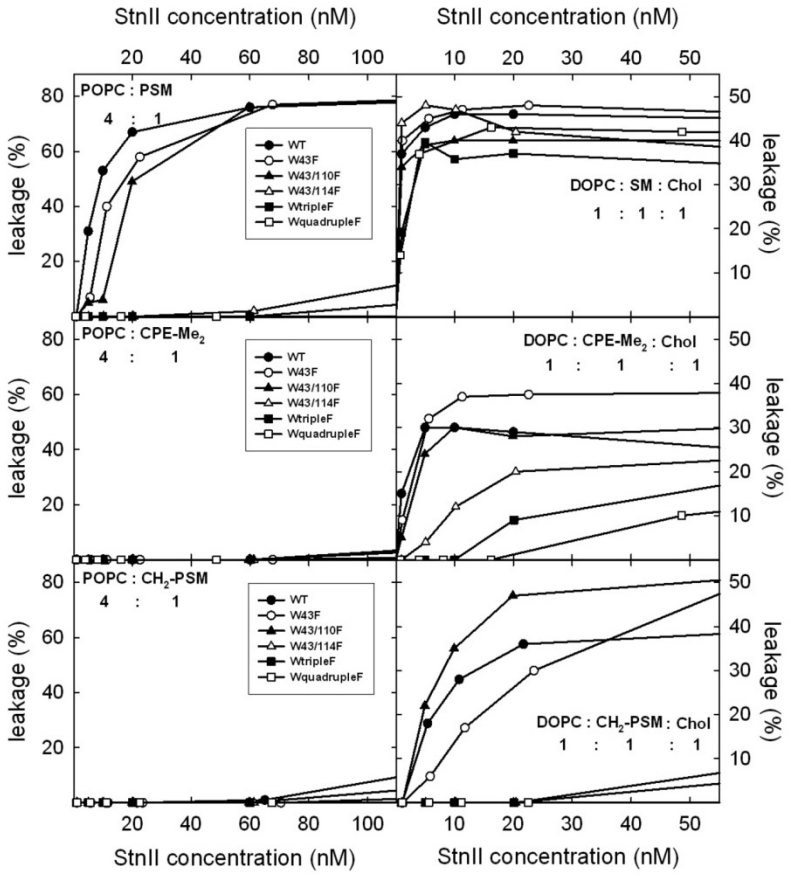

Figure 10. Calcein experiments showing the percentage of leakage 10 min after the addition of the studied proteins, which is represented vs the total protein concentration used. Calcein-containing LUVs of various lipidic compositions were employed, as indicated in each individual panel. The following proteins were assayed: wild-type StnII (●), W43F (○), W43/110F (▲), W43/114F (△), WtripleF (■), and WquadrupleF (□). Each plot was constructed from duplicate measurements with a maximum ± SEM value of 6%.

the participating residues but rather to the elimination of specific interactions involving the indolyl side chains.

Protein Structure and Stability. The first striking observation upon the construction of the planned W to F mutants was the deep impact of W146 replacement on protein solubility (Table 1). Eight of the 16 W mutants produced in *E. coli* showed a reduction in solubility, which rendered their purification difficult in a practical sense. All had at least W146 replaced with F (Table 1), in good agreement with the assigned role of W146 in stabilizing the correct protein−protein interactions needed to oligomerize and produce a pore in the presence of a membrane. The change to F in this position

DOI: 10.1021/acs.biochem.6b00935
Biochemistry XXXX, XXX, XXX−XXX

results in a more aggregation-prone protein molecule, suggesting that the role of W146 is not just to provide an adequate hydrophobic microenvironment but also to participate in specific protomer−protomer interactions.

The six mutant combinations that were purified in milligram amounts showed practically the same far-UV spectroscopic features as the wild-type StnII conformation (Figure 3), confirming the preservation of the overall wild-type conformational fold. On the other hand, near-UV CD (Figure S2) and fluorescence emission (Figure 4) spectra showed differences that were fully compatible with the mutations created. The reduction in the W fluorescence emission was proportional to the sequential elimination of the indolyl side chains and the simultaneous increase in the Y contribution (Figure 4 and Table 3), revealing the existence of nonradiative energy transfer between the W and Y residues in the wild-type protein.

The replacement of W110 with F yielded mutants (W43/110F and WtripleF) showing a quite significant increase in Y emission (Table 3). The report on StnII's crystalline structure showed the existence of an StnII−POC complex consisting of partly hydrophobic (V85, P105, Y111, and Y135) and partly hydrophilic (OH groups from S52, S103, Y131, Y135, and Y136) residues.[33] Within this POC binding site, W110 appears to be in the proximity of Y111 (Figure 1B). Therefore, in the absence of SM, it is safe to assume that the Y emission enhancement observed for these two mutants is due to the elimination of a nonradiative energy transfer phenomenon between Y111 and W110.

The WquadrupleF variant displayed W emissions well above the expected value for its only W residue, W146 [~2.3-fold higher (see Table 3)]. The side chain of this W115 is facing the β-sandwich interior and is in the proximity of the side chains of Y140 and H147 (Figure 1C), which are arranged in an intimate stackinglike interaction (Figure 1C). The substitution of indolyl W115 with a phenyl group probably perturbs this arrangement, releasing the conformational constraints of W146 and enhancing its fluorescence emission. Similarly, the aromatic ring of Y140 would also be responsible for the enhanced contribution of Y to the fluorescence spectra upon the removal of W115. In fact, the equivalent residue of H147 in StnI, another actinoporin from *S. helianthus* with a sequence 93.7% identical to that of StnII,[11] is tyrosine, a residue that can assume an identical stabilization function.

The WquadrupleF mutant also showed the lowest thermal stability, with a T_m value 14 °C lower than that of the wild-type protein (Table 2). This value is also 6 °C lower than the value obtained for WtripleF, confirming that W115 plays a major role in StnII structural stabilization. Interestingly, the only other mutant showing such a drastic decrease in T_m was W43F. As shown in Figures 1 and 2, W43 appears at the beginning of strand β2 with its indolyl side chain embedded within the sandwich's inner core and, most probably, contributing, like W115, to the stabilization of the protein. The other three mutants also showed reduced T_m values, but these were still much higher than those of W43F and WquadrupleF, indicating that replacing W110 and/or W114 with F results in a compensatory effect from the point of view of protein stability. Overall, these results can be interpreted as suggesting that the five W residues of StnII play a major role in maintaining the thermostability of StnII. All mutants, however, showed T_m values high above the temperatures used in all the other experiments performed, which allows us to discard denaturation as a possible explanation of the results obtained and discussed below.

Protein−Membrane Interactions. All W mutants showed very similar levels of hemolytic activity (Figure 5), which suggests that the hydrophobic effect is the major driving force regarding binding to the erythrocyte membranes. As reported previously for the equivalent mutant EqtII,[44] only the WquadrupleF mutant showed a small but significant reduction in hemolytic activity.

A very different picture emerged when the mutants were tested against much simpler systems, such as those represented by DOPC/SM/Chol (1:1:1) or POPC/PSM (4:1) vesicles. When assayed against the first type of vesicle, in which the relative Chol content was very similar to that found in sheep erythrocytes (~30%), all mutants displayed similar binding affinities, as shown by both their ITC thermograms (Figure 6) and their SPR sensorgrams (Figure 8). Thus, this result roughly paralleled the results of the hemolytic experiments. The ITC quantification of this interaction revealed, however, that W43F and W43/110F were even more effective than the wild-type protein, at least in terms of their relative membrane binding (RMB) values. The observed decrease in thermostability upon the substitution of F for W43 (Table 2) probably translates into an increased conformational flexibility, which eases the structural changes required for binding to the phospholipids. The other three mutants displayed slightly reduced values (Table 4), and as observed with the erythrocytes, this effect was also especially prominent for the WquadrupleF mutant.

On the other hand, when ITC was performed employing the POPC/PSM (4:1) vesicles, even the wild-type protein showed a 125-fold decrease in its RMB value (Table 4), as has been thoroughly described,[20,28,62] because it is now well-known that sterols facilitate StnII-induced pore formation.[20] The observation that benzyl alcohol was even more efficient than sterols in enhancing the pore formation process was then interpreted as an alteration of the hydrogen bonding network in the SM-containing bilayers,[20] probably facilitating the hydrophobic effect required for membrane binding. This would explain why the replacement of the membrane-interacting W residues with F exerts only a minor influence on StnII behavior in the presence of Chol. However, in the absence of this sterol, there would be a stronger SM interfacial hydrogen bonding network, which would then affect StnII membrane association, as recently shown by the reduced pore forming capacity of StnII in the presence of dihydro-SM vesicles.[19] Hence, binding and probably pore formation would, in this case, require the participation of key W residues in specific interactions, in addition to a general hydrophobic effect. This interpretation is, in fact, in perfect agreement with the results observed in this work, where all W mutants studied showed a decrease in RMB values compared to that of the wild-type protein assayed under identical conditions (Figure 6 and Table 4). Three of these mutants, W43/114F, WtripleF, and WquadrupleF, even failed to give a clearly detectable ITC signal (Figure 7). In other words, in the absence of Chol, the removal of W114 resulted in protein variants with highly impaired membrane binding ability, a result that could be expected given that W110 and W114 are part of the exposed cluster of aromatic amino acids, which has been reported to be necessary for membrane binding (Figure 2). This is consistent with the recent proposal that in EqtII, a stable cation−π interaction involving the choline headgroup of SM and the W116 [W114 in StnII (Table S1)] side chain exists.[65]

DOI: 10.1021/acs.biochem.6b00935
Biochemistry XXXX, XXX, XXX−XXX

The substitution of F for only W110 had, however, a much smaller impact on membrane affinity (see results for W43/110F). This is probably due to the fact that W110, which belongs to the loop connecting strands β6 and β7 (Figure 1), does penetrate the hydrophobic core of the membrane and this interaction would be only barely affected by the substitution of another highly hydrophobic amino acid such as F. This hypothesis is consistent with site-directed mutagenesis studies revealing that the equivalent residue [W112 (Table S1)] of EqtII is responsible for SM recognition and stabilizes the membrane-bound protein.[22] Consistently, both FraC W112 and W116 appear in the membrane binding region of the octameric crystalline pore structure reported for this protein and seem to interact directly with lipids. Furthermore, W112 would participate in recognizing the lipid located at one of the two high-affinity sites for SM described for FraC oligomers.[36] According to ITC results, the FraC mutant W112R/W116F, which introduces a positive charge at a position that is equivalent to that occupied by the indolyl side chain of W110 of StnII, lacks the ability to bind to SM/DOPC (1:1) liposomes, thus becoming completely inactive in hemolysis experiments.[36] NMR studies of StnI have confirmed that its W111 and W115 residues are inserted in dodecylphosphocholine (DPC) or dihexanoylphosphatidylcholine (DHPC) micelles.[66,67] Finally, the mutant StnI W111C was still able to permeabilize erythrocytes and liposomes, though at a concentration 10-fold higher than that of the wild-type protein because of its lower affinity for the membrane.[39] In good agreement with these observations, it has also been pointed out that the presence of a bulky hydrophobic amino acid side chain at this site plays a pivotal role in membrane binding.[22] Overall, these results suggest that the key role of membrane recognition assigned to the actinoporin's tryptophan represented by W110 of StnII would be based more on its participation in maintaining a hydrophobic effect that on the onset of interactions with specific SM chemical groups. Lending credence to this interpretation, W110 is conserved in only six of the 16 well-known actinoporin protein sequences, but it is replaced with L in seven and F in three of the other nine cases (Figure 2).

In a simplified version of actinoporins' pore formation mechanism, two major steps can be distinguished. First, the protein molecules bind to the membrane; second, they assemble into a functional oligomeric pore. Within the context of this simplified picture, it can be assumed that SPR or ITC assays are strongly influenced by the affinity of the proteins for the membrane,[27,68] although they are also influenced by the latter steps leading to pore formation. Thus, once the protein molecules are bound to the membrane, calcein leakage experiments can provide a better indication of the ability of actinoporin molecules to diffuse, oligomerize, and extend and insert their N-terminal α-helix (not necessarily in that order) within the hydrophobic core of the membrane, leading to the formation of a functional pore. As explained, it cannot be ignored that all these steps are also affected by the binding-to-the-membrane step.

Calcein leakage was measured recording not only the maximal rate of dye release as a function of protein concentration (Figure 9) but also the percentage of leakage after incubation for 10 min with the different concentrations of proteins used (Figure 10). Both sets of results were fully consistent with the interpretations described above. In the absence of Chol, all proteins studied, wild-type StnII included, showed very low rates of calcein release (Figure 9), which is in agreement with their highly impaired binding ability, as revealed by the ITC and SPR experiments. The three mutants displaying the lowest ITC RMB values (W43/114F, WtripleF, and WquadrupleF), for example, did not even produce a clearly detectable fluorescence signal after incubation for 10 min (Figure 10). The presence of Chol quite significantly increased the observed rates and resulted in indistinguishable percentages of calcein leakage when all mutants and the wild-type protein were compared, suggesting that replacing W residues of StnII has more impact on its membrane binding ability than on the subsequent steps leading to the formation of a functional pore. Therefore, these results confirm that actinoporin's W residues, more specifically those belonging to the cluster of aromatic amino acids, play a major role in membrane recognition and binding but have only a minor influence on the diffusion and oligomerization needed to assemble a pore, the only exception being W146 (see above).

Effect of PSM Analogues. Methylated SM analogues with reduced hydrogen bonding capability from 2NH and 3OH have been used to show that these groups were likely to form a hydrogen bond with StnII Tyr135. In addition, it appeared that Tyr111 and Tyr136 could donate hydrogen bonds to the phosphate oxygen of SM, thus stabilizing binding to the toxin.[23] It was then concluded that the interfacial hydrogen bonding properties of SM, in addition to the phosphocholine headgroup, were crucial for high-affinity SM−StnII interaction, a proposal that has recently been confirmed using dihydro versions of various SM variants.[19] To improve our comprehension of the specific interactions between actinoporins and SM molecules, two new SM analogues (CPE-Me_2 and CH_2-PSM) were included in this study (Figures 8 and 10).

The results confirm the extreme specificity of the interactions required for StnII to recognize SM-containing vesicles, as revealed by the absolute absence of any SPR signal (Figure 8) or calcein release (Figure 10) when the wild-type proteins and all the W mutants studied were assayed against lipid model vesicles in the absence of Chol, an impairment that was clearly circumvented by the presence of a large proportion of this sterol within the membrane (Figures 8 and 10). Also, in good accordance with the results discussed in the previous sections, only the WquadrupleF mutant showed a lack of activity that could not be rescued by the addition of Chol, regardless of which SM analogue was being employed. In the experiments in which the SM analogue employed contained a methylene group that was substituted for the oxygen atom binding to the ceramide moiety (CH_2-PSM), the presence of Chol rescued only the wild-type protein behavior for the W43 and W43/110F mutants (Figures 8 and 10). Some of the Chol effects with regard to the SM analogues used may relate to the presence of a partial gel phase (in the 4:1 bilayer composition) and its removal by cholesterol in the 1:1:1 composition. Removing methyl groups from SM has been shown to increase the thermostability of the SM gel phase.[69] With the PSM-CH_2 analogue, it is possible that headgroup orientation is different from that of PSM, and that the presence of cholesterol could affect headgroup orientation in a way that would make toxin−SM association more favorable. It is also possible that bonding of hydrogen to the oxygen linking the headgroup to the ceramide moiety can stabilize toxin−PSM interaction, and such interactions would not be possible in toxin−PSM-CH_2 interactions. This conclusion has been drawn on the basis of the fact that, as suggested by all the results discussed above,

DOI: 10.1021/acs.biochem.6b00935
Biochemistry XXXX, XXX, XXX−XXX

W43 is not involved in membrane recognition and W110 exerts an effect only on the basis of its highly hydrophobic nature, without apparently establishing any specific interactions with SM chemical groups.

■ CONCLUSIONS

The five W residues of StnII play a determining role in maintaining the high thermostability of StnII, with W43 and W115, which face the inner core of the β-sandwich, showing a larger contribution. W115 plays this major role in protein stabilization through an interaction with Y140 and H147, which also strongly influences the conformational freedom and microenvironment of W146. The function of this W146 residue is to provide not only a suitably hydrophobic microenvironment that favors protomer−protomer interactions but also specific interactions that cannot be fulfilled by the benzyl group of a phenylalanine residue. All W mutants studied showed similar behaviors against erythrocytes and Chol-containing model lipidic vesicles, which can be interpreted as the hydrophobic effect sustained by these residues, one of the major driving forces of binding to the membranes. However, in the absence of Chol, binding and probably pore formation require the participation of key W residues in specific interactions, in addition to a general hydrophobic effect. On the other hand, the key membrane recognition role assigned to StnII W110 is based on its participation in maintaining a hydrophobic effect, not on the establishment of specific interactions with SM moieties in a manner independent of the membrane lipid composition. These conclusions were also supported by the employment of two SM analogues with structural alterations in positions known to be important for StnII−SM interactions.

Overall, the results obtained are consistent with the conclusion that actinoporins' W residues belonging to the cluster of aromatic amino acids play a major role in membrane recognition and binding but have only a minor influence on the diffusion and oligomerization steps needed to assemble a functional pore.

■ ASSOCIATED CONTENT

Supporting Information

The Supporting Information is available free of charge on the ACS Publications website at DOI: 10.1021/acs.biochem.6b00935.

Materials and Methods used on small scale protein production and solubility assessment and near-UV CD spectra (PDF)

■ AUTHOR INFORMATION

Corresponding Author

*Departamento de Bioquímica y Biología Molecular I, Facultad de Ciencias Químicas, Universidad Complutense, 28040 Madrid, Spain. E-mail: alvaromp@quim.ucm.es. Telephone: 34 91 394 4259. Fax: 34 91 394 4159.

Funding

The work was funded by Grant BFU2012-32404 from the Spanish Ministerio de Ciencia e Innovación (to J.G.G. and A.M.-d.-P.) and by the Sigrid Juselius Foundation, the Ella and Georg Ehrnrooth Foundation, and the Magnus Ehrnrooth Foundation (to J.P.S.). FPU and UCM fellowships were granted to S.G.-L. and E.R.-d.-T., respectively.

Notes

The authors declare no competing financial interest.

■ ACKNOWLEDGMENTS

The two SM analogues assayed were a kind gift of Professor Katsumura (Kwansei Gakuin University, Sanda City, Hyogo, Japan).

■ ABBREVIATIONS

Chol, cholesterol; CD, circular dichroism; DOPC, 1,2-dioleoyl-*sn*-glycero-3-phosphocholine; Eqt, equinatoxin; Fra, fragaceatoxin; ITC, isothermal titration calorimetry; LUV, large unilamellar vesicle; PFTs, pore-forming toxins; POC, phosphocholine; POPC, 1-palmitoyl-2-oleoyl-*sn*-glycero-3-phosphocholine; PSM, palmitoyl-SM; CPE-Me_2, *N*-palmitoyl ceramide phosphoethanolamine-*N*,*N*-dimethyl; CH_2-PSM, PSM with its proximal esteric oxygen group replaced by a -CH_2- group; RHA, relative hemolytic activity; RMB, relative membrane binding; SEM, standard error of the mean; SM, sphingomyelin; Stn, sticholysin; WT, wild-type.

■ REFERENCES

(1) Anderluh, G., and Maçek, P. (2002) Cytolytic peptide and protein toxins from sea anemones (Anthozoa: Actiniaria). *Toxicon 40*, 111−124.

(2) Tejuca, M., Anderluh, G., Maçek, P., Marcet, R., Torres, D., Sarracent, J., Alvarez, C., Lanio, M. E., Dalla Serra, M., and Menestrina, G. (1999) Antiparasite activity of sea-anemone cytolysins on *Giardia duodenalis* and specific targeting with anti-*Giardia* antibodies. *Int. J. Parasitol. 29*, 489−498.

(3) Basulto, A., Pérez, V. M., Noa, Y., Varela, C., Otero, A. J., and Pico, M. C. (2006) Immunohistochemical targeting of sea anemone cytolysins on tentacles, mesenteric filaments and isolated nematocysts of *Stichodactyla helianthus*. *J. Exp. Zoolog. A Comp. Exp. Biol. 305A*, 253−258.

(4) Belmonte, G., Pederzolli, C., Maçek, P., and Menestrina, G. (1993) Pore Formation by the Sea Anemone Cytolysin Equinatoxin-II in Red Blood Cells and Model Lipid Membranes. *J. Membr. Biol. 131*, 11−22.

(5) Maçek, P., Belmonte, G., Pederzolli, C., and Menestrina, G. (1994) Mechanism of action of equinatoxin II, a cytolysin from the sea anemone *Actinia equina* L. belonging to the family of actinoporins. *Toxicology 87*, 205−227.

(6) Tejuca, M., Dalla Serra, M., Ferreras, M., Lanio, M. E., and Menestrina, G. (1996) Mechanism of membrane permeabilization by sticholysin I, a cytolysin isolated from the venom of the sea anemone *Stichodactyla helianthus*. *Biochemistry 35*, 14947−14957.

(7) Anderluh, G., Krizaj, I., Strukelj, B., Gubensek, F., Maçek, P., and Pungercar, J. (1999) Equinatoxins, pore-forming proteins from the sea anemone *Actinia equina*, belong to a multigene family. *Toxicon 37*, 1391−1401.

(8) De los Ríos, V., Oñaderra, M., Martínez-Ruiz, A., Lacadena, J., Mancheño, J. M., Martínez-del-Pozo, A., and Gavilanes, J. G. (2000) Overproduction in *Escherichia coli* and purification of the hemolytic protein sticholysin II from the sea anemone *Stichodactyla helianthus*. *Protein Expression Purif. 18*, 71−76.

(9) Wang, Y., Yap, L. L., Chua, K. L., and Khoo, H. E. (2008) A multigene family of Heteractis magnificalysins (HMgs). *Toxicon 51*, 1374−1382.

(10) Alegre-Cebollada, J., Oñaderra, M., Gavilanes, J. G., and Martínez-del-Pozo, A. (2007) Sea anemone actinoporins: the transition from a folded soluble state to a functionally active membrane-bound oligomeric pore. *Curr. Protein Pept. Sci. 8*, 558−572.

(11) García-Ortega, L., Alegre-Cebollada, J., García-Linares, S., Bruix, M., Martínez-del-Pozo, A., and Gavilanes, J. G. (2011) The behavior of

DOI: 10.1021/acs.biochem.6b00935
Biochemistry XXXX, XXX, XXX−XXX

sea anemone actinoporins at the water-membrane interface. *Biochim. Biophys. Acta, Biomembr. 1808*, 2275−2288.
(12) Rojko, N., Dalla Serra, M., Maček, P., and Anderluh, G. (2016) Pore formation by actinoporins, cytolysins from sea anemones. *Biochim. Biophys. Acta, Biomembr. 1858*, 446−456.
(13) Bellomio, A., Morante, K., Barlič, A., Gutiérrez-Aguirre, I., Viguera, A. R., and Gonzalez-Mañas, J. M. (2009) Purification, cloning and characterization of fragaceatoxin C, a novel actinoporin from the sea anemone *Actinia fragacea*. *Toxicon 54*, 869−880.
(14) Bakraç, B., and Anderluh, G. (2010) Molecular mechanism of sphingomyelin-specific membrane binding and pore formation by actinoporins. *Adv. Exp. Med. Biol. 677*, 106−115.
(15) Shin, M. L., Michaels, D. W., and Mayer, M. M. (1979) Membrane damage by a toxin from the sea anemone *Stoichactis helianthus*. II. Effect of membrane lipid composition in a liposome system. *Biochim. Biophys. Acta, Biomembr. 555*, 79−88.
(16) De los Ríos, V., Mancheño, J. M., Lanio, M. E., Oñaderra, M., and Gavilanes, J. G. (1998) Mechanism of the leakage induced on lipid model membranes by the hemolytic protein sticholysin II from the sea anemone *Stichodactyla helianthus*. *Eur. J. Biochem. 252*, 284−289.
(17) Valcarcel, C. A., Dalla Serra, M., Potrich, C., Bernhart, I., Tejuca, M., Martínez, D., Pazos, F., Lanio, M. E., and Menestrina, G. (2001) Effects of lipid composition on membrane permeabilization by sticholysin I and II, two cytolysins of the sea anemone *Stichodactyla helianthus*. *Biophys. J. 80*, 2761−2774.
(18) Martínez, D., Otero, A., Álvarez, C., Pazos, F., Tejuca, M., Eliana Lanio, M., Gutiérrez-Aguirre, I., Barlič, A., Iloro, I., Arrondo, J. L., González-Mañas, J. M., and Lissi, E. (2007) Effect of sphingomyelin and cholesterol on the interaction of St II with lipidic interfaces. *Toxicon 49*, 68−81.
(19) García-Linares, S., Palacios-Ortega, J., Yasuda, T., Astrand, M., Gavilanes, J. G., Martínez-Del-Pozo, A., and Slotte, J. P. (2016) Toxin-induced pore formation is hindered by intermolecular hydrogen bonding in sphingomyelin bilayers. *Biochim. Biophys. Acta, Biomembr. 1858*, 1189−1195.
(20) Palacios-Ortega, J., García-Linares, S., Astrand, M., Al Sazzad, M. A., Gavilanes, J. G., Martínez-Del-Pozo, A., and Slotte, J. P. (2016) Regulation of Sticholysin II-Induced Pore Formation by Lipid Bilayer Composition, Phase State, and Interfacial Properties. *Langmuir 32*, 3476−3484.
(21) Bernheimer, A. W., and Avigad, L. S. (1976) Properties of a toxin from the sea anemone *Stoichactis helianthus*, including specific binding to sphingomyelin. *Proc. Natl. Acad. Sci. U. S. A. 73*, 467−471.
(22) Bakraç, B., Gutiérrez-Aguirre, I., Podlesek, Z., Sonnen, A. F., Gilbert, R. J., Maçek, P., Lakey, J. H., and Anderluh, G. (2008) Molecular determinants of sphingomyelin specificity of a eukaryotic pore-forming toxin. *J. Biol. Chem. 283*, 18665−18677.
(23) Maula, T., Isaksson, Y. J., García-Linares, S., Niinivehmas, S., Pentikainen, O. T., Kurita, M., Yamaguchi, S., Yamamoto, T., Katsumura, S., Gavilanes, J. G., Martínez-del-Pozo, A., and Slotte, J. P. (2013) 2NH and 3OH are crucial structural requirements in sphingomyelin for sticholysin II binding and pore formation in bilayer membranes. *Biochim. Biophys. Acta, Biomembr. 1828*, 1390−1395.
(24) Barlič, A., Gutiérrez-Aguirre, I., Caaveiro, J. M., Cruz, A., Ruiz-Arguello, M. B., Pérez-Gil, J., and González-Mañas, J. M. (2004) Lipid phase coexistence favors membrane insertion of equinatoxin-II, a pore-forming toxin from *Actinia equina*. *J. Biol. Chem. 279*, 34209−34216.
(25) Varanda, W., and Finkelstein, A. (1980) Ion and nonelectrolyte permeability properties of channels formed in planar lipid bilayer membranes by the cytolytic toxin from the sea anemone. *J. Membr. Biol. 55*, 203−211.
(26) Alegre-Cebollada, J., Rodríguez-Crespo, I., Gavilanes, J. G., and Martínez-del-Pozo, A. (2006) Detergent-resistant membranes are platforms for actinoporin pore-forming activity on intact cells. *FEBS J. 273*, 863−871.
(27) Alegre-Cebollada, J., Cunietti, M., Herrero-Galán, E., Gavilanes, J. G., and Martínez-del-Pozo, A. (2008) Calorimetric scrutiny of lipid binding by sticholysin II toxin mutants. *J. Mol. Biol. 382*, 920−930.
(28) Alm, I., García-Linares, S., Gavilanes, J. G., Martínez-del-Pozo, A., and Slotte, J. P. (2015) Cholesterol stimulate and ceramide inhibit Sticholysin II-induced pore formation in complex bilayer membranes. *Biochim. Biophys. Acta, Biomembr. 1848*, 925−931.
(29) Pedrera, L., Gomide, A. B., Sánchez, R. E., Ros, U., Wilke, N., Pazos, F., Lanio, M. E., Itri, R., Fanani, M. L., and Álvarez, C. (2015) The Presence of Sterols Favors Sticholysin I-Membrane Association and Pore Formation Regardless of Their Ability to Form Laterally Segregated Domains. *Langmuir 31*, 9911−9923.
(30) Pedrera, L., Fanani, M. L., Ros, U., Lanio, M. E., Maggio, B., and Álvarez, C. (2014) Sticholysin I-membrane interaction: an interplay between the presence of sphingomyelin and membrane fluidity. *Biochim. Biophys. Acta, Biomembr. 1838*, 1752−1759.
(31) Athanasiadis, A., Anderluh, G., Maçek, P., and Turk, D. (2001) Crystal structure of the soluble form of equinatoxin II, a pore-forming toxin from the sea anemone *Actinia equina*. *Structure 9*, 341−346.
(32) Hinds, M. G., Zhang, W., Anderluh, G., Hansen, P. E., and Norton, R. S. (2002) Solution Structure of the Eukaryotic Pore-forming Cytolysin Equinatoxin II: Implications for Pore Formation. *J. Mol. Biol. 315*, 1219−1229.
(33) Mancheño, J. M., Martín-Benito, J., Martínez-Ripoll, M., Gavilanes, J. G., and Hermoso, J. A. (2003) Crystal and Electron Microscopy Structures of Sticholysin II Actinoporin Reveal Insights into the Mechanism of Membrane Pore Formation. *Structure 11*, 1319−1328.
(34) Mechaly, A. E., Bellomio, A., Gil-Carton, D., Morante, K., Valle, M., González-Mañas, J. M., and Guerin, D. M. (2011) Structural insights into the oligomerization and architecture of eukaryotic membrane pore-forming toxins. *Structure 19*, 181−191.
(35) García-Linares, S., Castrillo, I., Bruix, M., Menéndez, M., Alegre-Cebollada, J., Martínez-del-Pozo, A., and Gavilanes, J. G. (2013) Three-dimensional structure of the actinoporin sticholysin I. Influence of long-distance effects on protein function. *Arch. Biochem. Biophys. 532*, 39−45.
(36) Tanaka, K., Caaveiro, J. M., Morante, K., González-Mañas, J. M., and Tsumoto, K. (2015) Structural basis for self-assembly of a cytolytic pore lined by protein and lipid. *Nat. Commun. 6*, 6337.
(37) Malovrh, P., Viero, G., Serra, M. D., Podlesek, Z., Lakey, J. H., Maçek, P., Menestrina, G., and Anderluh, G. (2003) A novel mechanism of pore formation: membrane penetration by the N-terminal amphipathic region of equinatoxin. *J. Biol. Chem. 278*, 22678−22685.
(38) Rojko, N., Kristan, K. C., Viero, G., Zerovnik, E., Maçek, P., Dalla Serra, M., and Anderluh, G. (2013) Membrane damage by an α-helical pore-forming protein, Equinatoxin II, proceeds through a succession of ordered steps. *J. Biol. Chem. 288*, 23704−23715.
(39) Antonini, V., Perez-Barzaga, V., Bampi, S., Penton, D., Martinez, D., Dalla Serra, M., and Tejuca, M. (2014) Functional Characterization of Sticholysin I and W111C Mutant Reveals the Sequence of the Actinoporin's Pore Assembly. *PLoS One 9*, e110824.
(40) Rojko, N., Cronin, B., Danial, J. S., Baker, M. A., Anderluh, G., and Wallace, M. I. (2014) Imaging the Lipid-Phase-Dependent Pore Formation of Equinatoxin II in Droplet Interface Bilayers. *Biophys. J. 106*, 1630−1637.
(41) Baker, M. A., Rojko, N., Cronin, B., Anderluh, G., and Wallace, M. I. (2014) Photobleaching Reveals Heterogeneous Stoichiometry for Equinatoxin II Oligomers. *ChemBioChem 15*, 2139−2145.
(42) Subburaj, Y., Ros, U., Hermann, E., Tong, R., and García-Sáez, A. J. (2015) Toxicity of an α-pore-forming toxin depends on the assembly mechanism on the target membrane as revealed by single-molecule imaging. *J. Biol. Chem. 290*, 4856−4865.
(43) Morante, K., Bellomio, A., Gil-Cartón, D., Redondo-Morata, L., Sot, J., Scheuring, S., Valle, M., González-Mañas, J. M., Tsumoto, K., and Caaveiro, J. M. (2016) Identification of a membrane-bound prepore species clarifies the lytic mechanism of actinoporins. *J. Biol. Chem. 291*, 19210−19219.
(44) Malovrh, P., Barlič, A., Podlesek, Z., Maçek, P., Menestrina, G., and Anderluh, G. (2000) Structure-function studies of tryptophan

DOI: 10.1021/acs.biochem.6b00935
Biochemistry XXXX, XXX, XXX−XXX

mutants of equinatoxin II, a sea anemone pore-forming protein. *Biochem. J. 346*, 223−232.
(45) Hong, Q., Gutiérrez-Aguirre, I., Barlič, A., Malovrh, P., Kristan, K., Podlesek, Z., Maçek, P., Turk, D., González-Mañas, J. M., Lakey, J. H., and Anderluh, G. (2002) Two-step Membrane Binding by Equinatoxin II, a Pore-forming Toxin from the Sea Anemone, Involves an Exposed Aromatic Cluster and a Flexible Helix. *J. Biol. Chem. 277*, 41916−41924.
(46) Alegre-Cebollada, J., Lacadena, V., Oñaderra, M., Mancheño, J. M., Gavilanes, J. G., and Martínez-del-Pozo, A. (2004) Phenotypic selection and characterization of randomly produced non-hemolytic mutants of the toxic sea anemone protein sticholysin II. *FEBS Lett. 575*, 14−18.
(47) Pardo-Cea, M. A., Alegre-Cebollada, J., Martínez-del-Pozo, A., Gavilanes, J. G., and Bruix, M. (2010) ^{1}H, ^{13}C, and ^{15}N NMR assignments of StnII-Y111N, a highly impaired mutant of the sea anemone actinoporin Sticholysin II. *Biomol. NMR Assignments 4*, 69−72.
(48) Pardo-Cea, M. A., Castrillo, I., Alegre-Cebollada, J., Martínez-del-Pozo, A., Gavilanes, J. G., and Bruix, M. (2011) Intrinsic local disorder and a network of charge-charge interactions are key to actinoporin membrane disruption and cytotoxicity. *FEBS J. 278*, 2080−2089.
(49) Jaikishan, S., Björkbom, A., and Slotte, J. P. (2010) Sphingomyelin analogs with branched N-acyl chains: the position of branching dramatically affects acyl chain order and sterol interactions in bilayer membranes. *Biochim. Biophys. Acta, Biomembr. 1798*, 1987−1994.
(50) Björkbom, A., Yamamoto, T., Kaji, S., Harada, S., Katsumura, S., and Slotte, J. P. (2008) Importance of the phosphocholine linkage on sphingomyelin molecular properties and interactions with cholesterol; a study with phosphate oxygen modified sphingomyelin-analogues. *Biochim. Biophys. Acta, Biomembr. 1778*, 1501−1507.
(51) Green, M. R., and Sambrook, J. (2012) *Molecular cloning a laboratory manual*, 4th ed., Cold Spring Harbor Laboratory Press, Plainview, NY.
(52) Alegre-Cebollada, J., Clementi, G., Cunietti, M., Porres, C., Oñaderra, M., Gavilanes, J. G., and Martínez-del-Pozo, A. (2007) Silent mutations at the 5′-end of the cDNA of actinoporins from the sea anemone *Stichodactyla helianthus* allow their heterologous overproduction in *Escherichia coli*. *J. Biotechnol. 127*, 211−221.
(53) De Antonio, C., Martínez-del-Pozo, A., Mancheño, J. M., Oñaderra, M., Lacadena, J., Martínez-Ruiz, A., Pérez-Cañadillas, J. M., Bruix, M., and Gavilanes, J. G. (2000) Assignment of the contribution of the tryptophan residues to the spectroscopic and functional properties of the ribotoxin α-sarcin. *Proteins: Struct., Funct., Genet. 41*, 350−361.
(54) Mancheño, J. M., de los Ríos, V., Martínez-del-Pozo, A., Lanio, M. E., Oñaderra, M., and Gavilanes, J. G. (2001) Partially folded states of the cytolytic protein sticholysin II. *Biochim. Biophys. Acta, Protein Struct. Mol. Enzymol. 1545*, 122−131.
(55) Álvarez-García, E., Martínez-del-Pozo, A., and Gavilanes, J. G. (2009) Role of the basic character of α-sarcin's NH_2-terminal β-hairpin in ribosome recognition and phospholipid interaction. *Arch. Biochem. Biophys. 481*, 37−44.
(56) García-Linares, S., Richmond, R., García-Mayoral, M. F., Bustamante, N., Bruix, M., Gavilanes, J. G., and Martínez-del-Pozo, A. (2014) The sea anemone actinoporin (Arg-Gly-Asp) conserved motif is involved in maintaining the competent oligomerization state of these pore-forming toxins. *FEBS J. 281*, 1465−1478.
(57) De los Ríos, V., Mancheño, J. M., Martínez-del-Pozo, A., Alfonso, C., Rivas, G., Oñaderra, M., and Gavilanes, J. G. (1999) Sticholysin II, a cytolysin from the sea anemone *Stichodactyla helianthus*, is a monomer-tetramer associating protein. *FEBS Lett. 455*, 27−30.
(58) Heymann, J. B., Zakharov, S. D., Zhang, Y. L., and Cramer, W. A. (1996) Characterization of electrostatic and nonelectrostatic components of protein membrane binding interactions. *Biochemistry 35*, 2717−2725.
(59) Rouser, G., Fleischer, S., and Yamamoto, A. (1970) Two dimensional thin layer chromatographic separation of polar lipids and determination of phospholipids by phosphorus analysis of spots. *Lipids 5*, 494−496.
(60) Pace, C. N., Vajdos, F., Fee, L., Grimsley, G., and Gray, T. (1995) How to measure and predict the molar absorption coefficient of a protein. *Protein Sci. 4*, 2411−2423.
(61) Lacadena, J., Martínez-del-Pozo, A., Gasset, M., Patiño, B., Campos-Olivas, R., Vázquez, C., Martínez-Ruiz, A., Mancheño, J. M., Oñaderra, M., and Gavilanes, J. G. (1995) Characterization of the antifungal protein secreted by the mould *Aspergillus giganteus*. *Arch. Biochem. Biophys. 324*, 273−281.
(62) García-Linares, S., Alm, I., Maula, T., Gavilanes, J. G., Slotte, J. P., and Martínez-del-Pozo, A. (2015) The effect of cholesterol on the long-range network of interactions established among sea anemone Sticholysin II residues at the water-membrane interface. *Mar. Drugs 13*, 1647−1665.
(63) Morante, K., Caaveiro, J. M., Viguera, A. R., Tsumoto, K., and Gonzalez-Mañas, J. M. (2015) Functional characterization of Val60, a key residue involved in the membrane-oligomerization of fragaceatoxin C, an actinoporin from *Actinia fragacea*. *FEBS Lett. 589*, 1840−1846.
(64) Wimley, W. C., and White, S. H. (1996) Experimentally determined hydrophobicity scale for proteins at membrane interfaces. *Nat. Struct. Biol. 3*, 842−848.
(65) Weber, D. K., Yao, S., Rojko, N., Anderluh, G., Lybrand, T. P., Downton, M. T., Wagner, J., and Separovic, F. (2015) Characterization of the Lipid-Binding Site of Equinatoxin II by NMR and Molecular Dynamics Simulation. *Biophys. J. 108*, 1987−1996.
(66) Castrillo, I., Araujo, N. A., Alegre-Cebollada, J., Gavilanes, J. G., Martínez-del-Pozo, A., and Bruix, M. (2010) Specific interactions of sticholysin I with model membranes: an NMR study. *Proteins: Struct., Funct., Genet. 78*, 1959−1970.
(67) López-Castilla, A., Pazos, F., Schreier, S., and Ricardo Pires, J. (2014) Solution NMR analysis of the interaction between the actinoporin sticholysin I and DHPC micelles–correlation with backbone dynamics. *Proteins: Struct., Funct., Genet. 82*, 1022−1034.
(68) Rivera-de-Torre, E., Garcia-Linares, S., Alegre-Cebollada, J., Lacadena, J., Gavilanes, J. G., and Martinez-Del-Pozo, A. (2016) Synergistic Action of Actinoporin Isoforms from the Same Sea Anemone Species Assembled into Functionally Active Heteropores. *J. Biol. Chem. 291*, 14109−14119.
(69) Björkbom, A., Róg, T., Kaszuba, K., Kurita, M., Yamaguchi, S., Lönnfors, M., Nyholm, T. K., Vattulainen, I., Katsumura, S., and Slotte, J. P. (2010) Effect of sphingomyelin headgroup size on molecular properties and interactions with cholesterol. *Biophys. J. 99*, 3300−3388.
(70) DeLano, W. L. (2008) *The PyMOL Molecular Graphics System*, DeLano Scientific, San Diego.
(71) Pettersen, E. F., Goddard, T. D., Huang, C. C., Couch, G. S., Greenblatt, D. M., Meng, E. C., and Ferrin, T. E. (2004) UCSF Chimera–a visualization system for exploratory research and analysis. *J. Comput. Chem. 25*, 1605−1612.

DOI: 10.1021/acs.biochem.6b00935
Biochemistry XXXX, XXX, XXX−XXX

García-Linares *et al.*, 2016 ***Role of the Tryptophan Residues in the Specific Interaction of the Sea Anemone Stichodactyla helianthus's Actinoporin Sticholysin II with Biological Membranes***

SUPPLEMENTARY MATERIAL

Materials and Methods

Small scale protein production and solubility assessment

Freshly transformed RB791 *E. coli* colonies (W3110lac/qL8) containing the different plasmids constructed were grown in 5 ml of Luria-Bertani medium, containing 100µg/ml of ampicillin, up to an OD_{600} of 1.0. Then, isopropylthio-β-d-galactoside was added to 1.0 mM final concentration as inducer of the protein production and the culture was further incubated with vigorous shaking for 4 h at 37 ◦C. The cells were then pelleted at 5000×g for 30 min at room temperature. The cellular pellets were resuspended in 1.0 ml of water, exhaustively sonicated (seven pulses of 20 Kc for 1 min) in an ice bath, and centrifuged again at 14,000×g for 30 min at 4 ◦C. The supernatants thus obtained, containing the soluble recombinant proteins, as well as the corresponding cellular debris insoluble pellets, were then analyzed by means of 0.1% SDS – 15% PAGE [1].

Near-UV CD spectra

Near-UV circular dichroism (CD) spectra were obtained on a Jasco 715 spectropolarimeter at a 50 nm/min scanning speed. Optical path cells of 1.0 cm were employed. The proteins were dissolved in 15 mM MOPS buffer, pH 7.5, containing 100 mM NaCl (1.0 mg/mL protein concentration) [2]. At least four spectra were averaged to obtain the final spectrum.

Figures

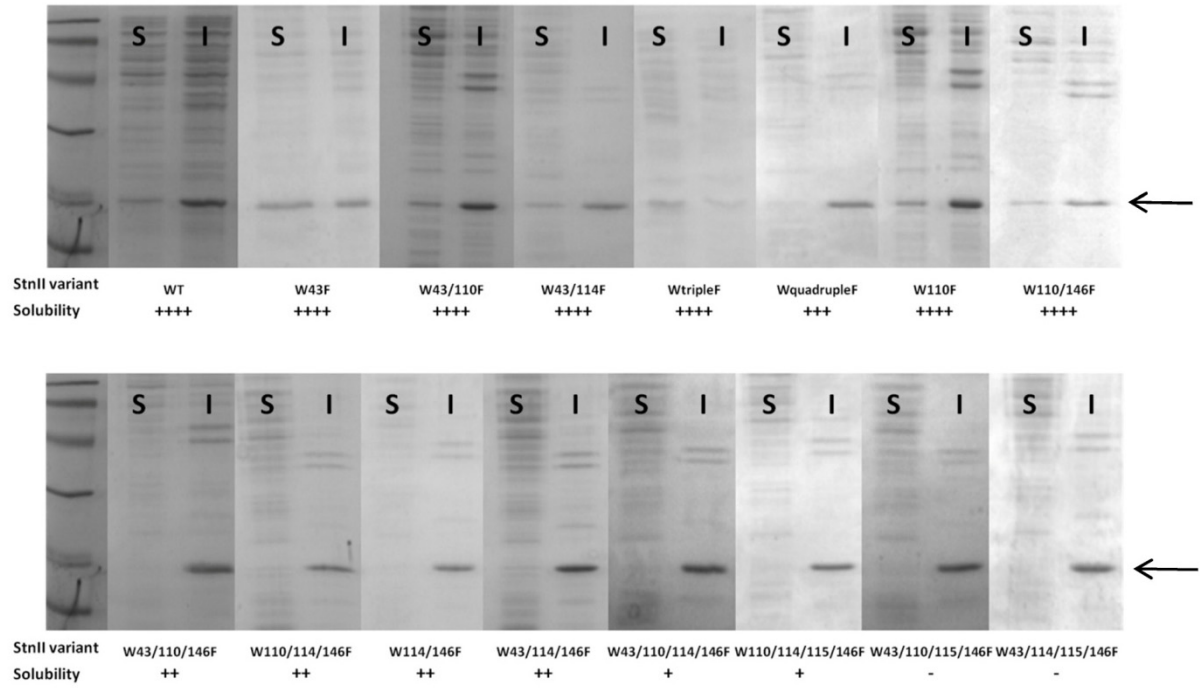

Figure S1.- 0.1% SDS – 15% PAGE analysis of small scale bacterial cultures harboring the plasmid responsible for the production of the wild-type StnII and the 15 different W mutants constructed. After induction with 1 mM IPTG, bacteria cells were collected by centrifugation, resuspended in water and lysed by exhaustive sonication. The soluble fraction (S) resulting from this treatment was recovered by centrifugation and the corresponding cellular debris insoluble pellet was again resuspended in water (I). The position of the StnII protein variants is indicated with arrows. BioRad Low Range Molecular weight marker (first row of both panels) values are 14.4, 21.5, 31.0, 45.0, 66.2, and 97.4 kDa. Relative solubility of all the proteins assayed by this procedure was qualitatively assessed using the wild-type protein as reference. This solubility is indicated by + or – symbols, where four ++++ indicates that solubility was estimated to be equal or larger than that of wild-type StnII. Identical notation is employed to denote solubility in Table 1 of the manuscript.

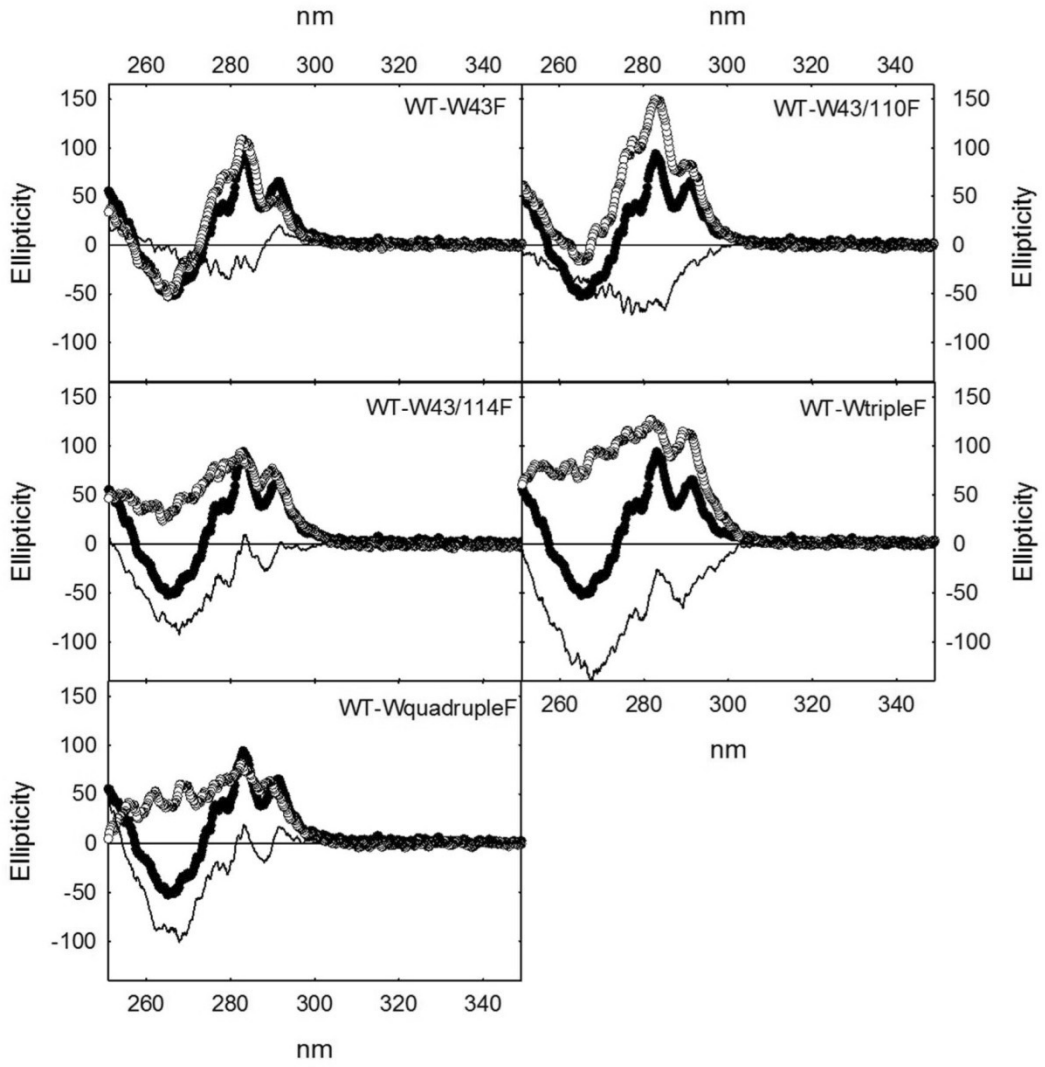

Figure S2. Near-UV circular dichroism spectra of wild-type StnII (black dots) and the various Trp mutants studied (white dots), as indicated in each panel. Black lines represent the calculated difference spectra for the wild-type minus the mutant. Mean residue weight ellipticity is expressed in units of degree x cm^2 x $dmol^{-1}$.

Table S1. Numbers corresponding to the position occupied by W residues along the sequences of the four best-characterized actinoporins: StnI, StnII, EqtII, and FraC.

StnI	StnII	EqtII	FraC
W44	W43	W45	W45
W111	W110	W112	W112
W115	W114	W116	W116
W116	W115	W117	W117
W147	W146	W149	W149

References

(1) Alegre-Cebollada, J., Clementi, G., Cunietti, M., Porres, C., Oñaderra, M., Gavilanes, J. G., and Martínez-del-Pozo, A. (2007) Silent mutations at the 5'-end of the cDNA of actinoporins from the sea anemone *Stichodactyla helianthus* allow their heterologous overproduction in *Escherichia coli*, *J. Biotechnol. 127*, 211-221.

(2) De Antonio, C., Martínez-del-Pozo, A., Mancheño, J. M., Oñaderra, M., Lacadena, J., Martínez-Ruiz, A., Pérez-Cañadillas, J. M., Bruix, M., and Gavilanes, J. G. (2000) Assignment of the contribution of the tryptophan residues to the spectroscopic and functional properties of the ribotoxin α-sarcin, *Proteins 41*, 350-361.

SECTION D

FROM PARTICULAR TO GENERAL:
ACTINOPORINS AS A FAMILY

ARTICLE IX

Differential effect of membrane composition on the pore-forming ability of four different sea anemone actinoporins

García-Linares, S., Rivera-de-Torre, E., Morante, K., Tsumoto, K., Caaveiro, J. M. M., Gavilanes, J. G., Slotte, J. P., Martínez-del-Pozo, Á. (2016). In press in *Biochemistry* (DOI: 10.1021/acs.biochem.6b01007).

Efecto de la composición de la membrana en la formación de poros por parte de cuatro actinoporinas diferentes de anémonas marinas

Las actinoporinas de anémonas marinas constituyen una familia multigénica de toxinas formadoras de poros. Equinatoxina II (EqtII), fragaceatoxina C (FraC), y esticolisinas I y II (StnI y StnII), producidas por tres especies distintas de anémonas, son las únicas que se han estudiado con detalle a nivel molecular. Las cuatro proteínas muestran una alta identidad de secuencia y su estructura tridimensional es prácticamente idéntica. Sin embargo, su capacidad para formar poros es muy distinta dependiendo del sistema lipídico que se utilice, un fenómeno que no se había estudiado en profundidad. Por tanto, el objetivo de este trabajo es evaluar, en condiciones idénticas, la influencia de distintas composiciones de membrana en la formación de poros por parte de las cuatro actinoporinas. Utilizando un sistema lipídico modelo complejo, como son los eritrocitos de carnero, StnII muestra una actividad hemolítica mucho más elevada que las otras tres proteínas estudiadas. Por otro lado, cuando se emplean vesículas unilamelares de DOPC:SM (4:1) la capacidad hemolítica decrece según el orden StnI > StnII > EqtII > FraC, siendo la unión a la membrana el paso limitante. Según lo esperado, cuando se utilizan vesículas unilamelares de DOPC:SM:Chol (1:1:1), la presencia del colesterol no sólo aumenta dos órdenes de magnitud las afinidades de unión a la membrana, sino que también revela que StnII produce liberación de calceína mucho más rápidamente que las otras tres actinoporinas. Este hecho concuerda con la hipótesis de que la diferencia de comportamiento de las actinoporinas radica en la alta variabilidad de secuencia en los 30 primeros residuos del extremo N-terminal. Finalmente, la influencia de los enlaces de hidrógeno que establecen la esfingomielina o la dihidro-esfingomielina en la interfase de la membrana afecta a todas las actinoporinas estudiadas. Se ha planteado que este comportamiento tan misceláneo puede ser consecuencia de las distintas afinidades o especificidades por la membrana, que podrían a su vez estar moduladas por la naturaleza de las membranas o incluso por la presencia de isotoxinas producidas por la misma especie de anémona que aún no han sido caracterizadas.

Differential effect of membrane composition on the pore-forming behavior of four different sea anemone actinoporins

Sara García-Linares[1,2], Esperanza Rivera-de-Torre[1], Tomaž Švigelj[3], Gregor Anderluh[3], Koldo Morante[4], Kouhei Tsumoto[4], José M.M. Caaveiro[4], José G. Gavilanes[1], J. Peter Slotte[2], Álvaro Martínez-del-Pozo[1,*]

[1]Departamento de Bioquímica y Biología Molecular I, Facultades de Química y Biología, Universidad Complutense, Madrid, Spain.
[2]Biochemistry, Faculty of Science and Engineering, Åbo Akademi University, Turku, Finland.
[3]Laboratory for Molecular Biology and Nanobiotechnology, National Institute of Chemistry, Hajdrihova 19, 1000 Ljubljana, Slovenia.
[4]Department of Bioengineering, Graduate School of Engineering, The University of Tokyo, 7-3-1 Hongo, Bunkyo-ku, Tokyo 113-8656, Japan.

*Corresponding author

Keywords: pore-forming-toxin, sticholysin, equinatoxin, fragaceatoxin, erythrocyte, oligomerization, lipid-protein interaction.

Abbreviations: CD, circular dichroism; DOPC, 1,2-dioleoyl-sn-glycero-3-phosphocholine; Eqt, equinatoxin; Fra, fragaceatoxin; ITC, isothermal titration calorimetry; LUV, large unilamellar vesicle; OSM, oleyl sphingomyelin; PFT, pore forming toxin; POPC, 1-palmitoyl-2-oleoyl-sn-glycero-3-phosphocholine; PSM, palmitoyl sphingomyelin; RHA, relative hemolytic activity; RMB, relative membrane binding; SM, sphingomyelin; SPR, surface plasmon resonance; Stn, sticholysin.

Abstract

Sea anemone actinoporins constitute a family of multigene pore-forming toxins. Equinatoxin II (EqtII), fragaceatoxin C (FraC), and sticholysins I and I (StnI and StnII), produced by three different sea anemone species, are the only ones which have been studied in deep molecular detail. The four proteins show high sequence identities and practically coincident three-dimensional structures. However, their pore-forming activity can be quite different depending on the model lipid system employed, a feature which has not been systematically studied before. Therefore, the aim of this work was to evaluate under identical conditions the influence of several distinct membrane compositions on their particular pore-forming behavior. Using a complex model lipid system, such as sheep erythrocytes, StnII showed much higher hemolytic activity than the other three actinoporins studied. On the other hand, this pore-forming ability decreased in the following order of StnI > StnII > EqtII > FraC when assayed against DOPC:SM (4:1) vesicles, being membrane binding the rate limiting step. As expected, when using DOPC:SM:Chol (1:1:1) LUVs, the presence of Chol not only enhanced membrane binding affinities by about two orders of magnitude but also revealed how StnII was much more faster than the other three actinoporins in

producing calcein release. This ability agrees with the proposal that explains this behavior in terms of their high sequence variability along their first 30 N-terminal residues. Finally, the influence of interfacial hydrogen bonding in SM or dihydro-SM containing bilayers was shown to be also a generalized feature of the four actinoporins studied. It was finally hypothesized that this observed miscellaneous behavior could be explained as a consequence of their distinct specificities and/or membrane binding affinities, which might eventually be modulated by the nature of their natural target membranes or even the presence of not yet characterized isotoxin forms from the same sea anemone species.

Introduction

Pore forming toxins (PFT) constitute a fascinating family of proteins because of their dual behavior at the water-membrane interface. In water they are mostly monomeric and remain stably folded as soluble globular proteins. However, upon interaction with lipid membranes of specific composition they become oligomeric integral membrane structures resulting in lytic pores that are lethal for their target cells. Given its small size and its rather simple three-dimensional structure, sea anemone actinoporins [1-6] represent a particularly optimal PFT system to study this transition from a soluble monomeric folded conformation to an oligomeric transmembrane protein.

Actinoporins incorporation into a membrane largely depends on its lipid bilayer composition and physicochemical state [6-13]. Both factors influence the molecular mechanism involved in the transition from the water media to the inserted state of the protein [14, 15]. It has been overtly demonstrated that high affinity recognition of sphingomyelin (SM) is crucial for the specific attachment of actinoporins to the membrane. However, the subsequent effects observed also depend on the physical properties derived from its particular composition and not only from its SM content [16-19]. Although still subject of study, the presence of cholesterol, coexistence of different phases or domains in the membrane, compactness and fluidity, and the hydrogen bonding network established among the different lipids present, seem to be important factors, if not necessarily for binding, at least for the final formation of the pore [4, 10, 12, 13, 16-18, 20-22].

Four different actinoporins, produced by three distinct sea anemone species, have been characterized in detail, including the resolution of their monomeric soluble three-dimensional structures. They are equinatoxin II (EqtII) from *Actinia equina* [23, 24], fragaceatoxin C (FraC) from *Actinia fragacea* [25, 26], and sticholysins I and II (StnI and StnII) from *Stichodactyla helianthus* [27, 28]. The four of them show almost identical conformation in good agreement with their high sequence identities (Fig. 1). A structure that can be described as a hydrophobic and compact β-sandwich core flanked on opposite sides by two α-helices (Fig. 2).

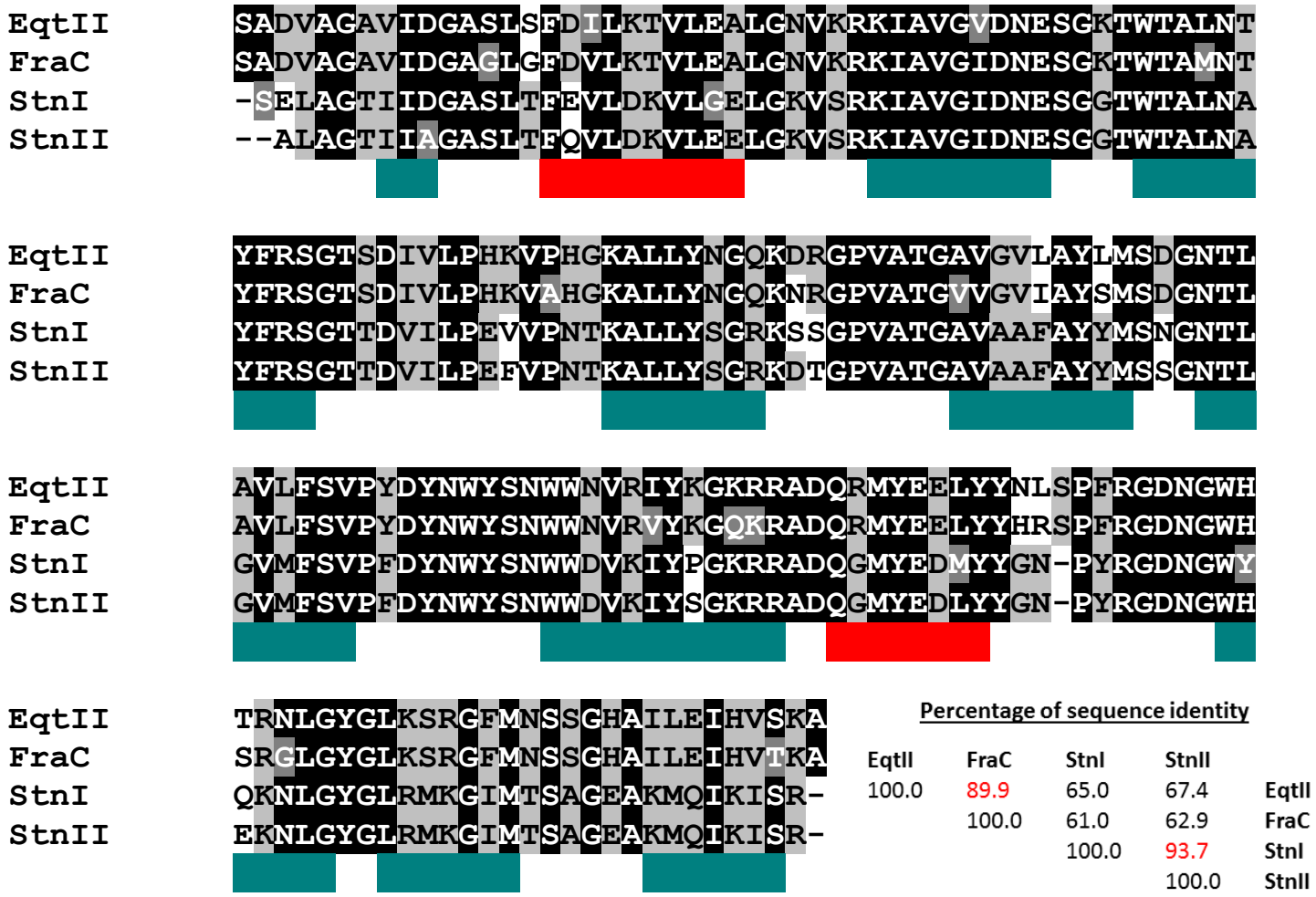

Figure 1. Sequence alignment of the four actinoporins studied. Black background represents the conserved residues, gray is for conservative changes and white for amino acid changes. Red rectangles correspond to the two α-helical segments while the green ones represent the β-strands. Sequences in between these elements appear as loops of non-regular structure. The degree of sequence identity among all four proteins studied, expressed as a percentage, is also shown at the bottom right side of the figure.

In spite of these almost identical structures, these four actinoporins can show quite different hemolytic activities. It has even been proposed that the SM dependence might vary among the different actinoporins studied [10, 15, 29, 30]. For example, it has been shown how cholesterol (Chol) can have profound influence on the behavior of some of these actinoporins [10, 12, 16-18, 31-33]. Strikingly, the functional and biophysical properties of these proteins have never been studied in detail under identical experimental conditions. Only recently their differences in activity were related to changes in the hydrophobicity of their NH_2-terminal ends [34]. This study was however mainly made using peptides mimicking the stretch containing only approximately the first 30 amino acids of each protein. The whole native actinoporins were only compared at the level of their hemolytic and permeabilizing PC:SM (50:50) vesicles activities [34]. In the present work we have measured and compared under identical conditions the spectroscopic features and pore-forming behavior in quite different lipidic environments of these four actinoporins which three-dimensional structure is known at atomic resolution. The major conclusion extracted from these results is that they show a differential sensitivity towards the distinct composition and/or biophysical state of their target membrane.

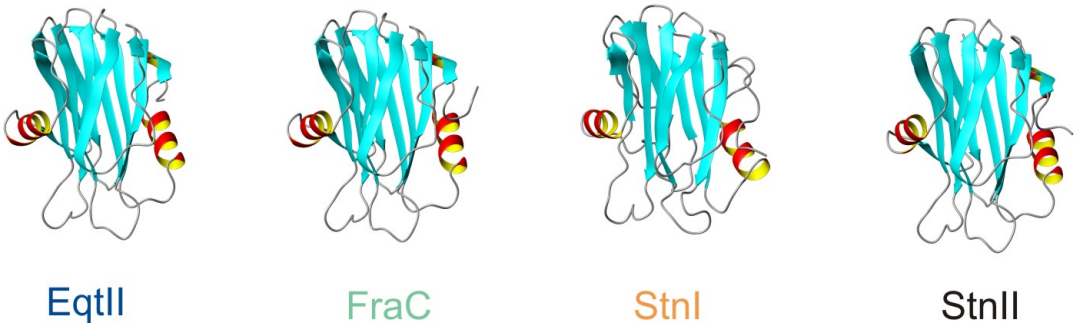

Figure 2. Diagrams representing the three-dimensional structures of the four actinoporins studied. EqtII (PDB 1IAZ), FraC (PDB 4WDC), StnI (PDB 2KS4), and StnII (PDB 1GWY), Diagrams were made using MOLMOL program [60].

Materials and methods

Materials. POPC, DOPC, Chol, porcine brain SM, and OSM were obtained from Avanti Polar Lipids (Alabaster, AL, USA). PSM was purified from egg SM as described previously [35]. Dihydro-PSM was prepared from PSM by hydrogenation using H_2-gas and palladium (10%) on charcoal (Sigma-Aldrich, St. Louis, MO, USA) as a catalyst, as described previously [36]. Dihydro-OSM was prepared from oleic acid anhydride (Sigma-Aldrich) and sphinganin–phosphorylcholine, as described previously [37]. Calcein was also obtained from Sigma-Aldrich. The preparation of the cDNA coding for the actinoporins, as well as the production and purification of the proteins, has been described before for EqtII [38], FraC [39], StnI, and StnII [40].

Homogeneity and spectroscopic characterization. Homogeneity of all protein samples used was confirmed by 0.1% (w/v) SDS/15% (w/v) PAGE performed with standard conditions [41]. After acid hydrolysis of the proteins (5.7 M HCl, 24 h, 110°C), amino acid analyses were performed on a Biochrom 20 automatic analyzer (Pharmacia, Pfizer, New York, NY). The results were used to estimate extinction coefficients for each actinoporin (Table 1) which were then used to calculate protein concentrations. All protein batches used were also characterized in terms of recording their far and near-UV circular dichroism (CD) spectra on a Jasco 715 spectropolarimeter (Easton, MD) and their fluorescence emission spectra on a SLM Aminco 8000 spectrofluorimeter (Urbana, IL), also as described before [42, 43].

Hemolysis assays. Hemolysis assays were performed in 96-multiwell plates as previously described [15, 40]. Briefly, erythrocytes from heparinized sheep blood were washed in 10 mM Tris buffer, pH 7.4, containing 0.145 M NaCl, to a final OD_{655} of 0.5 when mixing equal volumes of the cell suspension and buffer. The hemolysis was followed as a decrease in OD_{655} after addition of the erythrocyte suspension to different final concentrations of protein. An Expert 96 microplate reader (Asys Hitech, GmbH, Eugendorf, Austria) was employed to measure OD_{655}. The value obtained with 0.1% (w/v) Na_2CO_3 was considered as 100% hemolysis.

Isothermal Titration Calorimetry. The interaction between actinoporins and LUVs prepared from DOPC and SM (4:1 molar ratio, 100 nm diameter) or DOPC, SM and Chol (1:1:1 molar ratio, 100 nm diameter) was measured using isothermal titration calorimetry (ITC) as described before [15, 42, 44], using a VP-ITC calorimeter (Malvern MicroCal, Worcestershire, UK). Briefly, protein solutions at 1.5-10.0 µM concentration were titrated by injection of 20 µL aliquots of lipid suspensions (phospholipid concentration: 1.0-5.0 mM). The buffer employed was 10mM Tris, 100 mM NaCl, 1 mM EDTA, pH 7.5. Binding isotherms were adjusted to a model were the protein binds to the membrane involving "n" lipid molecules [15].

Surface Plasmon Resonance. The association of actinoporins with vesicle-coated gold chips was studied as described before [16, 44]. LUVs were prepared from DOPC:SM (4:1 molar ratio) or DOPC:SM:Chol (1:1:1 molar ratio) in Tris buffer (10 mM Tris, 140 mM NaCl, pH 7.4) by extrusion through 100 nm polycarbonate filters at 60 °. Actinoporins binding to the vesicles was studied at 23 °C with a BioNavis SPR Navi 200 instrument (BioNavis Ltd, Tampere, Finland). The sensor gold chip was coated with a carboxymethylated dextran layer which was treated with N-hydroxysuccinimide and N-ethyl-N' (dimethylaminopropyl) carbodiimide to activate the surface for capturing phospholipid membranes [45]. All solutions used for SPR were filtered through 0.2 µm membrane filters and degassed by bath sonication before use. The running buffer was 10 mM Tris, 140 mM NaCl, pH 7.4 and the flow rate was 5 µl/min. First, the chip

surface was cleaned with two injections of 10 mM CHAPS. Then extruded LUVs (0.5 mM lipid concentration) were applied on the surface (12 min injection) and unbound vesicles were removed by one (3 min) injection of 50 mM NaOH. Bovine serum albumin (0.1 mg/ml, 3 min injection) was used to verify that the chip did not have uncovered areas. Finally actinoporins (1.0 μM) was applied for 22–24 min after which buffer alone was injected for 10 min to study toxin dissociation. The chip was regenerated with CHAPS as in the beginning of the experiment.

Calcein leakage assay. Calcein-entrapped large unilamellar vesicles (LUVs) were prepared from DOPC and SM (4:1 molar ratio), DOPC, SM and Chol (1:1:1 molar ratio), POPC and OSM (4:1 molar ratio), POPC and PSM (4:1 molar ratio), POPC and dihydroOSM (4:1 molar ratio), or POPC and dihydroPSM (4:1 molar ratio) by extrusion through 200 nm filters at 60 °C [13]. Briefly, the desired lipids were mixed and dried under a stream of nitrogen. LUVs were separated from non-entrapped calcein by gel filtration on Sephacryl S200HR. The LUVs were used for permeabilization studies within 24 h following standardized protocols [16, 31]. Emission at 550 nm was followed at 23 °C as a function of time (Ex 480 nm). Fluorescence emission was measured on a PTI Quanta-Master spectrofluorimeter (Photon Technology International, Inc. NJ, USA). The released fraction of calcein was determined based on the maximum calcein release which was induced by LUV disintegration in 10% (v/v) Triton X-100. To ensure that no spontaneous leakage occurred, the emission was measured for each sample for 300 seconds before addition of toxin. A steady signal level, indicating intact vesicles, was observed for all samples.

Results

Structural and spectroscopic characterization

Far-UV CD characterization yielded very similar spectra for the four different actinoporins studied (Fig. 3). Given the high β-sheet structure content of actinoporins (Fig. 2), the small changes observed should not be attributed to significantly different conformations but rather would be the consequence of differences in terms of aromatic amino acid content and microenvironment (Table 1)[46, 47]. This interpretation was confirmed by the near-UV CD (Fig. 3) and fluorescence emission (Fig. 4) spectra, even though close inspection of the three-dimensional structures of the four proteins studied did not reveal obvious differences to explain the observed spectroscopic changes. The observed minor differences between StnI and StnII can however be explained just by the higher Tyr content of StnI (Table 1)[40].

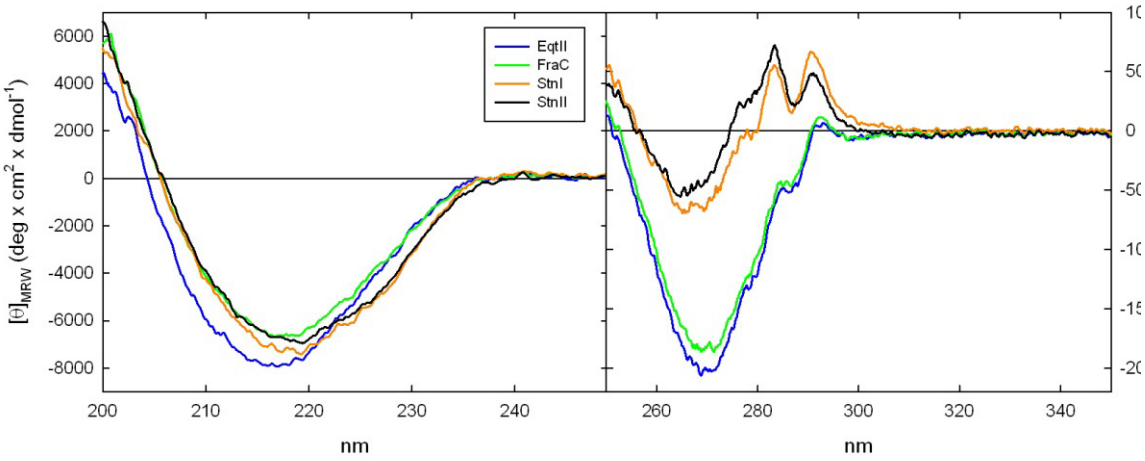

Figure 3. Circular dichroism characterization. Far- (*left panel*) and near-UV (*right panel*) circular dichroism spectra of the four actinoporins studied.

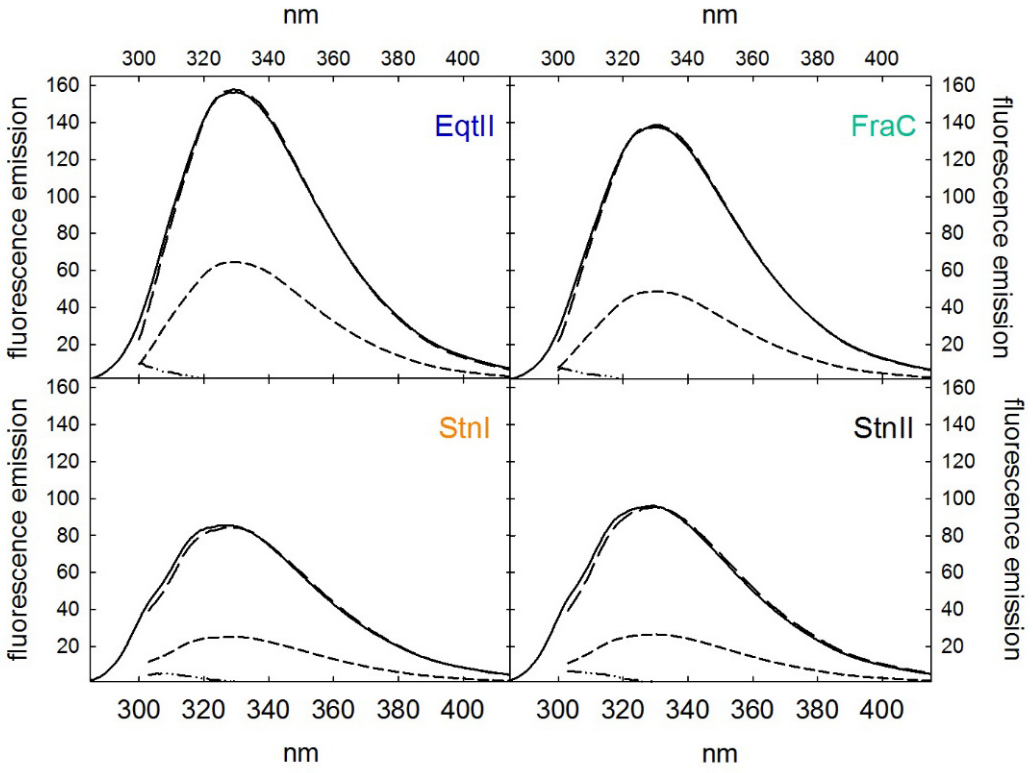

Figure 4. Fluorescence emission spectra of the four actinoporins studied. All spectra were recorded at identical protein concentrations. Experimental spectra resulted from excitation at 275 (solid lines) and 295 (short dashed lines) nm. These spectra obtained upon excitation at 295 nm were normalized at wavelengths above 380 nm to obtain the *Trp contributions* (long dashed lines). *Tyr contribution*s (dashed-point lines) were calculated by subtracting spectra representing the Trp contribution from those obtained upon excitation at 275 nm. Fluorescence emission units are arbitrary, expressed as percentages and referred to the maximum value of StnII when exciting at 275 nm.

This spectroscopic characterization allowed classifying the four actinoporins studied into two different pairs which would also match the degree of sequence identity found among them (Fig. 1). One pair would be StnI and StnII, showing almost identical CD (Fig. 2) and fluorescence emission (Fig. 3) spectra, displaying lower quantum yield values of the Trp emission (Fig. 4), and showing a high degree of sequence identity (Fig. 1). The other two actinoporins studied, EqtII and FraC, would constitute the second pair, showing also high sequence identity between them and almost identical near-UV CD (Fig. 3) and fluorescence emission (Fig. 4) spectra, but quite different in those three terms to those found for StnI and StnII.

Table 1.- Calculated extinction coefficients ($E^{0.1\%}$) of the four different actinoporins used in the study, content of Trp and Tyr residues, and HC_{50}, relative hemolytic activity (RHA) and theoretical pI values.

Actinoporin	**E (0.1%, 1 cm, 280 nm)**	**Number of Tyr**	**Number of Trp**	**HC_{50} (nM)**	**RHA[a]**	**Theoretical pI value**
Equinatoxin II	2.37	11	5	4.7	0.085	9.47
Fragaceatoxin C	2.16	11	5	4.5	0.089	9.57
Sticholysin I	2.55	13	5	3.0	0.133	8.96
Sticholysin II	2.54	12	5	0.4	1.000	8.99

[a]HC_{50}(StnII)/HC_{50}(other actinoporin)[15]

Hemolytic activity

The standard methods usually used to measure the hemolytic activity of actinoporins rely on recording the percentage of hemolysis observed after a fixed amount of time, being considered as 100% the hemolysis value obtained upon addition of Na_2CO_3 to a 0.1% (w/v) final concentration. This methodological approach artificially reduces the observed differences when actinoporin concentrations are high and, consequently, hemolysis takes place at high rate. Given that one of the purposes of the present work was to standardize the comparison among different actinoporins, in addition to the hemolysis percentage recorded after 10 min, the time needed to reach 50% of the final hemolysis value ($t_{1/2}$) was also registered. This second measurement represents a much more valuable parameter because it contains information about both kinetic and hemolytic proficiency. Both methods yielded very similar results (Fig. 5). StnII appeared as more hemolytic against sheep erythrocytes than the other three actinoporins studied (between 7-12 fold higher; Table 1) which, on the other hand, showed quantitatively similar hemolytic activities, at least in terms of their HC_{50} values or relative hemolytic activities (RHA) (Table 1).

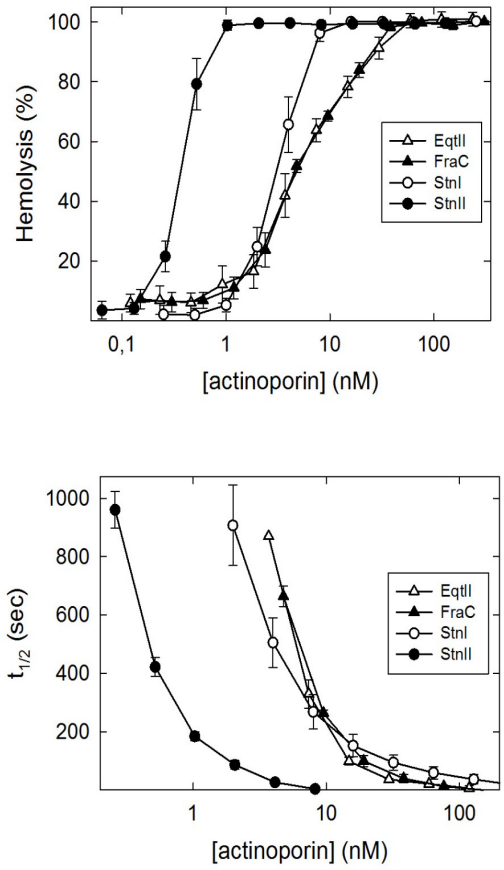

Figure 5. Hemolysis. Hemolytic activity of the four actinoporins studied, expressed as percentage of the hemolysis produced after 10 minutes (*upper panel*) or as the time needed ($t_{1/2}$, in seconds) to reach 50% of complete hemolysis (*lower panel*), versus the logarithm of protein concentration. The 100% value was calculated after addition of Na_2CO_3 to a 0.1% (w/v) final concentration.

Binding to different lipid model vesicles

Erythrocytes are rather complex systems which do not easily allow drawing conclusions about the nature of the lipid molecules involved in membrane binding and pore-formation. Therefore, the functional comparison was continued using LUVs of two different lipidic compositions: DOPC:SM (4:1) and DOPC:SM:Chol (1:1:1). Both types of vesicles can be considered as standard systems for actinoporins since they have been widely employed with the aim of studying actinoporin functional properties [13, 15, 16, 30, 31, 43, 44].

The actinoporins' pore-formation mechanism has been thoroughly studied but still some of its details need a better molecular definition [6, 26, 48-51]. In a simplified version of this mechanism, two major different steps can be distinguished: First, the protein molecules bind to the membrane and, second, assemble into a functional oligomeric pore. Within the context of this simplified picture, it can be assumed that SPR or ITC assays are highly influenced by the affinity of the proteins to the membrane [15], although they definitively measure the influence of the latter steps leading to pore-formation too.

SPR measurements revealed how StnI and StnII showed higher affinity for the DOPC:SM (4:1) vesicles than the other two actinoporins studied. This difference was however significantly reduced in the presence of Chol (Fig. 6, *right panel*), confirming the key role of this lipid for actinoporins functional activity. This experiment was performed at a single protein/lipid ratio value for the four actinoporins studied and should be considered just a semiquantitative result. Therefore, a quantitative analysis was performed using ITC (Fig. 7). All four actinoporins assayed showed the expected enthalpy driven process (Table 2) observed before for StnII [16, 31] and FraC [26, 32], suggesting the existence of a general mechanism of membrane interaction and pore-formation. However, consistently with the SPR results, in the absence of Chol, StnI and II showed very similar behaviors but bound to the vesicles with affinities 6 to 33 fold greater than FraC or EqtII, respectively, at least in terms of relative membrane binding (RMB) values (Table 2).

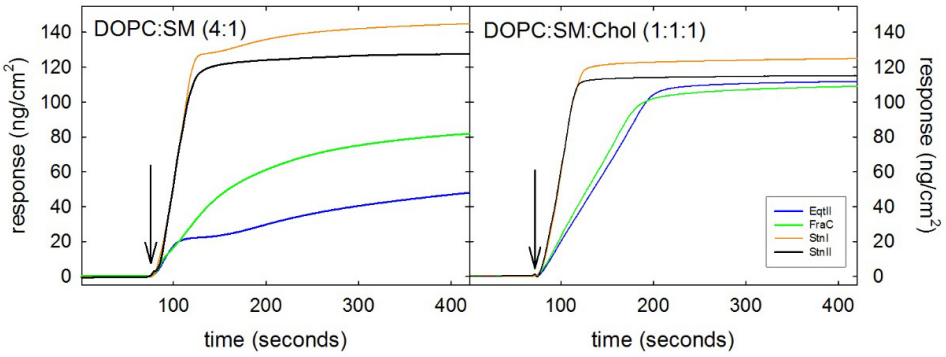

Figure 6. Surface Plasmon Resonance. Interaction of the actinoporins studied with supported bilayers of DOPC:SM (4:1) or DOPC:SM:Chol (1:1:1) as analyzed by SPR. Proteins were added at times indicated by arrows and the binding and formation of pores was determined as a function of time. The chip temperature was maintained at 23°C. Each value is average ± SEM from n=2.

On the other hand, and also as expected from the SPR experiments, Chol increased membrane affinity of all the toxins by about two orders of magnitude (Table 2), still remaining as an enthalpy driven mechanism. RMB values were now similar with differences in the order of no more than 4-fold lower of higher values (Table 2), confirming that Chol exerts a very similar influence on the membrane binding ability of the four actinoporins studied in accordance with the existence of a general mechanism for membrane binding and pore-formation.

In all cases studied, the higher differences were observed with regard to the number of n lipid molecules affected by binding of the different actinoporins studied (Table 2). Maybe this reflects different stoichiometries of a miscellaneous assembly of the oligomeric species appearing at the membrane, in good agreement with the proposal that this arrangement might not be uniformly distributed [48].

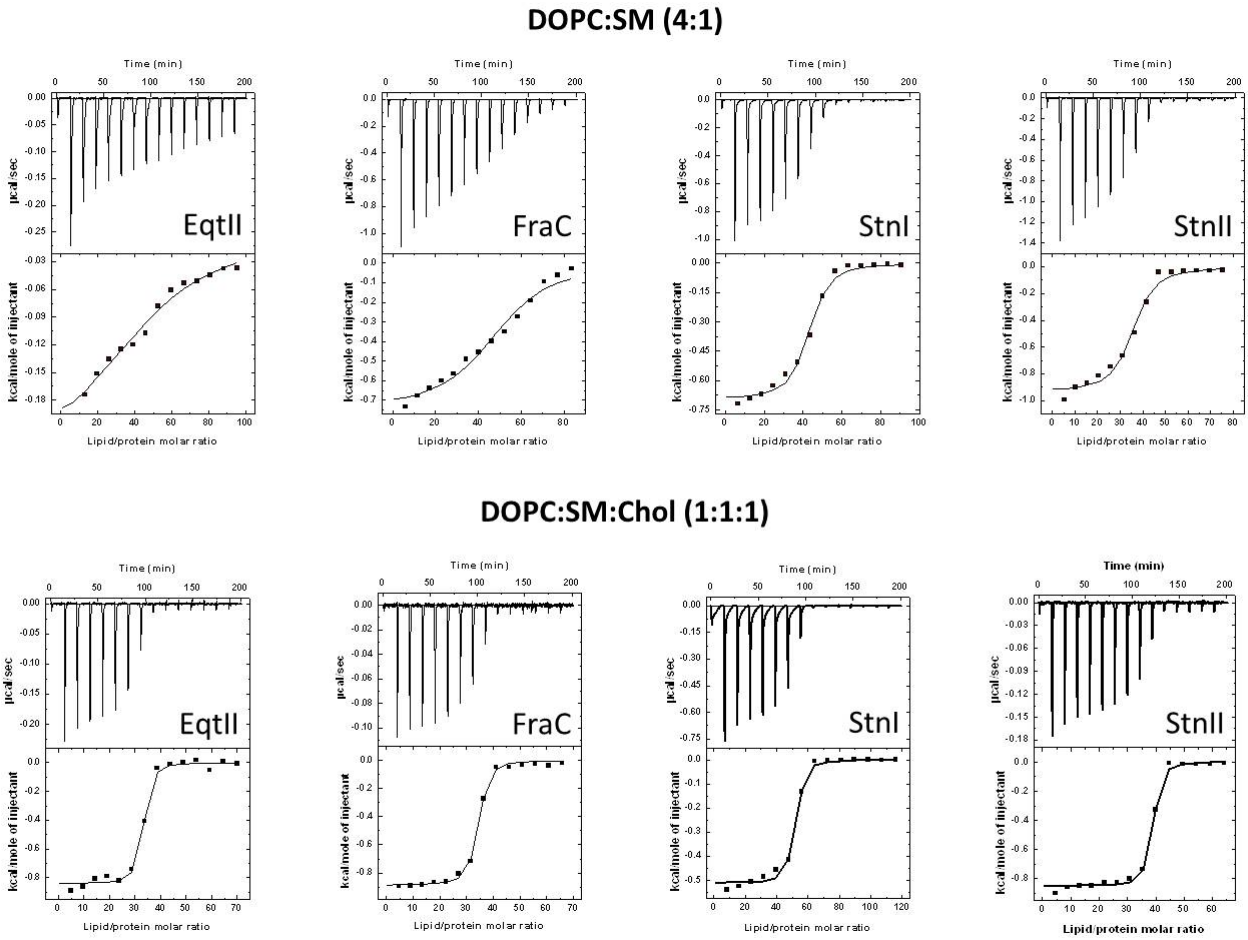

Figure 7. Isothermal Titration Calorimetry. Binding of the four actinoporins studied to DOPC:SM (4:1) or DOPC:SM:Chol (1:1:1) LUVs studied by ITC. Binding isotherms were adjusted to a model in which protein membrane binding involves the participation of "n" lipid molecules [15]. The c values ($c = K_b \times P_0$; where P_0 is the initial protein concentration) for all the graphs shown were in the range 1–1000.

Table 2. Analysis of the interaction between the four actinoporins studied and DOPC:PSM (4:1) or DOPC:SM:Chol (1:1:1) LUVs, as measured by ITC. Results shown are the average of at least two independent experiments.

DOPC:SM (4:1)						
Actinoporin	**n**	**K_b x 10^{-6} (M^{-1})**	**ΔG (kcal/mol)**	**ΔH (kcal/mol)**	**ΔS (cal/mol K)**	**RMB[a]**
EqtII	48 ± 5	0.29 ± 0.33	-5.3 ± 0.3	-12.2 ± 1.2	-23.0 ± 4.2	0.03
FraC	51 ± 3	1.61 ± 0.45	-6.2 ± 0.1	-37.3 ± 1.0	-104.2 ± 2.8	0.15
StnI	35 ± 9	6.89 ± 0.49	-7.4 ± 0.2	-26.2 ± 3.1	-63.4 ± 11.1	0.92
StnII	31 ± 5	6.62 ± 2.31	-7.4 ± 0.3	-33.6 ± 2.4	-88.0 ± 6.9	1.00
DOPC:SM:Chol (1:1:1)						
Actinoporin	**n**	**K_b x 10^{-8} (M^{-1})**	**ΔG (kcal/mol)**	**ΔH (kcal/mol)**	**ΔS (cal/mol K)**	**RMB[a]**
EqtII	32 ± 2	1.66 ± 1.15	-9.2 ± 0.5	-26.7 ± 0.7	-58.7 ± 4.0	1.19
FraC	26 ± 8	3.32 ± 1.12	-9.8 ± 0.1	-26.2 ± 4.3	-54.8 ± 14.5	2.93
StnI	47 ± 4	0.49 ± 0.15	-8.3 ± 0.2	-23.6 ± 1.6	-51.7 ± 5.7	0.23
StnII	39 ± 4	1.70 ± 0.90	-9.1 ± 0.5	-44.0 ± 3.0	-115.0 ± 9.0	1.00

[a]Relative Membrane Binding values calculated according to [n(StnII) × K(other actinoporin)]/[n(other actinoporin) × K(StnII)] as explained in [15]

Calcein-leakage

Once bound to the membrane, calcein-leakage experiments can give a good indication of the ability of actinoporins to diffuse, oligomerize, extend, and insert their N-terminal α-helix (not necessarily in that order), finally leading to the formation of a functional pore. In order to register these presumed kinetic differences, calcein leakage was measured as the maximum rate of dye release as a function of protein concentration (Fig. 8). In the absence of Chol, the proteins basically reproduced the same pattern observed by SPR and ITC measurements suggesting that binding would be the rate limiting step (Fig. 8, *left panel*).

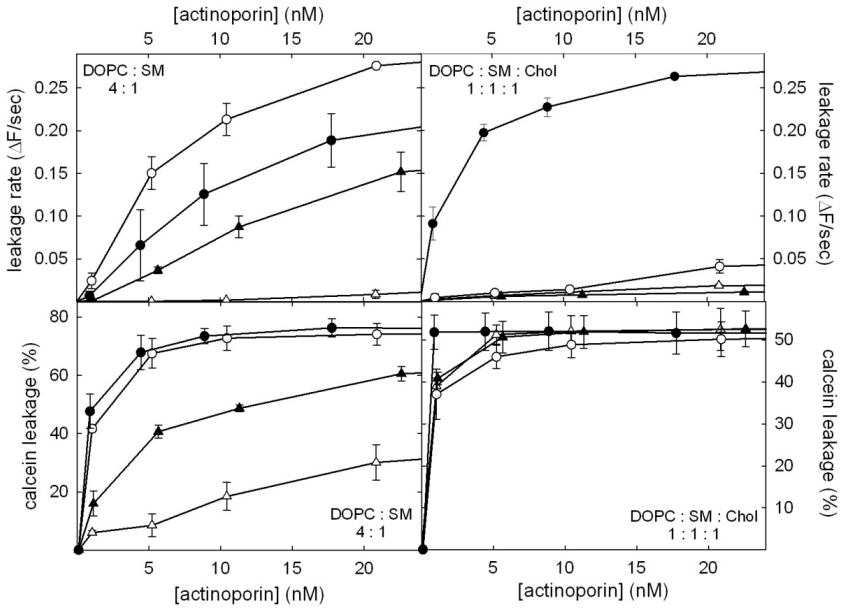

Figure 8. Calcein release. Maximum rate values of release (*upper panels*) or percentage of leakage after 10 minutes (*lower panels*) of calcein entrapped in DOPC: SM (4:1) or DOPC:SM:Chol (1:1:1) vesicles by EqtII (black triangles), FraC (white triangles), StnI (white circles), and StnII (black circles). Calcein-entrapped vesicles were prepared with extrusion and release was measured at 23 °C. All intensities were normalized. Towards the end of the measurement Triton X-100 was added to dissolve the LUVs and release all calcein. The results shown are representative of two different independent experiments. Each value is average ± SEM from n=2.

On the other hand, when Chol was present, StnII stood out as the most effective pore forming protein in kinetic terms. Given that the four proteins studied show similar and highly increased (about two orders of magnitude, Table 2) apparent binding affinities towards the DOPC:SM:Chol (1:1:1) vesicles, it seems reasonable to assume that in the presence of a large proportion of Chol (around 30%; very similar to the erythrocyte content) the rate limiting step would be some of the subsequent steps needed to produce a pore once the protein is bound to the membrane. In fact, and highly consistent with this interpretation after 10-15 min of protein addition, all four actinoporins showed identical percentage of final leakage (Fig. 8, *lower right panel*).

Finally, it has been recently shown how StnI and StnII formed pores in unilamellar vesicles containing PSM or OSM, but both toxins failed if vesicles were prepared from dihydro-PSM or dihydro-OSM [13]. This result was interpreted as the stronger intermolecular hydrogen bonding between dihydro-SM molecules increasing the energy barrier for toxin penetration into the interfacial region of the bilayer. Therefore this behavior was also tested for the four actinoporins studied measuring calcein release from POPC LUV containing one fifth (4:1 ratio) of PSM, OSM of their corresponding hydrogenated species (Fig. 9). As expected, all four proteins showed a highly impaired ability to release the encapsulated calcein when assayed against vesicles containing dihydro-PSM or dihydro-OSM, supporting the hypothesis that the intermolecular hydrogen bonding at the interfacial region prevented actinoporins from membrane binding and/or pore formation. Finally, as observed for the other calcein release experiments (Fig. 8) EqtII resulted much less efficient than the other three actinoporins characterized, even in the absence of the dihydro-SMs.

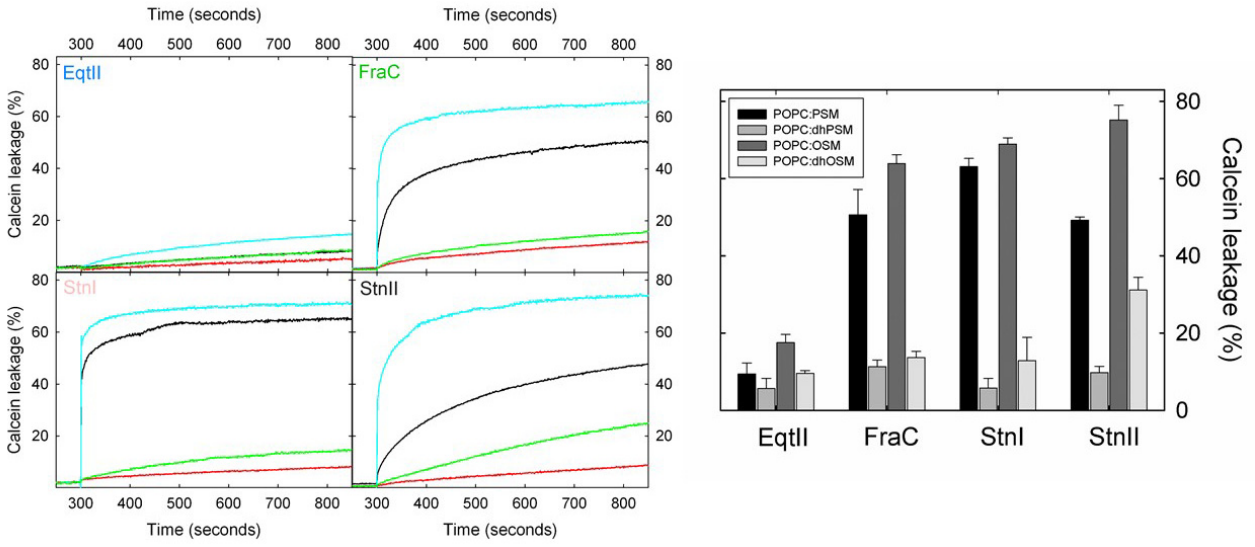

Figure 9. Calcein leakage in the presence of dihydro-SMs. (*Left panel*) Calcein release by EqtII, FraC, StnI, or StnII from POPC:PSM (black traces), POPC:dihydroPSM (red traces), POPC:OSM (blue traces), and POPC:dihydroOSM (green traces) lipid model vesicles. POPC:sphingolipid (4:1, molar ratios) LUVs were employed in all examples shown. After 300 seconds each indicated actinoporin was always added to give final concentration of 20 nM. The total lipid:actinoporin molar ratio was about 125:1. (*Right panel*) Bar diagrams showing the percentage of calcein release obtained in these experiments 500 seconds after protein addition. Each value is the average ± SEM from n=2.

Discussion

The four proteins studied have an identical number of Trp residues (Table 1) which are conserved along their sequences (Fig. 1) and occupy equivalent positions within their three-dimensional structures. Indeed, it is well accepted that these Trp play a key role in actinoporins binding to membranes [52-58]. Unexpectedly, and according to the spectroscopic characterization performed, these aromatic residues seem to appear in quite different microenvironment when comparing StnI and StnII to EqtII or FraC. An observation which correlates nicely with the degree of sequence identity among them. Differences which, however, do not seem to correlate with their hemolytic and membrane interaction behavior, maybe only reflecting minor local changes unrelated to the membrane interaction ability of these proteins, according to the protein-lipid interaction results obtained.

The hemolysis activity of all four actinoporins (Fig. 5) gave a very similar result as that one obtained before with human red blood cells [34], suggesting that the present observation might reflect a rather general behavior. However, although only the four proteins herein characterized have been produced in enough amount as to be characterized in deep detail, it must be remembered that these proteins appear as multigene families within each sea anemone species. That is to say, it should not be ruled out the possibility of the existence of other different isotoxins, not yet characterized, showing much different hemolytic activity than the four ones studied now. This possibility seems even more plausible in the light of the recent demonstration that StnI and StnII can act synergistically [59]. It can be then hypothesized that further characterization of new actinoporin isoforms might yield molecular species as hemolytic as StnII, for example.

The ability to produce calcein-leakage from DOPC:SM (4:1) vesicles roughly paralleled membrane binding affinity of the four proteins studied. In this system, binding to the membrane seemed to be the rate limiting step in order to produce a functional pore. On the contrary, membrane binding affinity for DOPC:SM:Chol (1:1:1) vesicles was similar for all them and about 100-fold higher when compared to the vesicles without Chol (Table 1). According to the results presented, all four actinoporins show an enhanced pore-forming ability in the presence of this membrane lipid. In this Chol-containing bilayer system, however, StnII was much faster in producing calcein leakage than the other three actinoporins studied (Fig. 8; *right panel*), a result which agrees with the differences observed in hemolytic activity (Fig. 5). Erythrocytes, after all, have a high content of Chol within their membranes of about 30%. This ability does not necessarily reflect a higher affinity for the membrane but rather an improved easiness to diffuse, oligomerize and penetrate the bilayer, given that membrane binding would not be now the rate-limiting step. This preference of

StnII for Chol had been already described [10, 16, 31] but not studied in relation to the other well-known actinoporins. Taking into account that DOPC:SM:Chol (1:1:1) vesicles are also a standard raft containing lipidic system the influence of lipid domains on this behavior cannot be ruled out, even considering that the latest findings suggest that the effect of Chol would be mainly due to its role modifying the physical state of the membrane and not to its participation in specific lipid-lipid or lipid-protein interactions[17, 21].

Comparison of the three-dimensional structures of the four actinoporins studied did not reveal major differences (Fig. 2), as expected from their very similar amino acid sequences (Fig. 1). Maybe it should be then concluded that the structures in solution do not reflect accurately the final conformation in the membrane-bound form. However, it has been recently reported that the hemolytic and permeabilizing activities of these actinoporins can be qualitatively reproduced by synthetic peptides resembling their first 30 amino acids [34]. These authors correlated this behavior with the hydrophobicity of the corresponding 1-10 N-terminal segment. Their data suggested that the N-terminus of StnII would be more deeply buried into the hydrophobic core of the bilayer than that of the other known actinoporins given the presence of a larger hydrophobic continuum along extended α-helix, which is proposed to penetrate the membrane. It is well known that the highest variability among these four proteins appears just along their first 30 N-terminal residues (Fig. 1). Neutron reflection studies of the interaction of EqtII with lipid membranes have revealed that Chol is required for the penetration of the 30 residues long extended N-terminal α-helix across the lipid bilayer [33]. Thus, the results obtained using the complete native proteins can be also explained in terms of the different hydrophobic character of this protein segment. Somehow, in the presence of Chol, StnII would more easily diffuse, oligomerize and/or penetrate the bilayer with its extended N-terminal α-helix. On the other hand, the effect of Chol on membrane thickness could be another factor which could differentially affect the behavior of the four actinoporins studied. Within this idea, the length of the N-terminal helix seems to be correlated with kinetic parameter in Chol-membranes. An experiment enlarging the N-terminal of StnII or shortening the other actinoporins could be an adequate approach to test this idea. Mutations that make the N-terminal of StnII more like that of EqtII/FraC could also offer valuable data.

Finally, it has been also very recently described how not only Chol but many other sterols facilitate StnII-induced pore formation markedly, although the efficiency does not appear to correlate with the sterol structures [21] but rather with the distortion of the hydrogen bonding network established among the different membrane lipids, with special emphasis on SM. This observation correlates nicely with the behavior of the four actinoporins when assayed against dihydro-SMs (Fig. 9). A behavior which had

been already described for StnII and attributed to effects on interfacial hydrogen bonding in SM or dihydro-SM containing bilayers [13]. An effect which now seems to be of general application to all actinoporins studied. Why this network perturbation should be less determinant on EqtII behavior is something that still remains to be explained and maybe is also related to the possibility of synergic interaction with some other isotoxins produced by *A. equina*.

In summary, we have shown that StnII from *S. helianthus* is the most hemolytic protein among the four actinoporins so far characterized in molecular detail. However, all they show quite different behavior when studied against simpler model systems such as LUVs containing Chol of dihydro-SM species, for example. This differential behavior might be a consequence of their distinct specificities and/or membrane binding affinities which might eventually be modulated by the nature of their natural target membranes or even the presence of not yet characterized isotoxin forms from the same sea anemone species.

Acknowledgements

We thank Mia Åstrand for her help in performing some of the experiments made with dihydro–SMs. Equinatoxin II was a kind gift from Drs. Tomaž Švigelj and Gregor Anderluh (Laboratory for Molecular Biology and Nanobiotechnology, National Institute of Chemistry of Ljubljana, Slovenia).

Funding

This work was funded by grant BFU2012–32404 from the Spanish Ministerio de Economía y Competitividad e Innovación, grants from the Academy of Finland, the Sigrid Juselius Foundation, the Ella and Georg Ehrnrooth Foundation, and the Magnus Ehrnrooth Foundation for JPS, by the Platform for Drug Discovery, Informatics and Structural Life Science from the Ministry of Ministry of Education, Culture, Sports, Science and Technology of Japan, and by Grants-in-Aid for Scientific Research C (16H02420 and 15K06962) from the Japan Society for the Promotion of Science. A FPU fellowship was granted to SGL and a UCM fellowship to ERT.

Notes

The authors declare no competing financial interest.

References

[1] Maček, P. (1992) Polypeptide cytolytic toxins from sea anemones (Actiniaria), *FEMS microbiology immunology 5*, 121-129.

[2] Anderluh, G., and Maček, P. (2002) Cytolytic peptide and protein toxins from sea anemones (Anthozoa: Actiniaria), *Toxicon 40*, 111-124.
[3] Alegre-Cebollada, J., Oñaderra, M., Gavilanes, J. G., and Martínez-del-Pozo, A. (2007) Sea anemone actinoporins: the transition from a folded soluble state to a functionally active membrane-bound oligomeric pore, *Curr Protein Pept Sci 8*, 558-572.
[4] Bakrač, B., and Anderluh, G. (2009) Molecular mechanism of sphingomyelin-specific membrane binding and pore formation by actinoporins, *Adv Exp Med Biol 677*, 106-115.
[5] García-Ortega, L., Alegre-Cebollada, J., García-Linares, S., Bruix, M., Martínez-del-Pozo, Á., and Gavilanes, J. G. (2011) The behavior of sea anemone actinoporins at the water-membrane interface, *Biochimica et biophysica acta 1808*, 2275-2288.
[6] Rojko, N., Dalla Serra, M., Macek, P., and Anderluh, G. (2016) Pore formation by actinoporins, cytolysins from sea anemones, *Biochim Biophys Acta 1858*, 446-456.
[7] Shin, M. L., Michaels, D. W., and Mayer, M. M. (1979) Membrane damage by a toxin from the sea anemone *Stoichactis helianthus*. II. Effect of membrane lipid composition in a liposome system, *Biochimica et biophysica acta 555*, 79-88.
[8] Belmonte, G., Pederzolli, C., Maček, P., and Menestrina, G. (1993) Pore formation by the sea anemone cytolysin equinatoxin-II in red blood cells and model lipid membranes, *J Membr Biol 131*, 11-22.
[9] Tejuca, M., Serra, M. D., Ferreras, M., Lanio, M. E., and Menestrina, G. (1996) Mechanism of membrane permeabilization by sticholysin I, a cytolysin isolated from the venom of the sea anemone *Stichodactyla helianthus*, *Biochemistry 35*, 14947-14957.
[10] De los Ríos, V., Mancheño, J. M., Lanio, M. E., Oñaderra, M., and Gavilanes, J. G. (1998) Mechanism of the leakage induced on lipid model membranes by the hemolytic protein sticholysin II from the sea anemone *Stichodactyla helianthus*, *Eur J Biochem 252*, 284-289.
[11] Valcarcel, C. A., Dalla Serra, M., Potrich, C., Bernhart, I., Tejuca, M., Martínez, D., Pazos, F., Lanio, M. E., and Menestrina, G. (2001) Effects of lipid composition on membrane permeabilization by sticholysin I and II, two cytolysins of the sea anemone *Stichodactyla helianthus*, *Biophys J 80*, 2761-2774.
[12] Martínez, D., Otero, A., Álvarez, C., Pazos, F., Tejuca, M., Lanio, M. E., Gutiérrez-Aguirre, I., Barlič, A., Iloro, I., Arrondo, J. L., González-Mañas, J. M., and Lissi, E. (2007) Effect of sphingomyelin and cholesterol on the interaction of St II with lipidic interfaces, *Toxicon 49*, 68-81.
[13] García-Linares, S., Palacios-Ortega, J., Yasuda, T., Åstrand, M., Gavilanes, J. G., Martínez-del-Pozo, A., and Slotte, J. P. (2016) Toxin-induced pore formation is hindered by intermolecular hydrogen bonding in sphingomyelin bilayers, *Biochim Biophys Acta - Biomembranes 1858*, 1189–1195.

[14] Menestrina, G., Cabiaux, V., and Tejuca, M. (1999) Secondary structure of sea anemone cytolysins in soluble and membrane bound form by infrared spectroscopy, *Biochemical and biophysical research communications 254*, 174-180.
[15] Alegre-Cebollada, J., Cunietti, M., Herrero-Galán, E., Gavilanes, J. G., and Martínez-del-Pozo, A. (2008) Calorimetric scrutiny of lipid binding by sticholysin II toxin mutants, *J Mol Biol 382*, 920-930.
[16] Alm, I., García-Linares, S., Gavilanes, J. G., Martínez-del-Pozo, A., and Slotte, J. P. (2015) Cholesterol stimulate and ceramide inhibit sticholysin II-induced pore formation in complex bilayer membranes, *Biochim Biophys Acta - Biomembranes 1848*, 925-931.
[17] Pedrera, L., Gomide, A. B., Sánchez, R. E., Ros, U., Wilke, N., Pazos, F., Lanio, M. E., Itri, R., Fanani, M. L., and Álvarez, C. (2015) The presence of sterols favors sticholysin I-membrane association and pore formation regardless of their ability to form laterally segregated domains, *Langmuir 31*, 9911-9923.
[18] Barlič, A., Gutiérrez-Aguirre, I., Caaveiro, J. M. M., Cruz, A., Ruiz-Argüello, M. B., Pérez-Gil, J., and González-Mañas, J. M. (2004) Lipid phase coexistence favors membrane insertion of equinatoxin-II, a pore-forming toxin from *Actinia equina*, *J Biol Chem 279*, 34209-34216.
[19] Schön, P., García-Sáez, A. J., Malovrh, P., Bacia, K., Anderluh, G., and Schwille, P. (2008) Equinatoxin II permeabilizing activity depends on the presence of sphingomyelin and lipid phase coexistence, *Biophysical journal 95*, 691-698.
[20] Caaveiro, J. M. M., Echabe, I., Gutiérrez-Aguirre, I., Nieva, J. L., Arrondo, J. L., and González-Mañas, J. M. (2001) Differential interaction of equinatoxin II with model membranes in response to lipid composition, *Biophys J 80*, 1343-1353.
[21] Palacios-Ortega, J., García-Linares, S., Åstrand, M., Al Sazzad, M. A., Gavilanes, J. G., Martínez-del-Pozo, A., and Slotte, J. P. (2016) Regulation of sticholysin II-induced pore formation by lipid bilayer composition, phase state, and interfacial properties, *Langmuir 32*, 3476-3484.
[22] Pedrera, L., Fanani, M. L., Ros, U., Lanio, M. E., Maggio, B., and Álvarez, C. (2014) Sticholysin I-membrane interaction: an interplay between the presence of sphingomyelin and membrane fluidity, *Biochimica et biophysica acta 1838*, 1752-1759.
[23] Athanasiadis, A., Anderluh, G., Maček, P., and Turk, D. (2001) Crystal structure of the soluble form of equinatoxin II, a pore-forming toxin from the sea anemone *Actinia equina*, *Structure 9*, 341-346.
[24] Hinds, M. G., Zhang, W., Anderluh, G., Hansen, P. E., and Norton, R. S. (2002) Solution structure of the eukaryotic pore-forming cytolysin equinatoxin II: implications for pore formation, *Journal of molecular biology 315*, 1219-1229.
[25] Mechaly, A. E., Bellomio, A., Gil-Carton, D., Morante, K., Valle, M., González-Mañas, J. M., and Guerin, D. M. (2011) Structural insights into the oligomerization and architecture of eukaryotic membrane pore-forming toxins, *Structure 19*, 181-191.

[26] Tanaka, K., Caaveiro, J. M. M., Morante, K., González-Mañas, J. M., and Tsumoto, K. (2015) Structural basis for self-assembly of a cytolytic pore lined by protein and lipid, *Nat Commun 6*, 6337.
[27] Mancheño, J. M., Martín-Benito, J., Martínez-Ripoll, M., Gavilanes, J. G., and Hermoso, J. A. (2003) Crystal and electron microscopy structures of sticholysin II actinoporin reveal insights into the mechanism of membrane pore formation, *Structure 11*, 1319-1328.
[28] García-Linares, S., Castrillo, I., Bruix, M., Menéndez, M., Alegre-Cebollada, J., Martínez-del-Pozo, A., and Gavilanes, J. G. (2013) Three-dimensional structure of the actinoporin sticholysin I. Influence of long-distance effects on protein function, *Arch Biochem Biophys 532*, 39-45.
[29] Alegre-Cebollada, J., Martínez-del-Pozo, Á., Gavilanes, J. G., and Goormaghtigh, E. (2007a) Infrared spectroscopy study on the conformational changes leading to pore formation of the toxin sticholysin II, *Biophysical journal 93*, 3191-3201.
[30] Alegre-Cebollada, J., Rodríguez-Crespo, I., Gavilanes, J. G., and Martínez-del-Pozo, A. (2006) Detergent-resistant membranes are platforms for actinoporin pore-forming activity on intact cells, *FEBS J 273*, 863-871.
[31] García-Linares, S., Alm, I., Maula, T., Gavilanes, J. G., Slotte, J. P., and Martínez-del-Pozo, Á. (2015) The effect of cholesterol on the long-range network of interactions established among sea anemone sticholysin II residues at the water-membrane interface, *Marine drugs 13*, 1647-1665.
[32] Morante, K., Caaveiro, J. M. M., Tanaka, K., Gonzalez-Mañas, J. M., and Tsumoto, K. (2015) A pore-forming toxin requires a specific residue for its activity in membranes with particular physicochemical properties, *J Biol Chem 290*, 10850-10861.
[33] Wacklin, H. P., Bremec, B. B., Moulin, M., Rojko, N., Haertlein, M., Forsyth, T., Anderluh, G., and Norton, R. S. (2016) Neutron reflection study of the interaction of the eukaryotic pore-forming actinoporin equinatoxin II with lipid membranes reveals intermediate states in pore formation, *Biochimica et biophysica acta 1858*, 640-652.
[34] Ros, U., Rodríguez-Vera, W., Pedrera, L., Valiente, P. A., Cabezas, S., Lanio, M. E., García-Sáez, A. J., and Álvarez, C. (2015b) Differences in activity of actinoporins are related with the hydrophobicity of their N-terminus, *Biochimie 116*, 70-78.
[35] Terova, B., Slotte, J. P., and Nyholm, T. K. (2004) Miscibility of acyl-chain defined phosphatidylcholineswith N-palmitoyl sphingomyelin in bilayermembranes, *Biochim Biophys Acta 1667*, 182-189.
[36] Kuikka, M., Ramstedt, B., Ohvo-Rekilä, H., Tuuf, J., and Slotte, J. P. (2001) Membrane properties of D-erythro-N-acyl sphingomyelins and their corresponding dihydro species, *Biophys J 80*, 2327-2337.
[37] Cohen, R., Barenholz, Y., Gatt, S., and Dagan, A. (1984) Preparation and characterization of well defined D-erythro sphingomyelins, *Chem Phys Lipids 35*, 371-384.

[38] Anderluh, G., Pungerear, J., Strukelj, B., Maček, P., and Gubensk, F. (1996) Cloning, sequencing and expression of equinatoxin II, *Biochemical and Biophysical Research Communications 220*, 437-442.
[39] Bellomio, A., Morante, K., Barlič, A., Gutiérrez-Aguirre, I., Viguera, A. R., and González-Mañas, J. M. (2009) Purification, cloning and characterization of fragaceatoxin C, a novel actinoporin from the sea anemone *Actinia fragacea*, *Toxicon 54*, 869-880.
[40] Alegre-Cebollada, J., Clementi, G., Cunietti, M., Porres, C., Oñaderra, M., Gavilanes, J. G., and Martínez-del-Pozo, A. (2007) Silent mutations at the 5'-end of the cDNA of actinoporins from the sea anemone Stichodactyla helianthus allow their heterologous overproduction in *Escherichia coli*, *J Biotechnol 127*, 211-221.
[41] Laemli, U. K. (1970) Cleavage of structural proteins during the assembly of the head of bacteriophage T4, *Nature 227*, 680-685.
[42] García-Linares, S., Richmond, R., García-Mayoral, M. F., Bustamante, N., Bruix, M., Gavilanes, J. G., and Martínez-del-Pozo, A. (2014) The sea anemone actinoporin (Arg-Gly-Asp) conserved motif is involved in maintaining the competent oligomerization state of these pore-forming toxins, *FEBS J 281*, 1465-1478.
[43] Pardo-Cea, M. A., Castrillo, I., Alegre-Cebollada, J., Martínez-del-Pozo, Á., Gavilanes, J. G., and Bruix, M. (2011) Intrinsic local disorder and a network of charge-charge interactions are key to actinoporin membrane disruption and cytotoxicity, *The FEBS journal 278*, 2080-2089.
[44] Maula, T., Isaksson, Y. J., García-Linares, S., Niinivehmas, S., Pentikainen, O. T., Kurita, M., Yamaguchi, S., Yamamoto, T., Katsumura, S., Gavilanes, J. G., Martínez-del-Pozo, Á., and Slotte, J. P. (2013) 2NH and 3OH are crucial structural requirements in sphingomyelin for sticholysin II binding and pore formation in bilayer membranes, *Biochimica et biophysica acta 1828*, 1390-1395.
[45] Löfås, S., and Johnsson, B. (1990) A novel hydrogel matrix on gold surfaces in surface plasmon resonance sensors for fast and efficient covalent immobilization of ligands, *J. Chem. Soc. Chem. Commun. 21*, 1524–1526.
[46] Woody, R. W. (1978) Aromatic side-chain contributions to the far ultraviolet circular dichroism of peptides and proteins, *Biopolymers 17*, 1451-1467.
[47] Lacadena, J., Martínez-del-Pozo, A., Gasset, M., Patiño, B., Campos-Olivas, R., Vázquez, C., Martínez-Ruiz, A., Mancheño, J. M., Oñaderra, M., and Gavilanes, J. G. (1995) Characterization of the antifungal protein secreted by the mould Aspergillus giganteus, *Arch Biochem Biophys 324*, 273-281.
[48] Subburaj, Y., Ros, U., Hermann, E., Tong, R., and García-Sáez, A. J. (2015) Toxicity of an a-pore-forming toxin depends on the assembly mechanism on the target membrane as revealed by single-molecule imaging, *J Biol Chem 290*, 4856-4865.
[49] Rojko, N., Kristan, K. C., Viero, G., Zerovnik, E., Macek, P., Dalla Serra, M., and Anderluh, G. (2013) Membrane damage by an α-helical pore-forming protein,

equinatoxin II, proceeds through a succession of ordered steps, *J Biol Chem 288*, 23704-23715.
[50] Ros, U., and García-Sáez, A. J. (2015a) More than a pore: The interplay of pore-forming proteins and lipid membranes, *The Journal of membrane biology 248*, 545-561.
[51] Cosentino, K., Ros, U., and García-Saez, A. J. (2015) Assembling the puzzle: Oligomerization of α-pore forming proteins in membranes, *Biochim Biophys Acta*. *1858*, 457-466.
[52] Anderluh, G., Barlič, A., Podlesek, Z., Maček, P., Pungercar, J., Gubensek, F., Zecchini, M. L., Serra, M. D., and Menestrina, G. (1999) Cysteine-scanning mutagenesis of an eukaryotic pore-forming toxin from sea anemone: topology in lipid membranes, *Eur J Biochem 263*, 128-136.
[53] Malovrh, P., Barlič, A., Podlesek, Z., Maček, P., Menestrina, G., and Anderluh, G. (2000) Structure-function studies of tryptophan mutants of equinatoxin II, a sea anemone pore-forming protein., *Biochem J 346*, 223-232.
[54] Alegre-Cebollada, J., Lacadena, V., Oñaderra, M., Mancheño, J. M., Gavilanes, J. G., and Martínez-del-Pozo, A. (2004) Phenotypic selection and characterization of randomly produced non-haemolytic mutants of the toxic sea anemone protein sticholysin II, *FEBS Lett 575*, 14-18.
[55] Anderluh, G., Razpotnik, A., Podlesek, Z., Maček, P., Separovic, F., and Norton, R. S. (2005) Interaction of the eukaryotic pore-forming cytolysin equinatoxin II with model membranes: ^{19}F NMR studies, *Journal of molecular biology 347*, 27-39.
[56] Castrillo, I., Araujo, N. A., Alegre-Cebollada, J., Gavilanes, J. G., Martínez-del-Pozo, Á., and Bruix, M. (2010) Specific interactions of sticholysin I with model membranes: an NMR study, *Proteins 78*, 1959-1970.
[57] Malovrh, P., Viero, G., Serra, M. D., Podlesek, Z., Lakey, J. H., Macek, P., Menestrina, G., and Anderluh, G. (2003) A novel mechanism of pore formation: membrane penetration by the N-terminal amphipathic region of equinatoxin, *J Biol Chem 278*, 22678-22685.
[58] Hong, Q., Gutiérrez-Aguirre, I., Barlič, A., Malovrh, P., Kristan, K., Podlesek, Z., Maček, P., Turk, D., González-Mañas, J. M., Lakey, J. H., and Anderluh, G. (2002) Two-step membrane binding by equinatoxin II, a pore-forming toxin from the sea anemone, involves an exposed aromatic cluster and a flexible helix, *The Journal of biological chemistry 277*, 41916-41924.
[59] Rivera-de-Torre, E., García-Linares, E., Alegre-Cebollada, J., Lacadena, J., Gavilanes, J. G., and Martínez-del-Pozo, A. (2016) Synergistic action of actinoporin isoforms from the same sea anemone species assembled into functionally active heteropores, *J Biol Chem 291*, 14109-14119.
[60] Koradi, R., Billeter, M., and Wuthrich, K. (1996) MOLMOL: a program for display and analysis of macromolecular structures, *Journal of molecular graphics 14*, 51-55, 29-32.

SECTION E

NANODISCS: A LIPID PLATFORM FOR PORE RECONSTITUTION

ARTICLE X

Reconstitution of a soluble StnII transmembrane pore into nanodiscs

In preparation.

Reconstitución de un poro transmembrana soluble de StnII en nanodiscos

Los nanodiscos son bicapas lipídicas autoensambladas y revestidas por una proteína de andamiaje derivada de la apolipoproteína A-1. Se han convertido en una herramienta muy importante en los sistemas modelo de membrana para reconstituir proteínas de membrana. En este trabajo se han empleado nanodiscos para reconstituir en ausencia de detergentes el poro transmembrana de StnII en estado soluble. El análisis de las imágenes obtenidas por criomicroscopía electrónica del complejo StnII/nanodisco han permitido la reconstrucción de un modelo tridimensional de la estructura del poro con 10 Å de resolución. Este modelo indica que el poro estaría formado por las hélices α N-terminal de ocho subunidades de StnII, permaneciendo los sándwiches β en el exterior de la bicapa, en contacto con las cabezas polares de los fosfolípidos e interaccionando entre ellos.

Introduction

Nanodiscs are self-assembled phospholipid bilayers encased within an engineered derivative of apolipoprotein A-1 scaffold protein *(Ritchie et al. 2009)*. They have become an important and versatile tool among model membrane systems to functionally reconstitute membrane proteins. We have employed this approach to try to reconstitute StnII transmembrane pore in a soluble state.

Experimental procedures

Materials. DOPC, porcine brain SM and Chol were obtained from Avanti Polar Lipids (Alabaster, AL, USA). The plasmid for the membrane scaffold protein (MSP1E3D1) was obtained from Addgene (Cambridge, MA, USA) and the expression and purification of the protein has been described elsewhere *(Ritchie et al. 2009)*. The preparation of the cDNA coding for StnII, as well as the production and purification of the protein has been described before *(Alegre-Cebollada et al. 2007)*.

Homogeneity and spectroscopic characterization. Homogeneity of protein samples used were confirmed by 0.1% (w/v) SDS / 15% (w/v) PAGE performed with standard conditions *(Laemmli 1970)*. All protein batches used were also characterized in terms of recording their far-UV circular dichroism (CD) spectrum on a Jasco 715 spectropolarimeter (Easton, MD) at 50 $nm \cdot min^{-1}$ scanning speed. Optical path cell of 0.1 cm was employed. Proteins were dissolved in 15 mM MOPS buffer, pH 7.5, containing 100 mM NaCl (0.2-1.0 $mg \cdot mL^{-1}$ protein concentration). At least four spectra were averaged to obtain the final spectrum.

Reconstitution of nanodiscs. Reconstitution considerations have been described before *(Ritchie et al. 2009)*. Lipid stocks of DOPC:SM:Chol (80:20:10 molar ratio) are prepared in chloroform at 50 mM. The desired amount of chloroform lipid stock is dispensed into a disposable glass culture tube and dried using a gentle stream of nitrogen gas. To remove residual solvent, the tube is placed in a vacuum desiccator under high vacuum for 3 h. Buffer containing 200 mM sodium cholate pH 8.0 is added to the dried lipid film. Typically, cholate is added up to twice the desired concentration of lipid. The tube is vortexed, heated under hot tap water (about 60 ºC), and sonicated in an ultrasonic bath until the solution is completely clear, and no lipid remains on the walls of the tube. Scaffold protein is added to cholate-solubilized phospholipid to yield desired lipid:protein ratio, ensuring that the final cholate concentration in the reconstitution mixture is between 12 and 40 mM. The mixture is incubated at room temperature for at least 15 min. Following detergent removal by dialysis the assembly is analyzed and purified by size-exclusion chromatography using a calibrated Superdex 200 column in 20 mM Tris buffer pH 7.4 containing 100 mM NaCl.

Cryo-electron microscopy. StnII is then added to the reconstituted nanodiscs and the mixture is analyzed by cryo-electron microscopy. For cryo-electron microscopy, 5µl aliquots of a solution containing StnII reconstituted in nanodiscs was applied to glow-discharged holey carbon grids (Quantifoil R 2/2, covered with an additional thin carbon layer) for 1 min, blotted for 5 sec, and frozen rapidly in liquid ethane at -180°C using a Leica EM CPC cryo-plunger system. Images were recorded automatically under minimum dose conditions in a Talos Arctica microscope (FEI company) equipped with a Falcon II Direct Detector at x99300 nominal magnification and between 1.5 and 2.5 µm underfocus. The final sampling ratio was 1.41 Å per pixel.

Results

Spectroscopic characterization of the purified proteins

Far-UV circular dichroism characterization of MSP1E3D1 protein was consistent with a polypeptide showing helical content probably arranged in short segments (Figure 1), which was expected since this protein is an engineered derivative of apolipoprotein A-1. On the other hand, far-UV CD of StnII was indistinguishable from the spectra published before for this protein *(De-los-Ríos et al. 2000)* and indicated a predominant β-sheet conformation (Figure 1), in good agreement with its known three-dimensional structure *(Mancheño et al. 2003)*.

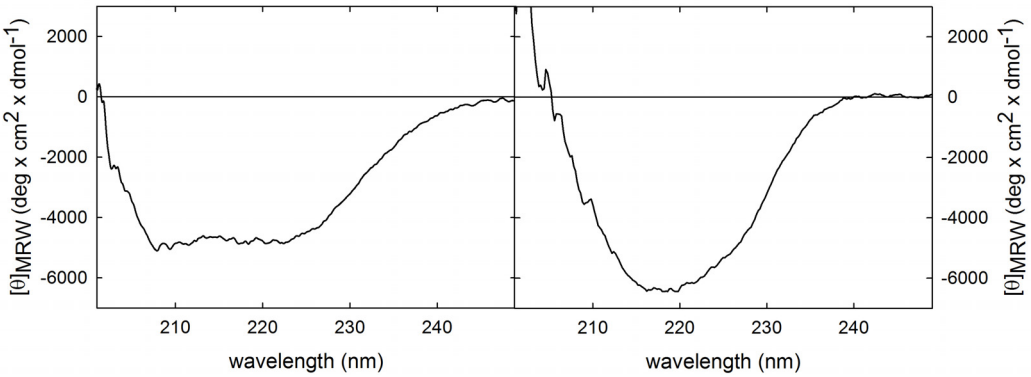

Figure 1. Far-UV circular dichroism spectra of MSP1E3D1 protein (*left panel*) and wild-type StnII (*right panel*).

Reconstitution of nanodiscs

After the dialysis of the lipid/MSP1E3D1 mixture to remove the detergent, far-UV CD characterization of the sample was performed (Figure 2). The spectrum obtained was indicative of an increase in the average length of the helical segments (see Figure 1) resulting from the MSP1E3D1 protein interaction with the mixture of phospholipids. An aliquot was taken to be analysed by 0.1% SDS (w/v) / 15% PAGE (w/v) (Figure 3).

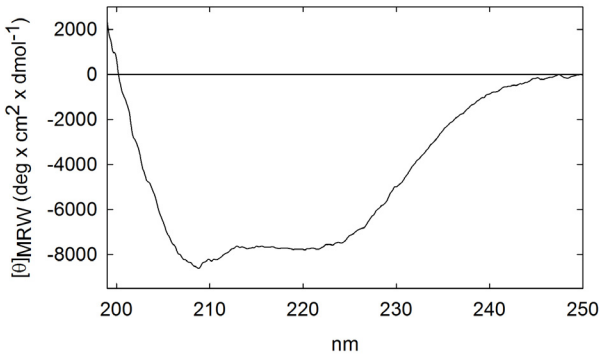

Figure 2. Far-UV circular dichroism spectra of reconstituted nanodiscs.

Once the detergent was removed, this sample was analyzed and purified by size-exclusion chromatography using a Superdex 200 column in 20 mM Tris buffer, pH 7.4 containing 100 mM NaCl. The chromatogram obtained displayed several peaks, one of them corresponding to the purified nanodiscs (Figure 4, arrow). The far-UV CD spectrum of the sample corresponding to this peak showed shape and high ellipticity negative values consistent with a high long α-helical conformation (Figure 5), in perfect agreement with the role that the MSP1E3D1 protein is supposed to fulfil when incorporated into nanodisc particles. An aliquot was also analysed by means of SDS-PAGE (Figure 3).

These purified and isolated nanodiscs were then mixed with a solution of homogenous StnII to a final StnII/MSP molar ratio of 10. This mixture was then analyzed by cryo-electron microscopy after taking another aliquot for SDS-PAGE analysis (Figure 3).

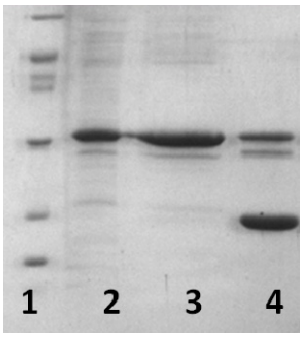

Figure 3. SDS/PAGE analysis of the different aliquots obtained during the reconstitution and purification of nanodiscs: Molecular mass markers (Bio-Rad) (lane 1), lipid/MSP mixture after dialysis (lane 2), the peak selected from the FPLC fractionation (lane 3), and purified nanodiscs with StnII (lane 4).

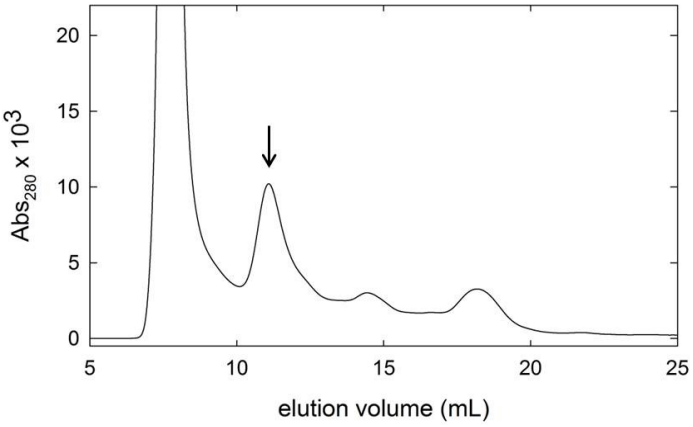

Figure 4. Elution profile of Superdex 200 column equilibrated with 20 mM Tris buffer, pH 7.4 containing 100 mM NaCl.

Image processing

Three-dimensional reconstruction of the assembled complex was performed using around 620.000 individual images of StnII-nanodiscs complexes which were selected automatically using SCIPION software *(De-la-Rosa-Trevín et al. 2016)* from the 516 plates recorded in the microscope. Images were two-dimensionally classified using the reference free algorithm implemented in RELION software *(Scheres 2012)*, showing that most of them (around 580.000) were end-on views, and the rest, side views (Figure 6). Side views were used to build an still preliminar three-dimensional structure of a StnII transmembrane pore at 10 Å resolution (Figure 7), using RELION software and starting from a initial model calculated using RANSAC software *(Vargas et al. 2014)* implemented in SCIPION.

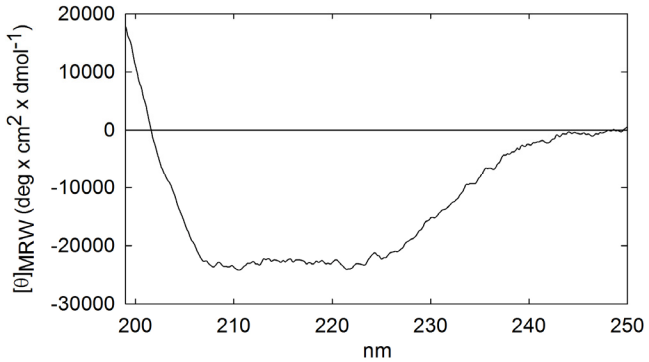

Figure 5. Far-UV circular dichroism spectra of purified nanodiscs.

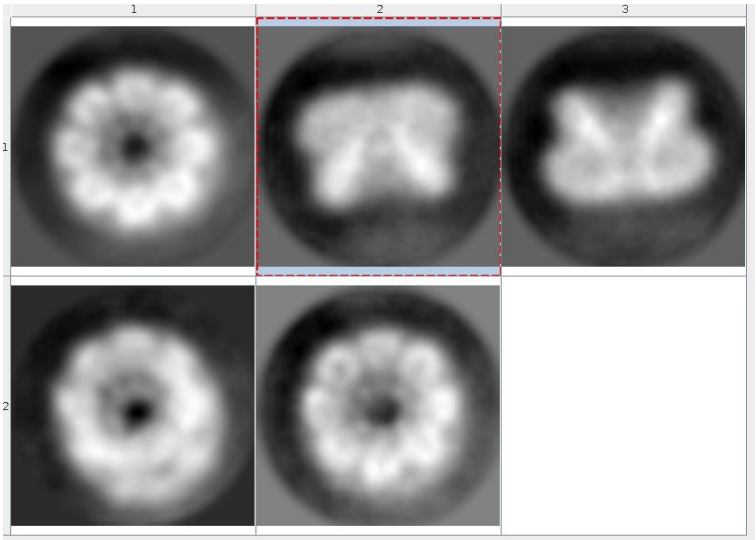

Figure 6. Some representative two dimensional class-averages obtained from images of frozen-hydrated samples of StnII containing nanodiscs, side and end-on views of the complex are clearly distinguishable.

The three-dimensional reconstruction obtained for StnII transmembrane pore structure seemed to indicate that the oligomer was made of eight StnII subunits (Figure 7A). The β-sandwich core of each molecule would remain outside the lipid bilayer in contact with the phospholipid head groups and in close interaction with each other, while the N-terminal α-helices would penetrate completely through the membrane (Figure 7B).

In Figure 7A we can observe the existence of gaps between the helices that most probably would be occupied by lipid molecules, as it has been previously seen with the crystalline pore-structure of FraC *(Tanaka et al. 2015)*. It is highly remarkable that, contrary to the mentioned FraC oligomeric structure, this StnII-pore reconstruction has been obtained in the absence of detergents and in the presence of Chol, a lipid which has been recently shown to be required for the correct formation of actinoporins' functional pores *(Alm et al. 2015, García-Linares et al. 2015, Wacklin et al. 2016)*. Work is in progress to yield a more refined structure at near-atomic resolution.

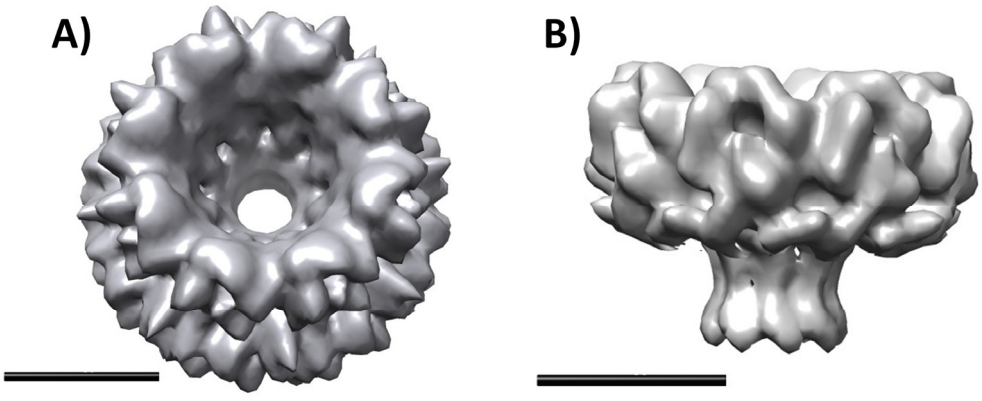

Figure 7. Three-dimensional reconstruction, using cryo-EM images, of a functional StnII pore assembled into nanodiscs containing SM and Chol. Scale bar is 50 Å. **A)** End-on view showing the octamer and the pore within the nanodisc. **B)** Side view of the StnII octamer excluding MSP1E3D1 and phospholipid molecules.

References

- Alegre-Cebollada, J., Clementi, G., Cunietti, M., Porres, C., Oñaderra, M., Gavilanes, J. G. and Martínez-del-Pozo, A. (2007). "Silent mutations at the 5'-end of the cDNA of actinoporins from the sea anemone *Stichodactyla helianthus* allow their heterologous overproduction in *Escherichia coli*". J Biotechnol 127(2): 211-221.

- Alm, I., García-Linares, S., Gavilanes, J. G., Martínez-del-Pozo, Á. and Slotte, J. P. (2015). "Cholesterol stimulates and ceramide inhibits sticholysin II-induced pore formation in complex bilayer membranes". Biochim Biophys Acta 1848(4): 925-931.

- De-la-Rosa-Trevín, J. M., Quintana, A., Del Cano, L., Zaldívar, A., Foche, I., Gutiérrez, J., Gómez-Blanco, J., Burguet-Castell, J., Cuenca-Alba, J., Abrishami, V., Vargas, J., Otón, J., Sharov, G., Vilas, J. L., Navas, J., Conesa, P., Kazemi, M., Marabini, R., Sorzano, C. O. and Carazo, J. M. (2016). "Scipion: A software framework toward integration, reproducibility and validation in 3D electron microscopy". J Struct Biol 195(1): 93-99.

- De-los-Ríos, V., Oñaderra, M., Martínez-Ruiz, A., Lacadena, J., Mancheño, J. M., Martínez-del-Pozo, Á. and Gavilanes, J. G. (2000). "Overproduction in *Escherichia coli* and purification of the hemolytic protein sticholysin II from the sea anemone *Stichodactyla helianthus*". Protein Expr Purif 18(1): 71-76.

- García-Linares, S., Alm, I., Maula, T., Gavilanes, J. G., Slotte, J. P. and Martínez-del-Pozo, Á. (2015). "The effect of cholesterol on the long-range network of interactions established among sea anemone sticholysin II residues at the water-membrane interface". Mar Drugs 13(4): 1647-1665.

- Laemmli, U. K. (1970). "Cleavage of structural proteins during the assembly of the head of bacteriophage T4". Nature 227(5259): 680-685.

- Mancheño, J. M., Martín-Benito, J., Martínez-Ripoll, M., Gavilanes, J. G. and Hermoso, J. A. (2003). "Crystal and electron microscopy structures of sticholysin II actinoporin reveal insights into the mechanism of membrane pore formation". Structure 11(11): 1319-1328.

- Ritchie, T. K., Grinkova, Y. V., Bayburt, T. H., Denisov, I. G., Zolnerciks, J. K., Atkins, W. M. and Sligar, S. G. (2009). "Chapter 11 - Reconstitution of membrane proteins in phospholipid bilayer nanodiscs". Methods Enzymol 464: 211-231.

- Scheres, S. H. (2012). "RELION: implementation of a Bayesian approach to cryo-EM structure determination". J Struct Biol 180(3): 519-530.

- Tanaka, K., Caaveiro, J. M. M., Morante, K., González-Mañas, J. M. and Tsumoto, K. (2015). "Structural basis for self-assembly of a cytolytic pore lined by protein and lipid". Nat Commun 6: 6337.

- Vargas, J., Álvarez-Cabrera, A. L., Marabini, R., Carazo, J. M. and Sorzano, C. O. (2014). "Efficient initial volume determination from electron microscopy images of single particles". Bioinformatics 30(20): 2891-2898.

- Wacklin, H. P., Bremec, B. B., Moulin, M., Rojko, N., Haertlein, M., Forsyth, T., Anderluh, G. and Norton, R. S. (2016). "Neutron reflection study of the interaction of the eukaryotic pore-forming actinoporin equinatoxin II with lipid membranes reveals intermediate states in pore formation". Biochim Biophys Acta 1858(4): 640-652.

DISCUSSION

NOTE: References to Figures appearing in the articles are indicated with Roman numerals referring to the article and the corresponding Arabic numerals which refer to the specific Figure within that article. Thus, for example, Fig. I-1 refers to Figure 1 of article numbered as I.

INTERACTION OF ACTINOPORINS WITH LIPID MEMBRANES: THE ROLE OF MEMBRANE COMPOSITION AND BIOPHYSICAL PROPERTIES

The contribution of lipids is relevant at each step of actinoporins' mechanism of action. Actinoporins bind to sphingomyelin containing membranes and show high binding specificity for this lipid. But membrane pore-forming ability is also affected by some other conditions, such as the presence of sterols, the coexistence of various phases or domains, compactness, fluidity, and the strength of the interfacial hydrogen bonding network.

Effects of sterols on StnII functionality

Chol has been widely proven to facilitate pore formation by actinoporins. This molecule is known to affect membrane fluidity by *(i)* increasing phospholipid acyl chain order when the membrane is in the physiological fluid state *(Feinstein et al. 1975, Jaikishan et al. 2010)*; *(ii)* facilitating lateral segregation of phospholipids, increasing the thermostability of both the gel and L_o domains *(Engberg et al. 2016)*; and *(iii)* interfering with intermolecular hydrogen bonding between SM molecules *(Róg et al. 2006)*. In addition, it also appears to affect the SM phosphocholine head group tilt and dynamics *(Niemela et al. 2004, Róg et al. 2006, Björkbom et al. 2010)*. As part of the work now presented, it has been shown that Chol increased pore formation kinetics by StnII (**Fig. II-1**; see previous note). Previous observations suggested that EqtII preferentially binds to molecules at the disordered/ordered domain interfaces *(Schön et al. 2008)* and oligomerizes to form pores at the liquid disordered phase *(Rojko et al. 2014)*. Moreover, ITC data suggested that StnII binding and pore formation led to an ordering effect in the bilayer, possibly reflecting in part ordering of the SM head group by StnII binding. However, PSM order increased only moderately in the presence of this lipid (**Fig. II-4**), so it is more likely that Chol altered more the SM head group tilt and dynamics (**Fig. 8A**) affecting StnII binding and/or oligomerization than producing a determinant effect on bilayer fluidity. Recent studies with StnI seem to indicate that this actinoporin binds and permeabilizes with higher efficiency sterol-containing membranes independently of their ability to form domains. Cholestenone, a non-inducing phase separation sterol but with a high propensity to induce non-lamellar phase, promoted toxin insertion, diffusion, and oligomerization leading to pore formation. *(Pedrera et al. 2015)*. On the other hand, Chol also affects membrane thickness, most probably facilitating N-terminal helix insertion (*Palacios-Ortega et al., in preparation*). In this regard, neutron reflection studies of the interaction of EqtII with lipid membranes have revealed that Chol is required for the penetration of the 30 residues long extended N-terminal α-helix across the lipid bilayer in order to make a functional pore *(Wacklin et al. 2016)*. Finally, Chol induces a negative curvature of the

membrane, which would facilitate the formation of the pore by reducing the stress caused by membrane distortion.

Addition of PCer to POPC:PSM bilayers inhibits StnII binding to the bilayer and consequent pore formation (**Figs. II-2** and **II-3**). It has not been yet fully elucidated the mechanism for how PCer addition to SM-domains hinder StnII-pore formation so markedly, but it is well known that PCer interacts with PSM leading to the formation of a highly ordered PCer and PSM rich domain *(Maula et al. 2012, Artetxe et al. 2013)*. This shift of PSM from a fluid to a gel like state would affect SM phosphocholine head group orientation and dynamics *(Metcalf et al. 2012)*, increase acyl chain order and lateral packing, and most likely also sequester SM diminishing its real availability for interaction with actinoporins. This observation would be in perfect agreement with the recent determination that StnII needs clusters of adjacent SMs in order to efficiently oligomerize and form pores *(Palacios-Ortega et al. 2016)*. These observations offer a new perspective on the StnII haemolysis inhibitory effect of sphingomyelinase addition to erythrocytes, which according to this new perspective could be caused more by ceramide generation than for factual depletion of SM.

Even though PCer has more affinity for PSM than Chol *(Alanko et al. 2005)*, this sterol was still able to partially reverse the inhibitory effect of PCer on StnII pore formation (**Fig. II-5**). Given the Chol concentration employed, it was more likely that Chol affected PSM properties (in the POPC-rich phase or at the gel phase boundary) than the over-all gel nature of the PSM-PCer domains. In summary, StnII-membrane interaction, leading to pore formation, may critically respond to changes in PSM head group properties, which can be efficiently modulated by Chol and/or ceramide. It cannot be discarded however that actinoporins' pore-formation is also affected by lipid-domain boundaries as initially had been proposed, a proposal which is perfectly compatible with the other proposals discussed in this Thesis *(Schön et al. 2008, Rojko et al. 2014)*.

Implication of the interfacial hydrogen bonding network of SM molecules

2NH and 3OH functional groups of SM seem to be important for giving specificity and high affinity for StnII-membrane interaction and for pore formation. Methylation of these groups has been shown to reduce SM gel-phase stability *(Björkbom et al. 2011)*, suggesting that hydrogen bonding involving the 2NH are important for SM-SM interlipid interactions (**Fig. 8B**). Also, sterol affinity for bilayers containing the methylated SM analogues was markedly lowered. Besides being of great importance for the biophysical membrane properties of SM, 2NH and 3OH are also implicated in specific interactions with actinoporins' residues. Molecular docking of SM to the POC binding site of StnII suggests that the phosphate oxygens interact with Tyr111 and Tyr136, while the 2NH and 3OH engage in electrostatic interactions with Tyr135. Additionally, the phosphate moiety could be further stabilized by the

cationic side chain of Arg51 (**Fig. III-4**). The lack of apparent membrane binding of 2NH and 3OH methylated SM analogues (**Figs. III-2** and **III-3**) and the failure to cause significant membrane permeabilization (**Fig. III-1**), suggested that these analogues failed to support stable membrane association of StnII. This would confirm that high affinity interaction between StnII and SM is required for stable membrane association of StnII.

The above paragraph discusses mostly the hydrogen bonding interactions established between specific protein residues side-chains and SM chemical groups. However, the importance of hydrogen bonding is also relevant in relation to the more general biophysical state of the membrane as it has been also demonstrated using dihydro-SM containing vesicles. As it has been previously shown, SM and dh-SM have different intermolecular hydrogen bonding properties and the obtained results suggest that this interaction is stronger in dihydro-SM bilayers *(Ferguson-Yankey et al. 2000, Talbott et al. 2000, Nyholm et al. 2003)*. Consequently, pore formation by StnI and StnII was markedly different in SM and dihydro-SM bilayers. Calcein leakage was highly attenuated when using dh-SM bilayers (**Fig. IV-1**). SPR and ζ-potential measurements also indicated that total binding of StnII was much weaker in supported bilayers or LUVs made of dh-OSM than OSM (**Figs. IV-2** and **IV-3**). Experiments with monolayers indicated that StnII penetration in dh-OSM was less efficient at high surface pressures compared to OSM (**Fig. IV-5**). Data obtained wit benzyl alcohol (BA), a well-known hydrogen-bonding small molecule with an affinity for bilayer interfaces *(Somerharju 2002)*, supported the implication of intermolecular hydrogen bonding in regulating membrane association of StnII. BA participates in hydrogen bonding similarly as Chol does *(Palacios-Ortega et al. 2016)* and induced strong activation of StnII-dependent calcein release from dihydro-OSM bilayers, while OSM bilayers were not affected, probably because pore formation was already maximal (**Fig. IV-6**).

THE ROLE OF PARTICULAR RESIDUES OF ACTINOPORINS

Actinoporins constitute a family of proteins with high degree of sequence identities but different haemolytic activities, suggesting that minor differences in conformational arrangements result in major functional changes. In order to analyze the influence of particular residues on the conformation and activity of these proteins, many mutant variants have been studied. All these mutations map to the previously mentioned functionally relevant regions because they are probably involved in conformational arrangements and specific interactions associated with pore formation. In the following lines the role of most relevant residues studied along this work are discussed in terms of their specific participation in binding to the membranes and pore-formation and also in relation to their strategic location regarding the aforementioned key functional protein regions. This distinction is just a resource

attempting to make this discussion more comprehensible because obviously proteins function as a whole and some of the actinoporins' specific residues can be classified within more than one of these regions *(García-Ortega et al. 2011)*.

Residue	Location / Function
StnII **A10**	30 first residues
StnI **G26**	30 first residues
StnI **V28**	30 first residues
StnII **R29**	30 first residues
StnII **W43**	Stabilization of β-sandwich
StnII **R51**	POC binding site
StnI **S53**	POC binding site
StnI **D57**	Detachment of α-helix
StnI **E62**	Detachment of α-helix
StnII **F106**	Aromatic cluster
StnII **W110**	Aromatic cluster
StnII **Y111**	POC binding site - Aromatic cluster
StnII **W114**	Aromatic cluster
StnII **W115**	Stabilization of β-sandwich
StnII **Y135**	POC binding site - Aromatic cluster
StnII **Y136**	POC binding site - Aromatic cluster
StnII **G142**	Oligomerization state
StnII **W146**	Protomer-protomer interactions

Table 1. Recompilation of all the mutants studied and discussed along this section and their location within the protein structure or their functional role.

Stn mutants affecting the 30 first residues stretch

Mutants affecting the amino terminal sequence stretch have confirmed that this region is crucial for pore formation but does not seem to be involved in the arrangements needed for membrane recognition. Substitution of Ala10 for Pro in StnII, for example, yielded a protein with identical membrane binding behaviour but with a highly decreased haemolysis and calcein leakage activities *(García-Linares et al. 2015)*. This could be explained by the conformational stiffness introduced by the Pro residue, which would hamper the extension of the α-helix *(Alegre-Cebollada et al. 2004, Kristan et al. 2004, Alegre-Cebollada et al. 2008)*. Moreover, membrane binding capability of A10P was identical to wild-type StnII using lipid vesicles with or without Chol (**Figs. VI-2** and **VI-3**), but haemolysis and calcein leakage, two phenomena which largely reflect the pore-forming ability of these proteins, were clearly reduced in the absence of this sterol (**Table VI-1** and **Fig. VI-4**). Interestingly, the presence of Chol allowed leakage of aqueous contents even though the helix could not be completely extended, favouring the hypothesis of the existence of a toroidal pore *(Rojko et al. 2014, Tanaka et al. 2015)* (**Fig. 9**). As was also observed with wild-type StnII, the A10P mutant did also show much higher affinity for Chol-containing membranes (**Table VI-2**). Overall, these observations reinforced the idea that pore formation, but not membrane recognition, was the step impaired in this mutant.

Another mutant studied was StnII Arg29 (**Figs. 6** and **VI-1**), corresponding to substitution of a conserved residue in most of the known actinoporins which has been proved to be involved in both membrane recognition and pore formation *(Alegre-Cebollada et al. 2008)*. This Arg29 and Phe106 establish a π-cation interaction which could not occur if the positively charged amino acid at position 29 was replaced by Gln. Thus, mutant R29Q showed an increased conformational freedom that led to distortion of the electrostatic potential along the interfacial binding site (**Fig. 12**). Again, Chol proved to be also crucial for correct binding and pore formation (**Figs. VI-2**, **VI-3** and **VI-4**).

In the case of StnI, five mutant variants obtained by random mutagenesis showed reduced haemolytic activity (**Fig. 3-V**). The residues mutated in these five examples were Gly26, Ser53, and Asp57, which are conserved in all known actinoporins; Val28, which is maintained in most of them; and Glu62, the most variable one (**Fig. I-1**). Two of these amino acids (Gly26 and Val28) are located within the 30 first residues stretch. Obviously, Asp57 and Glu62 are not therein located but they are included in this section of the Discussion because their substitution affects to the required N-terminal α-helix detachment. The fifth residue, Ser53, will be however discussed later, in a different section, since it belongs to the POC-binding site. All these five amino acids are located in regions with no ordered secondary structure (**Fig. V-2**, *right panel*) in good agreement with the assumption that changes within the β-barrel sandwich core or the two α-helices would involve such a high level of structural

disorganization that would impair its survival to the heat-shock step used during their phenotypic selection. That is to say, mutations on different regions than the ones found would render mutant species too unstable to be detected in the conditions employed. Nevertheless, NMR relaxation data indicated that these residues at positions 26, 53, 57 and 62 still belong to the rigid core of the protein (**Fig. V-2**, *left panel*).

StnI mutant variants G26D, V28E, D57A, and E62G did not show up at the membrane binding interface, which could explain the only very small changes observed in their membrane binding behaviour, very similar to that one displayed by wild-type StnI (**Fig. V-4**), but did not explain why they showed a reduced haemolytic activity (**Fig. V-3**). According to the more generally accepted mechanism for pore formation this could be interpreted as the mutations introduced affecting detachment of the α_1-helix. Careful inspection of the wild-type StnI structure reveals that Asp57 negatively charged side-chain is very close to Glu2 and Glu62 (**Fig. 13A**), most probably creating an electrostatic repulsion effect that should be important for the conformational change involving helix detachment. Substitution of Asp by Ala in position 57 would eliminate the load of negative charge around that region, favouring the interactions of the helix with the hinge loop or/and with the β-sandwich residues, most probably impairing helix detachment and thus decreasing the haemolytic activity of this mutant. This argument can be also used in identical terms to explain the behaviour of E62G mutant.

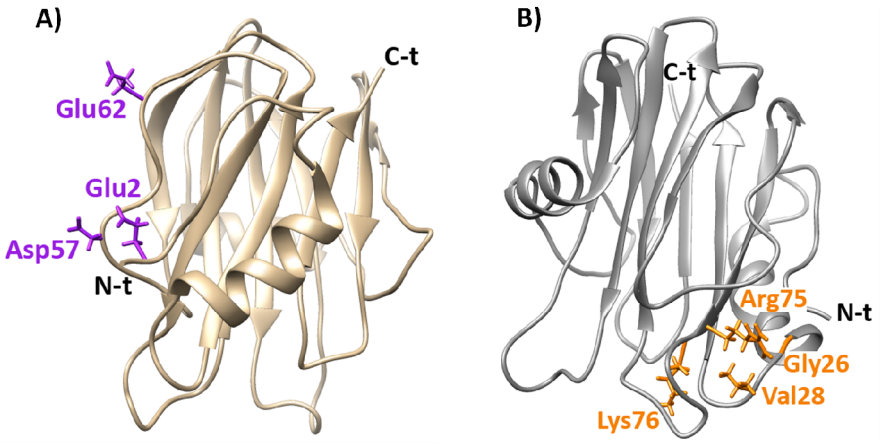

Figure 13. A) Diagram showing residues Glu2, Asp57 and Glu62 within the three-dimensional structure of StnI. Substitution of Asp by Ala would favor the interaction of the helix to the protein core. **B)** Diagram showing residues Gly26, Val28, Arg75 and Lys76 within the three-dimensional structure of StnI. Substitution of Gly by Asp or Val by Glu would hinder detachment of the helix. Both figures were made using UCSF Chimera program *(Pettersen et al. 2004)*.

Electrostatic interactions could also explain the reduced haemolytic activity of the G26D and V28E mutants. Side chains of Arg75 and Lys76 are really close to residues at positions 26 and 28 (**Fig. 13B**), therefore the substitution of Gly or Val for a negatively charged residue could result in an electrostatic interaction with Arg and/or

Lys side-chains. These new interactions could again hinder the detachment of the N-terminal helix required for pore formation. In summary, the lower haemolytic effect of four of the five mutations selected, altogether with their strategic situation in the vicinity of the N-terminal α-helix, could be interpreted as the result of impediments for its detachment and final pore-formation while leaving their membrane binding ability unaffected.

Overall, the results from this section can be summarized confirming that the N-terminal region of actinoporins is not directly involved in membrane recognition but it is required to make a functional pore.

Stn mutants affecting the POC-binding site

Regarding this structural site, we have prepared four mutants of StnII: R51Q, Y111N, Y135F and Y136F. According to the StnII-POC crystalline structure *(Mancheño et al. 2003)*, all of them establish interactions with the POC moiety and/or the 2NH and 3OH groups of SM *(Alegre-Cebollada et al. 2008, Pardo-Cea et al. 2010, Mechaly et al. 2011, Maula et al. 2013)*. The Tyr residues are simultaneously considered as part of the aromatic amino acids cluster. These four mutants showed reduced haemolytic activity (**Table VI-1**) and were incapable to interact with PSM-containing vesicles in the absence of Chol (**Fig. VI-3** and **Table VI-2**). Tyr136 was shown to interact specifically with the phosphate oxygens of the POC moiety *(Maula et al. 2013)* which would be essential for maintaining the SM molecule at the right position (**Fig. III-4**). But in the presence of Chol this interaction does not seem to be so crucial since the Y136F mutant is able to establish functional interactions, both in membrane binding (**Fig. VI-2** and **Table VI-2**) and calcein release activity (**Fig. VI-4A**). This observation might be related to the ability of Chol to reorient the SM head group (**Fig. 8A**). Employment of SM analogues revealed how Tyr135 interacts with the 2NH and 3OH groups of this lipid *(Maula et al. 2013)*, but both interactions would be absent in the Y135F mutant. This would explain the marked decrease in membrane binding affinity, calcein leakage and haemolytic activity even in the presence of Chol (**Figs. VI-2**, **VI-4** and **Table VI-1**). If Chol was not present in the vesicles, the mutant was completely unable to bind to the membrane, so we can suggest that Tyr135-SM interactions are also enhanced by this molecule.

R51Q and Y111N mutants showed diminished haemolytic activity (**Table VI-1**), low affinity for vesicles, with and without Chol (**Figs. VI-2**, **VI-3** and **Table VI-2**), and were inactive in calcein release experiments (**Fig. VI-4**). The POC moiety has been suggested to be stabilized by the cationic side chain of Arg51 *(Maula et al. 2013)* and the present results suggest that this interaction is strictly required for membrane recognition independently of the presence of Chol. Tyr111 is involved in the conformational change needed to bind to the POC and form the pore *(Mancheño et al. 2003)*. Y111N would fail to produce a functional pore even in the presence of Chol

because this mutant just does not bind to the membrane *(Alegre-Cebollada et al. 2008)*. Indeed, Tyr 111 is a key residue of cluster of aromatic residues (**Fig. 5**) and therefore its role in actinoporins' function is further discussed in the next section.

On the other hand, among the StnI mutant variants obtained by random mutagenesis that were described in a previous section, S53T was the only one that showed a reduced membrane binding capacity compared to the wild-type protein (**Fig. V-4**). However, although it is less haemolytic than StnI, it shows the highest haemolytic activity among all the other StnI mutants described above (**Fig. V-3**). The equivalent Ser52 in StnII is part of the phosphocholine binding site, which could explain why minimal changes at this position produce enough distortion in this region as to alter the membrane binding ability of the protein. Why this marked decrease in binding is not directly related to a much lower haemolytic activity seems to be a quite contradictory observation. But it could be that once the S53T mutant is bound to the membrane, it forms the pore more efficiently. Ser to Thr substitution could involve long-range conformational changes of residues placed around the hinge region that would facilitate N-terminal α-helix detachment.

In summary, single modifications of actinoporins' residues located at positions not involved in the interactions needed for membrane binding, or insertion, may also largely affect the proper functionality of these proteins by just altering the strictly required conformational freedom and/or electrostatic distribution of well-defined protein regions. As with the wild-type protein, Chol significantly facilitates interactions with the membrane of most mutants studied, most probably modifying the availability of SM molecules and the orientation of their head groups.

StnII mutants affecting the aromatic cluster

Four StnII mutants affecting residues from the aromatic cluster have been studied: F106L, Y111N, Y135F and Y136F. As it was mentioned before, Phe106 establishes an interaction with Arg29 side-chain in order to initiate the conformational changes needed for protein binding to the membrane *(Alegre-Cebollada et al. 2004, Pardo-Cea et al. 2011)*. This could be the reason why, in the absence of Chol, F106L is completely unable to bind to the lipid vesicles (**Fig. VI-3**) or induce calcein leakage (**Fig. VI-4B**) and, consequently, its haemolytic activity is quite impaired (**Table VI-1**). Even when Chol is present, membrane affinity is reduced compared to the wild-type StnII (**Table VI-2**).

The loop containing Tyr111 is completely disordered and shows high conformational flexibility, as it has been seen both in EqtII and StnII *(Athanasiadis et al. 2001, Hinds et al. 2002, Mancheño et al. 2003)*. In the soluble state, Tyr111 is exposed *(Castrillo et al. 2010)*, but in the StnII:POC complex appears pointing towards the POC moiety *(Mancheño et al. 2003)* a change that involves a dramatic change in the orientation of its aromatic side-chain (**Fig. 14**) . This residue is certainly crucial for

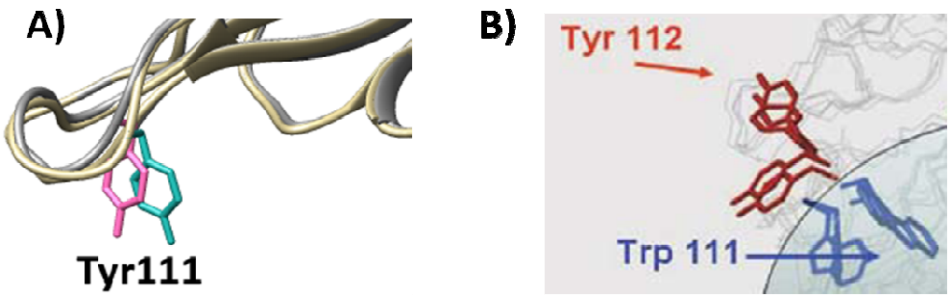

Figure 14. A) Stereo view of the superposition of free StnII (gray) and the StnII:POC complex (tan), showing Tyr111 residue rearrangement (magenta for free StnII and blue for StnII:POC complex) in the POC binding site. The image was made using UCSF Chimera program *(Pettersen et al. 2004)*. **B)** Potential orientations of the aromatic side chains of Trp111 and Tyr112 (Trp110 and Tyr111 in StnII) in the interaction of StnI with DPC micelles *(Castrillo et al. 2010)*.

membrane binding since its substitution by Asn completely blocked its membrane binding ability (**Fig. VI-3**), even in the presence of Chol (**Table VI-2**), and consequently its calcein release (**Fig. VI-4**) and haemolysis activities (**Table VI-1**).

Tyr135 and Tyr136, which role has been discussed in part in the above paragraphs, display a high motional flexibility, as it has been deduced by NMR analysis of StnI equivalent groups in the presence of DPC micelles *(Castrillo et al. 2010)*. In the absence of Chol, Y135F and Y136F are no longer capable of maintain the specific contacts (**Fig. VI-3**) but, since the mutations retain the hydrophobic character of the residues, these proteins can still interact in some degree with Chol-containing vesicles, especially the Y136F variant (**Fig. VI-2**).

The main conclusion of this set of results would be that key specific interactions between side-chains of particular actinoporin residues and definite SM chemical groups are strictly required for maintaining an efficient pore-forming functionality. However, especially in the presence of Chol, some of these interactions become dispensable as far as the hydrophobicity of these side-chains is essentially retained.

StnII mutant affecting the correct aggregation competent state for pore formation

As it has been stated in the lines above, actinoporins' N-terminal α-helix is involved in pore formation while specific regions at the β-sandwich are rather responsible for membrane recognition and binding. However, large regions of the protein still remain unexplored. Little is known about protein-protein interactions involving the oligomerization needed for pore formation, for example. Recent data from crystal structures of FraC at different stages of the lytic mechanism show that in the monomeric form of FraC, Phe16 is inserted in a hydrophobic cavity of the β-core. During the initial dimerization, the Val60 of a protein unit displaces the Phe16 of the other unit from its original position *(Tanaka et al. 2015)*, a process which seems to be critical for pore formation in cholesterol-rich membranes *(Morante et al. 2015b)*. But apart from this specific determination, many other key protein-protein interactions remain to be discovered.

Within this idea, one of the most intriguing observations regarding actinoporins is the presence of a rather conserved integrin-like binding RGD (Arg141-Gly142-Asp143) motif within their sequence. Therefore, it has been proposed long time ago that it mediates actinoporins binding to this kind of receptors on the cell surface explaining, for example, why these proteins are much more efficient against red blood cells than against naked lipid model vesicles *(Anderluh et al. 2002, Anderluh et al. 2003, Monastyrnaya et al. 2010)*. However, our results suggested that the RGD sequence region would be important for maintaining the correct oligomerization state of the protein and the convenient geometric arrangement of the protein monomers in order to form a functional pore rather than interacting with a non-yet identified integrin-like protein receptor *(García-Linares et al. 2014)*. Thus, it now seems that this RGD motif is important to maintain the solubility of the monomers and small oligomers since minimal changes of this sequence result in protein aggregates which very easily precipitate.

Within this idea, binding of a RAD mutant version of StnII to model lipid vesicles was indistinguishable from the wild-type protein behaviour (**Fig. VII-5**), confirming that this sequence is not directly involved in membrane recognition or binding. However, and in spite of this observation, this RAD mutant was much less haemolytic (**Fig. VII-4**). An observation that could not be explained in terms of loss of interaction between integrin-like receptors and the protein since not such receptors seem to exist on erythrocytes membranes. Consequently, we interpret our results as how the presence of Ala methyl group in the RAD mutant would distort not only a probably well-established ionic interaction between Arg141 and Asp143, but also the stabilization of Gly142 by the hydroxyl group of Ser163 (**Fig. 15**). Mutation to Ala would then lead to a more aggregation-prone protein.

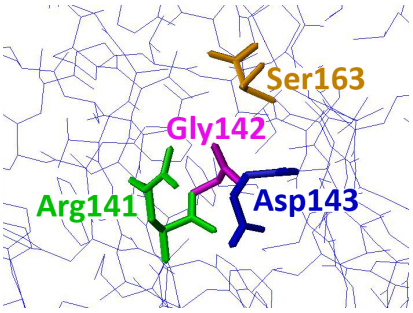

Figure 15. Diagram indicating the relative position of Arg141 (green), Gly142 (magenta), Asp143 (blue) and Ser163 (orange) within the three-dimensional structure of StnII (in lines). The image was generates with MOLMOL program *(Koradi et al. 1996)*.

Moreover, NMR characterization of this RAD mutant allowed the construction of a map revealing the residues involved in the interactions conducing to the tetramer species (**Figs. VII-2** and **VII-7**). This map was used to dock *in silico* the monomers into tetramers, obtaining a collection of different structures (**Fig. VII-8**). All of them displayed the N-terminal α-helix in an exposed position but unable to participate in pore formation. The geometry of the tetramers revealed that the elongation of this α-helix towards the membrane recognition face in one monomer was sterically blocked by the adjacent molecule and also suggested that these helices were too far apart to associate into a functional pore.

It was then concluded that RGD motif seemed to contribute to maintaining the proteins in the correct competent state of aggregation, both in their water-soluble state and in their membrane-bound configuration.

StnII mutants affecting Trp residues

Most of the known actinoporins contain five Trp residues which are generally proposed to play a key role in membrane binding and recognition *(Malovrh et al. 2000, Hong et al. 2002, Alegre-Cebollada et al. 2004, Alegre-Cebollada et al. 2007b, Alegre-Cebollada et al. 2008, Pardo-Cea et al. 2010, Pardo-Cea et al. 2011)* (**Fig. VIII-2**, *lower panel*). Following StnII numbering, and according to their location and arrangement within the soluble three-dimensional structure of this protein (**Fig. VIII-1**), Trp110 and Trp114 would belong to the cluster of aromatic residues *(Mancheño et al. 2003)* while Trp43 and Trp115 would play a major in the stabilization of the β-sandwich. In fact, their replacement yielded mutants which displayed the lowest T_m values. Finally, Trp146 would be implicated in specific protomer-protomer interactions, together with Val57, as has been proposed from the FraC octameric crystalline structure *(Tanaka et al. 2015, Morante et al. 2015b)*. Consequently, the replacement of Trp146 by Phe had a deep impact on protein solubility (**Table VIII-1**), in good agreement with this proposed role for this residue in stabilizing the correct protein-protein interactions needed to oligomerize and form the pore.

All the mutants studied had Trp residues replaced by Phe to different degrees of extent (**Table VIII-1**) but displayed far-UV CD spectra indistinguishable from wild-type StnII (**Fig. VIII-3**), meaning that they conserved the overall conformational fold. Near-UV CD spectra were much different from each other, as expected from the changed aromatic rings (**Fig. VIII-4**). The elimination of indolyl side chains resulted indeed in a decrease of Trp fluorescence emission and a simultaneous increase of Tyr fluorescence, most probably due to the disappearance of Tyr to Trp non-radiative energy transfer phenomena (**Fig. VIII-5**). For example, the elimination of Trp110 implicated an important increase in the emission of the close Tyr111 residue (**Figs. 5** and **VIII-11A**). In summary, all these mutants showed the expected spectroscopical properties given their protein location and the nature of the substitutions made.

Haemolysis activity of all these mutants was very similar to that one displayed by wild-type StnII (**Fig. VIII-6**), which suggested the hydrophobic effect as a major driving force in perforating the erythrocyte membranes. The only mutant that showed a significantly diminished haemolysis activity was WquadrupleF (**Fig. VIII-6**), in good agreement with previous results for EqtII *(Malovrh et al. 2000)*.

These mutants were also assayed against model lipid vesicles. When using DOPC:SM:Chol (1:1:1) LUVs the results where comparable with haemolysis experiments. This was not completely unexpected since the relative Chol content was very similar to that one found in sheep erythrocytes. All mutants displayed similar

binding affinities, as shown by ITC (**Fig. VIII-7**, *upper row*) and SPR measurements (**Fig. VIII-8**). When POPC:PSM (80:20) vesicles (no Chol present) were used, all proteins, including the wild-type, displayed a reduction in membrane affinity of around two fold (**Table VIII-4**). In the light of the highly hydrophobic nature of both Phe and Trp side-chains, these results in the absence of Chol were interpreted as the need of specific interactions established by Trp residues for membrane binding. Specific interactions beyond the hydrophobic effect that cannot be fulfilled by the benzyl ring of Phe. Those ones lacking Trp114 did not even give a measurable signal in ITC experiments. This was in agreement with Trp114 being part of the aromatic cluster (**Fig. 5**) and also concur with recent results that propose an interaction between the choline head group of SM and the Trp114 equivalent residue for EqtII *(Weber et al. 2015)*. On the other hand, even though Trp110 belongs to the aromatic cluster (**Fig. 5**), mutants affecting this residue showed a membrane affinity similar to that of the wild-type protein. This result was explained assuming that the interaction of Trp110 with the membrane is mainly hydrophobically driven and therefore, the substitution for another hydrophobic residue has not a significant effect. In fact, Trp 110 is not conserved in all known actinoporins but there is always a bulky hydrophobic residue at that position. This hypothesis is consistent with site-directed mutagenesis studies revealing that the equivalent residue (Trp112) of EqtII is needed for membrane recognition and stabilizes the membrane-bound protein *(Bakrač et al. 2008)*. Experiments carried out with FraC *(Tanaka et al. 2015)* and StnI *(Castrillo et al. 2010, López-Castilla et al. 2014)* also suggest that the equivalent residues of Trp110 and Trp114 appear in the membrane binding region and seem to interact directly with lipids.

Calcein release experiments in the absence of Chol showed that all protein Trp mutants studied displayed low pore-forming ability, as did wild-type StnII (**Figs. VIII-9** and **VIII-10**). Mutants lacking Trp114 were not even able to give a measurable signal. This set of results paralleled quite well with the aforementioned SPR and ITC assays. When these calcein leakage assays were performed with Chol-containing vesicles the observed rates were significantly increased and the percentages of final dye release were indistinguishable when mutants and wild-type StnII were compared (**Figs. VIII-9** and **VIII-10**). This means that replacing StnII Trp residues has more impact on its membrane binding ability than on the subsequent steps leading to the formation of a functional pore. Thus, it was proposed that Trp residues in actinoporins play a major role in membrane recognition and binding but have only a minor influence on the diffusion and oligomerization, with the only exception of Trp146, which is involved in protomer-protomer interactions as it was previously stated.

To go further into the specific interactions established between actinoporins and SM molecules two analogues of this lipid were included in the experiments: CPE-Me_2 and CH_2-PSM (**Fig. 16**). When the CPE-Me_2 analogue was assayed in the absence of Chol, none of the proteins (wild-type StnII included) were able to produce any measurable signal in SPR nor in calcein leakage assays. This impairment was circumvented by the presence of a large proportion of Chol within the membrane, except in the case of WquadrupleF mutant (**Figs. VIII-8** and **VIII-10**). When using CH_2-PSM analogue, mutants lacking Trp114 could not be rescued either (**Figs. VIII-8** and **VIII-10**). This could be explained because this SM analogue shows diminished hydrogen bonding ability (because of the substitution of an oxygen by a -CH_2- group) and it has been proven that the interfacial hydrogen-bonding properties of SM are a key factor in membrane recognition by actinoporins *(Maula et al. 2013)*. The different geometrical arrangements involved in a -O- or -CH_2- (tetrahedral) bond configurations may also lead to a different and less favourable SM head orientation at the membrane surface. The results confirm the extreme specificity of the interactions required for StnII to recognize SM-containing vesicles.

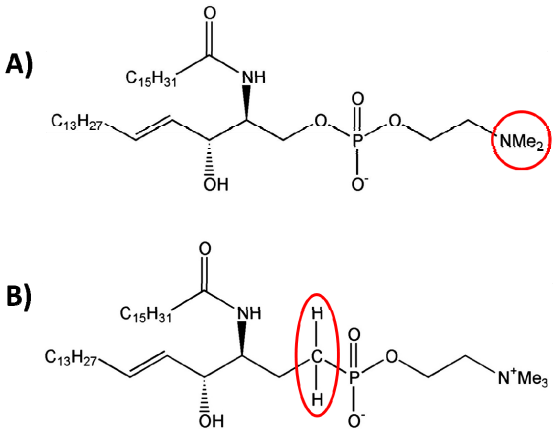

Figure 16. Schematic representation of the molecular structure of the analogues **A)** CPE-NMe_2 and **B)** CH_2-PSM. The structural particularity of each analogue is highlighted in red.

FROM PARTICULAR TO GENERAL: ACTINOPORINS AS A FAMILY

Only four of the many known actinoporins (**Fig. IX-1**) produced by different sea anemones, have been characterize in detail, including the resolution of their monomeric soluble three-dimensional structures: EqtII from *Actinia equina (Athanasiadis et al. 2001, Hinds et al. 2002)*, FraC from *Actinia fragacea (Mechaly et al. 2011, Tanaka et al. 2015)*, and StnI and StnII from *Stichodactyla helianthus (Mancheño et al. 2003, García-Linares et al. 2013)*. As it has been said previously, all of them show quite high sequence identity and therefore, almost identical conformation (**Fig. 2**). Nevertheless, they display different haemolysis activities and differential sensitivity towards the distinct composition and/or biophysical state of their target membranes. So far, however, functional and biophysical properties of these proteins had not been studied in detail under identical experimental conditions.

All four actinoporins showed almost identical three-dimensional soluble structures (**Fig. IX-2**), but near-UV circular dichroism suggested that, even though Trp

residues are conserved along their sequences, occupying equivalent positions, they must be in rather different microenvironment when comparing the pair EqtII/FraC to StnI/StnII (**Fig. IX-3**, *right panel*).

Haemolysis activities of EqtII, FraC and StnI were almost identical, while StnII proved to be much more efficient (**Fig. IX-5**). This observation correlates with the results obtained using synthetic peptides resembling actinoporins' first 30 amino acids *(Ros et al. 2015b)*. This behaviour was correlated with the hydrophobicity of the corresponding 1-10 N-terminal segment, being the N-terminus peptide analogue of StnII the most buried one into the hydrophobic core of the membrane among the rest of the actinoporins. Thus, the results obtained using the complete native proteins can be also explained in terms of the different hydrophobic character of this protein segment.

The behaviour of the four actinoporins both in membrane binding affinity and calcein leakage experiments yielded similar results when using DOPC:SM (4:1) vesicles (**Figs. IX-6**, **IX-7** and **IX-8**). On the other hand, all four actinoporins showed an enhanced and very similar pore-forming activity when using DOPC:SM:Chol (1:1:1) vesicles (**Fig. IX-8**), what allowed to infer that the pore-forming easiness induced by sterols *(Palacios-Ortega et al. 2016)* must be a general property of the actinoporins' toxic action. However, from the kinetic point of view, in the presence of Chol, StnII was much faster in producing calcein release than the other three wild-type proteins (**Fig. IX-8**), a behaviour very similar to that one observed in haemolysis. Somehow, in the presence of Chol, StnII would more easily diffuse, oligomerize and/or penetrate the bilayer with its extended N-terminal α-helix. Moreover, it has been recently described how many other sterols facilitate StnII-induced pore formation, independently of their structure *(Palacios-Ortega et al. 2016)*. This effect appears to be related with the capacity of these sterols to disrupt the hydrogen bonding network established mainly among SM molecules. This hypothesis is reinforced by the behaviour of the four actinoporins when assayed against dihydro-SMs. As it was previously observed with StnII *(García-Linares et al. 2016)*, membrane binding affinity and pore formation capacity of actinoporins are markedly diminished when using dhSM containing vesicles due to a tighter phospholipid packing (**Fig. IX-9**). This perturbation seems to be less determinant in EqtII, something that should be explained in the future.

In summary, the four actinoporins so far characterized in molecular detail show quite different behaviour when studied against simpler model systems. This differential behaviour might be a consequence of their distinct specificities and/or membrane binding affinities which might eventually be modulated by the nature of their natural target membranes or even the presence of not yet characterized isotoxin forms from the same sea anemone species, a possibility that seems even more feasible after the recent results that demonstrate how StnI and StnII can act synergistically *(Rivera-de-Torre et al. 2016)*.

NANODISCS: A LIPID PLATFORM FOR PORE RECONSTITUTION

Self-assembled phospholipid bilayer nanodiscs have become an important and versatile tool among model membrane systems to functionally reconstitute membrane proteins. Nanodiscs consist of a lipid bilayer encased within an engineered derivative of apolipoprotein A-1 scaffold protein (**Fig. 17**), which can be tailored to yield homogeneous preparations of disks with different diameters, and with epitope tags for exploitation in various purification strategies *(Ritchie et al. 2009)*.

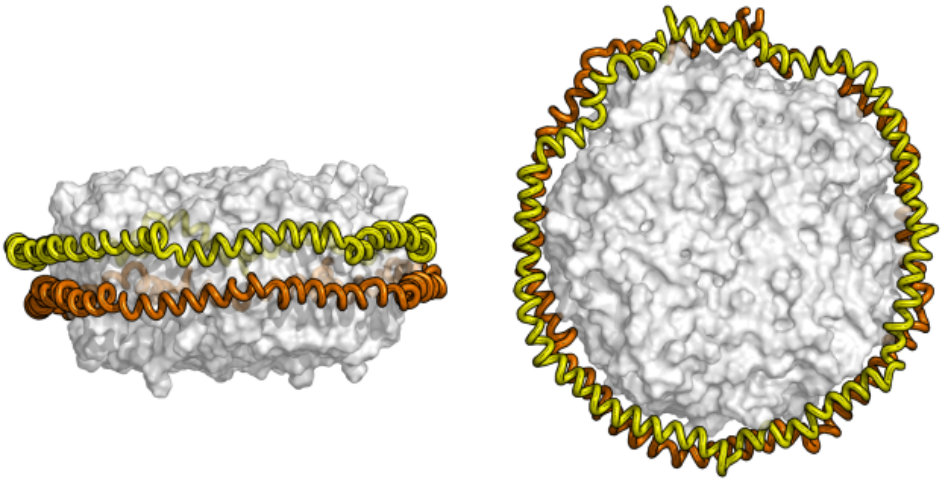

Figure 17. Side view (*left*) and frontal view (*right*) of a nanodisc. Modified from *(Ritchie et al. 2009)*.

Nanodiscs have been revealed as a perfect strategy to reconstitute the transmembrane pore structure of actinoporins in a soluble state. The StnII pores shown in this work are not only perfectly water soluble particles but have the additional advantage, when compared to the crystal structures obtained so far *(Mechaly et al. 2011, Tanaka et al. 2015)*, that the reconstruction has been made in a detergent-free environment. Thus, there are no elements present that could distort the membrane structure or membrane-proteins interactions.

Furthermore, StnII, instead of being present in the reconstitution mixture with the lipids and the scaffold protein, is added to already reconstituted and purified nanodiscs. This way, the formation of the pore has more resemblance to the real mode of action of StnII in nature.

An additional advantage is the lipid composition employed, since it contains both SM and Chol. No nanodiscs of this composition have been described before in the scientific literature, as far as we know. Therefore, we have first accomplished the construction of a completely new kind of nanodisc in terms of its lipidic composition. Additionally, Chol was not present in any of the previous actinoporin structures published so far, even though we now know that it is a required membrane component for the correct formation of the functional pore *(Wacklin et al. 2016)*. The three-dimensional model reconstructed from cryo-electron microscopy images (**Fig. X-**

7) shows a marked curvature of the membrane at the inner hole of the pore which should be explained by the presence of Chol favouring membrane monolayer bending and explaining, in part, why this lipid favours the formation of the pore.

Based on these cryo-electron microscopy preliminary results, the inclusion of the nanodiscs in the set of tools available to study the actinoporins' structure-function relationships would be probably revealed of a crucial importance.

CONCLUSIONS

Sphingomyelin has been long ago recognized to be crucial for actinoporins' membrane recognition and binding. However, one of the most important conclusions derived from the results presented now is that Chol also strongly modulates membrane binding affinity and pore formation ability of actinoporins by affecting membrane fluidity, interfering with the interfacial intermolecular hydrogen bonding among SM molecules and affecting the SM phosphocholine head group tilt and dynamics. The inhibitory effect of ceramides and the key role of specific amino acid side chains interactions with SM hydrogen bonding prone groups have been also established.

The three-dimensional structure of StnI has been solved with atomic resolution. Relevant protein regions for conformational changes associated with pore formation and involving long distant rearrangement of the polypeptide chain have been identified.

The production of mutant variants of StnI and StnII has led to a better understanding of the particular role of key residues located at particular regions of the protein that seem to be essential for the correct function of these actinoporins:

- Mutation of amino acids located at the 30 first residues stretch yielded mutants with a diminished pore formation capability.
- Changes in the POC binding site, the cluster of aromatic residues, or the array of basic amino acids generated proteins which, in general terms, were deficient in membrane recognition and binding.
- Mutations at the presumed integrin binding RGD motif revealed that this sequence is crucial for maintaining the actinoporins' pore-competent state of protein oligomerization.

It has been also determined that even modification of actinoporins' residues located at positions far away from the interactions needed for membrane binding, or insertion, did also largely affect the proper functionality of these proteins by altering the strictly required conformational freedom and/or electrostatic distribution of well-defined protein regions.

StnII has been shown to be the most powerful of all four actinoporins which structure is known at atomic resolution. This feature seems to be directly related with the particularly hydrophobic region of its amino-terminal stretch.

The employment of nanodiscs as lipid platforms to reconstitute the transmembrane pore of StnII in a soluble state has provided a high resolution structure of the pore. Work is in progress not only to improve the quality of this structure but also to include StnI and nanodiscs of different lipidic composition in this study.

BIBLIOGRAPHY

- Aittoniemi, J., Róg, T., Niemela, P., Pasenkiewicz-Gierula, M., Karttunen, M. and Vattulainen, I. (**2006**). "Tilt: major factor in sterols' ordering capability in membranes". *J Phys Chem B* 110(51): 25562-25564.

- Alanko, S. M., Halling, K. K., Maunula, S., Slotte, J. P. and Ramstedt, B. (**2005**). "Displacement of sterols from sterol/sphingomyelin domains in fluid bilayer membranes by competing molecules". *Biochim Biophys Acta* 1715(2): 111-121.

- Alegre-Cebollada, J., Lacadena, V., Oñaderra, M., Mancheño, J. M., Gavilanes, J. G. and Martínez-del-Pozo, Á. (**2004**). "Phenotypic selection and characterization of randomly produced non-haemolytic mutants of the toxic sea anemone protein sticholysin II". *FEBS Lett* 575(1-3): 14-18.

- Alegre-Cebollada, J., Rodríguez-Crespo, I., Gavilanes, J. G. and Martínez-del-Pozo, Á. (**2006**). "Detergent-resistant membranes are platforms for actinoporin pore-forming activity on intact cells". *FEBS J* 273(4): 863-871.

- Alegre-Cebollada, J., Martínez-del-Pozo, Á., Gavilanes, J. G. and Goormaghtigh, E. (**2007a**). "Infrared spectroscopy study on the conformational changes leading to pore formation of the toxin sticholysin II". *Biophys J* 93(9): 3191-3201.

- Alegre-Cebollada, J., Oñaderra, M., Gavilanes, J. G. and Martínez-del-Pozo, Á. (**2007b**). "Sea anemone actinoporins: the transition from a folded soluble state to a functionally active membrane-bound oligomeric pore". *Curr Protein Pept Sci* 8(6): 558-572.

- Alegre-Cebollada, J., Cunietti, M., Herrero-Galán, E., Gavilanes, J. G. and Martínez-del-Pozo, Á. (**2008**). "Calorimetric scrutiny of lipid binding by sticholysin II toxin mutants". *J Mol Biol* 382(4): 920-930.

- Alm, I., García-Linares, S., Gavilanes, J. G., Martínez-del-Pozo, Á. and Slotte, J. P. (**2015**). "Cholesterol stimulates and ceramide inhibits sticholysin II-induced pore formation in complex bilayer membranes". *Biochim Biophys Acta* 1848(4): 925-931.

- Álvarez, C., Casallanovo, F., Shida, C. S., Nogueira, L. V., Martínez, D., Tejuca, M., Pazos, I. F., Lanio, M. E., Menestrina, G., Lissi, E. and Schreier, S. (**2003**). "Binding of sea anemone pore-forming toxins sticholysins I and II to interfaces--modulation of conformation and activity, and lipid-protein interaction". *Chem Phys Lipids* 122(1-2): 97-105.

- Álvarez, C., Mancheño, J. M., Martínez, D., Tejuca, M., Pazos, F. and Lanio, M. E. (**2009**). "Sticholysins, two pore-forming toxins produced by the Caribbean Sea anemone *Stichodactyla helianthus*: their interaction with membranes". *Toxicon* 54(8): 1135-1147.

- Anderluh, G., Pungerčar, J., Križaj, I., Strukelj, B., Gubenšek, F. and Maček, P. (**1997**). "N-terminal truncation mutagenesis of equinatoxin II, a pore-forming protein from the sea anemone *Actinia equina*". *Protein Eng* 10(7): 751-755.

- Anderluh, G., Krizaj, I., Strukelj, B., Gubensek, F., Maček, P. and Pungercar, J. (**1999**). "Equinatoxins, pore-forming proteins from the sea anemone *Actinia equina*, belong to a multigene family". *Toxicon* 37(10): 1391-1401.

- Anderluh, G. and Maček, P. (**2002**). "Cytolytic peptide and protein toxins from sea anemones (Anthozoa: Actiniaria)". *Toxicon* 40(2): 111-124.

- Anderluh, G., Dalla-Serra, M., Viero, G., Guella, G., Maček, P. and Menestrina, G. (**2003**). "Pore formation by equinatoxin II, a eukaryotic protein toxin, occurs by induction of nonlamellar lipid structures". *J Biol Chem* 278(46): 45216-45223.

- Anderluh, G., Razpotnik, A., Podlesek, Z., Maček, P., Separovic, F. and Norton, R. S. (**2005**). "Interaction of the eukaryotic pore-forming cytolysin equinatoxin II with model membranes: ^{19}F NMR studies". *J Mol Biol* 347(1): 27-39.

- Anderluh, G. and Lakey, J. H. (**2008**). "Disparate proteins use similar architectures to damage membranes". *Trends Biochem Sci* 33(10): 482-490.

- Antonini, V., Pérez-Barzaga, V., Bampi, S., Pentón, D., Martínez, D., Dalla-Serra, M. and Tejuca, M. (**2014**). "Functional characterization of sticholysin I and W111C mutant reveals the sequence of the actinoporin's pore assembly". *PLoS One* 9(10): e110824.

- Artetxe, I., Sergelius, C., Kurita, M., Yamaguchi, S., Katsumura, S., Slotte, J. P. and Maula, T. (**2013**). "Effects of sphingomyelin headgroup size on interactions with ceramide". *Biophys J* 104(3): 604-612.

- Athanasiadis, A., Anderluh, G., Maček, P. and Turk, D. (**2001**). "Crystal structure of the soluble form of equinatoxin II, a pore-forming toxin from the sea anemone *Actinia equina*". *Structure* 9(4): 341-346.

- Baker, M. A., Rojko, N., Cronin, B., Anderluh, G. and Wallace, M. I. (**2014**). "Photobleaching reveals heterogeneous stoichiometry for equinatoxin II oligomers". *Chembiochem* 15(14): 2139-2145.

- Bakrač, B., Gutiérrez-Aguirre, I., Podlesek, Z., Sonnen, A. F., Gilbert, R. J., Maček, P., Lakey, J. H. and Anderluh, G. (**2008**). "Molecular determinants of sphingomyelin specificity of a eukaryotic pore-forming toxin". *J Biol Chem* 283(27): 18665-18677.

- Bakrač, B. and Anderluh, G. (**2010a**). "Molecular mechanism of sphingomyelin-specific membrane binding and pore formation by actinoporins". *Adv Exp Med Biol* 677: 106-115.

- Bakrač, B., Kladnik, A., Maček, P., McHaffie, G., Werner, A., Lakey, J. H. and Anderluh, G. (**2010b**). "A toxin-based probe reveals cytoplasmic exposure of Golgi sphingomyelin". *J Biol Chem* 285(29): 22186-22195.

- Barlič, A., Gutiérrez-Aguirre, I., Caaveiro, J. M. M., Cruz, A., Ruiz-Argüello, M. B., Pérez-Gil, J. and González-Mañas, J. M. (**2004**). "Lipid phase coexistence favors membrane insertion of equinatoxin-II, a pore-forming toxin from *Actinia equina*". *J Biol Chem* 279(33): 34209-34216.

- Basulto, A., Pérez, V. M., Noa, Y., Varela, C., Otero, A. J. and Pico, M. C. (**2006**). "Immunohistochemical targeting of sea anemone cytolysins on tentacles, mesenteric filaments and isolated nematocysts of Stichodactyla helianthus". *J Exp Zool A Comp Exp Biol* 305(3): 253-258.

- Bellomio, A., Morante, K., Barlič, A., Gutiérrez-Aguirre, I., Viguera, A. R. and González-Mañas, J. M. (**2009**). "Purification, cloning and characterization of fragaceatoxin C, a novel actinoporin from the sea anemone *Actinia fragacea*". *Toxicon* 54(6): 869-880.

- Belmonte, G., Pederzolli, C., Maček, P. and Menestrina, G. (**1993**). "Pore formation by the sea anemone cytolysin equinatoxin II in red blood cells and model lipid membranes". *J Membr Biol* 131(1): 11-22.

- Bernheimer, A. W. and Avigad, L. S. (**1976**). "Properties of a toxin from the sea anemone *Stoichacis helianthus*, including specific binding to sphingomyelin". *Proc Natl Acad Sci U S A* 73(2): 467-471.

- Björkbom, A., Róg, T., Kaszuba, K., Kurita, M., Yamaguchi, S., Lönnfors, M., Nyholm, T. K., Vattulainen, I., Katsumura, S. and Slotte, J. P. (**2010**). "Effect of sphingomyelin headgroup size on molecular properties and interactions with cholesterol". *Biophys J* 99(10): 3300-3308.

- Björkbom, A., Róg, T., Kankaanpää, P., Lindroos, D., Kaszuba, K., Kurita, M., Yamaguchi, S., Yamamoto, T., Jaikishan, S., Paavolainen, L., Päivärinne, J., Nyholm, T. K., Katsumura, S., Vattulainen, I. and Slotte, J. P. (**2011**). "N- and O-methylation of sphingomyelin markedly affects its membrane properties and interactions with cholesterol". *Biochim Biophys Acta* 1808(4): 1179-1186.

- Bruzik, K. S., Sobon, B. and Salamonczyk, G. M. (**1990**). "Nuclear magnetic resonance study of sphingomyelin bilayers". *Biochemistry* 29(16): 4017-4021.

- Caaveiro, J. M. M., Echabe, I., Gutiérrez-Aguirre, I., Nieva, J. L., Arrondo, J. L. and González-Mañas, J. M. (**2001**). "Differential interaction of equinatoxin II with model membranes in response to lipid composition". *Biophys J* 80(3): 1343-1353.

- Casallanovo, F., de Oliveira, F. J., de Souza, F. C., Ros, U., Martínez, Y., Pentón, D., Tejuca, M., Martínez, D., Pazos, F., Pertinhez, T. A., Spisni, A., Cilli, E. M., Lanio, M. E.,

Álvarez, C. and Schreier, S. (**2006**). "Model peptides mimic the structure and function of the N-terminus of the pore-forming toxin sticholysin II". *Biopolymers* 84(2): 169-180.

- Castrillo, I., Alegre-Cebollada, J., Martínez-del-Pozo, Á., Gavilanes, J. G. and Bruix, M. (**2009**). "(1)H, (13)C, and (15)N NMR assignments of StnII-R29Q, a defective lipid binding mutant of the sea anemone actinoporin sticholysin II". *Biomol NMR Assign* 3(2): 239-241.

- Castrillo, I., Araujo, N. A., Alegre-Cebollada, J., Gavilanes, J. G., Martínez-del-Pozo, Á. and Bruix, M. (**2010**). "Specific interactions of sticholysin I with model membranes: an NMR study". *Proteins* 78(8): 1959-1970.

- Celedón, G., González, G., Lissi, E., Cerda, T., Martínez, D., Soto, C., Pupo, M., Pazos, F., Lanio, M. E. and Álvarez, C. (**2009**). "Effect of calcium on the hemolytic activity of *Stichodactyla helianthus* toxin sticholysin II on human erythrocytes". *Toxicon* 54(6): 845-850.

- Celedón, G., González, G., Lissi, E., Cerda, T., Bascunant, D., Lepeley, M., Pazos, F., Lanio, M. E. and Álvarez, C. (**2011**). "Effect of pre-exposure of human erythrocytes to oxidants on the haemolytic activity of sticholysin II. A comparison between peroxynitrite and hypochlorous acid". *Free Radic Res* 45(4): 400-408.

- Cosentino, K., Ros, U. and García-Sáez, A. J. (**2016**). "Assembling the puzzle: Oligomerization of alpha-pore forming proteins in membranes". *Biochim Biophys Acta* 1858(3): 457-466.

- Cullis, P. R., De Kruyff, B. and Richards, R. E. (**1976**). "Factors affecting the motion of the polar headgroup in phospholipid bilayers. A ^{31}P NMR study of unsonicated phosphatidylcholine liposomes". *Biochim Biophys Acta* 426(3): 433-446.

- De-los-Ríos, V., Mancheño, J. M., Lanio, M. E., Oñaderra, M. and Gavilanes, J. G. (**1998**). "Mechanism of the leakage induced on lipid model membranes by the hemolytic protein sticholysin II from the sea anemone *Stichodactyla helianthus*". *Eur J Biochem* 252(2): 284-289.

- De-los-Ríos, V., Oñaderra, M., Martínez-Ruiz, A., Lacadena, J., Mancheño, J. M., Martínez-del-Pozo, Á. and Gavilanes, J. G. (**2000**). "Overproduction in *Escherichia coli* and purification of the hemolytic protein sticholysin II from the sea anemone *Stichodactyla helianthus*". *Protein Expr Purif* 18(1): 71-76.

- De-Planque, M. R., Kruijtzer, J. A., Liskamp, R. M., Marsh, D., Greathouse, D. V., Koeppe, R. E. n., de Kruijff, B. and Killian, J. A. (**1999**). "Different membrane anchoring positions of tryptophan and lysine in synthetic transmembrane alpha-helical peptides". *J Biol Chem* 274(30): 20839-20846.

- Drechsler, A., Potrich, C., Sabo, J. K., Frisanco, M., Guella, G., Dalla-Serra, M., Anderluh, G., Separovic, F. and Norton, R. S. (**2006**). "Structure and activity of the N-

terminal region of the eukaryotic cytolysin equinatoxin II". *Biochemistry* 45(6): 1818-1828.

- Drechsler, A., Miles, A. J., Norton, R. S., Wallace, B. A. and Separovic, F. (**2009**). "Effect of lipid on the conformation of the N-terminal region of equinatoxin II: a synchrotron radiation circular dichroism spectroscopic study". *Eur Biophys J* 39(1): 121-127.

- Engberg, O., Hautala, V., Yasuda, T., Dehio, H., Murata, M., Slotte, J. P. and Nyholm, T. K. (**2016**). "The Affinity of Cholesterol for Different Phospholipids Affects Lateral Segregation in Bilayers". *Biophys J* 111(3): 546-556.

- Fantini, J. and Barrantes, F. J. (**2013**). "How cholesterol interacts with membrane proteins: an exploration of cholesterol-binding sites including CRAC, CARC, and tilted domains". *Front Physiol* 4: 31.

- Feinstein, M. B., Fernandez, S. M. and Sha'afi, R. I. (**1975**). "Fluidity of natural membranes and phosphatidylserine and ganglioside dispersions. Effect of local anesthetics, cholesterol and protein". *Biochim Biophys Acta* 413(3): 354-370.

- Ferguson-Yankey, S. R., Borchman, D., Taylor, K. G., DuPré, D. B. and Yappert, M. C. (**2000**). "Conformational studies of sphingolipids by NMR spectroscopy. I. Dihydrosphingomyelin". *Biochim Biophys Acta* 1467(2): 307-325.

- García-Linares, S., Castrillo, I., Bruix, M., Menéndez, M., Alegre-Cebollada, J., Martínez-del-Pozo, Á. and Gavilanes, J. G. (**2013**). "Three-dimensional structure of the actinoporin sticholysin I. Influence of long-distance effects on protein function". *Arch Biochem Biophys* 532(1): 39-45.

- García-Linares, S., Richmond, R., García-Mayoral, M. F., Bustamante, N., Bruix, M., Gavilanes, J. G. and Martínez-del-Pozo, Á. (**2014**). "The sea anemone actinoporin (Arg-Gly-Asp) conserved motif is involved in maintaining the competent oligomerization state of these pore-forming toxins". *FEBS J* 281(5): 1465-1478.

- García-Linares, S., Alm, I., Maula, T., Gavilanes, J. G., Slotte, J. P. and Martínez-del-Pozo, Á. (**2015**). "The effect of cholesterol on the long-range network of interactions established among sea anemone sticholysin II residues at the water-membrane interface". *Mar Drugs* 13(4): 1647-1665.

- García-Linares, S., Palacios-Ortega, J., Yasuda, T., Åstrand, M., Gavilanes, J. G., Martínez-del-Pozo, Á. and Slotte, J. P. (**2016**). "Toxin-induced pore formation is hindered by intermolecular hydrogen bonding in sphingomyelin bilayers". *Biochim Biophys Acta* 1858(6): 1189-1195.

- García-Ortega, L., Alegre-Cebollada, J., García-Linares, S., Bruix, M., Martínez-del-Pozo, Á. and Gavilanes, J. G. (**2011**). "The behavior of sea anemone actinoporins at the water-membrane interface". *Biochim Biophys Acta* 1808(9): 2275-2288.

- Geny, B. and Popoff, M. R. (**2006**). "Bacterial protein toxins and lipids: pore formation or toxin entry into cells". *Biol Cell* 98(11): 667-678.

- González, M. R., Bischofberger, M., Pernot, L., van-der-Goot, F. G. and Frêche, B. (**2008**). "Bacterial pore-forming toxins: the (w)hole story?". *Cell Mol Life Sci* 65(3): 493-507.

- Gutiérrez-Aguirre, I., Barlič, A., Podlesek, Z., Maček, P., Anderluh, G. and González-Mañas, J. M. (**2004**). "Membrane insertion of the N-terminal alpha-helix of equinatoxin II, a sea anemone cytolytic toxin". *Biochem J* 384(Pt 2): 421-428.

- Heuck, A. P., Tweten, R. K. and Johnson, A. E. (**2001**). "Beta-barrel pore-forming toxins: intriguing dimorphic proteins". *Biochemistry* 40(31): 9065-9073.

- Hinds, M. G., Zhang, W., Anderluh, G., Hansen, P. E. and Norton, R. S. (**2002**). "Solution structure of the eukaryotic pore-forming cytolysin equinatoxin II: implications for pore formation". *J Mol Biol* 315(5): 1219-1229.

- Hong, Q., Gutiérrez-Aguirre, I., Barlič, A., Malovrh, P., Kristan, K., Podlesek, Z., Maček, P., Turk, D., González-Mañas, J. M., Lakey, J. H. and Anderluh, G. (**2002**). "Two-step membrane binding by equinatoxin II, a pore-forming toxin from the sea anemone, involves an exposed aromatic cluster and a flexible helix". *J Biol Chem* 277(44): 41916-41924.

- Iacovache, I., van-der-Goot, F. G. and Pernot, L. (**2008**). "Pore formation: an ancient yet complex form of attack". *Biochim Biophys Acta* 1778(7-8): 1611-1623.

- Jaikishan, S., Björkbom, A. and Slotte, J. P. (**2010**). "Sphingomyelin analogs with branched N-acyl chains: the position of branching dramatically affects acyl chain order and sterol interactions in bilayer membranes". *Biochim Biophys Acta* 1798(10): 1987-1994.

- Jiang, X. Y., Yang, W. L., Chen, H. P., Tu, H. B., Wu, W. Y., Wei, J. W., Wang, J., Liu, W. H. and Xu, A. L. (**2002**). "Cloning and characterization of an acidic cytolysin cDNA from sea anemone *Sagartia rosea*". *Toxicon* 40(11): 1563-1569.

- Koradi, R., Billeter, M. and Wuthrich, K. (**1996**). "MOLMOL: a program for display and analysis of macromolecular structures". *J Mol Graph* 14(1): 51-55, 29-32.

- Kristan, K. Č., Podlesek, Z., Hojnik, V., Gutiérrez-Aguirre, I., Guncar, G., Turk, D., González-Mañas, J. M., Lakey, J. H., Maček, P. and Anderluh, G. (**2004**). "Pore formation by equinatoxin, a eukaryotic pore-forming toxin, requires a flexible N-terminal region and a stable beta-sandwich". *J Biol Chem* 279(45): 46509-46517.

- Kristan, K. Č., Viero, G., Maček, P., Dalla-Serra, M. and Anderluh, G. (**2007**). "The equinatoxin N-terminus is transferred across planar lipid membranes and helps to stabilize the transmembrane pore". *FEBS J* 274(2): 539-550.

- Kristan, K. Č., Viero, G., Dalla-Serra, M., Maček, P. and Anderluh, G. (**2009**). "Molecular mechanism of pore formation by actinoporins". *Toxicon* 54(8): 1125-1134.

- Law, R. H., Lukoyanova, N., Voskoboinik, I., Caradoc-Davies, T. T., Baran, K., Dunstone, M. A., D'Angelo, M. E., Orlova, E. V., Coulibaly, F., Verschoor, S., Browne, K. A., Ciccone, A., Kuiper, M. J., Bird, P. I., Trapani, J. A., Saibil, H. R. and Whisstock, J. C. (**2010**). "The structural basis for membrane binding and pore formation by lymphocyte perforin". *Nature* 468(7322): 447-451.

- López-Castilla, A., Pazos, F., Schreier, S. and Pires, J. R. (**2014**). "Solution NMR analysis of the interaction between the actinoporin sticholysin I and DHPC micelles--correlation with backbone dynamics". *Proteins* 82(6): 1022-1034.

- Maček, P. (**1992**). "Polypeptide cytolytic toxins from sea anemones (Actiniaria)". *FEMS Microbiol Immunol* 5(1-3): 121-129.

- Maček, P., Belmonte, G., Pederzolli, C. and Menestrina, G. (**1994**). "Mechanism of action of equinatoxin II, a cytolysin from the sea anemone *Actinia equina l.* belonging to the family of actinoporins". *Toxicology* 87(1-3): 205-227.

- Malovrh, P., Barlič, A., Podlesek, Z., Maček, P., Menestrina, G. and Anderluh, G. (**2000**). "Structure-function studies of tryptophan mutants of equinatoxin II, a sea anemone pore-forming protein". *Biochem J* 346 Pt 1: 223-232.

- Malovrh, P., Viero, G., Dalla-Serra, M., Podlesek, Z., Lakey, J. H., Maček, P., Menestrina, G. and Anderluh, G. (**2003**). "A novel mechanism of pore formation: membrane penetration by the N-terminal amphipathic region of equinatoxin". *J Biol Chem* 278(25): 22678-22685.

- Mancheño, J. M., Martín-Benito, J., Martínez-Ripoll, M., Gavilanes, J. G. and Hermoso, J. A. (**2003**). "Crystal and electron microscopy structures of sticholysin II actinoporin reveal insights into the mechanism of membrane pore formation". *Structure* 11(11): 1319-1328.

- Mancheño, J. M., Martín-Benito, J., Gavilanes, J. G. and Vázquez, L. (**2006**). "A complementary microscopy analysis of sticholysin II crystals on lipid films: Atomic force and transmission electron characterizations". *Biophys Chem* 119(3): 219-223.

- Martín-Benito, J., Gavilanes, F., de-los-Ríos, V., Mancheño, J. M., Fernández, J. J. and Gavilanes, J. G. (**2000**). "Two-dimensional crystallization on lipid monolayers and three-dimensional structure of sticholysin II, a cytolysin from the sea anemone *Stichodactyla helianthus*". *Biophys J* 78(6): 3186-3194.

- Martínez, D., Otero, A., Álvarez, C., Pazos, F., Tejuca, M., Lanio, M. E., Gutiérrez-Aguirre, I., Barlič, A., Iloro, I., Arrondo, J. L., González-Mañas, J. M. and Lissi, E. (**2007**).

"Effect of sphingomyelin and cholesterol on the interaction of St II with lipidic interfaces". *Toxicon* 49(1): 68-81.

- Maula, T., Artetxe, I., Grandell, P. M. and Slotte, J. P. (**2012**). "Importance of the sphingoid base length for the membrane properties of ceramides". *Biophys J* 103(9): 1870-1879.

- Maula, T., Isaksson, Y. J., García-Linares, S., Niinivehmas, S., Pentikainen, O. T., Kurita, M., Yamaguchi, S., Yamamoto, T., Katsumura, S., Gavilanes, J. G., Martínez-del-Pozo, Á. and Slotte, J. P. (**2013**). "2NH and 3OH are crucial structural requirements in sphingomyelin for sticholysin II binding and pore formation in bilayer membranes". *Biochim Biophys Acta* 1828(5): 1390-1395.

- Mechaly, A. E., Bellomio, A., Gil-Carton, D., Morante, K., Valle, M., González-Mañas, J. M. and Guerin, D. M. (**2011**). "Structural insights into the oligomerization and architecture of eukaryotic membrane pore-forming toxins". *Structure* 19(2): 181-191.

- Meinardi, E., Florin-Christensen, M., Paratcha, G., Azcurra, J. M. and Florin-Christensen, J. (**1995**). "The molecular basis of the self/nonself selectivity of a coelenterate toxin". *Biochem Biophys Res Commun* 216(1): 348-354.

- Menestrina, G., Cabiaux, V. and Tejuca, M. (**1999**). "Secondary structure of sea anemone cytolysins in soluble and membrane bound form by infrared spectroscopy". *Biochem Biophys Res Commun* 254(1): 174-180.

- Metcalf, R. and Pandit, S. A. (**2012**). "Mixing properties of sphingomyelin ceramide bilayers: a simulation study". *J Phys Chem B* 116(15): 4500-4509.

- Monastyrnaya, M., Leychenko, E., Isaeva, M., Likhatskaya, G., Zelepuga, E., Kostina, E., Trifonov, E., Nurminski, E. and Kozlovskaya, E. (**2010**). "Actinoporins from the sea anemones, tropical Radianthus macrodactylus and northern Oulactis orientalis: Comparative analysis of structure-function relationships". *Toxicon* 56(8): 1299-1314.

- Morante, K., Caaveiro, J. M. M., Tanaka, K., González-Mañas, J. M. and Tsumoto, K. (**2015a**). "A pore-forming toxin requires a specific residue for its activity in membranes with particular physicochemical properties". *J Biol Chem* 290(17): 10850-10861.

- Morante, K., Caaveiro, J. M. M., Viguera, A. R., Tsumoto, K. and González-Mañas, J. M. (**2015b**). "Functional characterization of Val60, a key residue involved in the membrane-oligomerization of fragaceatoxin C, an actinoporin from *Actinia fragacea*". *FEBS Lett* 589(15): 1840-1846.

- Morante, K., Bellomio, A., Gil-Carton, D., Redondo-Morata, L., Sot, J., Scheuring, S., Valle, M., González-Mañas, J. M., Tsumoto, K. and Caaveiro, J. M. M. (**2016**). "Identification of a membrane-bound prepore species clarifies the lytic mechanism of actinoporins". *J Biol Chem*.

- Mueller, M., Grauschopf, U., Maier, T., Glockshuber, R. and Ban, N. (**2009**). "The structure of a cytolytic alpha-helical toxin pore reveals its assembly mechanism". *Nature* 459(7247): 726-730.

- Mueller, M. and Ban, N. (**2010**). "Enhanced SnapShot: Pore-forming toxins". *Cell* 142(2): 334, 334 e331.

- Niemela, P., Hyvonen, M. T. and Vattulainen, I. (**2004**). "Structure and dynamics of sphingomyelin bilayer: insight gained through systematic comparison to phosphatidylcholine". *Biophys J* 87(5): 2976-2989.

- Norton, R. S. (**2009**). "Structures of sea anemone toxins". *Toxicon* 54(8): 1075-1088.

- Nyholm, T., Nylund, M., Söderholm, A. and Slotte, J. P. (**2003**). "Properties of palmitoyl phosphatidylcholine, sphingomyelin, and dihydrosphingomyelin bilayer membranes as reported by different fluorescent reporter molecules". *Biophys J* 84(2 Pt 1): 987-997.

- Olivera, B. M., River, J., Clark, C., Ramilo, C. A., Corpuz, G. P., Abogadie, F. C., Mena, E. E., Woodward, S. R., Hillyard, D. R. and Cruz, L. J. (**1990**). "Diversity of Conus neuropeptides". *Science* 249(4966): 257-263.

- Palacios-Ortega, J., García-Linares, S., Åstrand, M., Al-Sazzad, M. A., Gavilanes, J. G., Martínez-del-Pozo, Á. and Slotte, J. P. (**2016**). "Regulation of sticholysin II-induced pore formation by lipid bilayer composition, phase state, and interfacial properties". *Langmuir* 32(14): 3476-3484.

- Pardo-Cea, M. A., Alegre-Cebollada, J., Martínez-del-Pozo, Á., Gavilanes, J. G. and Bruix, M. (**2010**). "(1)H, (13)C, and (15)N NMR assignments of StnII-Y111N, a highly impaired mutant of the sea anemone actinoporin sticholysin II". *Biomol NMR Assign* 4(1): 69-72.

- Pardo-Cea, M. A., Castrillo, I., Alegre-Cebollada, J., Martínez-del-Pozo, Á., Gavilanes, J. G. and Bruix, M. (**2011**). "Intrinsic local disorder and a network of charge-charge interactions are key to actinoporin membrane disruption and cytotoxicity". *FEBS J* 278(12): 2080-2089.

- Parker, M. W. and Feil, S. C. (**2005**). "Pore-forming protein toxins: from structure to function". *Prog Biophys Mol Biol* 88(1): 91-142.

- Pedrera, L., Fanani, M. L., Ros, U., Lanio, M. E., Maggio, B. and Álvarez, C. (**2014**). "Sticholysin I-membrane interaction: an interplay between the presence of sphingomyelin and membrane fluidity". *Biochim Biophys Acta* 1838(7): 1752-1759.

- Pedrera, L., Gomide, A. B., Sánchez, R. E., Ros, U., Wilke, N., Pazos, F., Lanio, M. E., Itri, R., Fanani, M. L. and Álvarez, C. (**2015**). "The presence of sterols favors sticholysin

I-membrane association and pore formation regardless of their ability to form laterally segregated domains". *Langmuir* 31(36): 9911-9923.

- Pettersen, E. F., Goddard, T. D., Huang, C. C., Couch, G. S., Greenblatt, D. M., Meng, E. C. and Ferrin, T. E. (**2004**). "UCSF Chimera--a visualization system for exploratory research and analysis". *J Comput Chem* 25(13): 1605-1612.

- Ritchie, T. K., Grinkova, Y. V., Bayburt, T. H., Denisov, I. G., Zolnerciks, J. K., Atkins, W. M. and Sligar, S. G. (**2009**). "Chapter 11 - Reconstitution of membrane proteins in phospholipid bilayer nanodiscs". *Methods Enzymol* 464: 211-231.

- Rivera-de-Torre, E., García-Linares, S., Alegre-Cebollada, J., Lacadena, J., Gavilanes, J. G. and Martínez-del-Pozo, Á. (**2016**). "Synergistic action of actinoporin isoforms from the same sea anemone species assembled into functionally active heteropores". *J Biol Chem* 291(27): 14109-14119.

- Róg, T. and Pasenkiewicz-Gierula, M. (**2006**). "Cholesterol-sphingomyelin interactions: a molecular dynamics simulation study". *Biophys J* 91(10): 3756-3767.

- Rojko, N., Kristan, K. Č., Viero, G., Žerovnik, E., Maček, P., Dalla-Serra, M. and Anderluh, G. (**2013**). "Membrane damage by an alpha-helical pore-forming protein, equinatoxin II, proceeds through a succession of ordered steps". *J Biol Chem* 288(33): 23704-23715.

- Rojko, N., Cronin, B., Danial, J. S., Baker, M. A., Anderluh, G. and Wallace, M. I. (**2014**). "Imaging the lipid-phase-dependent pore formation of equinatoxin II in droplet interface bilayers". *Biophys J* 106(8): 1630-1637.

- Rojko, N., Dalla-Serra, M., Maček, P. and Anderluh, G. (**2016**). "Pore formation by actinoporins, cytolysins from sea anemones". *Biochim Biophys Acta* 1858(3): 446-456.

- Ros, U. and García-Sáez, A. J. (**2015a**). "More than a pore: The interplay of pore-forming proteins and lipid membranes". *J Membr Biol* 248(3): 545-561.

- Ros, U., Rodríguez-Vera, W., Pedrera, L., Valiente, P. A., Cabezas, S., Lanio, M. E., García-Sáez, A. J. and Álvarez, C. (**2015b**). "Differences in activity of actinoporins are related with the hydrophobicity of their N-terminus". *Biochimie* 116: 70-78.

- Schön, P., García-Sáez, A. J., Malovrh, P., Bacia, K., Anderluh, G. and Schwille, P. (**2008**). "Equinatoxin II permeabilizing activity depends on the presence of sphingomyelin and lipid phase coexistence". *Biophys J* 95(2): 691-698.

- Shin, M. L., Michaels, D. W. and Mayer, M. M. (**1979**). "Membrane damage by a toxin from the sea anemone *Stoichactis helianthus*. II. Effect of membrane lipid composition in a liposome system". *Biochim Biophys Acta* 555(1): 79-88.

- Somerharju, P. (**2002**). "Pyrene-labeled lipids as tools in membrane biophysics and cell biology". *Chem Phys Lipids* 116(1-2): 57-74.

- Subburaj, Y., Ros, U., Hermann, E., Tong, R. and García-Sáez, A. J. (**2015**). "Toxicity of an alpha-pore-forming toxin depends on the assembly mechanism on the target membrane as revealed by single molecule imaging". *J Biol Chem* 290(8): 4856-4865.

- Talbott, C. M., Vorobyov, I., Borchman, D., Taylor, K. G., DuPré, D. B. and Yappert, M. C. (**2000**). "Conformational studies of sphingolipids by NMR spectroscopy. II. Sphingomyelin". *Biochim Biophys Acta* 1467(2): 326-337.

- Tanaka, K., Caaveiro, J. M. M., Morante, K., González-Mañas, J. M. and Tsumoto, K. (**2015**). "Structural basis for self-assembly of a cytolytic pore lined by protein and lipid". *Nat Commun* 6: 6337.

- Tejuca, M., Dalla-Serra, M., Ferreras, M., Lanio, M. E. and Menestrina, G. (**1996**). "Mechanism of membrane permeabilization by sticholysin I, a cytolysin isolated from the venom of the sea anemone *Stichodactyla helianthus*". *Biochemistry* 35(47): 14947-14957.

- Tejuca, M., Dalla Serra, M., Potrich, C., Álvarez, C. and Menestrina, G. (**2001**). "Sizing the radius of the pore formed in erythrocytes and lipid vesicles by the toxin sticholysin I from the sea anemone *Stichodactyla helianthus*". *J Membr Biol* 183(2): 125-135.

- Turk, T. (**1991**). "Cytolytic toxins from sea anemones". *Journal of Toxicology: Toxin Reviews* 10(3): 223-262.

- Uechi, G., Toma, H., Arakawa, T. and Sato, Y. (**2010**). "Molecular characterization on the genome structure of hemolysin toxin isoforms isolated from sea anemone Actineria villosa and Phyllodiscus semoni". *Toxicon* 56(8): 1470-1476.

- Valcárcel, C. A., Dalla-Serra, M., Potrich, C., Bernhart, I., Tejuca, M., Martínez, D., Pazos, F., Lanio, M. E. and Menestrina, G. (**2001**). "Effects of lipid composition on membrane permeabilization by sticholysin I and II, two cytolysins of the sea anemone *Stichodactyla helianthus*". *Biophys J* 80(6): 2761-2774.

- Valle, A., López-Castilla, A., Pedrera, L., Martínez, D., Tejuca, M., Campos, J., Fando, R., Lissi, E., Álvarez, C., Lanio, M. E., Pazos, F. and Schreier, S. (**2011**). "Cys mutants in functional regions of sticholysin I clarify the participation of these residues in pore formation". *Toxicon* 58(1): 8-17.

- Varanda, W. and Finkelstein, A. (**1980**). "Ion and nonelectrolyte permeability properties of channels formed in planar lipid bilayer membranes by the cytolytic toxin from the sea anemone *Stoichactis helianthus*". *J Membr Biol* 55(3): 203-211.

- Veitia, R., Tejuca, M., Álvarez, C., Lanio, M. E. and Pazos, I. F. (**1995**). "Kinetics of the hemolysis induced by a cytolysin from *Stichodactyla helianthus*: effect of temperature and divalent cations". *Biologia* 9: 15-21.

- Venable, R. M., Sodt, A. J., Rogaski, B., Rui, H., Hatcher, E., MacKerell, A. D., Jr., Pastor, R. W. and Klauda, J. B. (**2014**). "CHARMM all-atom additive force field for sphingomyelin: elucidation of hydrogen bonding and of positive curvature". *Biophys J* 107(1): 134-145.

- Wacklin, H. P., Bremec, B. B., Moulin, M., Rojko, N., Haertlein, M., Forsyth, T., Anderluh, G. and Norton, R. S. (**2016**). "Neutron reflection study of the interaction of the eukaryotic pore-forming actinoporin equinatoxin II with lipid membranes reveals intermediate states in pore formation". *Biochim Biophys Acta* 1858(4): 640-652.

- Wang, Y., Yap, L. L., Chua, K. L. and Khoo, H. E. (**2008**). "A multigene family of Heteractis magnificalysins (HMgs)". *Toxicon* 51(8): 1374-1382.

- Weber, D. K., Yao, S., Rojko, N., Anderluh, G., Lybrand, T. P., Downton, M. T., Wagner, J. and Separovic, F. (**2015**). "Characterization of the lipid-binding site of equinatoxin II by NMR and molecular dynamics simulation". *Biophys J* 108(8): 1987-1996.

ANNEX

Other articles related to the work carried out in this Doctoral Thesis:

- Palacios-Ortega, J., **García-Linares, S.**, Åstrand, M., Al-Sazzad, M. A., Gavilanes, J. G., Martínez-del-Pozo, Á. and Slotte, J. P. (2016). "Regulation of sticholysin II-induced pore formation by lipid bilayer composition, phase state, and interfacial properties". *Langmuir* 32(14): 3476-3484.

- Rivera-de-Torre, E., **García-Linares, S.**, Alegre-Cebollada, J., Lacadena, J., Gavilanes, J. G. and Martínez-del-Pozo, Á. (2016). "Synergistic action of actinoporin isoforms from the same sea anemone species assembled into functionally active heteropores". *J Biol Chem* 291(27): 14109-14119.

LANGMUIR Article
pubs.acs.org/Langmuir

Regulation of Sticholysin II-Induced Pore Formation by Lipid Bilayer Composition, Phase State, and Interfacial Properties

Juan Palacios-Ortega,[†,‡] Sara García-Linares,[†,‡] Mia Åstrand,[‡] Md. Abdullah Al Sazzad,[‡] José G. Gavilanes,[†] Álvaro Martínez-del-Pozo,[†] and J. Peter Slotte*[,‡]

[†]Departamento de Bioquímica y Biología Molecular I, Universidad Complutense, 28040 Madrid, Spain
[‡]Biochemistry, Faculty of Science and Engineering, Åbo Akademi University, 20500 Turku, Finland

Supporting Information

ABSTRACT: Sticholysin II (StnII) is a pore-forming toxin that uses sphingomyelin (SM) as the recognition molecule in targeting membranes. After StnII monomers bind to SM, several toxin monomers act in concert to oligomerize into a functional pore. The regulation of StnII binding to SM, and the subsequent pore-formation process, is not fully understood. In this study, we examined how the biophysical properties of bilayers, originating from variations in the SM structure, from the presence of sterol species, or from the presence of increasingly polyunsaturated glycerophospholipids, affected StnII-induced pore formation. StnII-induced pore formation, as determined from calcein permeabilization, was fastest in the pure unsaturated SM bilayers. In 1-palmitoyl-2-oleoyl-*sn*-glycero-3-phosphocholine (POPC)/saturated SM bilayers (4:1 molar ratio), pore formation became slower as the chain length of the saturated SMs increased from 14 up to 24 carbons. In the POPC/palmitoyl-SM (16:0-SM) 4:1 bilayers, SM could not support pore formation by StnII if dimyristoyl-PC was included at 1:1 stoichiometry with 16:0-SM, suggesting that free clusters of SM were required for toxin binding and/or pore formation. Cholesterol and other sterols facilitated StnII-induced pore formation markedly, but the efficiency did not appear to correlate with the sterol structure. Benzyl alcohol was more efficient than sterols in enhancing the pore-formation process, suggesting that the effect on pore formation originated from alcohol-induced alteration of the hydrogen-bonding network in the SM-containing bilayers. Finally, we observed that pore formation by StnII was enhanced in the PC/16:0-SM 4:1 bilayers, in which the PC was increasingly unsaturated. We conclude that the physical state of bilayer lipids greatly affected pore formation by StnII. Phase boundaries were not required for pore formation, although SM in a gel state attenuated pore formation.

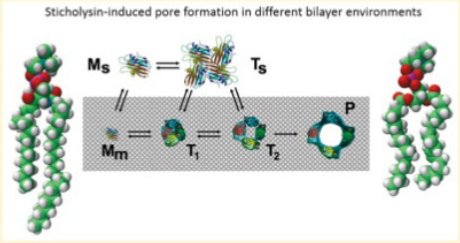

1. INTRODUCTION

The production of toxic proteins or peptides is a common feature of many pathogenic or sessile organisms, most probably to fulfill attack and/or defense functions. Some of these toxins have evolved to use various sphingolipids as "receptors" in their target membranes; these toxins include but are not limited to the cholera toxin (binds to GM1[1]) and the actinoporin family of toxins, which all appear to require the presence of sphingomyelin (SM) in their target membranes.[2−7] Actinoporins include toxins such as sticholysins I and II (StnI and StnII, from *Stichodactyla helianthus*[8,9]), equinatoxin II (EqtII, from *Actina equina*[10]), and fragaceatoxin C (FraC, from *Actina fragacea*[11]). In addition to actinoporins, lysenin from the earthworm *Eisenia fetida* has SM as its main target in membranes.[12] Actinoporins and lysenin are pore-forming toxins, but many more pore-forming toxins exist that do not use SM as a target.[13]

The water-soluble structure of sticholysin II (StnII) is known in detail.[14] It has a β-sandwich motif consisting of 10 β-strands flanked by two α-helices. These α-helices interact with both sides of the β-sandwich. For actinoporins, it is generally believed that monomeric peptides bind to the membrane interface (aided by SM) before oligomerization takes place, and a functional pore finally forms.[15] The structure of the pores is, in general, not experimentally well resolved, although the structure of a FraC transmembrane octameric pore has recently been reported.[16] More is known about how membrane or SM properties affect pore formation by different actinoporins. In the absence of cholesterol, pore formation by StnII requires hydrogen-bonding competent SM.[17] However, it has been reported that, in the presence of high cholesterol, pore formation could take place even in the absence of SM, for StnII and EqII.[2,8] The effect of cholesterol appears to be 2-fold: Cholesterol affects the apparent kinetics of pore formation[18] but also increases the apparent number of open StnII pores.[19] The actual mechanism by which cholesterol affects the rate and efficiency of pore formation is not fully understood. However, cholesterol is known to abolish a gel phase that saturated SMs could form in an unsaturated phospholipid bilayer in the absence of cholesterol. In so doing, cholesterol increases diffusion in the SM-rich domain but decreases diffusion in the unsaturated phospholipid domain.[20,21] Palmitoyl ceramide,

Received: January 22, 2016
Revised: March 15, 2016
Published: March 22, 2016

DOI: 10.1021/acs.langmuir.6b00082
Langmuir 2016, 32, 3476−3484

which interacts strongly with SM, induces gel-phase formation[22] and is known to abolish StnII-induced pore formation.[18]

SM has functional groups that are both acceptors and donors for hydrogen bonds, and many of its bilayer properties (e.g., interaction with other colipids) are affected by hydrogen bonding.[23] Intermolecular hydrogen bonding originating from the 2NH function of the sphingoid base is suggested to result in clustering of SMs in the bilayer phase.[24] Intramolecular hydrogen bonding involving the 3OH of the sphingoid base and phosphate oxygens of the phosphocholine headgroup is prevalent and is likely to regulate headgroup dynamics and orientation in SM.[25,26] The formation of StnII pores was abolished when hydrogen bonding from 2NH and 3OH was prevented by methylation.[17] This result was interpreted to be due to decreased binding of the toxin to methylated SM analogues. However, it is possible that intermolecular hydrogen bonding among SMs also may affect how pores are formed.

In this study, we examined how SM chain length and degree of unsaturation affected StnII-induced pore formation, as determined from the increased bilayer permeability to calcein. We also modulated the temperature and measured the resulting changes in the bilayer order and phase states, and we assessed the effects on pore formation by StnII. StnII-induced pore formation in the presence of different sterols was also determined, with the aim to elucidate possible structure/function correlations. Finally, we varied the degree of unsaturation of the phosphatidylcholines (PCs) used in the SM-containing bilayers, in order to determine the effects of mono- and polyunsaturation in bilayer lipids on StnII-induced pore formation. Our main findings suggest that the formation of StnII pores was most efficient in unsaturated SM bilayers, and the rate decreased with the length of the saturated chain length in SM. StnII binding and the pore-formation process appeared to require free clusters of SM, as a stoichiometric mixture of palmitoyl SM (16:0-SM) and dimyristoyl-PC (DMPC) in the 1-palmitoyl-2-oleoyl-*sn*-glycero-3-phosphocholine (POPC) bilayer failed to support pore formation. Interfacial hydrogen bonding appeared to greatly affect StnII-induced pore formation, as both sterols and benzyl alcohol unspecifically enhanced the process. We conclude that the physical state of bilayer lipids greatly affected pore formation by StnII. Phase boundaries were not required for pore formation, although SM in a gel state prevented pore formation.

2. MATERIALS AND METHODS

2.1. Materials. Calcein and benzyl alcohol (BA) were obtained from Sigma-Aldrich (St. Louis, MO). POPC, 1-palmitoyl-2-linoleoyl-*sn*-glycero-3-phosphocholine (PLPC), 1-palmitoyl-2-arachidonoyl-*sn*-glycero-3-phosphocholine (PAPC), and 1,2-dimyristoyl-*sn*-glycero-3-phosphocholine (DMPC) were obtained from Avanti Polar Lipids (Alabaster, AL). 16:0-SM and *N*-stearoyl-D-*erythro*-sphingomyelin (18:0-SM) were purified from egg and brain SM, respectively, using preparative high-performance liquid chromatography (HPLC) and elution with methanol. *N*-myristoyl-D-*erythro*-sphingomyelin (14:0-SM), *N*-lignoceroyl-D-*erythro*-sphingomyelin (24:0-SM), and *N*-oleoyl-D-*erythro*-sphingomyelin (18:1-SM) were synthesized from 14:0, 24:0, and 18:1 fatty acids, respectively, and lyso SM (Avanti Polar Lipids), with *N*,*N*′-dicyclohexylcarbodiimide (Sigma-Aldrich) as catalyst. *N*-C10-pyrene-D-*erythro*-sphingomyelin (Pyr-SM) was a gift from Dr. Pentti Somerharju (University of Helsinki). The sterols used (see Figure S1 for structures; cholesterol, 7-dehydrocholesterol, dihydrocholesterol, ergosterol, lathosterol (cholest-7-en-3β-ol), desmosterol, allocholesterol (cholest-4-en-3β-ol), and cholest-8(14)-en-3β-ol) were from Sigma-Aldrich or Steraloids (Newport, RI). *trans*-Parinaric acid (tPA) was prepared from α-linolenic acid, as described previously.[27]

2.2. Calcein release from LUVs. Calcein-entrapped large unilamellar vesicles (LUVs) were prepared with the indicated lipid compositions by extrusion through 200 nm filters at 60 °C. The glycerophospholipid content was 80 mol %, while the SM content was 20 mol %, unless otherwise indicated. The LUV compositions are indicated in each figure. The detailed method for preparation of calcein-entrapped LUVs has been previously described.[17] The buffer used was Tris buffer (10 mM Tris, 140 mM NaCl, pH 7.4) containing calcein at 100 mM. The LUVs were used for permeabilization studies within 8 h. The concentrations of LUV and StnII during the calcein-leakage experiments were 2.5 μM and 20 nM, respectively, unless otherwise indicated. Emission at 550 nm was followed at 23 °C as a function of time (the excitation wavelength was 480 nm). Fluorescence emission was measured in a PTI Quanta-Master spectrofluorimeter (Photon Technology International, Inc., Birmingham, NJ). The released fraction of calcein was determined based on the maximum calcein release that was induced by LUV disintegration using 10% Triton X-100. To ensure that no spontaneous leakage occurred, the emission was measured for each sample for 3−5 min before the toxin was added. A steady signal level, indicating intact vesicles, was observed for all samples. When benzoyl alcohol was used, it was added to preformed LUVs 30 min before the experiments were initiated.

2.3. Fluorescence lifetime analysis. For time-resolved fluorescence analysis of tPA, multilamellar vesicles were prepared with the indicated lipid compositions, in Tris buffer (50 mM Tris pH 7.4, 140 mM NaCl). The final lipid concentration was 0.1 mM, with tPA included at 1 mol %. The lifetime measurements were performed using a FluoTime 200 instrument (PicoQuant Gmb, Berlin, Germany) operated at 23 °C. The tPA was excited with a PLS LED laser with a maximum signal at 298 nm, and the emission was collected at 405 nm. The fluorescence decays were analyzed using FluoFit Pro software (PicoQuant Gmb).

2.4. Measurement of the excimer/monomer ratio of Pyr-SM in bilayer systems. For measurement of the excimer/monomer (E/M) ratio of Pyr-SM, the following setup was used: POPC LUVS were prepared to contain 6 mol % Pyr-SM. At 23 °C, the E/M ratio was determined as a function of time, after StnII was added (final lipid/StnII molar ratio 10:1). Pyr-SM was excited at 345 nm; the monomer emission was read at 392, and the excimer emission was read at 480.

2.5. Surface plasmon resonance measurements. The association of StnII with lipid bilayers on coated gold chips was examined as described previously.[17] Briefly, LUVs were prepared with the indicated lipid composition in Tris buffer by extrusion through 100 nm polycarbonate filters at 60 °C. StnII binding to the coated bilayers was studied at 23 °C with a BioNavis SPR Navi 200 instrument (BioNavis Ltd., Tampere, Finland). The sensor gold chip was coated with a carboxymethylated dextran layer that had been treated with *N*-hydroxysuccinimide and *N*-ethyl-*N*′(dimethylaminopropyl) carbodiimide to activate the surface for capturing phospholipid membranes. All solutions used for surface plasmon resonance (SPR) were filtered through 0.2 μm membrane filters and degassed with bath sonication before use. The running buffer was 10 mM Tris, 140 mM NaCl, pH 7.4, and the flow rate was 5 μL/min. First, the chip surface was cleaned with two injections of 10 mM 3-[(3-cholamidopropyl)-dimethylammonio]-1-propanesulfonate (CHAPS). Then extruded LUVs (0.5 mM lipid concentration) were applied on the surface (10 min injection), and unbound vesicles were removed by one (2 min) injection of 50 mM NaOH. Bovine serum albumin (0.1 mg/mL, 2 min injection) was used to verify that the chip did not have uncovered areas. Finally, StnII (1.0 μM) was applied for 10 min, after which buffer alone was injected for 2 min to study toxin dissociation. The chip was regenerated with CHAPS as in the beginning of the experiment.

DOI: 10.1021/acs.langmuir.6b00082
Langmuir 2016, 32, 3476−3484

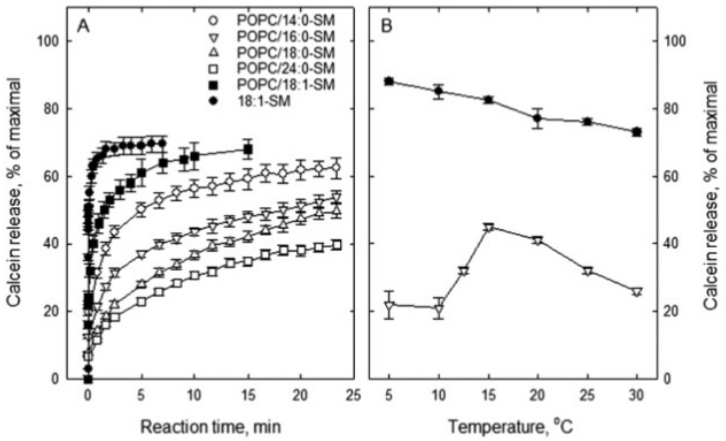

Figure 1. StnII-induced calcein release from LUVs of different compositions ((A) POPC/saturated SM 4:1, POPC/unsaturated SM 4:1, or pure 18:1-SM) and temperature dependence (B) on StnII-induced calcein release from 18:1-SM or POPC/16:0-SM (4:1) LUVs. Calcein release was determined at 23 °C (A) or at the indicated temperature (B). Symbols for (A) also apply to (B) (two compositions). The lipid/StnII molar ratio was about 125:1. Each value is the average ± SEM from $n = 2$.

3. RESULTS

3.1. SM chain length and phase behavior affect StnII-induced calcein release. To study how chain length and unsaturation in SM affected StnII-induced pore formation, as determined from increased bilayer permeability to calcein, we prepared bilayers with 80 mol % POPC and 20 mol % saturated SM chain length analogues. Such bilayers are mostly disordered, but as the SM saturated chain length increases, so does the bilayer order (in the SM-rich phase, when analyzed at constant temperature). When 18:1-SM was examined, the bilayers contained either POPC/18:1-SM (4:1) or pure 18:1-SM. In both cases, the bilayers were completely devoid of a gel phase (data not shown). Order in the SM-rich phase was determined from the lifetime analysis of tPA fluorescence, as this fatty acid preferentially partitions into ordered domains, and its excited-state lifetime is greatly affected by lipid packing and order in its vicinity.[28]

StnII-induced pore formation is greatly affected by the lipid/StnII ratio, and we normally used a fairly low ratio of 125:1 to avoid being close to the saturation levels of StnII. For bilayers with POPC and saturated SM chain length analogues, the StnII-induced calcein release became slower and less efficient (lower maximum calcein release %) as the SM chain length increased (Figure 1A). When the phase state of the SM-rich domain was assessed from the lifetime analysis of tPA (Table 1), it was evident that 14:0-SM and 16:0-SM at this concentration and temperature were fluid (or disordered). With 18:0-SM, the average lifetime was low, suggesting the absence of the gel phase, although the longest lifetime component of tPA had increased (indicative of some formation of an increasingly ordered phase[29]). With 24:0-SM, the average and the longest lifetime component of tPA were markedly increased, suggesting that 24:0-SM was at least in part present as an ordered, gel-like phase in the POPC bilayer. However, we do not imply that the 24:0-SM gel phase present in the POPC bilayer was a pure SM gel phase, as a much more elaborate analysis would be required to reach such conclusions. With monounsaturated 18:1-SM (both POPC/18:1-SM 4:1 and pure 18:1-SM), the StnII-induced calcein release was more rapid and efficient than seen with the saturated SM bilayers (Figure 1A). Further, calcein release was more efficient from pure 18:1-SM bilayers when compared to POPC/18:1-SM 4:1 bilayers (Figure 1A). These observations regarding acyl chain effects on StnII-induced pore formation suggest that differences in the lateral packing of the SM-rich domain were more influential in regulating StnII oligomerization and pore formation than the phase state was per se.

Table 1. Fluorescence Lifetime Analysis of tPA in POPC/SM Bilayers at 23 °C[a]

	τ_{AVG}	τ_{LC}
POPC/14:0-SM	6.1 ± 0.1	9.9 ± 1.0
POPC/16:0-SM	6.9 ± 02	9.5 ± 0.2
POPC/18:0-SM	8.2 ± 0.2	32.1 ± 3.8
POPC/24:0-SM	39.4 ± 0.1	58.7 ± 0.5
POPC/18:1-SM	5.5 ± 0.1	7.2 ± 0.1

[a]SMs with different acyl chain lengths were mixed with POPC (1:4 molar ratio) in multilamellar vesicles that contained 1 mol % tPA. The average lifetime (τ_{AVG} ± SD) and the longest lifetime component (τ_{LC} ± SD) are given ($n = 3$).

Next, we assessed the effect of temperature on StnII-induced pore formation and bilayer permeabilization. Using pure 18:1-SM vesicles, we observed that the maximum calcein release increased with decreasing temperature (Figure 1B). With the 16:0-SM in POPC, calcein release also increased with decreasing temperature, but below 15 °C, 16:0-SM formed a gel phase in the POPC bilayer and the StnII-induced calcein release was clearly attenuated. The gel-phase formation by 16:0-SM in POPC was ascertained from the markedly increased average and longest component lifetimes of tPA fluorescence, as the temperature was decreased below 15 °C (Figure S2). The finding that the calcein release % did not decrease to zero even when *N*-palmitoyl-D-*erythro*-sphingomyelin (PSM) was in the gel phase (Figure 1B) suggests that spontaneous leakage was responsible for the limited calcein release below 10 °C.

3.2. Effect of SM concentration on calcein release. To more closely study how the concentration of 16:0-SM in POPC affected StnII-induced calcein release, we measured calcein release at 23 °C as a function of the 16:0-SM concentration in the POPC bilayer (Figure 2A, black line). As shown in the

DOI: 10.1021/acs.langmuir.6b00082

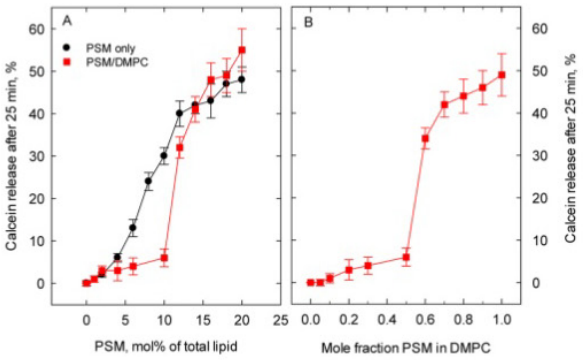

Figure 2. StnII-induced calcein release from LUVs of the indicated compositions. (A) Concentration of 16:0-SM in POPC was varied as indicated (black circles). (B) POPC content was 80 mol %, and the saturated phospholipid (DMPC + 16:0-SM) concentration was 20 mol %. However, the proportion of 16:0-SM/DMPC was varied in increments from all DMPC to all 16:0-SM as indicated on the bottom axis. The calcein release data (16:0-SM + DMPC) are also shown in (A) as red squares, as a function of 16:0-SM mol %. The lipid/StnII molar ratio was about 125:1. The experimental temperature was 23 °C. Each value is the average ± SEM from n = 2−3.

graph, the maximum calcein release (at 25 min after StnII was added) increased linearly with the 16:0-SM concentration from 2 mol % up to about 12 mol %, while the increase was less steep above this 16:0-SM level. It was observed that only about 2−3 mol % 16:0-SM was needed for StnII to cause calcein leakage (Figure 2A). The effect of SM concentration on actinoporin pore-formation efficiency has been addressed previously with mixed acyl-chain SMs.[8]

We have previously shown that 16:0-SM doped with 16:0-ceramide does not support StnII-induced pore formation.[18] It was assumed that 16:0-SM and the ceramide formed a tightly packed gel phase, which did not allow SM to participate with StnII in the oligomerization process, resulting in functional pores. We examined how doping of 16:0-SM with DMPC affected the capacity of SM to help StnII oligomerize and form pores that let calcein pass over the bilayer. DMPC was selected because it displays near-ideal miscibility with 16:0-SM. DMPC also does not induce gel-phase formation, as the gel−liquid crystalline phase transition temperature (T_m) of DMPC is ∼24 °C,[30] much lower than the T_m of ∼41 °C reported for 16:0-SM.[31] Interestingly, the concentration-corrected maximum calcein release induced by 16:0-SM was markedly attenuated up to ∼14 mol % 16:0-SM, if the bilayer also contained DMPC (Figure 2A). Looking at the ratio of 16:0-SM to DMPC, one can observe that if DMPC was in molar excess over 16:0-SM, it apparently hindered SM to participate efficiently in the StnII-induced pore-formation process (Figure 2B). When 16:0-SM was in molar excess relative to DMPC, it again became effective in supporting pore formation by StnII. Note that the proportions of POPC and saturated SM or saturated SM/PC were always equal in Figure 2A. These results show that, in molar excess, DMPC can mask SM and hinder it to activate StnII-induced pore formation. This effect was lost as soon as SM was in molar excess relative to DMPC. The results could indicate that StnII needs clusters of adjacent SMs in order to efficiently oligomerize and form pores; such SM clusters are not present in DMPC/16:0-SM alloys when 16:0-SM is not in molar excess over DMPC.

3.3. Pyrene excimer/monomer ratio during StnII-induced pore formation. To further examine the interaction between StnII and individual SM molecules, we examined how clustering or declustering of SM was affected by StnII. Clustering of SM was determined using Pyr-SM molecules. When the pyrenyl groups of two adjacent SM molecules are close to each other (within a few Å), they can form an excited-state dimer during excitation, and the emission from this excimer is red-shifted relative to the monomeric excited state.[32] Excimer fluorescence emission, therefore, is of diagnostic value when assessing molecular interaction in membranes. When POPC LUVs containing 6 mol % Pyr-SM were exposed to StnII (final lipid/StnII molar ratio 10:1) at 23 °C, and the effect on the Pyr-SM E/M ratio was measured (Figure 3), the E/M

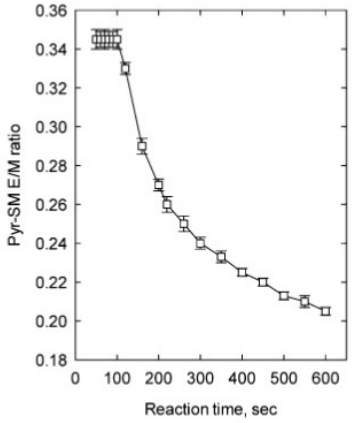

Figure 3. Excimer/monomer emission of Pyr-SM. Multilamellar vesicles were prepared from LUVs containing POPC with 6 mol % Pyr-SM. The E/M ratio of Pyr-SM is shown as a function of time at 23 °C, following the addition of StnII at time 100 s. The lipid/StnII ratio was 10:1. Each value is average ± SEM from n = 2.

ratio decreased as a function of time. The kinetics for the decrease in E/M ratio was similar to that observed for typical kinetics of StnII pore formation in bilayers with saturated SMs. This result suggests that StnII-induced pore formation leads to the extraction of Pyr-SM molecules from the Pyr-SM-rich domain, thus decreasing the likelihood of the Pyr-SM/Pyr-SM interaction resulting in excimers. One can presume that Pyr-SM was extracted from the Pyr-SM domain into the pore structure itself, where the Pyr-SMs were not close enough to each other to cause excimer formation.

3.4. Modulation of interfacial properties by benzyl alcohol. Benzyl alcohol (BA) is a hydrogen-bonding small molecule with an affinity for bilayer interfaces.[33] We have previously used BA to attenuate interlipid interactions in SM-containing domains in unsaturated phosphatidylcholine bilayers.[34] We now show that the addition of BA (5 mM) to LUVs prepared from POPC and 16:0-SM (4:1 molar ratio) dramatically increased kinetics and moderately increased the extent of the maximum calcein release (Figure 4), when BA-treated LUVs were exposed to StnII (20 nM). BA itself had no effect on spontaneous calcein leakage, and BA did not stimulate calcein release in POPC LUVs exposed to StnII (Figure 4). Although the main site of action of BA is at the bilayer interface, BA also affects acyl chain order as determined from diphenylhexatriene (DPH) anisotropy. However, the small change in the acyl chain order is not likely to explain the huge

DOI: 10.1021/acs.langmuir.6b00082

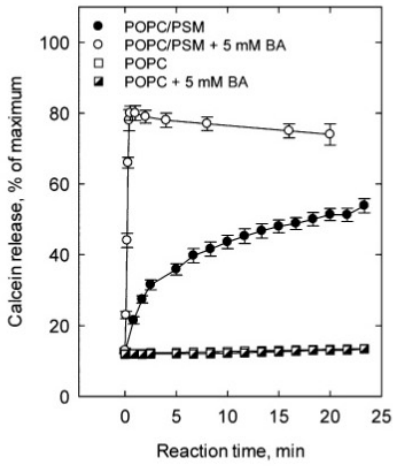

Figure 4. StnII-induced calcein release from LUVs at the indicated compositions. The LUVs contained either 100 mol % POPC or 80 mol % POPC and 20 mol % 16:0-SM. Some LUVs were exposed to 5 mM benzyl alcohol 30 min prior to treatment with StnII. The experimental temperature was 23 °C. The lipid/StnII molar ratio was about 125:1. Each value is the average ± SEM from n = 3. DPH anisotropy at 23 °C was 0.149 ± 0.003 in the POPC/16:0-SM bilayers and 0.115 ± 0.014 in the POPC/16:0-SM bilayers with 5 mM BA. The difference in anisotropy is statistically significant ($P < 0.001$).

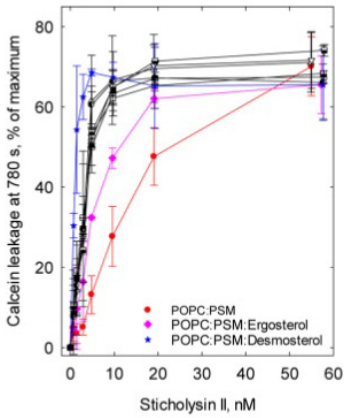

Figure 5. Sterol-enhanced calcein release in LUVs exposed to increasing concentrations of StnII. Calcein-entrapped LUVs, prepared from POPC/16:0-SM/sterol (4:1:0.5 by mole), were exposed to the indicated final concentrations of StnII, and the extent of calcein release after 13 min was determined. Each value is average ± SEM from n = 2. Symbols: red filled circle, POPC/PSM 4:1; open triangle (up), POPC/PSM with cholesterol; open triangle (down), with 7-dehydrocholesterol; open square, with dihydrocholesterol; pink filled diamond, with ergosterol; black/white circle, with lathosterol; blue filled star, with desmosterol; diagonally filled square, with allocholesterol; horizontally filled square, with 8(14)-cholesten-3β-ol.

activation of StnII pore formation. Instead, we assume that BA in the SM bilayers interfered with intermolecular hydrogen bonding among the SMs and that binding of StnII monomers to bilayers or the pore-formation process itself responded to such changes in intermolecular hydrogen bonding.

3.5. Effect of sterols on StnII-induced calcein release. Cholesterol is known to enhance pore formation by StnII.[8,35,36] We wanted to explore whether sterol activation of StnII-induced pore formation was specific relative to the structure of the sterol used or a more unspecific effect. We used 7 different sterols in addition to cholesterol (see Figure S1 for the structures). All sterols had a 3β hydroxyl group. As shown in Figure 5, when the LUVs prepared from POPC/16:0-SM (4:1) or POPC/16:0-SM/sterol (4:1:0.5 molar ratio) were exposed to increasing concentrations of StnII, all sterols enhanced calcein release (determined at 13 min after the toxin was added) relative to the control (no sterol added). Only two sterols stand out, ergosterol (blue line) and desmosterol (pink line). Ergosterol was slightly less effective than the other sterols, while desmosterol was most effective at low StnII concentrations. When the sterol effect was compared at the constant StnII concentration (10 nM) and at 100 s after the toxin was added, we observed that ergosterol again was less efficient than the other sterols (Figure 6A), but also 4-cholesten-3β-ol showed lower calcein-release activation than the other sterols. Desmosterol showed the highest activation of calcein release (Figure 6A).

To demonstrate a possible correlation between the sterol's capacity to enhance StnII-induced calcein release and the sterol's capacity to interact with the SM-rich phase, we performed tPA fluorescence lifetime analysis of the various LUV bilayers. If the tPA average lifetime becomes longer after the sterol is added (relative to the sterol-free control), one can conclude that the degree of order in the SM-rich domain was increased. From such an increase, one can infer that the sterol interacted with 16:0-SM in the bilayer. As shown in Figure 6B, all sterols tested increased the observable tPA average lifetime (from about 6 ns in control LUVs) to about 8−9 ns in the sterol-containing LUVs. Two sterols appeared to increase the tPA lifetime more than the others: dihydrocholesterol and lathosterol. Desmosterol, which activated StnII-induced calcein release the most, did not stand out when interaction with SM was assessed with tPA fluorescence lifetime analysis. We conclude that the effects of the sterols on StnII-induced calcein release, and their interactions with 16:0-SM in the LUVs, did not show a meaningful correlation between calcein release and sterol-induced bilayer ordering (Figure 6C). Therefore, it is possible that the sterol effect on StnII-induced calcein release is mediated via sterol-induced changes in the intermolecular hydrogen-bonding pattern among the SMs (comparable to the BA effect).

3.6. StnII interaction with 16:0-SM embedded in increasingly unsaturated PC bilayers. The properties of SM in a complex bilayer are likely to also be affected by the nature of the more unsaturated phospholipids in the bilayer.[29] This means that the StnII membrane binding and pore-formation process is likely to be affected by membrane lipids other than SM and cholesterol. Therefore, we examined how the degree of unsaturation among the PCs in the bilayer affected StnII-induced calcein release (Figure 7A) or StnII binding and pore formation, as determined with surface plasmon resonance on bilayers prepared from increasingly unsaturated PCs and 16:0-SM (Figure 7B). As observed for calcein release, StnII pore formation appeared to be much enhanced when 16:0-SM was dissolved in LUVs with two (PLPC) or four (PAPC) cis double bonds in the *sn*-2 acyl chain, compared to the POPC LUVs (Figure 7A). Qualitatively similar results were observed with SPR on supported bilayers made from 16:0-SM and POPC, PLPC, or PAPC (Figure 7B). These results show that the nature of the unsaturated

DOI: 10.1021/acs.langmuir.6b00082

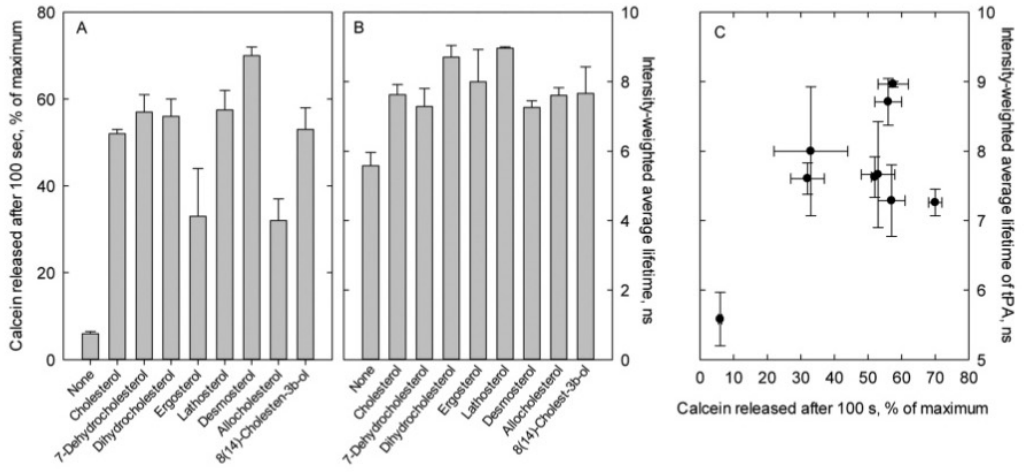

Figure 6. Effect of sterols on StnII-induced calcein release (A) and the average fluorescence lifetime of tPA (B). (C) Calcein release after 100 s (% of maximum, from (A)) plotted against the average tPA lifetime (ns, data from (B)). LUVs were prepared from POPC/16:0-SM/sterol (4:1:0.5 by mole) and contained entrapped calcein (A) or 1 mol % tPA (B). StnII was added to a final concentration of 20 nM (A), and calcein release after 100 s was determined. For (B), tPA fluorescence lifetime analysis was performed (with no addition of StnII). Values are average ± SEM from $n = 2–3$.

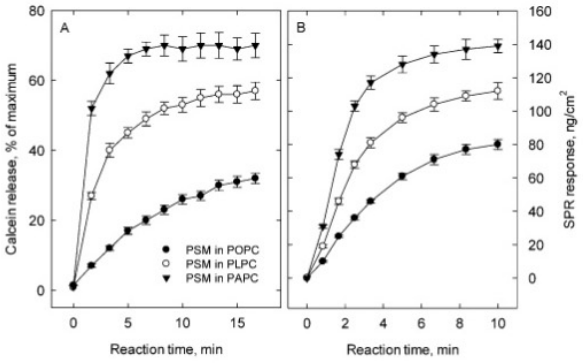

Figure 7. StnII interaction with PSM in mono- or polyunsaturated phosphatidylcholine bilayers. StnII-induced calcein release from LUVs of the indicated compositions is shown in (A). The LUVs were prepared to contain 80 mol % of the indicated unsaturated PC and 20 mol % of 16:0-SM. The lipid/StnII molar ratio was about 125:1. The experimental temperature was 23 °C. Each value is the average ± SEM from $n = 2$. (B) SPR sensogram of StnII association with supported bilayers prepared to the indicated lipid compositions. The experimental temperature was 23 °C. Each value is the average ± SEM from $n = 2–3$.

phosphatidylcholines affected StnII-induced pore formation, either via effects on 16:0-SM properties or via direct effects on the StnII oligomerization and pore-formation process independent of 16:0-SM.

4. DISCUSSION

We have addressed how bilayer acyl chain order and phase state, SM concentration, and interfacial hydrogen-bonding interactions, as well as sterols, affected pore formation and calcein leakage induced by the SM binding toxin StnII. In several previous reports concerning phase states and the effect of lateral domain boundaries on actinoporin-induced pore formation and bilayer permeabilization, it has been observed that phase boundaries may enhance pore formation[37,38] and sometimes even be required.[39] Although we do not question the results of previous reports, our results with StnII pore formation in 18:1-SM bilayers clearly show that at least StnII does not require phase boundaries for pore formation. The pore-formation process was most rapid and efficient in the 18:1-SM bilayers when compared to the POPC/saturated SM bilayers (Figure 1A). When the length of the saturated SM acyl chains was varied from 14 to 24 carbons, pore formation by StnII became increasingly difficult as the SM chain length increased. StnII probably did not react directly to the SM chain length, because StnII mainly binds to the interfacial parts of the SM molecule.[17] However, as the SM chain length increased, so did the acyl chain order (Table 1), and when acyl chain order increases, lateral packing usually becomes closer.[40] Closer lateral packing increases van der Waals interactions among the acyl chain, and the strengths of intermolecular hydrogen bonding also increase, as the strength of hydrogen bonding is also distance-dependent.[41] Hydrogen bonding is an important stabilizing force among SMs.[42] Stronger intermolecular hydrogen bonding would probably make pore formation by StnII (and other actinoporins) slower or more difficult, which is what we observed.

Variation in temperature can also affect phase states and lateral order in bilayer membranes. In the case of the 18:1-SM bilayers, the gel−liquid crystalline phase transition temperature was well below 0 °C (unpublished observations), which means that the 18:1-SM bilayers were fluid in all our experiments. However, as the temperature was decreased from 30 to 5 °C (Figure 1B), the acyl chain order increased.[43] Despite this increased acyl chain ordering, StnII-induced pore formation became slightly more efficient as the temperature was decreased. A similar temperature effect has been reported for pore formation by EqtII.[37] Apparently, the oligomerization process and/or final pore structure was stabilized by lowering the temperature, suggesting that hydrogen bonding among amino acid residues in the toxins could be an important cohesive and stabilizing force for the pore. In the case of the POPC/16:0-SM bilayers, decreasing temperature initially enhanced pore formation, but below 15 °C, a gel phase was formed (Figure S2); consequently, pore formation was attenuated (Figure 1B). Previously, we showed that palmitoyl

DOI: 10.1021/acs.langmuir.6b00082

ceramide turns 16:0-SM into a gel phase and completely inhibits StnI-induced pore formation,[18] even when the temperature was not altered.

The importance of SM for toxin binding to bilayers is well recognized. We observed that the extent of calcein release correlated almost linearly with the amount of 16:0-SM present in the POPC bilayer, up to the tested maximum level of 20 mol % (Figure 2A). Similar effects of SM concentration on bilayer permeabilization by actinoporins have been reported.[8] Interestingly, when the 16:0-SM was "complexed" with DMPC, the 16:0-SM lost most of its capacity to enhance pore formation by StnII (Figure 2). It is known that 16:0-SM and DMPC are almost ideally miscible, because of closely matching acyl chain length.[30] Only when the 16:0-SM was present in molar excess over DMPC did it regain its effect on pore formation by StnII. This finding may suggest that StnII needs clusters of 16:0-SM in order to form pores, as 16:0-SM was unlikely to be present as SM-SM clusters below a 1:1 stoichiometry with DMPC, due to the highly ideal mutual miscibility with DMPC. Above 1:1 stoichiometry, SM-SM clusters should become more prevalent. It has previously been suggested that, whereas actinoporins can bind to dispersed SM, lysenin requires clusters of SM before binding occurs.[5,44] Clusters would be assemblies of fewer than 10 SM molecules.[44] Maybe sticholysins also prefer SM clusters as interaction partners in target membranes?

In the absence of other saturated phospholipids, SM is known to cluster in unsaturated POPC bilayers. Our results with Pyr-SM also show clustering, which is evidenced by the formation of excited-state dimers in the POPC bilayers when Pyr-SM was present at 6 mol % (Figure 3).[45] For excited-state dimers to form, the pyrenoyl rings in the *N*-linked SM acyl chains must be in close proximity (within a few Å). During the exposure of POPC/Pyr-SM bilayers to StnII, the E/M ratio of Pyr-SM decreased with the kinetics resembling the pore-formation process (Figure 3B). This finding proves that SM-SM clusters existed in the POPC/Pyr-SM bilayers before StnII was added, as their proportion decreased after exposure to StnII. The finding also suggests that Pyr-SM was incorporated into the forming pore at locations that were further apart than was the case with SM-SM clusters. The recent structure of the FraC pore suggests that SMs occupy discrete sites along the rim of the pore.[16] Although the StnII pore may not be identical to the FraC pore, a similar distribution of bound SM around the pore structure is very likely. If that is the case, Pyr-SM would have occupied sites that either were not close in distance (a few Å) or had Pyr-SM oriented in a way such that the pyrenoyl rings were not close enough to each other to form excimers.

It has been shown previously that fatty acid alcohols may enhance pore formation by EqtII.[46] We have observed that BA also efficiently enhances pore formation by actinoporins. The effect of BA (5 mM) on StnII pore formation in POPC/16:0-SM bilayers was dramatic (Figure 4), with almost immediate permeabilization of the bilayers when compared to pore formation kinetics in the absence of BA. BA by itself did not compromise the permeability of LUV bilayers in the absence of either SM or StnII. It is possible that BA interferes with intermolecular hydrogen bonding among the SMs, in a way that lowers the energy barrier for toxin monomer diffusion and pore formation. We further suggest that the enhancing effect of sterols on actinoporin pore formation is similarly due to effects on intermolecular SM hydrogen bonding. This conclusion is drawn because sterols enhance pore formation in a way that is not dramatically related to either the sterol structure or the capacity of the sterols to interact with SM in the POPC/16:0-SM bilayers (Figures 5 and 6). Sterols are known to enhance pore formation by actinoporins.[35,36,47] With EqtII, it was shown that ergosterol was slightly more effective than cholesterol to increase bilayer permeability after exposure of the vesicles to EqtII.[37] For StnII, we observed that ergosterol was slightly less efficient than cholesterol in enhancing calcein release (Figure 5). Ergosterol was also slightly less efficient than cholesterol in enhancing bilayer permeability in StnI-treated bilayers.[48] Surprisingly, even cholestenone (4-cholesten-3-one) enhanced actinoporin-induced bilayer permeabilization,[37,48] although cholestenone lacks the 3β-hydroxyl. Apparently, the hydrogen-bond-accepting property of the sterol oxygen (on cholestenone) was more important than the hydrogen-bond-accepting/donating capacity of the sterol 3β-OH.

Finally, we examined how the properties of the unsaturated PC affected StnII-induced pore formation and calcein release from LUVs. In cell membranes, StnII would be expected to encounter some polyunsaturated glycerophospholipids, and their effect on membrane binding and pore formation could be direct or via effects on SM. It was recently shown that SM miscibility in mono- and polyunsaturated PCs is good, although the acyl chain order in the SM-rich domains became increasingly ordered as the degree of unsaturation in the PCs increased.[29] Our results suggest that pore formation by StnII was significantly enhanced when the number of cis double bonds in the *sn*-2 acyl chain of 1-palmitoyl-2-X-PC increased from one to two, and finally to four (Figure 7). At the same time, the 16:0-SM could become increasingly ordered, as less and less of the increasingly unsaturated PC is miscible in the SM-rich domain.[29] However, the lifetime of tPA does not show increased order in PSM domains (at 20 mol % PSM in unsaturated PC bilayers) as the PC unsaturation increased.[29] Therefore, it appears that the polyunsaturated PCs by themselves directly promoted pore formation. This could result from facilitated lateral diffusion of toxin monomers in the increasingly unsaturated PC-rich domain or from other stabilizing effects of the unsaturated PCs on the pore structure itself.

In conclusion, we have demonstrated that, although StnII monomer binding to membranes needed SM, the subsequent monomer diffusion and eventual pore-formation process was markedly affected by lipid packing and the acyl chain order in general, and by interfacial hydrogen-bonding properties in the membranes. It further appeared that glycerophospholipid unsaturation had a large effect on the pore-formation process, as evidenced from the effects on the calcein permeabilization of the bilayers. It is possible that non-SM lipids in the bilayers have a profound influence on how rapidly or efficiently pores form and may also influence the final structure of the pores formed.

■ ASSOCIATED CONTENT

Supporting Information

The Supporting Information is available free of charge on the ACS Publications website at DOI: 10.1021/acs.langmuir.6b00082.

Scheme depicting the molecular structures of all lipids used in the study and figure showing gel-phase formation in POPC/16:0-SM bilayers as a function of temperature (PDF)

DOI: 10.1021/acs.langmuir.6b00082

AUTHOR INFORMATION

Corresponding Author
*jpslotte@abo.fi.

Notes
The authors declare no competing financial interest.

ACKNOWLEDGMENTS

We thank Ida Alm-Ndiaye and Victor Hautala for help with some experiments and Dr. Pentti Somerharju for the kind gift of Pyr-SM. The work was funded by generous grants from the Academy of Finland, the Sigrid Juselius Foundation, the Åbo Akademi Foundation to J.P.S., and BFU2012-32404 from the Spanish Ministerio de Ciencia e Innovación to J.G.G. and A.M.P. An FPU fellowship was granted to S.G.-L.

ABBREVIATIONS

14:0-SM – *N*-myristoyl-D-*erythro*-sphingomyelin; 16:0-SM – *N*-palmitoyl-D-*erythro*-sphingomyelin; 18:0-SM – *N*-stearoyl-D-*erythro*-sphingomyelin; 18:1-SM – *N*-oleoyl-D-*erythro*-sphingomyelin; 24:0-SM – *N*-lignoceryl-D-*erythro*-sphingomyelin; BA – benzyl alcohol; DMPC – 1,2-dimyristoyl-*sn*-glycero-3-phosphocholine; E/M ratio – excimer/monomer emission ratio; EqtII – equinatoxin II; FraC – fragaceatoxin; HPLC – high-performance liquid chromatography; LUV – large unilamellar vesicle; PAPC – 1-palmitoyl-2-arachidonyl-*sn*-glycero-3-phosphocholine; PLPC – 1-palmitoyl-2-linoleyl-*sn*-glycero-3-phosphocholine; POPC – 1-palmitoyl-2-oleoyl-*sn*-glycero-3-phosphocholine; 16:0-SM – *N*-palmitoyl-D-*erythro*-sphingomyelin; Pyr-SM – *N*-C10-pyrene-D-*erythro*-sphingomyelin; SM – sphingomyelin; SPR – surface plasmon resonance; StnII – sticholysin II; tPA – *trans*-parinaric acid

REFERENCES

(1) van Heyningen, S. Cholera Toxin: Interaction of Subunits with Ganglioside GM1. *Science* **1974**, *183*, 656−657.
(2) Bakrač, B.; Gutierrez-Aguirre, I.; Podlesek, Z.; Sonnen, A. F.; Gilbert, R. J.; Maček, P.; Lakey, J. H.; Anderluh, G. Molecular determinants of sphingomyelin specificity of a eukaryotic pore-forming toxin. *J. Biol. Chem.* **2008**, *283*, 18665−18677.
(3) Alegre-Cebollada, J.; Onaderra, M.; Gavilanes, J. G.; Martínez-del-Pozo, A. Sea anemone actinoporins: the transition from a folded soluble state to a functionally active membrane-bound oligomeric pore. *Curr. Protein Pept. Sci.* **2007**, *8*, 558−572.
(4) Bakrač, B.; Anderluh, G. Molecular mechanism of sphingomyelin-specific membrane binding and pore formation by actinoporins. *Adv. Exp. Med. Biol.* **2010**, *677*, 106−115.
(5) Rojko, N.; Dalla Serra, M.; Maček, P.; Anderluh, G. Pore formation by actinoporins, cytolysins from sea anemones. *Biochim. Biophys. Acta, Biomembr.* **2016**, *1858*, 446−456.
(6) Maček, P. Polypeptide cytolytic toxins from sea anemones (Actiniaria). *FEMS Microbiol. Lett.* **1992**, *5*, 121−129.
(7) Anderluh, G.; Maček, P. Cytolytic peptide and protein toxins from sea anemones (*Anthozoa: Actiniaria*). *Toxicon* **2002**, *40*, 111−124.
(8) De Los Ríos, V.; Mancheño, J. M.; Lanio, M. E.; Oñaderra, M.; Gavilanes, J. G. Mechanism of the leakage induced on lipid model membranes by the hemolytic protein sticholysin II from the sea anemone *Stichodactyla helianthus*. *Eur. J. Biochem.* **1998**, *252*, 284−289.
(9) Tejuca, M.; Dalla Serra, M.; Ferreras, M.; Lanio, M. E.; Menestrina, G. Mechanism of membrane permeabilization by sticholysin I, a cytolysin isolated from the venom of the sea anemone *Stichodactyla helianthus*. *Biochemistry* **1996**, *35*, 14947−14957.
(10) Ferlan, I.; Lebez, D. Equinatoxin, a lethan protein from *Actinia equina* - purification and characterization. *Toxicon* **1974**, *12*, 57−61.
(11) Mechaly, A. E.; Bellomio, A.; Morante, K.; González-Mañas, J. M.; Guérin, D. M. Crystallization and preliminary crystallographic analysis of fragaceatoxin C, a pore-forming toxin from sea anemone. *Acta Crystallogr., Sect. F: Struct. Biol. Cryst. Commun.* **2009**, *65*, 357−360.
(12) Sekizawa, Y.; Kubo, T.; Kobayashi, H.; Nakajima, T.; Natori, S. Molecular cloning of cDNA for lysenin, a novel protein in the earthworm Eisenia foetida that causes contraction of rat vascular smooth muscle. *Gene* **1997**, *191*, 97−102.
(13) Ros, U.; García-Sáez, A. J. More Than a Pore: The Interplay of Pore-Forming Proteins and Lipid Membranes. *J. Membr. Biol.* **2015**, *248*, 545−561.
(14) Mancheño, J. M.; Martin-Benito, J.; Martinez-Ripoll, M.; Gavilanes, J. G.; Hermoso, J. A. Crystal and electron microscopy structures of sticholysin II actinoporin reveal insights into the mechanism of membrane pore formation. *Structure* **2003**, *11*, 1319−1328.
(15) Rojko, N.; Cronin, B.; Danial, J. S.; Baker, M. A.; Anderluh, G.; Wallace, M. I. Imaging the lipid-phase-dependent pore formation of equinatoxin II in droplets interface bilayer. *Biophys. J.* **2014**, *106*, 1630−1637.
(16) Tanaka, K.; Caaveiro, J. M.; Morante, K.; Gonzalez- Mañas, J. M.; Tsumoto, K. Structural basis for self-assembly of a cytolytic pore lined by protein and lipid. *Nat. Commun.* **2015**, *6*, 6337.
(17) Maula, T.; Isaksson, Y. J. E.; García-Linares, S.; Niinivehmas, S.; Pentikainen, O. T.; Kurita, M.; Yamaguchi, S.; Yamamoto, T.; Katsumura, S.; Gavilanes, J. G.; Martínez-del-Pozo, A.; Slotte, J. P. 2NH and 3OH are crucial strctural requirements in sphingomyelin for sticholysin II binding and pore formation in bilayer membranes. *Biochim. Biophys. Acta, Biomembr.* **2013**, *1828*, 1390−1395.
(18) Alm, I.; García-Linares, S.; Gavilanes, J. G.; Martínez-del-Pozo, A.; Slotte, J. P. Cholesterol stimulates and ceramide inhibits Sticholysin II-induced pore formation in complex bilayer membranes. *Biochim. Biophys. Acta, Biomembr.* **2015**, *1848*, 925−931.
(19) Islam, M. Z.; Alam, J. M.; Tamba, Y.; Karal, M. A.; Yamazaki, M. The single GUV method for revealing the function of antimicrobial, pore-forming toxin, and cell-penetrating peptides or proteins. *Phys. Chem. Chem. Phys.* **2014**, *16*, 15752−15767.
(20) Filippov, A.; Oradd, G.; Lindblom, G. Lipid lateral diffusion in ordered and disordered phases in raft mixtures. *Biophys. J.* **2004**, *86*, 891−896.
(21) Lindblom, G.; Oradd, G.; Filippov, A. Lipid lateral diffusion in bilayers with phosphatidylcholine, sphingomyelin, and cholesterol. An NMR study of dynamics and lateral phase separation. *Chem. Phys. Lipids* **2006**, *141*, 179−184.
(22) Silva, L.; de Almeida, R. F.; Fedorov, A.; Matos, A. P.; Prieto, M. Ceramide-platform formation and − induced biophysical changes in a fluid phospholipid membrane. *Mol. Membr. Biol.* **2006**, *23*, 137−148.
(23) Barenholz, Y.; Thompson, T. E. Sphingomyelins in bilayers and biological membranes. *Biochim. Biophys. Acta, Biomembr.* **1980**, *604*, 129−158.
(24) Mombelli, E.; Morris, R.; Taylor, W.; Fraternali, F. Hydrogen-bonding propensities of sphingomyelin in solution and in a bilayer assembly: a molecular dynamics study. *Biophys. J.* **2003**, *84*, 1507−1517.
(25) Ferguson-Yankey, S. R.; Borchman, D.; Taylor, K. G.; DuPre, D. B.; Yappert, M. C. Conformational studies of sphingolipids by NMR spectroscopy. I. Dihydrosphingomyelin. *Biochim. Biophys. Acta, Biomembr.* **2000**, *1467*, 307−25.
(26) Talbott, C. M.; Vorobyov, I.; Borchman, D.; Taylor, K. G.; DuPre, D. B.; Yappert, M. C. Conformational studies of sphingolipids by NMR spectroscopy. II. Sphingomyelin. *Biochim. Biophys. Acta, Biomembr.* **2000**, *1467*, 326−37.
(27) Kuklev, D. V.; Smith, W. L. Synthesis of four isomers of parinaric acid. *Chem. Phys. Lipids* **2004**, *131*, 215−222.

DOI: 10.1021/acs.langmuir.6b00082

(28) Sklar, L. A.; Hudson, B. S.; Simoni, R. D. Conjugated polyene fatty acids as fluorescent probes: synthetic phospholipid membrane studies. *Biochemistry* **1977**, *16*, 819−828.
(29) Kullberg, A.; Ekholm, O. O.; Slotte, J. P. Miscibility of Sphingomyelins and Phosphatidylcholines in Unsaturated Phosphatidylcholine Bilayers. *Biophys. J.* **2015**, *109*, 1907−1916.
(30) Terova, B.; Slotte, J. P.; Nyholm, T. K. Miscibility of acyl-chain defined phosphatidylcholines with N-palmitoyl sphingomyelin in bilayer membranes. *Biochim. Biophys. Acta, Biomembr.* **2004**, *1667*, 182−189.
(31) Barenholz, Y.; Suurkuusk, J.; Mountcastle, D.; Thompson, T. E.; Biltonen, R. L. A calorimetric study of the thermotropic behavior of aqueous dispersions of natural and synthetic sphingomyelins. *Biochemistry* **1976**, *15*, 2441−7.
(32) Lukacova, V.; Peng, M.; Tandlich, R.; Hinderliter, A.; Balaz, S. Partitioning of organic compounds in phases imitating the headgroup and core regions of phospholipid bilayers. *Langmuir* **2006**, *22*, 1869−1874.
(33) Somerharju, P. Pyrene-labeled lipids as tools in membrane biophysics and cell biology. *Chem. Phys. Lipids* **2002**, *116*, 57−74.
(34) Nagy, E.; Balogi, Z.; Gombos, I.; Akerfelt, M.; Bjorkbom, A.; Balogh, G.; Torok, Z.; Maslyanko, A.; Fiszer-Kierzkowska, A.; Lisowska, K.; Slotte, P. J.; Sistonen, L.; Horvath, I.; Vigh, L. *Proc. Natl. Acad. Sci. U. S. A.* **2007**, *104*, 7945−7950.
(35) Alegre-Cebollada, J.; Martínez-del-Pozo, A.; Gavilanes, J. G.; Goormaghtigh, E. Infrared spectroscopy study on the conformational changes leading to pore formation of the toxin sticholysin II. *Biophys. J.* **2007**, *93*, 3191−3201.
(36) García-Linares, S.; Alm, I.; Maula, T.; Gavilanes, J. G.; Slotte, J. P.; Martínez-del-Pozo, A. The effect of cholesterol on the long-range network interactions established among sea anemone Sticholysin II residues at the water-membrane interface. *Mar. Drugs* **2015**, *13*, 1647−1665.
(37) Barlic, A.; Gutierrez-Aguirre, I.; Caaveiro, J. M.; Cruz, A.; Ruiz-Arguello, M. B.; Perez-Gil, J.; Gonzalez- Mañas, J. M. Lipid phase coexistence favors membrane insertion of equinatoxin II, a pore forming toxin from Actinia equina. *J. Biol. Chem.* **2004**, *279*, 34209−34216.
(38) Pedrera, L.; Fanani, M. L.; Ros, U.; Lanio, M. E.; Maggio, B.; Alvarez, C. Sticholysin I-membrane interaction: an interplay between the presence of sphingomyelin and membrane fluidity. *Biochim. Biophys. Acta, Biomembr.* **2014**, *1838*, 1752−1759.
(39) Schön, P.; García-Saez, A. J.; Malovrh, P.; Bacia, K.; Anderluh, G.; Schwille, P. Equinatoxin II permeabilizing activity depends on the presence of sphingomyelin and lipid phase coexistence. *Biophys. J.* **2008**, *95*, 691−698.
(40) Cannon, B.; Heath, G.; Huang, J.; Somerharju, P.; Virtanen, J. A.; Cheng, K. H. Time-resolved fluorescence and fourier transform infrared spectroscopic investigations of lateral packing defects and superlattice domains in compositionally uniform cholesterol/phosphatidylcholine bilayers. *Biophys. J.* **2003**, *84*, 3777−91.
(41) Jeffrey, G. A.; Saenger, W. *Hydrogen bonding in biological structures*; Springer Verlag: 1991.
(42) Schmidt, C. F.; Barenholz, Y.; Thompson, T. E. A nuclear magnetic resonance study of sphingomyelin in bilayer systems. *Biochemistry* **1977**, *16*, 2649−56.
(43) Kuikka, M.; Ramstedt, B.; Ohvo-Rekila, H.; Tuuf, J.; Slotte, J. P. Membrane properties of Derythro-N-acyl sphingomyelins and their corresponding dihydro species. *Biophys. J.* **2001**, *80*, 2327−2337.
(44) Makino, A.; Abe, M.; Murate, M.; Inaba, T.; Yilmaz, N.; Hullin-Matsuda, F.; Kishimoto, T.; Schieber, N. L.; Taguchi, T.; Arai, H.; Anderluh, G.; Parton, R. G.; Kobayashi, T. Visualization of the heterogenous membrane distribution of sphingomyelin associated with cytokinesis, cell polarity, and sphingolipidosis. *FASEB J.* **2015**, *29*, 477−493.
(45) Somerharju, P. J.; Virtanen, J. A.; Eklund, K. K.; Vainio, P.; Kinnunen, P. K. 1-Palmitoyl-2-pyrenedecanoyl glycerophospholipids as membrane probes: evidence for regular distribution in liquid-crystalline phosphatidylcholine bilayers. *Biochemistry* **1985**, *24*, 2773−81.
(46) Maček, P.; Zecchini, M.; Stanek, K.; Menestrina, G. Effect of membrane partitioned n-alcohols and fatty acids on pore-forming activity of a sea anemone toxin. *Eur. Biophys. J.* **1997**, *25*, 155−162.
(47) Alvarez, C.; Mancheño, J. M.; Martínez, D.; Tejuca, M.; Pazos, F.; Lanio, M. E. Sticholysins, two pore-forming toxins produced by the Caribbean Sea anemone, Stichodactyla heliantus: their interactions with membranes. *Toxicon* **2009**, *54*, 1135−1147.
(48) Pedrera, L.; Gomide, A. B.; Sanchez, R. E.; Ros, U.; Wilke, N.; Pazos, F.; Lanio, M. E.; Itri, R.; Fanani, M. L.; Alvarez, C. The presence of sterols favors sticholysin I-membrane association and pore formation regardless of their ability to form laterally segregated domains. *Langmuir* **2015**, *31*, 9911−9923.

■ NOTE ADDED AFTER ASAP PUBLICATION

This paper was published on the Web on March 29, 2016, with an error in the Supporting Information. The corrected version was reposted on April 4, 2016.

DOI: 10.1021/acs.langmuir.6b00082

Synergistic Action of Actinoporin Isoforms from the Same Sea Anemone Species Assembled into Functionally Active Heteropores*

Received for publication, December 14, 2015, and in revised form, April 26, 2016 Published, JBC Papers in Press, April 27, 2016, DOI 10.1074/jbc.M115.710491

Esperanza Rivera-de-Torre[‡], Sara García-Linares[‡], Jorge Alegre-Cebollada[§], Javier Lacadena[‡], José G. Gavilanes[‡1], and Álvaro Martínez-del-Pozo[‡2]

From the [‡]Departamento de Bioquímica y Biología Molecular I, Facultades de Química y Biología, Universidad Complutense, 28040 Madrid and [§]Centro Nacional de Investigaciones Cardiovasculares Carlos III, 28029 Madrid, Spain

Among the toxic polypeptides secreted in the venom of sea anemones, actinoporins are the pore-forming toxins whose toxic activity relies on the formation of oligomeric pores within biological membranes. Intriguingly, actinoporins appear as multigene families that give rise to many protein isoforms in the same individual displaying high sequence identities but large functional differences. However, the evolutionary advantage of producing such similar isotoxins is not fully understood. Here, using sticholysins I and II (StnI and StnII) from the sea anemone *Stichodactyla helianthus*, it is shown that actinoporin isoforms can potentiate each other's activity. Through hemolysis and calcein releasing assays, it is revealed that mixtures of StnI and StnII are more lytic than equivalent preparations of the corresponding isolated isoforms. It is then proposed that this synergy is due to the assembly of heteropores because (i) StnI and StnII can be chemically cross-linked at the membrane and (ii) the affinity of sticholysin mixtures for the membrane is increased with respect to any of them acting in isolation, as revealed by isothermal titration calorimetry experiments. These results help us understand the multigene nature of actinoporins and may be extended to other families of toxins that require oligomerization to exert toxicity.

Actinoporins, single polypeptide chains of around 175 amino acids, constitute a family of toxic proteins produced by different sea anemone species. They show basic isoelectric point values and are usually cysteineless (1–4). Actinoporins belong to a much larger group of widely distributed proteins, known as pore-forming toxins, whose toxic activity relies on the formation of pores within biological membranes (5–9). All pore-forming toxins show a very similar dual behavior by which they remain mostly monomeric and stably folded in aqueous solution but become oligomeric integral proteins when encountering membranes (2–4, 10–23).

The incorporation of actinoporins into the membrane largely depends on lipid bilayer composition and membrane physicochemical state (18, 24–29). Both factors influence the conformational changes occurring during the transition from the water media to the inserted states of the protein (30, 31). Thus, high affinity recognition of sphingomyelin (SM)[3] is crucial for specific attachment to a membrane, but the subsequent effects observed also depend on the physical properties derived from its particular composition and not only from its SM content (23, 32). In fact, although still controversial, the presence of cholesterol and the coexistence of different phases in the membrane seem to be important factors, if not for binding then at least for the final formation of the pore (23, 28, 29, 32–36).

Actinoporins have been isolated from more than 20 different sea anemone species (1, 3, 37–41) in agreement with their rather ubiquitous distribution within the Actinaria order (1). They display high sequence identities (between 60 and 80%) and appear as multigene families, giving rise to many protein isoforms within the same individual (42–46). Despite the small number of amino acid changes between them, actinoporin isoforms usually result in substantial functional differences in terms of solubility and lytic activity (38, 45, 47–51), as exemplified by StnI and StnII, produced by *Stichodactyla helianthus*, and also two of the best characterized actinoporins (3, 4, 20, 22, 24, 47–50, 52).

The reason why a single anemone produces several isoforms of actinoporins in its venom is still not fully understood. One possible explanation would be to expand the range of prey susceptible of being attacked (53). Such a strategy would extend and modulate the range of action of sea anemones. It has even been proposed an analogy with immunoglobulins, which suggests that sea anemone tentacles could produce many actinoporin isoforms because they would represent the embryo of a rudimentary defense system (45). However, so far the possibility that these different isoforms show synergistic activity has not been explored. This possibility is interesting because it would lead to more efficient venoms. The results presented here not only prove that StnI and StnII potentiate their lytic activity when they act together but also indicate that they can

* This work was supported by Grant BFU2012-32404 from the Spanish Ministerio de Ciencia e Innovación (to A. M. P.), a Formación de Personal Universitario fellowship (to S. G. L.), a Universidad Complutense de Madrid collaboration fellowship (to E. R. T.), and Ramón y Cajal Award RYC-2014-16604) (to J. A. C.). The authors declare that they have no conflicts of interest with the contents of this article.

[1] To whom correspondence may be addressed. Tel.: 34-913944158; Fax: 34-913944159; E-mail: ppgf@bbm1.ucm.es.

[2] To whom correspondence may be addressed. Tel.: 34-913944158; Fax: 34-913944159; E-mail: alvaromp@quim.ucm.es.

[3] The abbreviations used are: SM, sphingomyelin; 6HStnII, sticholysin II tagged with six histidine residues at the N terminus; DOPC, 1,2-dioleoyl-*sn*-glycero-3-phosphocholine; DSS, disuccinimidyl suberate; ITC, isothermal titration calorimetry; LUV, large unilamellar vesicle; Stn, sticholysin; Chol, cholesterol.

establish functional heteropores, suggesting that actinoporins have a more deeply regulated physiological mode of action than previously believed.

Experimental Procedures

Materials—1,2-Dioleoyl-*sn*-glycero-3-phosphocholine (DOPC), cholesterol (Chol), and porcine brain SM were obtained from Avanti Polar Lipids. Disuccinimidyl suberate (DSS) was purchased from Pierce (Thermo Scientific). The preparation of the cDNA coding for StnI, StnII, and the six His-tagged version of StnII (6HStnII), as well as the production and purification of the three different proteins, has been described before (30, 50, 54). Homogeneity of all protein samples used was analyzed by 0.1% (w/v) SDS-12–15% PAGE (w/v) performed under standard conditions (55) and amino acid analysis after acid hydrolysis of the proteins (5.7 M HCl, 24 h, 110 °C). These amino acid analyses were performed on a Biochrom 20 automatic analyzer (GE Healthcare). All protein batches used were also previously characterized in terms of recording their far-UV circular dichroism (CD) spectra on a Jasco 715 spectropolarimeter, also as described (20, 21, 56, 57).

Hemolysis—Hemolysis assays were performed in 96-multiwell plates as described previously (30, 50). Briefly, erythrocytes from heparinized sheep blood were washed in 10 mM Tris buffer, pH 7.4, containing 145 mM NaCl, to a final A_{655} of 0.5 when mixing equal volumes of the cell suspension and buffer. The hemolysis was followed as a decrease in A_{655} after addition of the erythrocyte suspension to different final concentrations of protein. An Expert 96 microplate reader (Asys Hitech, GmbH, Eugendorf, Austria) was employed to measure A_{655}. The value obtained with 0.1% (w/v) Na_2CO_3 was considered as 100% hemolysis.

Lipid Vesicle Preparation—DOPC/SM/Chol (1:1:1) phospholipid vesicles were prepared as described previously (20, 23, 58). A phospholipid (0.1–1.0 mg) solution in 2:1 (v/v) chloroform/methanol was dried under a flow of nitrogen, and the dry film obtained was used to prepare a lipid dispersion by adding 0.5–2.0 ml of Tris-NaCl (10 mM Tris-HCl, pH 7.4, 140 mM NaCl), briefly vortex mixing, and incubating for 1 h at 37 °C. This suspension of multilamellar vesicles was further subjected to five cycles of extrusion at 37 °C through polycarbonate filters (100-nm pore size) to obtain a homogeneous population of unilamellar vesicles.

Calcein Leakage Assays—Calcein-entrapped DOPC/SM/Chol (1:1:1) large unilamellar vesicles (LUVs) were prepared as described (23) by extrusion through 100-nm filters (Nucleopore, Whatman) at 37 °C. Briefly, the desired lipids were mixed and dried under a stream of nitrogen. The lipids were re-dissolved in chloroform and dried again before removal of any traces of remaining solvent in vacuum for 60 min. Prior to extrusion, the dry lipid films were hydrated for 1 h at 37 °C in Tris buffer (10 mM Tris, 140 mM NaCl, 0.5 mM EDTA, pH 7.4), containing 100 mM calcein. The total lipid concentration was 1.25 mM. LUVs were separated from non-entrapped calcein by gel filtration on Sephacryl S200HR. These LUVs were used for permeabilization studies within 24 h. Phospholipid concentration was determined from measurement of phosphorus (59) after elution of vesicles during isolation. The concentrations of LUV phospholipids and protein during calcein leakage experiments were about 7.5 μM and 1–80 nM, respectively. Emission at 550 nm was followed at 23 °C as a function of time (excitation at 480 nm). Fluorescence emission was measured with an SLM Aminco 8000 spectrofluorimeter. To ensure that no major spontaneous leakage occurred, the emission was measured for each sample during 5 min before addition of toxin. A steady signal level, indicating intact vesicles, was observed for all samples. Maximum calcein release was determined upon LUV disintegration induced by 10% Triton X-100.

Cross-linking Experiments—Cross-linking was performed essentially as described before (60). DSS was used as the cross-linking reagent in a reaction that was performed by adding a small aliquot of a concentrated freshly prepared cross-linker solution to the protein sample at the required concentrations. Protein (wild-type StnI and a His_6-tagged version of StnII (6HStnII)) (50) and vesicle mixtures were prepared in 15 mM MOPS, pH 7.4, containing 50 mM NaCl, at the following final molar concentrations: 2.0 μM StnI, 0.5 μM 6HStnII, 0.1 μM (lipid concentration) DOPC/SM/Chol (1:1:1) phospholipid vesicles, and 0.04 μM DSS. The final concentration of each protein employed in this case was independent of the presence or not of the other actinoporin. A second set of cross-linking experiments was made with mixtures containing a constant concentration of 6HStnII and increasing amounts of StnI up to a StnI/6HStnII molar ratio of 95:5. The cross-linker was dissolved in dimethyl sulfoxide (DMSO). The protein/lipid reaction mixtures were incubated at 37 °C for 1 h, then the cross-linker was added and kept for 30 min at room temperature, and finally the mixtures were quenched for 15 min by adding an aliquot of the same buffer but containing 50 mM Lys. After addition of the corresponding electrophoresis loading buffer to each aliquot, they were boiled for 20 min in the presence of 0.5% (v/v) β-mercaptoethanol, and the cross-linked products were analyzed by SDS-PAGE following standard procedures (55). Western immunoblotting was used to detect 6HStnII using a mouse monoclonal anti-polyhistidine-peroxidase antibody from Sigma.

Protein Binding to Lipid Vesicles—Binding was measured using isothermal titration calorimetry (ITC) as described before (21, 30, 61), using a VP-ITC calorimeter (MicroCal). Briefly, protein solutions at 1.5–10.0 μM concentration were titrated by injection of 10- or 20-μl aliquots of lipid suspensions (phospholipid concentration, 0.85–5.00 mM). Binding isotherms were adjusted to a model where the protein binds to the membrane involving "*n*" lipid molecules (30).

Results

StnI and StnII Show Synergistic Hemolytic Activity—A hemolysis experiment was designed to study the potential formation of StnI/StnII heteropores and its functional consequences. With this idea, sheep erythrocyte hemolysis was assayed in the presence of isolated StnI or StnII at different concentrations or for a mixture of StnI/StnII at 80:20 constant molar ratio (Fig. 1). This experiment was so designed given the lower hemolytic activity of StnI. Inspection of results shown in Fig. 1 reveal how the mixture produced higher hemolysis rates

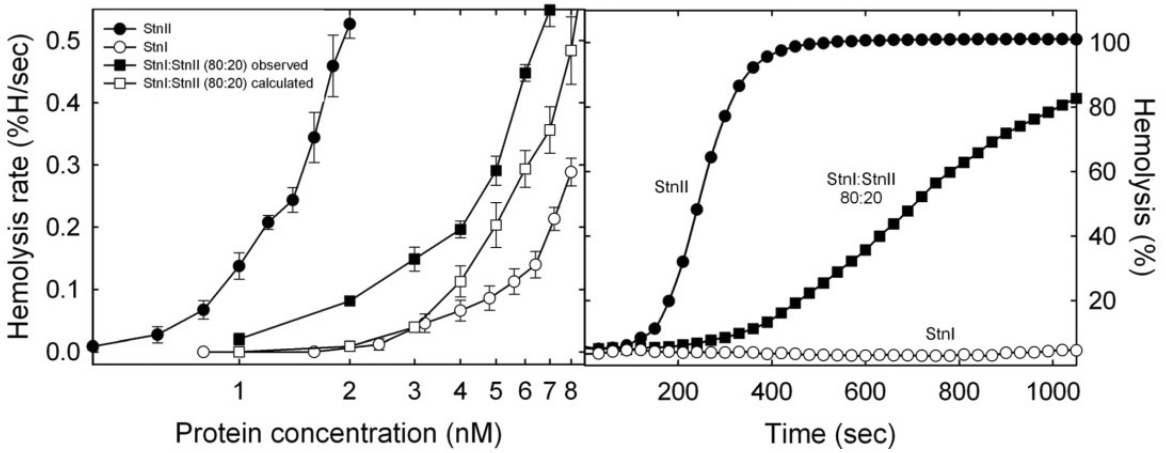

FIGURE 1. *Left panel,* maximum hemolytic rate values (expressed as percentage of hemolysis/s) are represented *versus* the logarithm of total protein concentration: StnI (*white dots*), StnII (*black dots*), and the StnI/StnII (80:20) mixture (*black squares*). The *white squares line* was obtained as the arithmetical addition of the rates obtained with the individual proteins for the real concentration of each one in the different mixtures employed. Results shown are the average of four independently performed experiments. Each of these experiments was made in duplicate. *Error bars* represent ±S.D. *Right panel,* as a representative example, the hemolytic activity curves of StnI (*white dots*), StnII (*black dots*), or a StnI/StnII (80:20) mixture (*black squares*), at a total protein concentration of 2 nM, are also shown.

than that one resulting from the arithmetical combination of the corresponding values obtained with the individual proteins.

To evaluate the specificity of this observation, two different StnII mutants were employed as controls. First, the same experiment as that described in Fig. 1 was made using StnII A10PS28P instead of the wild-type protein. This mutant has been previously described as retaining its full membrane binding activity but showing a highly diminished pore-forming ability due to its inability to extend the needed α-helical stretch (30). As shown in Fig. 2*A*, even though the mutant was completely unable to lyse the erythrocytes within the full concentration range assayed, the mixture still produced higher hemolysis rates than those resulting from the arithmetical combination of the corresponding values obtained with the individual proteins (wild-type StnI and A10PS28P StnII at a 80:20 ratio).

In the second control experiment performed, the StnII mutant used was Y111N. In this StnII variant a key residue of the so-called phosphocholine-binding site has been replaced rendering a protein that cannot bind to the membrane and therefore shows a dramatically reduced hemolytic activity (30, 54). It can be seen how in this case (Fig. 2*B*) the synergistic effect of StnII is not observed. Overall, the three sets of experiments suggest not only the existence of synergistic action between both actinoporin isoforms, StnI and StnII, but also that this synergy seems to occur at the membrane binding step of the pore formation mechanism.

StnI and StnII Show Synergistic Lytic Activity toward Lipid Model Vesicles—Erythrocytes are a rather complex model system to study protein-lipid interactions and assembly of pores at the membrane. Therefore, an experiment was designed to study leakage of calcein-containing DOPC/SM/Chol (1:1:1) phospholipid vesicles upon addition of different actinoporin concentrations. This type of vesicle represents one of the standard models most widely used to characterize StnI and StnII pore formation behavior (18, 20, 23, 28, 30, 54, 62). As can be observed in Fig. 3, the results obtained were similar to those corresponding to the hemolysis assays. The mixture of StnI and StnII produced higher calcein release rates than that resulting from the arithmetical combination of the corresponding values obtained with the individual proteins.

StnI and StnII Can Be Cross-linked in the Presence of Lipid Membranes—The results obtained from both sets of activity experiments, hemolysis and calcein release assays, show that StnI and StnII display synergistic activity. One explanation for this synergy would be the formation of active StnI/StnII heteropores. If this were the case, molecules from both proteins studied should be in close enough proximity as to be cross-linked using a short bifunctional reagent such as DSS (spacer arm, 1.1 nm), which reacts against exposed primary amines. Consequently, mixtures of StnI and StnII were incubated in the presence or absence of DOPC/SM/Chol (1:1:1) phospholipid vesicles and then DSS was added, following a standard protocol (63). The resulting mixture of proteins was analyzed by means of SDS-PAGE followed by Western blotting and immunodetection. For this purpose, instead of the wild-type protein, a His_6-tagged version of StnII (6HStnII) was employed. This protein has been described to retain the general features and molecular mechanism of wild-type StnII (50, 64). This 6HStnII variant shows two advantages for cross-linking experiments. First, the presence of the N-terminal poly(His) tag shifts its electrophoretic mobility to the point where it can be unequivocally distinguished from wild-type StnI (50). Second, it can be identified by an anti-poly-His antibody without cross-reactivity from StnI (18). Therefore, the results presented in blots of Figs. 4 and 5 reveal only the presence of 6HStnII, independently of the amount of StnI present.

In the absence of vesicles, only 6HStnII is detected in Fig. 4, *lanes 1* and *2*, despite the presence of a 4-fold higher concentration of StnI or the previous addition, or not, of the cross-linking agent. Fig. 4, *lanes 3* and *4*, shows the same set of results, cross-linked or not, but this time after incubation of both pro-

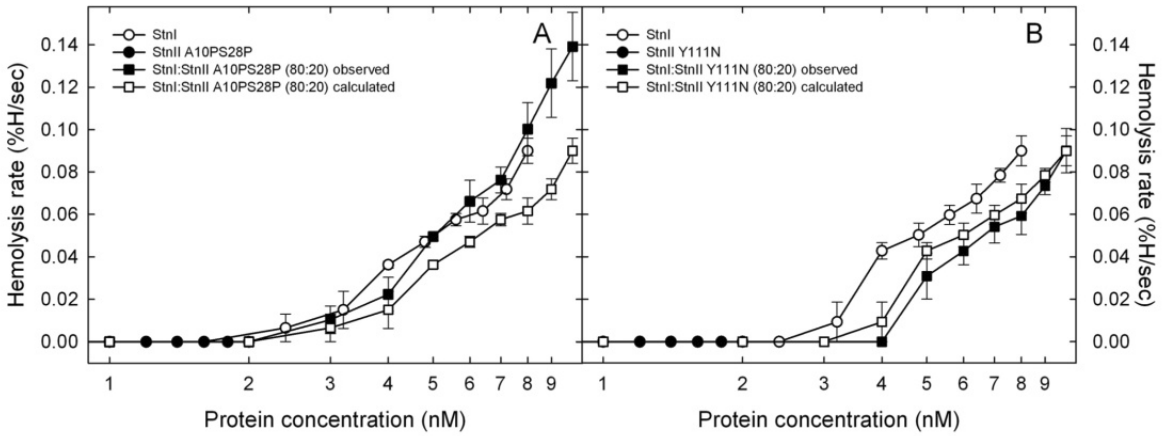

FIGURE 2. **Maximum hemolytic rate values (expressed as percentage of hemolysis/s) are represented *versus* the logarithm of total protein concentration of individual and two different actinoporin mixtures: wild-type StnI and A10PS28P (*A*) or Y111N (*B*) StnII mutants.** Both panels show the behavior of StnI (*white dots*), the StnII mutant (*black dots*), and the StnI/StnII mutant (80:20) mixture (*black squares*). The *white squares* line was obtained as the arithmetical addition of the rates obtained with the individual proteins for the real concentration of each one in the different mixtures employed. Results shown are the average of four independently performed experiments. Each of these experiments was made in duplicate. *Error bars* represent ±S.D.

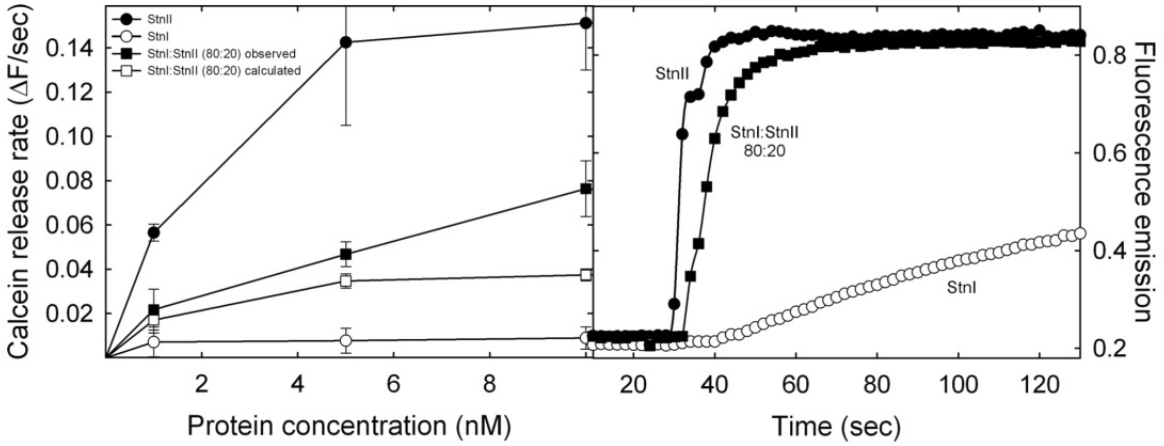

FIGURE 3. *Left panel,* calcein release of maximal rates (expressed as normalized fluorescence intensity increment/s) are represented *versus* the total protein concentration: StnI (*white dots*), StnII (*black dots*), and the StnI/StnII (80:20) mixture (*black squares*). The *white squares line* was obtained as the arithmetical addition of the rates obtained with the individual proteins taking into account the real concentration of each one of them in the different mixtures employed. Results shown are the average of three independently performed experiments. Each of these experiments was made in duplicate. *Error bars* represent ± S.D. *Right panel,* as a representative example, the calcein leakage traces of StnI (*white dots*), StnII (*black dots*), or an StnI/StnII (80:20) mixture (*black squares*), at a total protein concentration of 5 nM, are also shown.

teins with DOPC/SM/Chol (1:1:1) vesicles. Thus, again, in the absence of DSS, no other band but that one corresponding to monomeric 6HStnII was observed (Fig. 4, *lane 3*). However, when the cross-linker was present, new bands of different electrophoretic mobility were evident (Fig. 4, *lane 4*). At least two of these bands were not observed if 6HStnII (Fig. 4, *lane 5*) or StnI (*lane 6*) were the only proteins present. Therefore, they can only correspond to hetero-oligomers made of 6HStnII and wild-type StnI, the only situation that would explain their immunodetection by the anti-poly(His) antibody together with their singular electrophoretic mobility. It has been well determined that the presence of the six His tags at the N-terminal end of sticholysins has a deep impact on their electrophoretic mobility (50).

To show further evidence of the assembly of StnI and 6HStnII into cross-linkable heteropores, the titration experiment shown in Fig. 5 was performed. Again, under these conditions and in the absence of vesicles, only 6HStnII was detected in Fig. 5, *lane 1*. However, when cross-linker and vesicles were present, 6HStnII cross-linked oligomers could be detected (Fig. 5, *lane 2*). In fact, the observed distribution pattern is very similar to the one reported previously for equinatoxin II under almost identical conditions (25, 65). As shown in Fig. 5, *lanes 2–5*, upon increasing the StnI/6HStnII ratio, the appearance of the bands corresponding to cross-linked proteins is increasingly evident altogether with a decrease of the monomeric 6HStnII species. This second set of results not only confirms the presence of cross-linkable

	1	2	3	4	5	6
StnI (80)	+	+	+	+	-	+
6HStnII (20)	+	+	+	+	+	-
Vesicles	-	-	+	+	+	+
Cross-linker	-	+	-	+	+	+

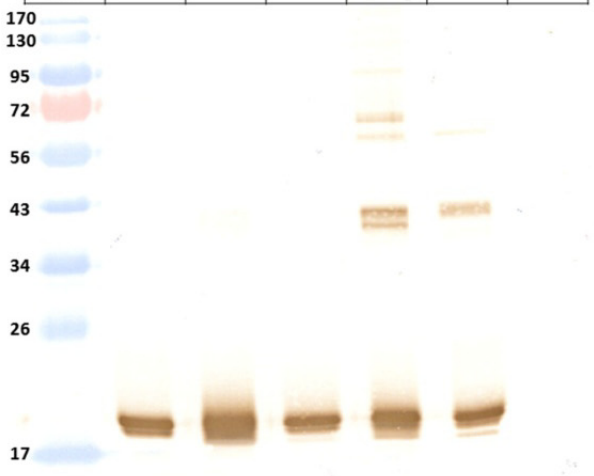

FIGURE 4. **Immunoblotting detection of 6HStnII previously incubated in the presence, or not, of wild-type StnI, DOPC/SM/Chol (1:1:1) phospholipid vesicles, and/or DSS, as indicated.** Proteins were detected using a mouse monoclonal anti-polyhistidine-peroxidase antibody. The amount of 6HStnII loaded was 2.5 pmol. The StnI:6HStnII molar ratio employed was 80:20 in all instances shown. Molecular weight standards (EZ-RUN™ pre-stained Rec Protein Ladder) were also loaded, and the corresponding molecular masses are indicated in kDa at the *left margin*.

	1	2	3	4	5	6
StnI (pmol)	0.0	0.0	10.0	22.5	47.5	47.5
6HStnII (pmol)	2.5	2.5	2.5	2.5	2.5	0.0
StnI:6HStnII	0.0	0.0	80:20	90:10	95:5	-
Vesicles	-	+	+	+	+	-
Cross-linker	-	+	+	+	+	-

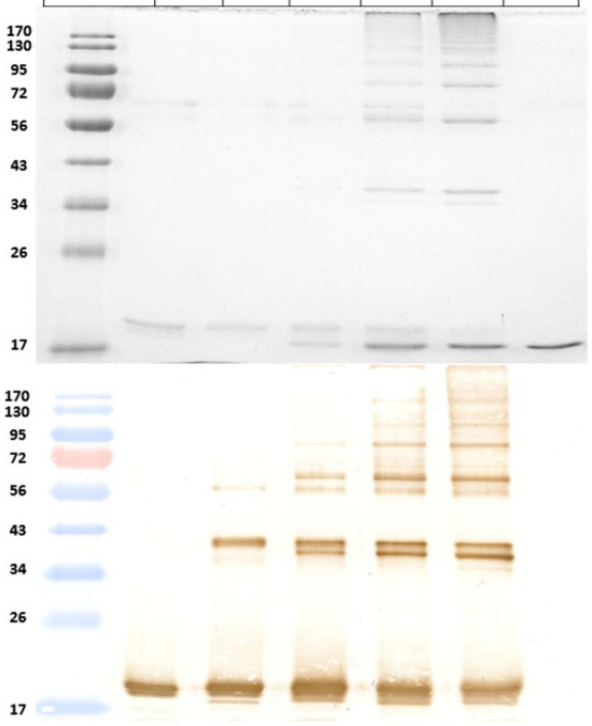

FIGURE 5. **Coomassie Blue-stained gel (*upper panel*) and the corresponding immunoblotting detection (*lower panel*) of 6HStnII titrated with increasing amounts of StnI are shown.** The proteins, and also the mixtures assayed, were incubated in the presence, or not, of wild-type StnI, DOPC/SM/Chol (1:1:1) phospholipid vesicles, and/or DSS, as indicated. Proteins were detected using a mouse monoclonal anti-polyhistidine-peroxidase antibody. The amount of 6HStnII loaded was 2.5 pmol in all instances shown. The StnI/6HStnII molar ratio employed is also indicated. Molecular weight standards (EZ-RUN™ pre-stained Rec Protein Ladder) were also loaded, and the corresponding molecular masses are indicated in kDa at the *left margin*.

heteropores on the bilayer but also its marked protein concentration and StnI/6HStnII ratio dependence. The presence of other hetero-oligomers of lower electrophoretic mobility is also detected but, given the inherent influence of the DSS reaction on band electrophoretic mobility and sharpness (60), it is not possible to assign specific stoichiometries. We also used Coomassie staining to analyze the results of cross-linking. Compared with the Western blotting results, we found that the lower mobility heterooligomer bands at around 40 kDa that become apparent at higher StnI/6HStnII ratios have a lower reactivity against the anti-His antibody, in agreement with the lower content of His tags in the heterooligomers. In summary, this set of experiments allowed us to conclude that, in the presence of membranes, actinoporins StnI and StnII are close enough as to be cross-linked by a short cross-linking agent, suggesting that heteropores of StnI and StnII are formed.

Mixtures of StnI and StnII Show Increased Membrane Affinity—The actinoporins pore formation mechanism has been thoroughly studied although some of its details are still the subject of dispute (17, 32, 66–70). In a simplified version of this mechanism, two different steps can be distinguished. First, the protein binds to the membrane, and second, it assembles into a functional oligomeric pore (18, 30). Within the context of this simplified picture, it can be assumed that binding assays by ITC measure the affinity of the proteins to the membrane (30). As observed in Fig. 6, the affinity of StnI for DOPC/SM/Chol (1:1:1) phospholipid vesicles is lower than that corresponding to StnII (Table 1). In terms of relative membrane binding affinity, StnII binding to the vesicles is 4-fold higher, a result that is good enough by itself to explain the long known differences in terms of hemolytic and calcein leakage activities between StnI and StnII (26, 71).

To explore whether improved binding could contribute to the synergistic lytic activity shown by sticholysins, we performed ITC binding experiments in which a total actinoporin concentration was fixed, but different StnI/StnII molar ratios were assayed (Fig. 7). Quite surprisingly, the binding affinity of

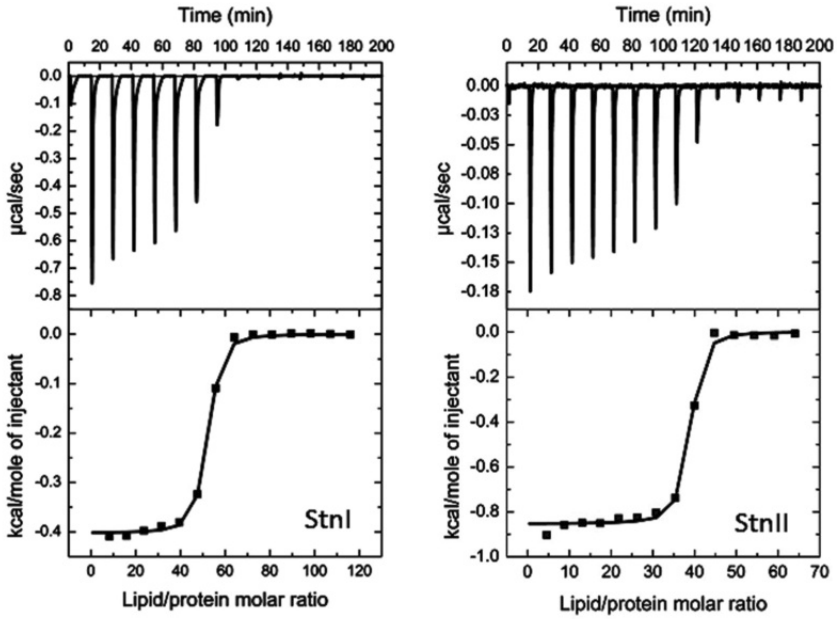

FIGURE 6. **Binding of StnI and StnII to DOPC/SM/Chol (1:1:1) vesicles studied by ITC.** Reactant concentrations were those ones shown in Table 1. Binding isotherms were adjusted to a model in which protein membrane binding involves the participation of "*n*" lipid molecules (30). The *c* values ($c = K_a \times P_0$) for the graphs shown are within the range 1–1000.

TABLE 1

Binding of StnI, StnII, or different StnI/StnII mixtures to DOPC/SM/Chol (1:1:1) vesicles studied by ITC

Thermodynamic parameters for protein mixtures StnI/StnII (95:5), StnI/StnII (90:10), and StnI/StnII (80:20) (Fig. 7) should be considered only as estimations and are shown only for trend consistency purposes because binding affinities were so high that keeping the *c* values within range involved dilutions below the recommended detection limits of the instrument. Therefore, the corresponding *c* values of the three mixtures containing the higher proportion of StnII are higher than the recommended ones. Results shown are the average of at least three separate experiments.

	StnI/StnII (100:0)	StnI/StnII (0:100)[a]	StnI/StnII (99:1)	StnI/StnII (95:5)	StnI/StnII (90:10)	StnI/StnII (80:20)
n	49 ± 1	39 ± 4	38 ± 1	42 ± 1	38 ± 1	47 ± 9
K_a (M^{-1}) × 10^{-8}	0.41 ± 0.03	1.70 ± 0.90	2.84 ± 0.91	33.90 ± 41.90	23.20 ± 19.90	237.00 ± 29.30
ΔG (kcal/mol)	−8.21 ± 0.03	−9.10 ± 0.50	−10.90 ± 0.48	−10.89 ± 0.48	−10.73 ± 0.37	−11.54 ± 1.29
ΔH (kcal/mol)	−20.9 ± 2.1	−44.0 ± 3.0	−9.1 ± 0.1	−11.1 ± 0.1	−14.0 ± 0.1	−27.3 ± 3.2
ΔS (cal/mol·K)	−42.84 ± 6.78	−115 ± 9.00	−1.2 ± 0.73	−0.8 ± 2.0	−14.0 ± 1.7	−52.9 ± 6.4
[Protein]	10.0 µM	1.5 µM	1.5 µM	1.5 µM	1.5 µM	1.0 µM
$c = K_a \times$ [Protein]	410	255	426	5090	3480	23700
RBM[b]	0.19	1.00	1.71	5.50	4.20	115.7

[a] See Ref. 30.
[b] Relative membrane binding $(n_{(StnII)} \times K_{(other)})/(n_{(other)} \times K_{(StnII)})$ as explained in Ref. 30.

mixtures of StnI and StnII was always higher than for any of the two actinoporins acting in isolation. This effect was already detected in the presence of trace amounts (1.0%) of StnII and correlated with increased relative membrane binding (Fig. 7 and Table 1). It is difficult to conceive how the binding affinity could increase without direct interaction between StnI and StnII. Hence, the ITC experiments lend additional support to the hypothesis that StnI and StnII can assemble into functional heteropores, leading to synergistic lytic activity.

Finally, given the large effect on affinity of only traces of StnII in the mixtures, we studied whether this increase in binding affinity was directly correlated with an enhancement of function. As can be seen in Fig. 8, just 1.0% of StnII in the mixtures was enough to dramatically improve their hemolytic activity, as revealed by the hemolysis assays performed with different StnI/StnII (99:1) mixtures over a 1–10 nM concentration range (Fig. 8).

Discussion

Sea anemones produce a wide variety of toxic compounds that are mainly stored in their nematocysts (72). Among them, actinoporins constitute a well studied family of toxic pore-forming proteins (3, 4, 70). It has long been known that individual sea anemone species produce many different actinoporin isoforms that, indeed, are very differently represented in terms of the amount present in their venomous secretions. In this regard, actinoporins represent a well established example of a multigenic protein family (38, 39, 43, 45, 46, 51, 73). They are not, however, the only example of toxic pore-forming multigene protein families (74), suggesting that the results shown now could be of larger significance and not only restricted to the actinoporin family. In fact, it has been very recently suggested that the pore responsible for damaging mitochondria during apoptosis could be made of hetero-oligomers of the Bax and Bak proteins (75). The natural biological function of this

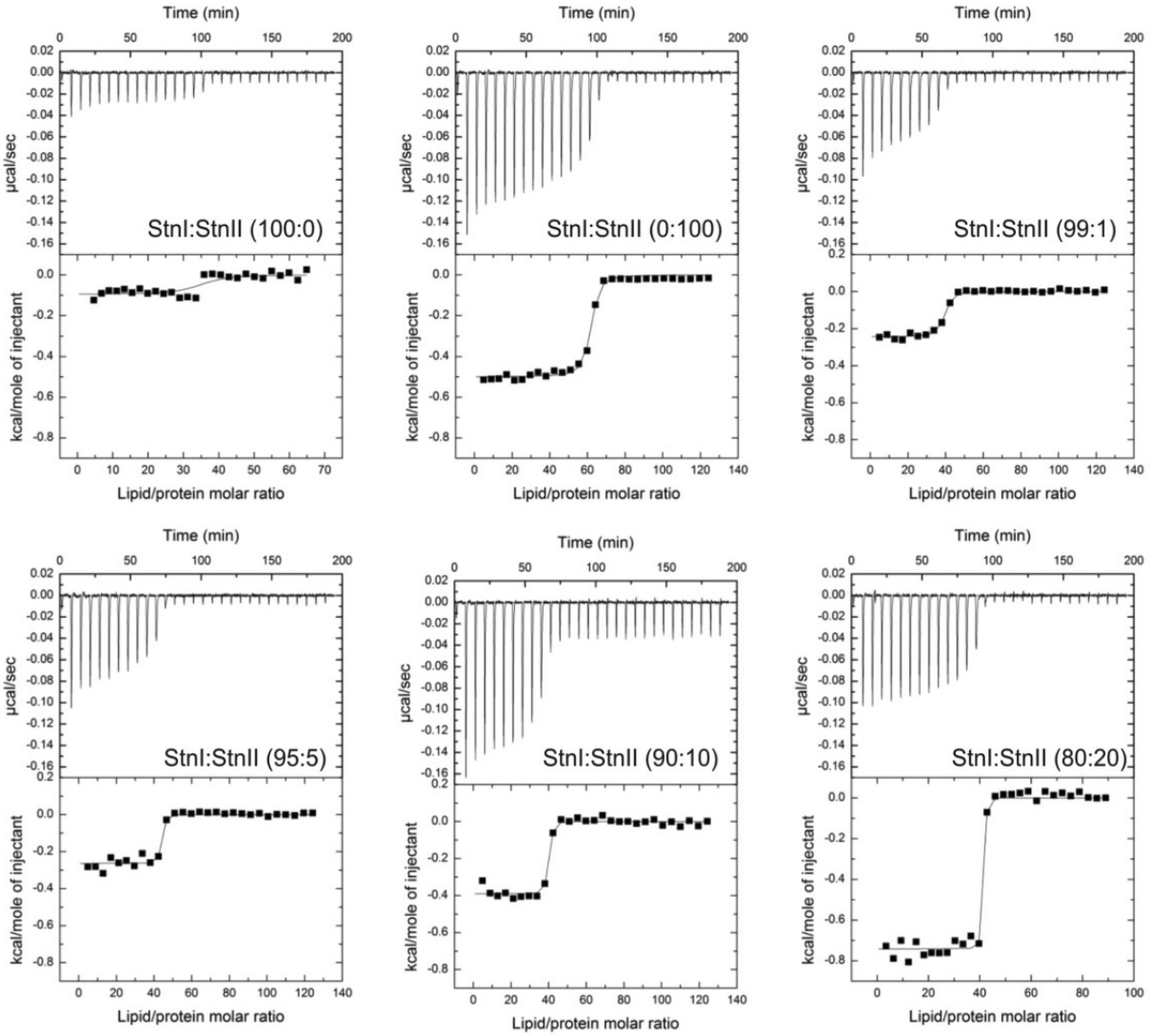

FIGURE 7. **Binding of StnI, StnII, and different StnI/StnII mixtures (molar ratios as indicated) to DOPC/SM/Chol (1:1:1) vesicles studied by ITC.** Reactant concentrations for the examples shown are $P_0 = 1.5\ \mu M$ and $L_0 = 0.85$ mM for all experiments, where P_0 refers to the initial total protein concentration within the calorimeter cell and L_0 is the lipid concentration within the dispensing auto-pipette. Binding isotherms were adjusted to a model in which protein membrane binding involves the participation of "*n*" lipid molecules (30). The *c* values ($c = K_a \times P_0$) for the graphs shown were in the 1–1000 range only for the StnI/StnII (0:100), StnI/StnII (99:1), and StnI/StnII (100:0). In the other three thermograms shown the binding affinities were so high that keeping the *c* values within range involved dilutions below the recommended detection limits of the instrument.

genetic multiplicity is indeed far from being understood. Regarding the actinoporin family, it has been proposed that the existence of multiple isoforms would broaden the range of possible prey for a given species (38, 39, 43, 45, 46, 51, 73). In this regard, actinoporins might be similar to immunoglobulins, which require a plethora of highly diverse genes to counteract foreign antigens (45).

Here, we propose a complementary hypothesis to explain the evolutionary advantage of multigenic actinoporins, formation of mixed functional pores. This mechanism would enable a much wider and finely tuned modulation of their toxicity and specificity. These results support the feasibility of this novel hypothesis.

StnI and StnII are two of the best well studied actinoporins and also constitute an optimum example of two almost identical isoforms (they share 91.0% of amino acid sequence identity) produced by the same sea anemone species but showing very different hemolytic activities (24, 47, 50, 76). Consequently, they were the model proteins chosen to study the possibility of molecularly different actinoporins assembling into the same functional pore structure. Indeed, the employment of independently produced and isolated recombinant protein species excludes artifacts produced by traces of cross-contamination in the experiments shown that were made with only one single protein component.

Actinoporin pore structure and stoichiometry are still highly controversial and far from being solved (22, 36, 66, 69,

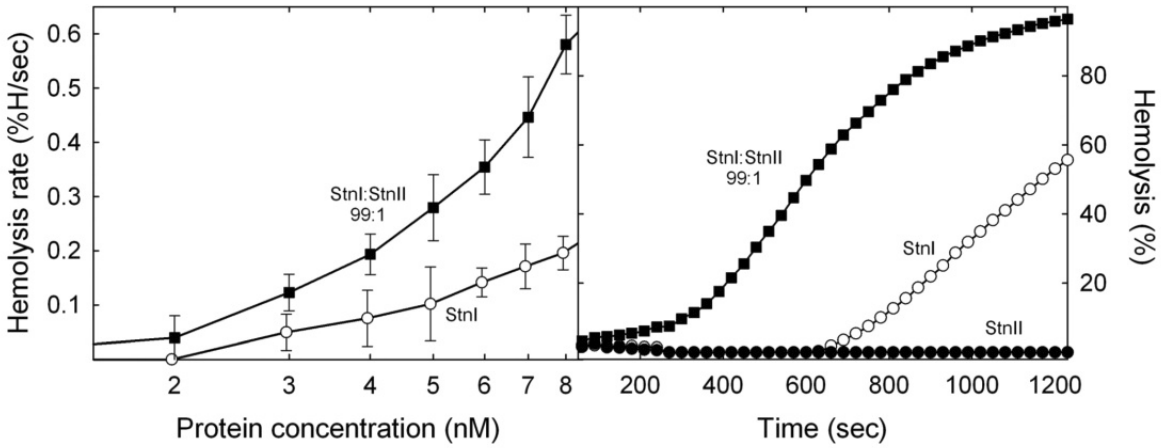

FIGURE 8. *Left panel,* maximum hemolytic rate values (expressed as percentage of hemolysis/s) are represented *versus* the logarithm of total protein concentration of StnI (*white dots*) and an StnI/StnII (99:1) mixture (*black squares*). In these experiments the amount of StnII present in all the mixtures was so low that, when assayed in the absence of StnI, its hemolytic activity was undetectable in the time range measured. Results shown are the average of four independently performed experiments. Each of these experiments was made in duplicate. *Error bars* represent ±S.D. *Right panel,* as a representative example, the hemolytic activity curves of StnI at 3.96 nM (*white dots*), StnII at 0.04 nM (*black dots*), and the corresponding StnI/StnII (99:1) 4 nM mixture (*black squares*) are also shown.

70, 77–79). The latest actinoporin pore-like oligomeric structure published is a crystalline octameric ensemble of FraC (66). According to those results, the two side-chain residues showing more buried surface upon oligomerization would be FraC Val-60 and Trp-149 (66, 80). These residues have their corresponding counterparts in StnI (Ile-59 and Trp-149) and StnII (Ile-58 and Trp-146). Both amino acids could nicely perform an identical function in the StnI-StnII mixed oligomers. Therefore, from a molecular point of view there would not be impediments for the formation of StnI-StnII heteropores.

Synergistic activity of StnI and StnII in both hemolysis and calcein-release experiments suggested that both proteins are in fact able to interact within the same pore structure (Figs. 1–3). Cross-linking experiments further support this observation because, and only in the presence of lipid vesicles, both StnI and StnII could be cross-linked with a short cross-linking agent (Figs. 4 and 5). Finally, we have also shown that mixtures of StnI and StnII show increased affinity for lipid vesicles, in agreement with the fact that both isoforms interact in the process of membrane binding and pore formation (Fig. 7). ITC and hemolytic experiments also show that 1.0% of StnII dramatically enhances StnI binding to lipid model vesicles driving a dramatic improvement of hemolytic activity. Taking into account the only moderate effects observed in calcein-leakage experiments, and the hemolysis results obtained with the two different StnII mutants used as control (Fig. 2), it can be also suggested that synergy between StnI and StnII could mostly be due to a better interaction with the membrane, although the final step of pore formation would not be strongly affected.

As stated above, actinoporins represent multigene families. However, only two or three different isoforms are usually produced by the same sea anemone species in amounts large enough to be detected and purified. For example, up to 19 different cDNA sequences have been detected for *S. helianthus*, the sea anemone producing StnI and StnII (43). Thus, taking into account this discrepancy between the number of actinoporin encoding genes found in sea anemones and the amount and diversity of isotoxins made, it is tempting to speculate that the less represented isoforms might play a role in regulating and/or potentiating the activity and specificity of those ones produced in larger amounts. Maybe this is just a strategy to fulfill a much more modulated and specific cytotoxic action against potential prey and/or predators.

Conclusions

Overall, the results presented here show that two different actinoporins produced by the same sea anemone species act in synergy, most probably interacting to form functional pores made of distinct protein isoforms. As far as we know, this observation has not been reported before. This interaction has sound consequences in terms of the biological functionality of actinoporins and suggests that it could represent a more general strategy employed by other pore-forming proteins. According to the results reported now, it can be speculated that one of the reasons for actinoporins being multigene families is the possibility of interaction among different isotoxins to exert a much more modulated and/or potentiated action against their prey and/or predators. This possibility would translate into more versatile defense and/or attack responses in their natural environment.

Author Contributions—E. R. T., S. G. L., and J. A. C. conducted the experiments. E. R. T., S. G. L., J. A. C., J. L., J. G. G., and A. M. P. conceived and designed the experiments, analyzed and discussed the results, wrote and corrected the manuscript, and suggested modifications.

References

1. Macek, P. (1992) Polypeptide cytolytic toxins from sea anemones (*Actiniaria*). *FEMS Microbiol. Immunol.* **5,** 121–129
2. Anderluh, G., and Macek, P. (2002) Cytolytic peptide and protein toxins from sea anemones (Anthozoa: *Actiniaria*). *Toxicon* **40,** 111–124
3. Alegre-Cebollada, J., Oñaderra, M., Gavilanes, J. G., and del Pozo, A.

(2007) Sea anemone actinoporins: the transition from a folded soluble state to a functionally active membrane-bound oligomeric pore. *Curr. Protein Pept. Sci.* **8,** 558–572
4. García-Ortega, L., Alegre-Cebollada, J., García-Linares, S., Bruix, M., Martínez-Del-Pozo, A., and Gavilanes, J. G. (2011) The behavior of sea anemone actinoporins at the water-membrane interface. *Biochim. Biophys. Acta* **1808,** 2275–2288
5. Parker, M. W., and Feil, S. C. (2005) Pore-forming protein toxins: from structure to function. *Prog. Biophys. Mol. Biol.* **88,** 91–142
6. Gonzalez, M. R., Bischofberger, M., Pernot, L., van der Goot, F. G., and Frêche, B. (2008) Bacterial pore-forming toxins: the (w)hole story? *Cell. Mol. Life Sci.* **65,** 493–507
7. Bischofberger, M., Iacovache, I., and van der Goot, F. G. (2012) Pathogenic pore-forming proteins: function and host response. *Cell Host Microbe* **12,** 266–275
8. Iacovache, I., van der Goot, F. G., and Pernot, L. (2008) Pore formation: an ancient yet complex form of attack. *Biochim. Biophys. Acta* **1778,** 1611–1623
9. Gouaux, E. (1997) Channel-forming toxins: tales of transformation. *Curr. Opin. Struct. Biol.* **7,** 566–573
10. Anderluh, G., Dalla Serra, M., Viero, G., Guella, G., Macek, P., and Menestrina, G. (2003) Pore formation by equinatoxin II, a eukaryotic protein toxin, occurs by induction of nonlamellar lipid structures. *J. Biol. Chem.* **278,** 45216–45223
11. Athanasiadis, A., Anderluh, G., Macek, P., and Turk, D. (2001) Crystal structure of the soluble form of equinatoxin II, a pore-forming toxin from the sea anemone *Actinia equina*. *Structure* **9,** 341–346
12. Kristan, K. C., Viero, G., Dalla Serra, M., Macek, P., and Anderluh, G. (2009) Molecular mechanism of pore formation by actinoporins. *Toxicon* **54,** 1125–1134
13. Gilbert, R. J., Dalla Serra, M., Froelich, C. J., Wallace, M. I., and Anderluh, G. (2014) Membrane pore formation at protein-lipid interfaces. *Trends Biochem. Sci.* **39,** 510–516
14. Hinds, M. G., Zhang, W., Anderluh, G., Hansen, P. E., and Norton, R. S. (2002) Solution structure of the eukaryotic pore-forming cytolysin equinatoxin II: implications for pore formation. *J. Mol. Biol.* **315,** 1219–1229
15. Marchioretto, M., Podobnik, M., Dalla Serra, M., and Anderluh, G. (2013) What planar lipid membranes tell us about the pore-forming activity of cholesterol-dependent cytolysins. *Biophys. Chem.* **182,** 64–70
16. Rojko, N., Cronin, B., Danial, J. S., Baker, M. A., Anderluh, G., and Wallace, M. I. (2014) Imaging the lipid-phase-dependent pore formation of equinatoxin II in droplet interface bilayers. *Biophys. J.* **106,** 1630–1637
17. Rojko, N., Kristan, K. Č., Viero, G., Žerovnik, E., Maček, P., Dalla Serra, M., and Anderluh, G. (2013) Membrane damage by an α-helical pore-forming protein, Equinatoxin II, proceeds through a succession of ordered steps. *J. Biol. Chem.* **288,** 23704–23715
18. Alegre-Cebollada, J., Rodríguez-Crespo, I., Gavilanes, J. G., and del Pozo, A. (2006) Detergent-resistant membranes are platforms for actinoporin pore-forming activity on intact cells. *FEBS J.* **273,** 863–871
19. Castrillo, I., Araujo, N. A., Alegre-Cebollada, J., Gavilanes, J. G., Martínez-del-Pozo, A., and Bruix, M. (2010) Specific interactions of sticholysin I with model membranes: an NMR study. *Proteins* **78,** 1959–1970
20. García-Linares, S., Castrillo, I., Bruix, M., Menéndez, M., Alegre-Cebollada, J., Martínez-del-Pozo, Á., and Gavilanes, J. G. (2013) Three-dimensional structure of the actinoporin sticholysin I. Influence of long-distance effects on protein function. *Arch. Biochem. Biophys.* **532,** 39–45
21. García-Linares, S., Richmond, R., García-Mayoral, M. F., Bustamante, N., Bruix, M., Gavilanes, J. G., and Martínez-Del-Pozo, A. (2014) The sea anemone actinoporin (Arg-Gly-Asp) conserved motif is involved in maintaining the competent oligomerization state of these pore-forming toxins. *FEBS J.* **281,** 1465–1478
22. Mancheño, J. M., Martín-Benito, J., Martínez-Ripoll, M., Gavilanes, J. G., and Hermoso, J. A. (2003) Crystal and electron microscopy structures of sticholysin II actinoporin reveal insights into the mechanism of membrane pore formation. *Structure* **11,** 1319–1328
23. Alm, I., García-Linares, S., Gavilanes, J. G., Martínez-Del-Pozo, Á., and Slotte, J. P. (2015) Cholesterol stimulates and ceramide inhibits sticholysin II-induced pore formation in complex bilayer membranes. *Biochim. Biophys. Acta* **1848,** 925–931
24. Valcarcel, C. A., Dalla Serra, M., Potrich, C., Bernhart, I., Tejuca, M., Martinez, D., Pazos, F., Lanio, M. E., and Menestrina, G. (2001) Effects of lipid composition on membrane permeabilization by sticholysin I and II, two cytolysins of the sea anemone *Stichodactyla helianthus*. *Biophys. J.* **80,** 2761–2774
25. Belmonte, G., Pederzolli, C., Macek, P., and Menestrina, G. (1993) Pore formation by the sea anemone cytolysin equinatoxin-II in red blood cells and model lipid membranes. *J. Membr. Biol.* **131,** 11–22
26. Tejuca, M., Serra, M. D., Ferreras, M., Lanio, M. E., and Menestrina, G. (1996) Mechanism of membrane permeabilization by sticholysin I, a cytolysin isolated from the venom of the sea anemone *Stichodactyla helianthus*. *Biochemistry* **35,** 14947–14957
27. Shin, M. L., Michaels, D. W., and Mayer, M. M. (1979) Membrane damage by a toxin from the sea anemone *Stoichactis helianthus*. II. Effect of membrane lipid composition in a liposome system. *Biochim. Biophys. Acta* **555,** 79–88
28. de los Rios, V., Mancheño, J. M., Lanio, M. E., Oñaderra, M., and Gavilanes, J. G. (1998) Mechanism of the leakage induced on lipid model membranes by the hemolytic protein sticholysin II from the sea anemone *Stichodactyla helianthus*. *Eur. J. Biochem.* **252,** 284–289
29. Martínez, D., Otero, A., Alvarez, C., Pazos, F., Tejuca, M., Lanio, M. E., Gutiérrez-Aguirre, I., Barlic, A., Iloro, I., Arrondo, J. L., González-Mañas, J. M., and Lissi, E. (2007) Effect of sphingomyelin and cholesterol on the interaction of St II with lipidic interfaces. *Toxicon* **49,** 68–81
30. Alegre-Cebollada, J., Cunietti, M., Herrero-Galán, E., Gavilanes, J. G., and Martínez-del-Pozo, A. (2008) Calorimetric scrutiny of lipid binding by sticholysin II toxin mutants. *J. Mol. Biol.* **382,** 920–930
31. Menestrina, G., Cabiaux, V., and Tejuca, M. (1999) Secondary structure of sea anemone cytolysins in soluble and membrane bound form by infrared spectroscopy. *Biochem. Biophys. Res. Commun.* **254,** 174–180
32. Pedrera, L., Gomide, A. B., Sánchez, R. E., Ros, U., Wilke, N., Pazos, F., Lanio, M. E., Itri, R., Fanani, M. L., and Alvarez, C. (2015) The presence of sterols favors sticholysin I-membrane association and pore formation regardless of their ability to form laterally segregated domains. *Langmuir* **31,** 9911–9923
33. Bakrac, B., and Anderluh, G. (2010) Molecular mechanism of sphingomyelin-specific membrane binding and pore formation by actinoporins. *Adv. Exp. Med. Biol.* **677,** 106–115
34. Barlic, A., Gutiérrez-Aguirre, I., Caaveiro, J. M., Cruz, A., Ruiz-Argüello, M. B., Pérez-Gil, J., and González-Mañas, J. M. (2004) Lipid phase coexistence favors membrane insertion of equinatoxin-II, a pore-forming toxin from *Actinia equina*. *J. Biol. Chem.* **279,** 34209–34216
35. Caaveiro, J. M., Echabe, I., Gutiérrez-Aguirre, I., Nieva, J. L., Arrondo, J. L., and González-Mañas, J. M. (2001) Differential interaction of equinatoxin II with model membranes in response to lipid composition. *Biophys. J.* **80,** 1343–1353
36. Wacklin, H. P., Bremec, B. B., Moulin, M., Rojko, N., Haertlein, M., Forsyth, T., Anderluh, G., and Norton, R. S. (2016) Neutron reflection study of the interaction of the eukaryotic pore-forming actinoporin equinatoxin II with lipid membranes reveals intermediate states in pore formation. *Biochim. Biophys. Acta* **1858,** 640–652
37. Bellomio, A., Morante, K., Barlic, A., Gutiérrez-Aguirre, I., Viguera, A. R., and González-Mañas, J. M. (2009) Purification, cloning and characterization of fragaceatoxin C, a novel actinoporin from the sea anemone *Actinia fragacea*. *Toxicon* **54,** 869–880
38. Monastyrnaya, M., Leychenko, E., Isaeva, M., Likhatskaya, G., Zelepuga, E., Kostina, E., Trifonov, E., Nurminski, E., and Kozlovskaya, E. (2010) Actinoporins from the sea anemones, tropical *Radianthus macrodactylus* and northern *Oulactis orientalis*: comparative analysis of structure-function relationships. *Toxicon* **56,** 1299–1314
39. Monastyrnaya, M. M., Zykova, T. A., Apalikova, O. V., Shwets, T. V., and Kozlovskaya, E. P. (2002) Biologically active polypeptides from the tropical sea anemone *Radianthus macrodactylus*. *Toxicon* **40,** 1197–1217
40. Leichenko, E. V., Monastirnaya, M. M., Zelepuga, E. A., Tkacheva, E. S., Isaeva, M. P., Likhatskaya, G. N., Anastyuk, S. D., and Kozlovskaya, E. P. (2014) Hct-A is a new actinoporin family from the *Heteractis crispa* sea anemone. *Acta Naturae* **6,** 89–98

41. Hu, B., Guo, W., Wang, L. H., Wang, J. G., Liu, X. Y., and Jiao, B. H. (2011) Purification and characterization of gigantoxin-4, a new actinoporin from the sea anemone *Stichodactyla gigantea*. *Int. J. Biol. Sci.* **7,** 729–739
42. Anderluh, G., Barlic, A., Podlesek, Z., Macek, P., Pungercar, J., Gubensek, F., Zecchini, M. L., Serra, M. D., and Menestrina, G. (1999) Cysteine-scanning mutagenesis of an eukaryotic pore-forming toxin from sea anemone: topology in lipid membranes. *Eur. J. Biochem.* **263,** 128–136
43. de los Ríos, V., Oñaderra, M., Martínez-Ruiz, A., Lacadena, J., Mancheño, J. M., Martínez del Pozo, A., and Gavilanes, J. G. (2000) Overproduction in *Escherichia coli* and purification of the hemolytic protein sticholysin II from the sea anemone *Stichodactyla helianthus*. *Protein Expr. Purif.* **18,** 71–76
44. Turk, T. (1991) Cytolytic toxins from sea anemones. *J. Toxicol. Toxin Rev.* **10,** 223–262
45. Wang, Y., Yap, L. L., Chua, K. L., and Khoo, H. E. (2008) A multigene family of *Heteractis* magnificalysins (HMgs). *Toxicon* **51,** 1374–1382
46. Anderluh, G., Krizaj, I., Strukelj, B., Gubensek, F., Macek, P., and Pungercar, J. (1999) Equinatoxins, pore-forming proteins from the sea anemone *Actinia equina*, belong to a multigene family. *Toxicon* **37,** 1391–1401
47. Alvarez, C., Mancheño, J. M., Martínez, D., Tejuca, M., Pazos, F., and Lanio, M. E. (2009) Sticholysins, two pore-forming toxins produced by the Caribbean sea anemone *Stichodactyla helianthus*: their interaction with membranes. *Toxicon* **54,** 1135–1147
48. del Monte-Martínez, A., González-Bacerio, J., Romero, L., Aragón, C., Martínez, D., de Los Á Chávez, M., Álvarez, C., Lanio, M. E., Guisán, J. M., and Díaz, J. (2014) Improved purification and enzymatic properties of a mixture of sticholysin I and II: isotoxins with hemolytic and phospholipase A activities from the sea anemone *Stichodactyla helianthus*. *Protein Expr. Purif.* **95,** 57–66
49. Martínez, D., Morera, V., Alvarez, C., Tejuca, M., Pazos, F., García, Y., Raida, M., Padrón, G., and Eliana Lanio, M. (2002) Identity between cytolysins purified from two morphos of the Caribbean sea anemone *Stichodactyla helianthus*. *Toxicon* **40,** 1219–1221
50. Alegre-Cebollada, J., Clementi, G., Cunietti, M., Porres, C., Oñaderra, M., Gavilanes, J. G., and Pozo, A. M. (2007) Silent mutations at the 5′-end of the cDNA of actinoporins from the sea anemone *Stichodactyla helianthus* allow their heterologous overproduction in *Escherichia coli*. *J. Biotechnol.* **127,** 211–221
51. Uechi, G., Toma, H., Arakawa, T., and Sato, Y. (2010) Molecular characterization on the genome structure of hemolysin toxin isoforms isolated from sea anemone *Actineria villosa* and *Phyllodiscus semoni*. *Toxicon* **56,** 1470–1476
52. Ros, U., Pedrera, L., Diaz, D., Karam, J. C., Sudbrack, T. P., Valiente, P. A., Martinez, D., Cilli, E. M., Pazos, F., Itri, R., Lanio, M. E., Schreier, S., and Ávarez, C. (2011) The membranotropic activity of N-terminal peptides from the pore-forming proteins sticholysin I and II is modulated by hydrophobic and electrostatic interactions as well as lipid composition. *J. Biosci.* **36,** 781–791
53. Olivera, B. M., Rivier, J., Clark, C., Ramilo, C. A., Corpuz, G. P., Abogadie, F. C., Mena, E. E., Woodward, S. R., Hillyard, D. R., and Cruz, L. J. (1990) Diversity of *Conus* neuropeptides. *Science* **249,** 257–263
54. Alegre-Cebollada, J., Lacadena, V., Oñaderra, M., Mancheño, J. M., Gavilanes, J. G., and del Pozo, A. M. (2004) Phenotypic selection and characterization of randomly produced non-haemolytic mutants of the toxic sea anemone protein sticholysin II. *FEBS Lett.* **575,** 14–18
55. Laemmli, U. K. (1970) Cleavage of structural proteins during the assembly of the head of bacteriophage T4. *Nature* **227,** 680–685
56. Alegre-Cebollada, J., Martínez del Pozo, A., Gavilanes, J. G., and Goormaghtigh, E. (2007) Infrared spectroscopy study on the conformational changes leading to pore formation of the toxin sticholysin II. *Biophys. J.* **93,** 3191–3201
57. Pardo-Cea, M. A., Castrillo, I., Alegre-Cebollada, J., Martínez-del-Pozo, Á., Gavilanes, J. G., and Bruix, M. (2011) Intrinsic local disorder and a network of charge-charge interactions are key to actinoporin membrane disruption and cytotoxicity. *FEBS J.* **278,** 2080–2089
58. Martínez-Ruiz, A., García-Ortega, L., Kao, R., Lacadena, J., Oñaderra, M., Mancheño, J. M., Davies, J., Martínez del Pozo, A., and Gavilanes, J. G. (2001) RNase U2 and α-sarcin: A study of relationships. *Methods Enzymol.* **341,** 335–351
59. Bartlett, G. R. (1959) Colorimetric assay methods for free and phosphorylated glyceric acids. *J. Biol. Chem.* **234,** 469–471
60. Oñaderra, M., Mancheño, J. M., Lacadena, J., de los Rios, V., Martínez del Pozo, A., and Gavilanes, J. G. (1998) Oligomerization of the cytotoxin α-sarcin associated with phospholipid membranes. *Mol. Membr. Biol.* **15,** 141–144
61. Maula, T., Isaksson, Y. J., García-Linares, S., Niinivehmas, S., Pentikäinen, O. T., Kurita, M., Yamaguchi, S., Yamamoto, T., Katsumura, S., Gavilanes, J. G., Martínez-del-Pozo, A., and Slotte, J. P. (2013) 2NH and 3OH are crucial structural requirements in sphingomyelin for sticholysin II binding and pore formation in bilayer membranes. *Biochim. Biophys. Acta* **1828,** 1390–1395
62. García-Linares, S., Alm, I., Maula, T., Gavilanes, J. G., Slotte, J. P., and Martínez-Del-Pozo, Á. (2015) The effect of cholesterol on the long-range network of interactions established among sea anemone Sticholysin II residues at the water-membrane interface. *Mar. Drugs* **13,** 1647–1665
63. de los Ríos, V., Mancheño, J. M., Martínez del Pozo, A., Alfonso, C., Rivas, G., Oñaderra, M., and Gavilanes, J. G. (1999) Sticholysin II, a cytolysin from the sea anemone *Stichodactyla helianthus*, is a monomer-tetramer associating protein. *FEBS Lett.* **455,** 27–30
64. Pazos, I. F., Martínez, D., Tejuca, M., Valle, A., del Pozo, A., Alvarez, C., Lanio, M. E., and Lissi, E. A. (2003) Comparison of pore-forming ability in membranes of a native and a recombinant variant of Sticholysin II from *Stichodactyla helianthus*. *Toxicon* **42,** 571–578
65. Macek, P., Belmonte, G., Pederzolli, C., and Menestrina, G. (1994) Mechanism of action of equinatoxin II, a cytolysin from the sea anemone *Actinia equina* L. belonging to the family of actinoporins. *Toxicology* **87,** 205–227
66. Tanaka, K., Caaveiro, J. M., Morante, K., González-Mañas, J. M., and Tsumoto, K. (2015) Structural basis for self-assembly of a cytolytic pore lined by protein and lipid. *Nat. Commun.* **6,** 6337
67. Cosentino, K., Ros, U., and García-Sáez, A. J. (2016) Assembling the puzzle: oligomerization of α-pore forming proteins in membranes. *Biochim. Biophys. Acta* **1858,** 457–466
68. Ros, U., and García-Sáez, A. J. (2015) More than a pore: the interplay of pore-forming proteins and lipid membranes. *J. Membr. Biol.* **248,** 545–561
69. Subburaj, Y., Ros, U., Hermann, E., Tong, R., and García-Sáez, A. J. (2015) Toxicity of an α-pore-forming toxin depends on the assembly mechanism on the target membrane as revealed by single-molecule imaging. *J. Biol. Chem.* **290,** 4856–4865
70. Rojko, N., Dalla Serra, M., Maček, P., and Anderluh, G. (2016) Pore formation by actinoporins, cytolysins from sea anemones. *Biochim. Biophys. Acta* **1858,** 446–456
71. Martinez, D., Campos, A. M., Pazos, F., Alvarez, C., Lanio, M. E., Casallanovo, F., Schreier, S., Salinas, R. K., Vergara, C., and Lissi, E. (2001) Properties of St I and St II, two isotoxins isolated from *Stichodactyla helianthus*: a comparison. *Toxicon* **39,** 1547–1560
72. Wong, E. S., and Belov, K. (2012) Venom evolution through gene duplications. *Gene* **496,** 1–7
73. Valle, A., Alvarado-Mesén, J., Lanio, M. E., Álvarez, C., Barbosa, J. A., and Pazos, I. F. (2015) The multigene families of actinoporins (part I): isoforms and genetic structure. *Toxicon* **103,** 176–187
74. Brinkman, D. L., Konstantakopoulos, N., McInerney, B. V., Mulvenna, J., Seymour, J. E., Isbister, G. K., and Hodgson, W. C. (2014) *Chironex fleckeri* (box jellyfish) venom proteins: expansion of a cnidarian toxin family that elicits variable cytolytic and cardiovascular effects. *J. Biol. Chem.* **289,** 4798–4812
75. Dewson, G. (2016) Doughnuts, daisy chains and crescent moons: the quest for the elusive apoptotic pore. *EMBO J.* **35,** 371–373
76. Ros, U., Rodríguez-Vera, W., Pedrera, L., Valiente, P. A., Cabezas, S., Lanio, M. E., García-Sáez, A. J., and Alvarez, C. (2015) Differences in activity of actinoporins are related with the hydrophobicity of their N terminus. *Biochimie* **116,** 70–78
77. Martín-Benito, J., Gavilanes, F., de Los Ríos, V., Mancheño, J. M., Fernández, J. J., and Gavilanes, J. G. (2000) Two-dimensional crystal-

lization on lipid monolayers and three-dimensional structure of sticholysin II, a cytolysin from the sea anemone *Stichodactyla helianthus*. *Biophys. J.* **78,** 3186–3194

78. Mechaly, A. E., Bellomio, A., Gil-Cartón, D., Morante, K., Valle, M., González-Mañas, J. M., and Guérin, D. M. (2011) Structural insights into the oligomerization and architecture of eukaryotic membrane pore-forming toxins. *Structure* **19,** 181–191
79. Baker, M. A., Rojko, N., Cronin, B., Anderluh, G., and Wallace, M. I. (2014) Photobleaching reveals heterogeneous stoichiometry for equinatoxin II oligomers. *Chembiochem* **15,** 2139–2145
80. Morante, K., Caaveiro, J. M., Viguera, A. R., Tsumoto, K., and González-Mañas, J. M. (2015) Functional characterization of Val60, a key residue involved in the membrane-oligomerization of fragaceatoxin C, an actinoporin from *Actinia fragacea*. *FEBS Lett.* **589,** 1840–1846